

General Disclaimer

One or more of the Following Statements may affect this Document

- This document has been reproduced from the best copy furnished by the organizational source. It is being released in the interest of making available as much information as possible.
- This document may contain data, which exceeds the sheet parameters. It was furnished in this condition by the organizational source and is the best copy available.
- This document may contain tone-on-tone or color graphs, charts and/or pictures, which have been reproduced in black and white.
- This document is paginated as submitted by the original source.
- Portions of this document are not fully legible due to the historical nature of some of the material. However, it is the best reproduction available from the original submission.

NASA CR NO. 72967 V.2

VOLUME II

EXPERIMENTAL QUIET ENGINE PROGRAM

Contract No. NAS3-12430

PHASE I

ENGINE DESIGN REPORT

VOLUME II

March 15, 1970

Prepared for:

National Aeronautics and Space Administration
Lewis Research Center
Cleveland, Ohio, 44135

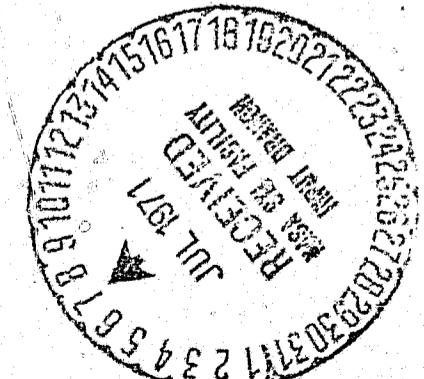
N71-29188

FACILITY FORM 602	(ACCESSION NUMBER) 305	(PAGES) CR-72967 v0/II	(THRU) 3
			(CODE) 28
			(CATEGORY)

ADVANCED TECHNOLOGY PROGRAMS DEPARTMENT

GENERAL  ELECTRIC

CINCINNATI, OHIO 45215



VOLUME II

EXPERIMENTAL QUIET ENGINE PROGRAM

Contract No. NAS3-12430

PHASE I

ENGINE DESIGN REPORT

VOLUME II

March 15, 1970

ADVANCED TECHNOLOGY PROGRAMS DEPARTMENT

GENERAL  ELECTRIC

CINCINNATI, OHIO 45215

TABLE OF CONTENTS

VOLUME II

<u>Section</u>	<u>Page</u>
7.0 TURBINE AND EXHAUST NOZZLE MECHANICAL DESIGN	337
7.1 LOW PRESSURE TURBINE ROTOR DESIGN	337
7.1.1 Summary	337
7.1.1.1 Fans A and B Turbine	337
7.1.1.1.1 Turbine Rotor	337
7.1.1.1.2 Turbine Cooling	339
7.1.1.1.3 Turbine Rotor Materials	341
7.1.1.1.4 Design Requirements	341
7.1.1.1.5 Design Analysis	349
7.1.1.2 Fan C Turbine	409
7.1.1.2.1 Turbine Rotor	416
7.1.1.2.2 Turbine Cooling	416
7.1.1.2.3 Turbine Rotor Materials	417
7.1.1.2.4 Design Analysis	417
7.2 LOW PRESSURE TURBINE STATOR DESIGN	455
7.2.1 Summary	455
7.2.2 Turbine Stator, Fans A and B	457
7.2.2.1 Turbine Nozzles	457
7.2.2.2 Turbine Casing	466
7.2.2.3 Turbine Shrouds	466
7.2.2.4 Interstage Seals	478
7.2.2.5 Axial Clearances	479
7.2.3 Turbine Stator, Fan C	481
7.2.3.1 Turbine Nozzle, Stage 2	481
7.2.3.2 Turbine Casing	486
7.2.3.3 Turbine Shrouds	486
7.2.3.4 Interstage Seal	492
7.3 LOW PRESSURE TURBINE FRAME AND EXHAUST NOZZLE DESIGN	493
7.3.1 Summary	493
7.3.1.1 Material Selection, Frames and Exhaust Nozzles	493
7.3.1.2 Engine A/B Frame and Nozzle Design	496
7.3.1.2.1 Engine A/B Midframe Design	496
7.3.1.2.2 Engine A/B Rear Frame Design	496
7.3.1.2.3 Engine A/B Exhaust Nozzle Design	496
7.3.1.3 Engine C Turbine Frame and Exhaust Nozzle Design	496
7.3.1.3.1 Engine C Turbine Midframe Design	496

TABLE OF CONTENTS (CONTINUED)

<u>Section</u>		<u>Page</u>
	7.3.1.3.2 Engine C Turbine Rear Frame Design	510
	7.3.1.3.3 Engine C Exhaust Nozzle Design	510
7.3.1.4	Thermal and Mechanical Stress Analysis - Turbine Frames and Exhaust Nozzles	510
	7.3.1.4.1 Analysis, A/B Turbine Midframe	512
	7.3.1.4.2 Analysis, A/B Turbine Rear Frame	512
	7.3.1.4.3 Analysis, A/B Exhaust Nozzle	528
	7.3.1.4.4 Analysis, Engine C Turbine Midframe	528
	7.3.1.4.5 Analysis, Engine C Turbine Rear Frame	536
	7.3.1.4.6 Analysis, Engine C Exhaust Nozzle	546
8.0	TURBINE THRUST BALANCE AND PARASITIC FLOW ANALYSIS	551
8.1	SUMMARY	551
8.2	METHOD OF ANALYSIS	551
8.3	RESULTS OF ANALYSIS	552
9.0	BEARINGS AND SEALS DESIGN	565
9.1	SUMMARY	565
9.2	FULL SCALE FAN COMPONENT BEARINGS AND SEALS DESIGN	565
9.2.1	Bearing Design	565
9.2.2	Lube and Scavenge System Design	569
9.3	CF6 BEARINGS, SEALS, AND DRIVES DESIGN	569
9.3.1	Bearings and Seals	569
9.3.2	Accessory Drives	574
9.4	CF6 LUBRICATION SYSTEM	575
9.4.1	Lubrication Subsystems	576
9.4.1.1	Lube Supply	577
9.4.1.2	Lube Scavenge	577
9.4.1.3	Sump Air Pressurization	581
9.4.1.4	Vent Air	582
9.5	EXPERIMENTAL QUIET ENGINE BEARINGS AND SEALS DESIGN	583
9.5.1	Sumps and Accessory Drives	583
9.5.2	Bearing and Seal Design	583
9.5.3	Lubrication System	584
10.0	CONTROLS AND ACCESSORIES AND CONFIGURATION DESIGN	585
10.1	SUMMARY	585

TABLE OF CONTENTS (CONCLUDED)

<u>Section</u>		<u>Page</u>
10.1.1	Power Control System	585
10.1.2	Fuel Supply System	586
10.1.3	Electrical System	586
10.1.4	Configuration Design	586
11.0	INSTALLATION AERODYNAMICS AND PERFORMANCE	591
11.1	SUMMARY	591
11.1.1	Inlet Cowl and Diffuser Aerodynamic Design	591
11.1.2	Fan Bypass Duct and Nozzle Aerodynamic Design	591
11.1.3	Core Duct and Nozzle Aerodynamic Design	594
11.1.4	Core Cowl Aerodynamic Design	600
11.1.5	Aircraft Pylon and Lower Pylon Fairing Aerodynamic Design	600
11.1.6	NASA-Lewis Facility Installation Aerodynamic Design	604
12.0	TEST AND INSTRUMENTATION	611
12.1	SUMMARY	611
12.2	FULL SCALE COMPONENT TESTING OF FANS A, B, C, AND X	611
12.2.1	Test Objectives	611
12.2.2	Instrumentation	612
12.2.2.1	Aerodynamic Instrumentation	612
12.2.2.2	Acoustic Instrumentation	615
12.2.2.3	Safety Instrumentation	615
12.3	SCALE MODEL ACOUSTIC TESTING OF CONFIGURATIONS B AND C	616
12.3.1	Test Objectives	616
12.3.2	Acoustic Instrumentation	616
12.3.2.1	Aerodynamic Instrumentation	616
12.3.2.2	Acoustic Instrumentation	618
12.3.2.3	Safety Instrumentation	618
12.4	FULL SCALE ENGINE TESTING	618
12.4.1	Test Objectives	619
12.4.2	Instrumentation	619
12.4.2.1	Aerodynamic Instrumentation	619
12.4.2.2	Acoustic Instrumentation	621
12.4.2.3	Safety Instrumentation	622
13.0	ENGINE CYCLE PERFORMANCE	623
13.1	SUMMARY	623
13.2	ENGINE CYCLE PERFORMANCE	623
14.0	REFERENCES	627

LIST OF ILLUSTRATIONS

VOLUME II

<u>Figure</u>		<u>Page</u>
191	Low Pressure Turbine for Fans A and B	338
192	Low Pressure Turbine Blade Retainer Design	340
193	Temperature Profiles for the Fans A and B Low Pressure Turbine	345
194	Hot Flowpath for the Fan C Low Pressure Turbine	346
195	Temperature Profiles for the Fan C Low Pressure Turbine Blades	348
196	Blade Nomenclature for the Fans A, B, and C Low Pressure Turbines	350
197	Fans A/B Stage 1 Turbine Blade Steady State Stress	352
198	Fans A/B Stage 2 Turbine Blade Steady State Stress	353
199	Fans A/B Stage 3 Turbine Blade Steady State Stress	354
200	Fans A/B Stage 4 Turbine Blade Steady State Stress	355
201	Campbell Diagram for the Fans A/B Stage 1 Turbine Rotor	356
202	Campbell Diagram for the Fans A/B Stage 2 Turbine Rotor	357
203	Campbell Diagram for the Fans A/B Stage 3 Turbine Rotor	358
204	Campbell Diagram for the Fans A/B Stage 4 Turbine Rotor	359
205	Stress Distribution for the Fans A/B Stage 1 Turbine, 444 CPS, 1st Flexural, In-Phase	361
206	Stress Distribution for the Fans A/B Stage 1 Turbine, 1067 CPS, 1st Axial, Out-of-Phase	362
207	Stress Distribution for the Fans A/B Stage 1 Turbine, 4315 CPS, 2nd Flexural, Out-of-Phase	363
208	Stress Distribution for the Fans A/B Stage 1 Turbine, 2041 CPS, 1st Flexural, Out-of-Phase	364
209	Stress Distribution for the Fans A/B Stage 1 Turbine, 2206 CPS, 1st Torsional, Out-of-Phase	365

LIST OF ILLUSTRATIONS (CONTINUED)

<u>Figure</u>		<u>Page</u>
210	Stress Distribution for the Fans A/B Stage 2 Turbine, 321 CPS, 1st Flexural, In-Phase	366
211	Stress Distribution for the Fans A/B Stage 2 Turbine, 801 CPS, 1st Axial, Out-of-Phase	367
212	Stress Distribution for the Fans A/B Stage 2 Turbine, 1430 CPS, 1st Flexural, Out-of-Phase	368
213	Stress Distribution for the Fans A/B Stage 2 Turbine, 1992 CPS, 1st Torsional, Out-of-Phase	369
214	Stress Distribution for the Fans A/B Stage 3 Turbine, 224 CPS, 1st Flexural, In-Phase	370
215	Stress Distribution for the Fans A/B Stage 3 Turbine, 657 CPS, 1st Axial, Out-of-Phase	371
216	Stress Distribution for the Fans A/B Stage 3 Turbine, 940 CPS, 1st Flexural, Out-of-Phase	372
217	Stress Distribution for the Fans A/B Stage 3 Turbine, 1365 CPS, 1st Torsional, Out-of-Phase	373
218	Stress Distribution for the Fans A/B Stage 3 Turbine, 2633 CPS, 2nd Flexural, Out-of-Phase	374
219	Stress Distribution for the Fans A/B Stage 4 Turbine, 168 CPS, 1st Flexural, In-Phase	375
220	Stress Distribution for the Fans A/B Stage 4 Turbine, 521 CPS, 1st Axial, Out-of-Phase	376
221	Stress Distribution for the Fans A/B Stage 4 Turbine, 666 CPS, 1st Flexural, Out-of-Phase	377
222	Stress Distribution for the Fans A/B Stage 4 Turbine, 1207 CPS, 1st Torsional, Out-of-Phase	378
223	Stress Distribution for the Fans A/B Stage 4 Turbine, 1860 CPS, 2nd Flexural, Out-of-Phase	379
224	Blade Dovetail Schematic	380
225	Fans A/B, LP Turbine Rotor, Dovetail Stress Analysis, Stage 1	386
226	Fans A/B, LP Turbine Rotor, Dovetail Stress Analysis, Stage 2	387

LIST OF ILLUSTRATIONS (CONTINUED)

<u>Figure</u>		<u>Page</u>
227	Fans A/B, LP Turbine Rotor, Dovetail Stress Analysis, Stage 3	388
228	Fans A/B, LP Turbine Rotor, Dovetail Stress Analysis, Stage 4	389
229	Fans A/B, LP Turbine Rotor, Stage 1 Steady State Stress, 3236 RPM	392
230	Fans A/B, LP Turbine Rotor, Stage 1 Steady State Stress, 3830 RPM	393
231	Fans A/B, LP Turbine Rotor, Stage 2 Steady State Stress, 3236 RPM	394
232	Fans A/B, LP Turbine Rotor, Stage 2 Steady State Stress, 3830 RPM	395
233	Fans A/B, LP Turbine Rotor, Stage 3 Steady State Stress, 3236 RPM	396
234	Fans A/B, LP Turbine Rotor, Stage 3 Steady State Stress, 3830 RPM	397
235	Fans A/B, LP Turbine Rotor, Stage 4 Steady State Stress, 3236 RPM	398
236	Fans A/B, LP Turbine Rotor, Stage 4 Steady State Stress, 3830 RPM	399
237	Fans A/B, LP Turbine Steady State Disc Temperature	400
238	Fans A and B Turbine Rotor Multishell Analysis, Effective Surface Stress, KSI	406
239	Fans A/B LP Turbine, Stage 1 Campbell Diagram	410
240	Fans A/B LP Turbine, Stage 2 Campbell Diagram	411
241	Fans A/B LP Turbine, Stage 3 Campbell Diagram	412
242	Fans A/B LP Turbine, Stage 4 Campbell Diagram	413
243	Fans A and B LP Turbine Rotor Steady State Temperatures	414
244	Fan C Low Pressure (LP) Turbine	415

LIST OF ILLUSTRATIONS (CONTINUED)

<u>Figure</u>		<u>Page</u>
245	Fan C LP Turbine Stage 1 Blade, Steady State Stress	420
246	Fan C LP Turbine Stage 2 Blade, Steady State Stress	421
247	Fan C LP Turbine, Stage 1 Campbell Diagram	423
248	Fan C LP Turbine, Stage 2 Campbell Diagram	424
249	Stress Distribution for the Fan C Stage 1 Turbine, 378 CPS, 1st Flexural, In-Phase	428
250	Stress Distribution for the Fan C Stage 1 Turbine, 748 CPS, 1st Axial, In-Phase	429
251	Stress Distribution for the Fan C Stage 1 Turbine, 1601 CPS, 1st Flexural, Out-of-Phase	430
252	Stress Distribution for the Fan C Stage 1 Turbine, 2351 CPS, 1st Torsional, Out-of-Phase	431
253	Stress Distribution for the Fan C Stage 1 Turbine, 4241 CPS, 2nd Flexural, Out-of-Phase	432
254	Stress Distribution for the Fan C Stage 2 Turbine, 234 CPS, 1st Flexural, In-Phase	433
255	Stress Distribution for the Fan C Stage 2 Turbine, 642 CPS, 1st Axial, In-Phase	434
256	Stress Distribution for the Fan C Stage 2 Turbine, 868 CPS, 1st Flexural, Out-of-Phase	435
257	Stress Distribution for the Fan C Stage 2 Turbine, 1645 CPS, 1st Torsional, Out-of-Phase	436
258	Stress Distribution for the Fan C Stage 2 Turbine, 2392 CPS, 2nd Flexural, Out-of-Phase	437
259	Fan C, LP Turbine Rotor, Dovetail Stress Analysis, Stage 1	438
260	Fan C, LP Turbine Rotor, Dovetail Stress Analysis, Stage 2	439

LIST OF ILLUSTRATIONS (CONTINUED)

<u>Figure</u>	<u>Page</u>
261 Fan C, LP Turbine Rotor, Stage 1 Steady State Stress, 4604 RPM	443
262 Fan C, LP Turbine Rotor, Stage 2 Steady State Stress, 4604 RPM	444
263 Fan C, LF Turbine Rotor, Stage 1 Steady State Stress, 5440 RPM (Overspeed)	445
264 Fan C, LP Turbine Rotor, Stage 2 Steady State Stress, 5440 RPM (Overspeed)	446
265 Fan C LP Turbine Steady State Disc Temperature	447
266 Fan C LP Turbine Rotor Multishell Analysis, Effective Surface Stress, KSI (4605 RPM)	451
267 Fan C Interstage Seal Campbell Diagram	453
268 Fan C Pressure Balance Seal Campbell Diagram	454
269 Fan C LP Turbine Rotor Steady State Temperatures	456
270 Radial Temperature Profile Entering the Fan A and B LP Turbine Nozzles	458
271 Cast Material Properties, Rene' 80 (C50TF28), 3 Standard Deviations	460
272 Fans A and B LP Turbine Stator Details	461
273 Fans A and B Stage 1 Vane, Gas Load Stresses	462
274 Fans A and B Stage 2 Vane, Gas Load Stresses	463
275 Fans A and B Stage 3 Vane, Gas Load Stresses	464
276 Fans A and B Stage 4 Vane, Gas Load Stresses	465
277 Campbell Diagram for the Fans A/B Stage 1 Vane, In-Phase Modes	467
278 Campbell Diagram for the Fans A/B Stage 1 Vane, Out-of-Phase Modes	468
279 Campbell Diagram for the Fans A/B Stage 2 Vane, In-Phase Modes	469

LIST OF ILLUSTRATIONS (CONTINUED)

<u>Figure</u>		<u>Page</u>
280	Campbell Diagram for the Fans A/B Stage 2 Vane, Out-of-Phase Modes	470
281	Campbell Diagram for the Fans A/B Stage 3 Vane, In-Phase Modes	471
282	Campbell Diagram for the Fans A/B Stage 3 Vane, Out-of-Phase Modes	472
283	Campbell Diagram for the Fans A/B Stage 4 Vane, In-Phase Modes	473
284	Campbell Diagram for the Fans A/B Stage 4 Vane, Out-of-Phase Modes	474
285	LP Turbine Casing Temperatures for Fans A and B	475
286	LP Turbine Casing Stresses for Fans A and B	476
287	Forced Inconel 718 Material Properties	477
288	Vibration Analysis of Static Interstage Seals for LP Turbine Stages 1 through 4, Fans A and B	480
289	Flowpath, Fan C Low Pressure Turbine	482
290	Radial Temperature Profile for the Fan C Low Pressure Turbine Stage 2 Vane, Inlet Temperature	483
291	Tangential Load Stop for the Fan C LP Turbine Stage 2 Vane	484
292	Fan C Stage 2 Vane, Gas Load Stresses	485
293	Campbell Diagram for the Fan C Stage 2 Vane, In-Phase Modes	487
294	Campbell Diagram for the Fan C Stage 2 Vane, Out-of-Phase Modes	488
295	Turbine Casing Metal Temperatures for the Fan C Low Pressure Turbine	489
296	Turbine Casing Maximum Stresses for the Fan C Low Pressure Turbine	490

LIST OF ILLUSTRATIONS (CONTINUED)

<u>Figure</u>		<u>Page</u>
297	Tangential Load Stop for the Fan C LP Turbine Stage 1 Shroud	491
298	Vibration Analysis of the Stage 2 Seal for the Fan C LP Turbine	494
299	Engine A and B Low Pressure Turbine Frame Assembly	498
300	Engine A and B Exhaust Nozzle Assembly	501
301	Engine A and B Turbine Midframe Isometric	503
302	Engine A and B Turbine Midframe Bolt Connection of Frame Struts	504
303	Turbine Rear Frame Assembly	505
304	Engine C Low Pressure Turbine Frame and Exhaust Nozzle Assembly	507
305	Fan C Turbine Midframe Strut Casting (311788)	509
306	Turbine Midframe Maximum Mount Loads	513
307	Bearing Cone Stresses	514
308	Flight Maneuver Loading Diagram	517
309	Engine A/B Turbine Axial Loads, Pounds	519
310	Maximum Stresses Engine A/B Turbine Midframe	520
311	Strut Maximum Stresses, Turbine Midframe	521
312	Turbine Midframe Mount Stress Summary	522
313	Inconel 718 Sheet Material Properties, 30 Deviation	523
314	Inconel 718 Cast Material Properties, 30 Deviation	524
315	Rene' 41 Cast Material Properties, 30 Deviation	525
316	Engine A Integrated Profile of Peaks	526

LIST OF ILLUSTRATIONS (CONTINUED)

<u>Figure</u>		<u>Page</u>
317	Engine B Integrated Profile of Peaks	527
318	Engine A/B Turbine Rear Frame Maximum Stresses	529
319	Turbine Rear Frame Maximum Strut Stresses	530
320	Frame Temperatures, Engine A/B	532
321	Inconel 718 Cast Material Properties, 3 σ Deviation	533
322	Engine A/B Exhaust Nozzle Shell Stability	534
323	Hastelloy X Yield and Rupture Stresses with 3 σ Deviation	535
324	Engine C Frame Temperatures	538
325	Engine C Turbine Midframe Outer and Inner Ring Stresses	539
326	Cast Rene' 41 Material Properties, 3 σ Deviation (Engine C Turbine Midframe Maximum Stresses)	540
327	A-286 Forged Material Properties, 3 σ Deviation	541
328	Inconel 718 Material Properties, 3 σ Deviation (Engine C Turbine Midframe Maximum Stresses)	542
329	Engine C Turbine Axial Loads, Pounds	543
330	Engine C LP Turbine Stage 1 Vane Natural Frequencies	544
331	Engine C Integrated Profile of Peaks	545
332	Engine C Turbine Rear Frame Maximum Stresses	547
333	Inconel 718 Cast Material Properties, 3 σ Deviation (Engine C Turbine Rear Frame Maximum Stress)	548
334	Engine C Exhaust Nozzle Shell Stability	549
335	Engine Forward Cavity Pressures and Flows, Fans A/B	555
336	Engine Forward Cavity Pressures and Flows, Fan C	556
337	Engine Mid-Cavity Pressures and Flows, Fan A	557
338	Engine Mid-Cavity Pressures and Flows, Fan B	558

LIST OF ILLUSTRATIONS (CONTINUED)

<u>Figure</u>		<u>Page</u>
339	Engine Mid-Cavity Pressures and Flows, Fan C	559
340	Engine Aft Cavity Pressures and Flows, Fan A	560
341	Engine Aft Cavity Pressures and Flows, Fan B	561
342	Engine Aft Cavity Pressures and Flows, Fan C	563
343	Full Scale Fan Component and Test Facility Assembly	567
344	CF6 B Sump	571
345	CF6 Bearing Arrangements	573
346	Lube System Schematic	579
347	Left Side, CF6 Engine	587
348	Right Side, CF6 Engine	587
349	Schematic of the Thick-Lip Inlet for Engine B	592
350	Fan B Inlet Diffuser and Equivalent Conical Diffusion Angle With and Without the 13-Inch Cylindrical Section	593
351	Schematic of the Experimental Quiet Engine Installation	595
352	Fan Duct and Nozzle Mach Number Distribution for Distribution for Engines A, B, and C at Cruise Conditions	596
353	Fan Duct and Nozzle Mach Number Distribution for Engines A, B, and C at Take-off Conditions ($M_{\infty} = 0$)	597
354	Flow Area Distributions for Engines A, B, and C Fan Duct and Nozzle	598
355	Core Duct and Nozzle Mach Number Distribution for Engines A, B, and C at Cruise Conditions	601
356	Core Duct and Nozzle Mach Number Distribution for Engines A, B, and C at Take-off Conditions ($M_{\infty} = 0$)	602
357	Flow Area Distributions for Engines A, B, and C Core Duct and Nozzle	603

LIST OF ILLUSTRATIONS (CONCLUDED)

<u>Figure</u>		<u>Page</u>
358	Schematic of the NASA-Lewis Installations Bypass Ducts, Indicating Common Parts and the Proposed Locations of Splitters Used to Increase the Amount of Duct Acoustic Treatment	605
359	Bypass Duct Flow Area Distribution of the NASA-Lewis Installation for Fans A and B	606
360	Bypass Duct Flow Area Distribution of the NASA-Lewis Installation for Fan C	607
361	Core Duct Flow Area Distribution of the NASA-Lewis Installation for Fans A, B, and C	608
362	Bypass Duct Mach Number Distributions for the NASA-Lewis Installations	609
363	Full Scale Fan Instrumentation Schematic	613
364	Instrumentation Planes, Acoustic Scale Model Vehicles	617
365	Typical Station Designations for Aerodynamic Instrumentation	620

LIST OF TABLES

<u>Section</u>	<u>VOLUME II</u>	<u>Page</u>
LII.	Rotor Material List	342
LIII.	LP Turbine Rotor Blade Summary, Fans A and B	344
LIV.	Fan C LP Turbine Rotor Blade Summary	347
LV.	Fan A and B LP Turbine Rotor Stage 1 Blade Dovetail Stress Analysis (3500 RPM)	381
LVI.	Fan A and B LP Turbine Rotor Stage 2 Blade Dovetail Stress Analysis (3500 RPM)	382
LVIII.	Fan A and B LP Turbine Rotor Stage 3 Blade Dovetail Stress Analysis (3500 RPM)	383
LVIII.	Fan A and B LP Turbine Rotor Stage 4 Blade Dovetail Stress Analysis (3500 RPM)	384
LIX.	Fan A and B LP Turbine Rotor Stage 1 Disc Dovetail Stress Analysis (3500 RPM)	402
LX.	Fan A and B LP Turbine Rotor Stage 2 Disc Dovetail Stress Analysis (3500 RPM)	403
LXI.	Fan A and B LP Turbine Rotor Stage 3 Disc Dovetail Stress Analysis (3500 RPM)	404
LXII.	Fan A and B LP Turbine Rotor Stage 4 Disc Dovetail Stress Analysis (3500 RPM)	405
LXIII.	LP Turbine Shaft and Bolt Stress Summary, SLS - Standard Day	408
LXIV.	Fan C Rotor Material List	418
LXV.	Fan C LP Turbine Rotor Stage 1 Blade Dovetail Stress Analysis (4605 RPM)	426
LXVI.	Fan C LP Turbine Rotor Stage 2 Blade Dovetail Stress Analysis (4605 RPM)	427
LXVII.	Fan C LP Turbine Rotor Stage 1 Disc Dovetail Stress Analysis (4605 RPM)	448
LXVIII.	Fan C LP Turbine Rotor Stage 2 Disc Dovetail Stress Analysis (4605 RPM)	449

LIST OF TABLES (CONTINUED)

<u>Section</u>		<u>Page</u>
LXIX.	Turbine Nozzle Inlet Temperature and Pressures	457
LXX.	Fans A and B Gas-Loaded Stresses	459
LXXI.	Seal Pressures and Temperatures, Fans A and B	478
LXXII.	Fans A and B LP Turbine Stator Critical Axial Clearances	479
LXXIII.	Fan C Shroud Nominal Radial Clearances	492
LXXIV.	Material Selection for Turbine Frames and Exhaust Nozzles	495
LXXV.	Frame Spring Constants	511
LXXVI.	Maximum Maneuver Load Combinations	515
LXXVII.	Fan A/B Turbine Midframe Unit Loads	516
LXXVIII.	Unit Bearing Loads for Maneuver Case	518
LXXIX.	Frame Temperatures, °F	531
XXC.	Fan C Turbine Midframe Unit Loads	531
XIXC.	Flow Network Boundary Conditions	553
XVIIIC.	Bearing Thrust Loads	554
XVIIC.	Full Scale Fans A, B, and C Roller Bearing Data	568
XVIC.	Experimental Quiet Engine Installation Exhaust Losses	599
XVC.	NASA-Lewis Facility Installation Duct Losses	610
XIVC.	Predicted Cycle Performance Data	624

7.0 TURBINE AND EXHAUST NOZZLE MECHANICAL DESIGN

7.1 LOW PRESSURE TURBINE ROTOR DESIGN

7.1.1 Summary

This section presents the methods and procedures used in the mechanical design of the low pressure turbine rotors for Experimental Quiet Engine Configurations A, B, and C.

The Fans A and B low pressure turbine rotor uses the first four stages of the CF6 five-stage low pressure turbine rotor. The Fans A and B rotor mechanical requirements are substantially reduced when compared to the CF6 engine, because of the lower rotor temperatures and speed. This results in increased design margin on all Fan A and B rotor components.

The Fan C low pressure turbine rotor is a new two-stage design. The design of the rotor blading, discs, and shafts utilizes proven CF6 design concepts.

The Fan C rotor is an overhung design, being supported on a single conical shaft. The blading tip speeds have been maintained at a level which is lower than that of the CF6. All blades have tip shrouds to insure adequate mechanical damping for prevention of excessive airfoil vibration.

The materials used in both the A and B rotor and the C rotor are the same as those used on the CF6-6 to take maximum advantage of CF6-6 experience.

7.1.1.1 Fans A and B Turbine

The low pressure turbine (LPT) for configurations A and B consists of four stages which extract energy from the primary gas stream to drive the fan. The general arrangement of this turbine is shown in Figure 191.

7.1.1.1.1 Turbine Rotor

The LP turbine rotor for Fans A and B consists of four blade and disc assemblies, two shafts, four interstage seals, and a heat shield.

Each disc has a large bore and integral spacer arms with mating flanges on the ends.

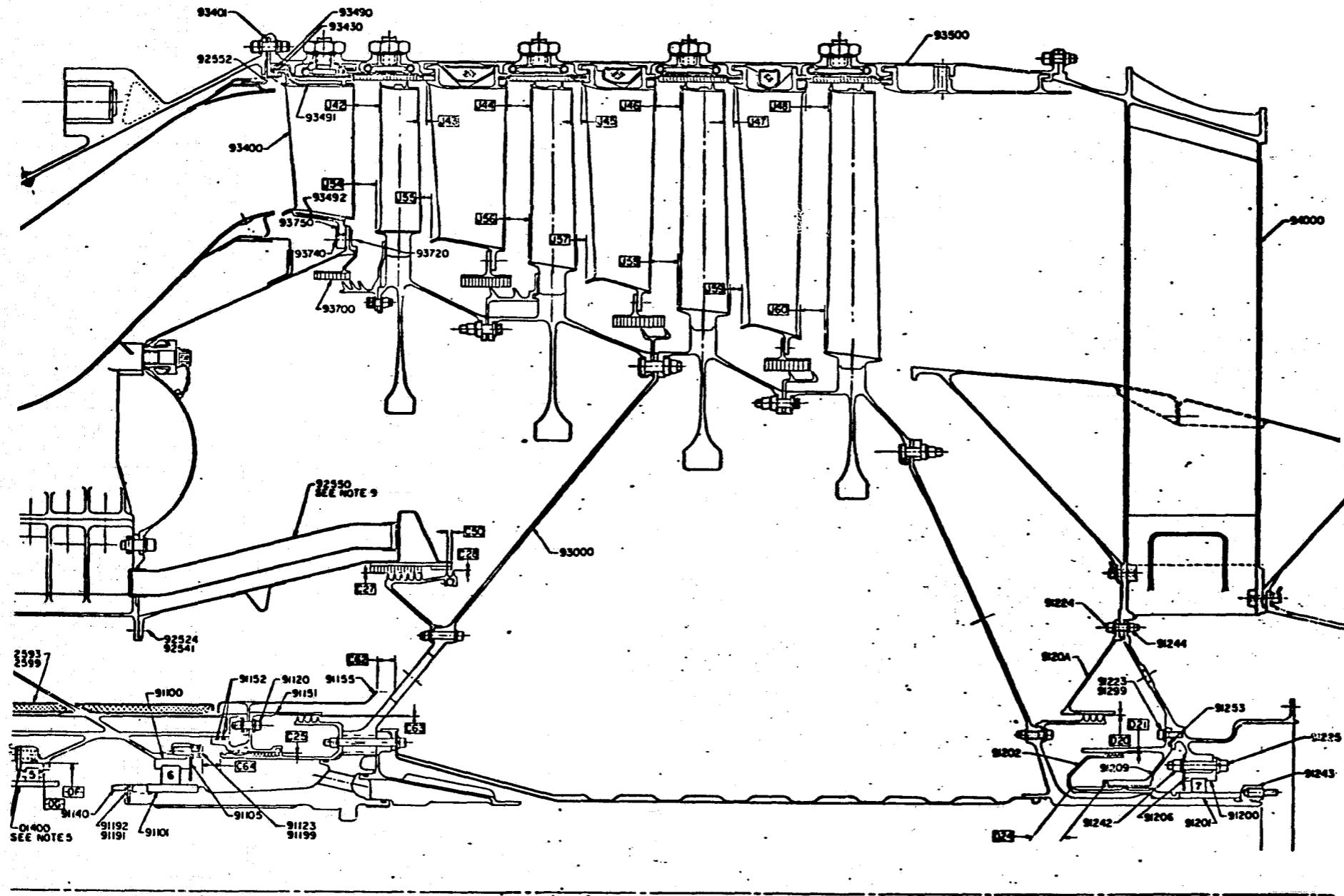


Figure 191. Low Pressure Turbine for Fans A and

The blades have integral tip shrouds which are interlocked by a "Z" form with their neighbors. This arrangement prevents high vibratory stress of the blading. The "Z" form is deep to prevent unlatching, and the mating surfaces are built up in size and hardfaced with chromium carbide to prevent wear. Each tip shroud also has two labyrinth seal teeth to oppose the stator shroud to minimize tip leakage.

The blades are retained in the disc by modified "dogbone" retainers (see Figure 192). The retainers are bent into place during assembly.

The two shafts are conical to provide stiffness. The forward shaft is attached to the fan shaft by a differential, threaded coupling bolt and supports the front end of the turbine on the Number 6 bearing in the turbine midframe. The OD flange of this shaft sandwiches between the second and third stage disc flanges.

The aft shaft supports the aft end of the turbine on the Number 7 bearing in the turbine rear frame. The OD flange of this shaft is attached to the aft disc spacer flange of Stage 4.

The interstage seals are separate parts which also sandwich between the disc spacer flanges. Each seal, except a three-tooth stage 1, consists of two slanted labyrinth seal teeth which are aluminum oxide hardfaced for wear resistance. The two-tooth seals are spaced such that their wear grooves in the stator seal will not overlap and cause high leakage. The slanted teeth are to reduce leakage.

In addition, the Stage 2 seal extends aft to form a plenum on the face of the Stage 2 disc rim. A small amount of coolant, bled into this plenum, cools the second-stage disc rim and dovetail area.

All of the flange bolting is done with close-tolerance bolts, which assure rotor alignment and power transmission.

The final part of the LP turbine rotor is a heat shield tube, which is installed in the center of the rotor for the purpose of channeling sump air to the turbine rear frame and preventing this air from being heated by the rotor.

7.1.1.1.2 Turbine Cooling

The turbine cooling paths are shown in Figure 191 and include a small amount of coolant for both rotor and stator.

The rotor uses ninth-stage bleedflow from the piston balance seal to cool the first two stages. This coolant is a combination of seal leakage plus flow through holes in the side of the balance piston seal. There are two cooling paths:

340

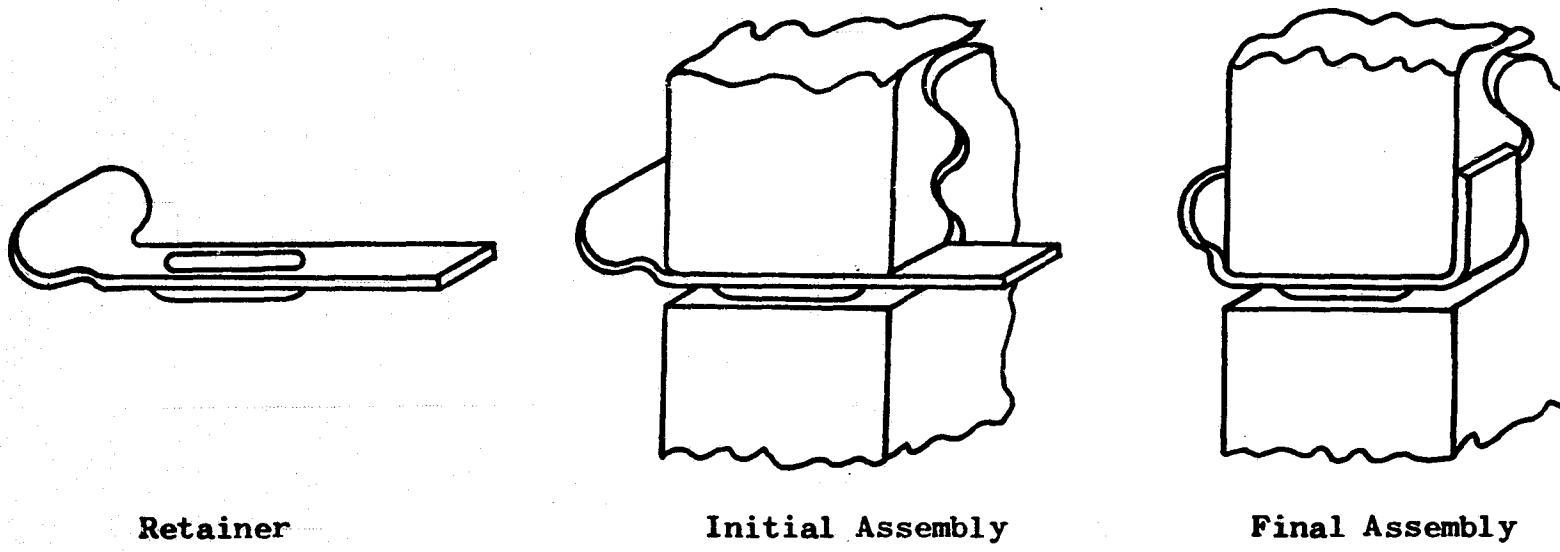


Figure 192. Low Pressure Turbine Blade Retainer Design

1. First-Stage Cooling. The first-stage stator seal opposes a single seal tooth projection on the first-stage disc. This is a "leak positive" seal, sized such that it never closes and flows 0.20 lb/sec to cool the rim of the first-stage disc.
2. Second-Stage Cooling. The second-stage rotor interstage seal forms a cavity with the second-stage disc spacer arm and the face of the disc. Coolant is bled into this cavity through the dovetail slots, thus cooling the disc rim. The quantity of coolant is 0.187 lb/sec.

Since much of this coolant flow (balance seal leakage and CDP recoup) would be a loss to the cycle, whether or not it is used for cooling, the cost to the cycle is very small for cooling the low pressure turbine.

7.1.1.1.3 Turbine Rotor Materials

Materials used in the low pressure turbine are all commercially-available alloys with good records of successful use. Each material was carefully selected for strength and the best balance of life, weight, cost, and resistance to environmental deterioration.

Because of the material selection and the relatively mild environmental conditions, it was not found necessary to protective coat the airfoils to resist corrosive/erosive effects. The only protective coatings of any kind used on the turbine are for wear resistance. These are chromium carbide on the blade tip shroud interlock mating faces and aluminum oxide on the rotor interstage seal teeth.

The material list that follows (see Table LII) tabulates the materials used in the LP turbine parts. Each material is designated by its common name plus the AMS or General Electric Specification Number which is used to control its use.

7.1.1.1.4 Design Requirements

The design of the low pressure turbines (Fans A/B and C), is based on the maximum operating conditions as specified for the engines. This requirement results in two important design limits:

- a) For LP turbine for Fans A and B, the maximum stress and temperature occur at the engine condition of sea level static, hot day, at which point the turbine conditions are $P_{5.4} = 52.8$ psia, $T_{5.4} = 1271^{\circ}\text{F}$, and $N_F = 3414$ rpm.
- b) For LP turbine for Fan C, the maximum stress and temperature occur at the engine condition of sea level static, hot day, at which point the turbine conditions are $P_{5.4} = 54.3$ psia, $T_{5.4} = 1297^{\circ}\text{F}$, and $N_F = 4843$ rpm.

Table LII. Rotor Material List

Part	Qty	Material	
		Name	Spec. No.
Discs - All Stages	4	IN 718	C50TF6
Blades - All Stages	546	R77*	C50TF15 Cl B
Shaft - Forward	1	IN 718	C50TF6
Shaft - Aft	1	A-286	C50T41D
Interstage Seals, Stages 2, 3, 4	3	IN 718**	C50TF6 Cl B
Forward Seal, Stage 1	1	IN 718**	C50TF6 Cl B
Retainers, Blade	546	IN 718	B50TF14 Cl A
Heat Shield	1	321	AMS 5510
Flange Bolts	355	IN 718	C50T82
Nuts	355	Waspalloy	AMS 5709

* Tip shroud interlock contact surface plasma sprayed with chromium carbide per General Electric Specification P50T30D.

** Seal teeth plasma sprayed with aluminum oxide per General Electric Specification Pl 6TF3 Cl B with B50TF58 Cl A material.

The aerodynamic design requirements for both the low pressure turbines follow:

- a) For LP turbine for Fans A and B, the aerodynamic design requirements were determined by the power and speed requirements of the fan and by the need to hold a relatively low tip diameter to obtain an optimum boat trail angle on the cowl aft of the fan discharge; coupled with this, was high efficiency as required by the engine thermodynamic cycle. The result was a low-tip-speed turbine, utilizing 4 stages for optimum power extraction and efficiency. The turbine is derived by removing the last stage from the 5-stage CF6 LP turbine. This produces a low stage loading which, together with the relatively low tip speed, results in an inherently low-stressed design.

The resulting geometry of the turbine is shown in Table LIII, which tabulates important design parameters such as number of blades, chords, etc. The rotor blade temperature profiles are shown in Figure 193. These blade temperatures were obtained by scaling the CF6 blade temperatures with the appropriate interstage data from the two turbines. The temperatures shown are average stage temperatures and are based on cycle analysis without any adders for deterioration, control error, etc.

- b) For LP turbine for Fan C, the aerodynamic design requirements were determined by the power and speed requirement of Fan C and by the design intention to remove the gooseneck flowpath between the HP and LP turbines such as found in engines A and B. Coupled with this was high efficiency as required by the engine thermodynamic cycle. The result was a low-tip-speed turbine, utilizing a two-stage turbine. This produces a nominal over-all loading on the turbine with the first stage highly loaded and the second stage lightly loaded. However, the turbine has airfoil requirements such that the mechanical design is inherently low stressed.

The resulting turbine hot flowpath is shown in Figure 194. Table LIV tabulates important design parameters such as number of blades, chords, etc. The rotor blade temperature profiles are shown in Figure 195. These temperatures were scaled similarly to the temperatures for the LP turbine on Fans A and B. The blade temperatures shown are average stage temperatures and are based on cycle analysis without any adders for deterioration, control error, etc.

Table LIII. LP Turbine Rotor Blade Summary, Fans A and B

345

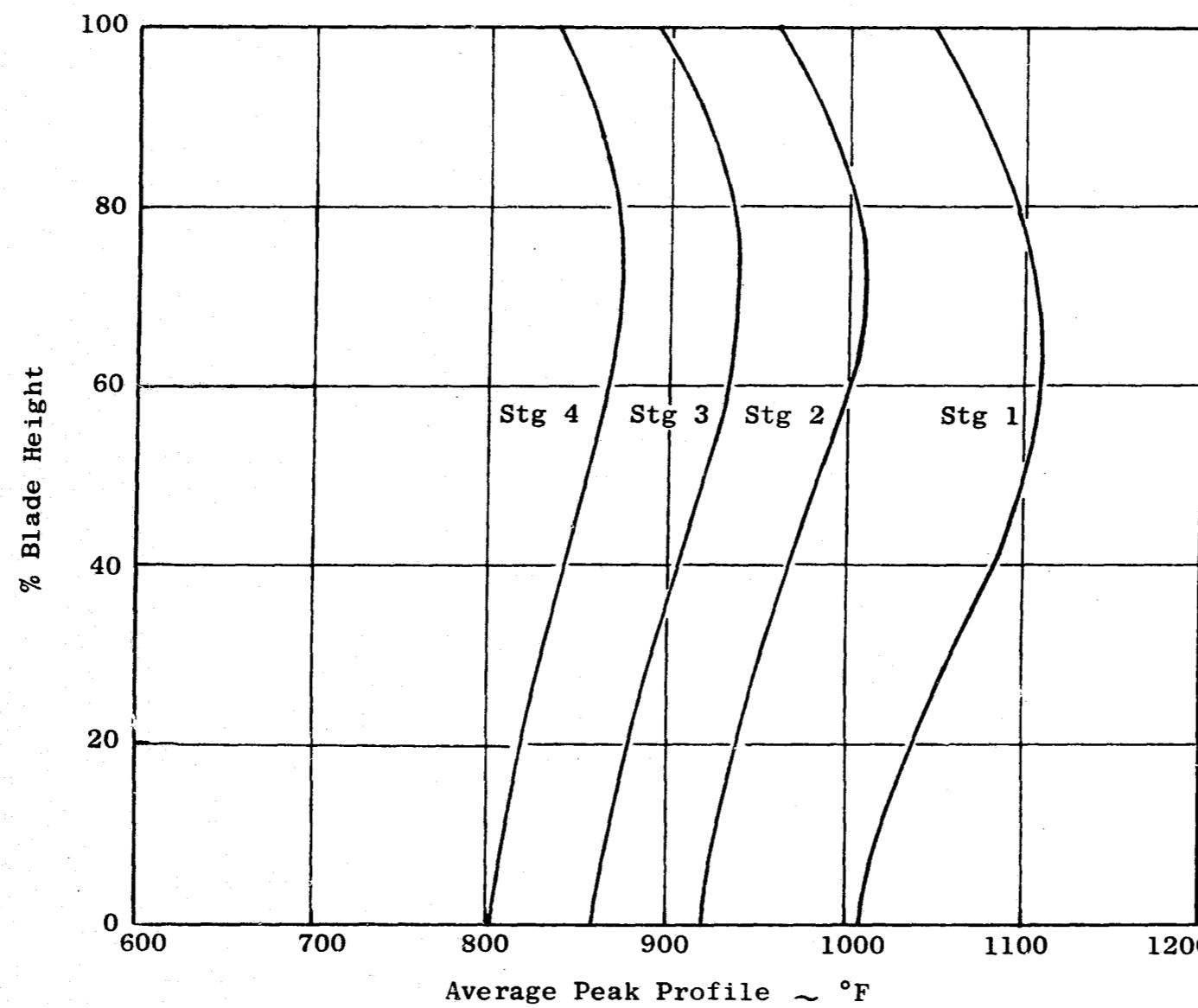


Figure 193. Temperature Profiles for the Fans A and B Low Pressure Turbine Blades

34

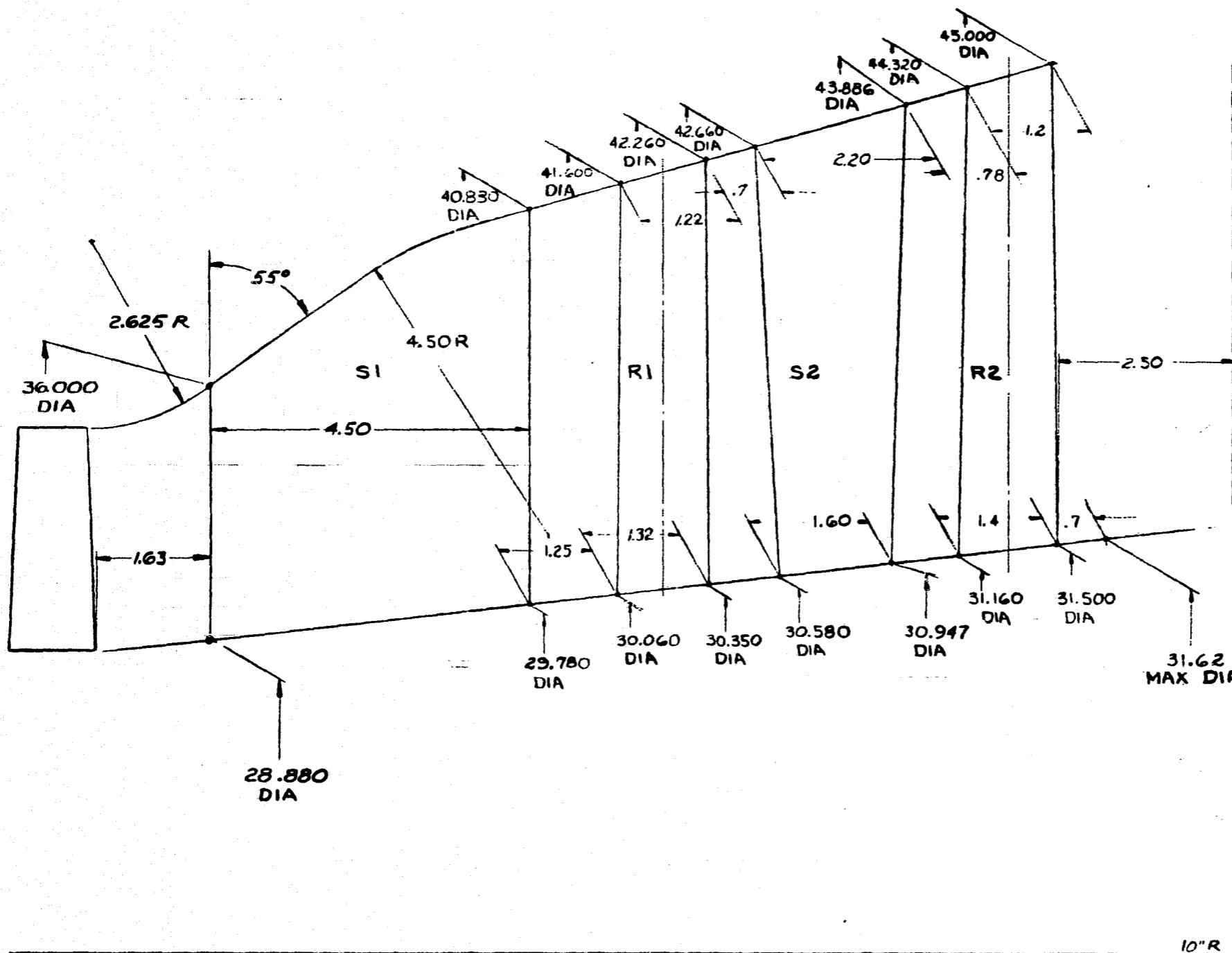


Figure 194. Hot Flowpath for the Fan C Low Pressure Turbine

Table LIV. Fan C LP Turbine Rotor Blade Summary

Stage	1			2		
Section	Root	Pitch	Tip	Root	Pitch	Tip
No. of Blades		118			130	
Material		R-77			R-77	
Blade Temperature (°F)		1106			921	
Chord (Inches)	1.324	1.325	1.409	1.405	1.348	1.379
Maximum Thickness (Inch)	0.265	0.215	0.145	0.167	0.132	0.114
Rad to Flowpath (Inches) Q	14.919	17.941	20.963	15.467	18.902	22.338
Blade Height Average (Inches)		6.044			6.871	
Aspect Ratio		4.55			5.09	
Solidity	1.650	1.320	1.085	1.860	1.410	1.10
Airfoil Weight (Stage)		39.6			37.8	
Pretwist Angle, ° (Nominal)		0.45			0.45	
Tip Moment (Mz)		-59.95			-29.93	
Tangential Tilt		0.018			0.010	
Axial Offset		-0.030			-0.014	
Centrifugal Stress	17200	12200	5600	19600	13000	3300
LE Resultant Stress	23000	13100	4500	21600	13400	3100
TE Resultant Stress	14500	10400	6300	18500	12200	3900
CX Resultant Stress	16100	12000	3800	19300	13200	3700
Allowable Vib Stress		16400			34800	
Dovetail Neck Temp (°F)		1000			831	
Maximum D/T Heywood Stress		37750			27450	
D/T to A/F Vib Stress Ratio - 1st Flexural (Free)		2.06			0.95	
1st Flexural (Free) Frequency		380			235	
1st Flexural (OOP) Frequency		1720			890	
Shroud Interlock Bearing Stress		2280			1220	

347

348

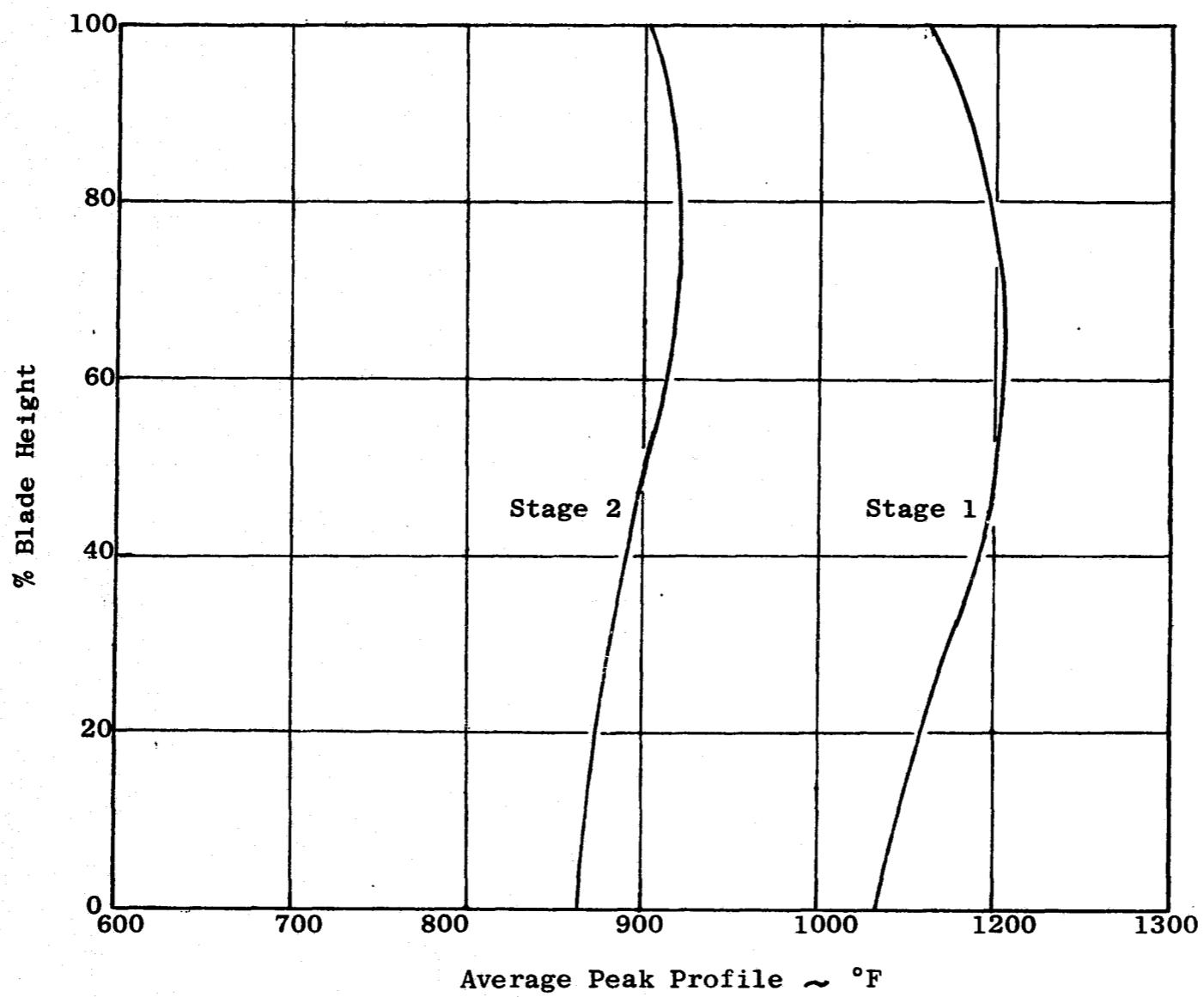


Figure 195. Temperature Profiles for the Fan C Low Pressure Turbine Blades

7.1.1.1.5 Design Analysis

This section presents the details of the stress and temperature analysis of the low pressure turbine components for Fans A and B. Included in this section are the following:

- Blades
- Discs
- Blade Retainers
- Shaft
- Seals
- Disc-Blade Vibration
- Temperature Distribution

The rotor, because of its low tip speed and low temperature environment is not creep or rupture limited. Another reason for this is that the airfoils are sized for the low-aerodynamic-loading condition of the turbine and, as such, are much too large to be highly stressed.

- Blade Design

The LP turbine blades (see Figure 196 for typical blade) have tip shrouds and two-tang dovetails. The blades also have long shanks to place the dovetail as remote as possible from the hot gas stream. In addition, all stages have shank "skirts" to prevent leakage across the stage and to provide a smooth wheel face for low windage losses.

The tip shroud is of special importance to high-aspect-ratio (length over chord) blading to prevent high vibratory stress. This is a "Z" form, with the middle leg of the "Z" being the contact surface between adjacent blades while the other legs form clearance for thermal closure during transients. The contact surfaces are enlarged radially and hardfaced for wear resistance with sprayed chromium carbide. This interlock is at an angle of 75° from the engine axis, which is the approximate angle of the first flexural mode of vibration, thus assuring good damping in this important mode.

Finally, there are two labyrinth seal teeth on each tip shroud for leakage control across the stage. The pitch between these teeth is such that the wear tracks in the opposing stator shroud will not overlap to cause excessive leakage.

- Steady State Stress

Turbine blade steady state stresses are determined by a Twisted Blade Analysis Computer Program. The procedure for calculating stresses consists of a computer input of the necessary airfoil section properties such as area, moments of inertia, elastic modulus, torsional stiffness and blade tip loads, rotational speed, tilt and offset. The computer then calculates stress at 4 points on a given airfoil section: (1) the leading edge, (2) the trailing edge, and the concave (3) and convex (4) maximum thickness points. Steady state stresses are a combination

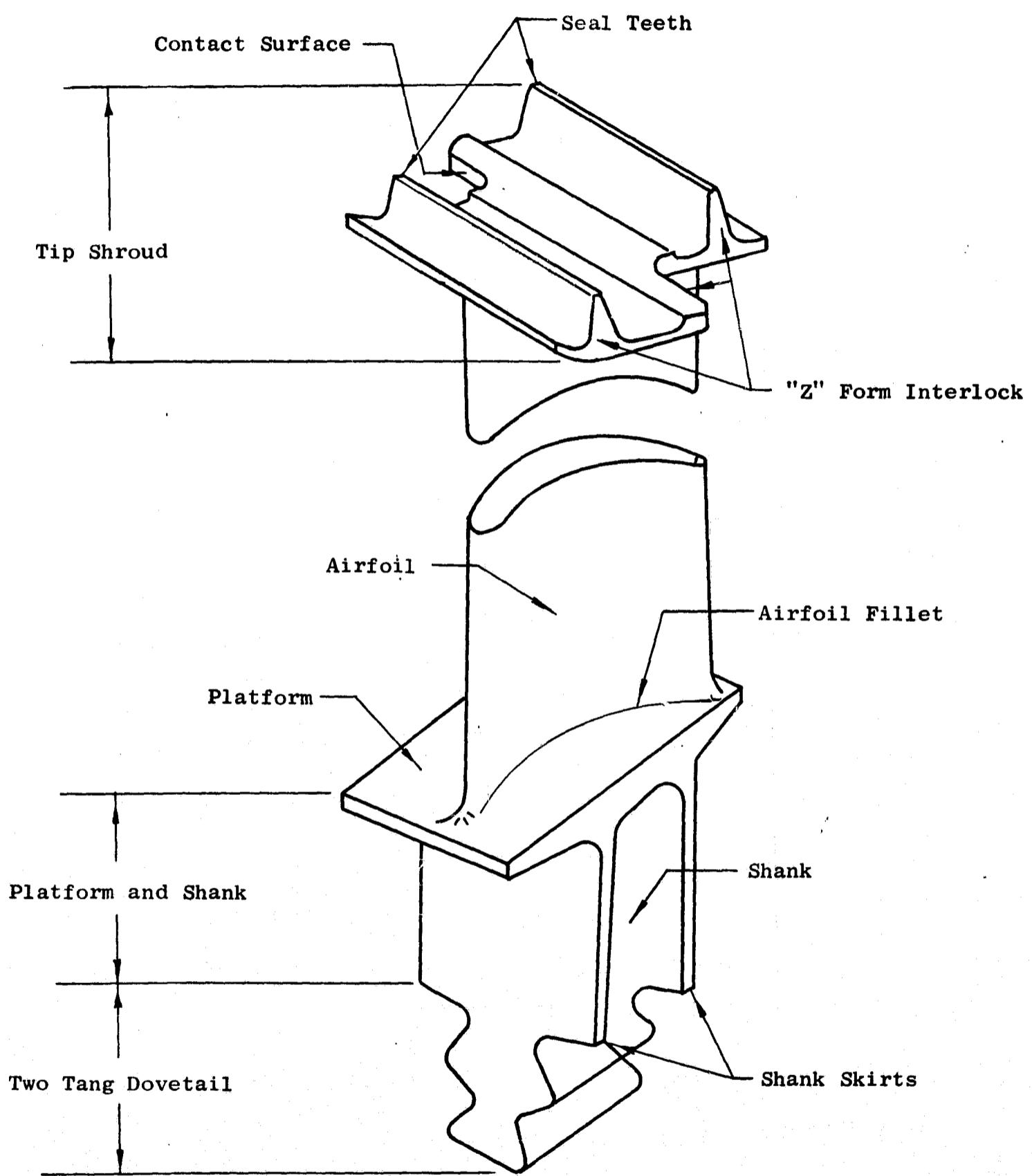


Figure 196. Blade Nomenclature for the Fans A, B, and C Low Pressure Turbines

of centrifugal, bending, induced tensile, and shear stresses. These stresses are then combined to give an effective stress at each of the previously mentioned points.

Of importance to the computer program is the condition of end restraint. The blade is assumed built in at the neck of the dovetail. At the tip shroud, twist, and moments and shears (both axially and tangentially) are set at zero.

The resulting steady-state-stress levels at the leading edge, trailing edge, and concave and convex maximum thickness points are plotted in Figures 197, 198, 199 and 200. The engine condition in each plot is at a rotor speed of 3500 rpm.

- Vibratory Stress and Frequency

Blade natural frequencies and vibratory stress distribution are also calculated with the Twisted Blade Analysis Computer Program. The program calculates the resonant frequencies by determining at what frequency the reciprocal of blade deflection or moment reaches zero.

The calculation of the blade natural frequencies was carried out by the Twisted Blade Program for two blade-tip boundary conditions. These tip restraint conditions greatly affect the resonant frequencies of the blade. The first frequency search was done for the in-phase tip condition, for which all axial and tangential deflections and rotations are permitted holding the rotation about a radial line to zero. The in-phase vibration modes are quite similar to a free-tip cantilever condition yielding the lowest possible blade frequencies. The second frequency search was done for the out-of-phase tip condition. Here the blade tip is restricted from movement in the tangential direction while maintaining no rotation about a radial line. The out-of-phase vibration modes are best correlated with engine data for shrouded turbines and are, therefore, considered the prime frequencies.

The result of this calculation is twofold:

1. Campbell diagrams (Figures 201 through 204) are plotted to show the relationship of natural frequency and rotor speed. Frequency of resonance varies with speed (centrifugal stiffening) and temperature (spring affect as determined by Young's modulus) in the following manner:

$$f = \left[f_0 + \beta \omega^2 \right] \sqrt{\frac{E}{E_0}}$$

where:

f is frequency

β is a configuration constant

ω is speed

E is Young's Modulus

Subscript o is base or room

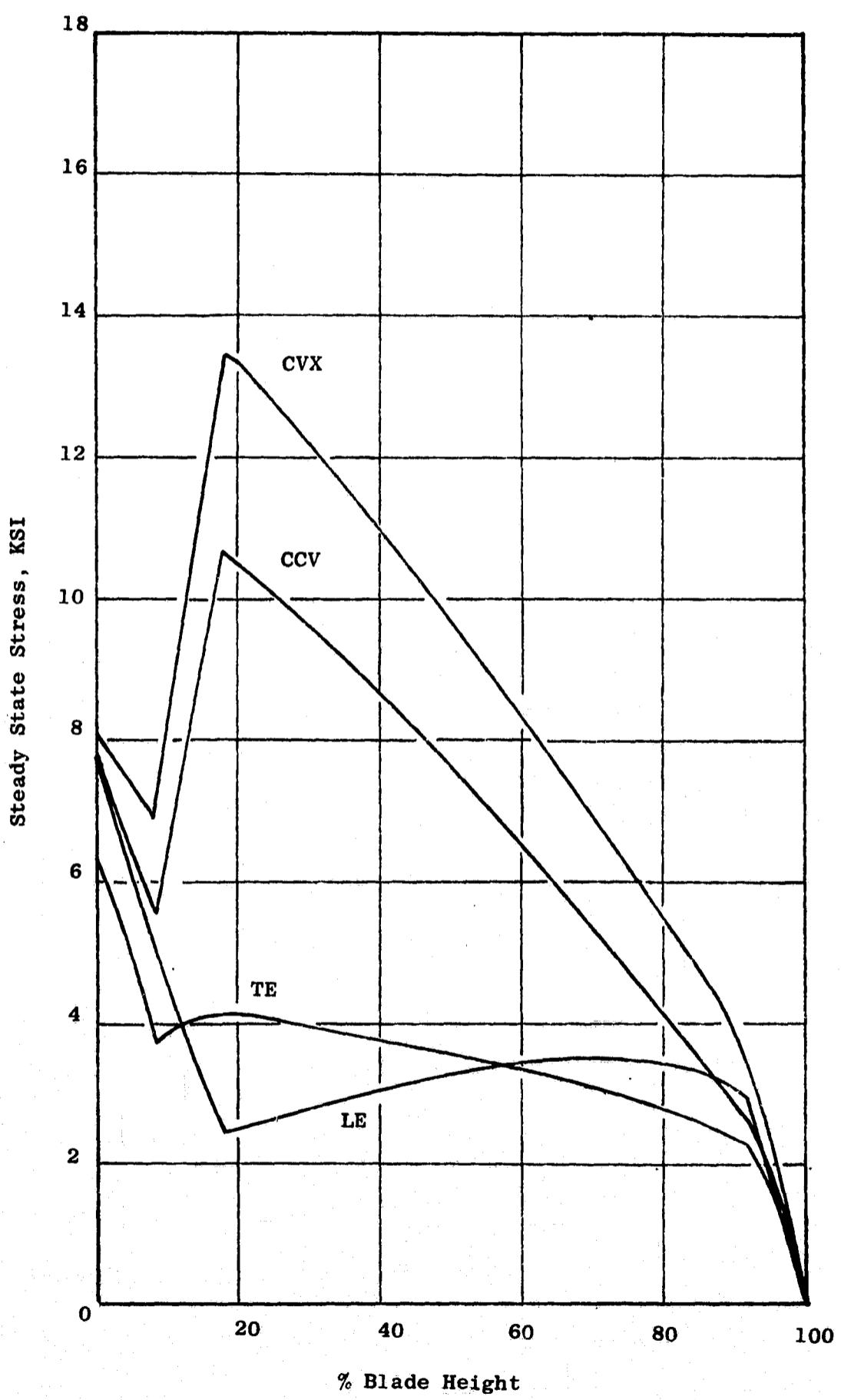


Figure 197. Fans A/B Stage 1 Turbine Blade Steady State Stress

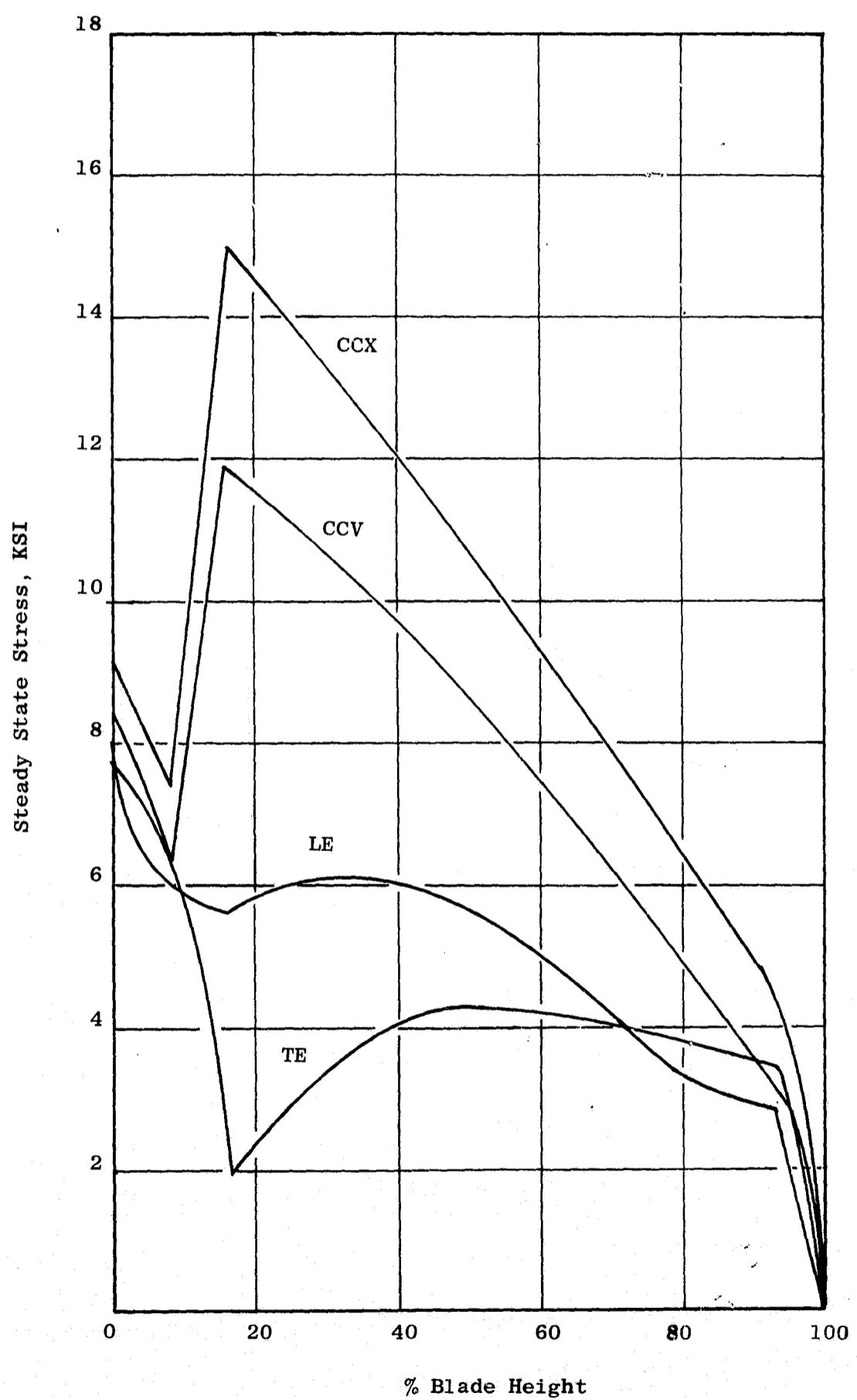


Figure 198. Fans A/B Stage 2 Turbine Blade Steady State Stress

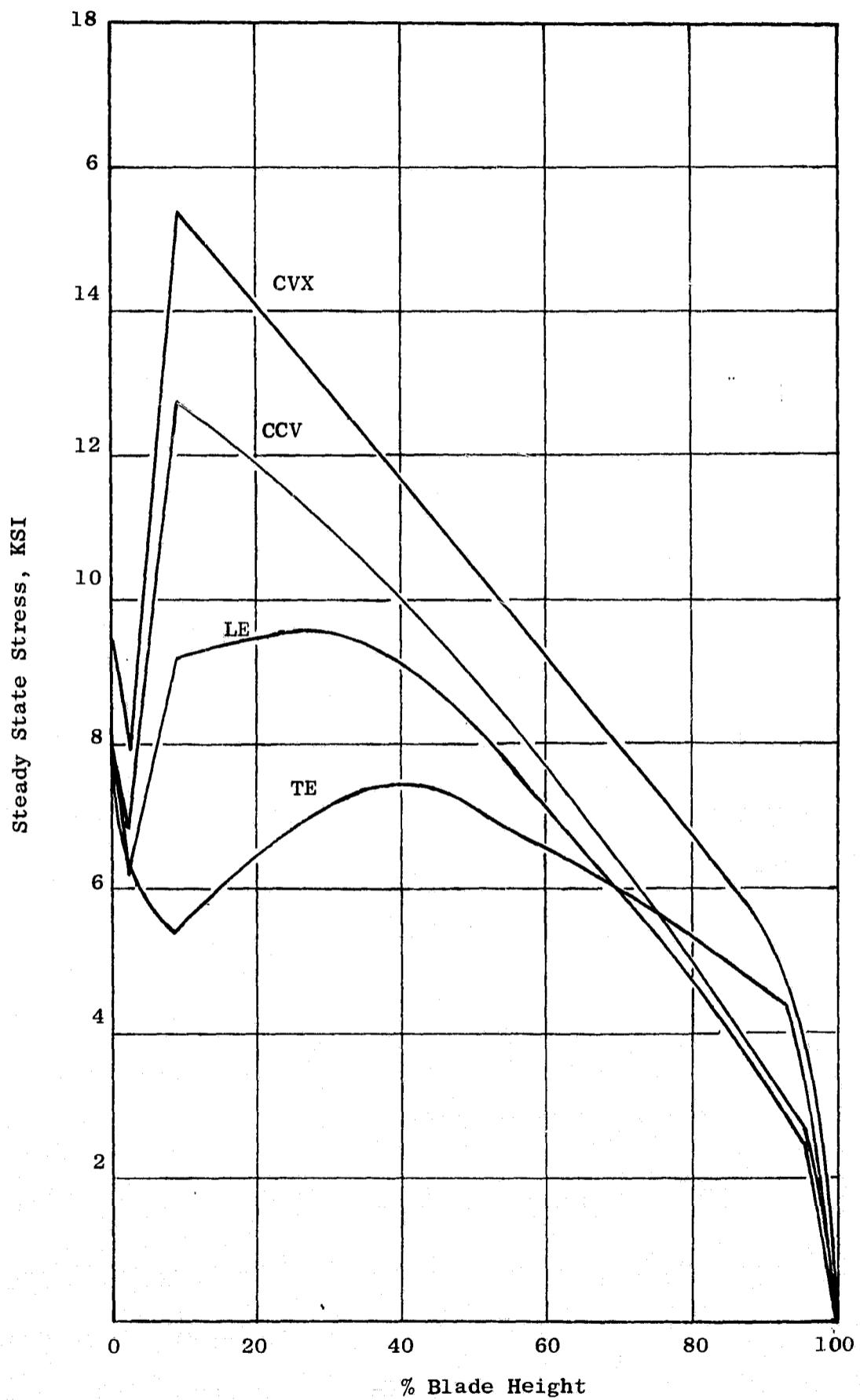


Figure 199. Fans A/B Stage 3 Turbine Blade Steady State Stress

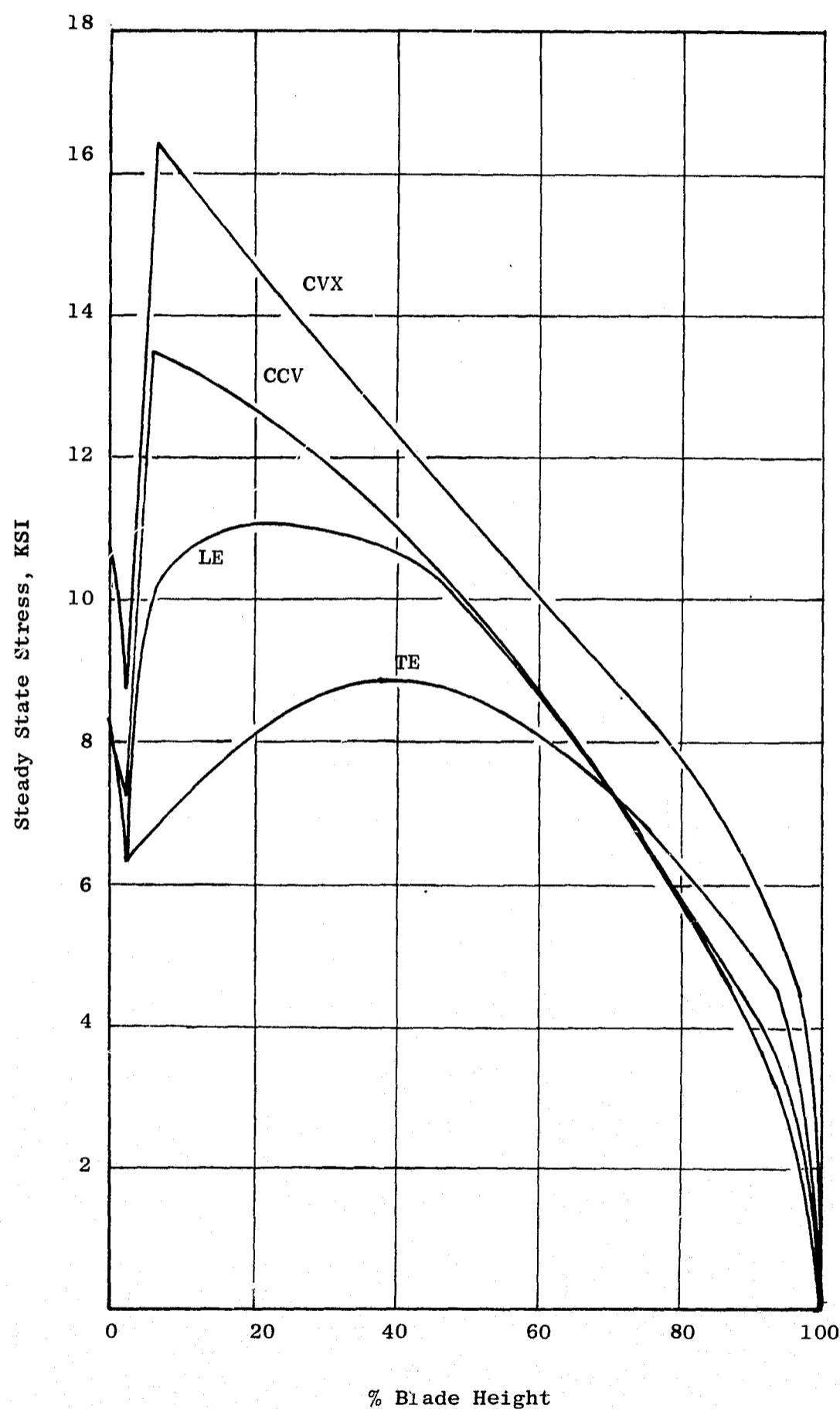


Figure 200. Fans A/B Stage 4 Turbine Blade Steady State Stress

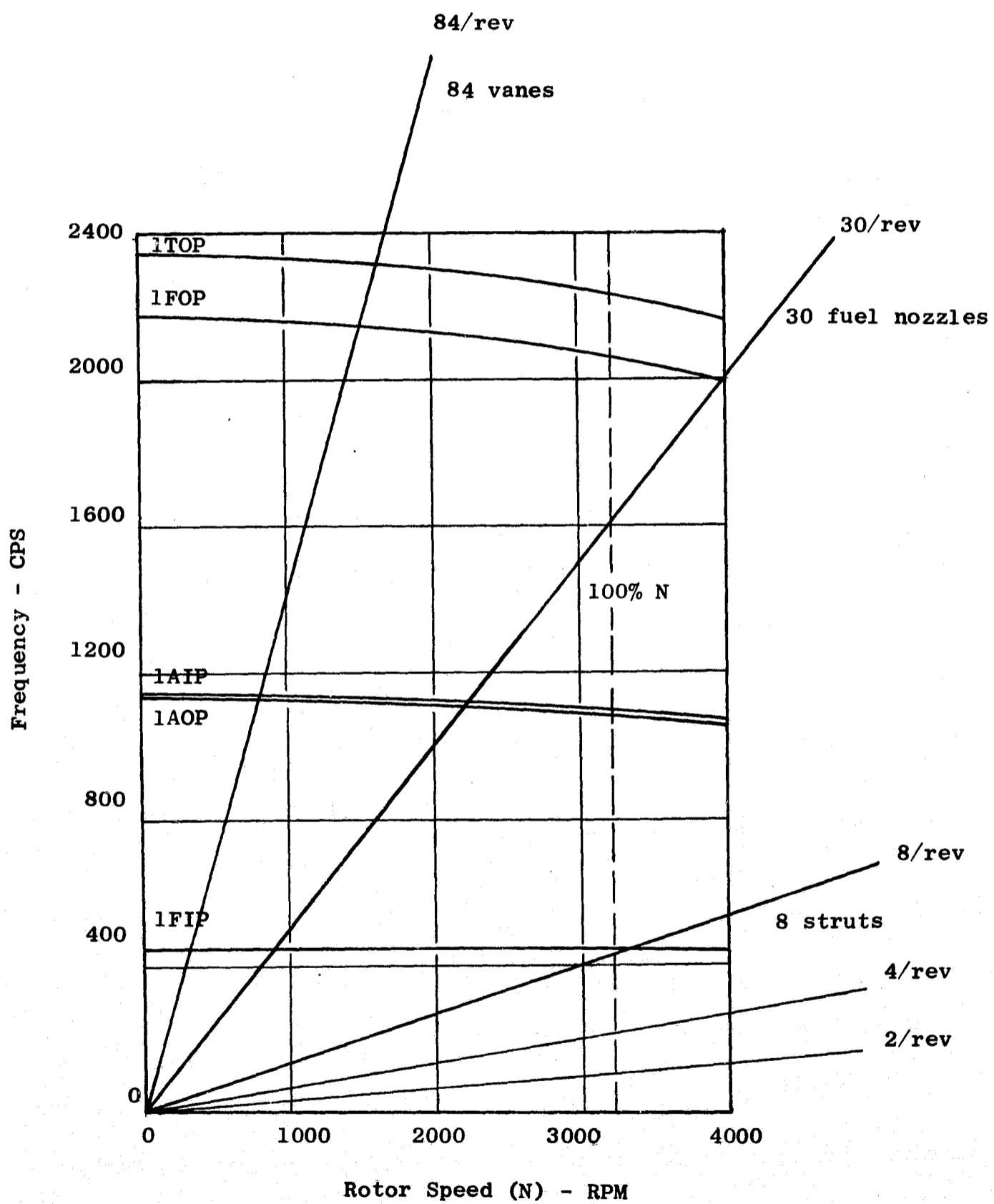


Figure 201. Campbell Diagram for the Fans A/B Stage 1 Turbine Rotor

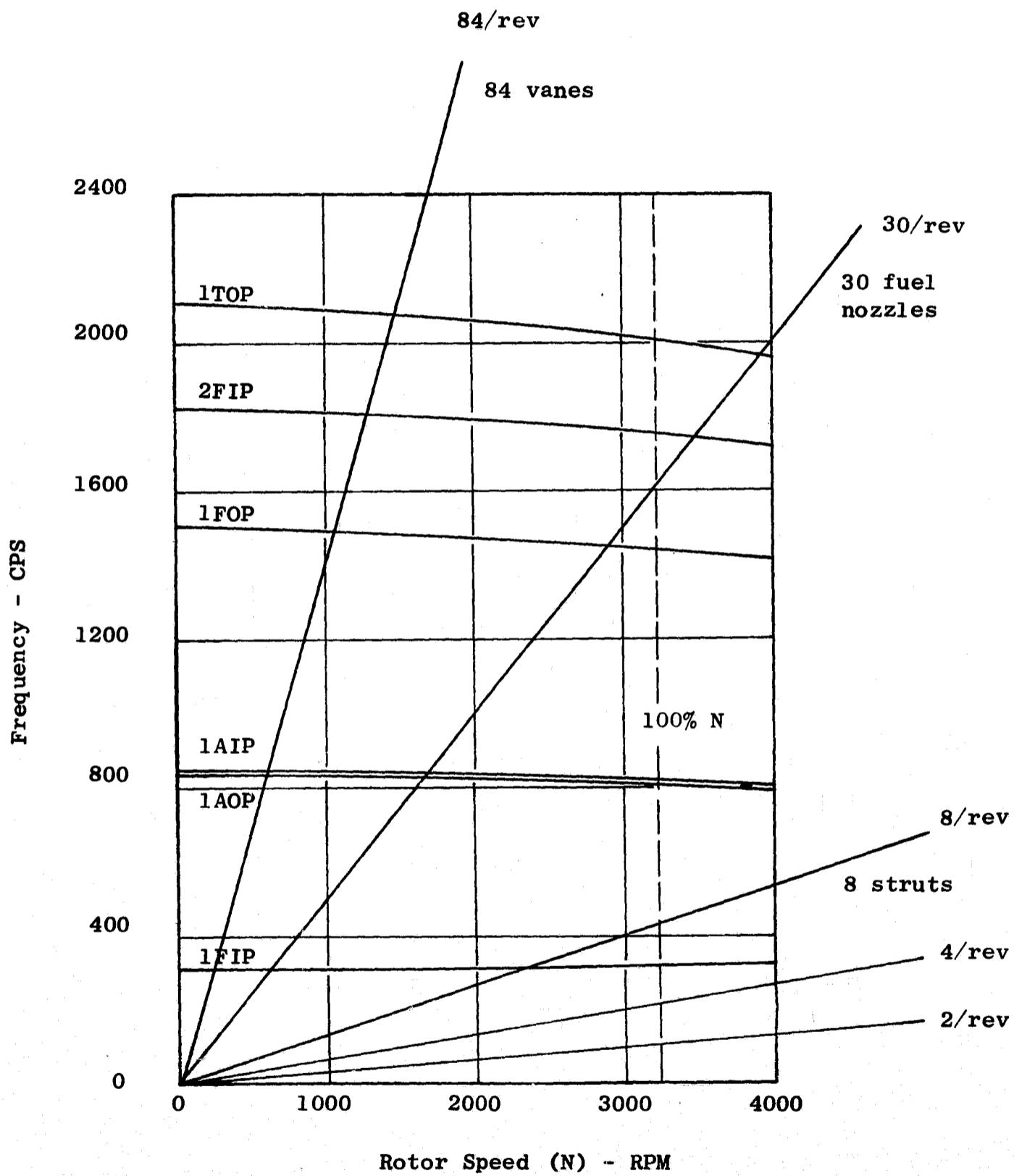


Figure 202. Campbell Diagram for the Fans A/B Stage 2 Turbine Rotor

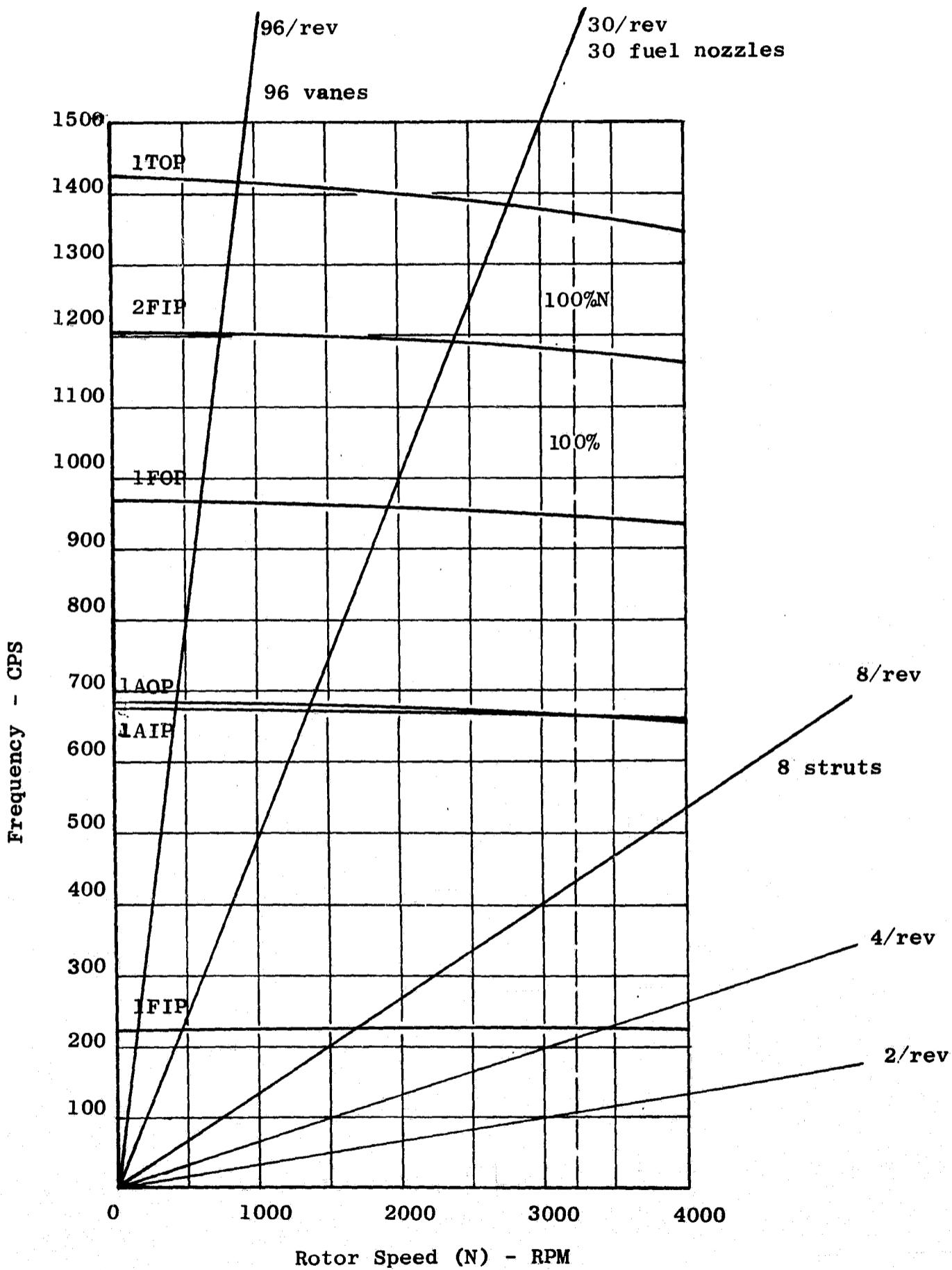


Figure 203. Campbell Diagram for the Fans A/B Stage 3 Turbine Rotor

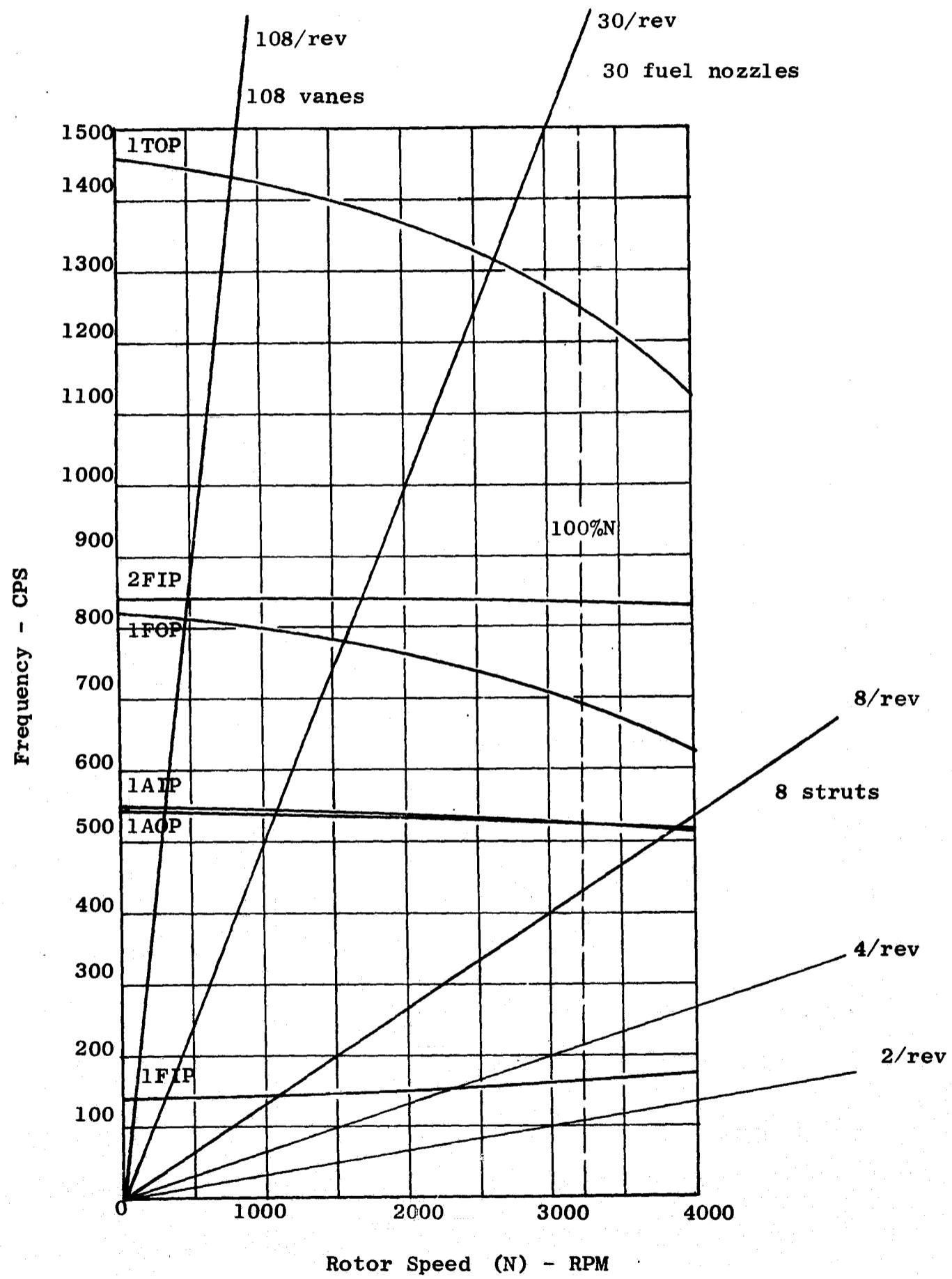


Figure 204. Campbell Diagram for the Fans A/B Stage 4 Turbine Rotor

The blade frequencies plotted on the Campbell diagram were obtained from bench test results at 0 rpm and Twisted Blade Analysis at 3500 rpm.

The Campbell diagram has "per rev" lines illustrating various possible excitation stimuli which could exist to cause resonant vibration at the engine speed where the natural frequency intersects with these lines. The low-order excitation lines can exist in any engine, while the higher-order lines indicate passing frequencies of such things as fuel nozzles or vanes. Such diagrams are used to avoid potentially dangerous interferences in the initial design and to identify modes of vibration during engine test.

2. Stress distribution charts are also produced from the computer analysis. By this means, the maximum stress in the airfoil can be identified in relation to any other point in the airfoil. These plots are used during engine stress surveys, where one or two strain gages are applied to convert the gage reading to maximum stress.

The stress distribution charts for all four stages are shown in Figures 205 through 223 for the more important modes of first flexural in-phase and restrained modes out-of-phase of first flexural, first axial, first torsional, and second flexural.

- Dovetails

All four stages use two-tang dovetails which are scaled from a common design. For convenience, the same size dovetail is used for Stages 1 and 2 and for Stages 3 and 4. The two-tang design was chosen because of the good experience available with this dovetail on the TF39 and CF6 engines.

The dovetails are analyzed using the R.B. Heywood method, which involves the use of geometric construction of the plane-of-bending in the fillet sections and is based on photoelastic studies of plastic models.

Steady state forces acting on the dovetail include centrifugal force, shear due to gas load, bending due to gas load, and blade offset and tilt (see Figure 224). Tables LV through LVIII tabulate the important steady state stress levels in each stage. All stress levels are at a rotor speed of 3500 rpm. As noted in the tables and on the figures, results are given at six points on the dovetail tangs. These points are located on the four extreme corners (Points 1 - 4) and halfway between the corners (Points 5 and 6).

193

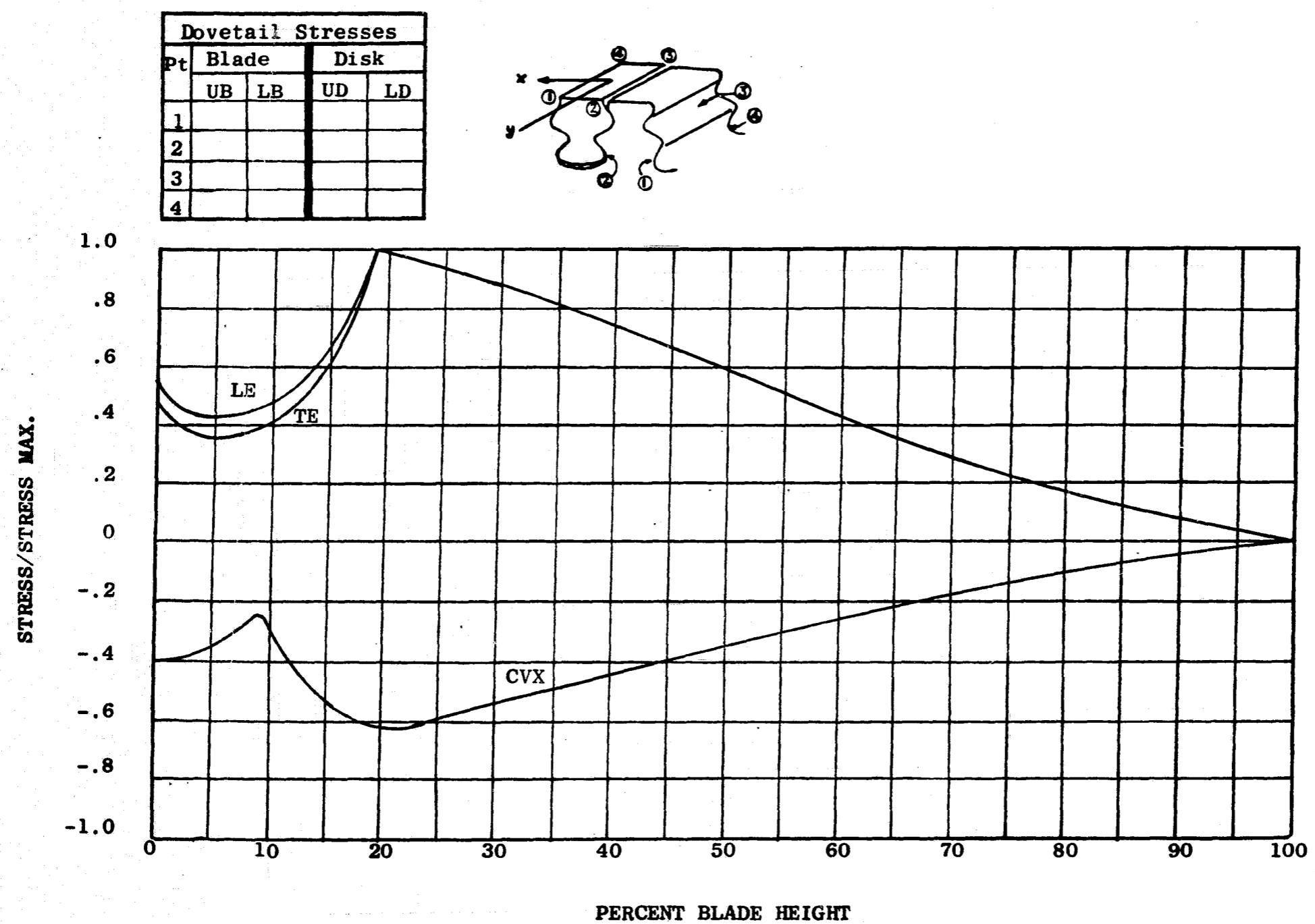


Figure 205. Stress Distribution for the Fans A/B Stage 1 Turbine, 444 CPS, 1st Flexural, In-Phase

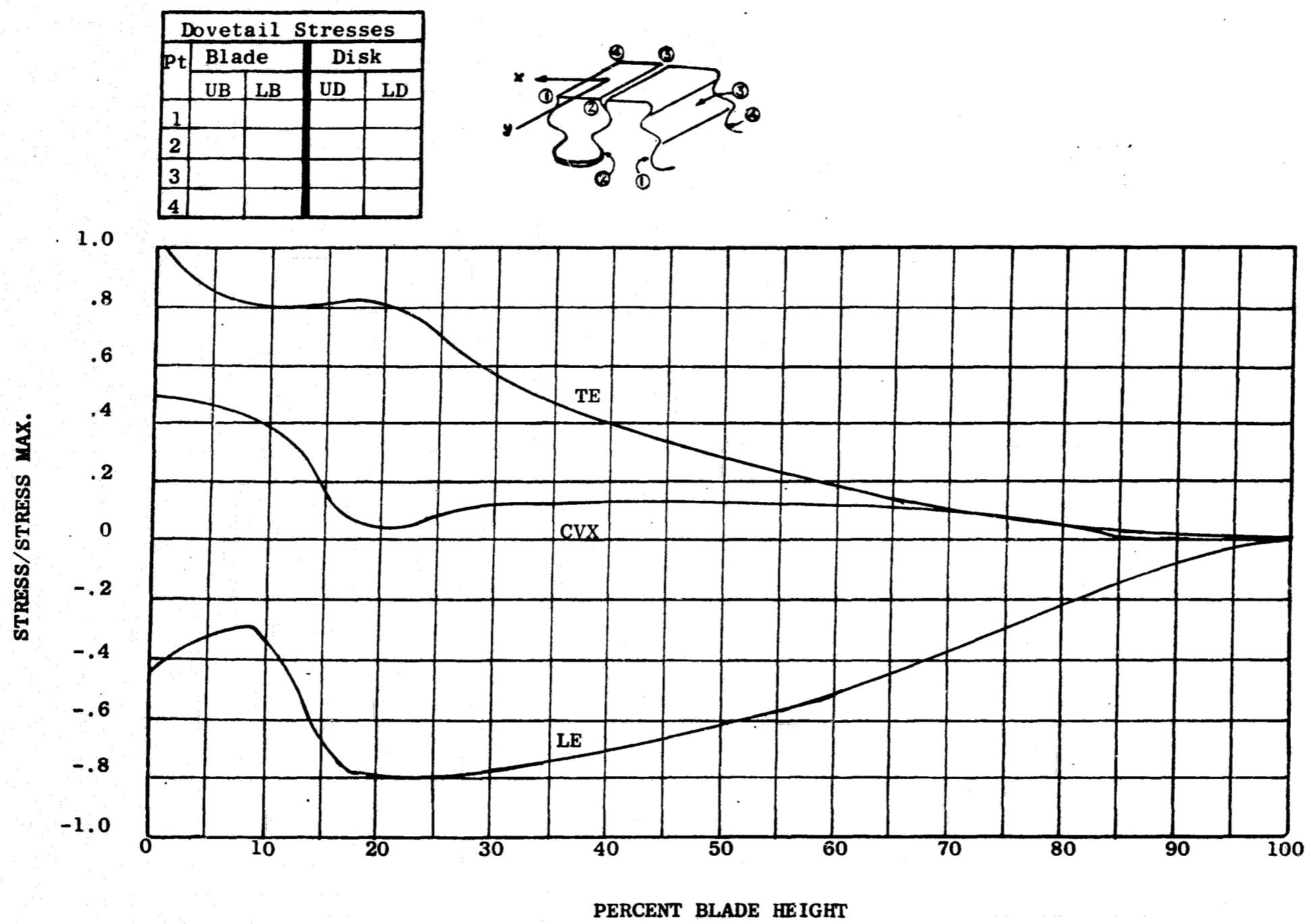


Figure 206. Stress Distribution for the Fans A/B Stage 1 Turbine, 1067 CPS, 1st Axial, Out-of-Phase

Dovetail Stresses				
Pt	Blade		Disk	
	UB	LB	UD	LD
1				
2				
3				
4				

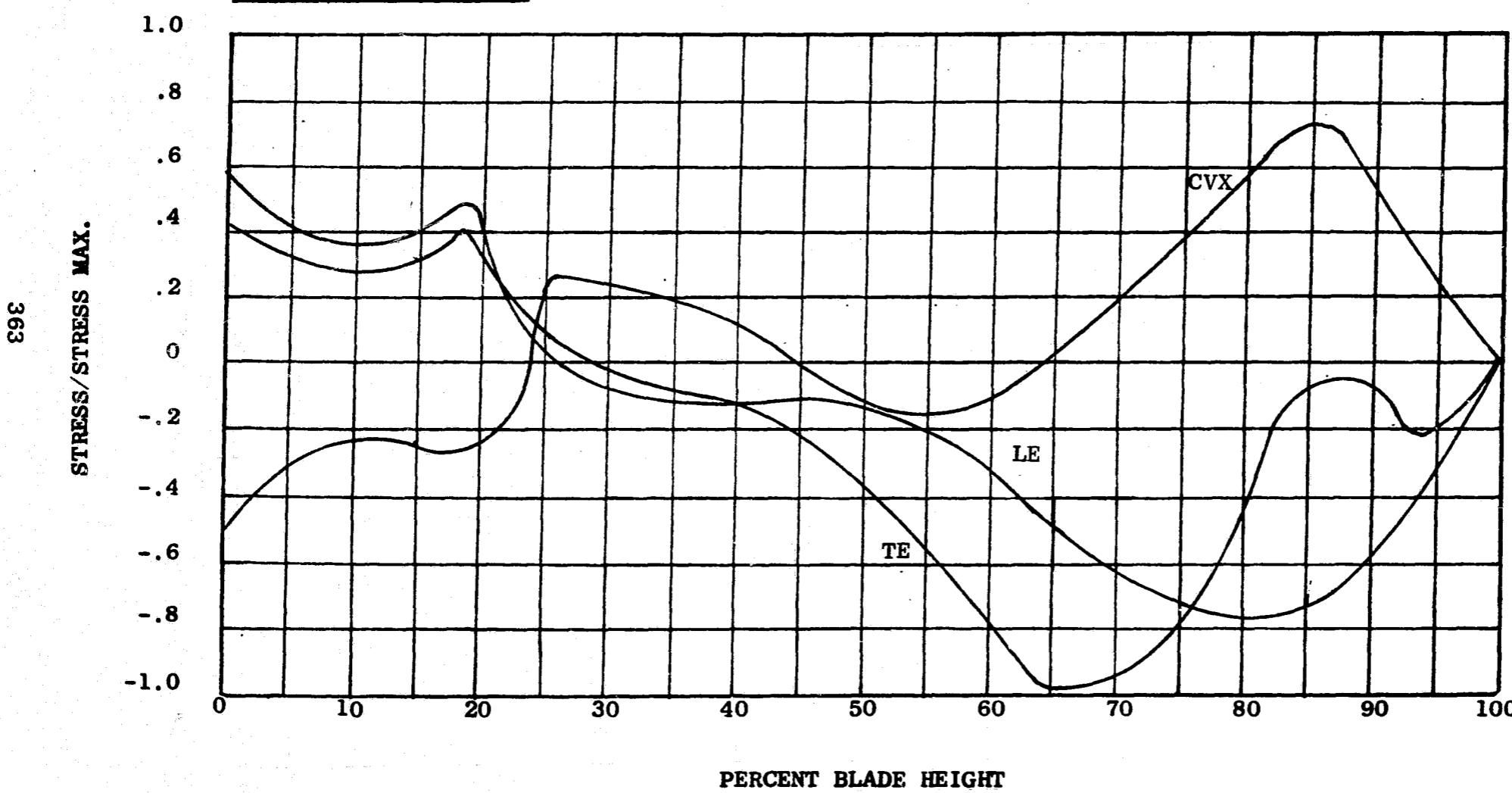
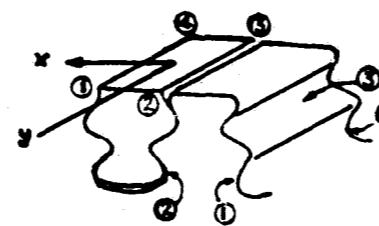


Figure 207. Stress Distribution for the Fans A/B Stage 1 Turbine, 4315 CPS, 2nd Flexural, Out-of-Phase

968

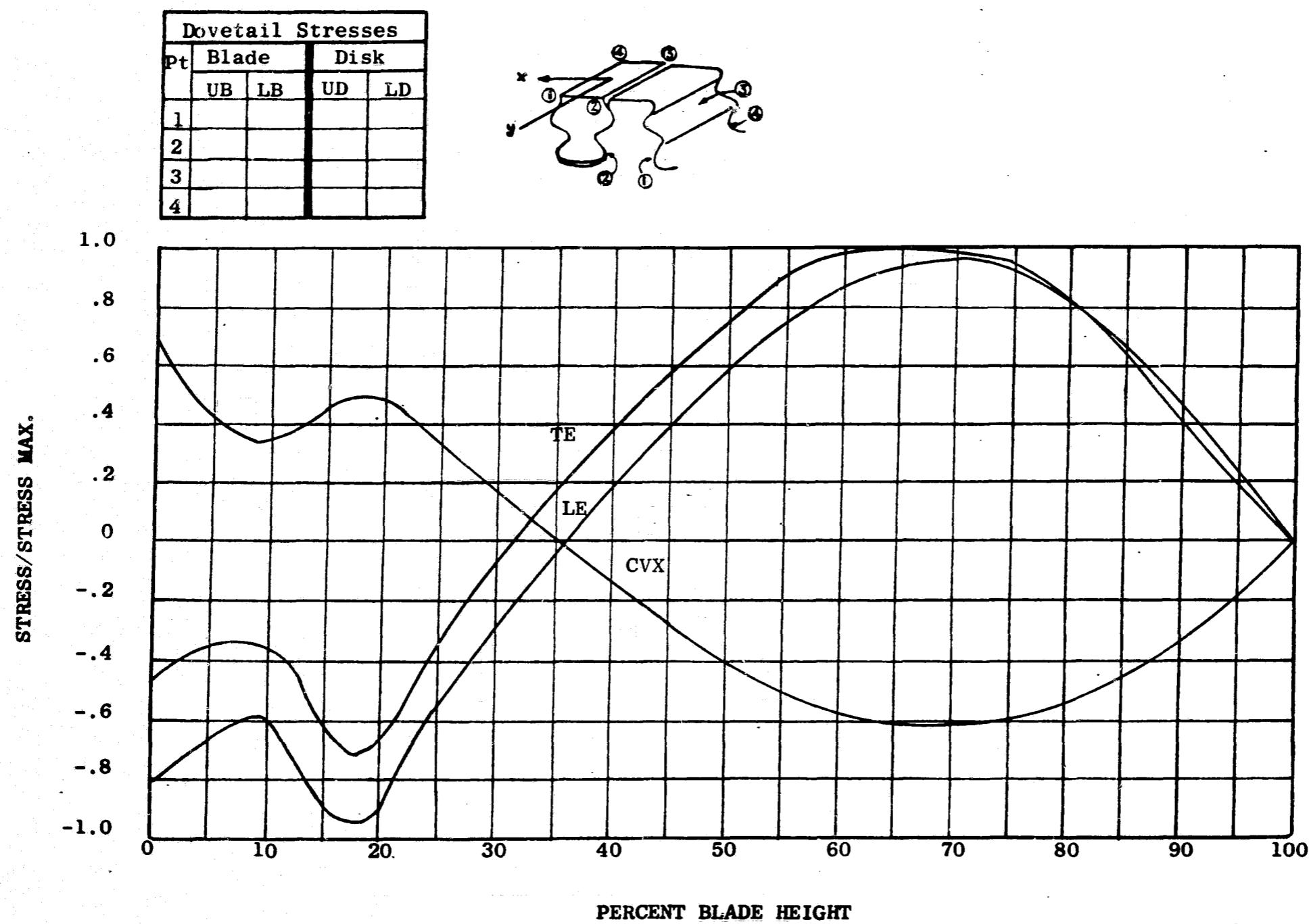


Figure 208. Stress Distribution for the Fans A/B Stage 1 Turbine, 2041 CPS, 1st Flexural, Out-of-Phase

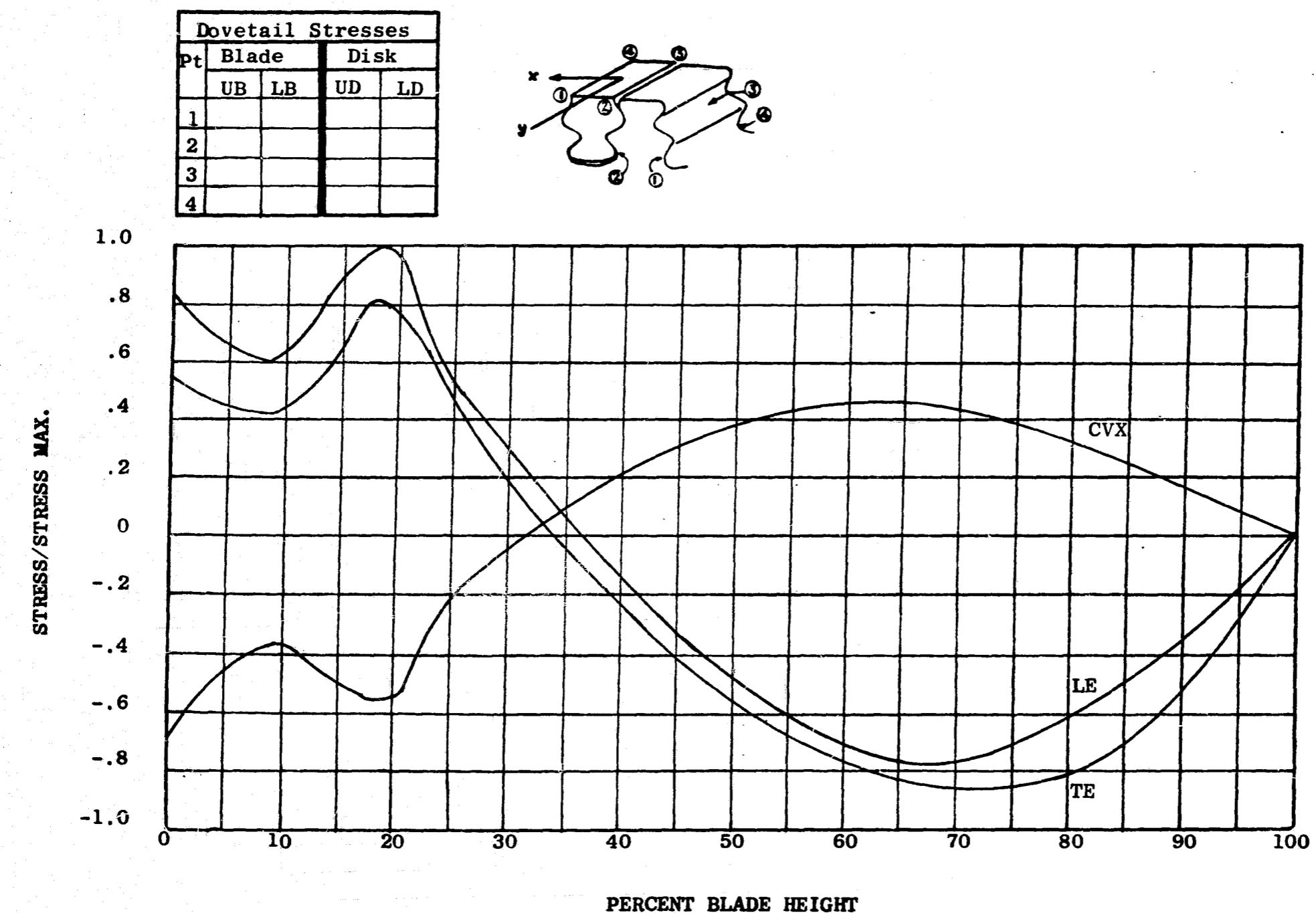


Figure 209. Stress Distribution for the Fans A/B Stage 1 Turbine, 2206 CPS, 1st Torsional, Out-of-Phase

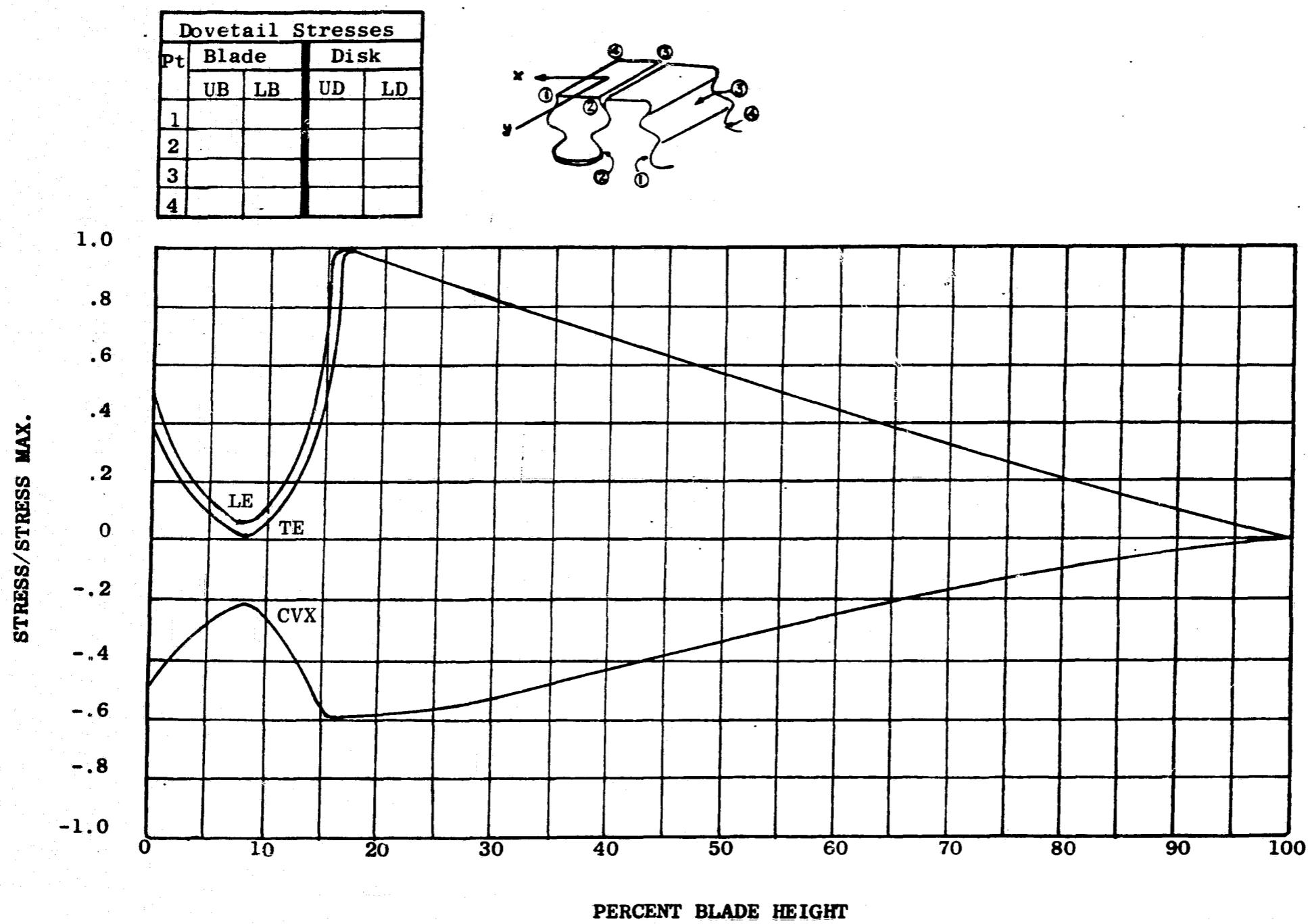


Figure 210. Stress Distribution for the Fans A/B Stage 2 Turbine, 321 CPS, 1st Flexural, In-Phase

798

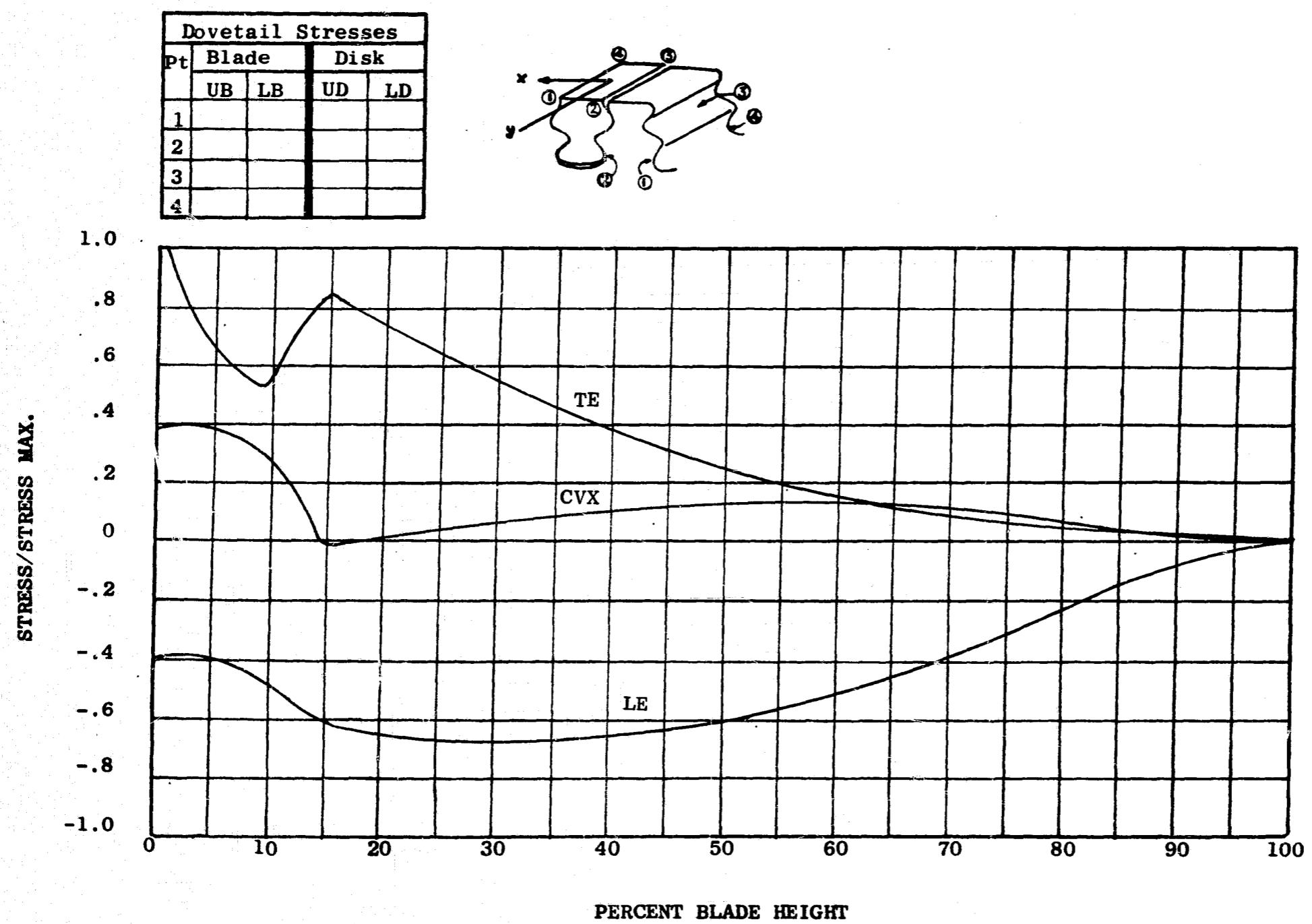


Figure 211. Stress Distribution for the Fans A/B Stage 2 Turbine, 801 CPS, 1st Axial, Out-of-Phase

89c

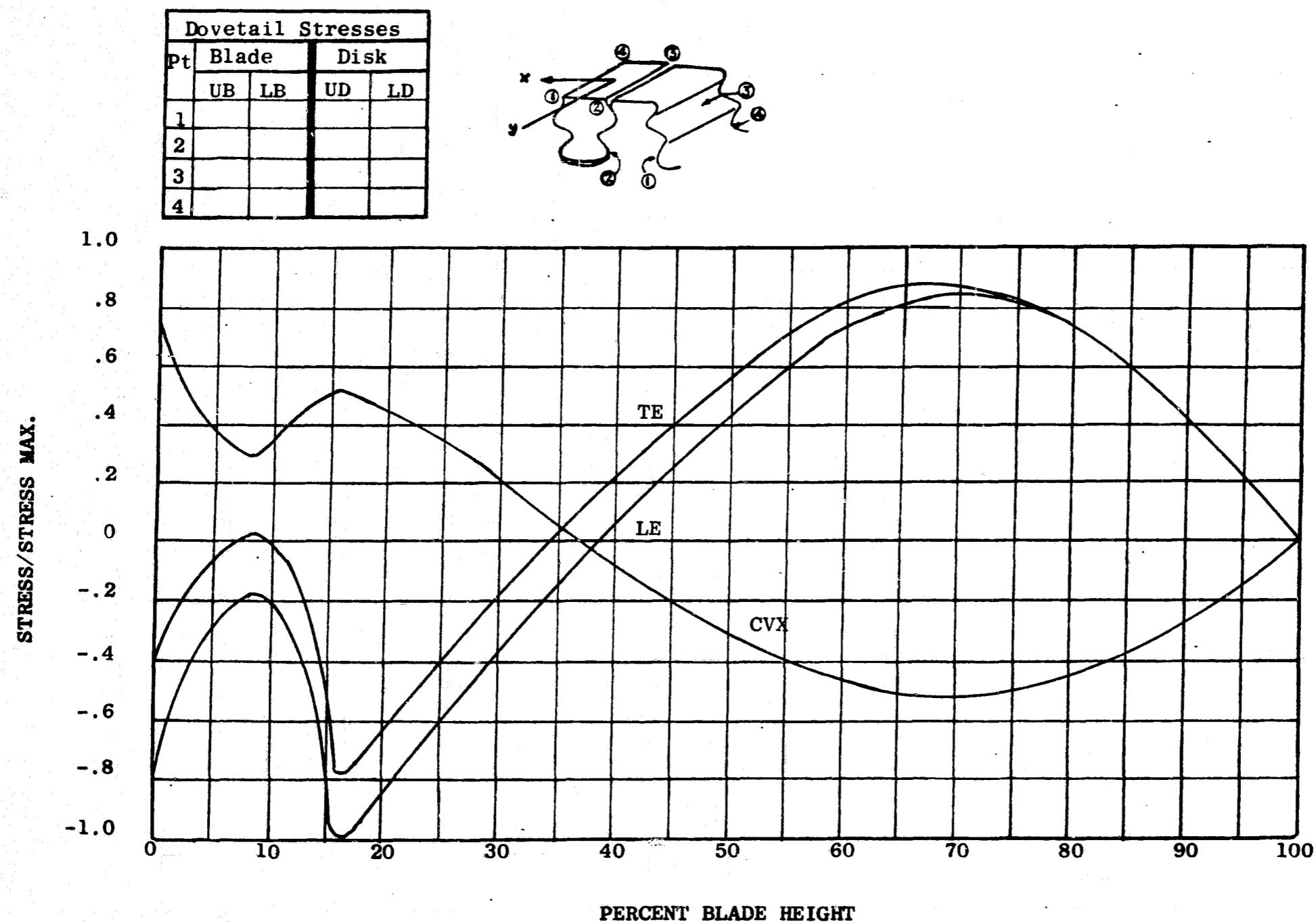


Figure 212. Stress Distribution for the Fans A/B Stage 2 Turbine, 1430 CPS, 1st Flexural, Out-of-Phase

369

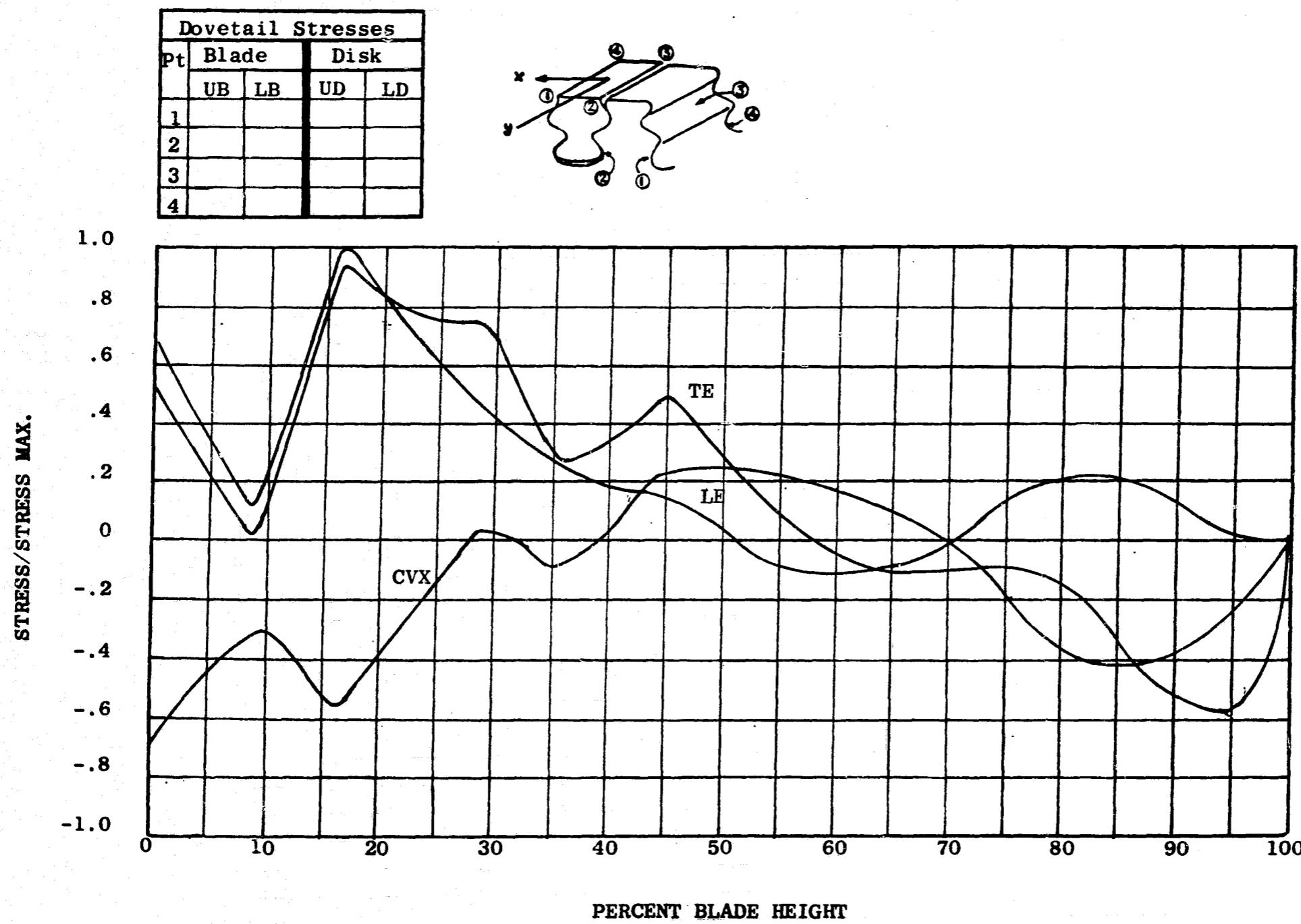


Figure 213. Stress Distribution for the Fans A/B Stage 2 Turbine, 1992 CPS, 1st Torsional, Out-of-Phase

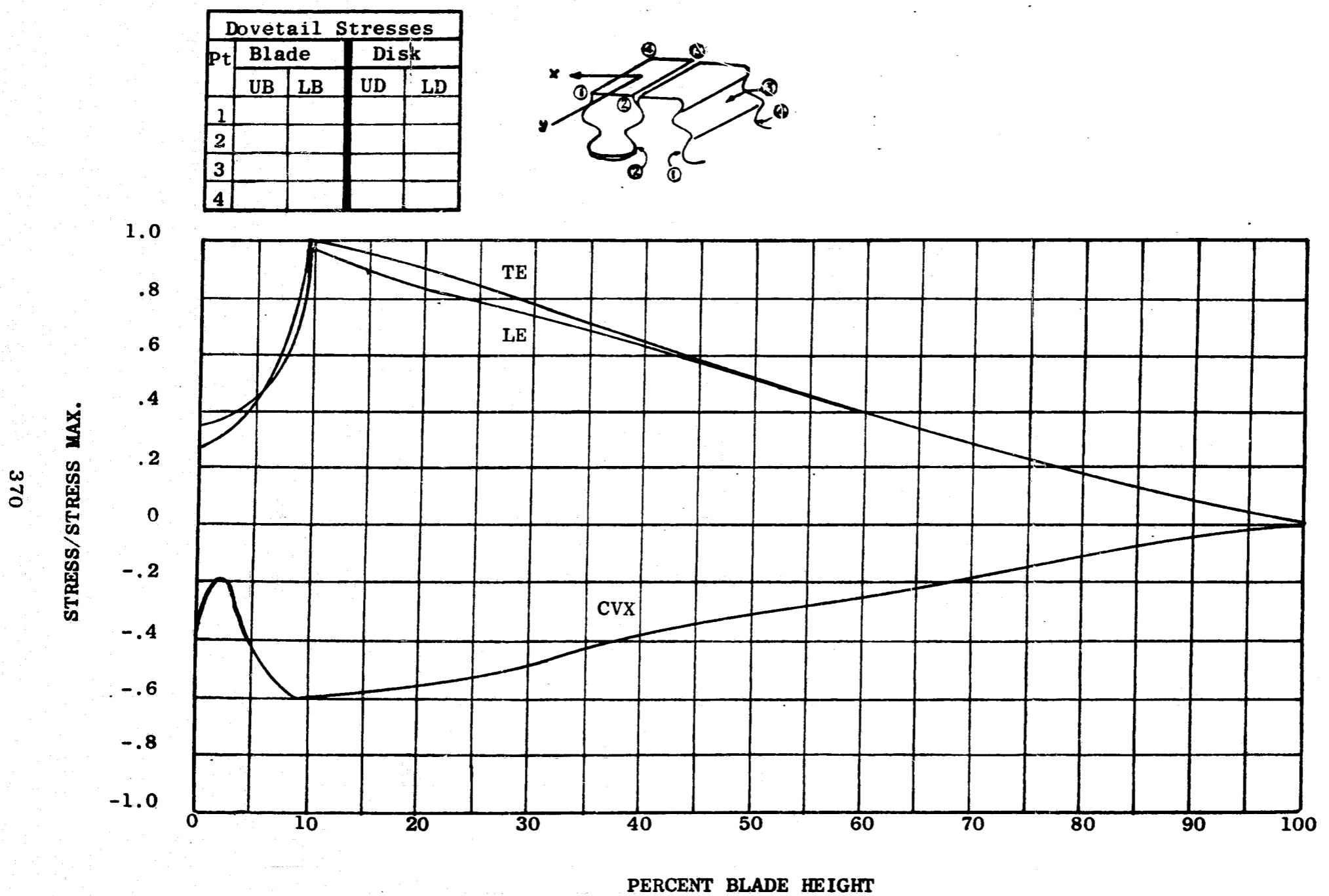


Figure 214. Stress Distribution for the Fans A/B Stage 3 Turbine, 224 CPS, 1st Flexural, In-Phase

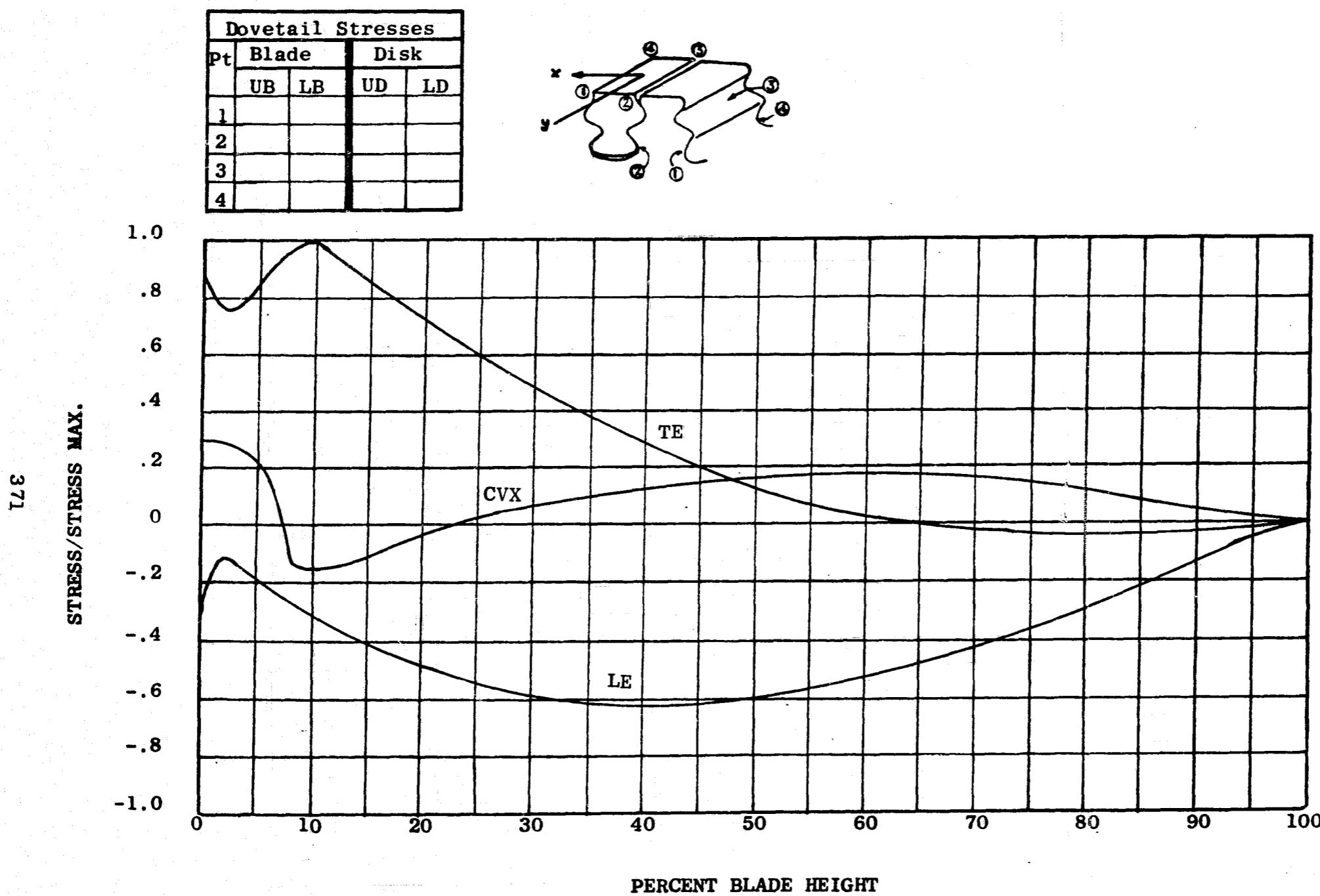


Figure 215. Stress Distribution for the Fans A/B Stage 3 Turbine, 657 CPS, 1st Axial, Out-of-Phase

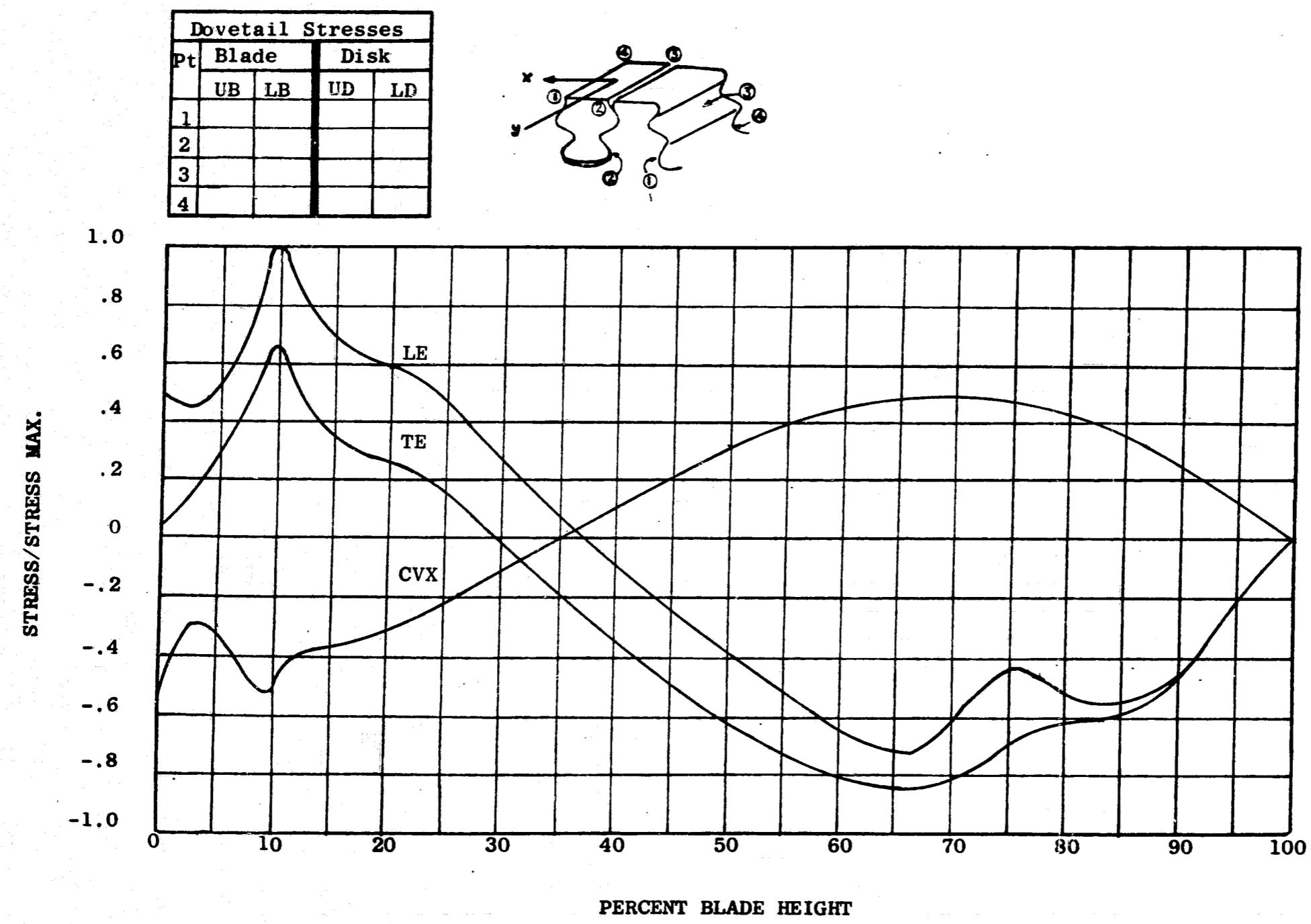


Figure 216. Stress Distribution for the Fans A/B Stage 3 Turbine, 940 CPS, 1st Flexural, Out-of-Phase

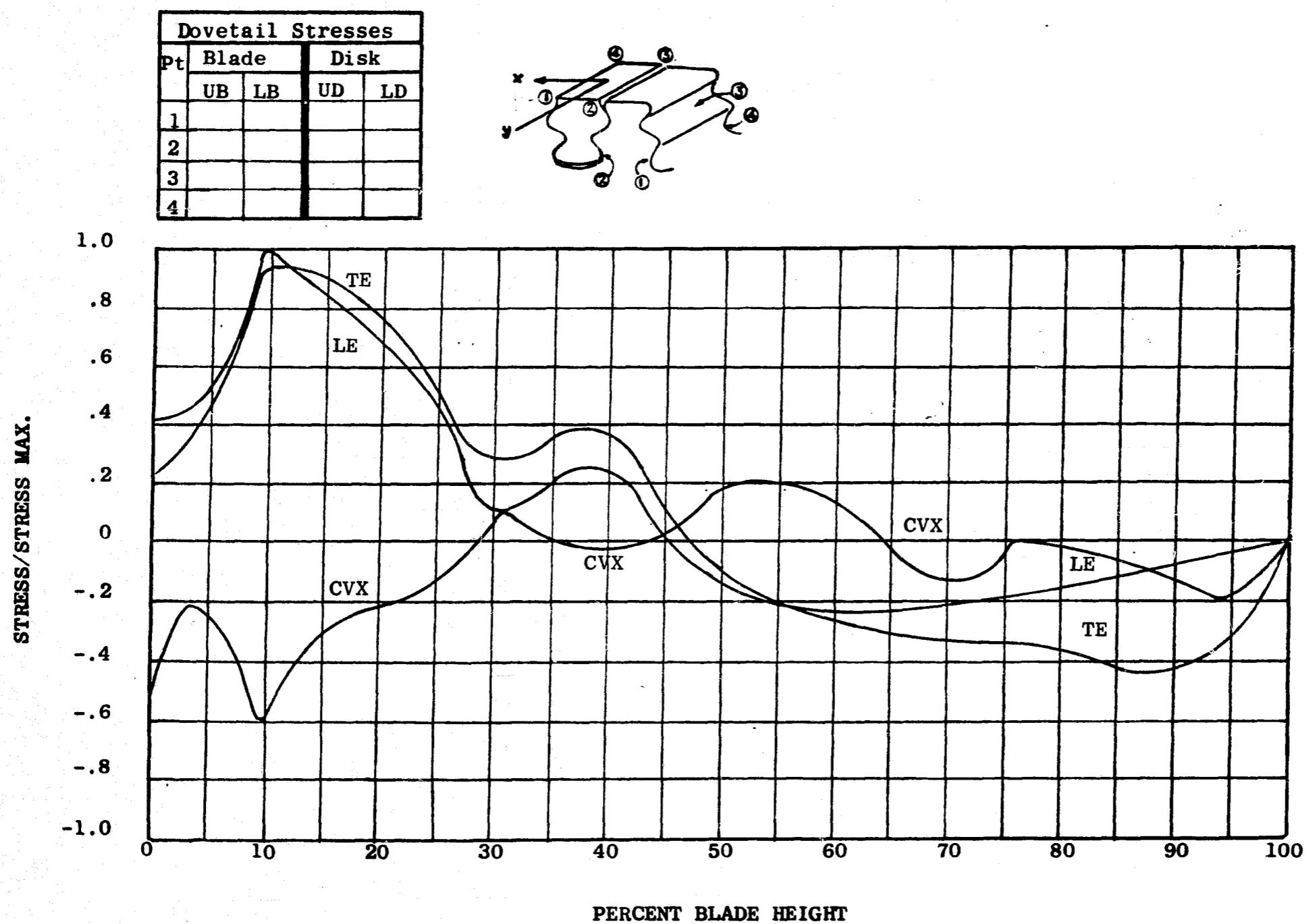


Figure 217. Stress Distribution for the Fans A/B Stage 3 Turbine, 1365 CPS, 1st Torsional, Out-of-Phase

374

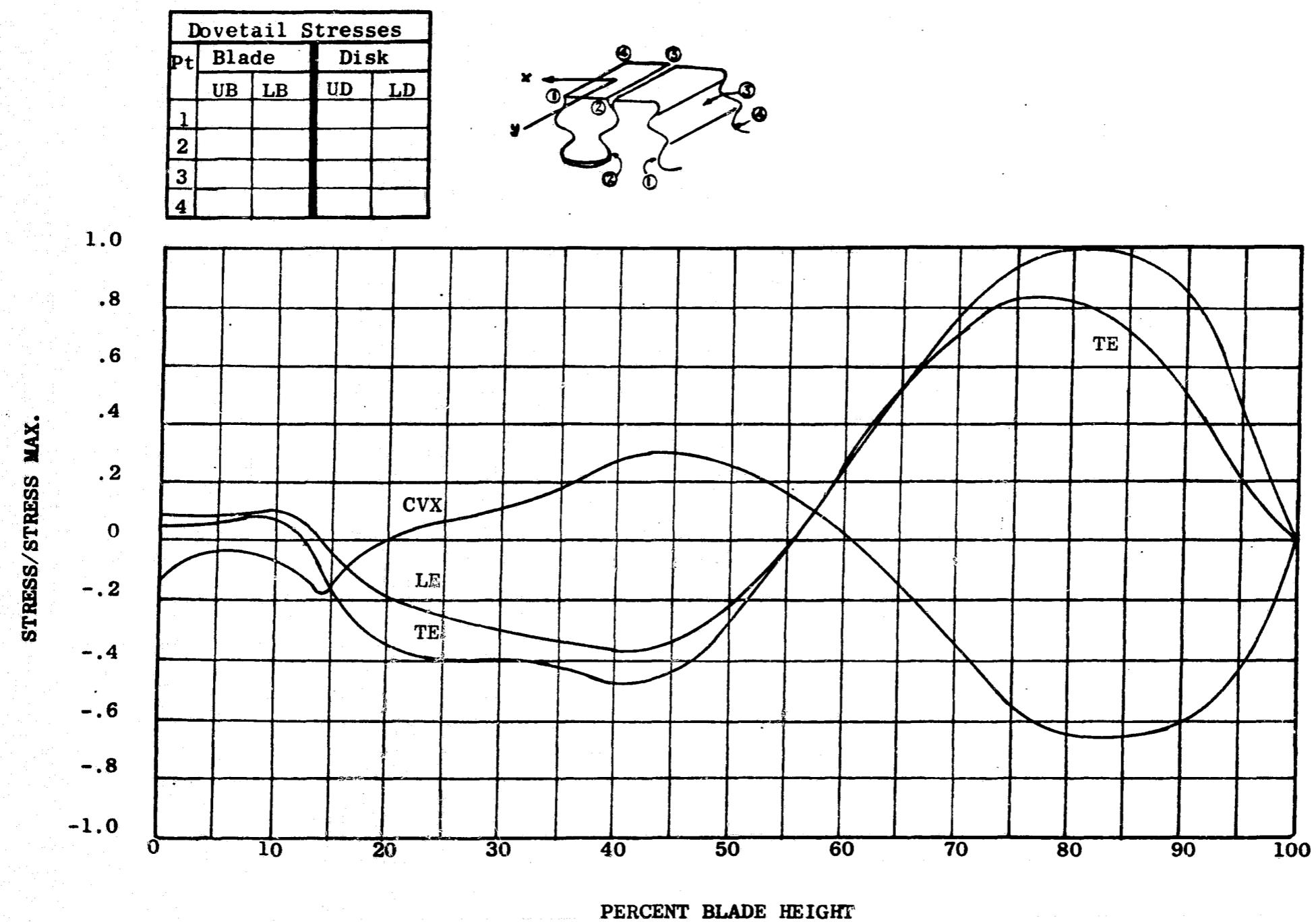


Figure 218. Stress Distribution for the Fans A/B Stage 3 Turbine, 2633 CPS, 2nd Flexural, Out-of-Phase

375

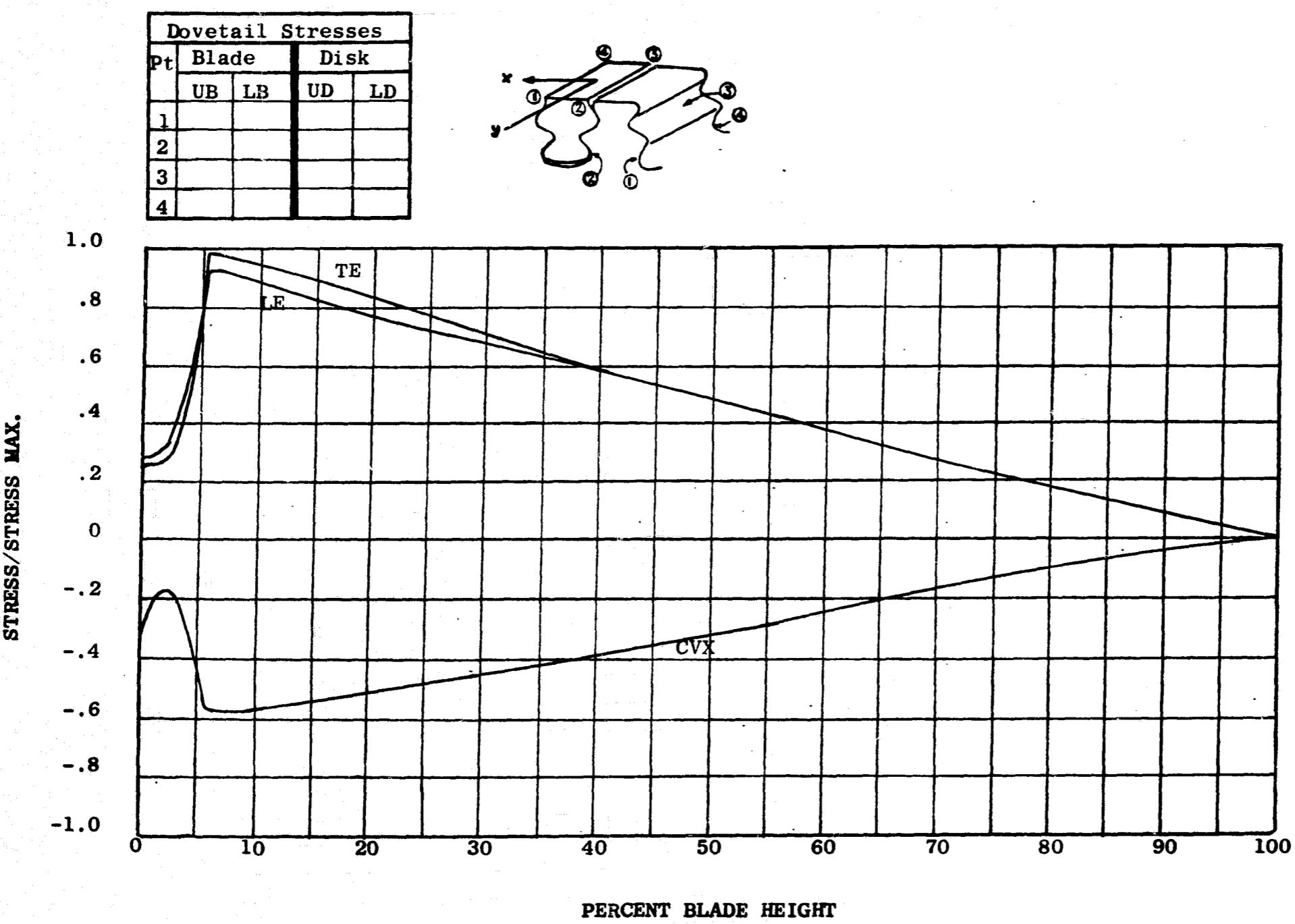


Figure 219. Stress Distribution for the Fans A/B Stage 4 Turbine, 168 CPS, 1st Flexural, In-Phase

948

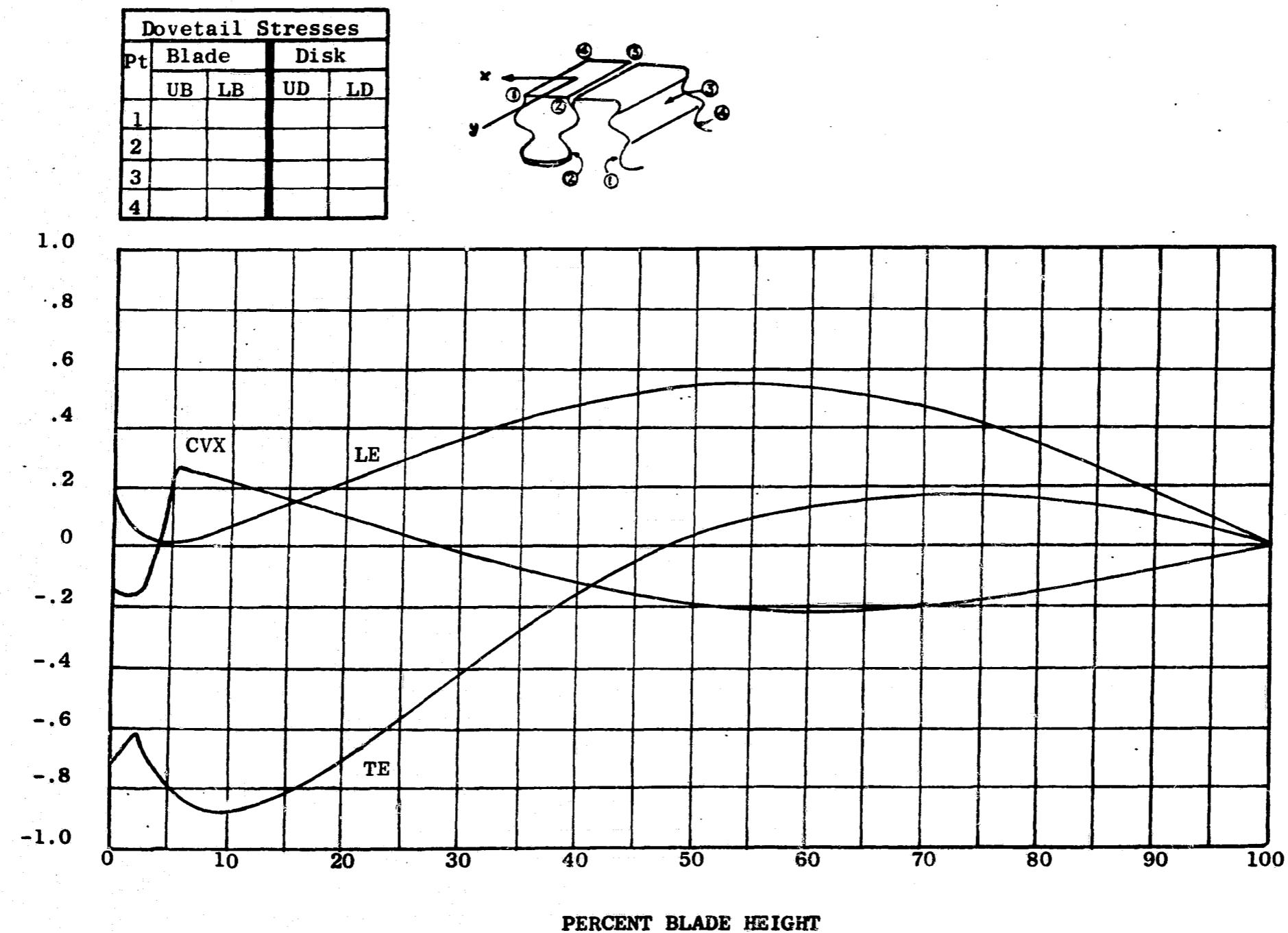


Figure 220. Stress Distribution for the Fans A/B Stage 4 Turbine, 521 CPS, 1st Axial, Out-of-Phase

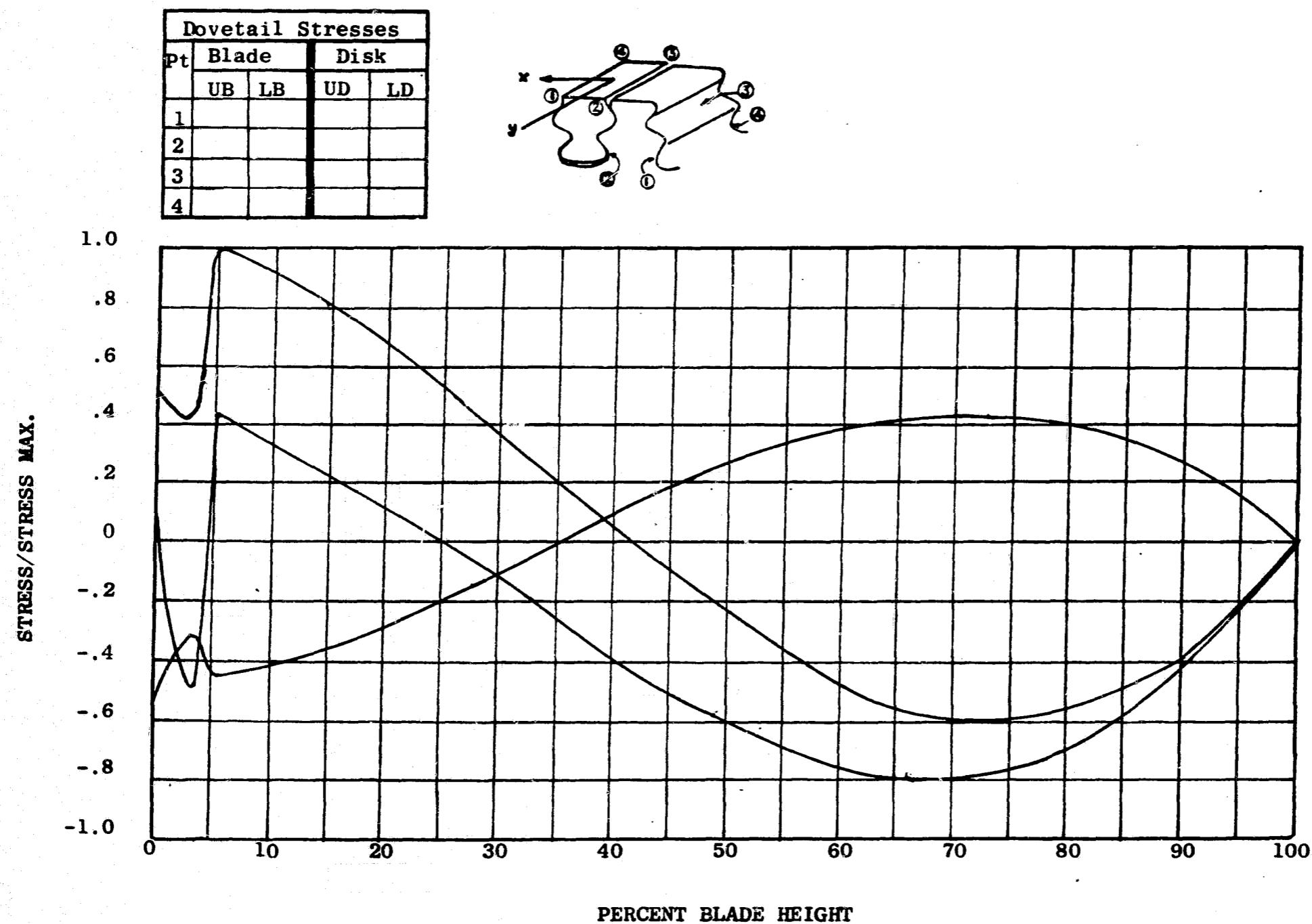


Figure 221. Stress Distribution for the Fans A/B Stage 4 Turbine, 666 CPS, 1st Flexural, Out-of-Phase

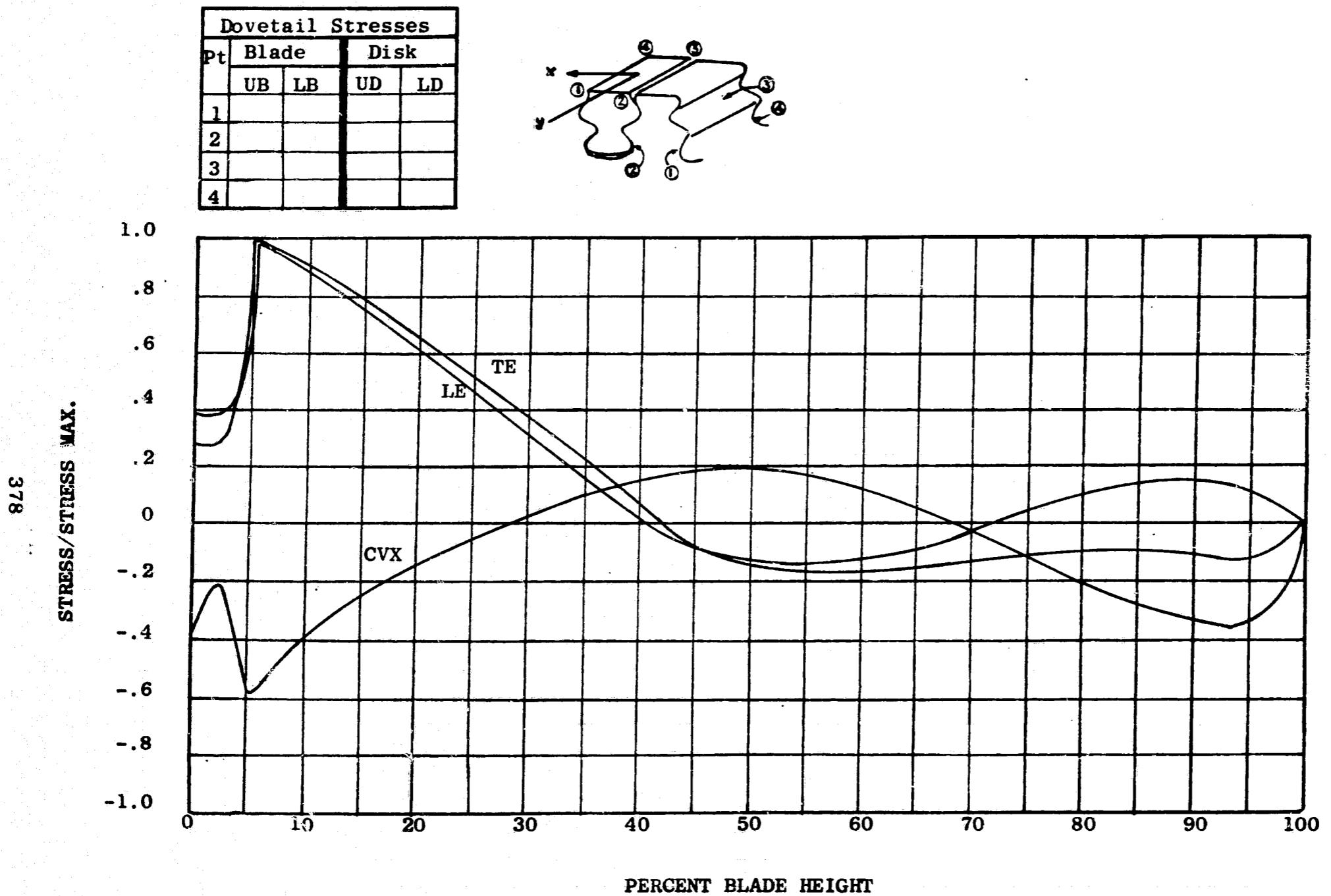


Figure 222. Stress Distribution for the Fans A/B Stage 4 Turbine, 1207 CPS, 1st Torsional, Out-of-Phase

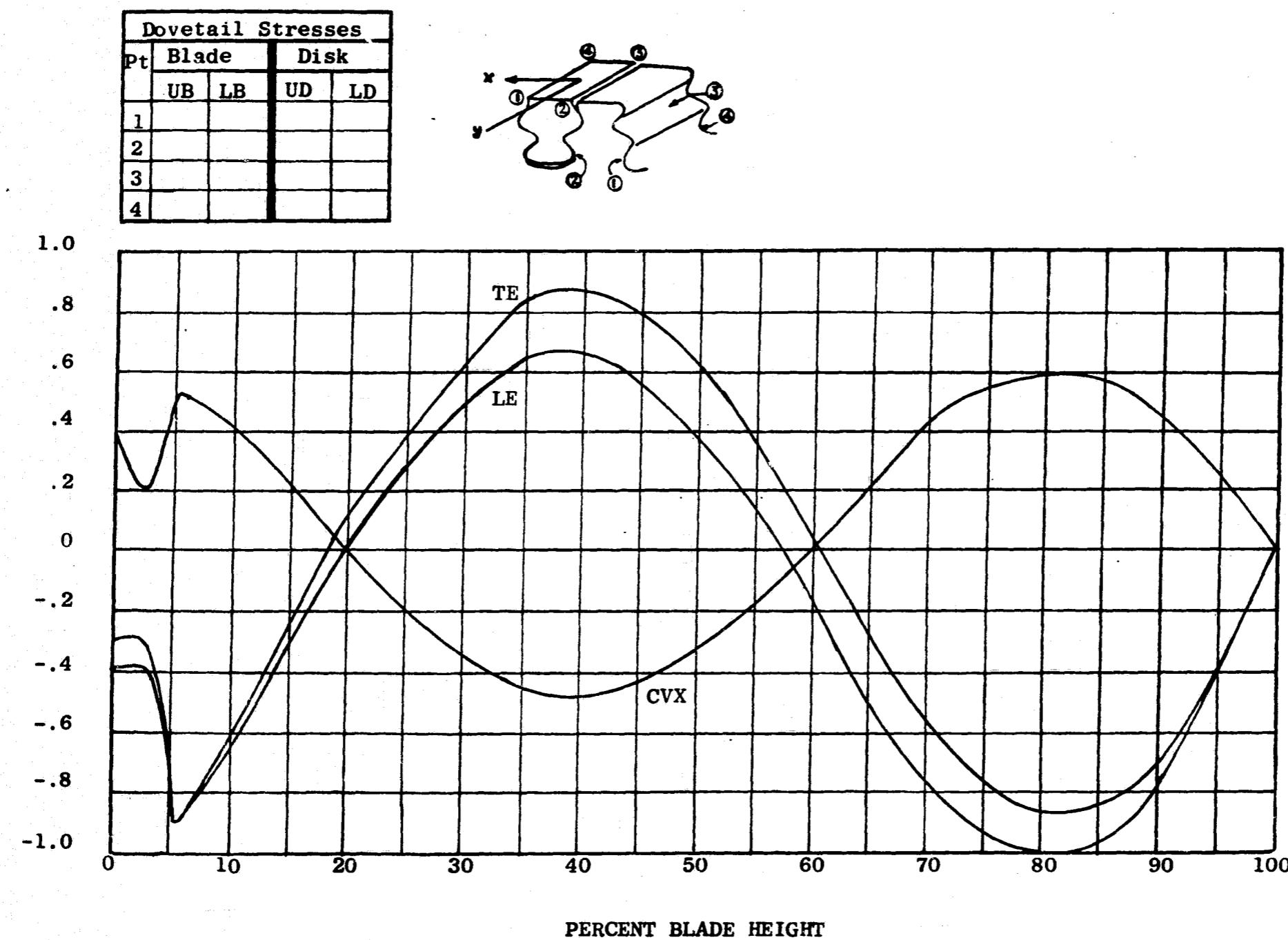


Figure 223. Stress Distribution for the Fans A/B Stage 4 Turbine, 1860 CPS, 2nd Flexural, Out-of-Phase

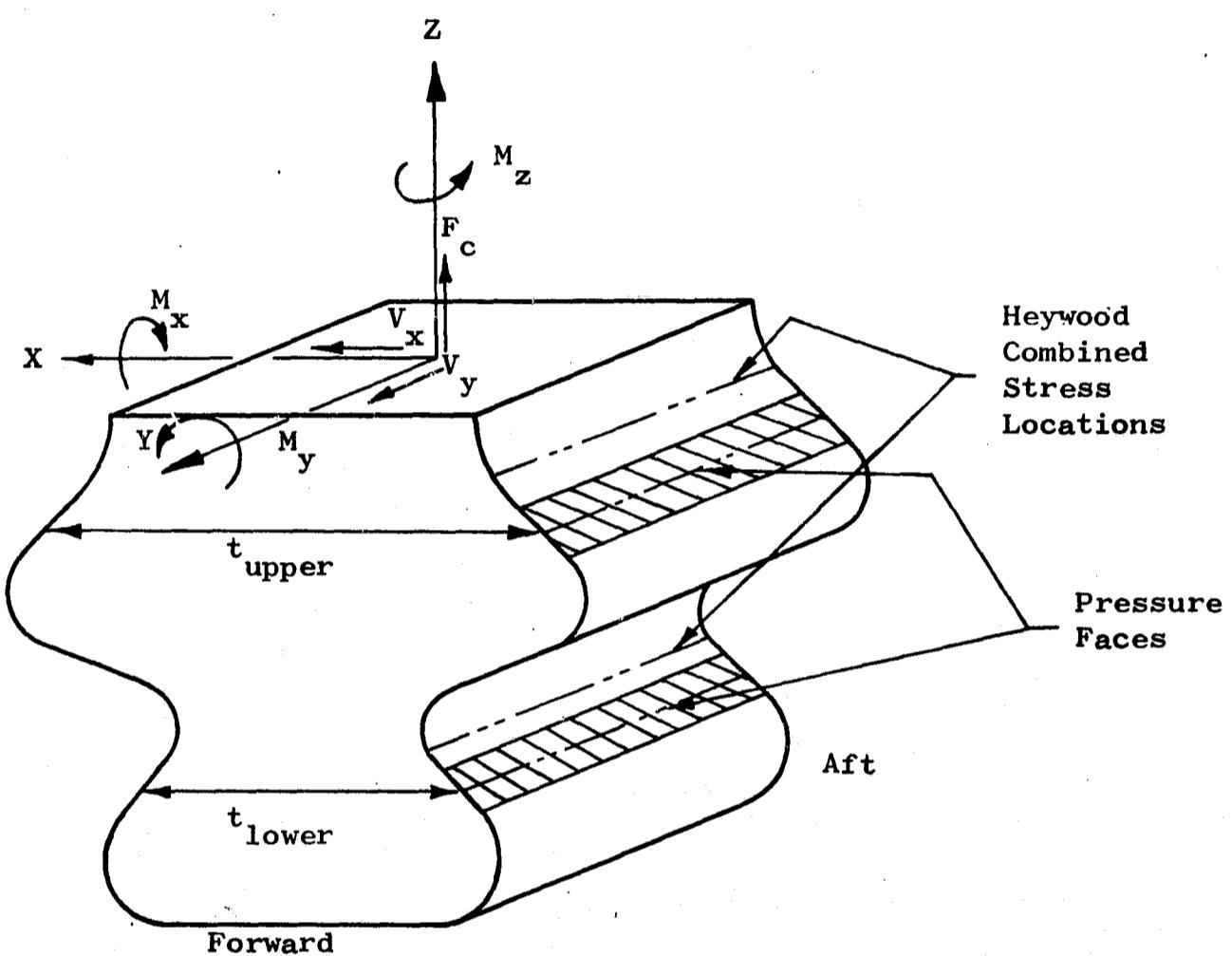


Figure 224. Blade Dovetail Schematic

Table LV. Fan A and B LP Turbine Rotor Stage 1 Blade Dovetail Stress Analysis
 (3500 RPM)

Point	σ_c	σ_{mx}	σ_{my}	σ_{neck}	σ_{tang}	σ_{total}
<u>Upper Tang</u>						
1	6503	-2036	112	4579	10750	13025
2	6503	-2036	-112	4355	10930	12800
3	6503	2036	112	8426	19000	23480
4	6503	2036	112	8650	18900	23720
5	6503	0	-112	6391	14950	18140
6	6503	0	112	6615	14850	18400
<u>Lower Tang</u>						
1	5631	-1685	-181	3766	8260	10350
2	5631	-1685	181	4127	8485	10975
3	5631	1685	181	7497	14963	19640
4	5631	1685	-181	7136	14738	19020
5	5631	0	181	5812	11724	15310
6	5631	0	-181	5451	11500	14685

Table LVI. Fan A and B LP Turbine Rotor Stage 2 Blade Dovetail Stress Analysis
(3500 RPM)

Point	σ_c	σ_{mx}	σ_{my}	σ_{neck}	σ_{tang}	σ_{total}
<u>Upper Tang</u>						
1	8163	-1806	515	6872	16000	19465
2	8163	-1806	-515	5842	15450	17660
3	8163	1806	-515	9454	23000	27390
4	8163	1806	515	10484	23550	29160
5	8163	0	-515	7648	19250	22540
6	8163	0	515	8678	19800	24330
<u>Lower Tang</u>						
1	7070	-1426	53	5697	11734	15165
2	7070	-1426	-53	5590	11636	14960
3	7070	1426	-53	8443	17067	22260
4	7070	1426	53	8550	17166	22470
5	7070	0	-53	7016	14351	18610
6	7070	0	53	7123	14450	18820

Table LVII. Fan A and B LP Turbine Rotor Stage 3 Blade Dovetail Stress Analysis
(3500 RPM)

Point	σ_c	σ_{mx}	σ_{my}	σ_{neck}	σ_{tang}	σ_{total}
<u>Upper Tang</u>						
1	10730	-2100	715	9343	12000	19790
2	10730	-2100	-715	7913	11500	17750
3	10730	2100	-715	12110	16550	26390
4	10730	2100	715	13540	16900	28300
5	10730	0	-715	10010	14050	22090
6	10730	0	715	11440	14500	24080
<u>Lower Tang</u>						
1	7575	-1630	360	6305	11338	15700
2	7575	-1630	-360	5585	11081	14600
3	7575	1630	-360	8845	15483	21710
4	7575	1630	360	9565	15740	22790
5	7575	0	-360	7215	13282	18160
6	7575	0	360	7935	13540	19240

Table LVIII. Fan A and B LP Turbine Rotor Stage 4 Blade Dovetail Stress Analysis
(3500 RPM)

Point	σ_c	σ_{mx}	σ_{my}	σ_{neck}	σ_{tang}	σ_{total}
<u>Upper Tang</u>						
1	9500	-1570	1145	9075	11370	19000
2	9500	-1570	-1145	6785	10500	15690
3	9500	1570	-1145	9925	14200	22100
4	9500	1570	1145	12215	15100	25420
5	9500	0	-1145	8355	12350	18900
6	9500	0	1145	9645	13200	21040
<u>Lower Tang</u>						
1	8240	0	750	8990	13120	20210
2	8240	0	-750	7490	12520	18000
3	8240	0	-750	7490	16690	20750
4	8240	0	750	8990	17300	23130
5	8240	0	-750	7490	14600	19400
6	8240	0	750	8990	15200	21700

Vibratory stress distributions in the dovetails are shown on the blade stress distribution charts of Figures 205 through 223. These are determined by imposing moments and shear forces taken from the blade analysis on the dovetail and analyzing the dovetail by the previously mentioned Heywood analysis. Results of the vibratory analysis on the dovetail are presented as an alternating stress ratio (relative to a chosen point on the airfoil surface) which, in this case, was the airfoil root leading edge.

Vibratory stress results are given for the first flexural in-phase mode in Figures 225, 226, 227, and 228. The four maximum combinations of steady state stress and alternating stress ratio for each stage are shown relative to the airfoil root stress.

It will be noted that, in general, the vibratory stress in the dovetail is higher than in the airfoil. This is caused by the low force levels created by the low tip speed and the large airfoils required for aerodynamic performance. The dovetails, which already have very low stress levels by aircraft standards, would have to be made abnormally large to reverse this situation. This would serve no useful purpose, since the vibratory levels of the shrouded blades are so low that the dovetails are completely safe with the present design.

The procedure for analysis of the double-tang dovetail using the Single-Tang Dovetail Computer Program was the following: each component of stress on each tang (upper and lower) was analyzed separately. The assumptions made for the loads for each stress component were:

1. The upper blade tang supports the entire load at its neck, and, therefore, 100 percent of all blade loads are used for the neck stress calculation. These loads are the centrifugal (F_C), the bending (M_x and M_y), and the shear (V_x and V_y).
2. Assuming that 50 percent of the F_C , M_x and M_z loads are taken out by the upper tang of the disc and that the M_y moment is distributed between upper and lower tangs according to the following relations:

$$M_y \text{ upper} = M_y \text{ total } (t^2_{\text{upper}})/(t^2_{\text{upper}} + t^2_{\text{lower}})$$

and

$$M_y \text{ lower} = M_y \text{ total } (t^2_{\text{lower}})/(t^2_{\text{upper}}),$$

the tang-bending stress calculation of the upper tang of both blade and disc can be made. The effect on moments M_x and M_y , due to shear loads V_x and V_y , are neglected.

3. The lower blade neck stress calculation is made by using the remainder of the loads transmitted to the lower blade tang, which is 50 percent of F_C , M_x and M_z , with M_y lower computed in Step 2.

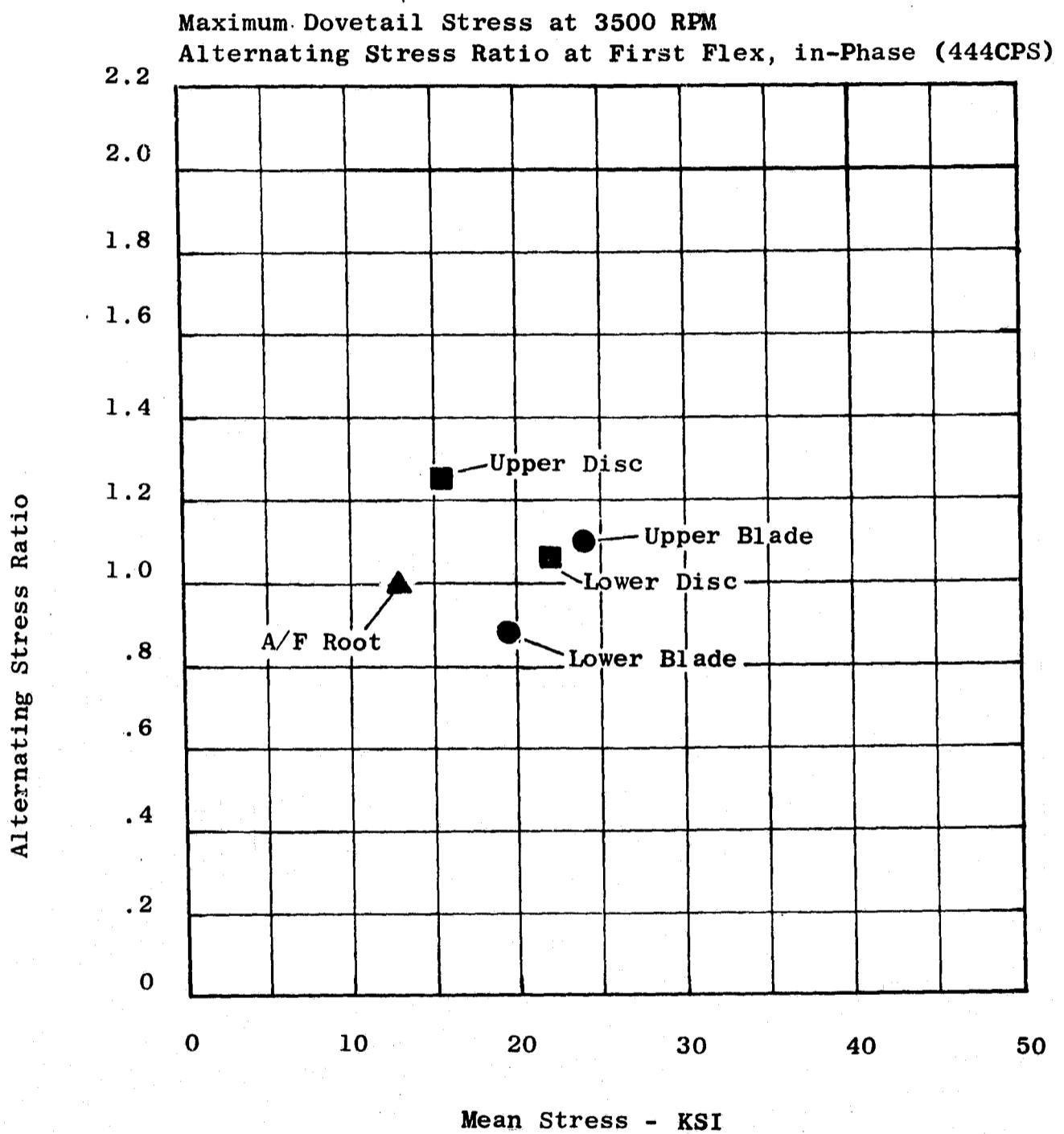
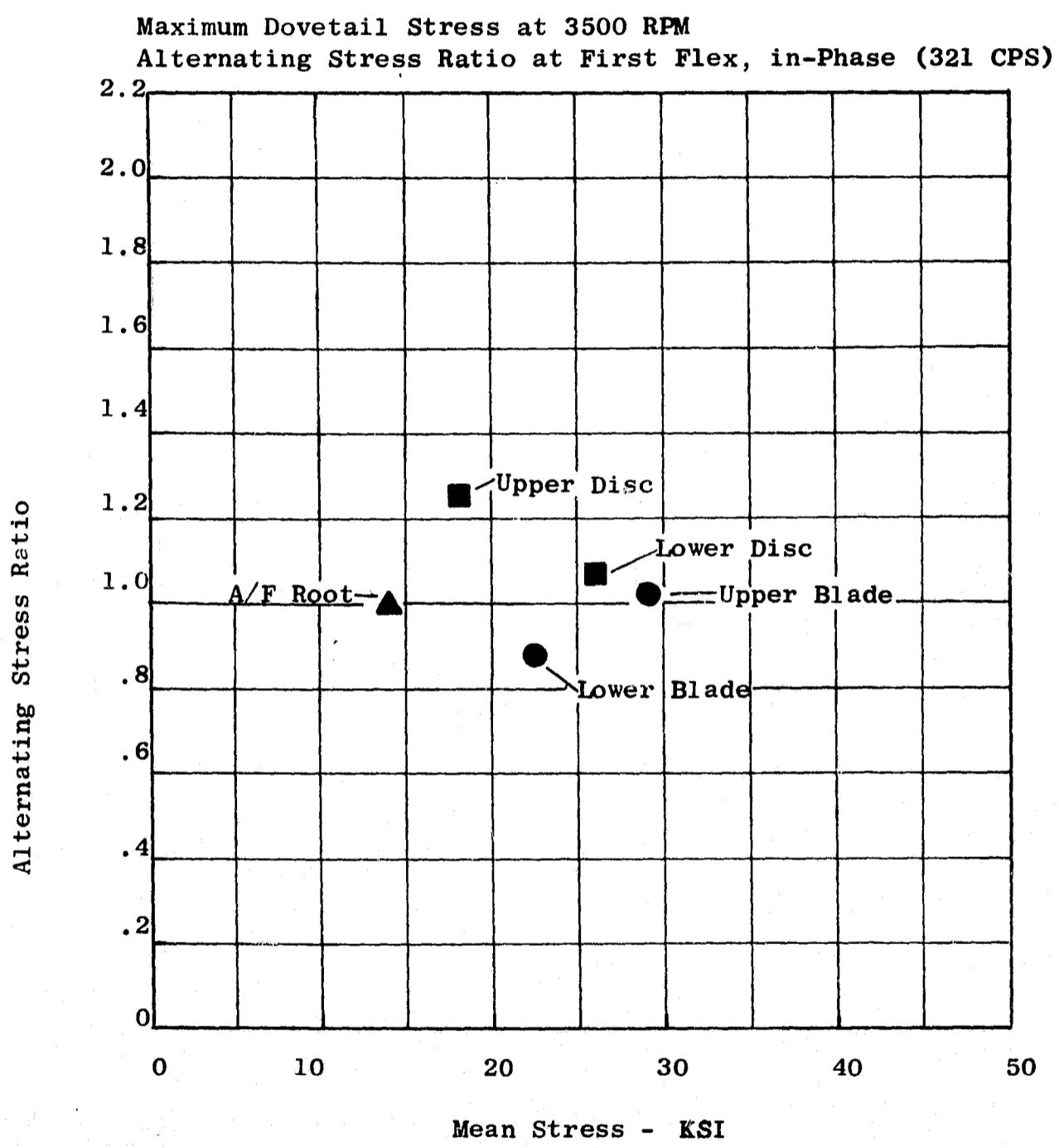
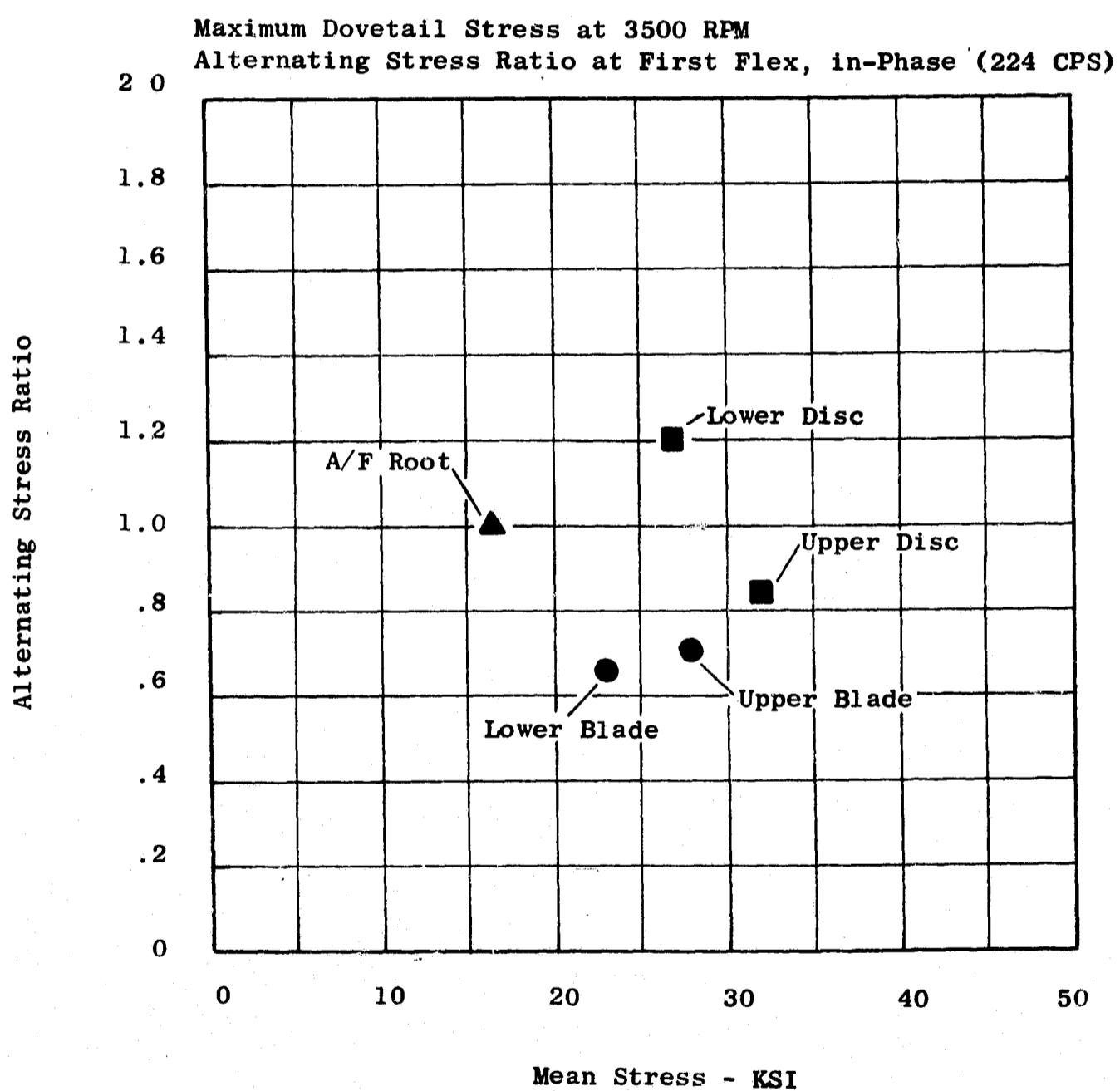


Figure 225. Fans A/B, LP Turbine Rotor, Dovetail Stress Analysis, Stage 1



**Figure 226. Fans A/B, LP Turbine Rotor, Dovetail Stress Analysis,
 Stage 2**



**Figure 227. Fans A/B, LP Turbine Rotor, Dovetail Stress Analysis,
Stage 3**

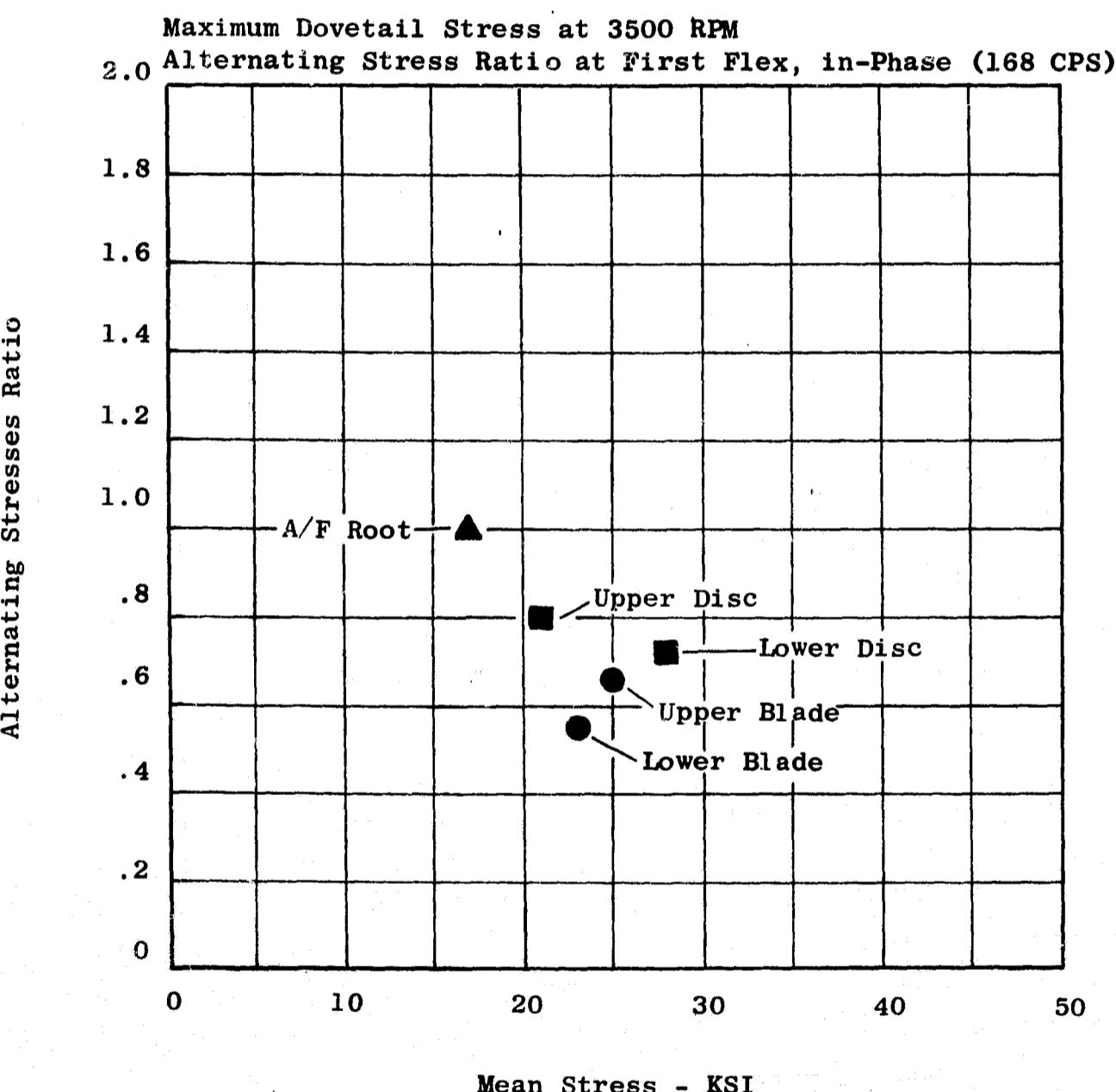


Figure 228. Fans A/B, LP Turbine Rotor, Dovetail Stress Analysis, Stage 4

4. The lower blade tang stress calculation used the same load as the neck stress in Step 3, since the lower blade tang is identical to a single-tang dovetail.
5. The upper disc neck stress is calculated using the same loads as used for the upper disc tang stress, since it is also identical to a single-tang dovetail.
6. The lower disc neck stress takes on the entire blade load plus an increment of F_c from the dovetail weight itself.
7. The lower disc tang stress calculation used the loads obtained in Step 3.

A modification to the tang-bending stress calculations was required on the upper blade tang and lower disc tang because of the geometry of these particular tangs. The tang functions, which are generated by the computer program and are used directly to obtain tang stress, are calculated based on a vertical plane through the Heywood point typical of single-tang dovetails. The error is introduced in the value of (j), the moment arm of the tang load.

The corrected tang functions were ratioed to the computer values and the adjusted tang stresses were 2.27 times higher for the upper blade tang and 1.47 times higher for the lower disc tang.

Neck stress and tang stress components on corresponding tangs were combined by the Heywood method which is:

$$\sigma_{\text{total}} = \sigma_{\text{neck}} + \sigma_{\text{tang}}$$

where,

$$T = \frac{1}{1 + 0.1162 \frac{\sigma_{\text{neck}}}{\sigma_{\text{tang}}}}$$

Vibratory stress calculations were handled in the same manner except stress concentration factors for the upper and lower tangs were:

	<u>Upper</u>	<u>Lower</u>
Blade	1.69	1.63
Disc	1.52	1.61

- Discs

The LP turbine discs feature integral spacer arms and high bore diameters. By placing the bolted flanges at the extremities of the spacer arms, the stress concentration effects of holes are removed from the disc. The high bore diameter is used to maintain a high rim tangential stress, to offset the thermal stress created by the rim being at a higher temperature than the bore. Both effects are especially desirable to improve the disc low cycle fatigue capability.

All the LP turbine discs are made of IN718, the strongest available alloy in the intermediate temperature range.

- Stress Analysis

The discs are designed to survive overspeed to a design speed of 3830 rpm. To analyze for this condition, the elastic disc analysis computer program was used. No allowance is made in the program for the disc spacer arms, although these tend to retard disc growth and consequently lower the disc stresses. The program output is stresses in the radial and tangential directions plus effective stress, which is the stresses combined by the method known as the Hencky-Von Mises Theory of Failure. A detailed stress analysis on the spacer arms is covered later in this report.

The resulting stresses for two operating conditions are shown. The first condition is at 3236 rpm. The disc stresses are shown in Figures 229, 231, 233 and 235. This represents the typical operating conditions that the discs will encounter. Figures 230, 232, 234 and 236 show the stresses that the discs would encounter at overspeed to 3830 rpm. The analysis established that the rotor is safe at these operating conditions. The low pressure steady state disc temperature is shown in Figure 237. The resulting stress levels are judged against the criteria strength listed below:

Stress	Stages			
	1	2	3	4
Bore Stress				
Calculated	85,525	86,050	71,520	81,690
120% x 0.2% yield	157,000	156,000	156,000	156,000
% Margin	83.7	81.3	118	91
Average Tangential Stress				
Calculated	72,100	71,270	60,150	70,690
0.2% yield	111,000	110,000	110,500	111,000
% Margin	54	54.3	83.5	57
Maximum Rim Stress				
Calculated	53,450	38,150	28,150	44,050
0.02% yield	110,000	109,000	109,500	110,000
% Margin	229	186	290	150

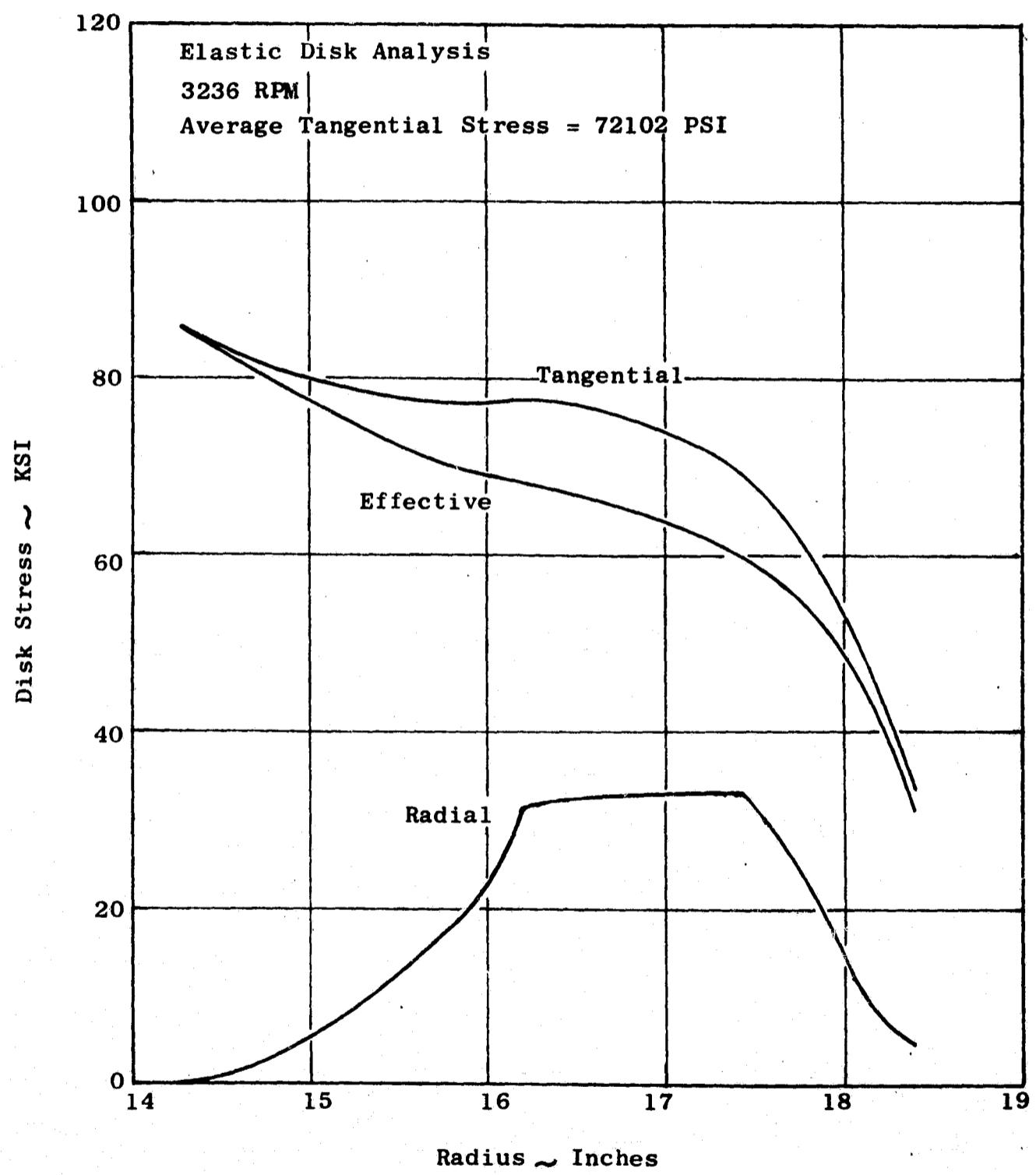


Figure 229. Fans A/B, LP Turbine Rotor, Stage 1 Steady State Stress, 3236 RPM

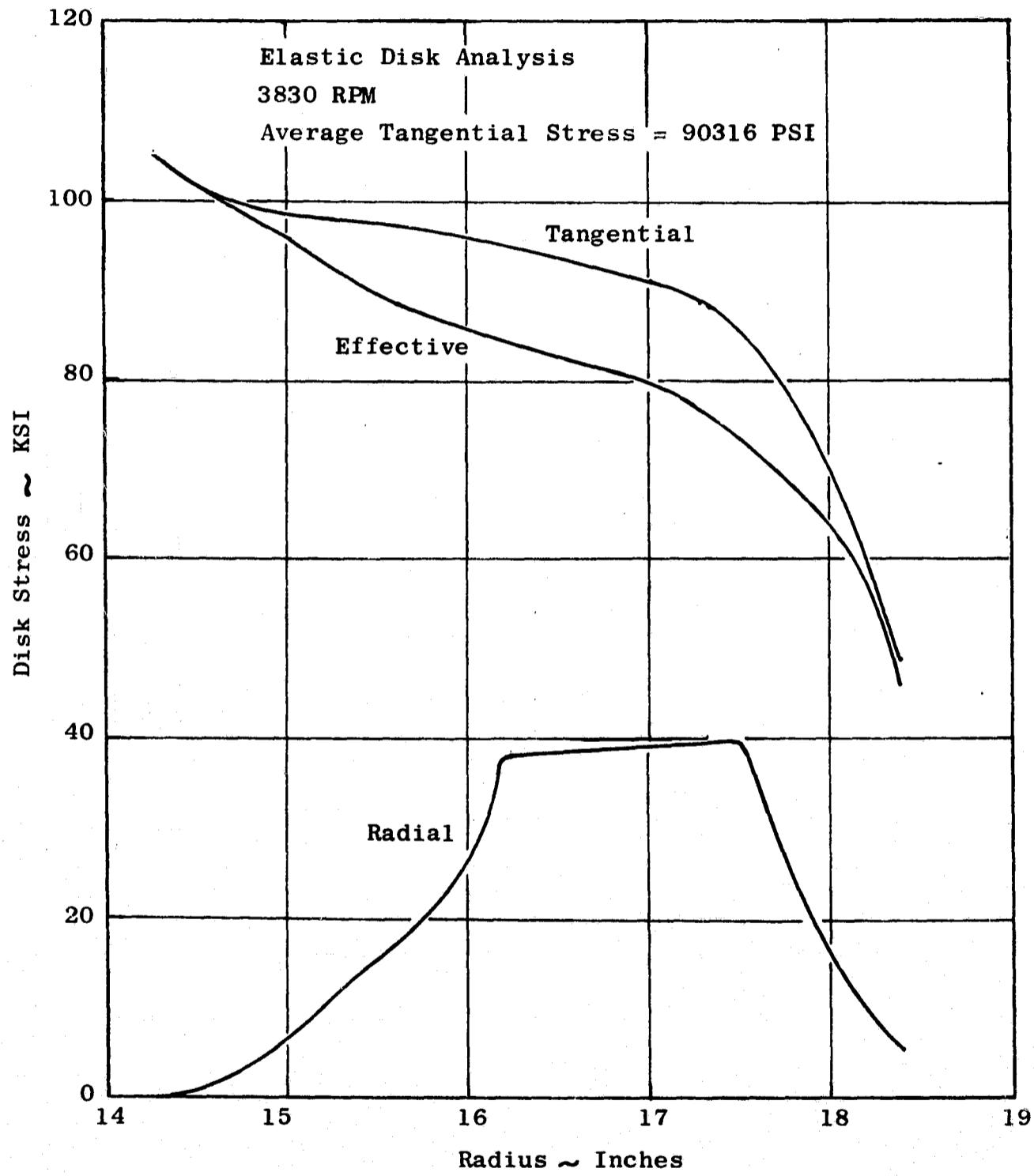


Figure 230. Fans A/B, LP Turbine Rotor, Stage 1 Steady State Stress, 3830 RPM

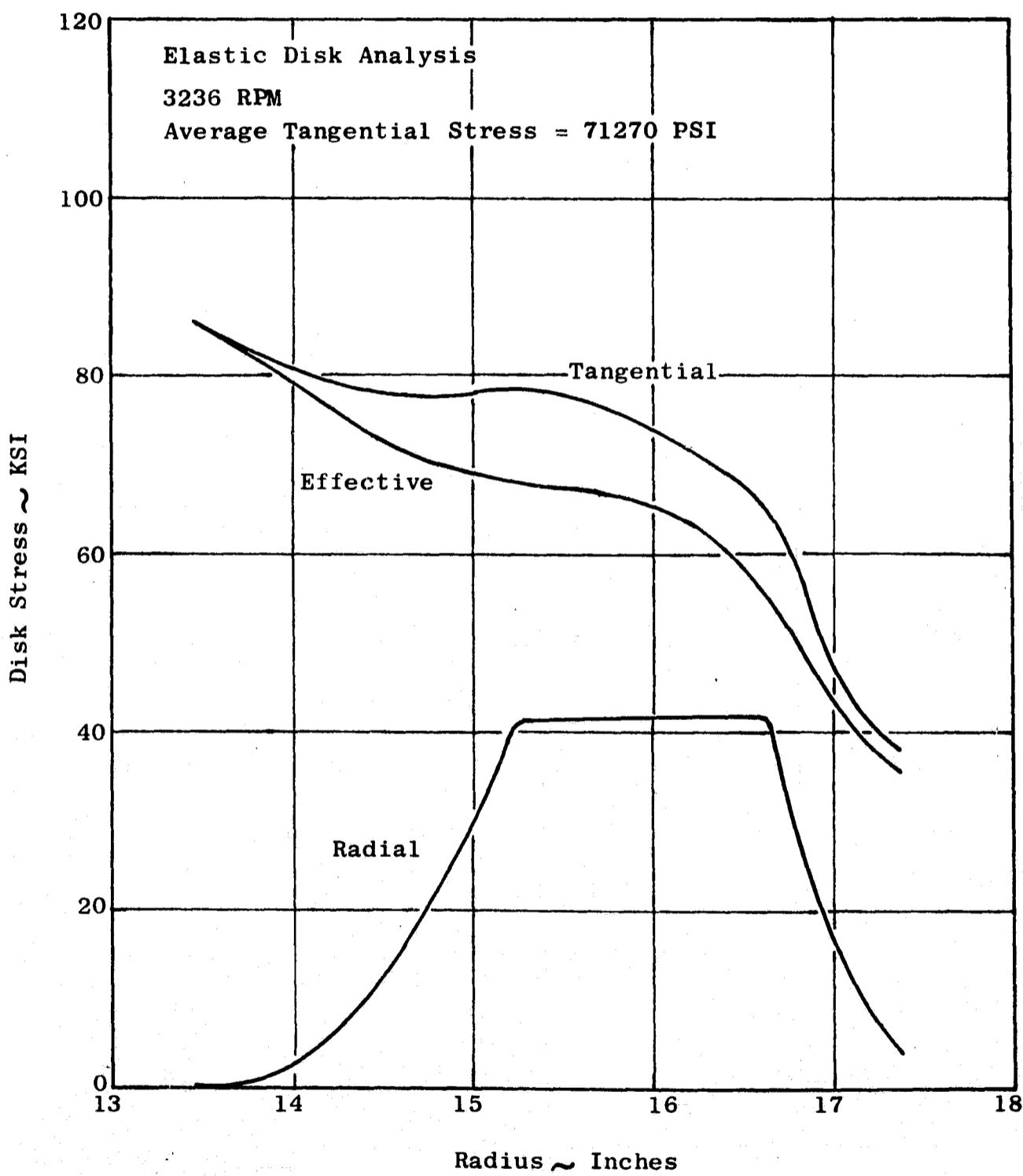


Figure 231. Fans A/B, LP Turbine Rotor, Stage 2 Steady State Stress,
3236 RPM

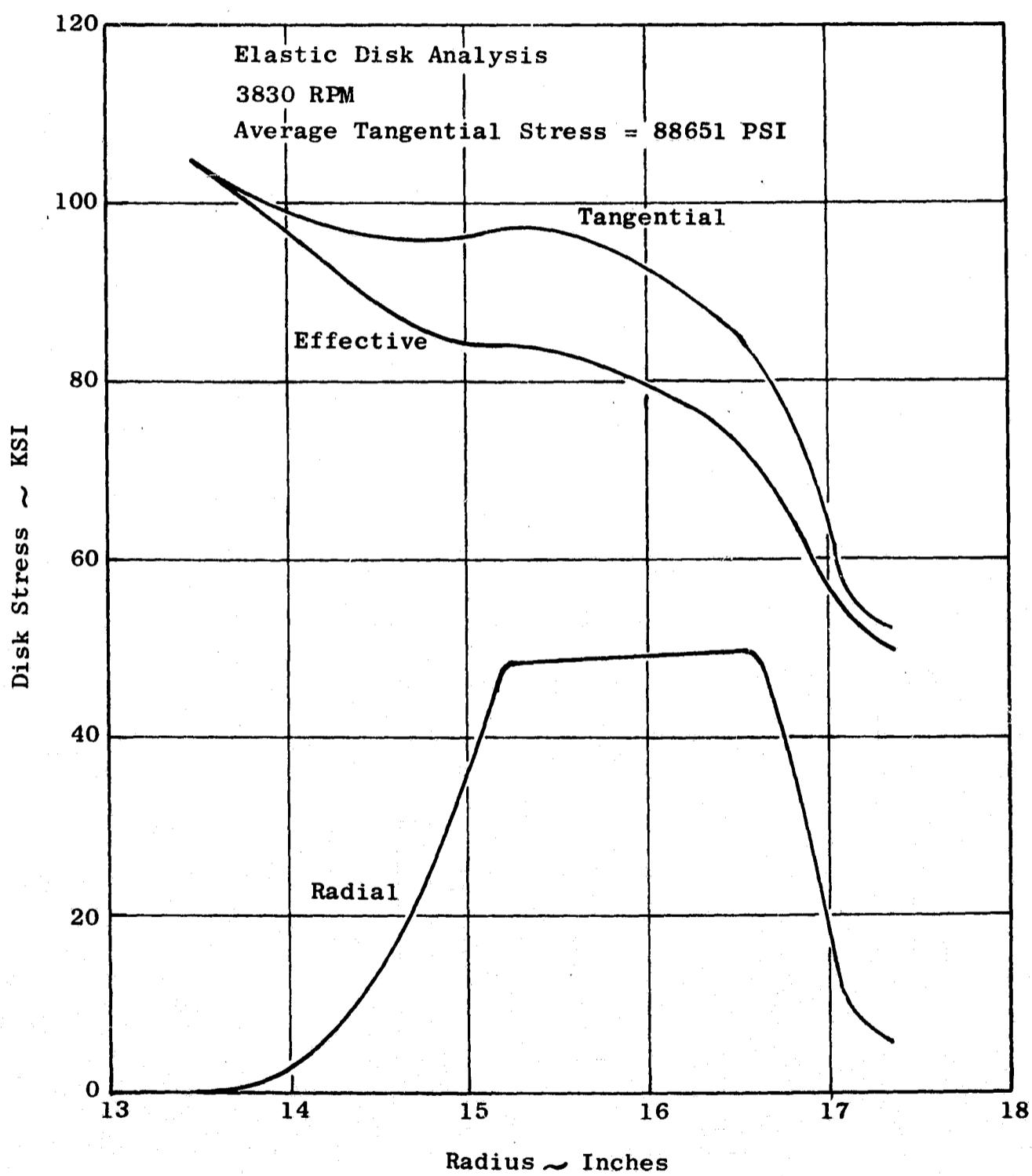


Figure 232. Fans A/B, LP Turbine Rotor, Stage 2 Steady State Stress, 3830 RPM

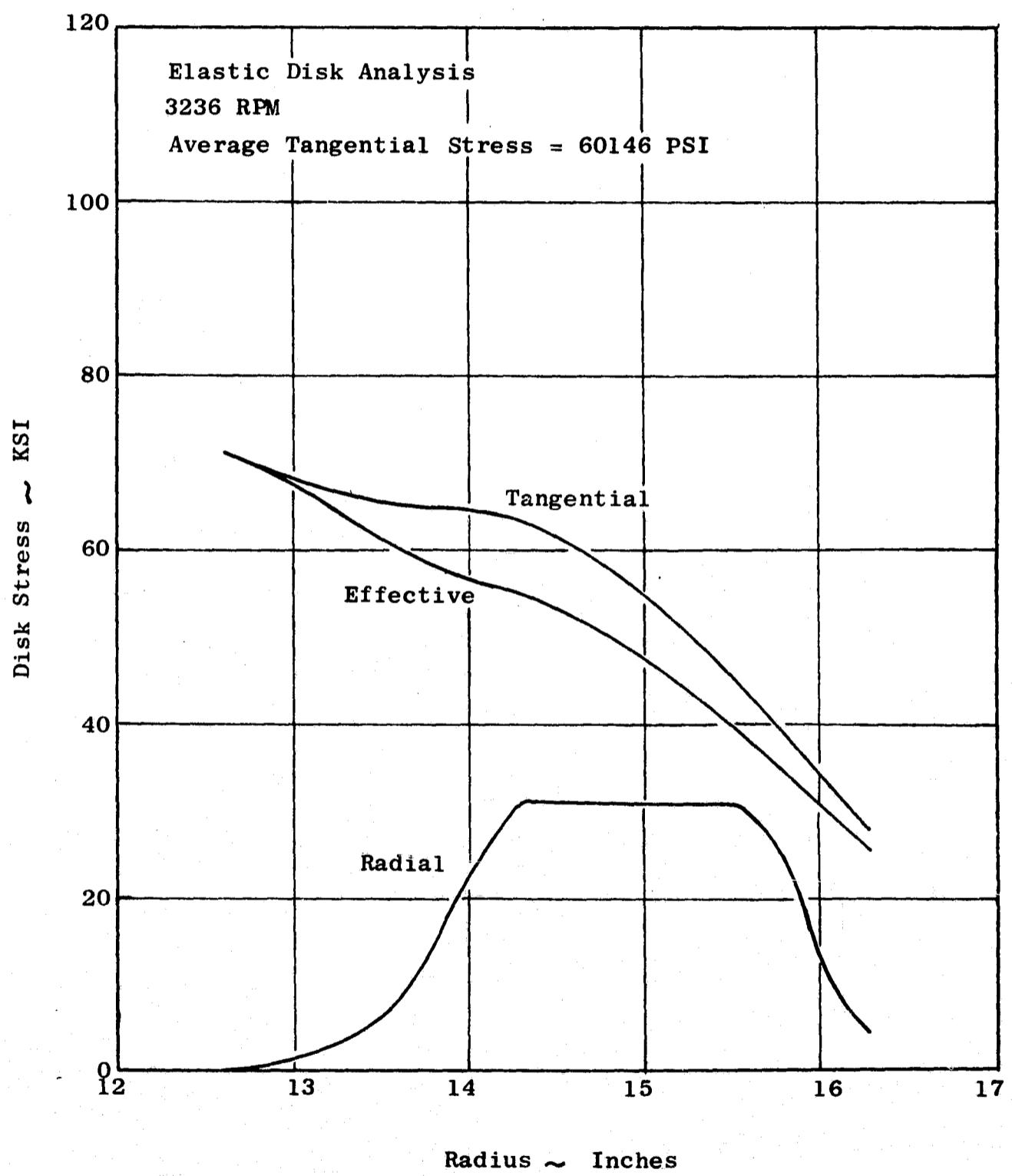


Figure 233. Fans A/B, LP Turbine Rotor, State 3 Steady State Stress,
3236 RPM

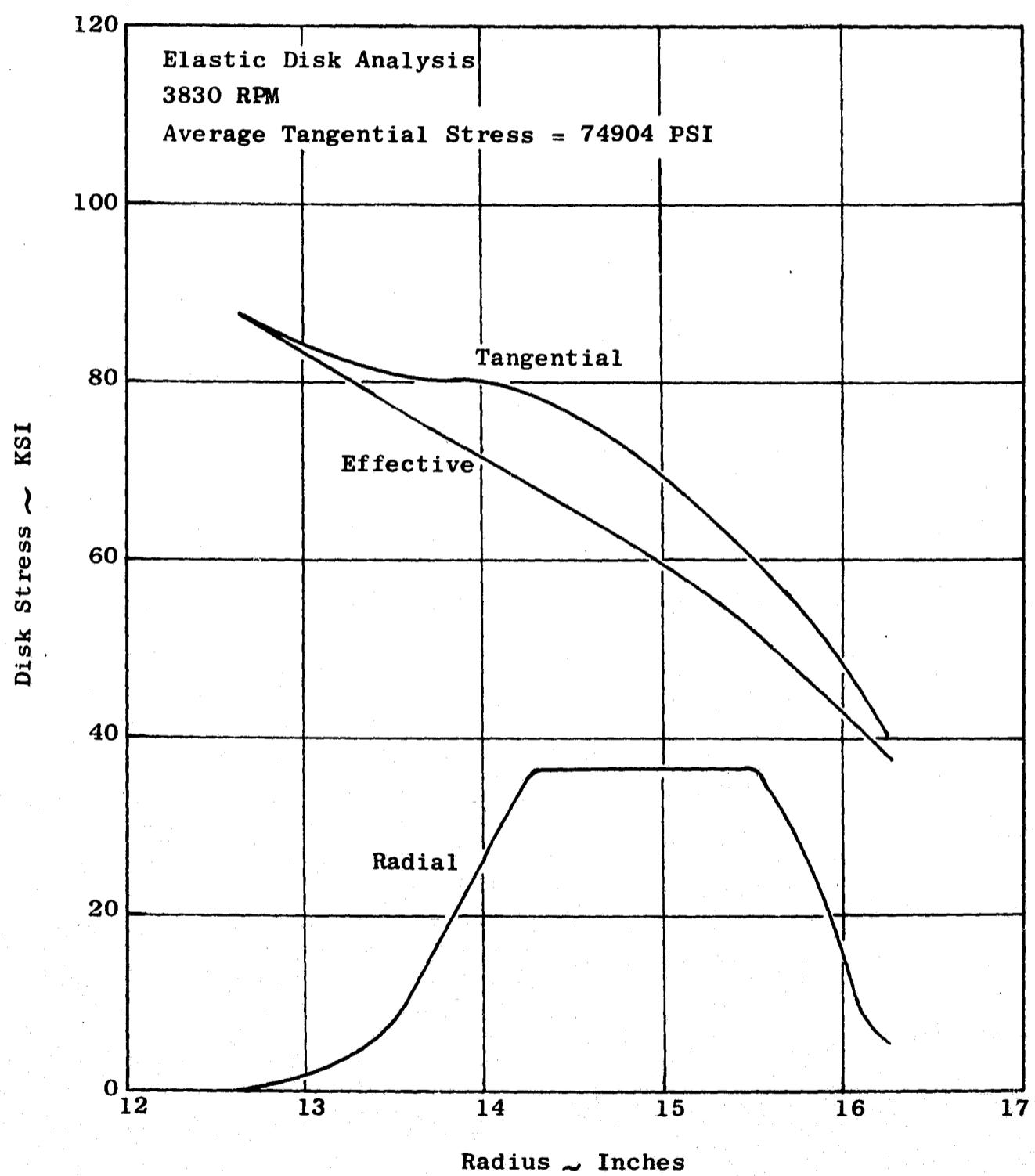


Figure 234. Fans A/B, LP Turbine Rotor, Stage 3 Steady State Stress,
3830 RPM

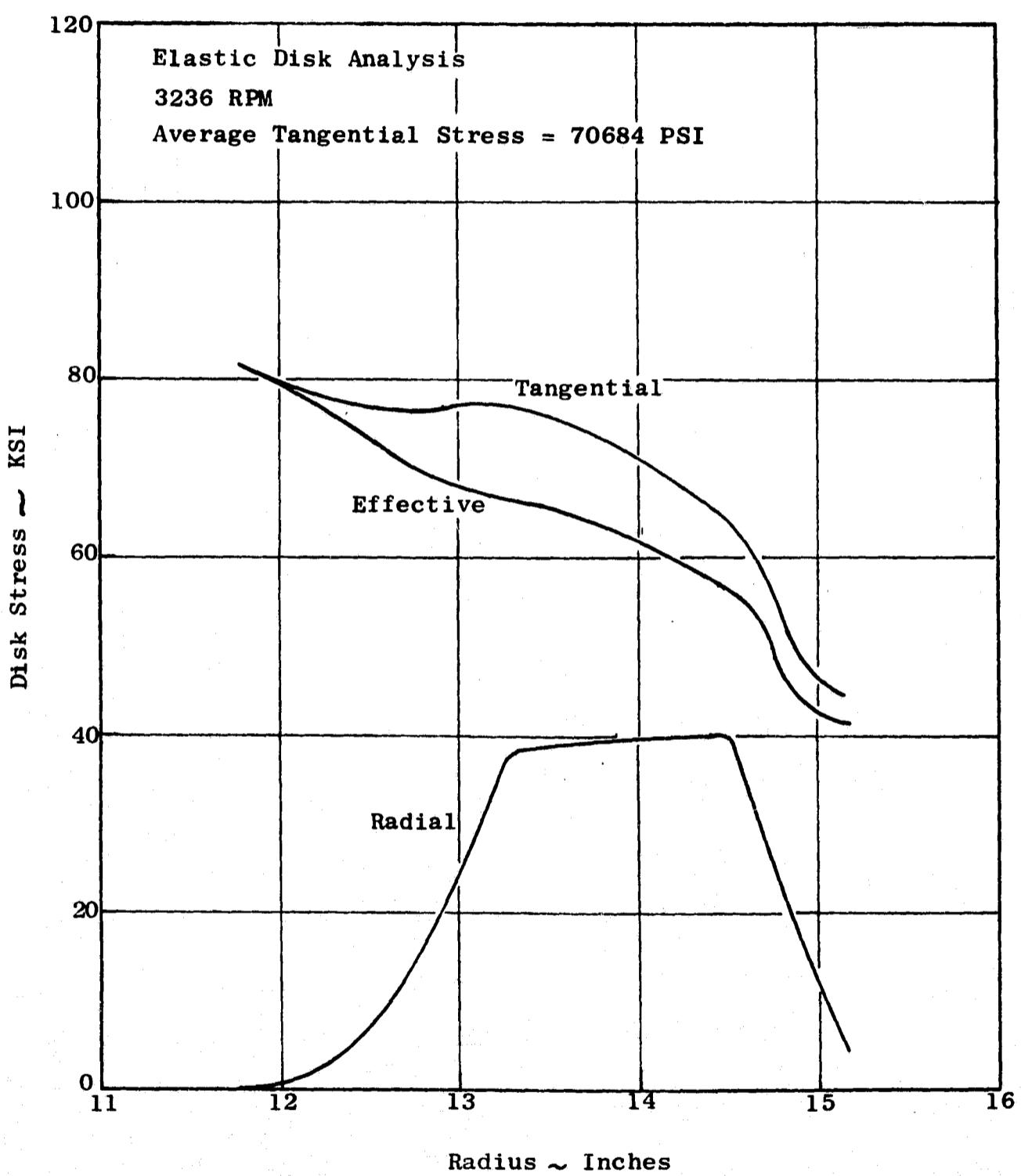


Figure 235. Fans A/B, LP Turbine Rotor, Stage 4 Steady State Stress, 3236 RPM

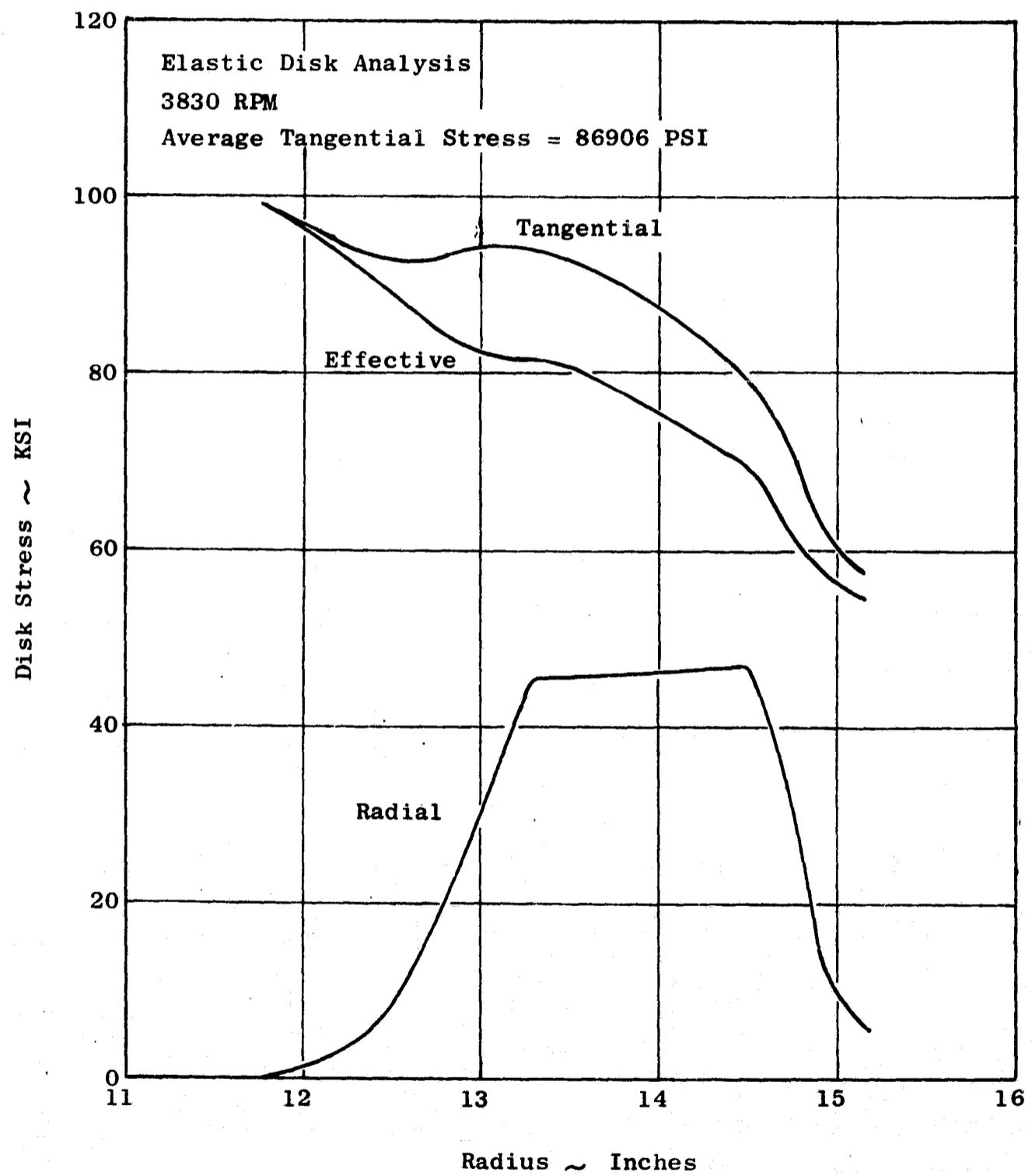


Figure 236. Fans A/B, LP Turbine Rotor, Stage 4 Steady State Stress, 3830 RPM

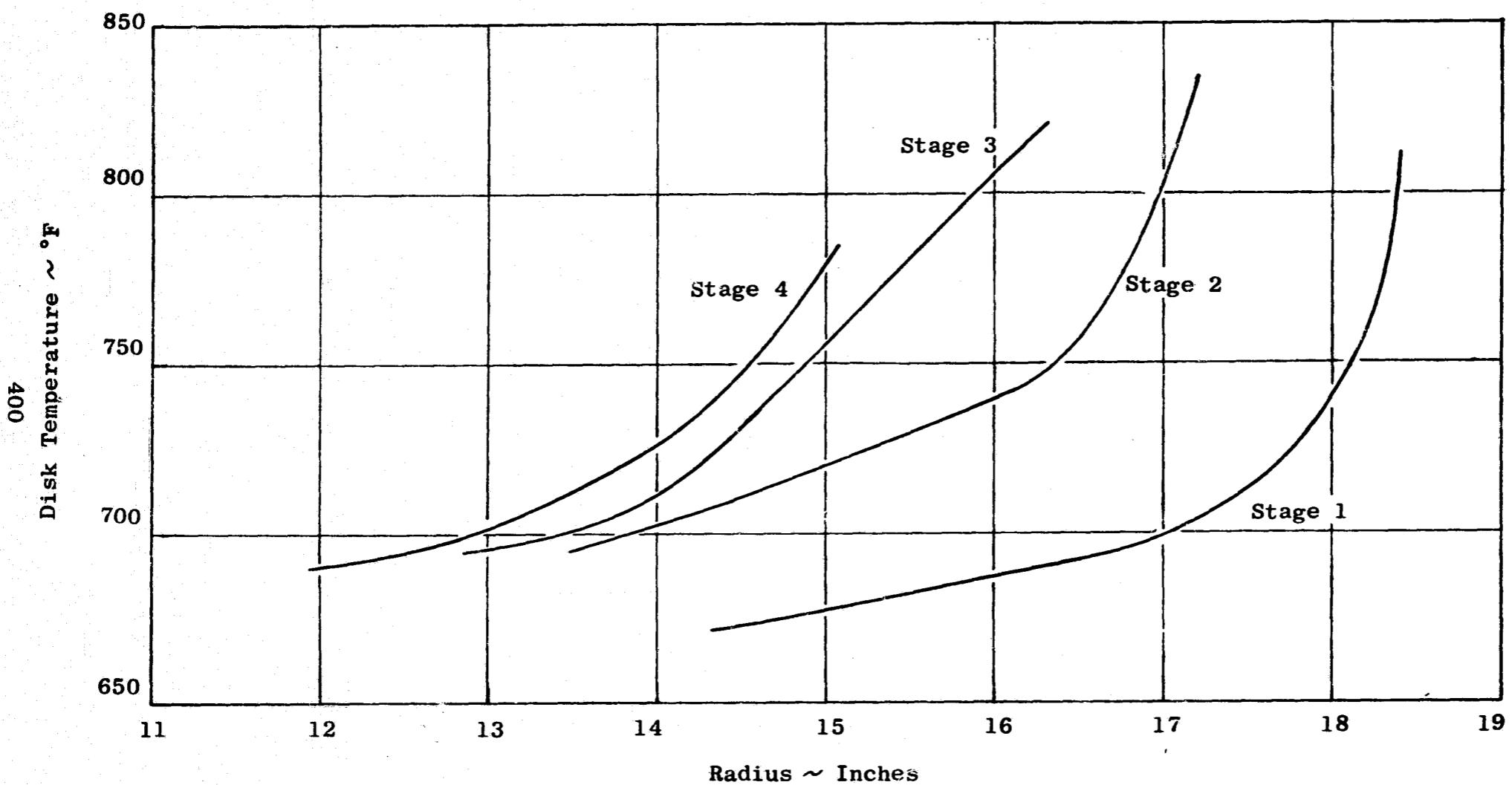


Figure 237. Fans A/B LP Turbine Steady State Disc Temperature

The disc dovetail stresses were analyzed using the same procedure as the blade stresses covered earlier in the report. Both stages, of course, use the two-tang dovetail to match the blades. The steady state stresses included in the analysis are the centrifugal force, shear due to gas load, bending due to gas load, and blade offset and tilt. Tables LIX, LX, LXI, and LXII tabulate the important steady state stress levels in each stage. All stress levels are at the engine condition of sea level static, standard day and at a rotor speed of 3500 rpm. As noted in the tables, the results are given at six points on the dovetail tangs. These points are located similar to the blade dovetail.

Vibratory stress distributions in the dovetails are shown with the blade dovetail stress distribution in Figures 225 through 228. Results of the vibratory analysis on the dovetail are presented as an alternating stress ratio relative to a chosen point on the airfoil (which, in this case, was the airfoil root leading edge). Vibratory results are given for the first flexural in-phase mode.

- Blade Retainers

The blade retainers are direct copies of retainers presently being used on the TF39 and CF6 engines and are not expected to cause any problems based on test experience to date.

- Shafts

The rotor structure, including shaft, disc flanges, and seals, was analyzed with the Multishell Computer Program which is used for complicated axisymmetrical bodies. The modeling procedure consists of breaking up a part to be analyzed into geometrically regular elements such as cones, cylinders, and rings. The program then computes influence coefficients for each end of each submember. It also computes free-end deflections for the centrifugal and thermal loads imposed. When the member ends are jointed, compatible deflections are imposed and the required end loads are computed. These end loads, together with the internal loads, completely define the loads, stresses, and deflections throughout the member.

The forward shaft is bolted between the Stage 2 and 3 disc flanges and extends forward to the No. 6 bearing. The hub of the shaft splines to the midshaft. The shaft is made of a one-piece Inconel 718 forging. The steady state stresses are shown in Figure 238. The maximum stress in the outer cone of the shaft is 46,000 psi compared to a 0.2 percent offset yield strength of 128,000 psi at the maximum temperature of 800°F.

Table LIX. Fan A and B LP Turbine Rotor Stage 1 Disc Dovetail Stress Analysis
(3500 RPM)

Point	σ_c	σ_{mx}	σ_{my}	σ_{neck}	σ_{tang}	σ_{total}
<u>Upper Tang</u>						
1	8085	-2492	-426	5294	3373	8435
2	8085	-2492	426	6019	3325	9145
3	8085	2492	426	11004	6767	17310
4	8085	2492	-426	10152	6755	16420
5	8085	0	426	8511	5041	13230
6	8085	0	-426	7659	5039	12340
<u>Lower Tang</u>						
1	8140	-2247	-1036	4857	8400	11850
2	8140	-2247	1036	6929	8650	14485
3	8140	2247	1036	11422	15230	24610
4	8140	2247	-1036	9350	15000	21990
5	8140	0	1036	9175	11940	19545
6	8140	0	-1036	7103	11700	16925

Table LX. Fan A and B LP Turbine Rotor Stage 2 Disc Dovetail Stress Analysis
(3500 RPM)

Point	σ_c	σ_{mx}	σ_{my}	σ_{neck}	σ_{tang}	σ_{total}
<u>Upper Tang</u>						
1	9728	-1786	-3	7939	5023	12620
2	9728	-1786	+3	7944	4861	12480
3	9728	+1786	+3	11517	7301	18320
4	9728	+1786	-3	11511	7466	18450
5	9728	0	+3	9731	6081	15400
6	9728	0	-3	9725	6243	15335
<u>Lower Tang</u>						
1	9972	-1993	-736	7243	10900	16520
2	9972	-1993	+736	8714	12250	19245
3	9972	+1993	+736	12701	18400	28450
4	9972	+1993	-736	11230	17100	25760
5	9972	0	+736	10708	15400	23900
6	9972	0	-736	9237	14000	21140

Table LXI. Fan A and B LP Turbine Rotor Stage 3 Disc Dovetail Stress Analysis
(3500 RPM)

Point	σ_c	σ_{mx}	σ_{my}	σ_{neck}	σ_{tang}	σ_{total}
<u>Upper Tang</u>						
1	8040	16910	372	25320	7717	32775
2	8040	16910	-372	24575	7333	31660
3	8040	-16910	-372	12330	10560	21935
4	8040	-16910	372	-8495	10940	4370
5	8040	0	-372	7670	8946	15550
6	8040	0	372	8413	9329	16675
<u>Lower Tang</u>						
1	9375	-1654	482	8201	12700	18965
2	9375	-1654	-482	7238	12500	17650
3	9375	1654	-482	10546	18300	25775
4	9375	1654	482	11509	18500	27100
5	9375	0	-482	8892	15400	21710
6	9375	0	482	9855	15600	23030

Table LXII. Fan A and B LP Turbine Rotor Stage 4 Disc Dovetail Stress Analysis
(3500 RPM)

Point	σ_c	σ_{mx}	σ_{my}	σ_{neck}	σ_{tang}	σ_{total}
<u>Upper Tang</u>						
1	8645	-1221	903	8326	8709	16090
2	8645	-1221	-903	6521	8027	13545
3	8645	1221	-903	8963	10980	18575
4	8645	1221	903	10770	11662	21130
5	8645	0	-903	7742	9504	16060
6	8645	0	903	9547	10186	18610
<u>Lower Tang</u>						
1	10120	-1517	300	8902	13950	20700
2	10120	-1517	-300	8301	14300	20215
3	10120	1517	-300	11336	19600	27650
4	10120	1517	300	11937	19250	28150
5	10120	0	-300	9819	16950	23940
6	10120	0	300	10420	16600	24420

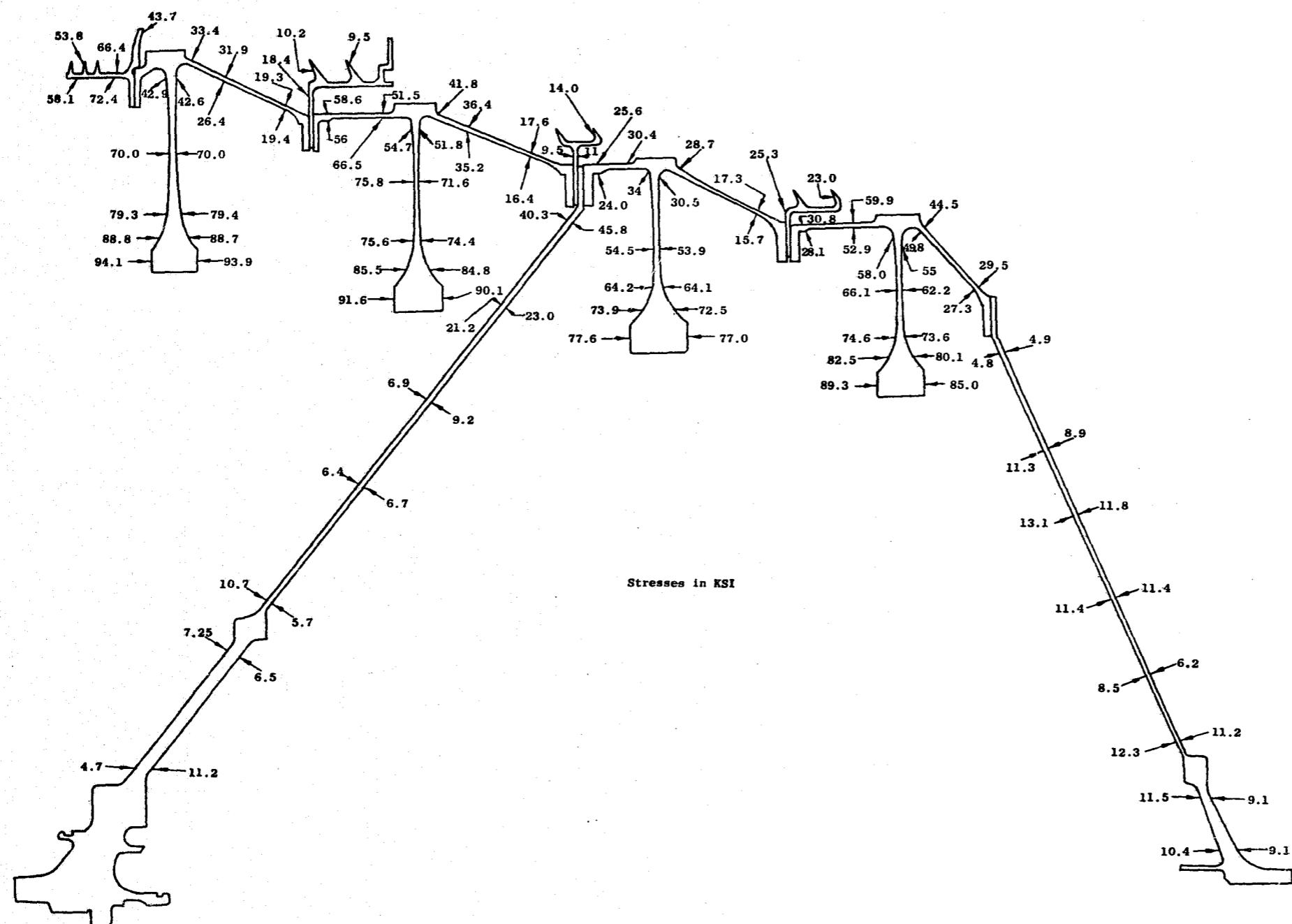


Figure 238. Fans A and B LP Turbine Rotor Multishell Analysis, Effective Surface Stress, KSI

The rear shaft is bolted to the aft spacer arm of the Stage 4 disc and extends aft to the Number 7 bearing. The rear shaft is loaded by rotating, thermal, and maneuver loads only; it transmits no torque. The shaft is made from A-286 forging. Maximum shaft temperature is 730°F for a minimum 0.2 percent offset yield strength of 70,500 psi compared to the maximum stress in the shaft of 13,100 psi.

The spacer arms are integral with the discs and, thus, are also Inconel 718 material. The conical arms are tapered near the disc rims to increase stiffness and to reduce stresses. Spacer arm steady state stresses are shown in Figure 238.

A summary of the significant low pressure rotor forward shaft stresses, and its bolted connection between the second and third rotor stages, is shown in Table LXIII. The table also presents for comparison the corresponding shaft and bolt stresses for the Fan C rotor.

- Seals

There are three interstage rotor seals. These seals are made of Inconel 718 and have two teeth slanted forward at approximately 30°. The seals are designed to rub into the honeycomb in the stator seals, and the teeth are spaced so that the wear track of one tooth does not enter the wear track of the other tooth during engine operation. By this means, seal clearance is kept to a minimum for reduced leakage. The outer surfaces of the teeth are coated with aluminum oxide as a hardcoating to permit the seal to "rub in" without wearing away the rotating seal. Seal stresses are generally low and are shown on Figure 238. These stresses are at a rotor speed of 3500 rpm. The maximum allowable stress 0.2% offset yeild strength is 126,000 psi at the maximum seal temperature of 900°F.

The three-tooth seal on the forward site of the Stage 1 disc is used to restrict the airflow from the forward rotor cavity. The forward rotor cavity must have a continuous flow of purge air, and no hot gas from the gas stream may be allowed to enter the cavity. Stresses, as shown in Figure 238, are at a rotor speed of 3500 rpm. The 0.2 percent offset yield strength is 127,000 psi at the seal temperature of 870°F.

- Disc-Blade Vibration

Coupled blade-disc natural frequencies were calculated using the Blade-Disc System Vibration Program. This program is an extension of the Twisted Blade Program used for the blade analysis, where now the disc profile and rim configuration can be added to the input. The program performs a frequency search for the particular mode desired at a specified rpm level. The modes investigated were the first and second "O"-diameter modes (umbrella mode) and the circumferential modes from the two-diameter up to the eight-diameter mode.

Table LXIII. LP Turbine Shaft and Bolt Stress Summary, SLS - Standard Day

Parameter		Fan A/B	Fan C
Fan HP		16 068	18 626
RPM		3 236	4 606
Torque		312 820	254 760
Upper Cone	σ_{max} .	45 800	37 000
	T_{max} .	1 910	2 500
	σ_{total}	46 000	38 000
	Temperature, °F	800	750
	0.2Y σ allowable	128 000	129 000
Lower Cone	σ_{max} .	11 200	58 900
	σ_{max} @ hole	27 800	22 800
	T_{max} .	9 670	7 800
	σ_{total}	39 000	81 700
	Temperature, °F	550	500
	0.2Y σ allowable	131 000	132 500
Bolt T_{max} .		3 300	6 000
5/16 bolt torque, in./lbs		300	300
Clamp force, lbs		6 000	6 000
$\sigma_{tensile}$		104 000	104 000
σ_{total}		104 000	104 200
Temperature, °F		800	800
0.02Y σ allowable		111 500	111 500

The umbrella or first O-diameter mode is the fundamental frequency and, therefore, is the lowest natural frequency of the blade-disc system. This mode can only be excited by strong axial pressure pulses in the engine such as a compressor stall. Engine experience on both the TF39 and CF6 has shown no resonant conditions with the umbrella modes anywhere in the operating range.

The circumferential modes become resonant only at the operating point where the particular diameter mode crosses its corresponding per rev line, such as indicated on the Campbell diagram for the 6- and 8-diameter modes in Figure 239. Although the analysis indicates resonance at the frequencies shown in Figures 239 through 242, no significant vibratory stress has ever been recorded for the blade disc systems within the operating range of the CF6 and TF39 engines.

- Temperature Distribution

Calculation of the LP turbine rotor temperatures was made by use of the GE 635 Computer Program, THTD.

Briefly, THTD is a very general program which gives a finite difference analysis of three-dimensional steady state or transient heat flow, employing the implicit form of the heat balance equations. The method of analysis consists of representing the geometry of the problem by elemental bits of geometry called nodes, connected in a manner prescribed by format with the appropriate convection, radiation, or heat generation boundary conditions impressed on them.

The LP turbine node network extended axially through the rotor, forward to aft. The network extended radially from the inner radius of the LP turbine shaft to the rotor and then to the blade platforms. The blade platforms were assumed to be at the local gas temperature as given in the design requirements. The inner radius of the LP shaft was assumed to be at sump temperature. Boundary conditions imposed on the other nodes were obtained from classical heat transfer convection equations.

Figure 243 shows the calculated temperature distribution of the turbine rotor.

7.1.1.2 Fan C Turbine

The low pressure turbine (LPT) for experimental engine configuration C consists of two stages which extract energy from the primary gas stream to drive the fan. The general arrangement of this turbine is shown in Figure 244.

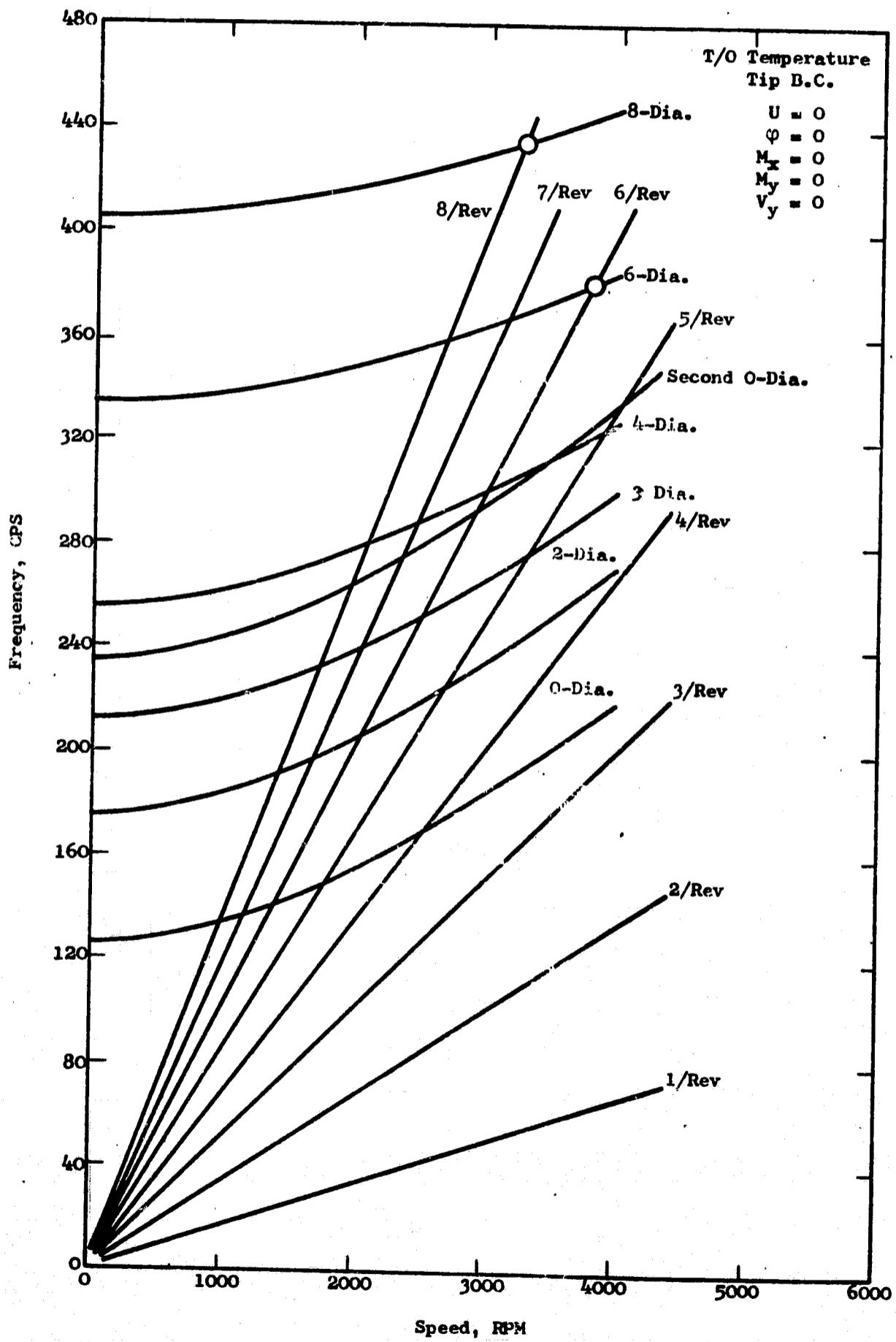


Figure 239. Fans A/B LP Turbine, Stage 1 Campbell Diagram

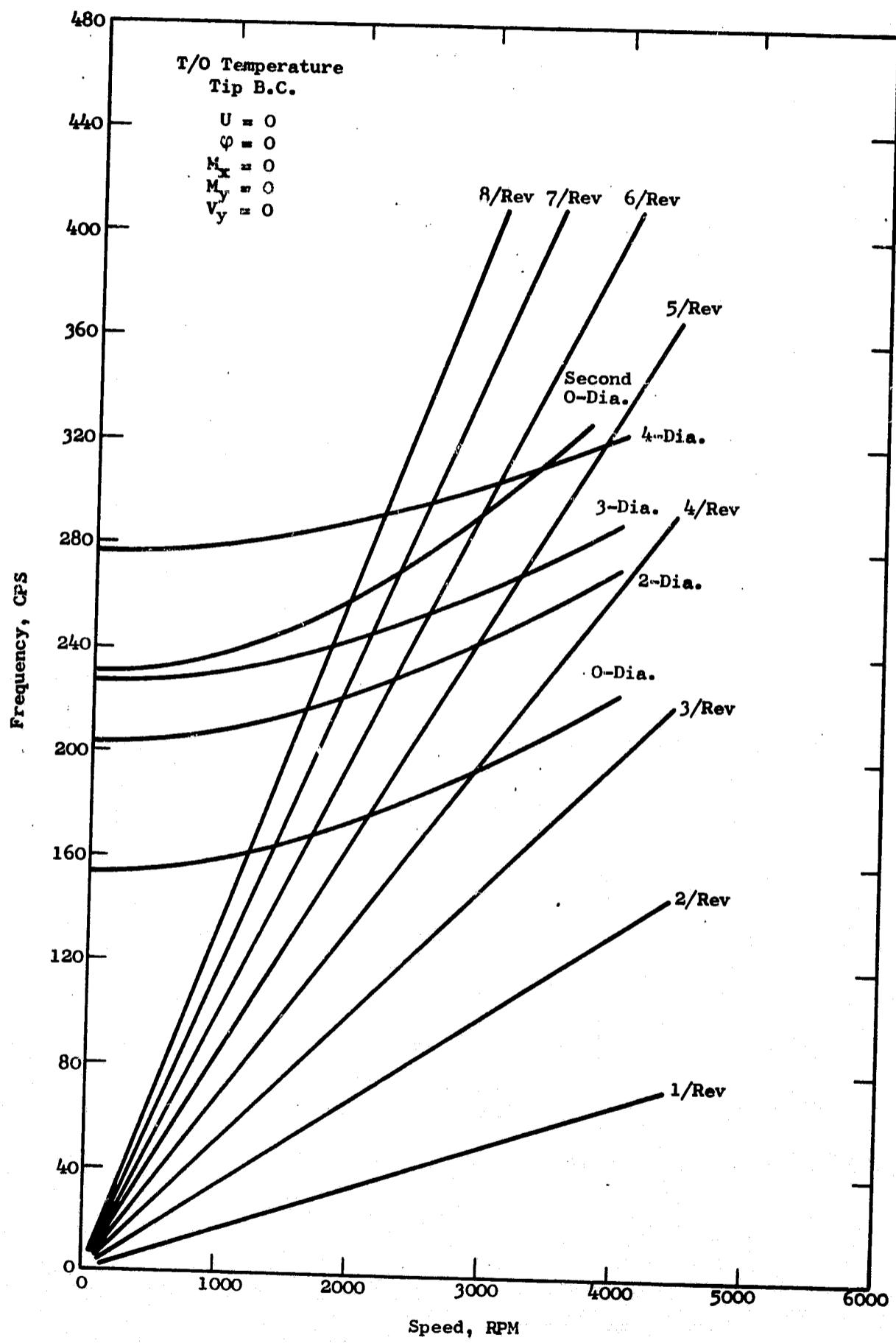


Figure 240. Fans A/B LP Turbine, Stage 2 Campbell Diagram

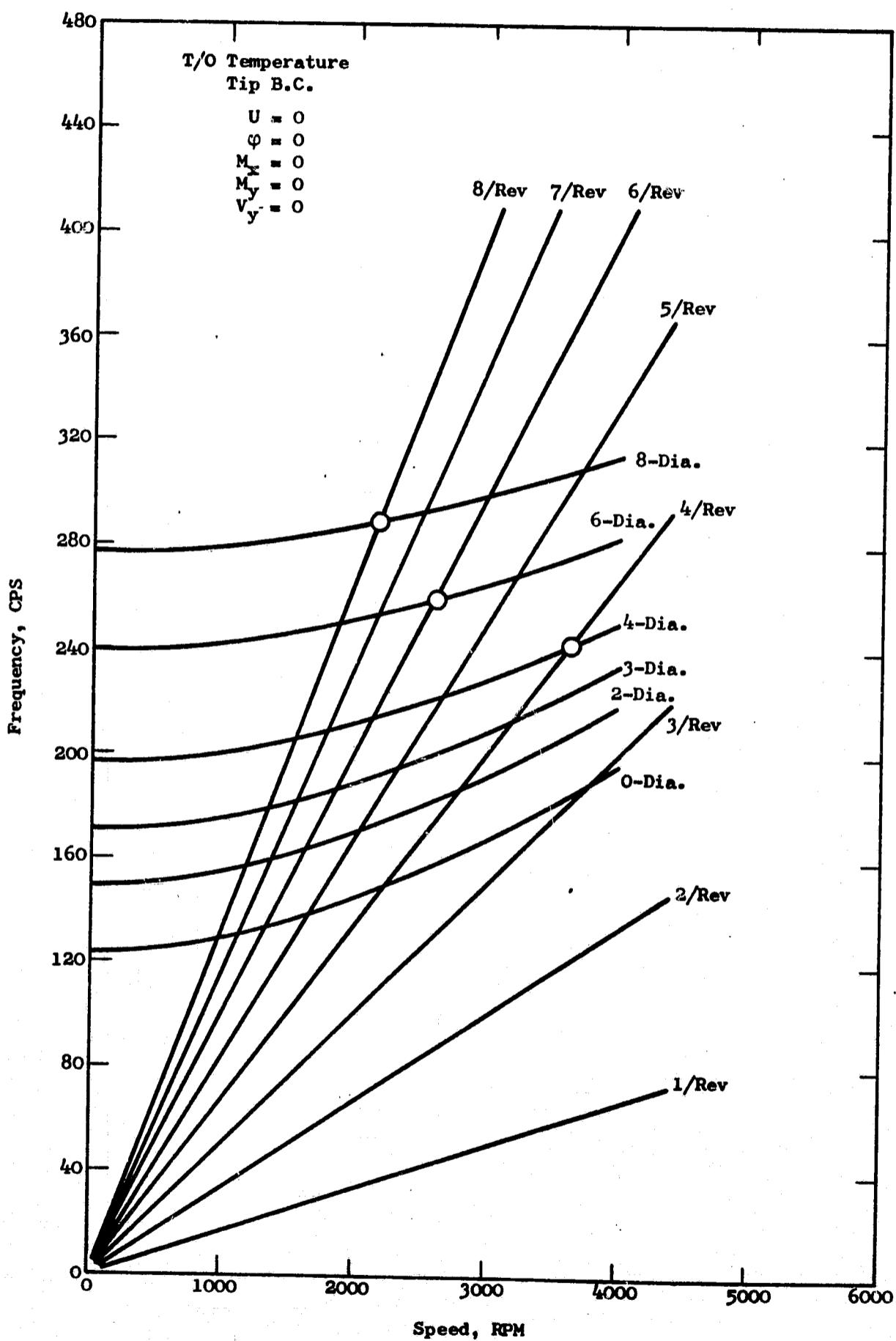


Figure 241. Fans A/B LP Turbine, Stage 3 Campbell Diagram

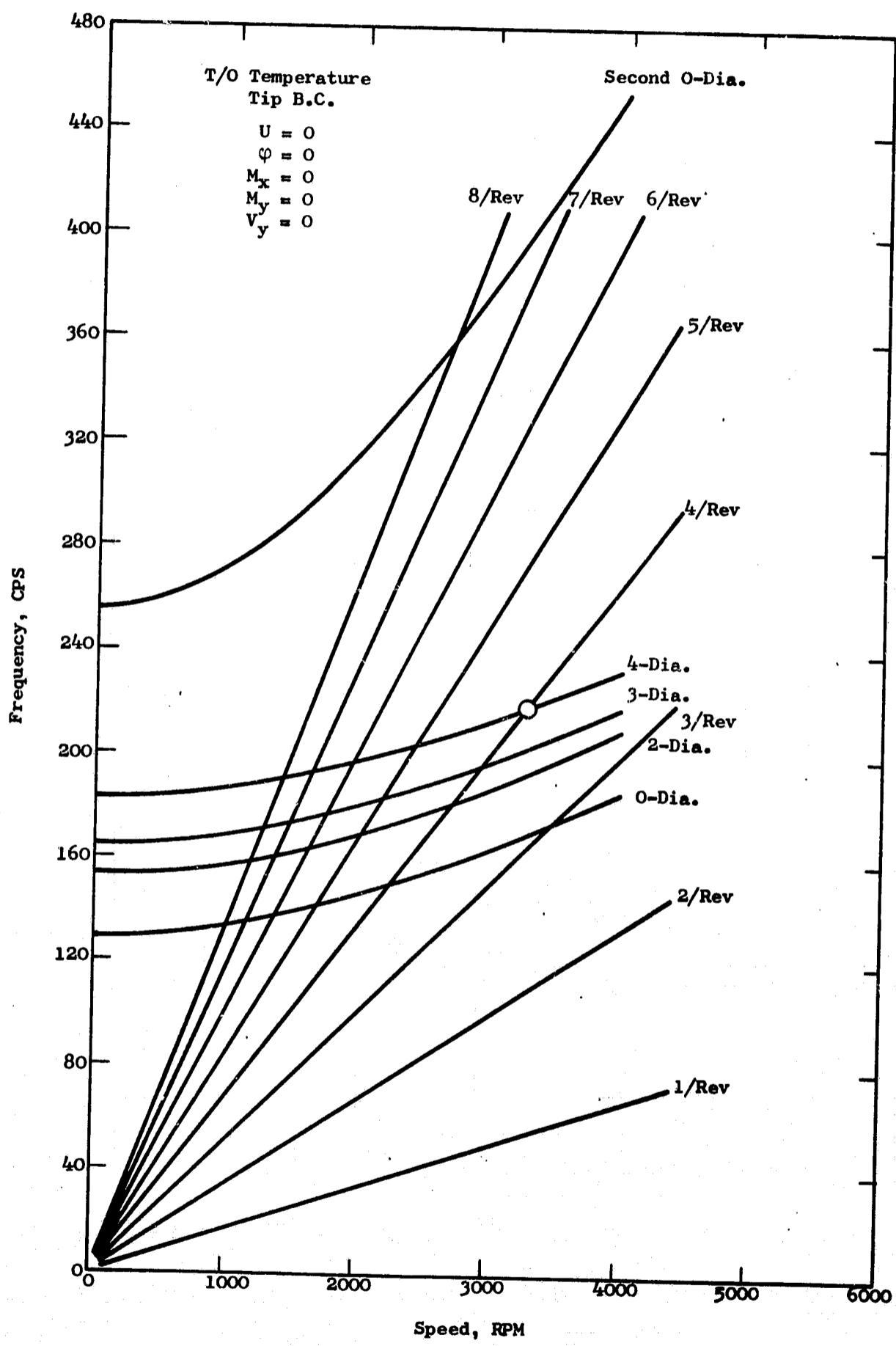


Figure 242. Fans A/B IP Turbine, Stage 4 Campbell Diagram

414

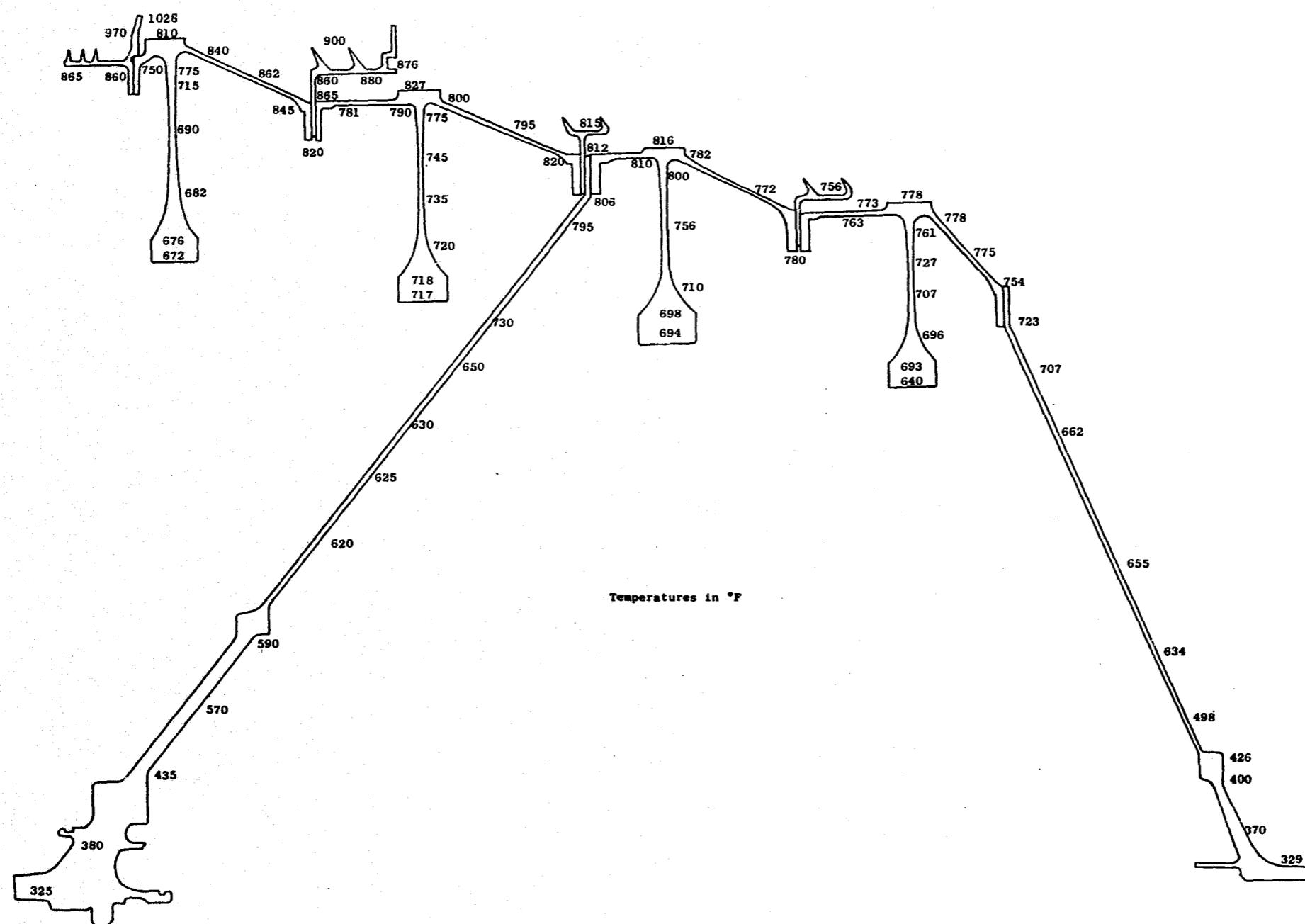


Figure 243. Fans A and B LP Turbine Rotor Steady State Temperatures

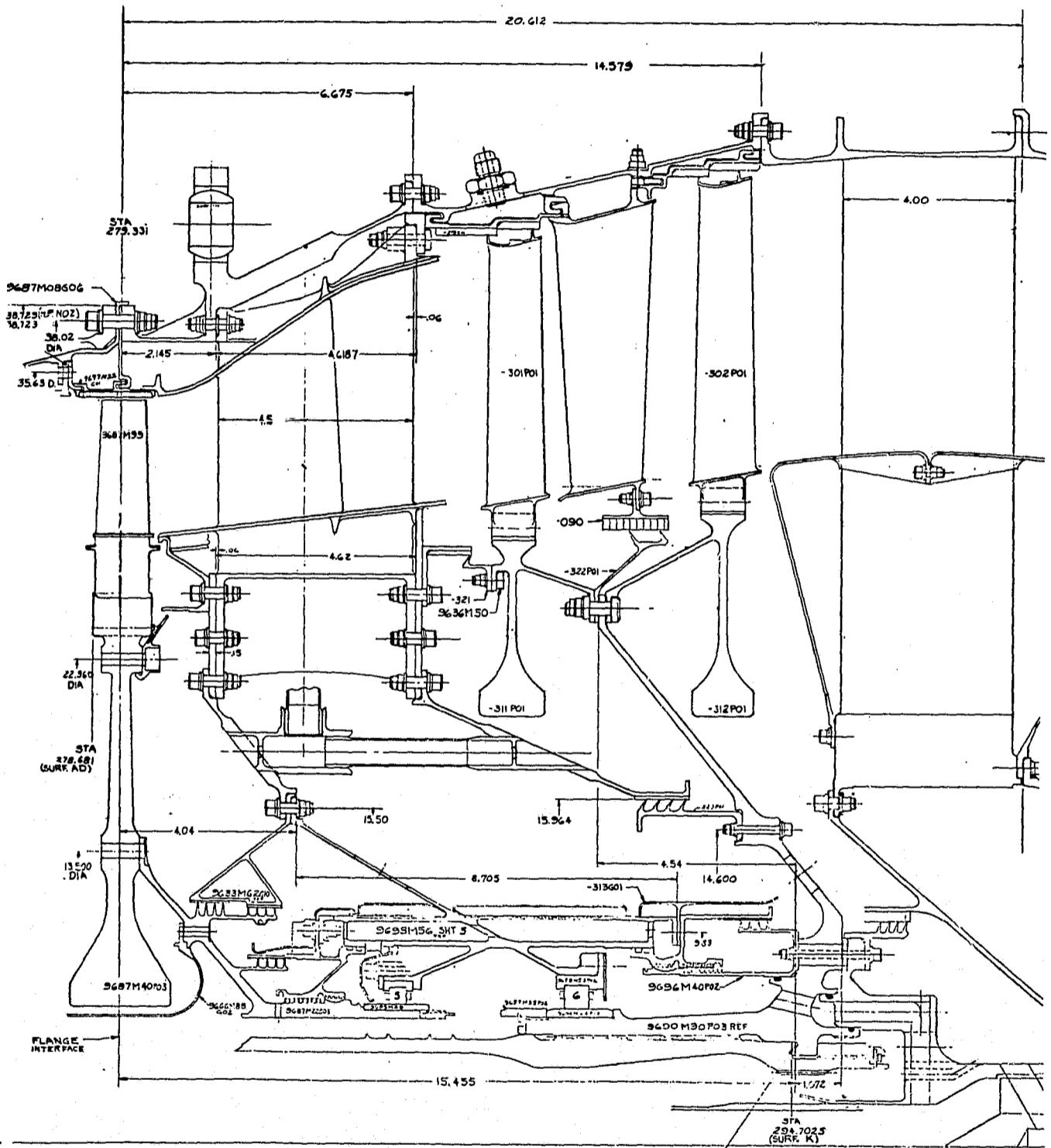


Figure 244. Fan C Low Pressure (LP) Turbine

7.1.1.2.1 Turbine Rotor

The LP turbine rotor for Fan C consists of two blade and disc assemblies, one shaft, and one interstage seal.

Each disc has a large bore and integral spacer arms with mating flanges on the ends.

The blades are attached to the discs by two-tang dovetails. The shank between the dovetail and blade has "skirts" to prevent leakage across the stage and to provide a smooth fore and aft face to eliminate windage losses. The blade also has relatively long shanks to isolate the dovetail from the hot gas stream.

All blades have integral tip shrouds which are interlocked by a "Z" form with their neighbors. This arrangement prevents high vibratory stress of the blading. The "Z" form is deep to prevent unlatching, and the mating surfaces are built up in size and hardfaced with chromium carbide to prevent wear. Each tip shroud also has two labyrinth seal teeth to oppose the stator shroud to minimize tip leakage.

The blades are retained in the disc by modified "dogbone" retainers (see Figure 192). The retainers are bent into place during assembly.

The shaft is conical to provide stiffness. The shaft is attached to the fan shaft by a differential, threaded coupling bolt and supports the turbine on the No. 6 bearing in the turbine midframe. The OD flange of this shaft sandwiches between the first and second stage disc flanges.

The interstage seal is a separate part which also is sandwiched between the disc spacer flanges. The seal consists of two slanted labyrinth seal teeth which are aluminum oxide hardfaced for wear resistance. The two-tooth seal is spaced such that the wear grooves in the stator seal will not overlap and cause high leakage. The slanted teeth are to reduce leakage.

The main flange bolting is done with 5/16-inch close-tolerance bolts, which assure rotor alignment and power transmission.

7.1.1.2.2 Turbine Cooling

The turbine cooling paths are shown in Figure 244 and include a small amount of coolant for both rotor and stator.

The rotor uses ninth-stage bleed flow from the piston balance seal to cool the rotor cavity. This coolant is a combination of seal leakage plus flow through holes in the side of the balance piston seal.

The first-stage stator seal opposes a single seal tooth projection on the first stage disc. This is a "leak positive" seal, sized such that it never closes, and is used to purge the rotor cavity.

Since much of this coolant (balance seal leakage and CDP recoup) would be mostly a loss whether or not it is used for cooling, the cost to the cycle is very small for cooling the low pressure turbine.

7.1.1.2.3 Turbine Rotor Materials

Materials used in the low pressure turbine are all commercially available alloys with good records of successful use. Each material was carefully selected, not only for strength, but for the best balance of life, weight, cost, and resistance to environmental deterioration.

Because of the material selection and the relatively mild environmental conditions, it was not found necessary to protective coat the airfoils to resist corrosive/erosive effects. The only protective coatings of any kind used on the turbine are for wear resistance. These are chromium carbide on the blade tip shroud interlock mating faces and aluminum oxide on the rotor interstage seal teeth.

The material list that follows (see Table LXIV) tabulates the materials used in the LP turbine parts. Each material is designated by its common name plus the AMS or General Electric Specification number which is used to control its use.

7.1.1.2.4 Design Analysis

This section presents the details of the stress and temperature analysis of the low pressure turbine components. Included in this section are the following:

- Blades
- Discs
- Blade Retainers
- Shaft
- Seals
- Disc-Blade Vibration
- Temperature Distribution

The rotor, because of its low tip speed and low temperature environment, is not creep or rupture limited.

Table LXIV. Fan C Rotor Material List

Part	Qty	Material	
		Name	Spec. No.
Discs - All Stages	2	IN 718	C50TF6
Blades - All Stages	248	R77*	C50TF15 Cl B
Shaft	1	IN 718	C50TF6
Interstage Seal	1	IN 718**	C50TF6 Cl B
Forward Seal, Stage 1	1	IN 718**	C50TF6 Cl B
Retainers, Blade	248	IN 718	B50TF14 Cl A
Flange Bolts	172	IN 718	C50T82
Nuts	172	Waspalloy	AMS 5709

* Tip shroud interlock contact surface plasma-sprayed with chromium carbide per General Electric Specification P50T30D.

** Seal teeth plasma-sprayed with aluminum oxide per General Electric Specification P16TF3 Cl B with B50TF58 Cl A material.

- Blade Design

The LP turbine blades (see Figure 196 for typical blade) all have tip shrouds and two-tang dovetails. Blade shanks were made short because of the low gas stream temperature and to provide a balanced dovetail design between blade and disc. In addition, all stages have shank "skirts" to prevent leakage across the stage and to provide a smooth wheel face for low windage losses.

The tip shroud is of special importance to such high-aspect-ratio (length over chord) blading to prevent high vibratory stress. This is a "Z" form, with the middle leg of the "Z" being the contact surface between adjacent blades while the other legs form clearance for thermal closure during transients. The contact surfaces are enlarged radially and hardfaced for wear resistance with plasma-sprayed chromium carbide. This interlock was chosen because of the reliability of the design as proven by the engine experience of the TF39 and CF6. The 75° angle of the interlock from the engine axis provides good frictional damping in the first flexural mode.

Finally, there are two labyrinth seal teeth on each tip shroud for leakage control across the stage. The pitch between these teeth is such that the wear tracks in the opposing stator shroud will not overlap to cause excessive leakage.

- Steady State Stress

Turbine blade steady state stresses are determined by a Twisted Blade Analysis Computer Program. The procedure for calculating stresses consists of a computer input of the necessary airfoil section properties such as area, moments-of-inertia, elastic modulus, torsional stiffness and blade tip loads, rotational speed, and offset. The computer then calculates stresses at 4 points on a given airfoil section: (1) the leading edge, (2) the trailing edge, and the concave (3) and convex (4) maximum thickness points. Steady state stresses are a combination of centrifugal, bending, induced tensile, and shear stresses. These stresses are then combined to give an effective stress at each of the previously mentioned points.

Of importance to the computer program is the condition of end restraint. The blade is assumed built in at the tip of the dovetail. At the tip shroud, twist, and moments and shears (both axially and tangentially) are set at zero.

The resulting steady state stress levels at the leading edge, trailing edge, and concave and convex maximum thickness points are plotted in Figures 245 and 246. The engine condition in each plot is at a rotor speed of 4605 rpm.

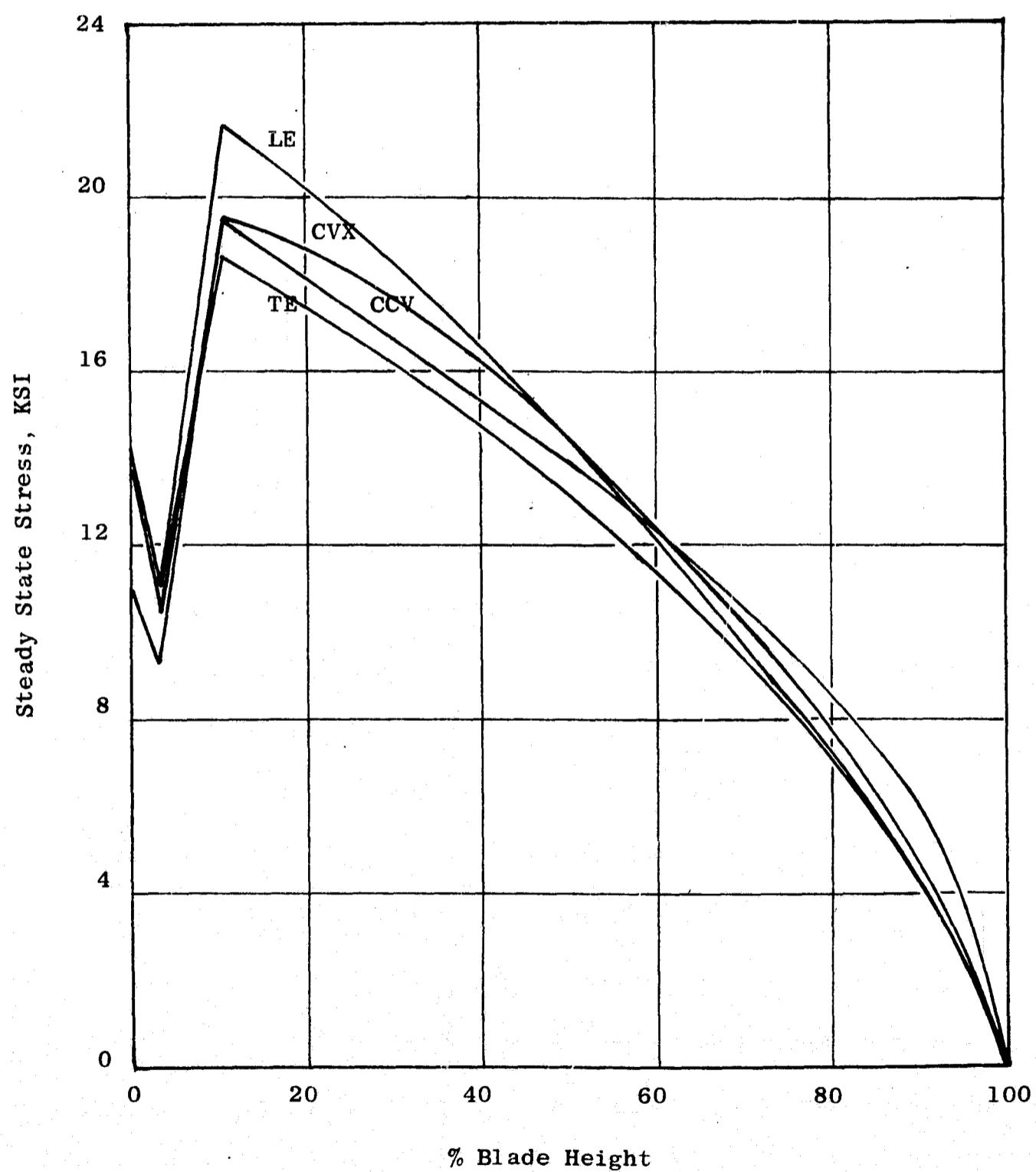


Figure 245. Fan C LP Turbine Stage 1 Blade, Steady State Stress

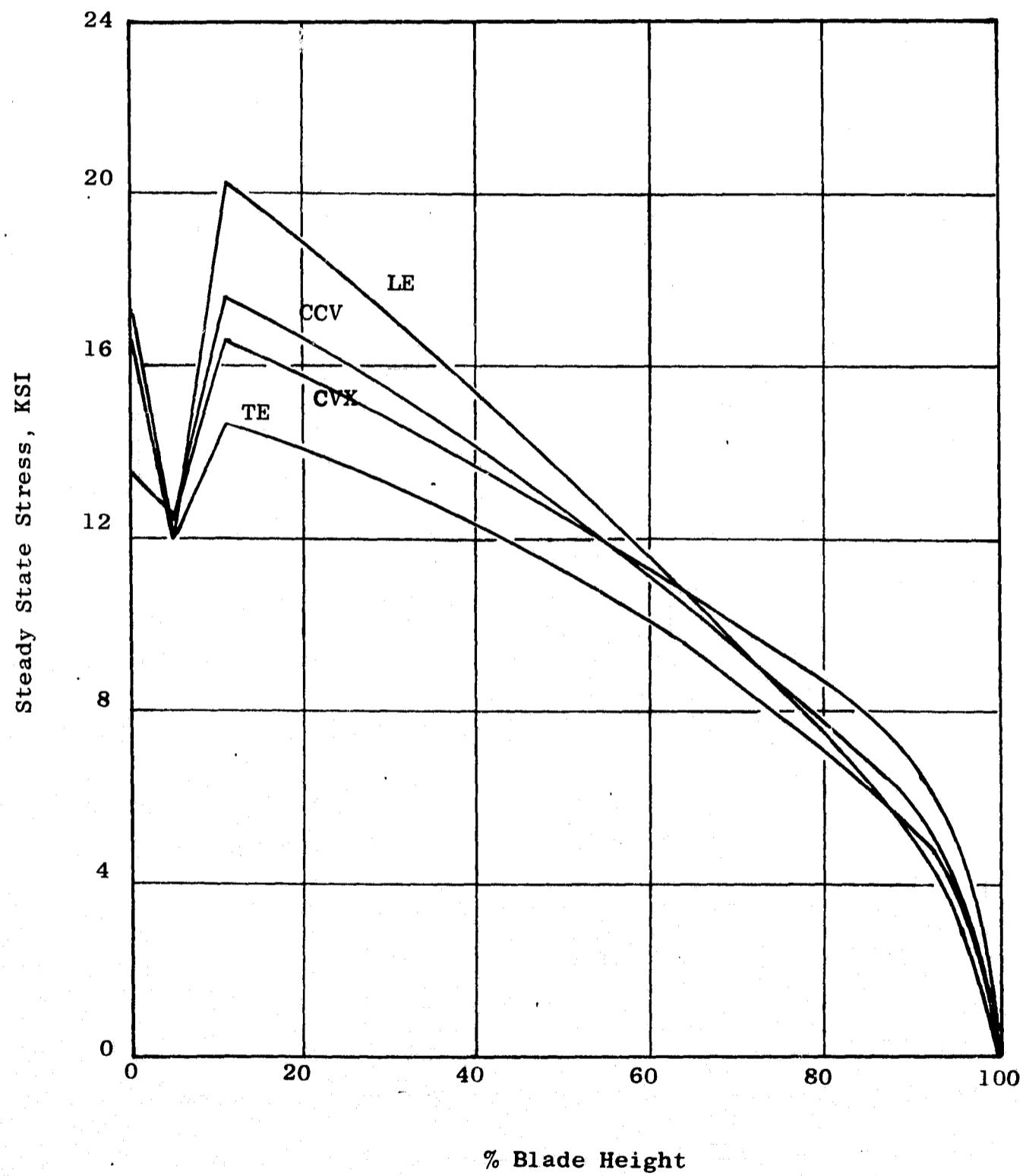


Figure 246. Fan C LP Turbine Stage 2 Blade, Steady State Stress

- Vibratory Stress and Frequency

Blade natural frequencies and vibratory stress distribution are also calculated with the Twisted Blade Analysis Computer Program. The program calculates the resonant frequencies by determining at what frequency the reciprocal of blade deflection or moment reaches zero.

The calculation of the blade natural frequencies was carried out by the Twisted Blade Program for two blade/tip boundary conditions. These tip-restraint conditions greatly affect the resonant frequencies of the blade. The first frequency search was done for the in-phase tip condition, for which all axial and tangential deflections and rotations are permitted holding the rotation about a radial line to zero. The in-phase vibration modes are quite similar to a free-tip cantilever condition, yielding the lowest possible blade frequencies. The second frequency search was done for the out-of-phase tip condition. Here the blade tip is restricted from movement in the tangential direction while maintaining no rotation about a radial line. The out-of-phase vibration modes are best correlated with engine data for shrouded turbines and are, therefore, considered the prime frequencies.

The result of this calculation is twofold:

1. Campbell diagrams (Figures 247 and 248) are plotted to show the relationship of natural frequency and rotor speed. Frequency of resonance varies with speed (centrifugal stiffening) and temperature (spring effect as determined by Young's Modulus) in the following manner:

$$f = \left[f_0 + \beta \omega^2 \right] \sqrt{\frac{E}{E_0}}$$

where:

f is frequency

β is a configuration constant

ω is speed

E is Young's Modulus

Subscript $_0$ is base or room

Each Campbell diagram has "per rev" lines illustrating various possible excitation stimuli which could exist to cause resonant vibration at the engine speed where the natural frequency intersects with these lines. The low-order excitation lines can exist in any engine, while the higher-order lines indicate passing frequencies of such things as fuel nozzles or vanes. Such diagrams are used to avoid potentially dangerous interferences in the initial design and to identify modes of vibration during engine test.

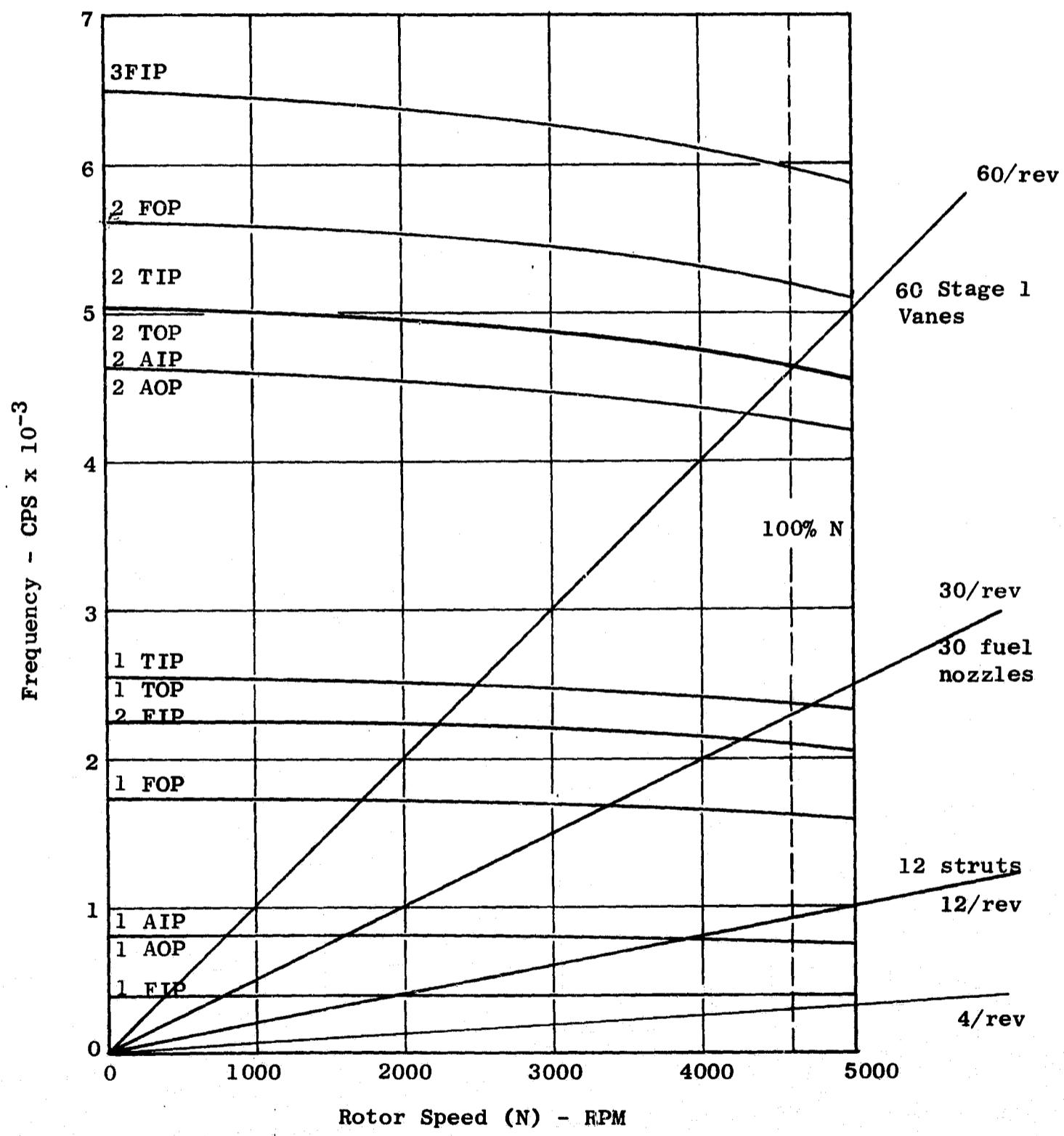


Figure 247. Fan C LP Turbine, Stage 1 Campbell Diagram

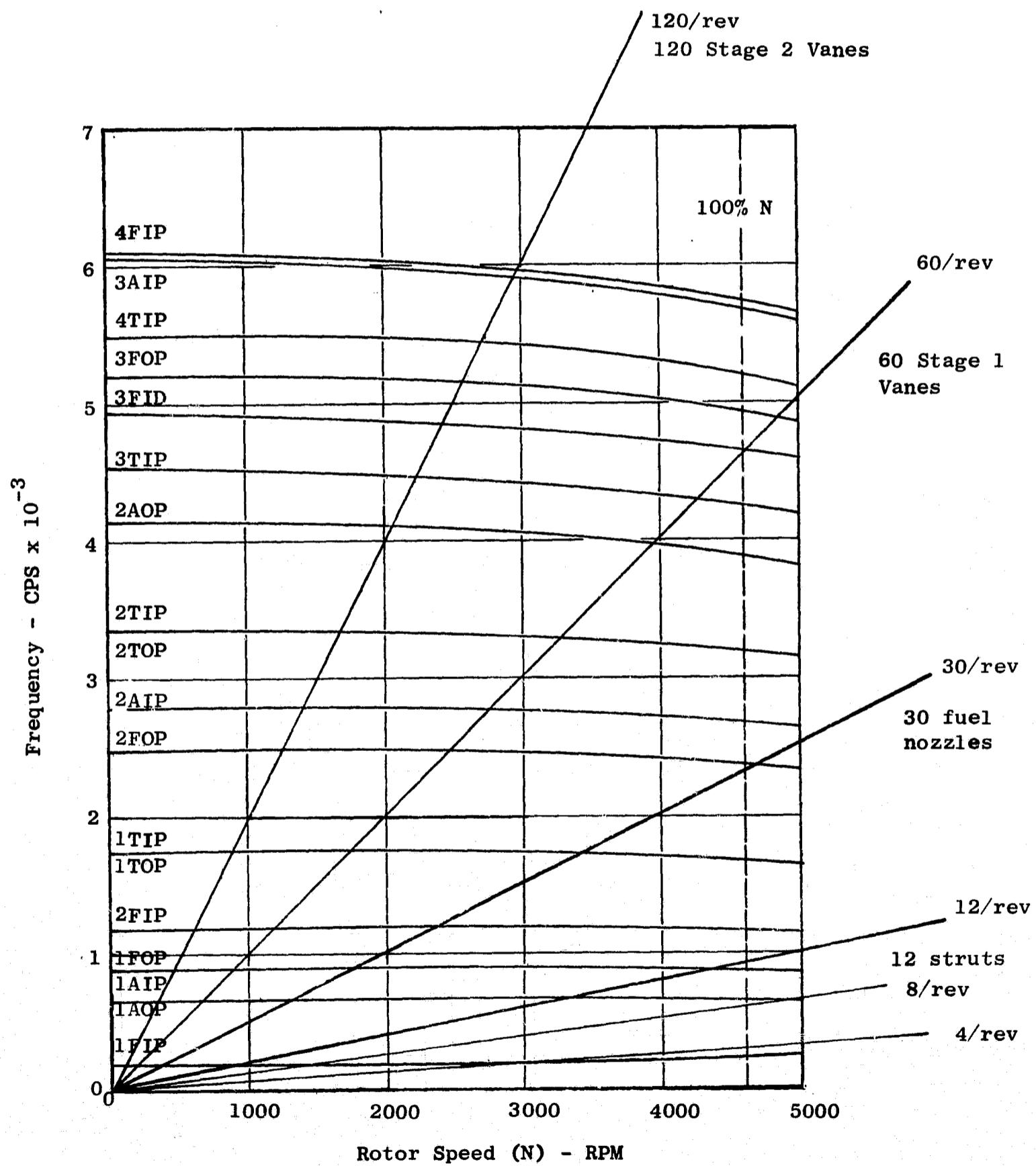


Figure 248. Fan C LP Turbine, Stage 2 Campbell Diagram

2. Stress distribution charts are also produced from the computer analysis. By this means, the maximum stress in the airfoil can be identified in relation to any other point in the airfoil. These plots are used during engine stress surveys, where one or two strain gages are applied, to convert the gage reading to maximum stress.

The stress distribution charts for both stages are shown in Figures 249 through 258 for the more important modes of first flexural (in-phase) and restrained modes of first flexural, first axial, first torsional, and second flexural.

- Dovetails

Both stages use two-tang dovetails which are scaled from a common design. For convenience and cost reasons, the same size dovetail is used for Stages 1 and 2. The two-tang design was chosen because of the good experience available with this dovetail on the TF39 and CF6 engines.

The dovetails are analyzed using the RB Heywood method, which involves the use of geometric construction of the plane of bending in the fillet sections and is based on photoelastic studies of plastic models.

Steady state forces acting on the dovetail include centrifugal force, shear due to gas load, bending due to gas load, and blade offset and tilt. (see Figure 224). Tables LXV and LXVI tabulate the important steady state stress levels in each stage. All stress levels are at a rotor speed of 4605 rpm. As noted in the tables on the figures, results are given at six points on the dovetail tangs. These points are located on the four extreme corners (Points 1-4) and halfway between the corners (Points 5-6).

Vibratory stress distributions in the dovetails are shown on the blade stress distribution charts of Figures 249 through 258. These are determined by imposing moments and shear forces taken from the blade analysis on the dovetail and analyzing the dovetail by the previously mentioned Heywood analysis. Results of the vibratory analysis on the dovetail are presented as an alternating stress ratio (relative to a chosen point on the airfoil surface) which, in this case, was the airfoil root leading edge. Vibratory stress results are given for the first flexural in-phase mode in Figures 259 and 260. The four maximum combinations of steady state stress and alternating stress ratio for each stage are shown relative to the airfoil root stress.

It will be noted that, in general, the vibratory stress in the dovetail is higher than in the airfoil. This is caused by the low force levels created by the low tip speed and the large airfoils required for aerodynamic performance. The dovetails, which already have very low stress levels by aircraft standards, would have to be made abnormally large to reverse this situation. This would serve no useful purpose, since the vibratory levels

Table LXV. Fan C LP Turbine Rotor Stage 1 Blade Dovetail Stress Analysis (4605 RPM)

Point	σ_c	σ_{mx}	σ_{my}	σ_{neck}	σ_{tang}	σ_{total}
<u>Upper Tang</u>						
1	15800	+212	-1230	14780	15200	28357
2	15800	+212	+1230	17240	15600	31355
3	15800	-212	+1230	16818	15700	30972
4	15800	-212	-1230	14350	14500	27326
5	15800	0	+1230	17030	15300	30851
6	15800	0	-1230	14570	14700	27650
<u>Lower Tang</u>						
1	13700	+175	-1120	12755	28300	35253
2	13700	+175	+1120	14995	27700	37748
3	13700	-175	+1120	14645	27100	36948
4	13700	-175	-1120	12405	27100	34017
5	13700	0	+1120	14820	27800	37618
6	13700	0	-1120	12580	26900	34125

Table LXVI. Fan C LP Turbine Rotor Stage 2 Blade Dovetail Stress Analysis (4605 RPM)

Point	σ_c	σ_{mx}	σ_{my}	σ_{neck}	σ_{tang}	σ_{total}
<u>Upper Tang</u>						
1	12450	+69	-1460	11059	11400	21239
2	12450	+69	+1460	13970	12800	25538
3	12450	-69	+1460	13800	12650	25234
4	12450	-69	-1460	10921	11200	20927
5	12450	0	+1460	13910	12750	25432
6	12450	0	-1460	10990	11300	21083
<u>Lower Tang</u>						
1	10800	+413	-2560	8280	14200	20120
2	10800	+413	+2560	13400	16000	27450
3	10800	-413	+2560	13320	16000	27360
4	10800	-413	-2560	8200	14200	20020
5	10800	0	+2560	13360	16000	27405
6	10800	0	-2560	8240	14100	20001

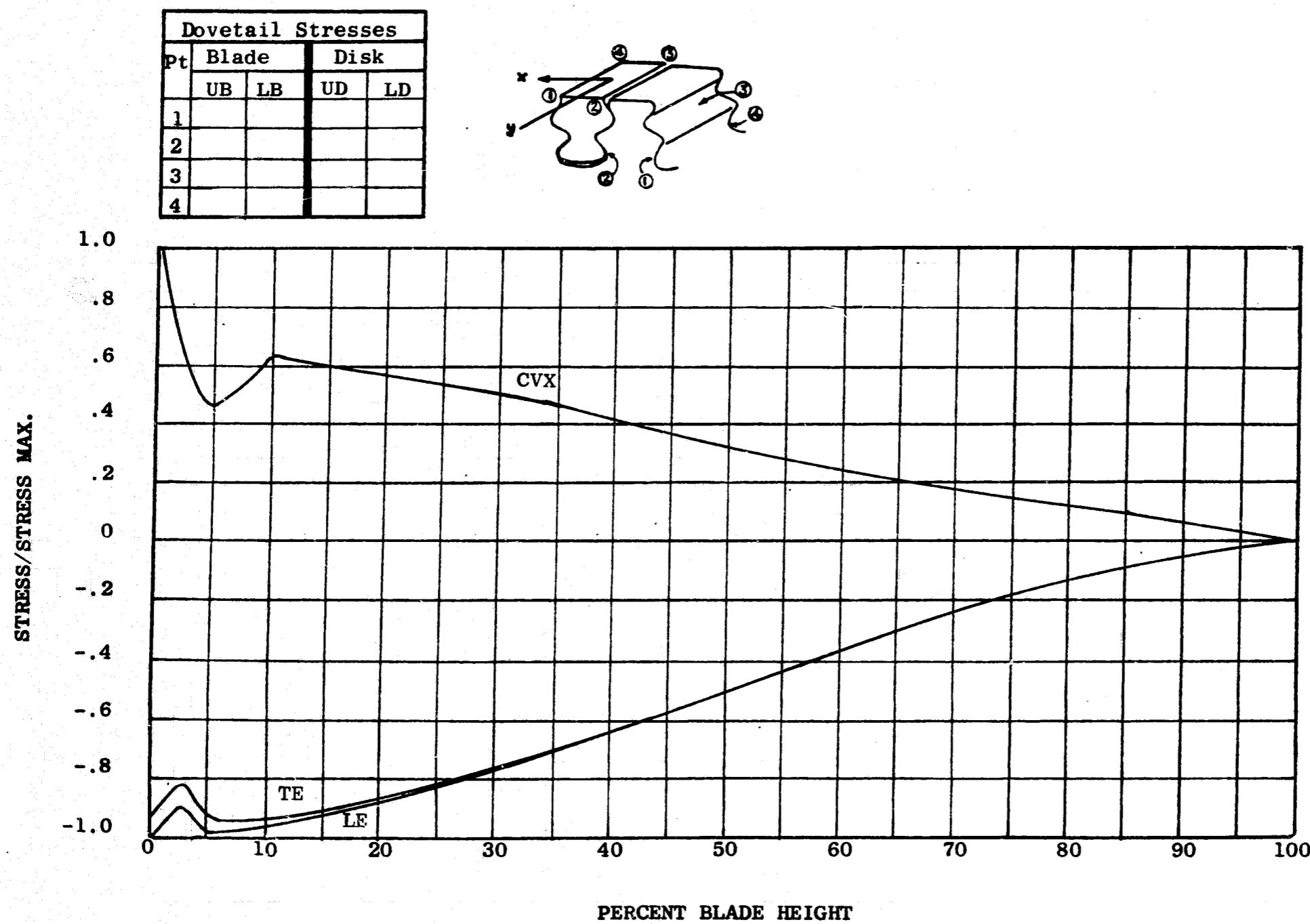


Figure 249. Stress Distribution for the Fan C Stage 1 Turbine, 378 CPS, 1st Flexural, In-Phase

429

Dovetail Stresses				
Pt	Blade		Disk	
	UB	LB	UD	LD
1				
2				
3				
4				

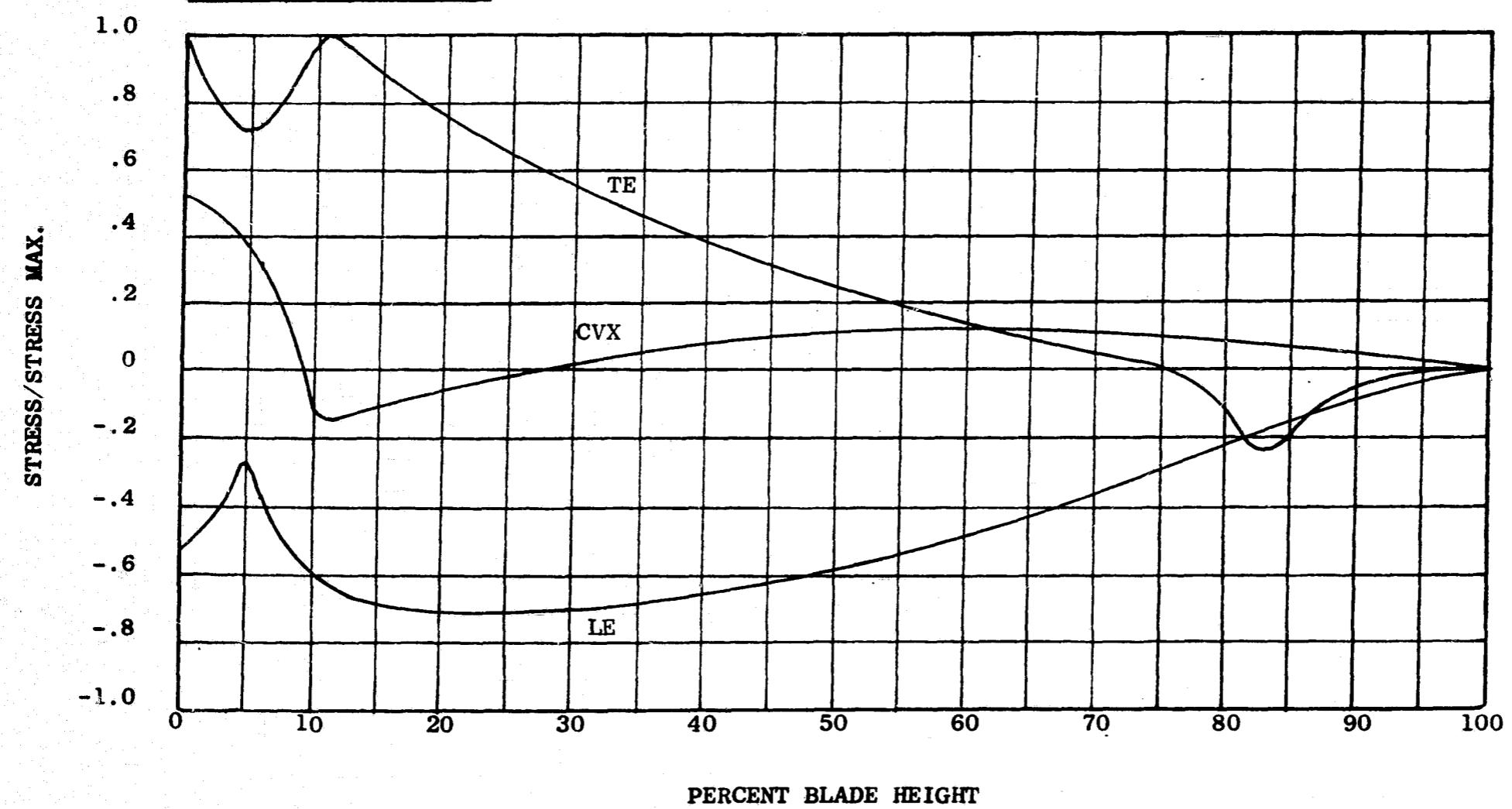
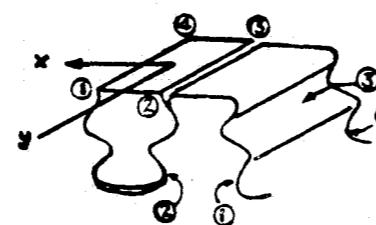


Figure 250. Stress Distribution for the Fan C Stage 1 Turbine, 748 CPS, 1st Axial, In-Phase

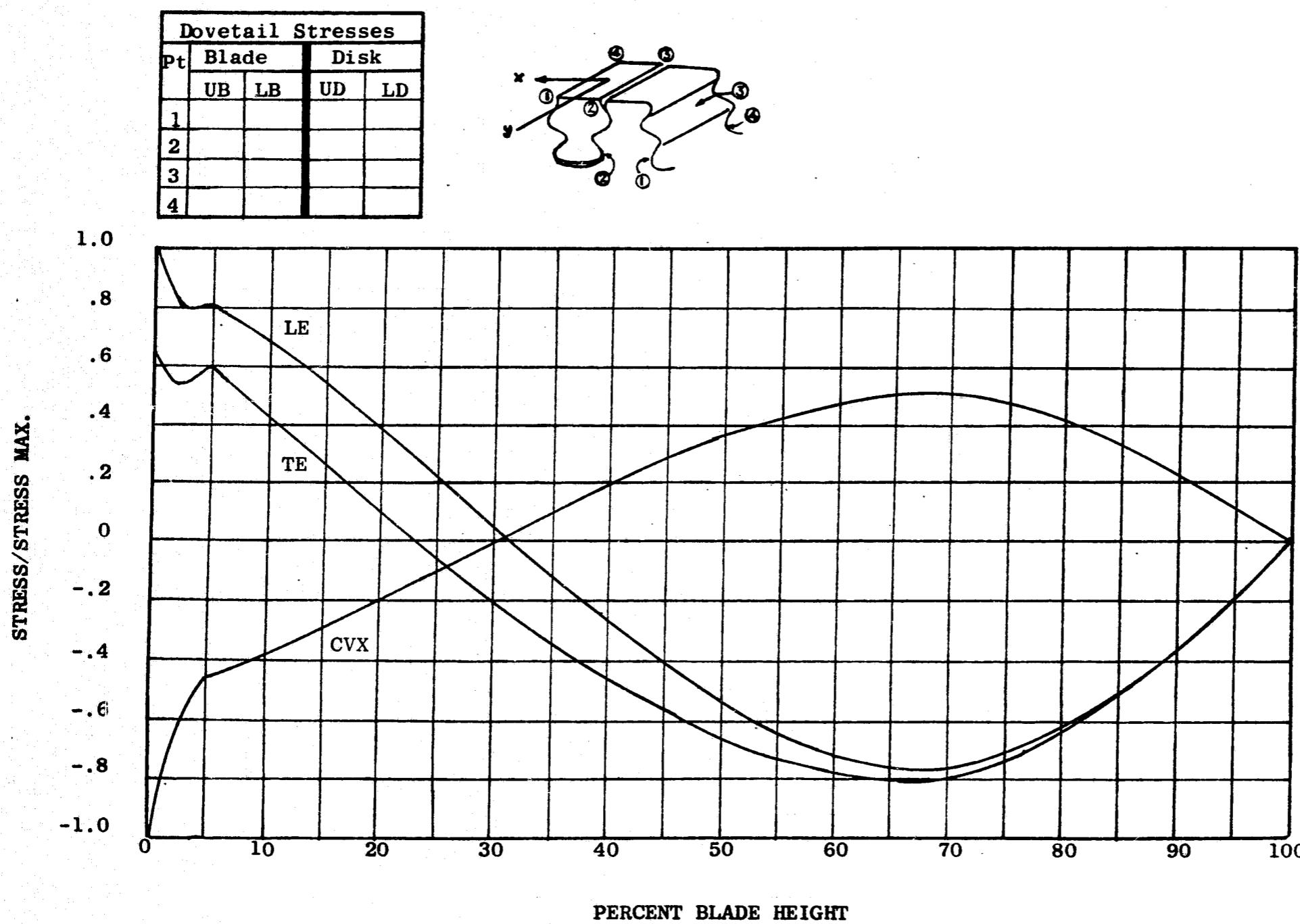


Figure 251. Stress Distribution for the Fan C Stage 1 Turbine, 1601 CPS, 1st Flexural, Out-of-Phase

431

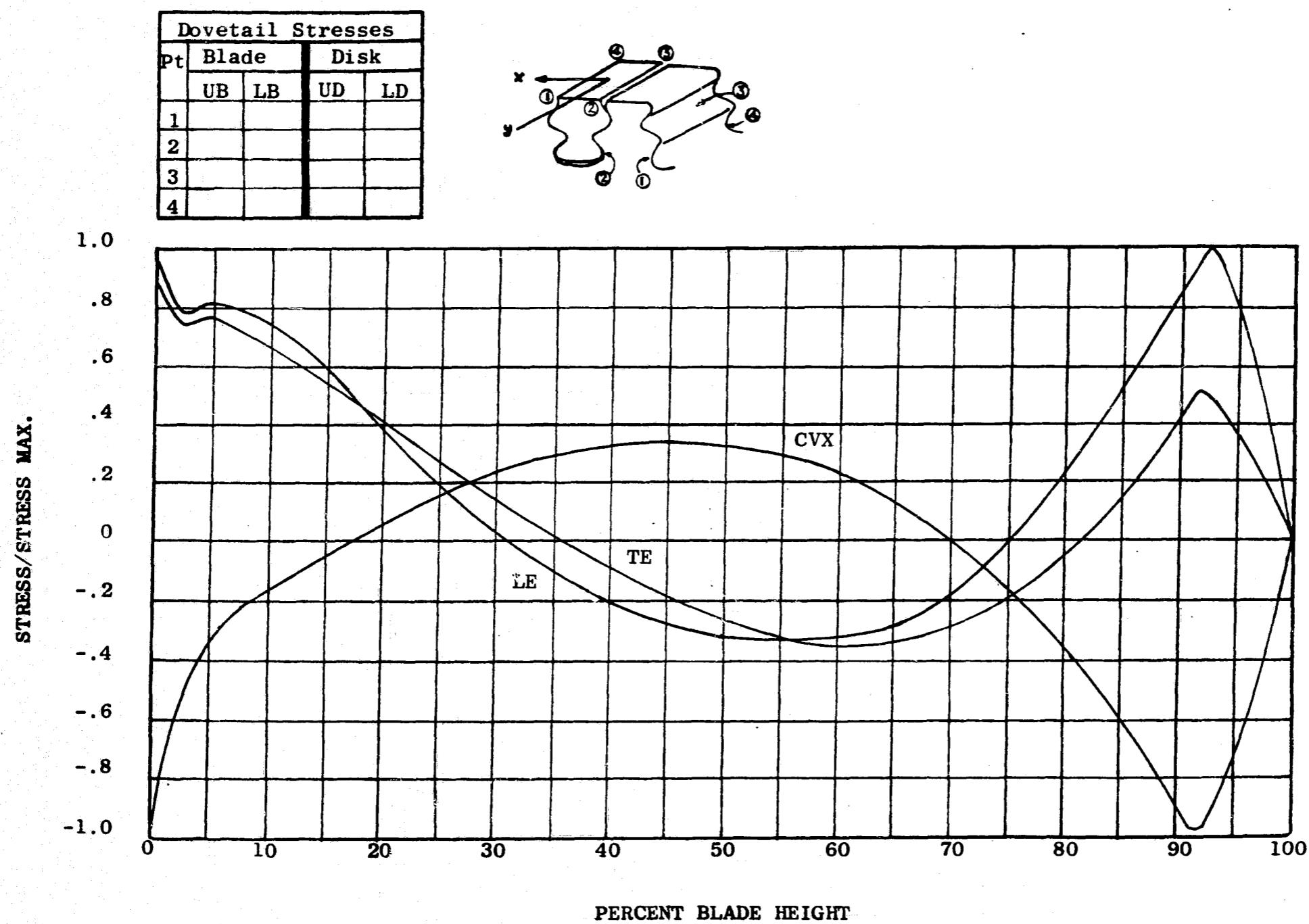


Figure 252. Stress Distribution for the Fan C Stage 1 Turbine, 2351 CPS, 1st Torsional, Out-of-Phase

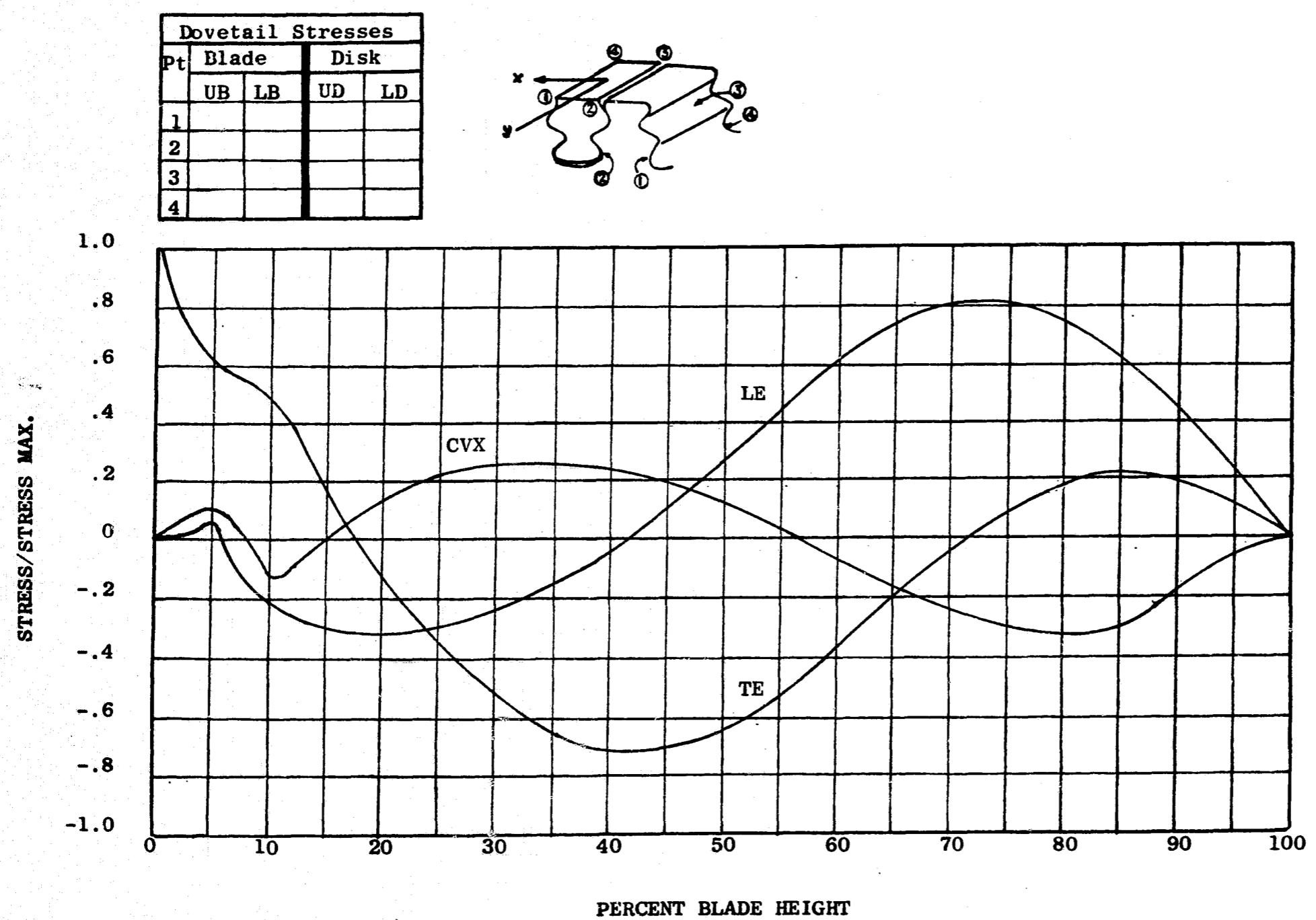


Figure 253. Stress Distribution for the Fan C Stage 1 Turbine, 4241 CPS, 2nd Flexural, Out-of-Phase

433

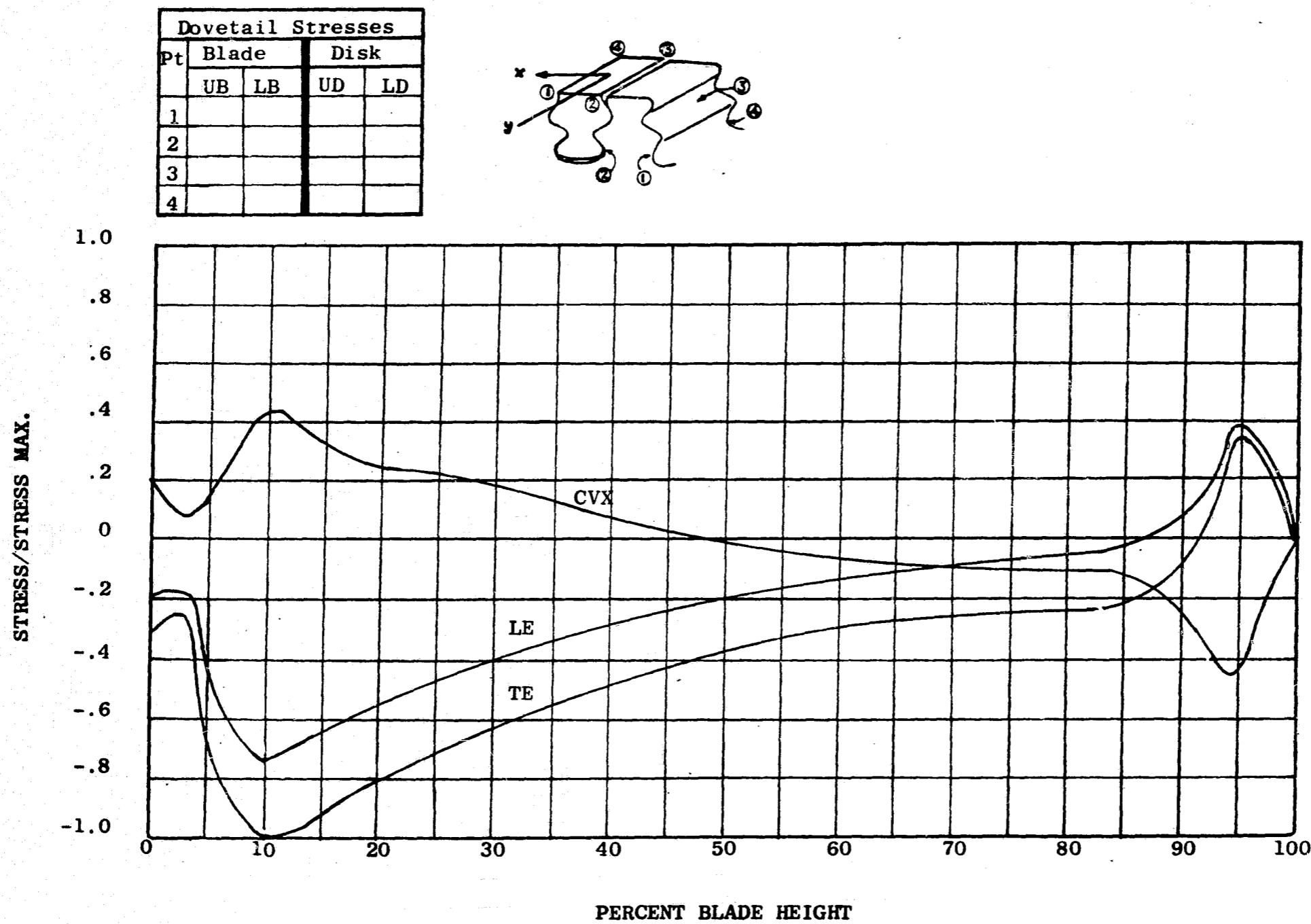


Figure 254. Stress Distribution for the Fan C Stage 2 Turbine, 234 CPS, 1st Flexural, In-Phase

1 2 3 4 5 6 7 8 9 10 11 12 13 14 15 16 17 18 19 20 21 22 23 24 25 26 27 28 29 30 31 32 33 34 35 36 37 38 39 40 41 42 43 44 45 46 47 48 49 50 51 52 53 54 55 56 57 58 59 50 51 52 53 54 55 56 57 58 59 60 61 62 63 64 65 66 67 68 69 60 61 62 63 64 65 66 67 68 69

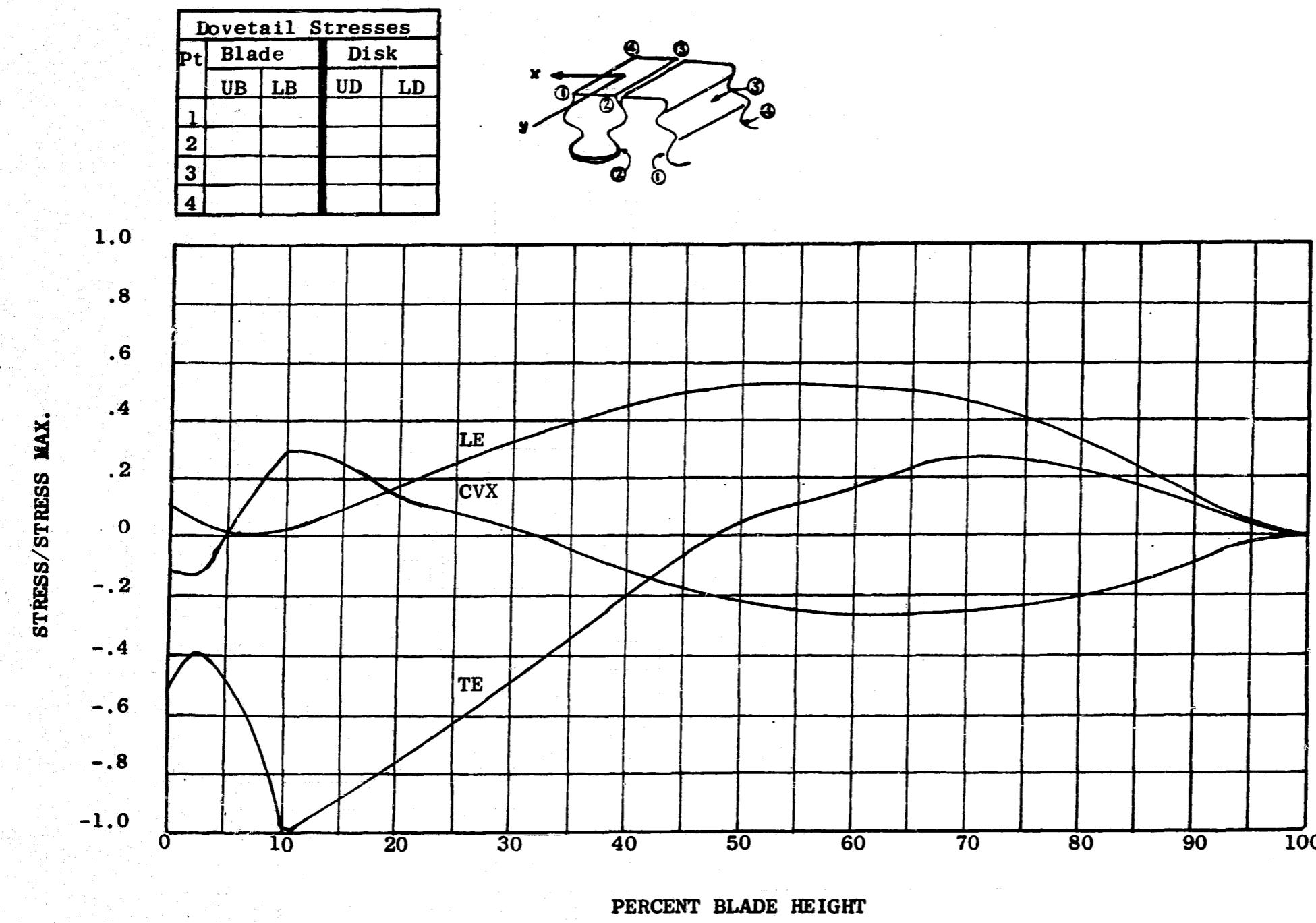


Figure 255. Stress Distribution for the Fan C Stage 2 Turbine, 642 CPS, 1st Axial, In-Phase

435

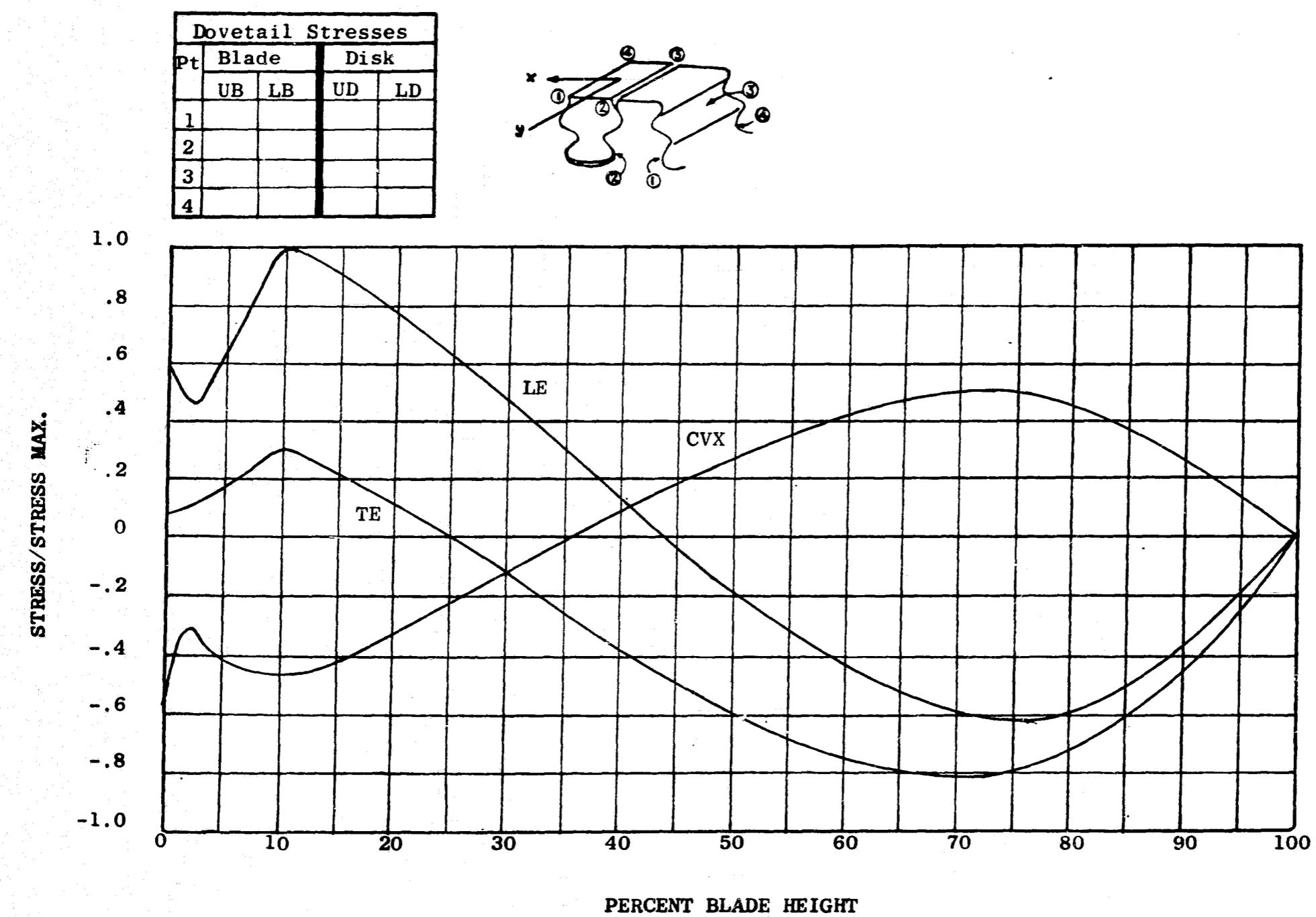


Figure 256. Stress Distribution for the Fan C Stage 2 Turbine, 868 CPS, 1st Flexural, Out-of-Phase

436

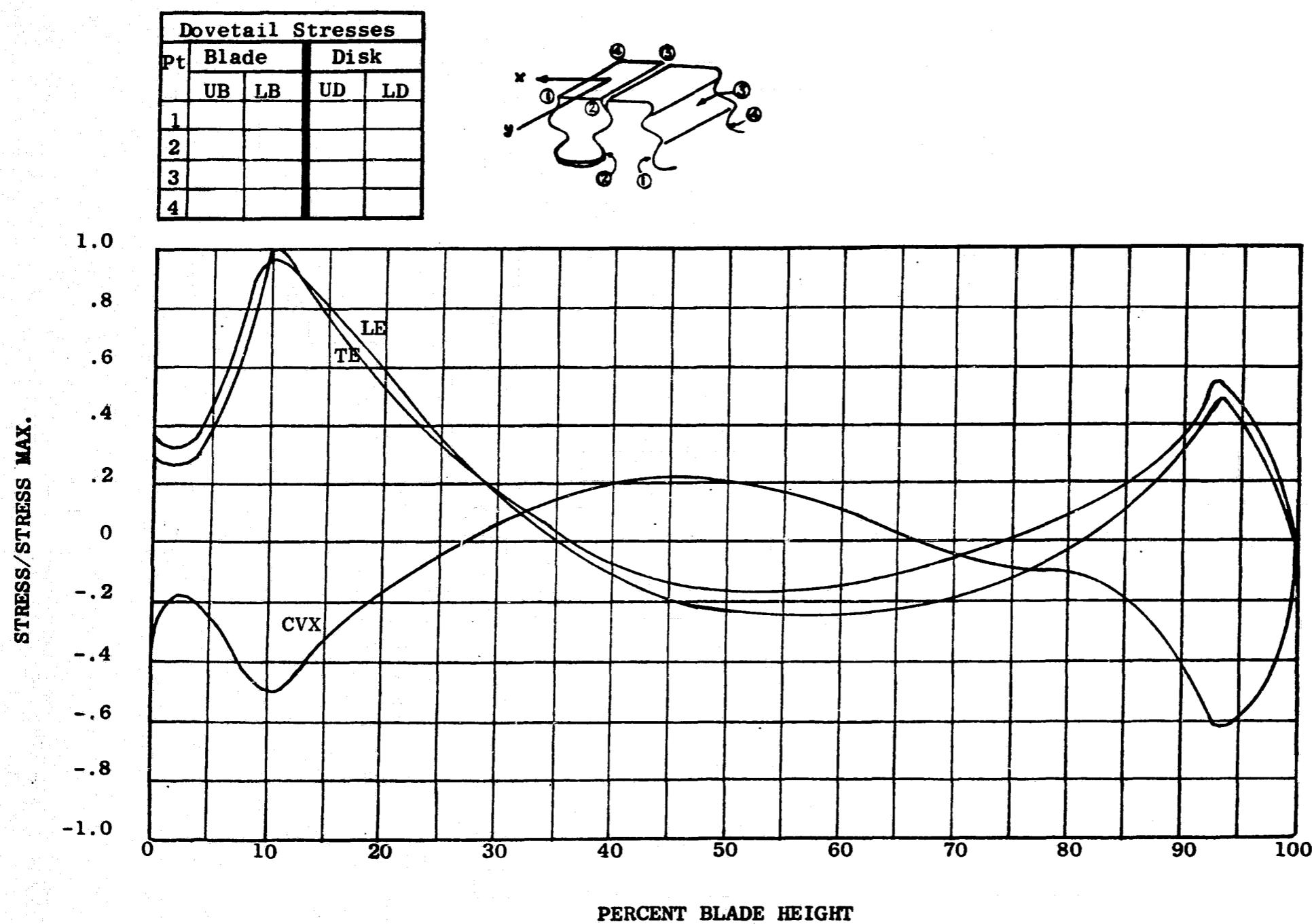


Figure 257. Stress Distribution for the Fan C Stage 2 Turbine, 1645 CPS, 1st Torsional, Out-of-Phase

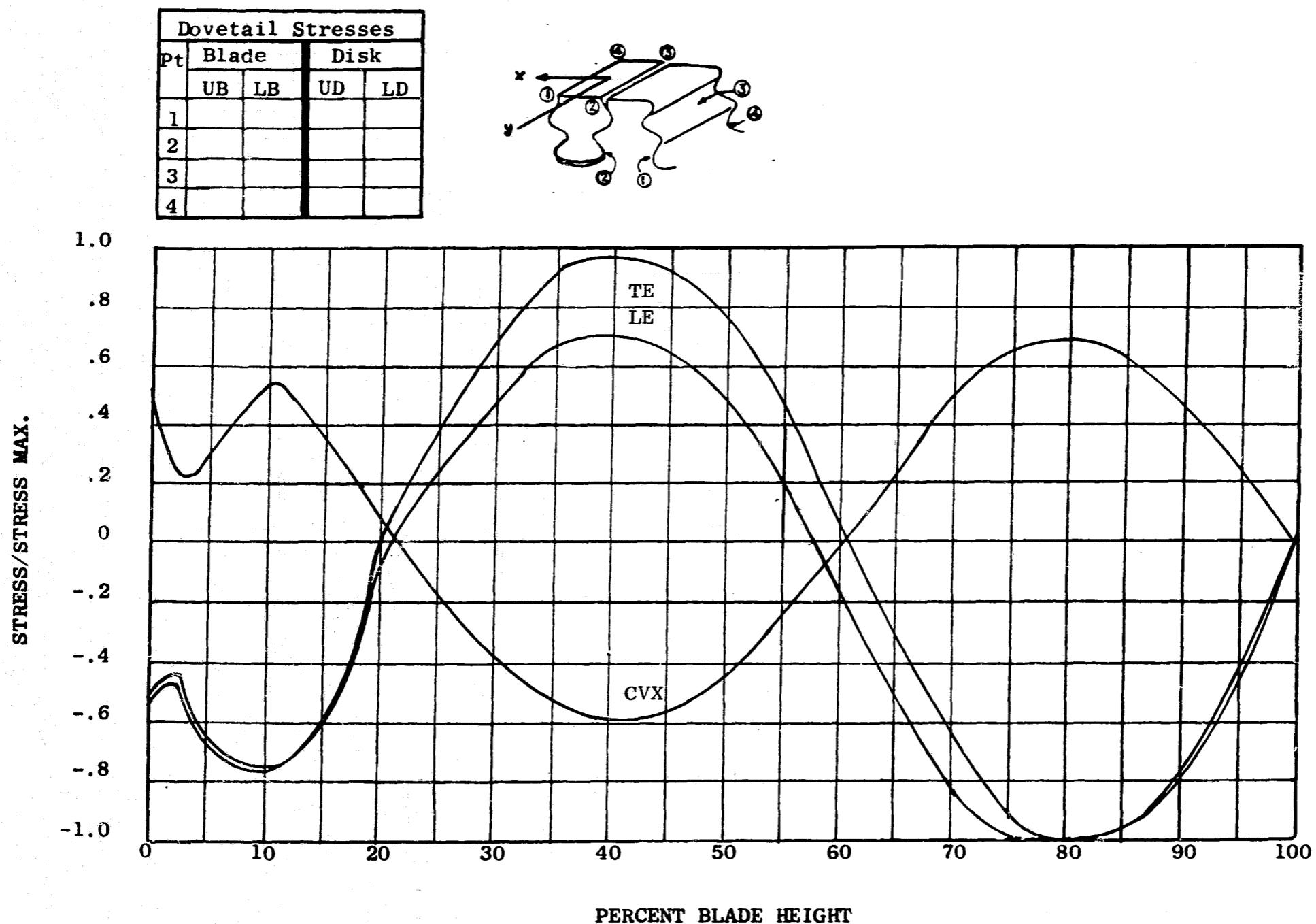


Figure 258. Stress Distribution for the Fan C Stage 2 Turbine, 2392 CPS, 2nd Flexural, Out-of-Phase

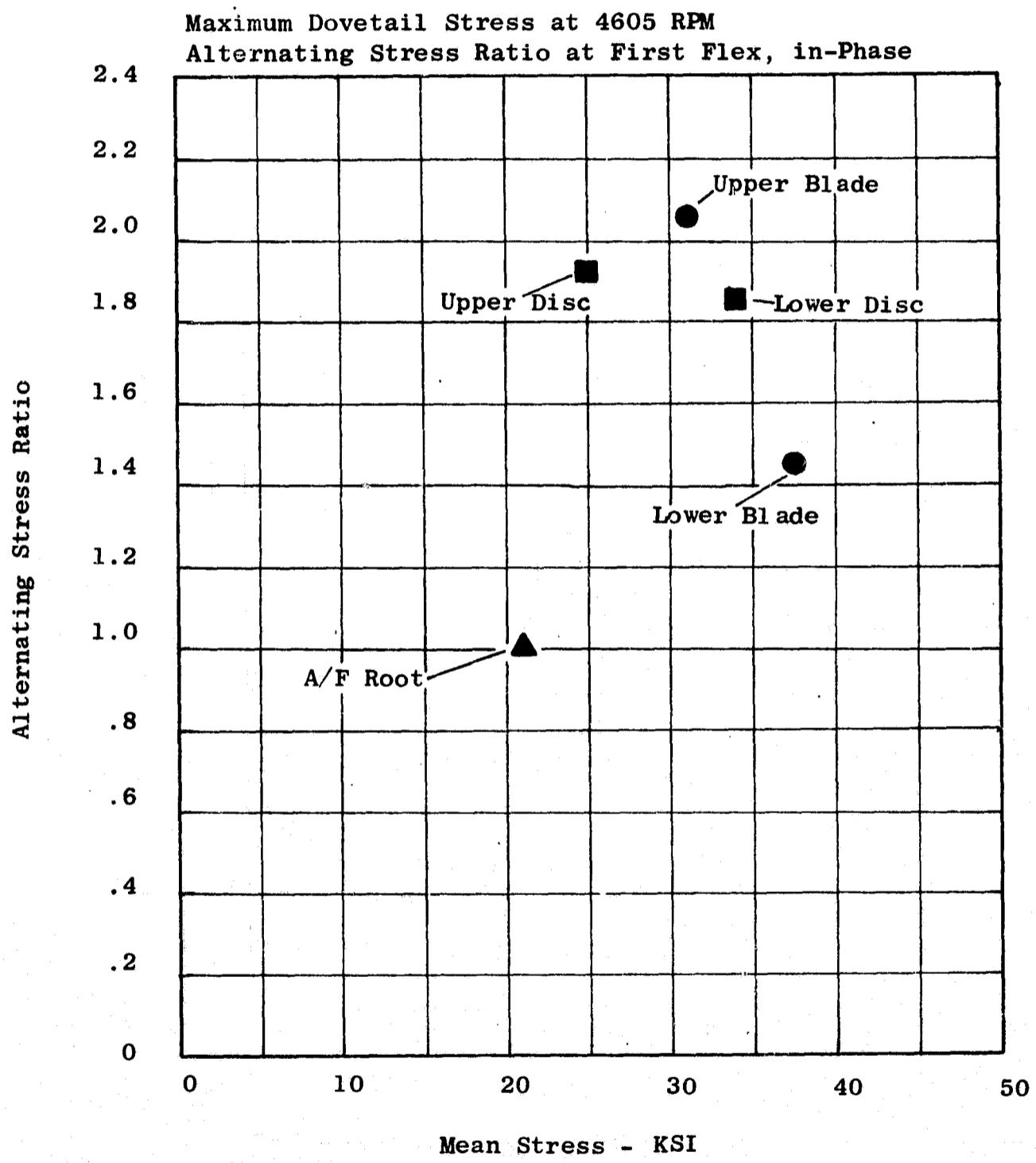


Figure 259. Fan C, LP Turbine Rotor, Dovetail Stress Analysis, Stage 1

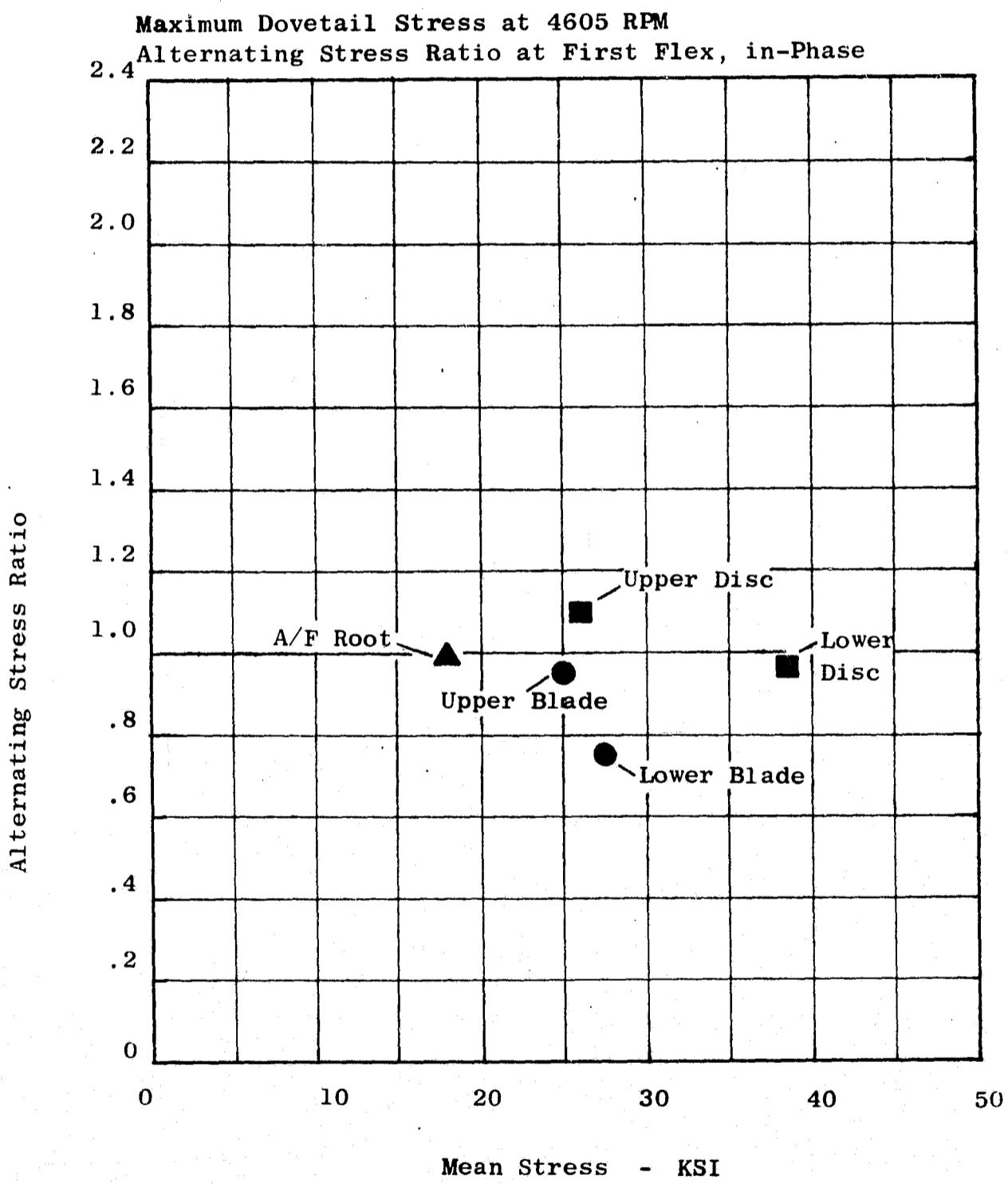


Figure 260. Fan C, LP Turbine Rotor, Dovetail Stress Analysis,
Stage 2

of the shrouded blades are so low that the dovetails are completely safe with the present design.

The procedure for analysis of the double-tang dovetail using the Single-Tang Dovetail Computer Program was the following:

Each component of stress on each tang (upper and lower) was analyzed separately. The assumptions made for the loads for each stress component were:

- a. The upper blade tang supports the entire load at its neck, and, therefore, 100 percent of all blade loads are used for the neck stress calculation. These loads are the centrifugal (F_c), the bending (M_x and M_y), torsion (M_z), and the shear (V_x and V_y).
- b. Assuming 50 percent of the F_c , M_x and M_y loads are taken out by the upper tang of the disc and that the M_y moment is distributed between upper and lower tangs according to the following relations:

$$M_y \text{ upper} = M_y \text{ total } (t^2 \text{ upper}) / (t^2 \text{ upper} + t^2 \text{ lower})$$

and

$$M_y \text{ lower} = M_y \text{ upper } (t^2 \text{ lower}) / (t^2 \text{ upper}),$$

the tang-bending stress calculation of the upper tang of both blade and disc can be made. Shear loads V_x and V_y are neglected.

- c. The lower blade neck stress calculation is made by using the remainder of the loads transmitted to the lower blade tang, which is 50 percent of F_c , M_x , and M_z , with M_y lower computed in Step b.
- d. The lower blade tang stress calculation uses the same loads as the neck stress in Step c, since the lower blade tang is identical to a single-tang dovetail.
- e. The upper disc neck stress is calculated using the same loads as used for the upper disc tang stress, since it is also identical to a single-tang dovetail.
- f. The lower disc neck stress takes on the entire blade load plus an increment of F_c from the dovetail weight itself.

g. The lower disc tang stress calculation used the loads obtained in Step c.

A modification to the tang-bending stress calculations was required on the upper blade tang and lower disc tang due to the geometry of these particular tangs. The tang functions, which are generated by the computer program and are used directly to obtain tang stress, are calculated based on a vertical plane through the Heywood point typical of single-tang dovetails. The error is introduced in the value of (j), the moment arm of the tang load.

The corrected tang functions were ratioed to the computer values, and the adjusted tang stresses were 2.27 times higher for the upper blade tang and 1.45 times higher for the lower disc tang. Neck stress and tang stress components on corresponding tangs were combined by the Heywood method which is:

$$\sigma_{\text{total}} = \sigma_{\text{neck}} + T \sigma_{\text{tang}}$$

where,

$$T = \frac{1}{1 + 0.1162 \frac{\sigma_{\text{neck}}}{\sigma_{\text{tang}}}}$$

- Discs

The LP turbine discs feature integral spacer arms and high bore diameters. By placing the bolted flanges at the extremities of the spacer arms, the stress concentration effects of holes are removed from the disc. The high bore diameter is used to maintain a high rim tangential stress to offset the thermal stress created by the rim being at a higher temperature than the bore. Both effects are especially desirable to improve the disc low cycle fatigue capability.

All the LP turbine discs are made of IN 718, the strongest available alloy in the intermediate temperature range.

- Stress Analysis

The discs are designed to survive overspeed to a design speed of 5440 rpm. To analyze for this condition, the elastic disc analysis computer program was used. No allowance is made in the program for the disc spacer arms, although these tend to retard disc growth and consequently lower the disc stresses. The program output is stresses in the radial and tangential directions, plus effective stress which is the stress combined by the method known as the Hencky-Von Mises Theory of Failure. A detailed stress analysis on the spacer arms is covered later in this report.

The resulting stresses for two operating conditions are shown in Figures 261 to 264. The first condition is at 4604 rpm. The disc stresses are shown in Figures 261 and 262; this represents the typical operating conditions that the discs will encounter. Figures 263 and 264 show the stresses that the discs would encounter at overspeed to 5440 rpm. The analysis establishes that the rotor is safe at these operating conditions. Disc temperature is shown in Figure 265.

The resulting disc stress levels are judged against the criteria strength listed as follows:

Stress	Stages	
	1	2
<u>Bore Stress</u>		
Calculated	96,250	85,900
120% x 0.2% Yield	157,000	156,000
% Margin	63	81.5
<u>Average Tangential Stress</u>		
Calculated	76,100	70,400
0.02% Yield	109,500	110,000
% Margin	44	56.3
<u>Maximum Rim Stress</u>		
Calculated	7,500	35,300
0.02% Yield	107,000	109,000
% Margin	1,428	309

The disc dovetail stresses were analyzed using the same procedure as the blade stresses covered earlier in the report. Both stages, of course, use the two-tang dovetail to match the blades. The steady state stresses included in the analysis are the centrifugal force, shear due to gas load, bending due to gas load, and blade offset and tilt. Tables LXVII and LXVIII tabulate the important steady state stress levels in each stage. All stress levels are at a rotor speed of 4605 rpm. As noted in the tables, the results are given at six points on the dovetail tangs. These points are located similar to the blade dovetail.

Vibratory stress distribution in the dovetails are shown with the blade dovetail stress distribution in Figures 259 and 260. Results of the

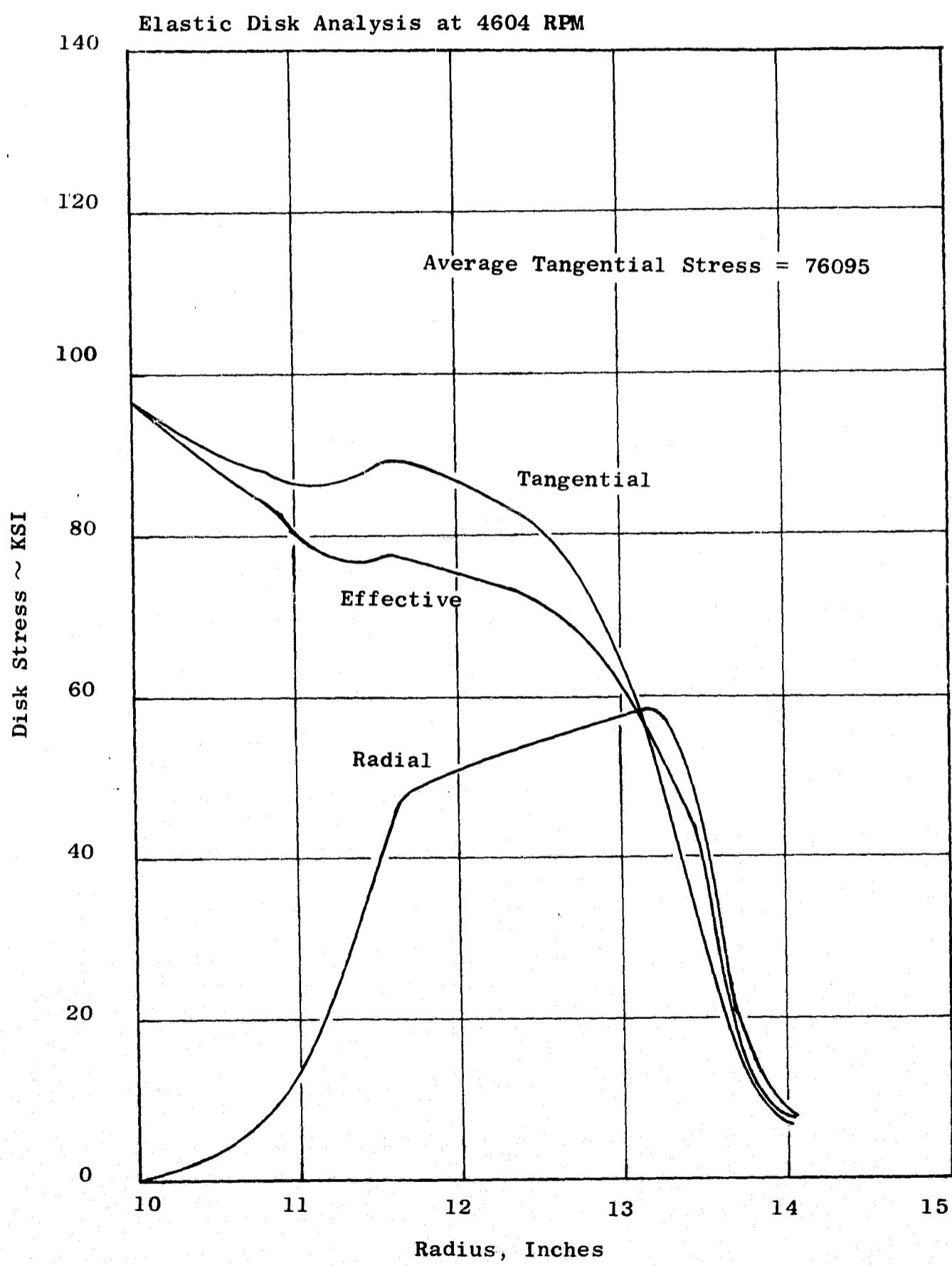


Figure 261. Fan C, LP Turbine Rotor, Stage 1 Steady State Stress, 4604 RPM

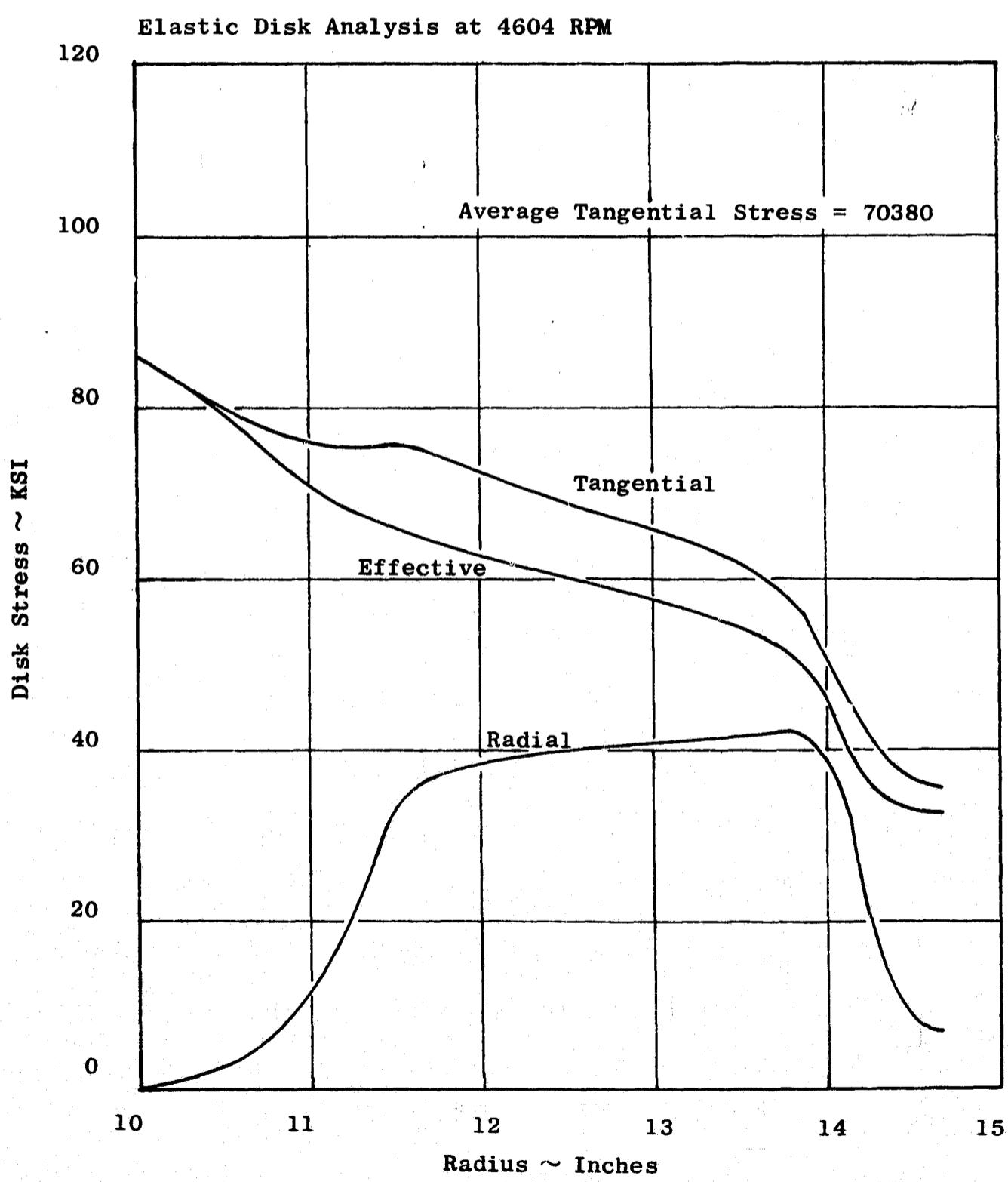


Figure 262. Fan C, LP Turbine Rotor, Stage 2 Steady State Stress, 4604 RPM

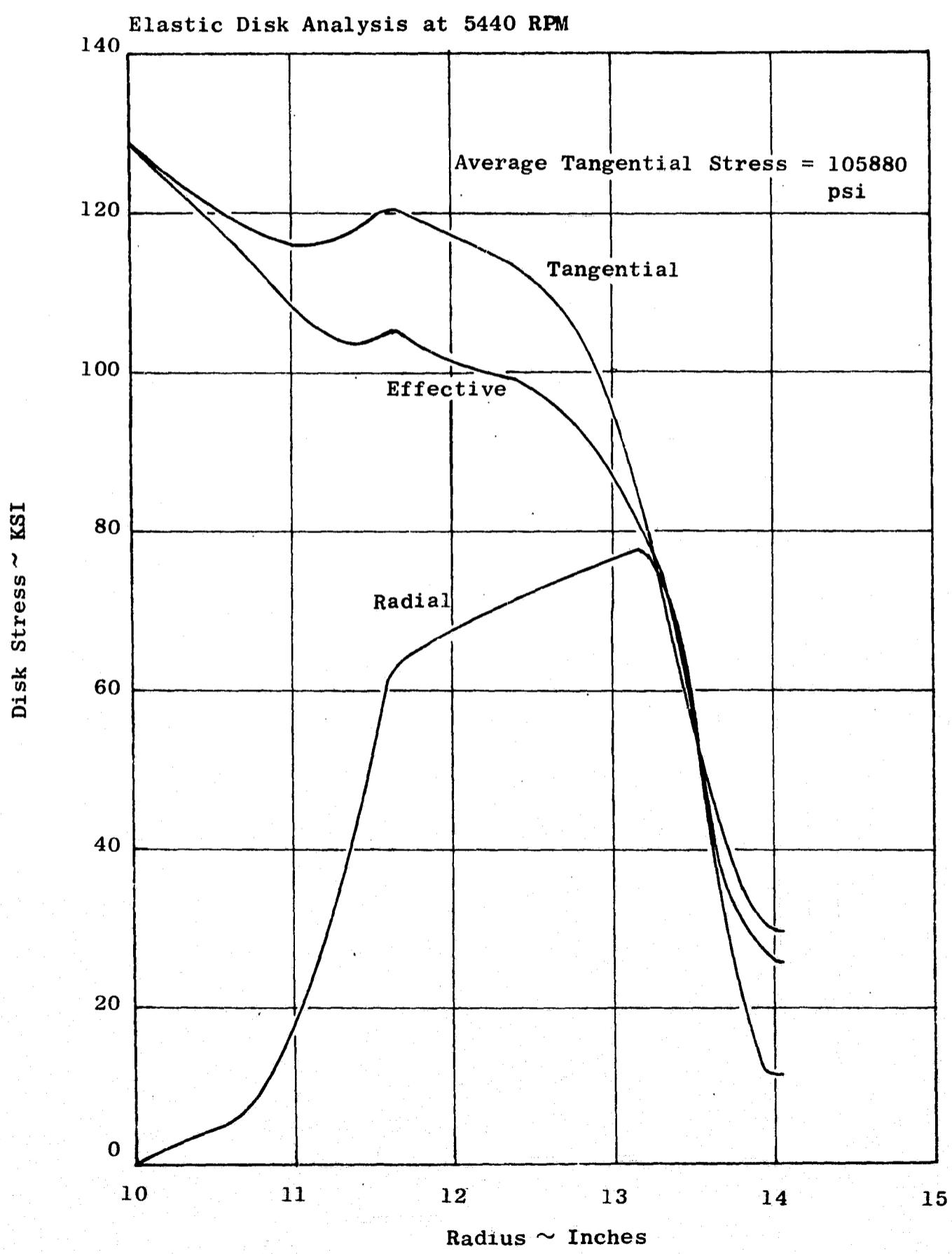


Figure 263. Fan C, LP Turbine Rotor, Stage 1 Steady State Stress, 5440 RPM (Overspeed)

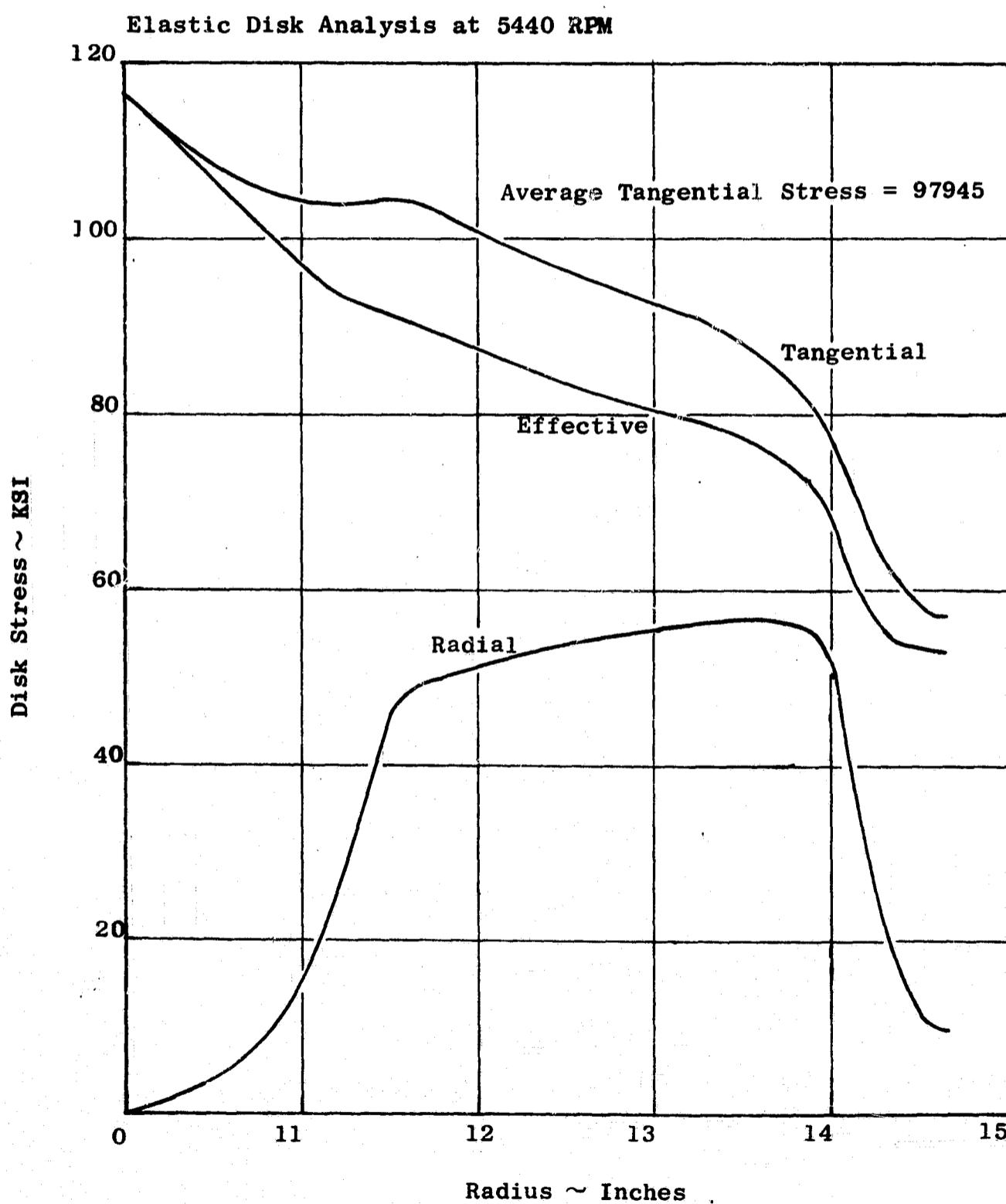


Figure 264. Fan C, LP Turbine Rotor, Stage 2 Steady State Stress,
5440 RPM (Overspeed)

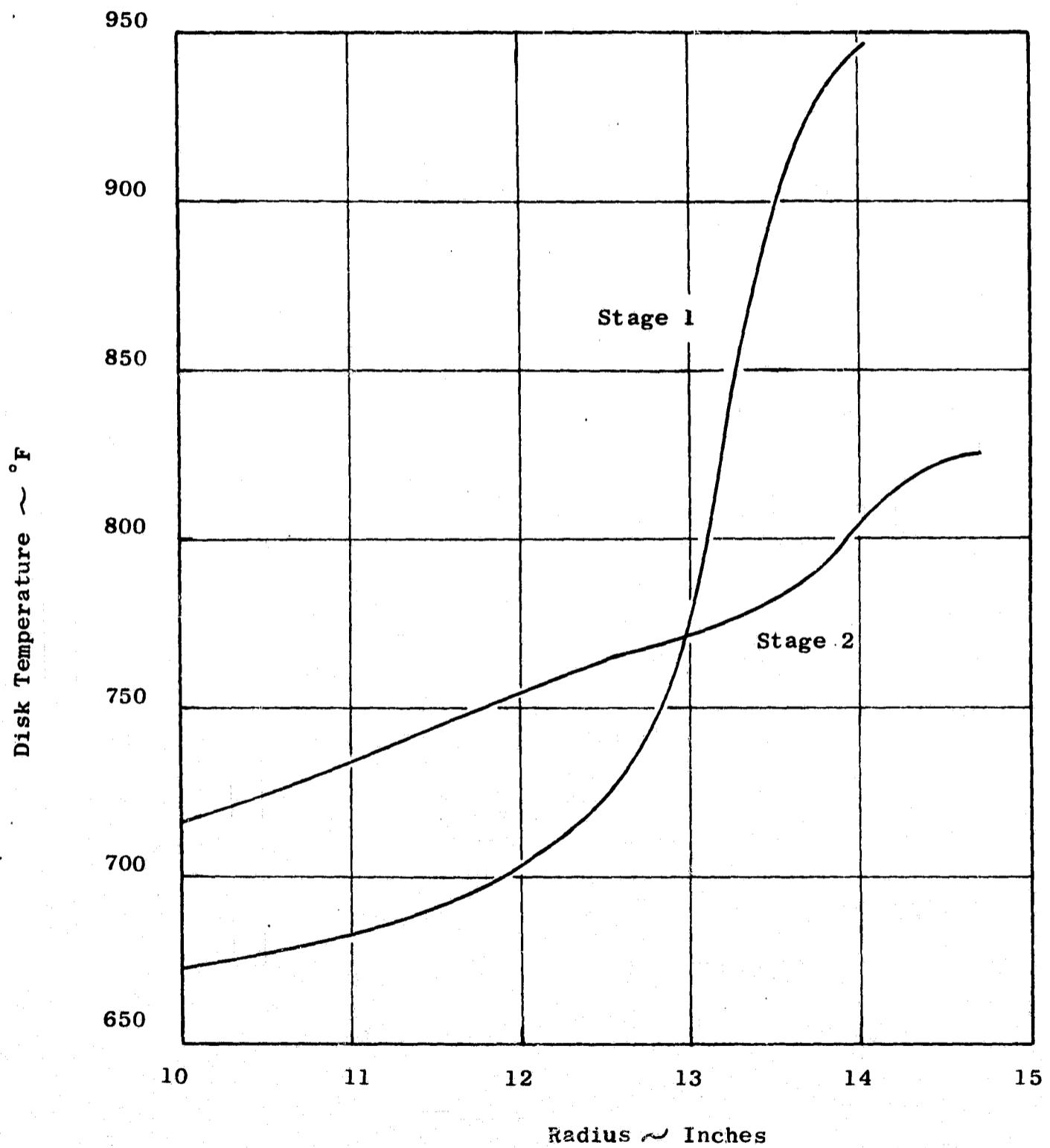


Figure 265. Fan C LP Turbine Steady State Disc Temperature

Table LXVII. Fan C LP Turbine Rotor Stage 1 Disc Dovetail Stress Analysis (4605 RPM)

Point	σ_c	σ_{mx}	σ_{my}	σ_{neck}	σ_{tang}	σ_{total}
<u>Upper Tang</u>						
1	13600	+152	-1040	12712	11900	23444
2	13600	+152	+1040	14792	11610	25325
3	13600	-152	+1040	14480	11100	24672
4	13600	-152	-1040	12408	11100	22454
5	13600	0	+1040	14640	11800	25429
6	13600	0	-1040	12560	11300	22790
<u>Lower Tang</u>						
1	16100	+192	-910	16292	18900	32946
2	16100	+192	+910	17200	19500	34429
3	16100	-192	+910	16900	18900	33626
4	16100	-192	-910	14998	18300	31025
5	16100	0	+910	17010	19200	33983
6	16100	0	-910	15190	18600	31472

Table LXVIII. Fan C LP Turbine Rotor Stage 2 Disc Dovetail Stress Analysis (4605 RPM)

Point	J_c	σ_{mx}	σ_{my}	σ_{neck}	σ_{tang}	σ_{total}
<u>Upper Tang</u>						
1	13400	+64	-4860	8600	8750	16424
2	13400	+64	+4860	18320	9800	27546
3	13400	-64	+4860	18200	9700	27334
4	13400	-64	-4860	18480	8660	26692
5	13400	0	+4860	18260	9800	27484
6	13400	0	-4860	8540	8660	16287
<u>Lower Tang</u>						
1	14500	+74	-7600	6974	11650	16730
2	14500	+74	+7600	22174	18600	39121
3	14500	-74	+7600	22026	18600	38963
4	14500	+74	-7600	6830	11650	16552
5	14500	0	+7600	22100	18600	39042
6	14500	0	-7600	6900	11650	16639

vibratory analysis on the dovetail are presented as an alternating stress ratio, relative to a chosen point on the airfoil, which in this case was the airfoil root leading edge. Vibratory results are given for the first flexural in-phase mode.

- Blade Retainers

The blade retainers are direct copies of retainers presently being used on the TF39 and CF6 engines and are not expected to cause any problems based on test experience to date.

- Shaft

The rotor structure (including shaft, disc flanges, and seals) was analyzed with the Multishell Computer Program which is used for complicated axisymmetrical bodies. The modeling procedure consists of breaking up a part to be analyzed into geometrically regular elements such as cones, cylinders, and rings. The Program then computes influence coefficients for each end of each submember. It also computes free-end deflections for the centrifugal and thermal loads imposed. When the member ends are jointed, compatible deflections are imposed, and the required end loads are computed. These end loads, together with the internal loads, completely define the loads, stresses, and deflections throughout the member.

The shaft, which carries the overhung rotor, is bolted between the Stage 1 and 2 disc flanges and extends forward to the No. 6 bearing. The hub of the shaft splines to the midshaft. The shaft is made of a one-piece Inconel 718 forging. The steady state stresses are shown in Figure 266. The maximum stress in the outer cone of the shaft is 37,000 psi compared to a 0.2 percent offset yield strength of 120,000 psi at the maximum temperature of 750°F.

The spacer arms are integral with the discs and, thus, are also Inconel 718 material. The conical arms are tapered near the disc rims to increase stiffness and to reduce stresses. Spacer arm steady state stresses also are shown in Figure 266. The highest stress in the spacer arms occurs in the Stage 1 forward seal extension and is 54,000 psi. The local temperature is 850°F, which gives a minimum 0.2 percent offset yield strength of 127,500 psi. The maximum temperature along the rotor is 860°F in the aft spacer arm of the Stage 1 disc. The minimum yield strength at this temperature is 127,500 psi.

- Seals

There is one interstage rotor seal on the Fan C low pressure turbine. The seal is made of Inconel 718 and has two teeth slanted forward at approximately 30°. The seal is designed to rub into the honeycomb in the stator seal, and the teeth are spaced so that the wear track of one tooth does not

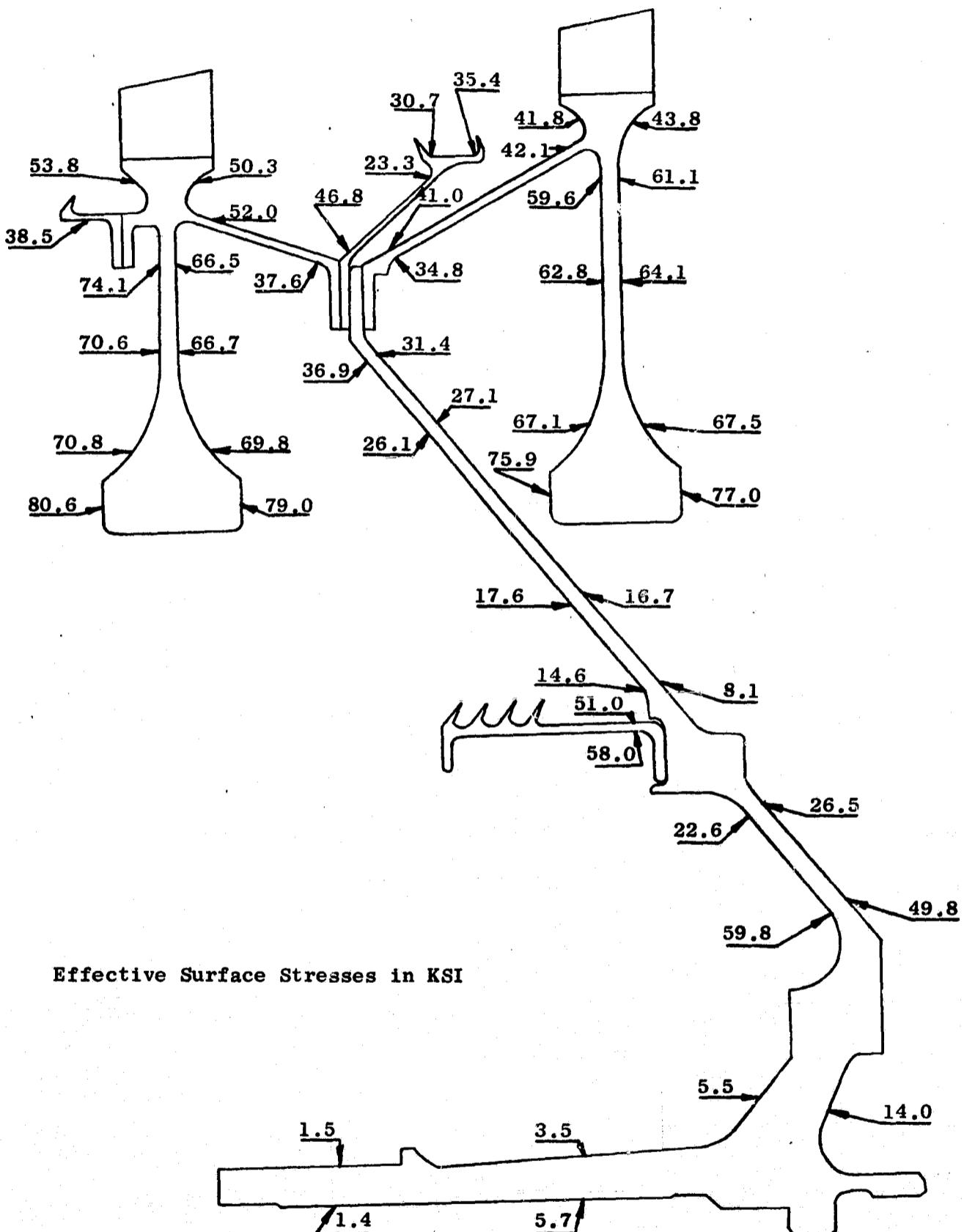


**Figure 266. Fan C LP Turbine Rotor Multishell Analysis,
Effective Surface Stress, KSI (4605 RPM)**

enter the wear track of the other tooth during engine operation. By this means, seal clearance is kept to a minimum for reduced leakage. The outer surfaces of the teeth are coated with aluminum oxide as a hardcoating, to permit the seal to "rub in" without wearing away the rotating seal. Seal stresses are general low and are shown on Figure 266. These stresses are at a rotor speed of 4605 rpm. The allowable stress, 0.2 percent offset yield strength, is 127,500 psi at the seal temperature of 850°F.

The single-tooth seal on the forward side of the Stage 1 disc is used to restrict the airflow from the forward rotor cavity. The forward rotor cavity must have a continuous flow of purge air, and hot gas from the gas stream must not be allowed to enter the cavity. Seal stresses are generally low and are shown in Figure 266. These stresses are at a rotor speed of 4606 rpm. The 0.2 percent offset yield strength, at the seal temperature of 850°F, is 127,500 psi.

A pressure balance seal is located on the forward side of the LP turbine shaft. Ninth stage compressor bleed air, which is piped through the turbine midframe, is supplied to the forward rotor cavity. This air is then throttled across the four-tooth pressure balance seal, permitting the compressor bleed air to purge the lower and rear rotor cavities. This seal is made of Inconel 718, and the seal teeth will be hardcoated with aluminum oxide to reduce wear. The maximum seal stress, at 4605 rpm, is 58,000 psi. The allowable stress, 0.2 percent offset yield strength is 132,000 psi at a temperature of 630°F.

The interstage seal and pressure balance seal were analyzed to determine if any seal natural frequencies fell within the operating range of the Fan C LP turbine. Briefly, the seal is modeled into an equivalent cylinder with end conditions imposed to best represent the seal design. The two seals analyzed here used clamp-free end conditions. Next, both beam-mode and ring-mode frequencies are calculated on the equivalent cylinder for a range of circumferential wave numbers. The calculated beam and ring frequencies are added together at each circumferential wave number and the result plotted on a Campbell diagram. Figures 267 and 268 show that seal resonance falls way outside of the operating range of the Quiet Engine Fan-C version.

● Disc-Blade Vibration

The disc-blade vibration is in process for the LP turbine for Fan C. No problems are expected to be encountered in this area.

● Temperature Distribution

Calculation of the LP turbine rotor temperatures was made by use of the GE 635 Computer Program, THTD.

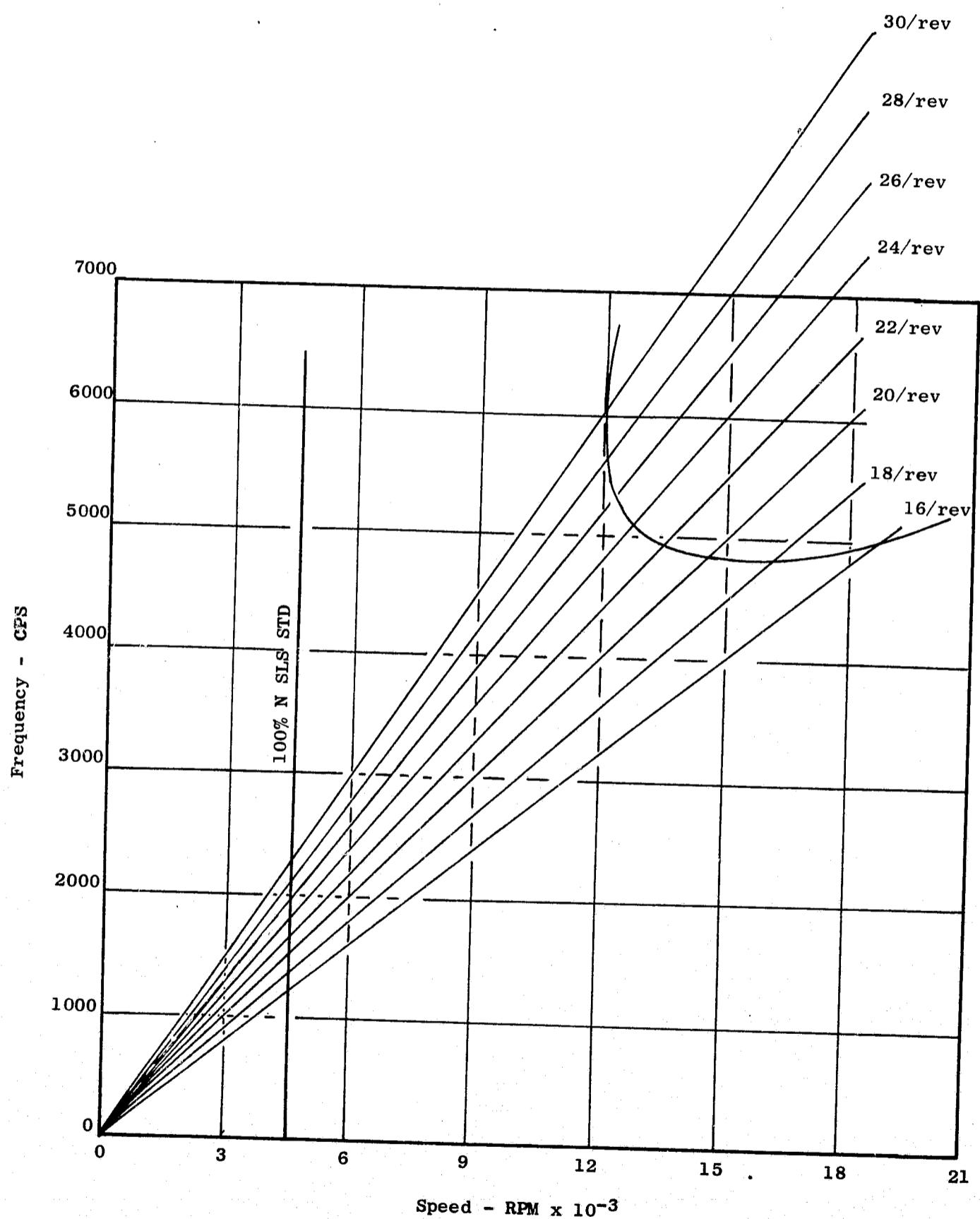


Figure 267. Fan C Interstage Seal Campbell Diagram

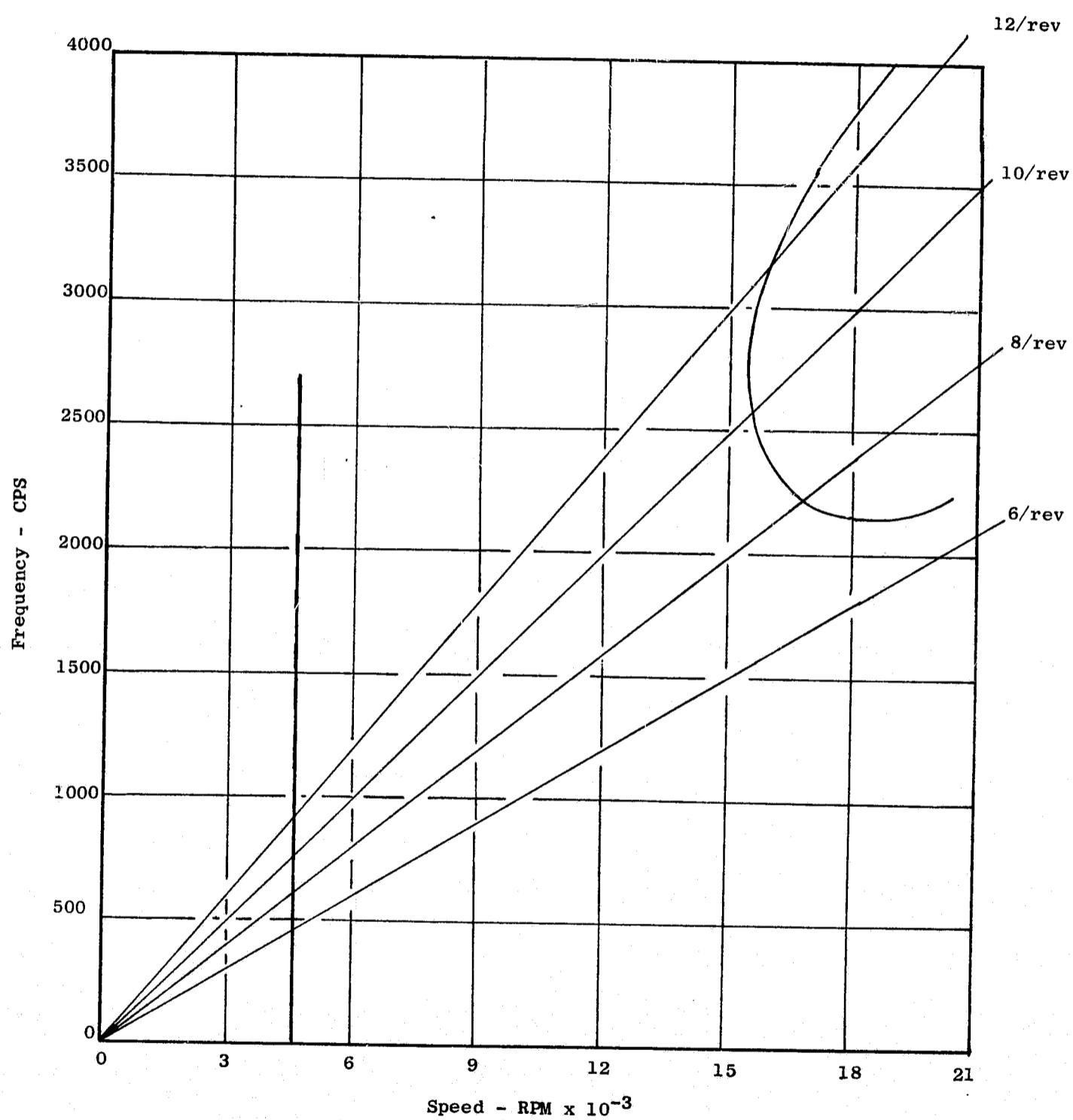


Figure 268. Fan C Pressure Balance Seal Campbell Diagram

Briefly, THTD is a very general program which gives a finite difference analysis of three-dimensional steady state or transient heat flow, employing the implicit form of the heat balance equations. The method of analysis consists of representing the geometry of the problem by elemental bits of geometry called nodes, connected in a manner prescribed by format with the appropriate convection, radiation, or heat generation boundary conditions impressed on them.

The LPT turbine node network extended axially through the rotor, forward to aft. The network extended radially from the inner radius of the low pressure shaft of the rotor to the blade platforms. The blade platforms were assumed to be at the local gas temperature. The inner radius of the low pressure shaft was assumed to be at sump temperature. Boundary conditions imposed on the other nodes were obtained from classical heat transfer convection equations.

Figure 269 shows the calculated temperature distribution of the turbine rotor.

7.2 LOW PRESSURE TURBINE STATOR DESIGN

7.2.1 Summary

This section presents the methods and procedures used in the mechanical design of the low pressure turbine stators for Experimental Quiet Engine Configurations A, B, and C.

The Fan A and B low pressure turbine stator uses the first four stages of the CF6-6 five-stage low pressure turbine stator. In order to make the two stator assemblies compatible, a flowpath segment is bolted to the casing to take the place of the CF6-6 fifth-stage hardware. In addition, the flow area of the Stage 1 turbine nozzle is reduced from that of the CF6-6 to meet the Fan A and B cycle requirements.

The Fan C low pressure turbine stator is a new two-stage design. The hardware is somewhat more elaborate, as the flowpath is conical for Fan C as compared to cylindrical for Fans A and B and the CF6-6. Also, the turbine vane solidity is higher, resulting in the vane-to-vane spacing being smaller.

The materials used in both the A and B stator and the C stator are identical to those used in the CF6-6 to take maximum advantage of CF6-6 experience.

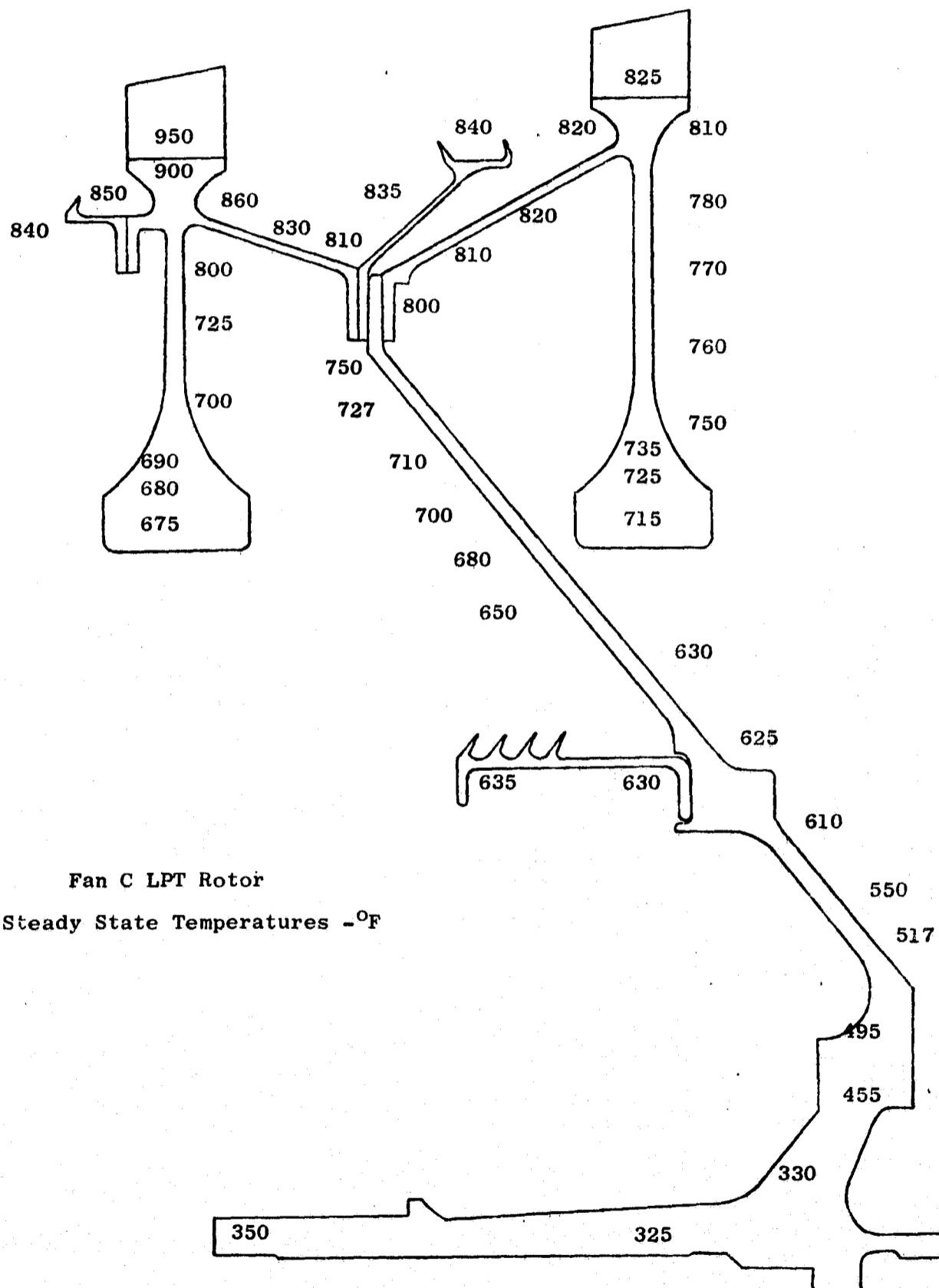


Figure 269. Fan C LP Turbine Rotor Steady State Temperatures

7.2.2 Turbine Stator, Fans A and B

The LP turbine stator used in the Fans A and B engine (see Figure 191) is composed of the first four stages of the CF6-6 stator plus a new flowpath segment component which is bolted to the casing to fill the gap created by removal of the CF6 Stage 5 blade and vane. In addition, the Stage 1 LP turbine nozzle flow area is reduced by 7.8 percent as required by the engine cycle.

The turbine casing is split at the horizontal centerline for ease of assembly and so that one-half may be removed to inspect the LP turbine. The turbine casing rails, from which the turbine nozzles and shrouds are supported, are impingement cooled with 9th-stage compressor air to maintain good control of operating clearances at the turbine blade tip shrouds.

Inlet temperature and pressure to each turbine nozzle stage are shown in Table LXIX.

Table LXIX. Turbine Nozzle Inlet Temperatures and Pressures

Stage	Temperature, °F	Pressure, psia
	Fans A & B	Fans A & B
1	1231	52
2	1090	38.2
3	985	29.2
4	901	20.0

Radial temperature profiles, of hot gas entering each of the four stages of turbine nozzles, are shown in Figure 270.

7.2.2.1 Turbine Nozzles

Steady state temperatures of the turbine nozzles, since they are not cooled, can be determined from Figure 270. Stage 1 operates at an average temperature of 1231°F with a peak temperature of 1326°F occurring at 65 percent of span height.

458

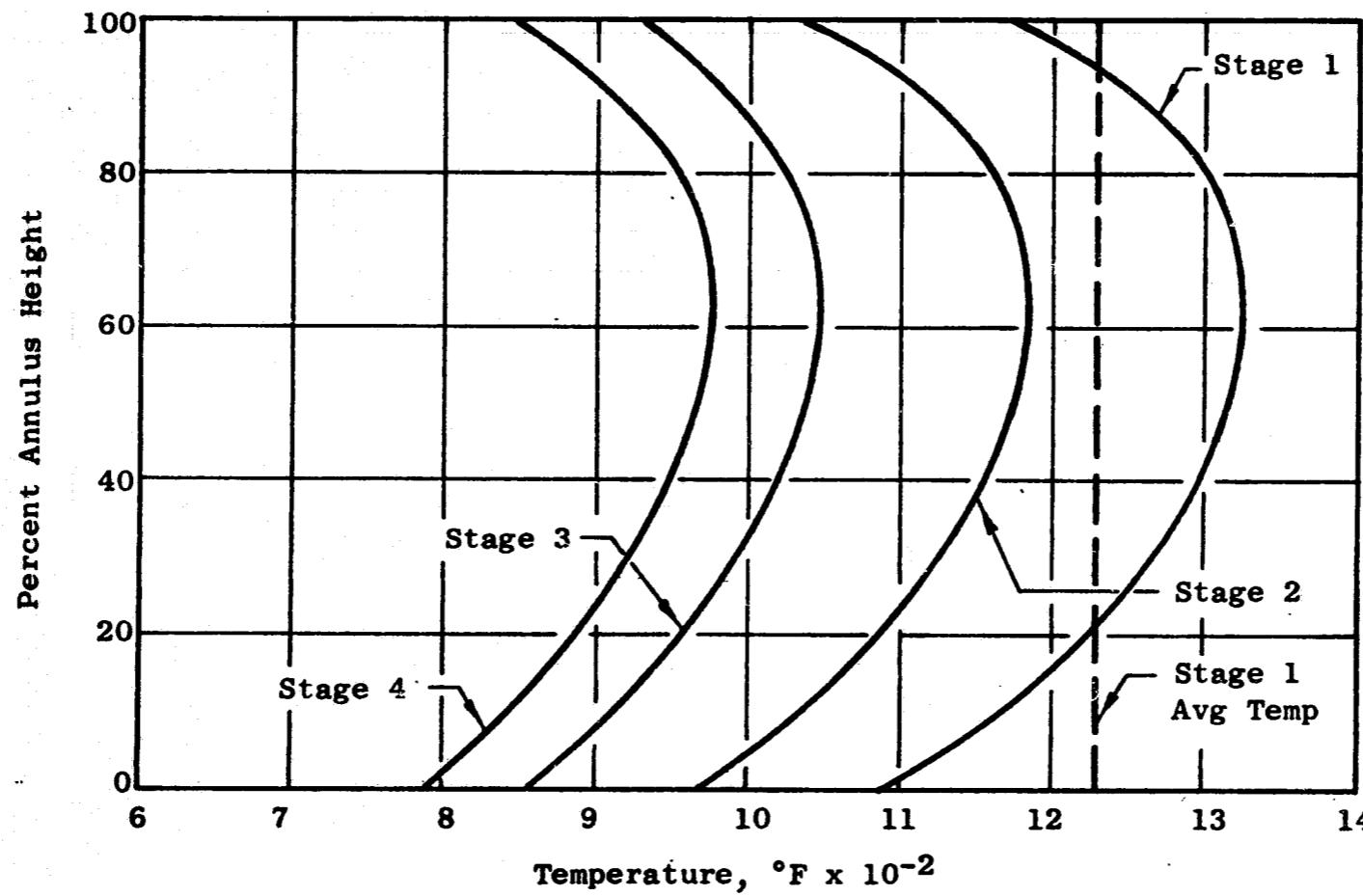


Figure 270. Radial Temperature Profile Entering the Fan A and B LP Turbine Nozzles

Vane material is cast Rene' 80, a nickel-base superalloy which possesses excellent strength at high temperature. As is the case for most of the materials in the turbine stator, the temperatures of the Quiet Engine cycle do not require as exotic a material as is actually being used. But, since the CF6 components are "off-the-shelf", they provide reliable and economical hardware. Figure 271 shows the allowable strength of Rene' 80 material as a function of temperature.

Turbine nozzles are precision, investment-cast, six-vane segments. They are supported from rails on the casing and are accurately machined on the casing/nozzle mating surface. Tangential load stops position the segments circumferentially and prevent rotation caused by the tangential gas load on the vanes (see Sections L-L and K-K of Figure 272. Figure 272 also shows (in Section Y-Y and View X) the method of using sealing strips to prevent leakage between segments. View M shows a section thru a boroscope port which permits inspection of the LP turbine without removing the casing. The segmented turbine nozzles permit replacement of nozzle sections in the event of local damage in the turbine.

To achieve the 7.8 percent reduction in flow area required in the Stage 1 nozzle, without incurring an expensive tooling change, the Stage 1 nozzle waxes will be modified in the trailing edge area.

The Twisted Blade Computer Program was used to determine gas-load stresses in the turbine vanes. These are plotted as a function of radial height in Figures 273 through 276. An additional thermal stress is induced in the vanes during transients (throttle bursts and chops), because of the difference in thermal response between the vane trailing edge and the leading edge or the convex side. A determination of this stress was made based on testing performed on the TF39 vanes. Maximum gas-load and thermal stresses for each of the four stages of vanes are shown in Table LXX.

LXX. Fans A and B Gas-Load Stresses

Stage	Fans A & B		
	Max. Gas-Load Stress, PSI	Max. Thermal Stress, PSI	Life, Hours
1	2,200	38,000	Infinite
2	5,400	31,100	Infinite
3	11,300	25,900	Infinite
4	12,100	22,400	Infinite

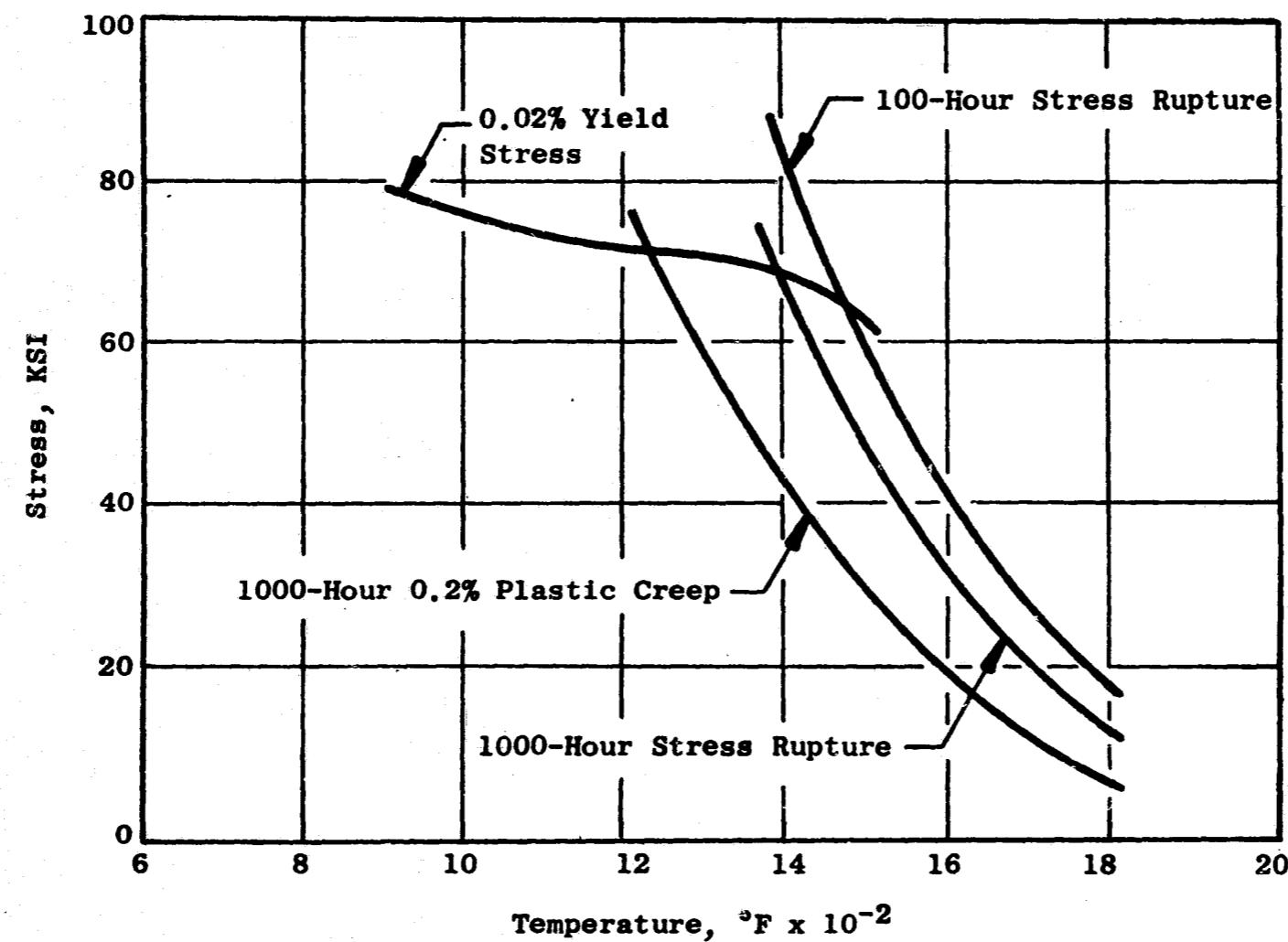


Figure 271. Cast Material Properties, Rene' 80 (C50TF28), 3 Standard Deviations

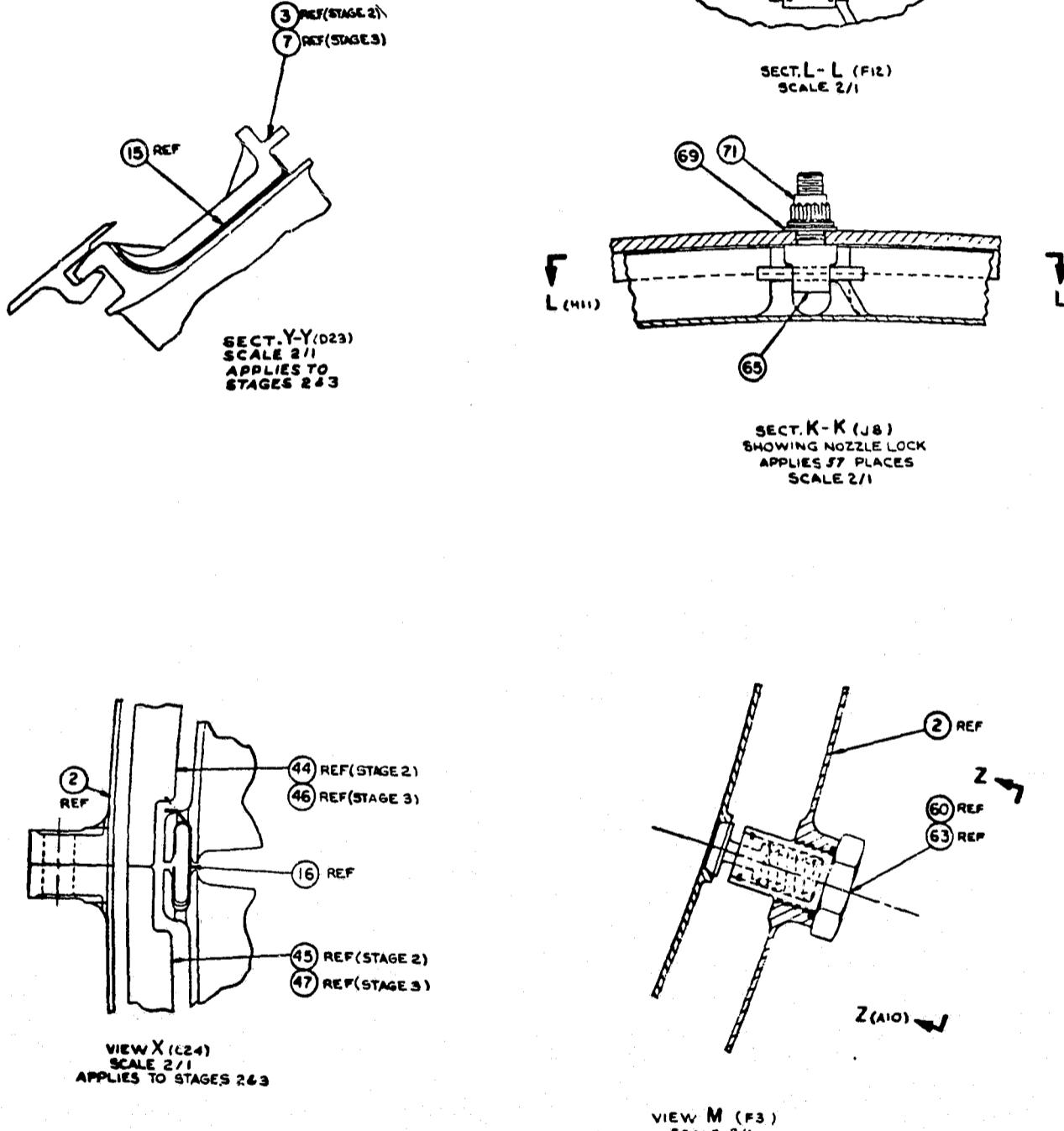


Figure 272. Fans A and B LP Turbine Stator Details

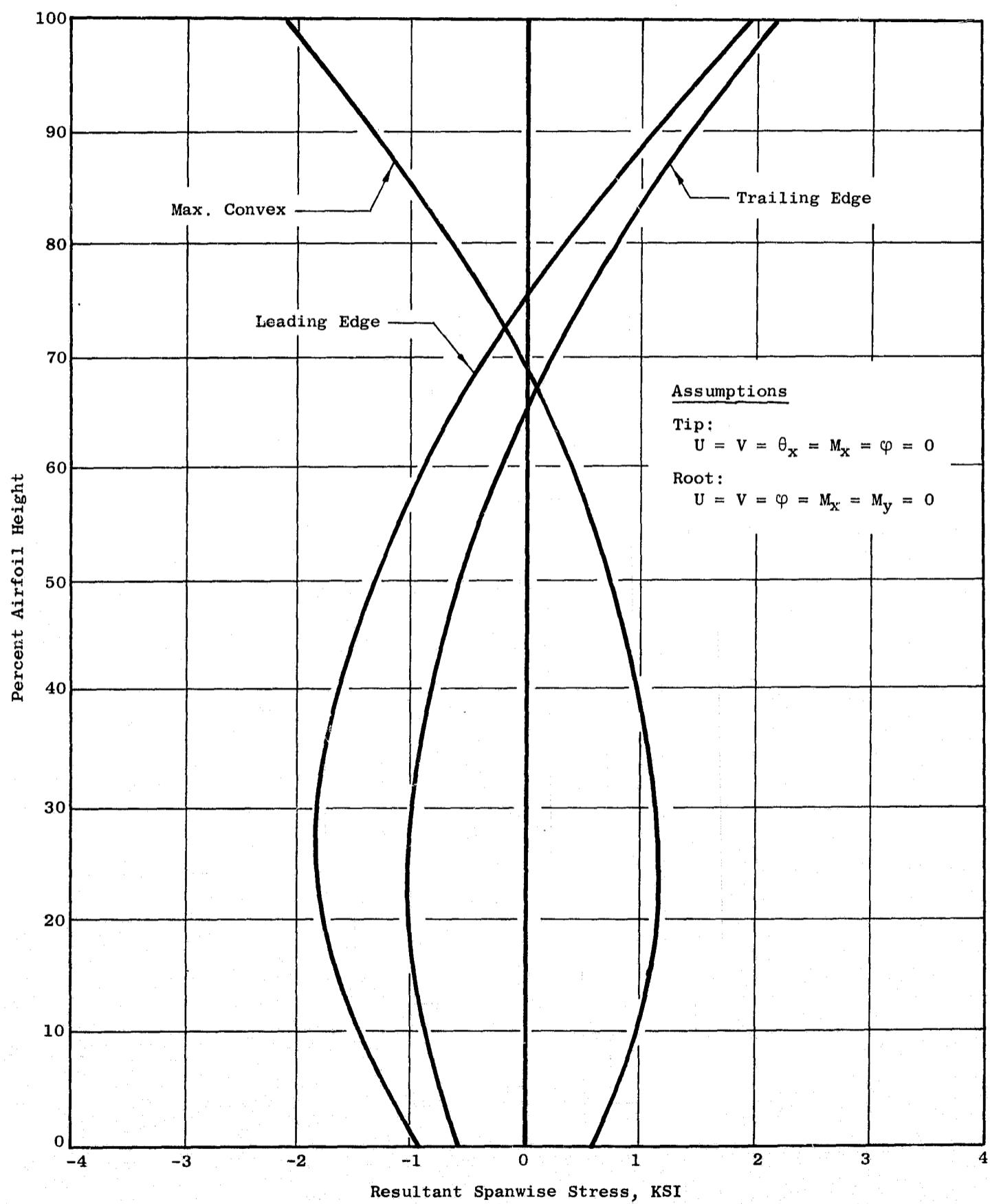


Figure 273. Fans A and B Stage 1 Vane, Gas Load Stresses

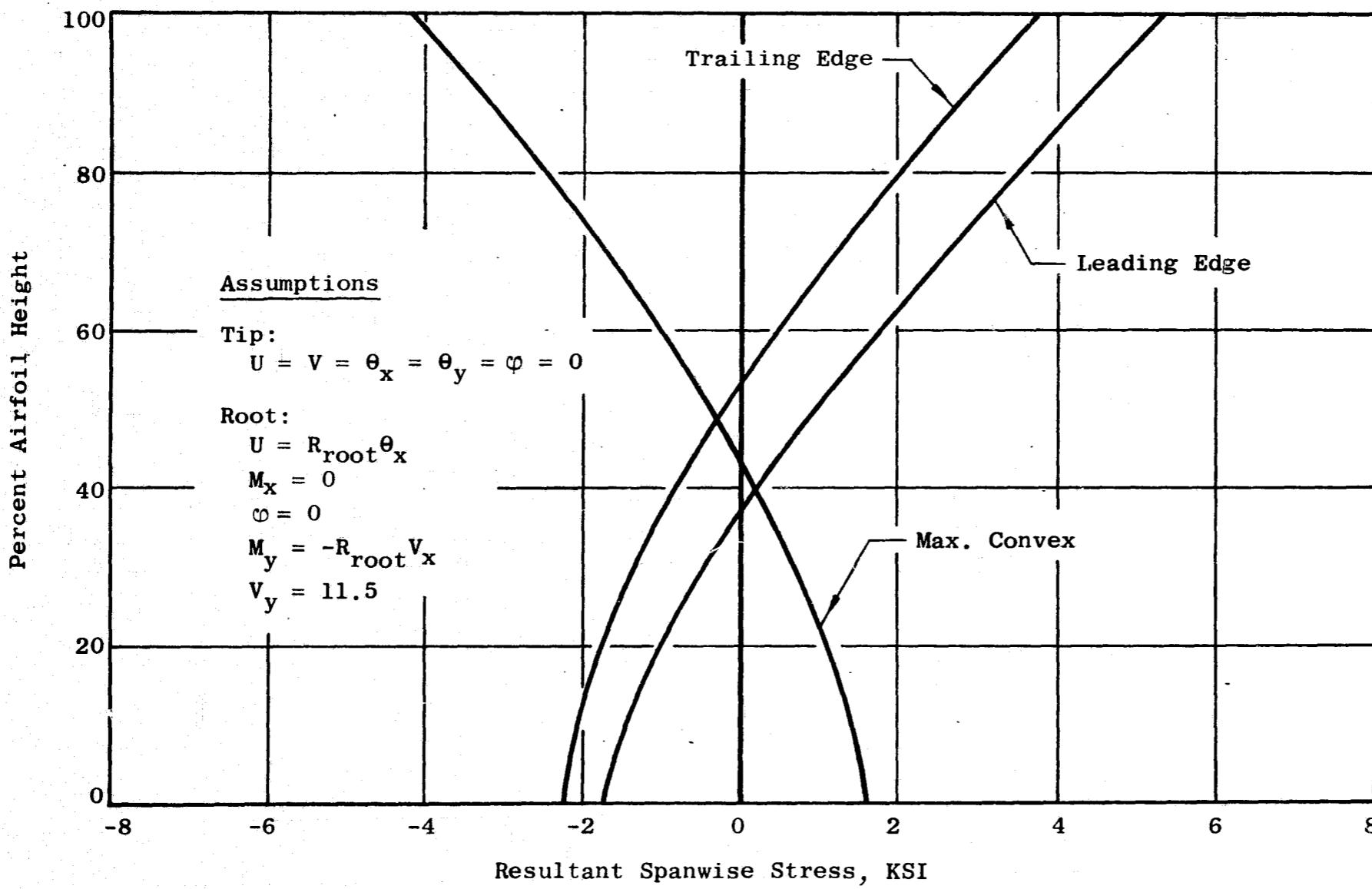


Figure 274. Fans A and B Stage 2 Vane, Gas Load Stresses

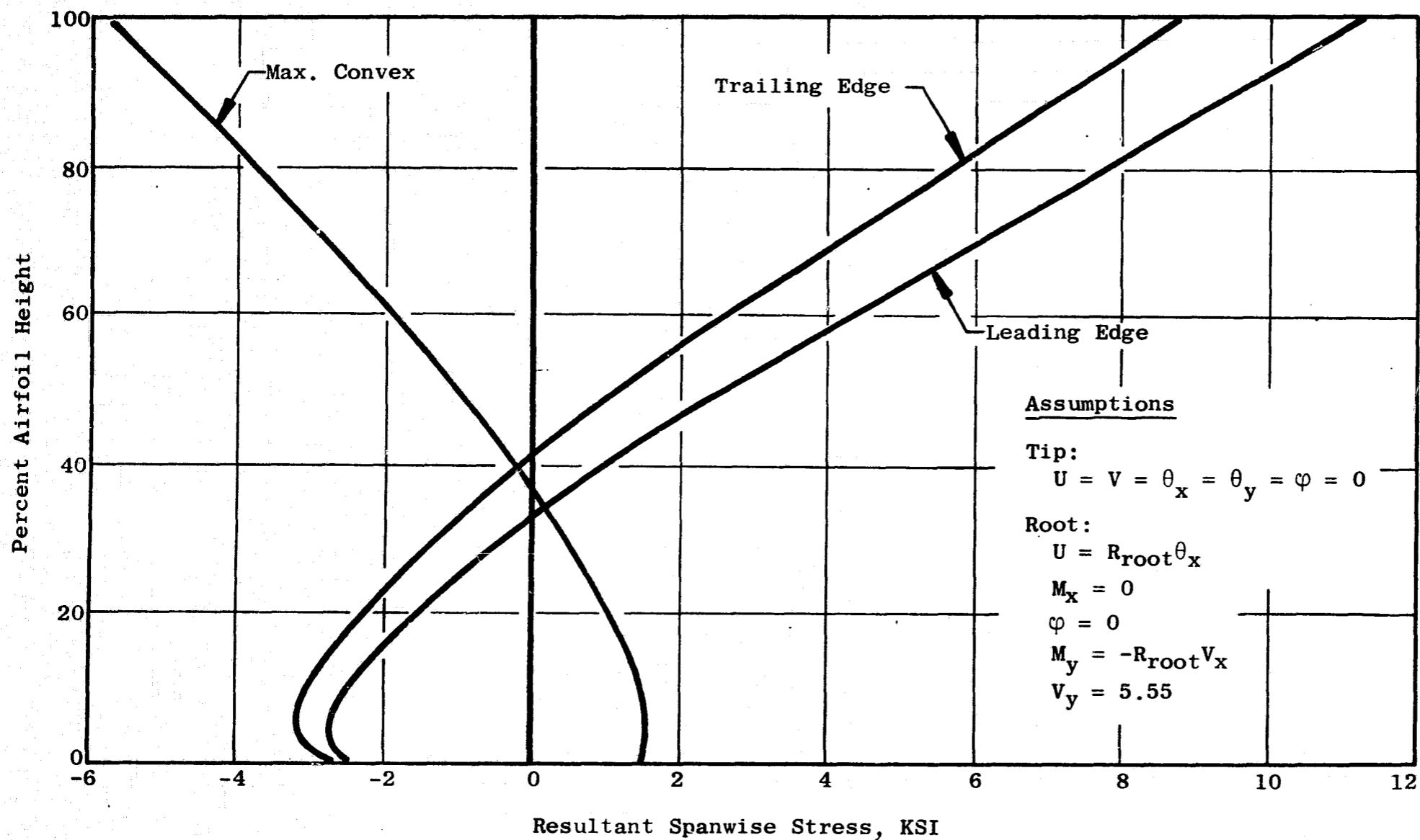


Figure 275. Fans A and B Stage 3 Vane, Gas Load Stresses

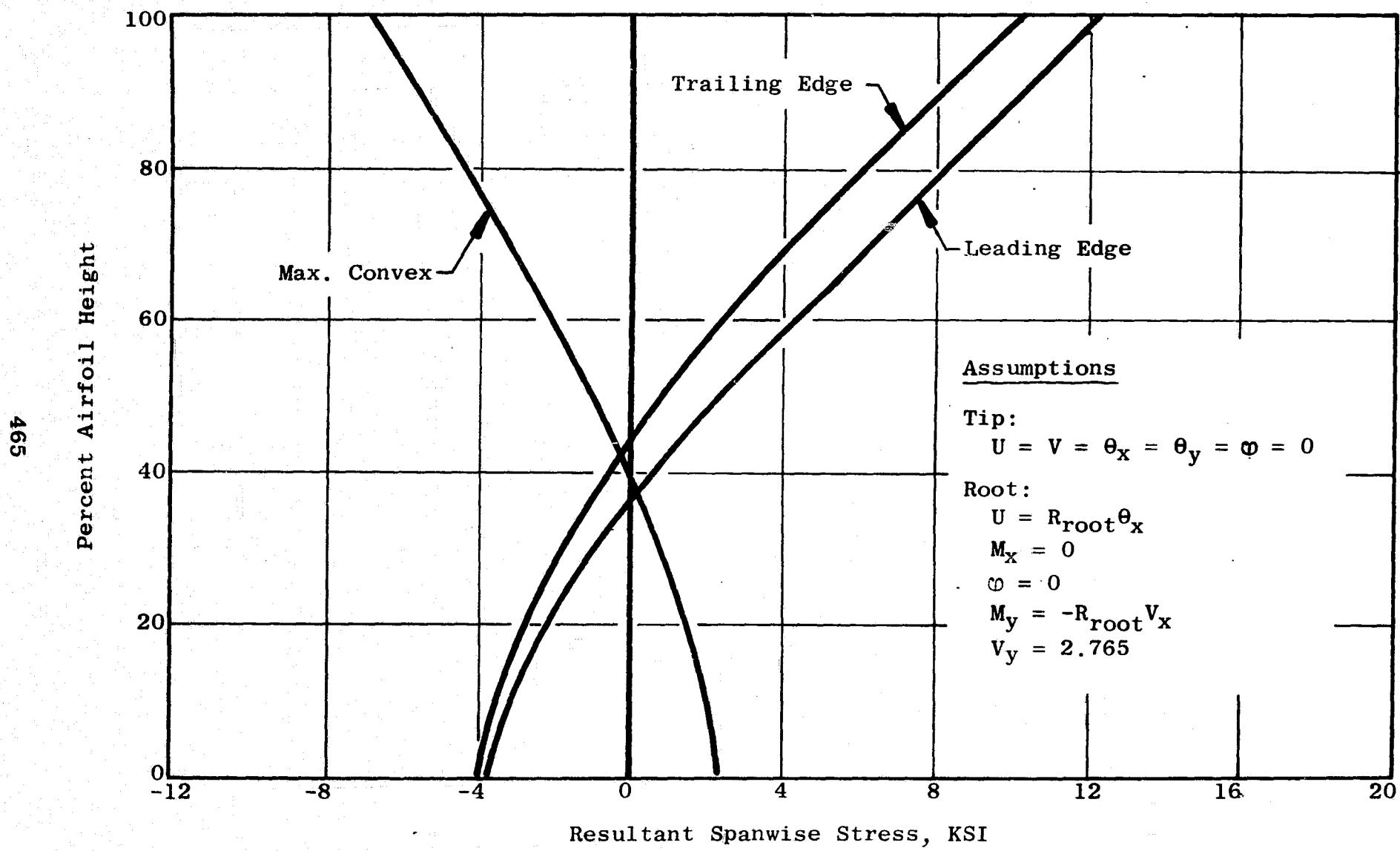


Figure 276. Fans A and B Stage 4 Vane, Gas Load Stresses

A frequency analysis of the vanes was made for both in-phase and out-of-phase modes. Campbell diagrams, showing the results for each stage, are shown in Figures 277 thru 284 inclusive.

All vanes have a minimum frequency of greater than 4 per rev. Stages 2 and 4 show a possible resonance with the passing frequency of the preceding stage of rotor blades. This is not considered to be a problem, however, because:

- (a) For a 2 percent error in calculated frequency, the vanes are not in resonance; and,
- (b) It is difficult to excite such high frequencies (Stage 2 = 9000 cps and Stage 4 = 6800 cps).

As a precaution, these vanes will be instrumented and monitored during testing.

7.2.2.2 Turbine Casing

The turbine casing is fabricated of Inconel 718 material and is comprised of forged rings welded to sheet metal cylinders and cones. It is made up of two halves, bolted together at the horizontal split line. After premachining and welding, the component is heat treated for maximum strength and then final machined to close-tolerance dimensions.

The rails, which support the turbine nozzles and shrouds, are impingement cooled by means of 9th-stage compressor air at 500°F. This maintains close control of blade-tip-to-shroud clearances, which produces high turbine efficiency. Cooling air ports (one per stage) and boroscope ports (one per stage) are welded to the casing.

The maximum stresses in the turbine casing were determined using the Multishell III SNAP Computer Program. This program stress analyzes shells of revolution with axisymmetric loading. Temperatures at various locations along the casing are given in Figure 285. A tabulation of maximum stresses is shown in Figure 286. These may be compared with the allowable strength of Inconel 718 as shown in Figure 287.

7.2.2.3 Turbine Shrouds

The turbine shrouds are cylindrical components placed over the turbine blade tips and made of Hastelloy X material, for good oxidation resistance and desirable brazing properties. Each stage is segmented with cold buildup tangential gaps between segments for thermal expansion reasons. The turbine blade side is faced with 1/16-inch-cell honeycomb, 0.0025/0.004 inch in stock thickness, to provide minimum resistance to the blade tip seal teeth which rub into the honeycomb during transients. Segments may be replaced when

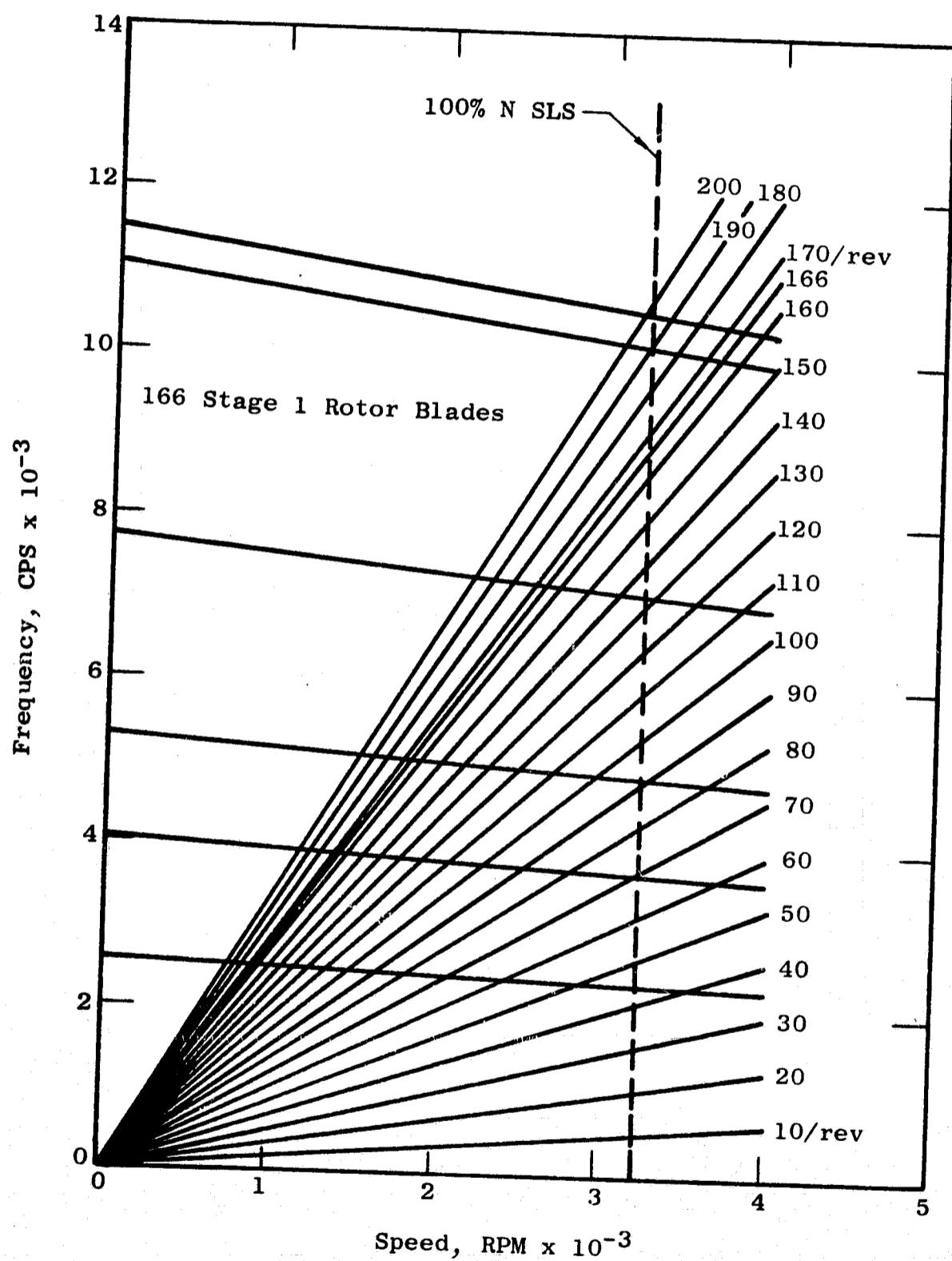


Figure 277. Campbell Diagram for the Fans A/B Stage 1 Vane, In-Phase Modes

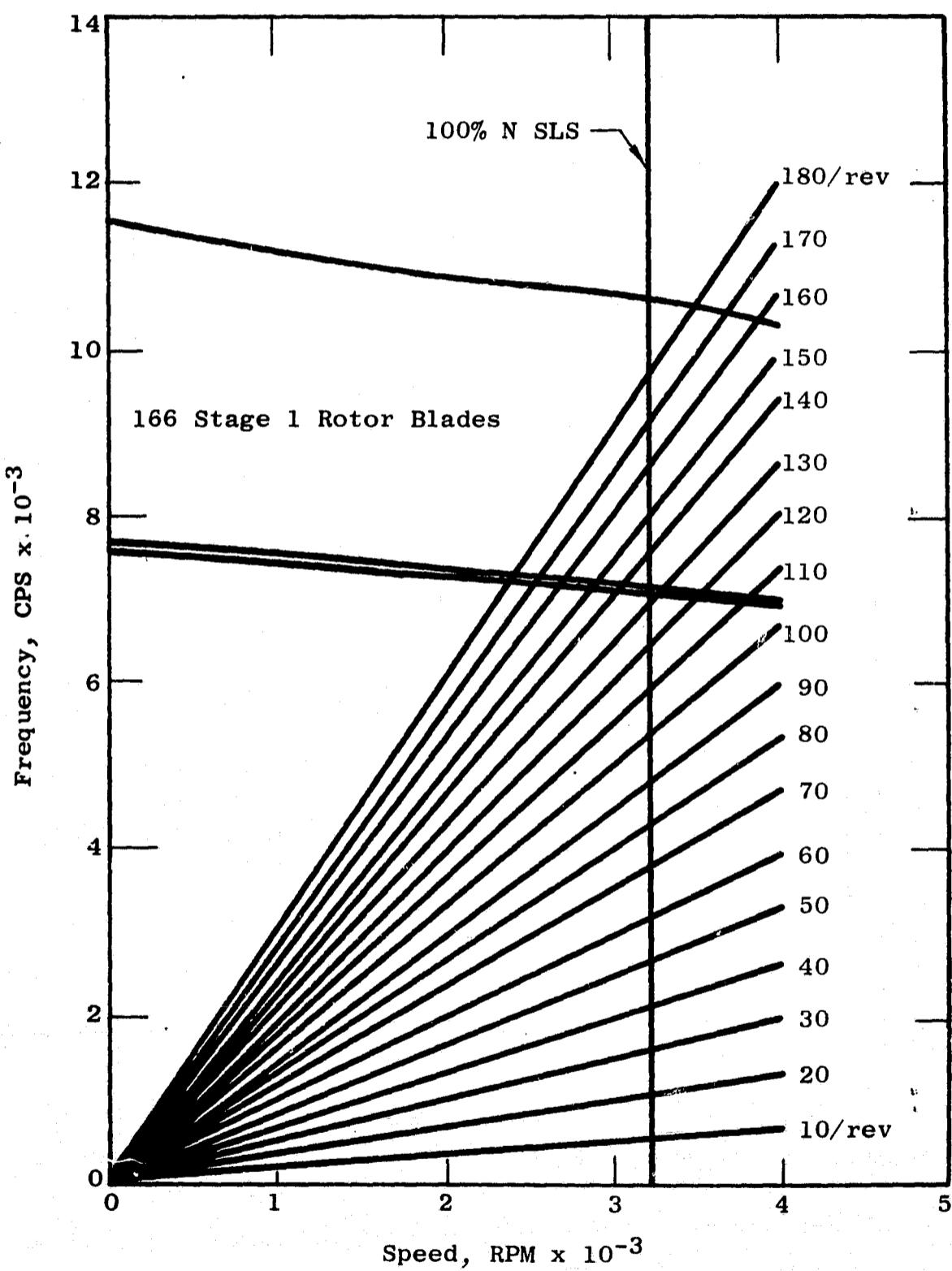


Figure 278. Campbell Diagram for the Fans A/B Stage 1 Vane, Out-of-Phase Modes

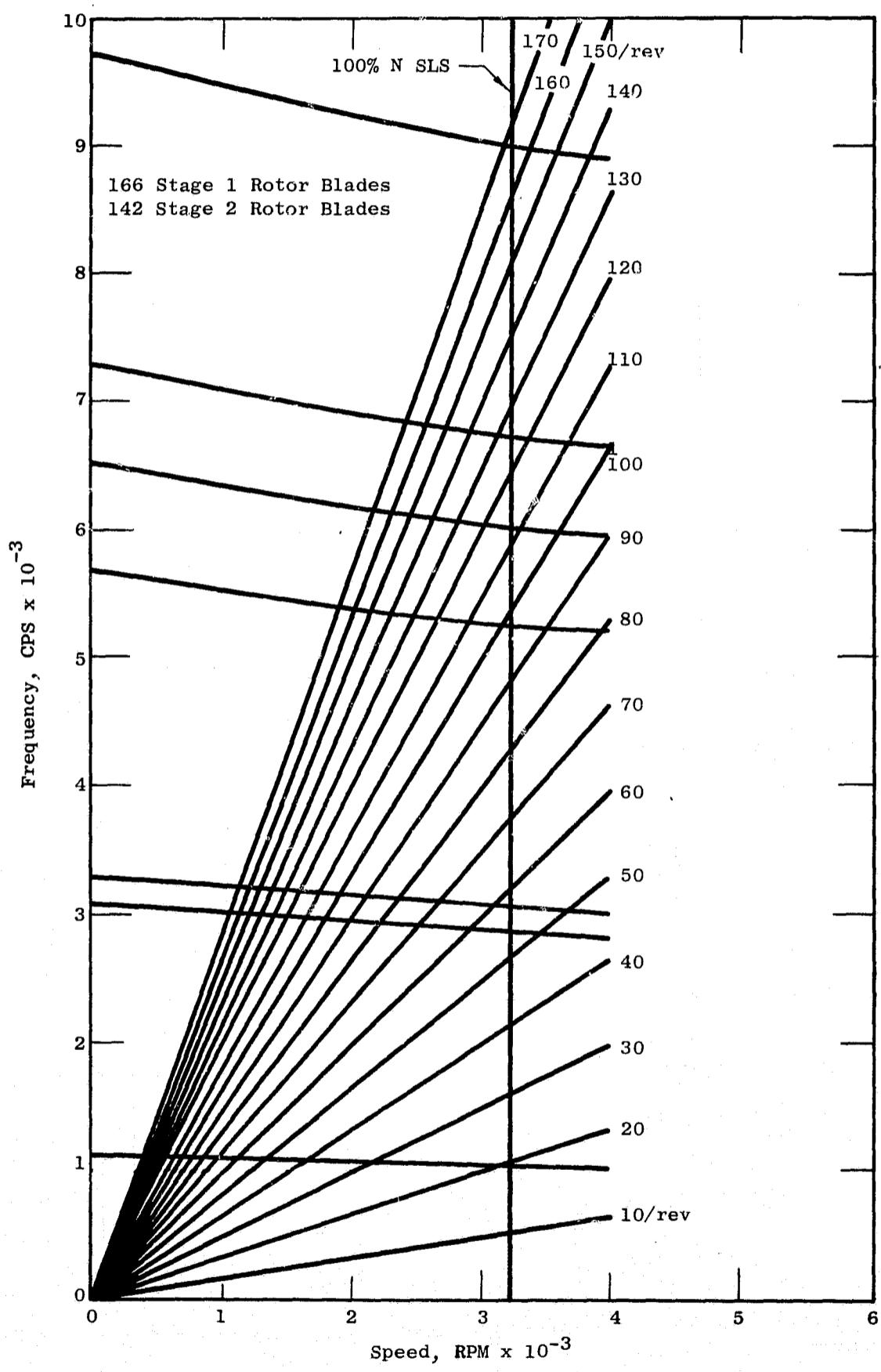


Figure 279. Campbell Diagram for the Fans A/B Stage 2 Vane, In-Phase Modes

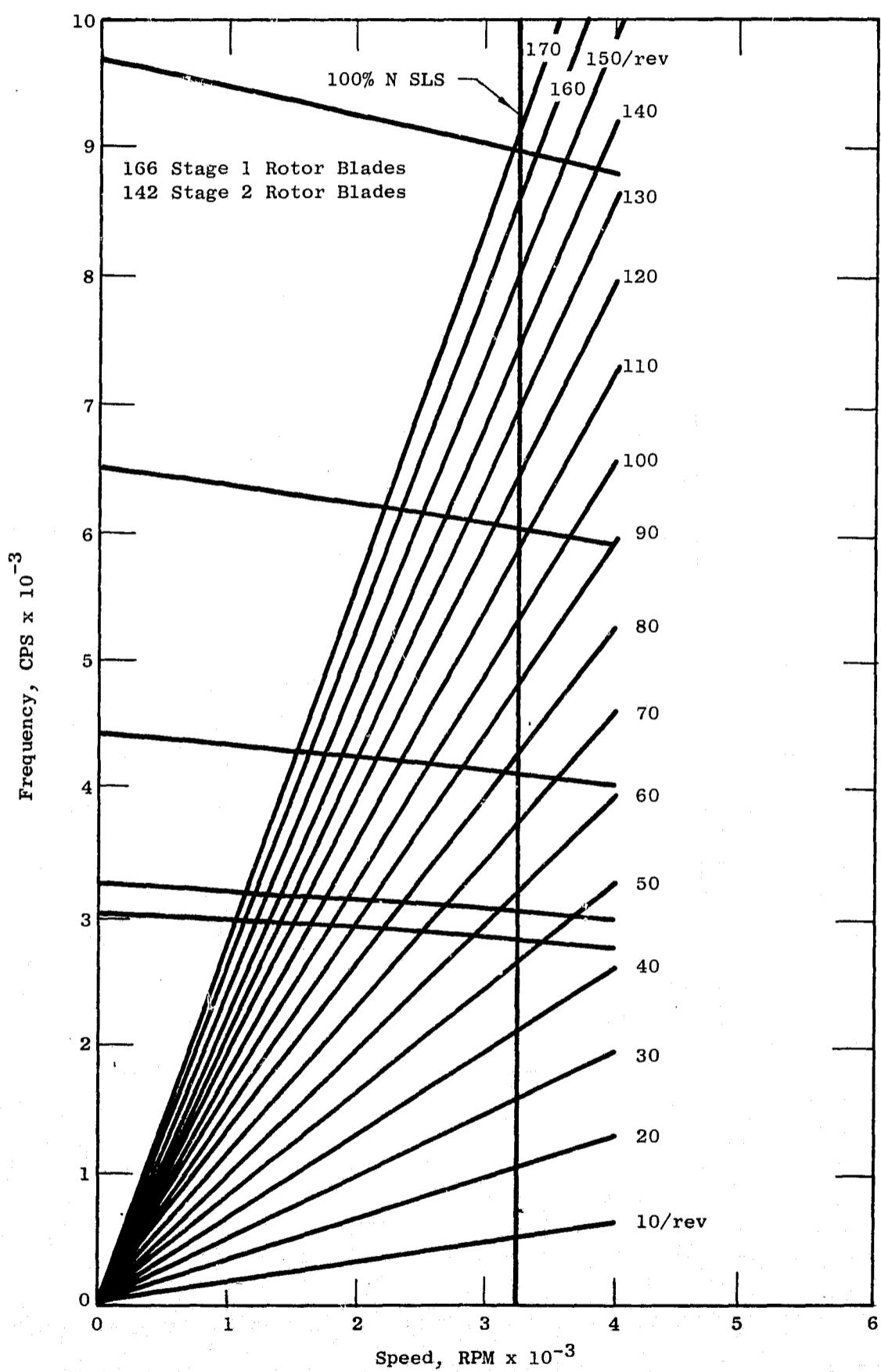


Figure 280. Campbell Diagram for the Fans A/B Stage 2 Vane, Out-of-Phase Modes

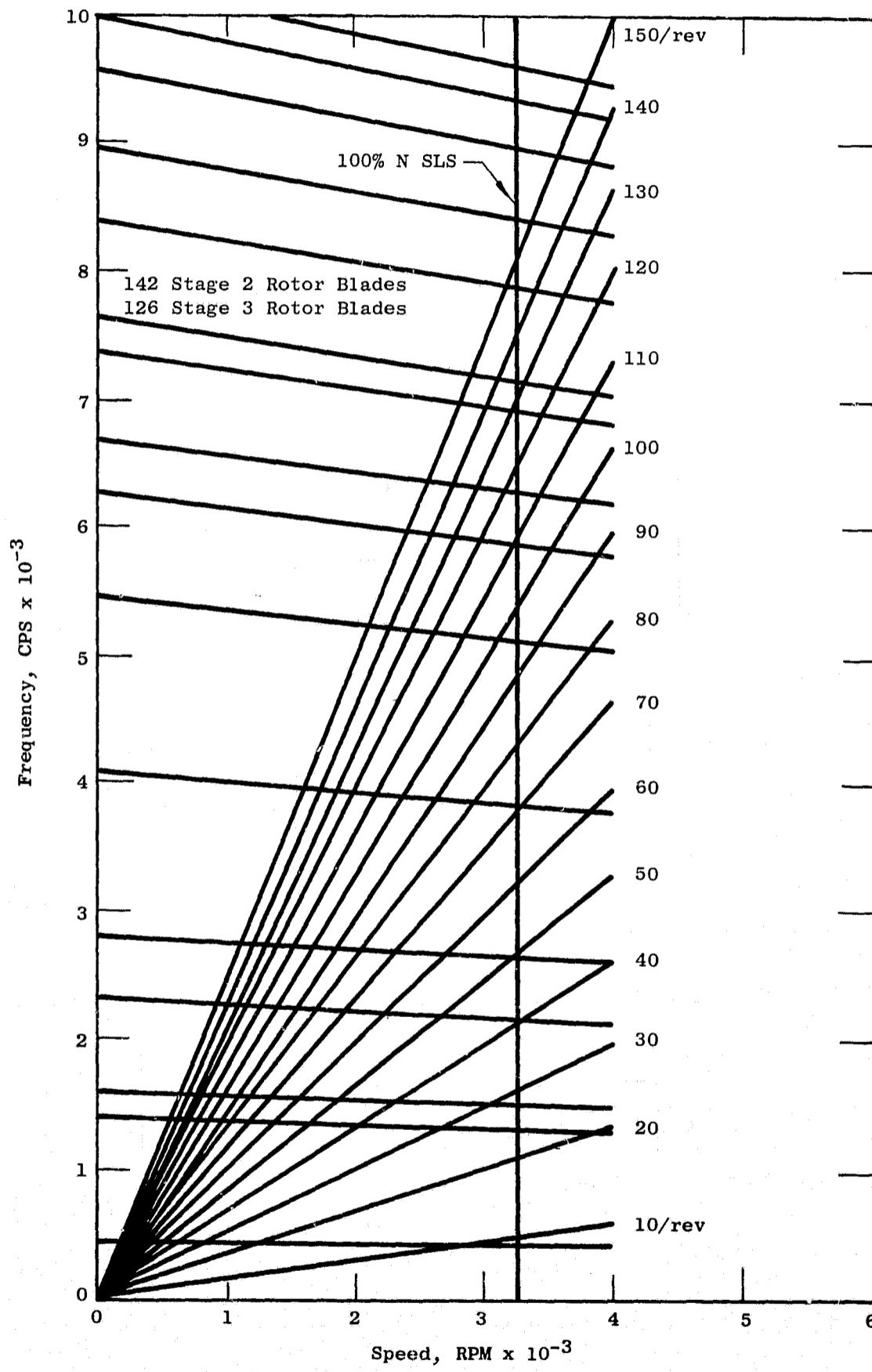


Figure 281. Campbell Diagram for the Fans A/B Stage 3 Vane, In-Phase Modes

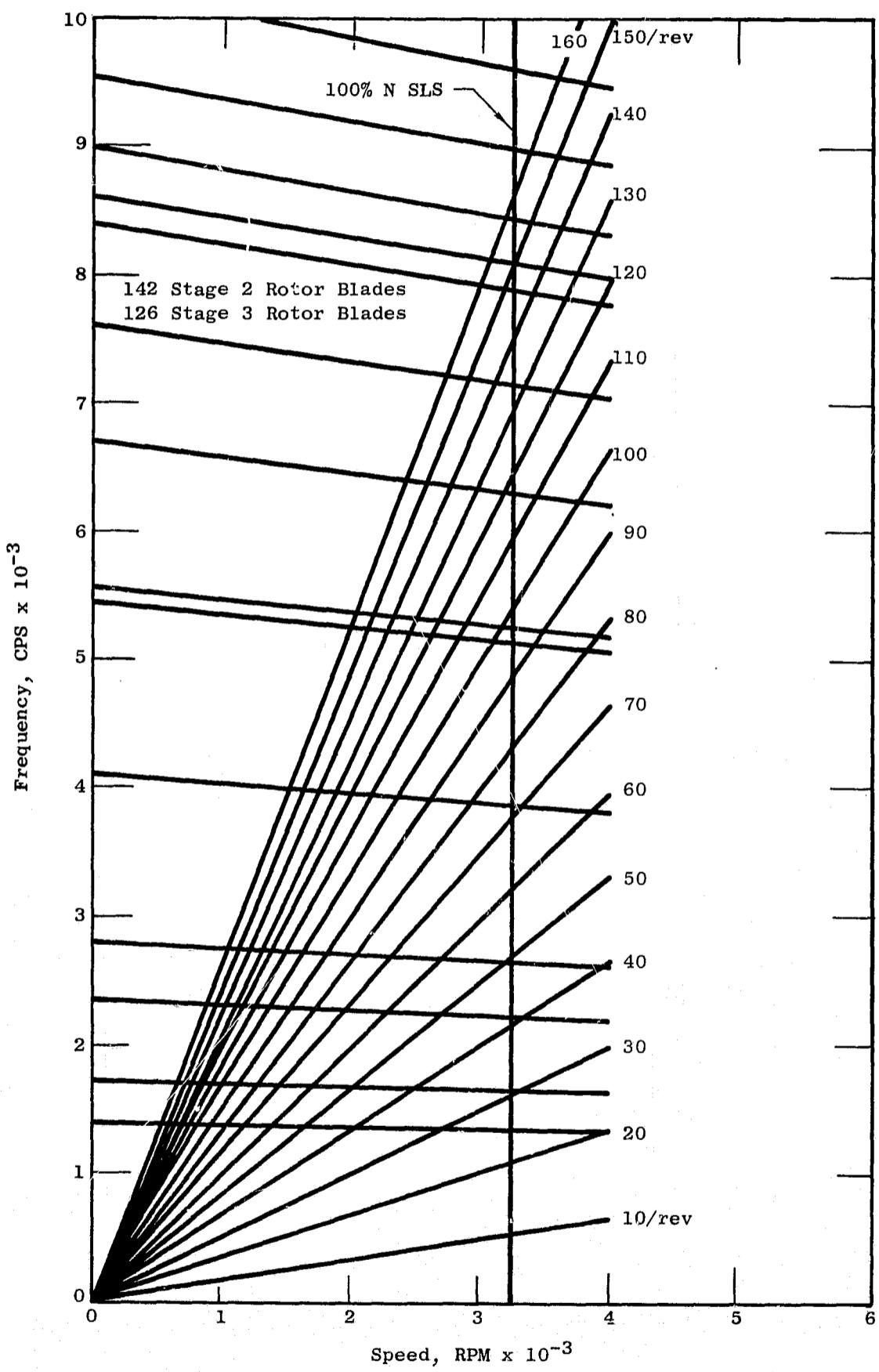


Figure 282. Campbell Diagram for the Fans A/B Stage 3 Vane, Out-of-Phase Modes

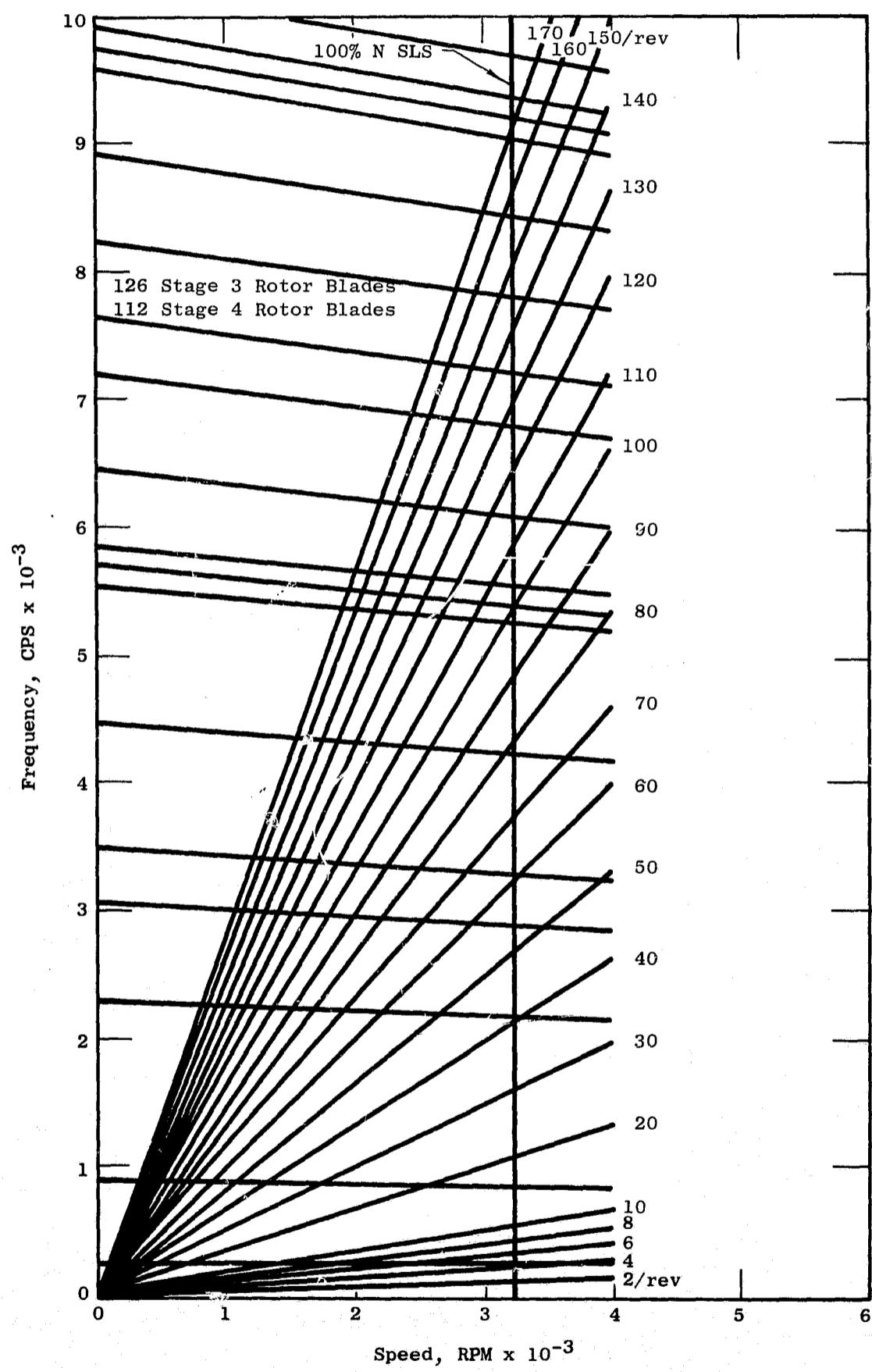


Figure 283. Campbell Diagram for the Fans A/B Stage 4 Vane, In-Phase Modes

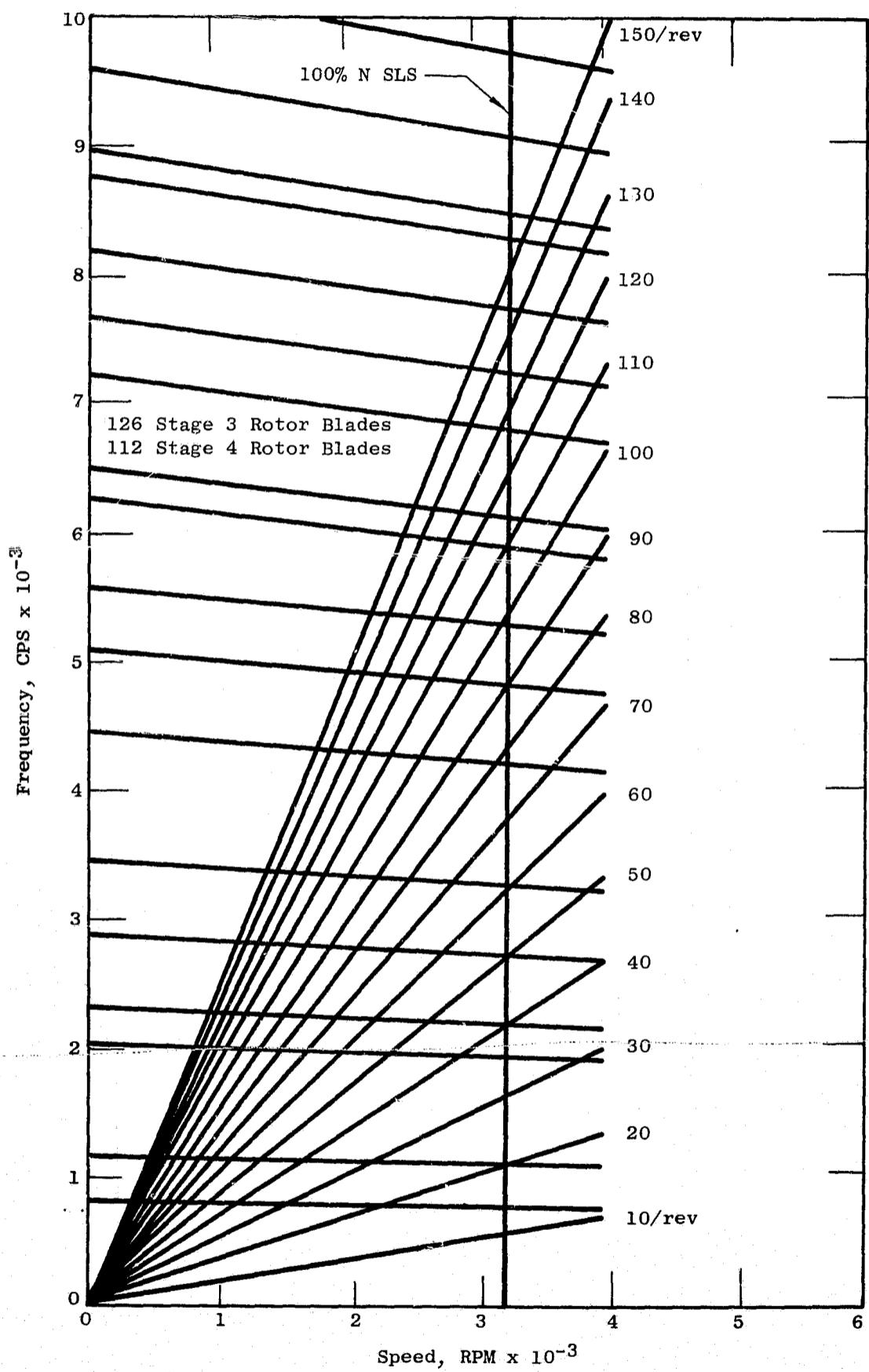
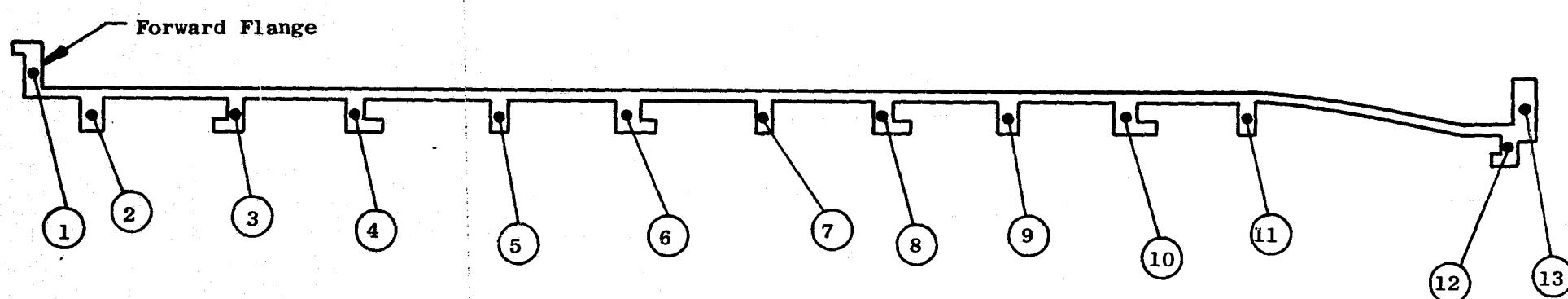


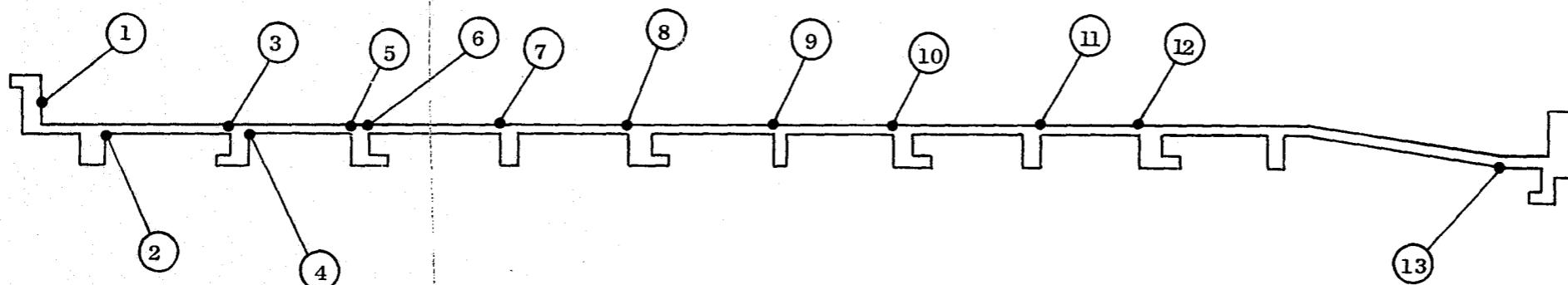
Figure 284. Campbell Diagram for the Fans A/B Stage 4 Vane, Out-of-Phase Modes

475



Location	Temperature (°F)
1	815
2	798
3	723
4	760
5	750
6	710
7	737
8	660
9	718
10	610
11	586
12	650
13	536

Figure 285. LP Turbine Casing Temperatures for Fans A and B



Location	Stress (PSI)
1	8,610
2	9,693
3	6,820
4	8,228
5	14,942
6	15,687
7	6,774
8	15,190
9	11,300
10	11,400
11	7,314
12	9,139
13	7,710

Figure 286. LP Turbine Casing Stresses for Fans A and B

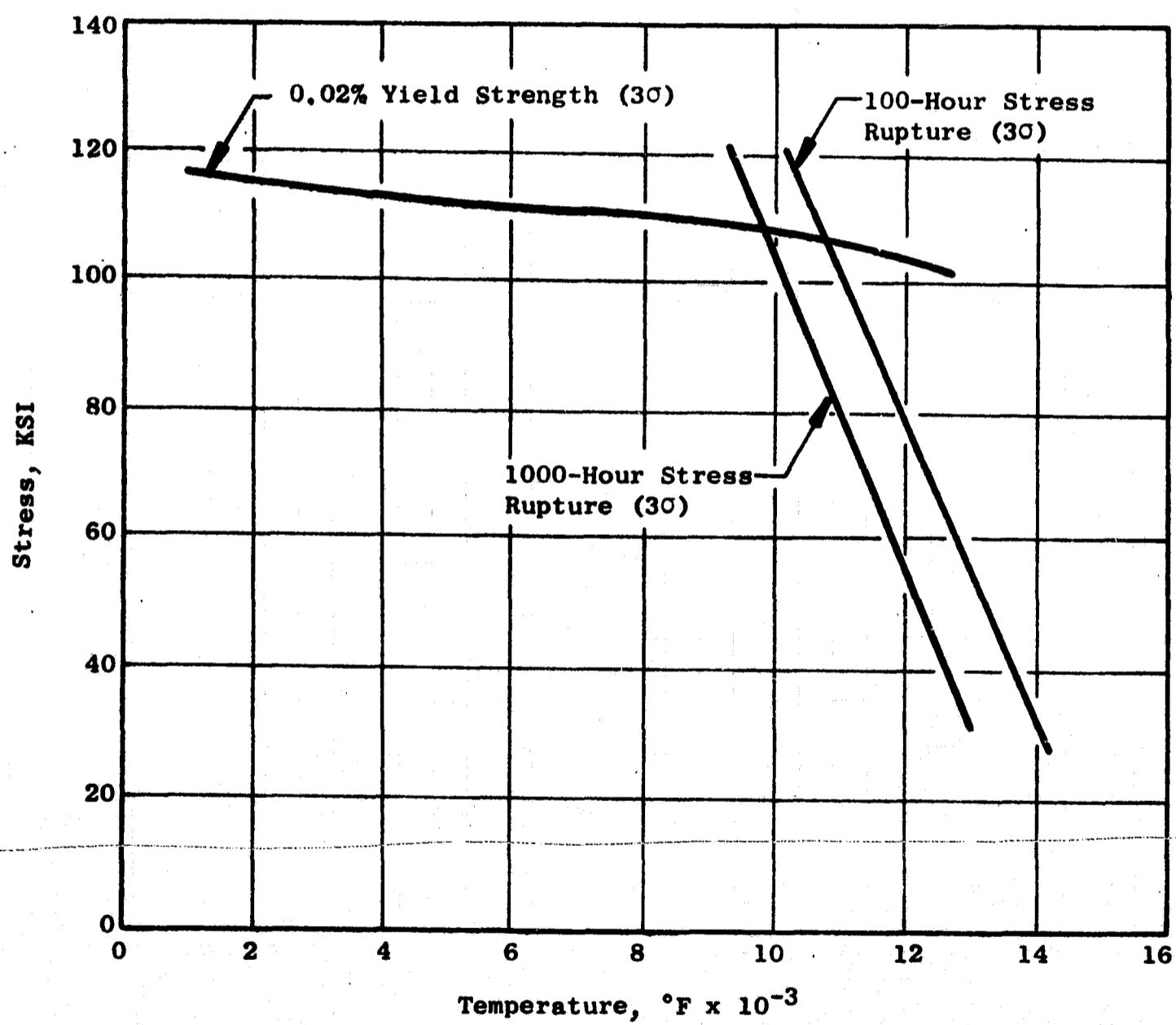


Figure 287. Forced Inconel 718 Material Properties

long-time running causes the shroud diameter to be over limits. Shrouds are prevented from moving tangentially during rubs by a tang on the shroud, which fits against a machined shoulder on the turbine nozzles.

Cold buildup radial blade tip clearances are:

<u>Stage</u>	<u>Nominal Cold Clearance, Inch</u>
1	0.030
2	0.038
3	0.049
4	0.039

Under throttle-burst conditions, blade seal teeth will rub into the honeycomb of the shrouds by 0.040 inch to 0.050 inch.

7.2.2.4 Interstage Seals

Interstage seals prevent leakage of the hot gas stream around the root end of the turbine nozzles. In construction, they are similar to the shrouds in that they are a brazed, honeycomb-type segment designed to absorb rubs from the rotor seal teeth during transients.

Pressures and temperatures at the seals are shown in Table LXXI.

Table LXXI. Seal Pressures and Temperatures, Fans A and B

Stage	Temperature, °F Fans A & B	Pressure Drop Across Seal, PSI
		Fans A & B
1	1000	12.0
2	900	7.4
3	815	4.7
4	755	3.0

A vibration analysis of the seals on a very conservative basis shows that there will be no resonance in the engine operating range. Figure 288 is a frequency response plot of the four stages of seals. Cold radial build-up clearance (nominal) is:

<u>Stage</u>	<u>Nominal Cold Clearance, Inch</u>
1	0.0175
2	0.009
3	0.030
4	0.020

7.2.2.5 Axial Clearances

Critical axial clearances for the cold buildup condition are shown on Figure 191 and are listed in Table LXXII. In the hot-running condition, the turbine casing will move aft relative to the rotor. Clearance between the Stage 1 vane and turbine blade, for example, will decrease by 0.290 inch, while the clearances aft of this will be reduced progressively less.

Table LXXII. Fans A and B LP Turbine Stator Critical Axial Clearances

Number	Minimum	Maximum
J42	0.722	0.913
J43	0.169	0.297
J44	0.694	0.812
J45	0.171	0.282
J46	0.735	0.852
J47	0.188	0.274
J48	0.708	0.824
J49	0.176	0.278
J50	0.861	0.997
J54	0.677	0.863
J55	0.202	0.338
J56	0.735	0.876
J57	0.202	0.317
J58	0.800	0.920
J59	0.233	0.327
J60	0.729	0.862

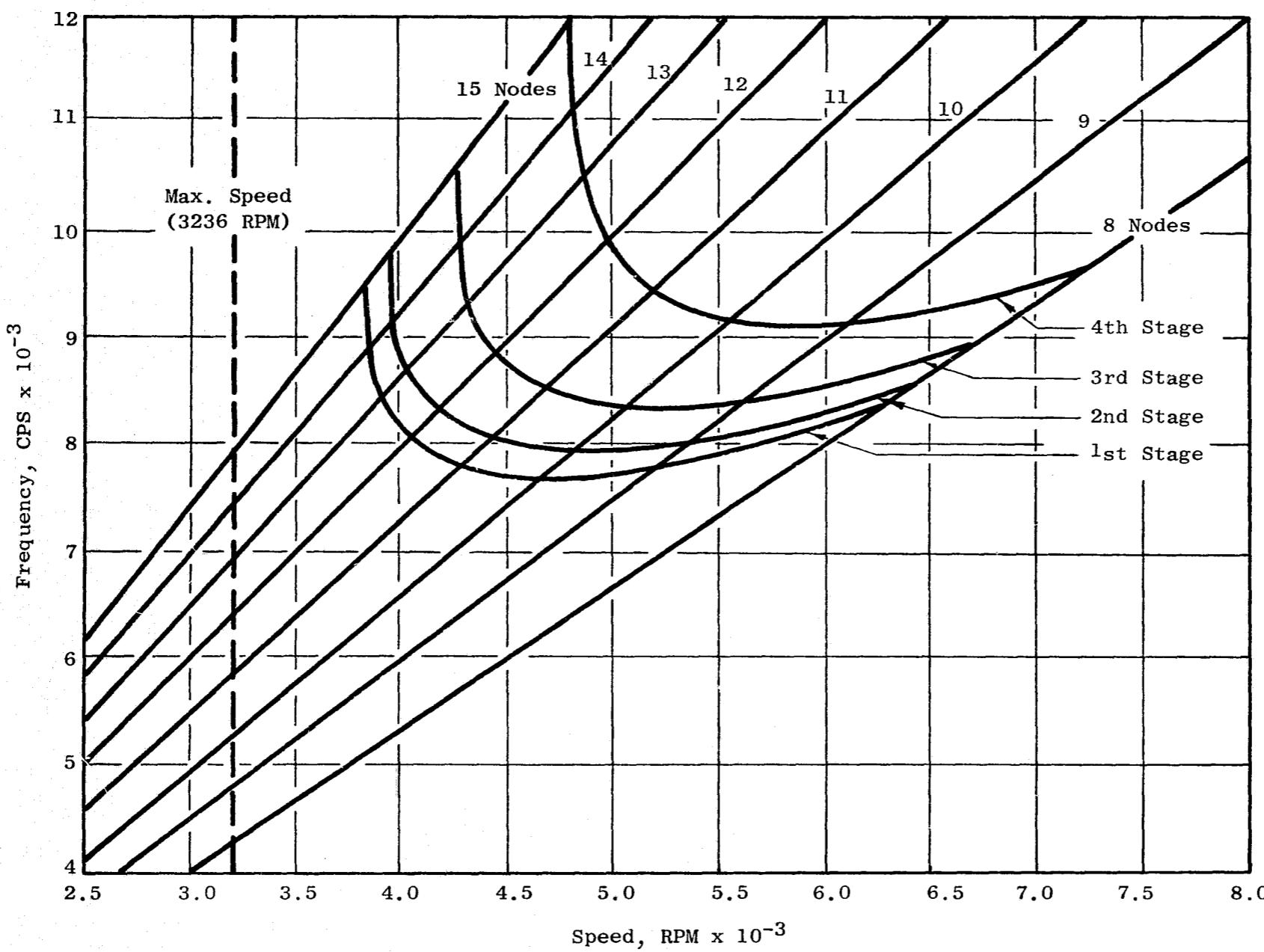


Figure 288. Vibration Analysis of Static Interstage Seals for LP Turbine Stages 1 through 4, Fans A and B

7.2.3 Turbine Stator, Fan C

The Fan C LP turbine stator consists of the turbine casing, the Stage 2 turbine nozzle (the Stage 1 turbine nozzle is an integral part of the midframe), Stage 1 and Stage 2 turbine shrouds, and the interstage seal (see Figure 244). Design data for the turbine stator is as follows and as shown on the flowpath drawing, Figure 289.

Stage 2 average inlet temperature	-	967°F
Stage 2 inlet total pressure	-	26.5 psia
Number of vanes, Stage 2 nozzle	-	120

The radial temperature profile entering the Stage 2 turbine nozzle is shown in Figure 290.

To provide a reliable and problem-free turbine stator, the type of design used successfully in the TF39 and CF6 engines was utilized. The same materials were also used, in order to benefit from the experience, learning curves, tooling, and manufacturing process development. Because of the lower temperature and to produce lower-cost components, a single purge-type cooling method is used for the casing.

7.2.3.1 Turbine Nozzle, Stage 2

The Stage 2 turbine nozzle is assembled from 6-vane, precision-investment-cast segments of Rene' 80 material. Segments are accurately machined to achieve a close fit where they are supported from the rails of the turbine casing. Thermal expansion requires gaps between segments. The gaps are sealed against leakage during reduced-power conditions, by thin sheet metal seals which slide into slots in the vane segments of the extremities of the outer band. The tangential load stop is the TF39-type design which uses off-the-shelf hardware. Figure 291 shows enlarged sectional views through the stop. The axial view shows how the Stage 2 shroud supports the aft leg of the turbine nozzle during assembly and until the gas load is applied.

The material selected for the vane castings is Rene' 80. Although the temperature capability of Rene' 80 is well above that required for this application; the good casting qualities, the extensive experience that vendors have with it, and the availability of the alloy, were main factors considered for the material selection.

Gas-load stresses on the vane, which are shown in Figure 292, were determined by means of the Twisted Blade Computer Program. Thermal stress is induced during a transient which produces a maximum temperature difference of 324 degrees between the vane trailing edge and the convex side. The temperature gradient was determined (as in the case of the Fan A and B vane) based on TF39 testing. A maximum stress summary (trailing edge) is as follows:

289

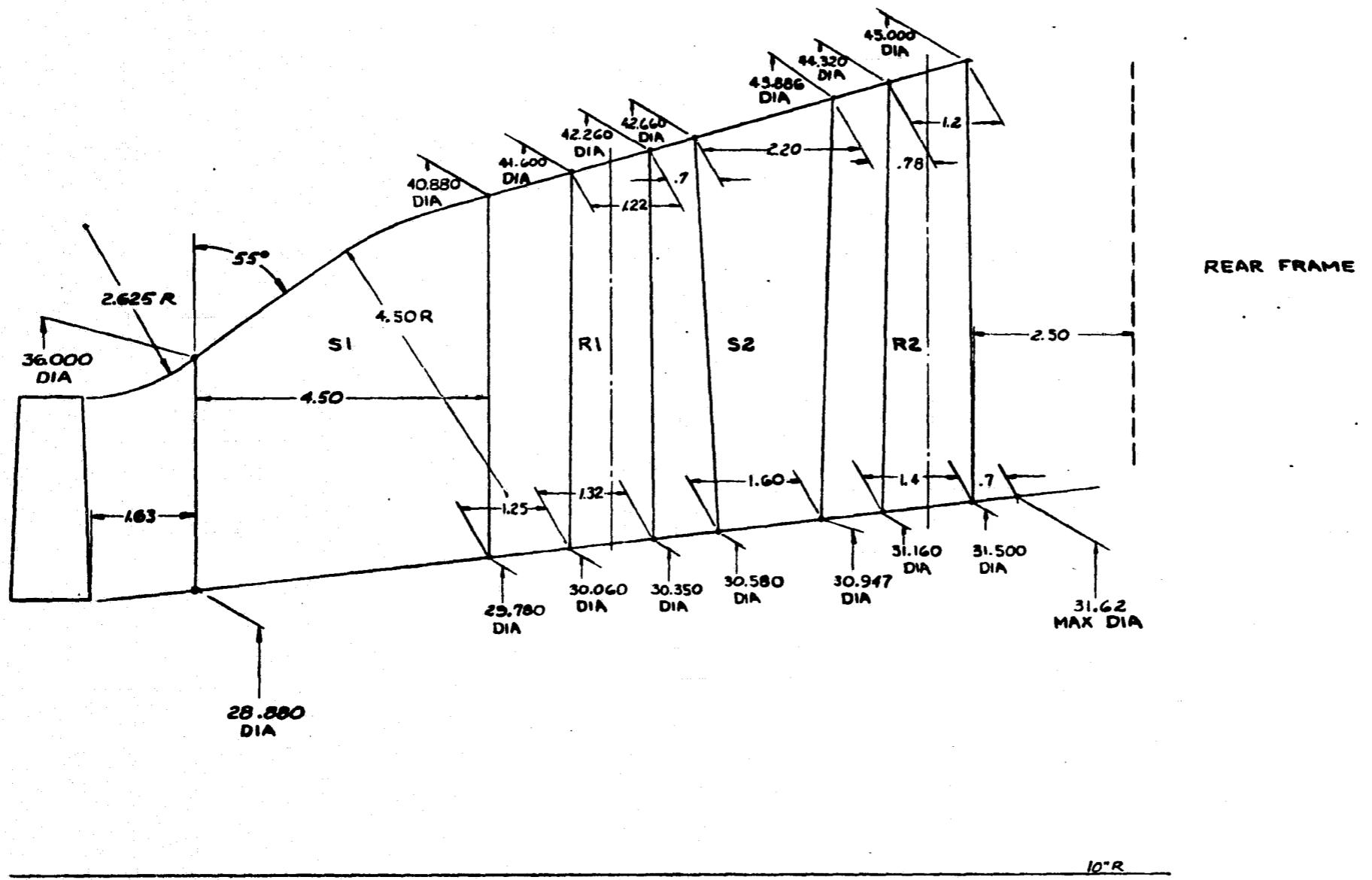


Figure 289. Flowpath, Fan C Low Pressure Turbine

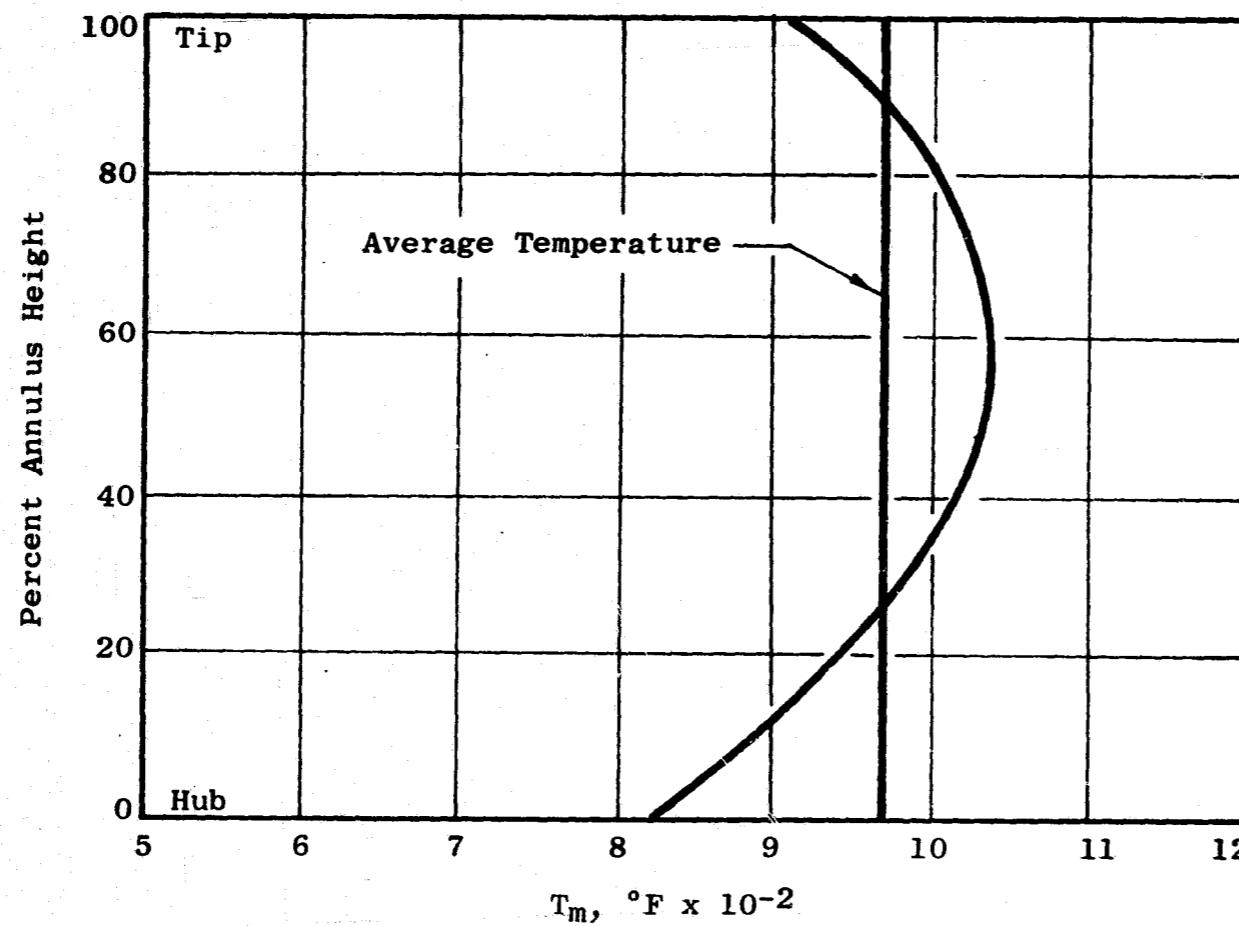
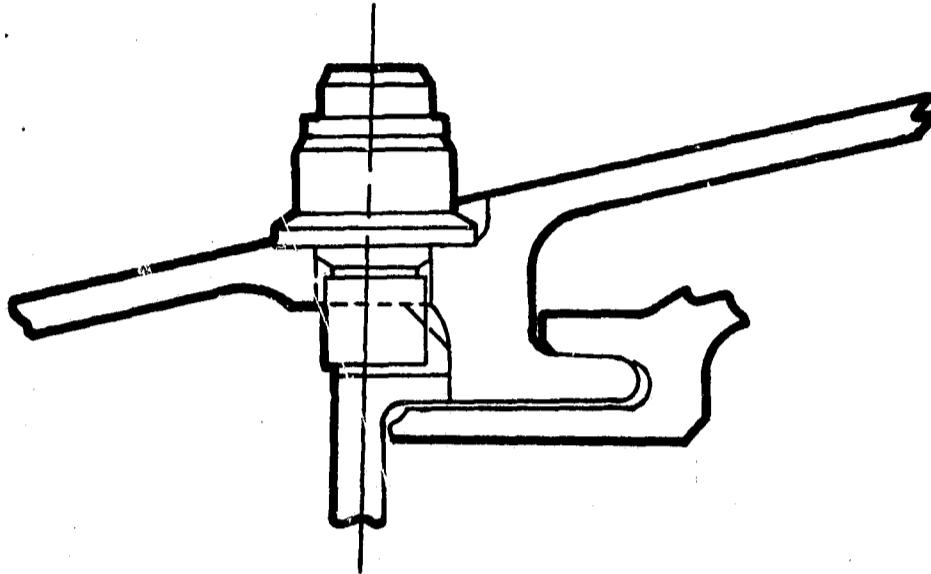
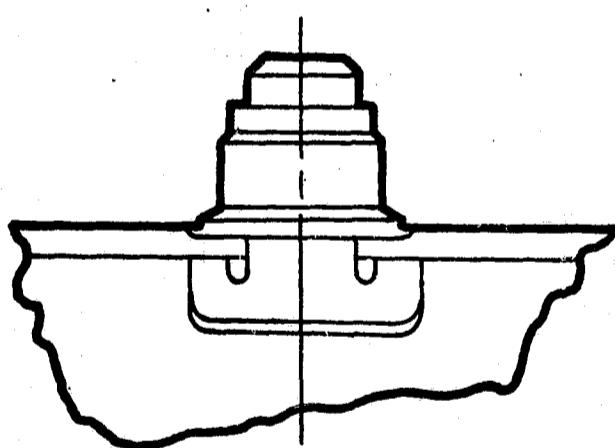


Figure 290. Radial Temperature Profile for the Fan C Low Pressure
Turbine Stage 2 Vane, Inlet Temperature



Axial View



Circumferential View

**Figure 291. Tangential Load Stop for the Fan C
LP Turbine Stage 2 Vane**

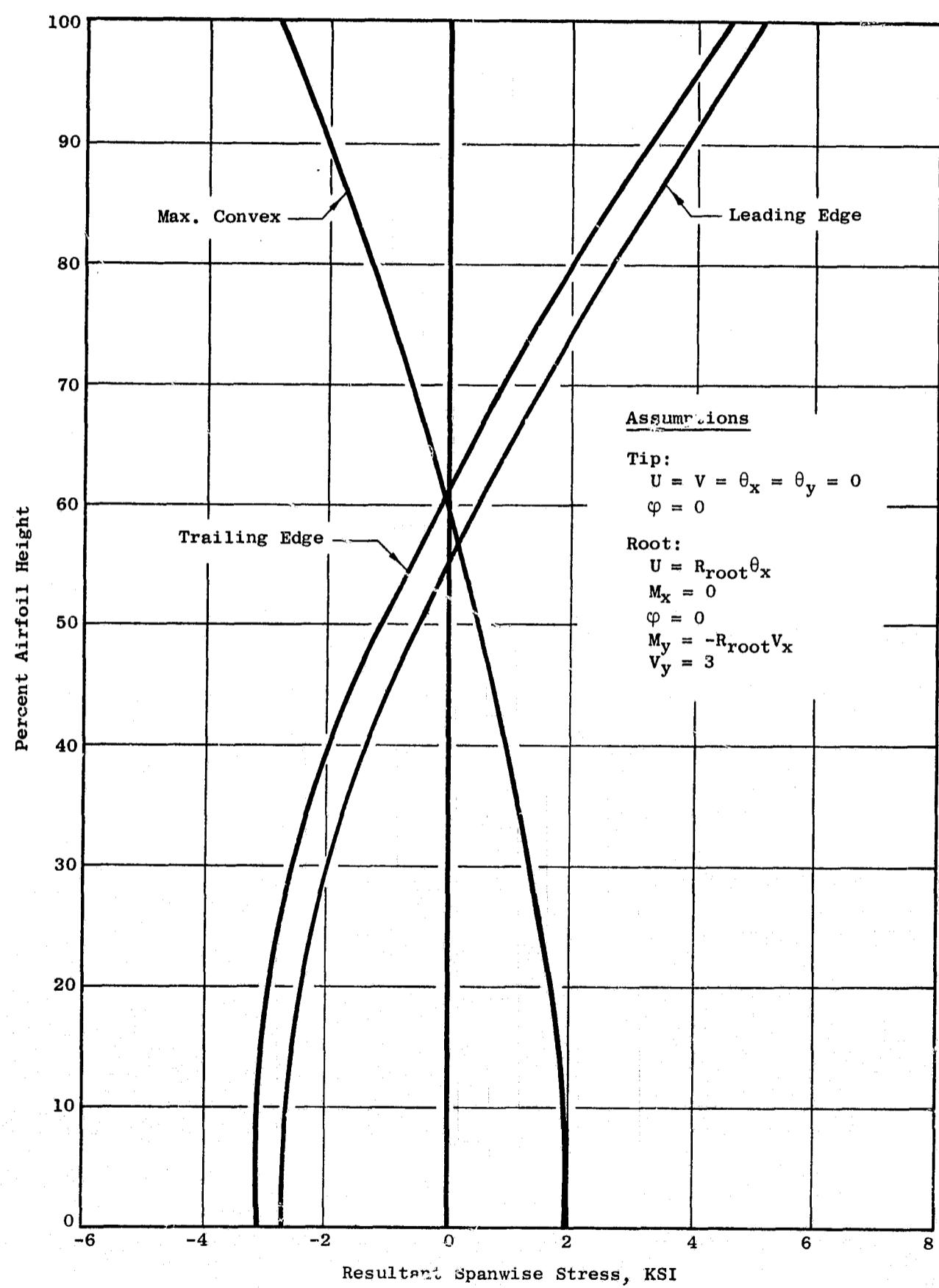


Figure 292. Fan C Stage 2 Vane, Gas Load Stresses

Gas load stress	-	4,500 psi
Thermal stress	-	34,800 psi
Total stress	-	39,300 psi
0.2% creep life	-	Infinite

A vibration analysis of the turbine vanes was made for both the in-phase and the out-of-phase modes. The Campbell diagrams (see Figures 293 and 294) show that there is no resonance with the passing frequency of the 118 Stage-1 rotor blades, or the 130 Stage-2 rotor blades.

7.2.3.2 Turbine Casing

The LP turbine casing is machined from an Inconel 718 forging. It is a two-piece design, split in two halves on the horizontal centerline. The horizontal flanges which are welded to each half are aligned relative to each other by means of body-bound bolts. As in the case of the Fan A and B casing, cooling air ports and a boroscope port are included in the casing.

Metal temperatures of the flanges and rails are shown in Figure 295. The SNAP Computer Program was used to determine stresses in the casing; strategic maximum stresses are shown in Figure 296. Allowable stresses for the Inconel 718 casing material are shown in Figure 287. The low temperature of the casing results in the 0.02 percent yield strength being the limiting criteria.

7.2.3.3 Turbine Shrouds

The Stage 1 and Stage 2 turbine shrouds are Hastelloy-X segments which are supported from the rails of the casing. Honeycomb is brazed to the side that faces the turbine blades, in order to form a wearing surface for the seal teeth of the blades. While the cold buildup clearance between seal teeth and shrouds is 0.020 inch, transient conditions can cause the blade teeth to rub into the honeycomb to a maximum depth of 0.044 inch. Small-cell honeycomb (1/16 inch) is used to provide effective sealing. To create minimum resistance to a rub, however, the stock thickness of the honeycomb is small (0.0025/0.004 inch).

To position the shrouds, and to prevent tangential motion during a rub, a tang on the Stage 1 shroud fits against a shoulder which is machined into the aft leg of the turbine nozzle (see Figure 297). The tang of the Stage 2 shroud rests against a similar shoulder on the aft rail of the turbine casing.

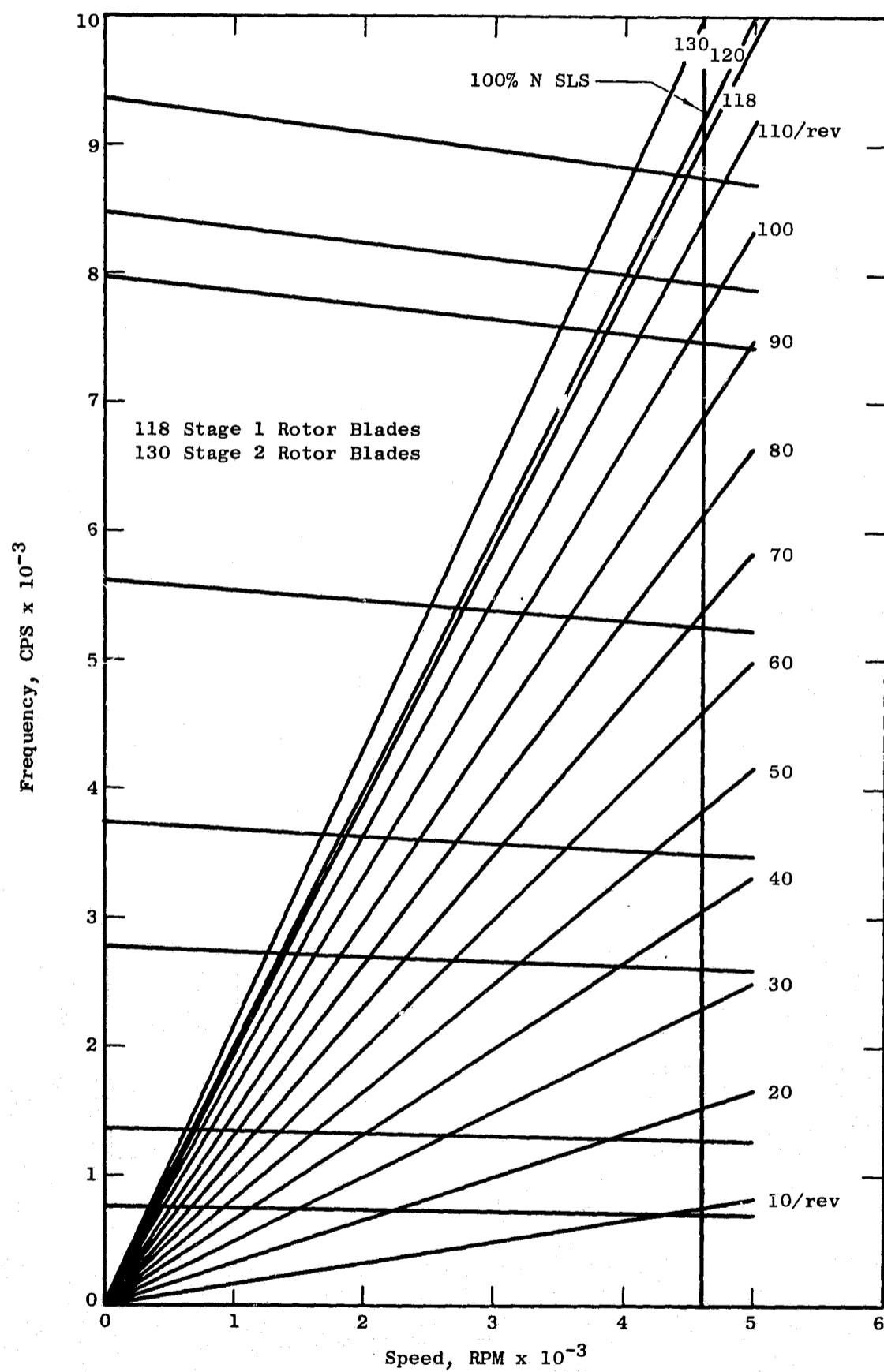


Figure 293. Campbell Diagram for the Fan C Stage 2 Vane, In-Phase Modes

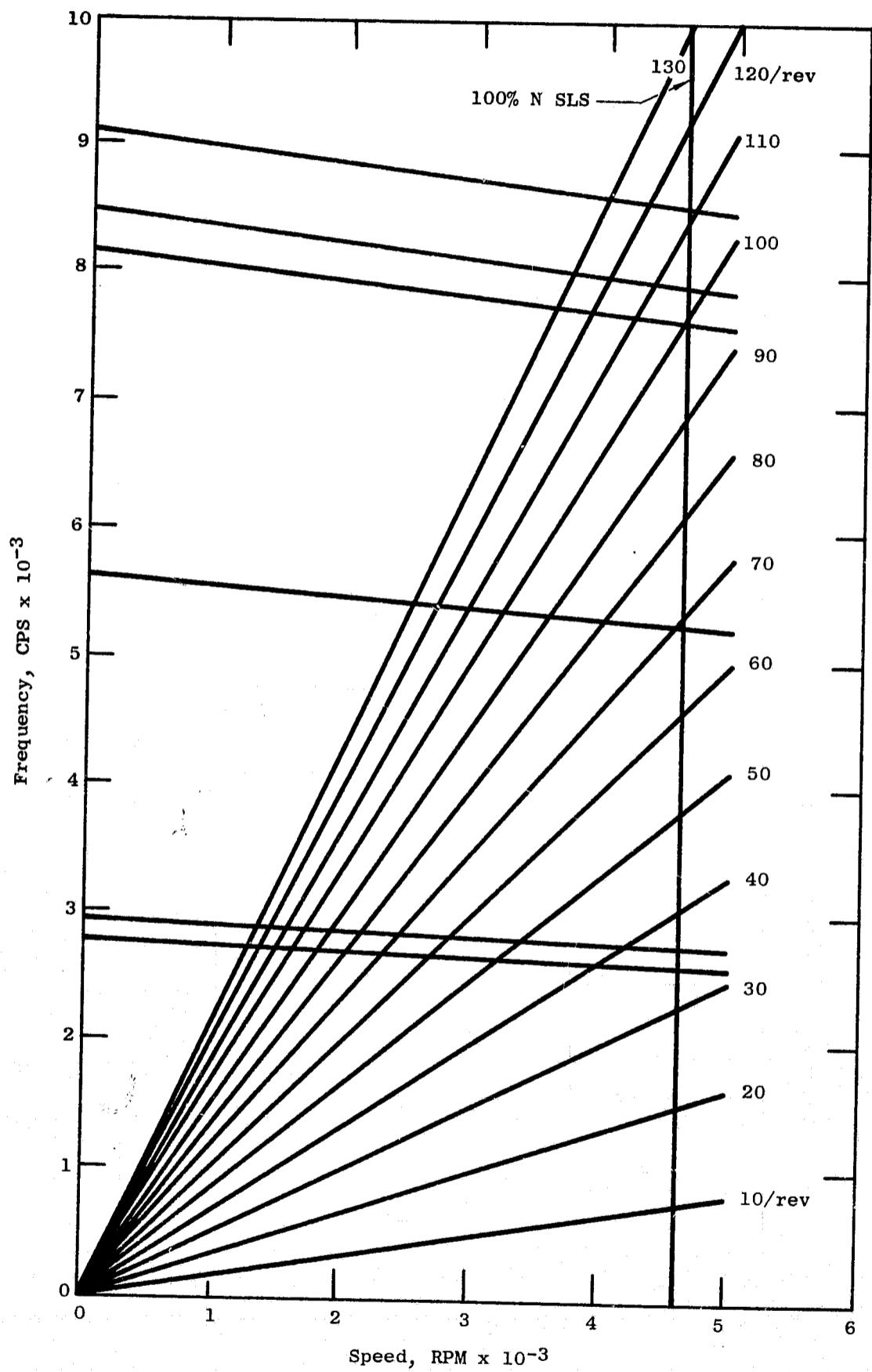
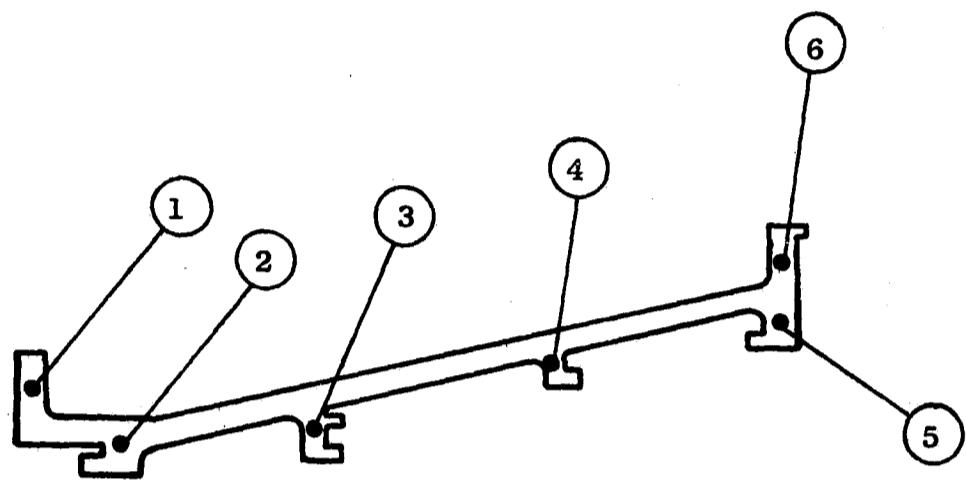
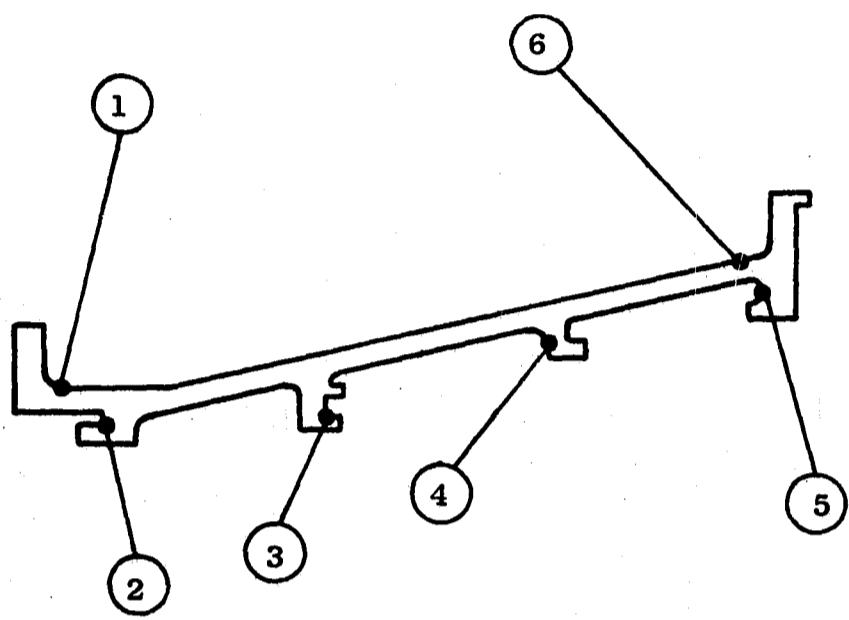


Figure 294. Campbell Diagram for the Fan C Stage 2 Vane, Out-of-Phase Modes



Location	Temperature (°F)
1	750
2	910
3	858
4	855
5	750
6	747

Figure 295. Turbine Casing Metal Temperatures for the Fan C Low Pressure Turbine



<u>Location</u>	<u>Stress (PSI)</u>
1	7,410
2	3,160
3	9,440
4	328
5	629
6	5,490

**Figure 296. Turbine Casing Maximum Stresses
for the Fan C Low Pressure Turbine**

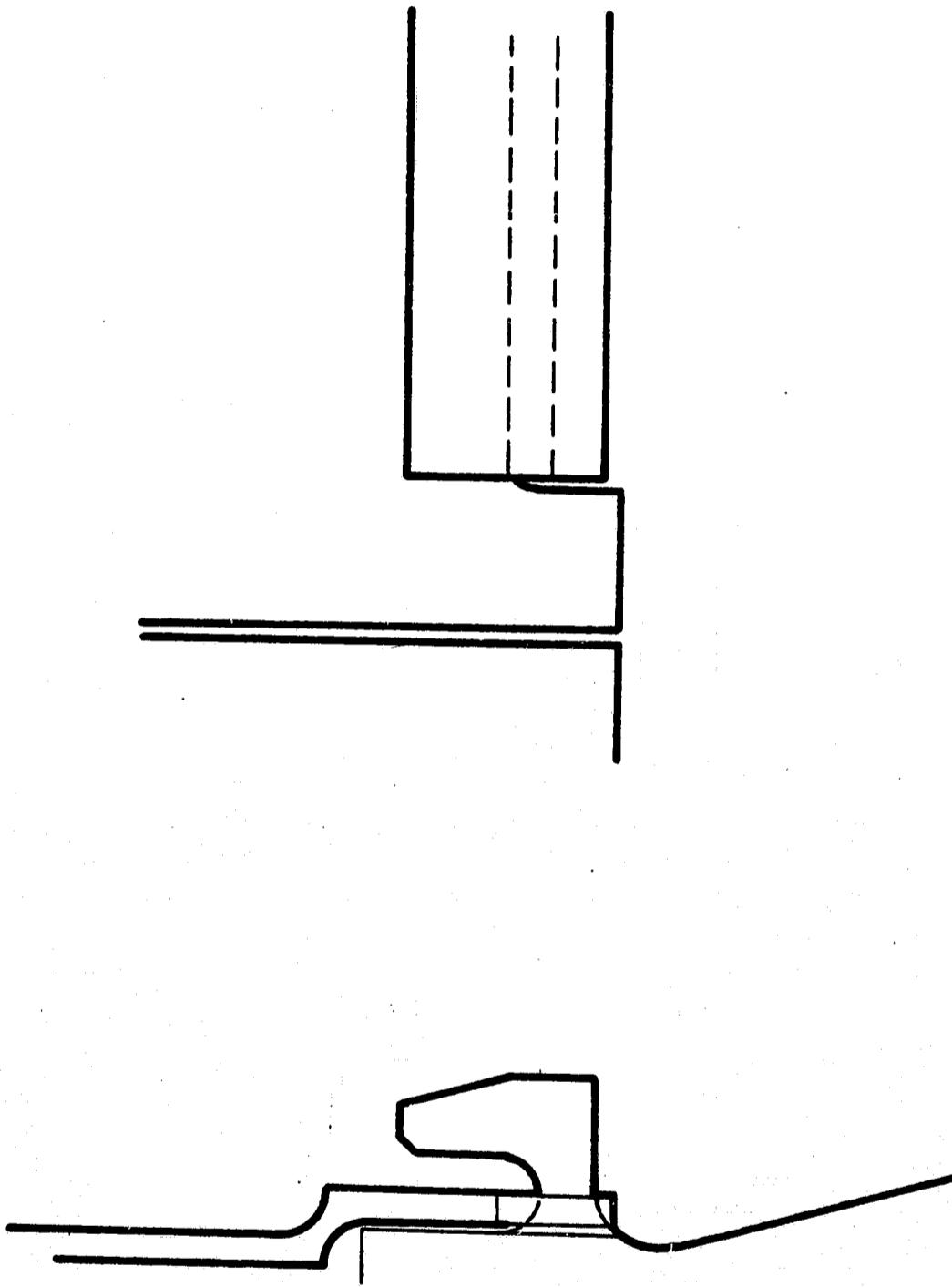


Figure 297. Tangential Load Stop for the Fan C LP Turbine Stage 1 Shroud

Shroud nominal radial clearances, with respect to the blade seal teeth, are shown in Table LXXIII.

Table LXXIII. Fan C Shroud Nominal Radial Clearances

Clearance	Stage 1		Stage 2	
	Fwd Tooth	Aft Tooth	Fwd Tooth	Aft Tooth
Cold Buildup	0.020	0.020	0.020	0.020
Steady State	-0.019	-0.030	-0.012	-0.025
During Accel	-0.041	-0.044	-0.031	-0.036
During Decel	0.046	0.034	0.040	0.027

Note: negative values indicate rubs

7.2.3.4 Interstage Seal

The function of the interstage seal is to prevent or minimize hot-gas flow in the cavity below the 2nd stage turbine nozzle. Similar to the shrouds, the seal is made in segments with honeycomb brazed to the inner surface. The segments are bolted to the inner band flange of the turbine nozzle, so that one seal segment spans two nozzle segments. Design data for the seal are as follows:

Maximum temperature	967°F
Pressure difference across seal	4 psi
Material	Hastelloy X
Seal leakage	0.80 lb/sec

Seal nominal radial clearances, with respect to the rotor seal teeth, are as follows:

Condition	Clearance
Cold buildup	0.020
Steady state	-0.014
During accel	-0.037
During decel	0.044

A vibration analysis was made for the seal which is extremely conservative. It was assumed that the seal is a fully-annular, 360-degree ring (instead of its actual configuration of 10 individual segments). On this basis, and using the traveling-wave criteria reported by J.S. Alford in ASME Paper No. 63-AHGT-9 (Protection of Labyrinth Seals from Flexural Vibration), the Campbell diagram of Figure 298 was plotted. Even on this highly conservative assumption, there would be no resonance with the speed of the rotor.

7.3 LOW PRESSURE TURBINE FRAME AND EXHAUST NOZZLE DESIGN

7.3.1 Summary

The Experimental Quiet Engine has two low pressure turbine support structures, or frames, and one exhaust nozzle for engine Configuration A and B and engine Configuration C. The functions of these structures are:

- a) Turbine Midframe - includes the rear main engine mount, provides support for the rear of the high pressure turbine rotor and the front of the low pressure turbine rotor, provides an aerodynamic flowpath transition between the high and low pressure turbines, supports the low pressure turbine casing, provides piping for lubrication and pressurization for the C-sump, and contains access ports for inspection of the low pressure turbine inlet.
- b) Turbine Rear Frame - provides support for the rear of the low pressure turbine rotor, primary stream exhaust nozzle and plug, supports the instrumentation slip ring assembly, and provides lead-out passages for the slip ring assembly and cooling air.
- c) Exhaust Nozzle - provides an accelerating flowpath for the low pressure turbine exhaust gases.

The low pressure turbine frames and exhaust nozzles are either CF6 components or are new components designed in accordance with CF6 design practices. Loads and temperatures imposed on these frames and nozzles are equal to or less than CF6 loads and temperatures.

7.3.1.1 Material Selection, Frames and Exhaust Nozzles

Table LXXIV lists the materials selected for the frames and exhaust nozzles of the Experimental Quiet Engine designs and compares these materials with those used in the equivalent CF6 structures.

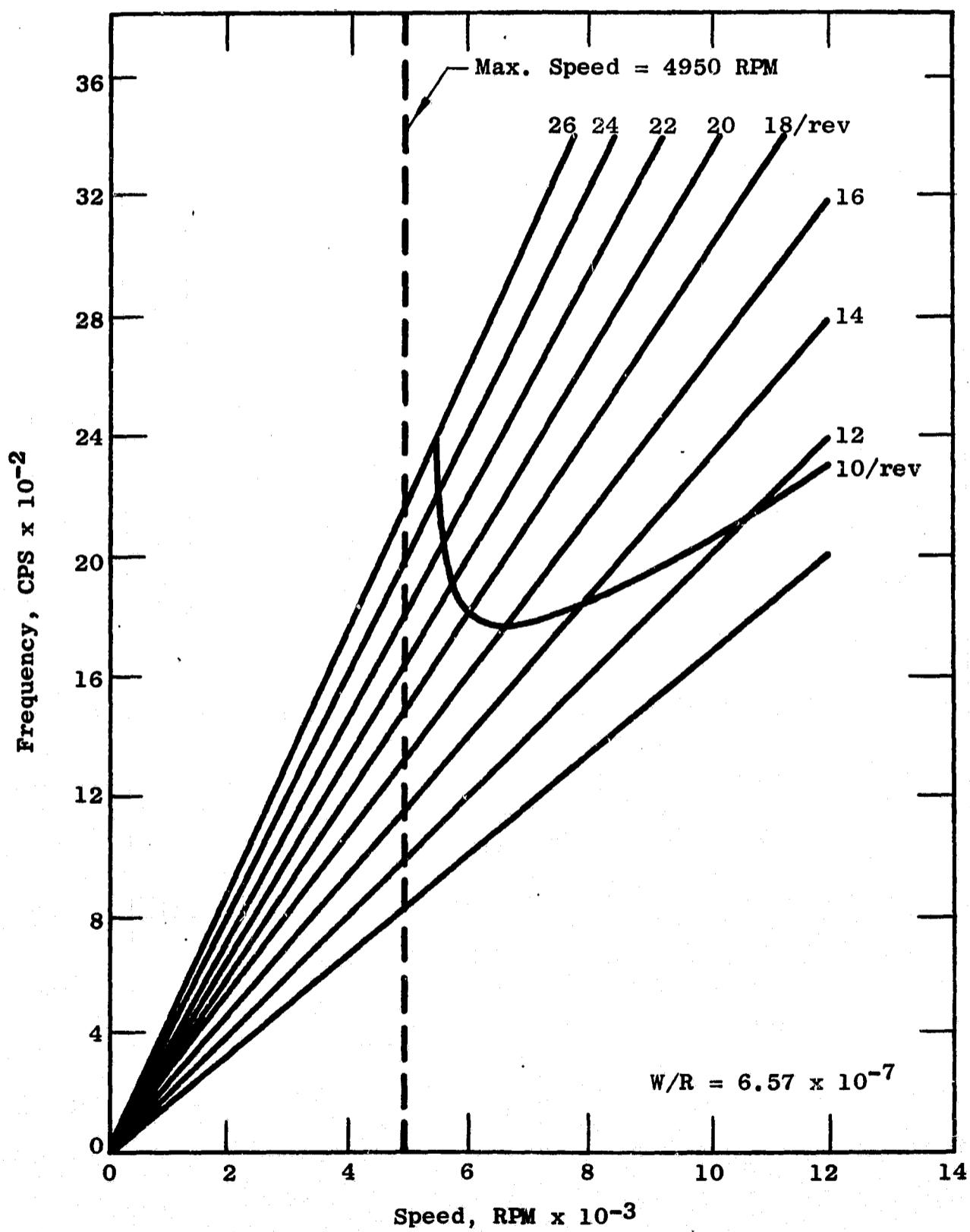


Figure 298. Vibration Analysis of the Stage 2 Seal for the Fan C LP Turbine

Table LXXIV. Material Selection for Turbine Frames and Exhaust Nozzles

Component	Configuration		
	CF6	A and B	C
<u>Turbine Midframe</u>			
Casing	Inco 718	Inco 718	A-286
Aft Outer Ring	---	---	A-286
Strut	R-41	R-41	R-41
Hub Ring	Inco 718	Inco 718	Inco 718
Sump	17-4PH	17-4PH	17-4PH
Liner	Hast X	Hast X	Integral with Strut
Nozzle Support	Inco 718 and R-41	Inco 718 and R-41	---
Bearing Cone	---	---	Inco 718
Seals	---	---	Hast X
Tubes	321 Stainless	321 Stainless	321 Stainless
<u>Turbine Rear Frame</u>			
Frame Structure	Inco 718	Inco 718	Inco 718
Flowpaths	Hast X	Hast X	Hast X
Sumps	17-4PH	17-4PH	17-4PH
Nozzle Support Cone	Inco 718	Inco 718	Inco 718
<u>Exhaust Nozzle</u>			
Outer Flowpath	Hastelloy X	Hastelloy X	Hastelloy X
Inner Flowpath	Hastelloy X	Hastelloy X	Hastelloy X
Support Cones	Hastelloy X	Hastelloy X	Hastelloy X

7.3.1.2 Engine A/B Frame and Nozzle Design

Engine A/B uses an off-the-shelf CF6 turbine midframe and a CF6 turbine rear frame structure with a new rear frame flowpath and exhaust nozzle. These designs are shown in Figures 299 and 300.

7.3.1.2.1 Engine A/B Midframe Design

The turbine midframe design features for A/B are shown in Figures 301 and 302. A similar midframe is used on the TF39 engine. The difference between the frame designs is that the TF39 has a thrust mount on the frame casing vertical centerline, while the A/B frame has a mount for engine side loads at this location.

7.3.1.2.2 Engine A/B Rear Frame Design

The turbine rear frame for Engine A/B is shown in Figure 303. The frame is a CF6 structure with a new Hastelloy-X inner flowpath. Like the A/B midframe, this structure is similar to the TF39 frame (the differences being flowpath and strut chord length). The A/B frame strut chord is four inches vs a six-inch strut chord for the TF39.

7.3.1.2.3 Engine A/B Exhaust Nozzle Design

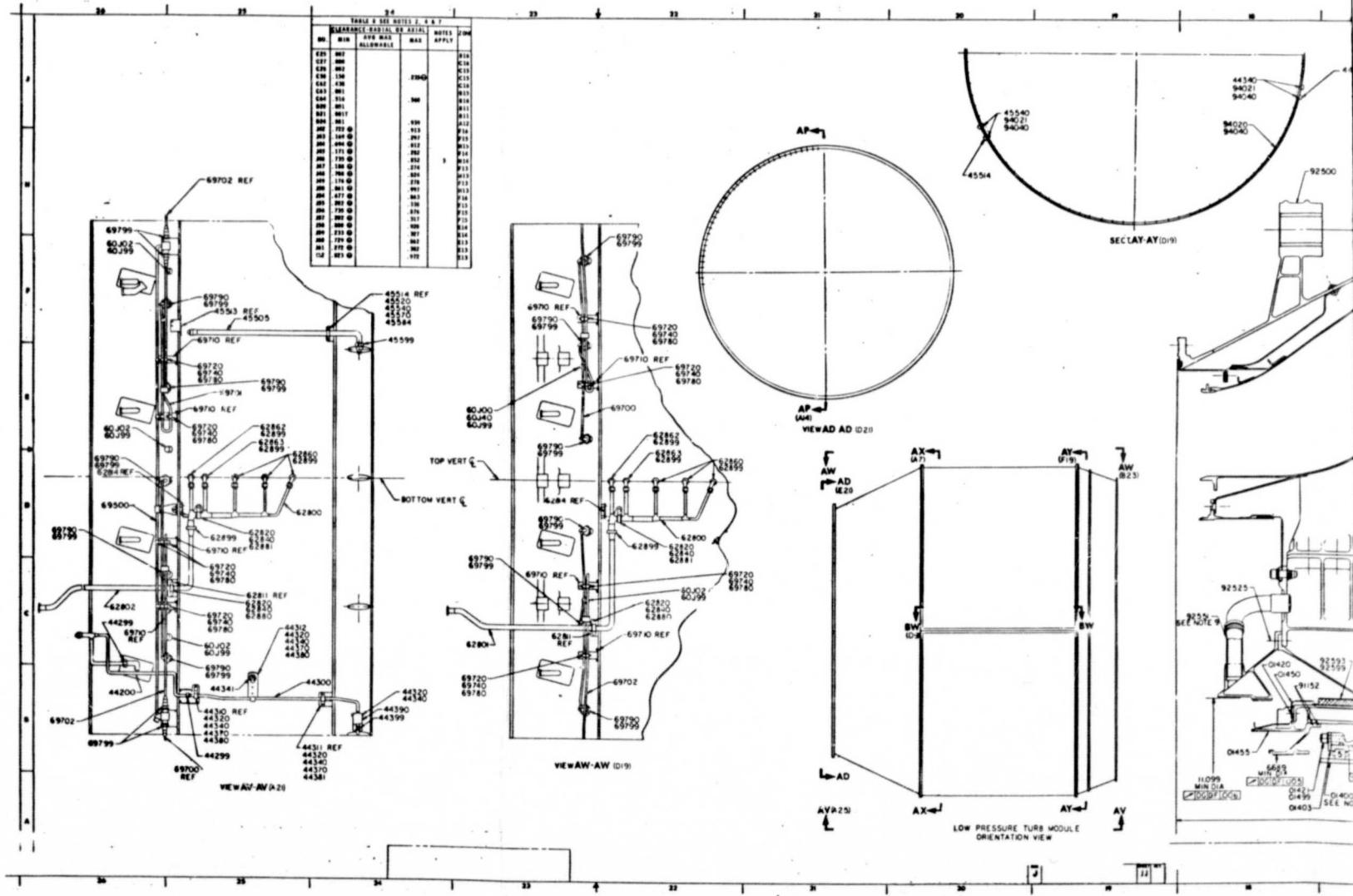
The exhaust nozzle design for engine A/B is a simple Hastelloy X shell-type convergent nozzle similar to the CF6 design. Hastelloy X was selected for the nozzle material because of its corrosion resistance and thermal expansion compatibility with the turbine rear frame.

7.3.1.3 Engine C Turbine Frame and Exhaust Nozzle Design

Engine C uses a newly designed turbine midframe and a rear frame and exhaust nozzle similar in configuration to the A/B rear frame and exhaust nozzle. These designs are shown in Figure 304.

7.3.1.3.1 Engine C Turbine Midframe Design

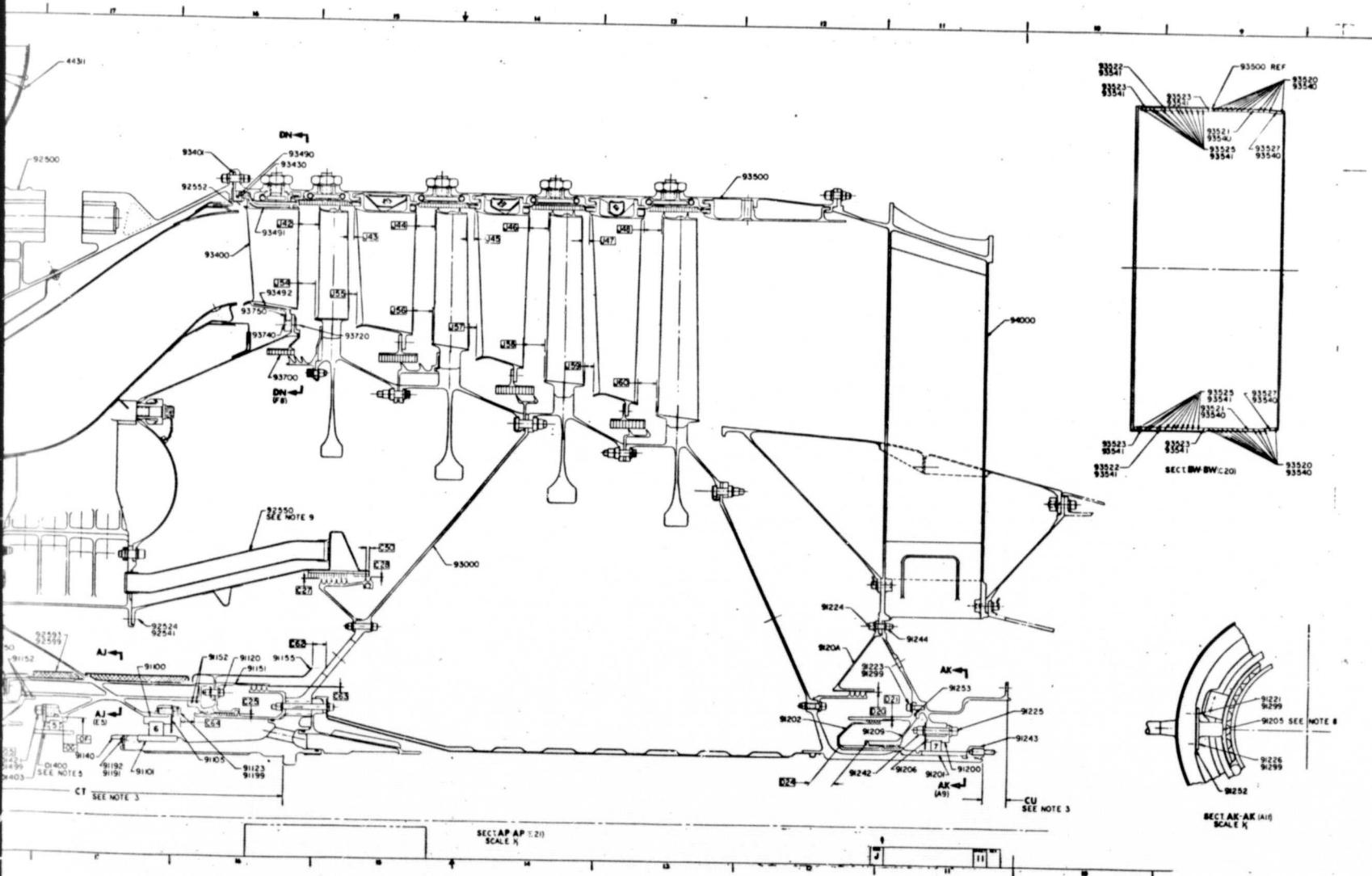
The turbine midframe for Engine C is a bolted structure consisting of twelve integral strut/vane R-41 castings bolted to axially-spaced inner and outer rings. Figure 305 is a model of the strut/vane casting.



PRECEDING PAGE BLANK NOT FILMED

Figure 299. Engine A and B Low

FOLDOUT FRAME



Low Pressure Turbine Frame Assembly

FOLDOUT FRAME 2

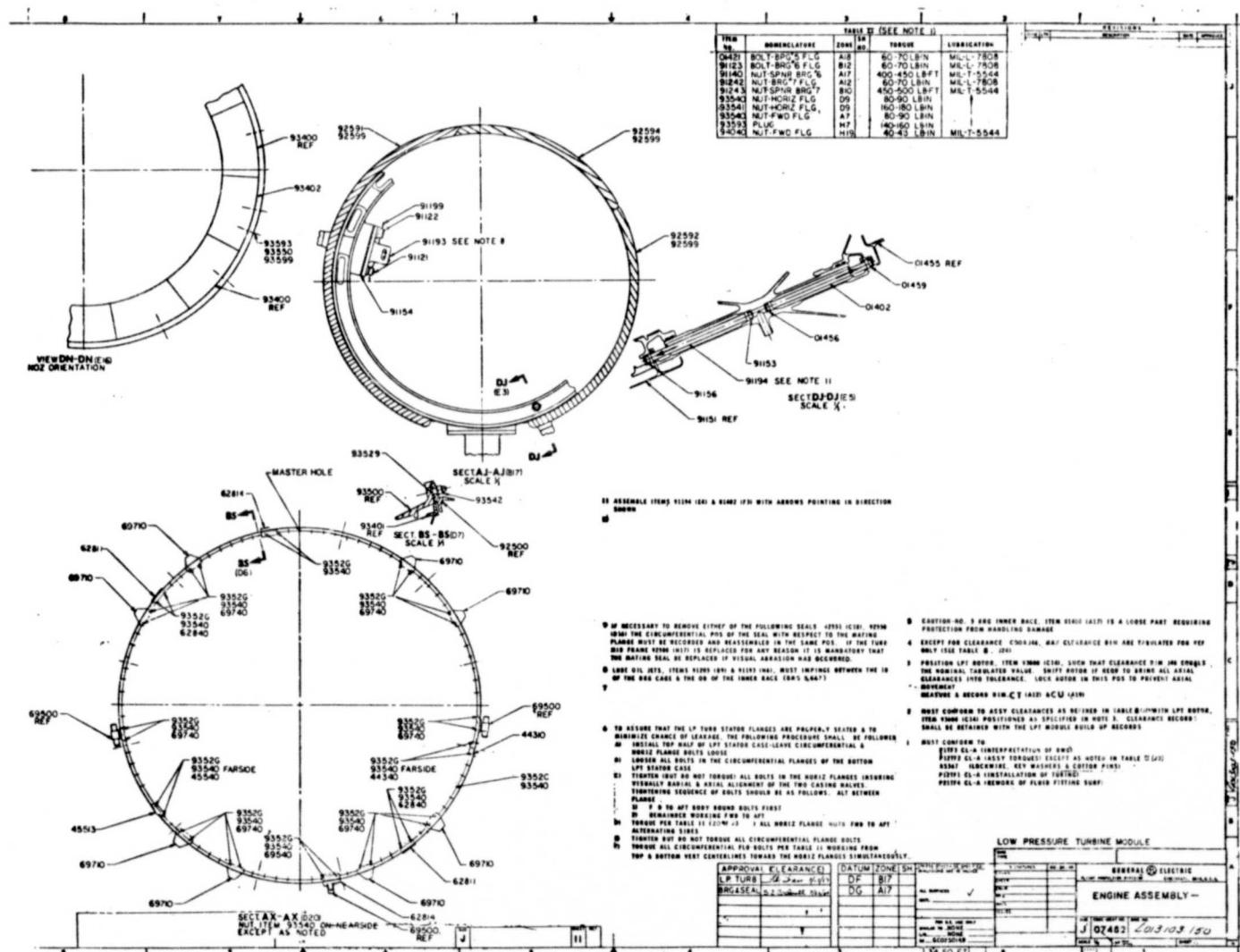
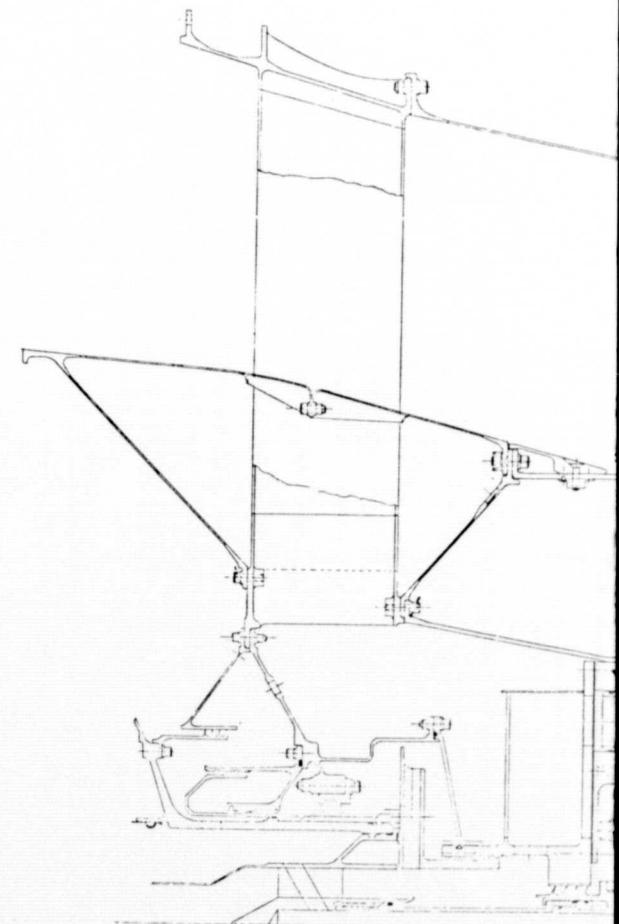
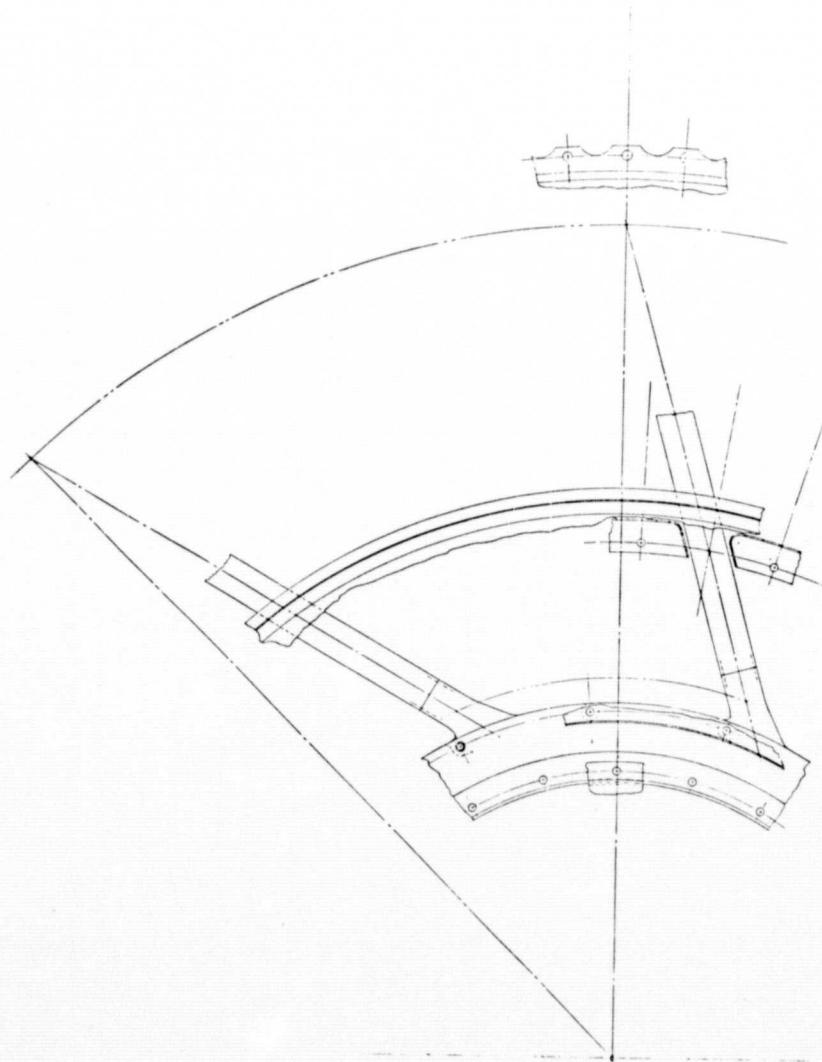


Figure 299. Engine A and B Low Pressure Turbine Frame Assembly (Concluded)

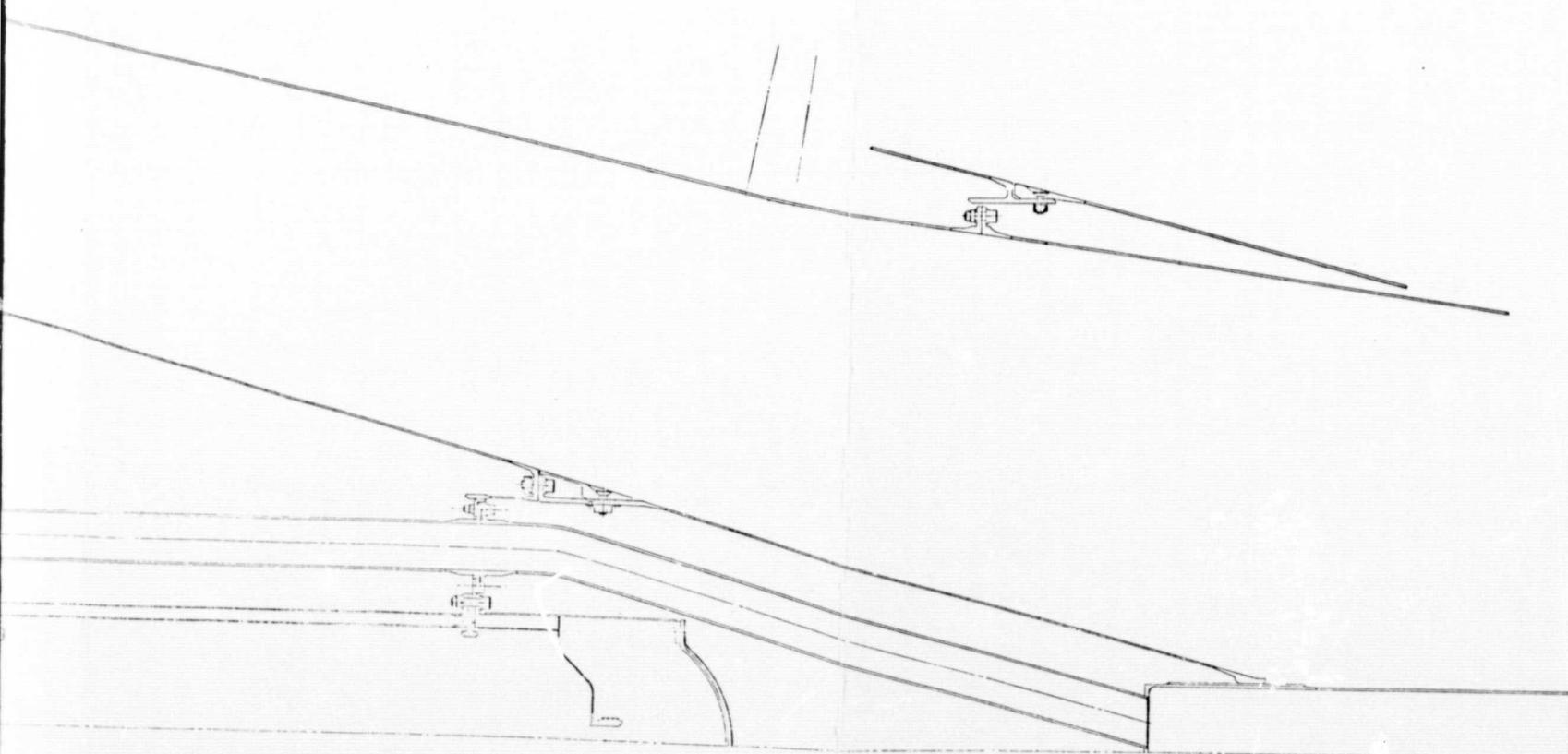
22 | 21 ↓ 20 | 19 | 18 | 17 | 16 | 15 |



FOLDOUT FRAME

Figure 300. Engine A an

13 | 12 | 11 | 10 | 9 | 8 | 7 | 6 |



FOLDOUT FRAME

2

PRECEDING PAGE BLANK NOT FILMED

B Exhaust Nozzle Assembly

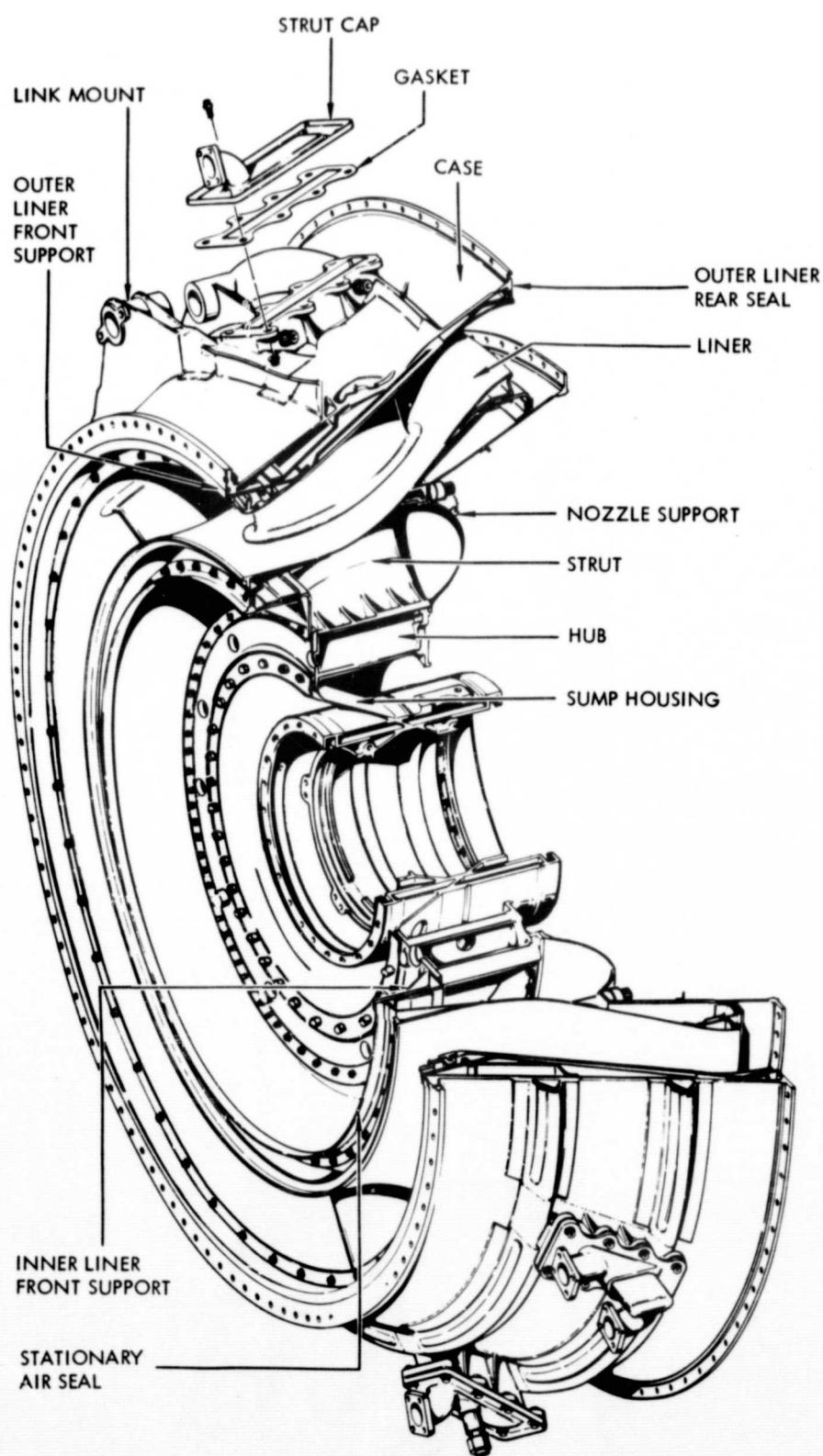
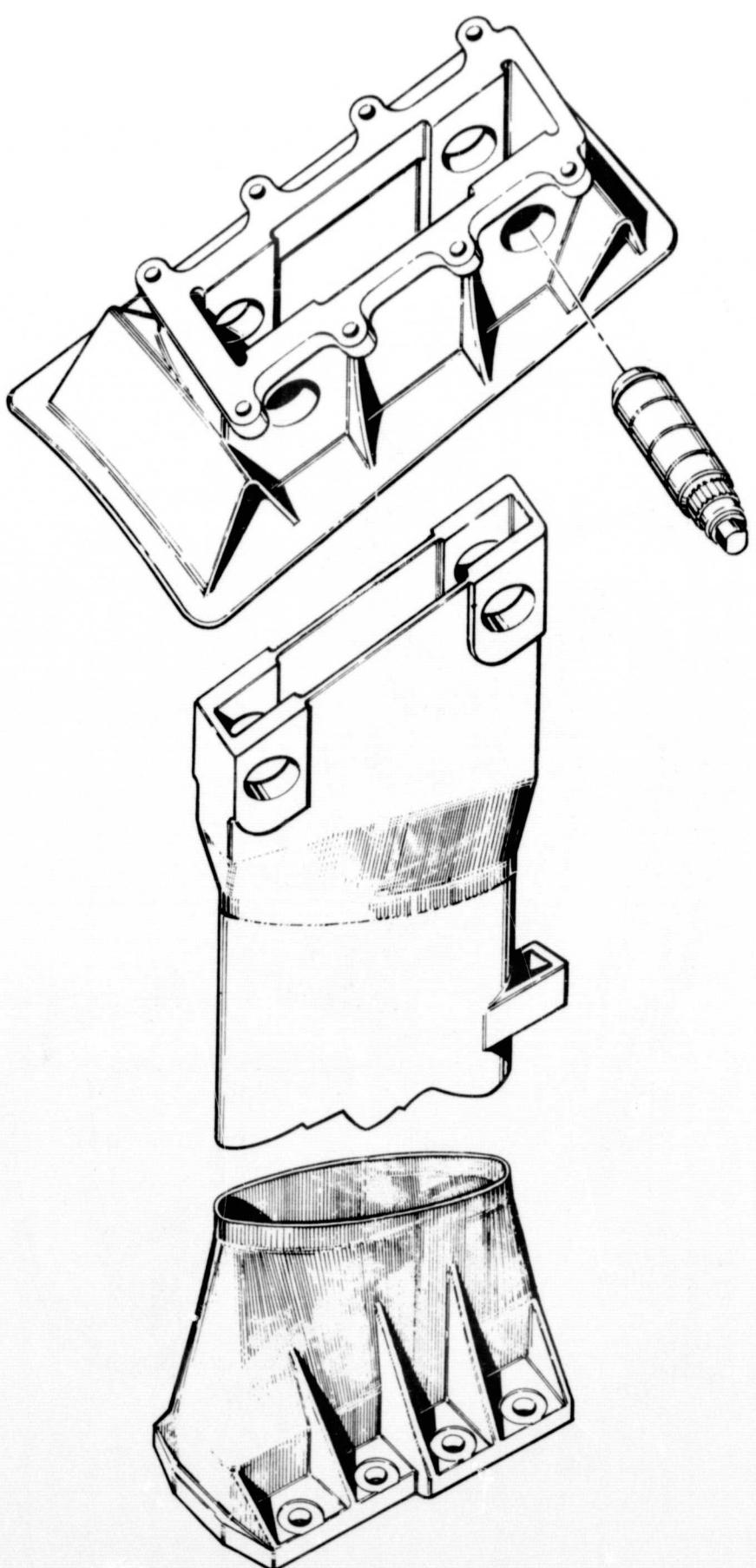
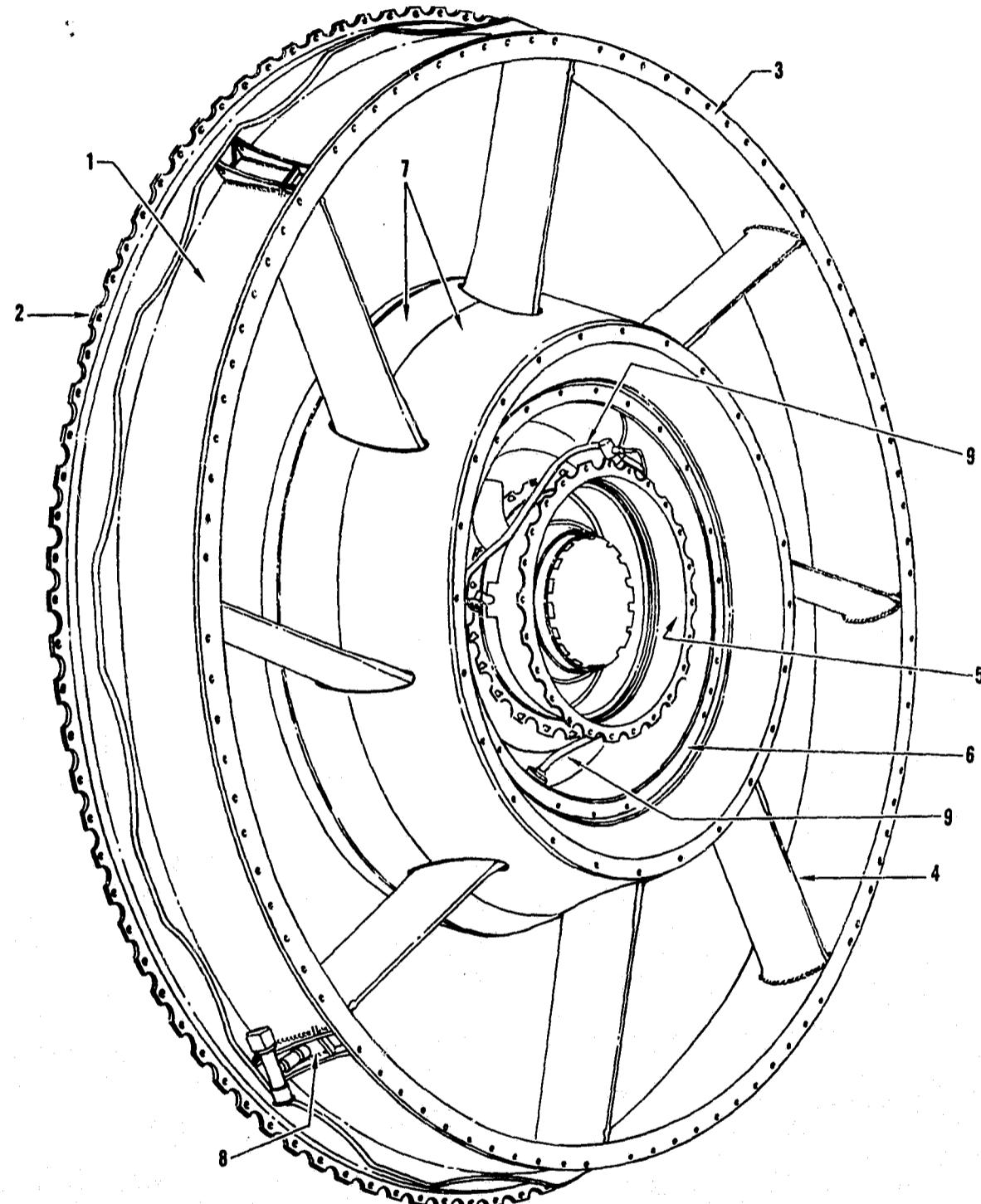


Figure 301. Engine A and B Turbine Midframe Isometric



**Figure 302. Engine A and B Turbine Midframe
Bolt Connection of Frame Struts**



- | | |
|-------------------|--------------------------|
| 1. OUTER CASING | 6. HUB |
| 2. FORWARD FLANGE | 7. INNER LINER (2 PIECE) |
| 3. AFT FLANGE | 8. SERVICE TUBE PAD |
| 4. STRUTS (8) | 9. OIL TUBES |
| 5. SUMP HOUSING | |

Figure 303. Turbine Rear Frame Assembly.

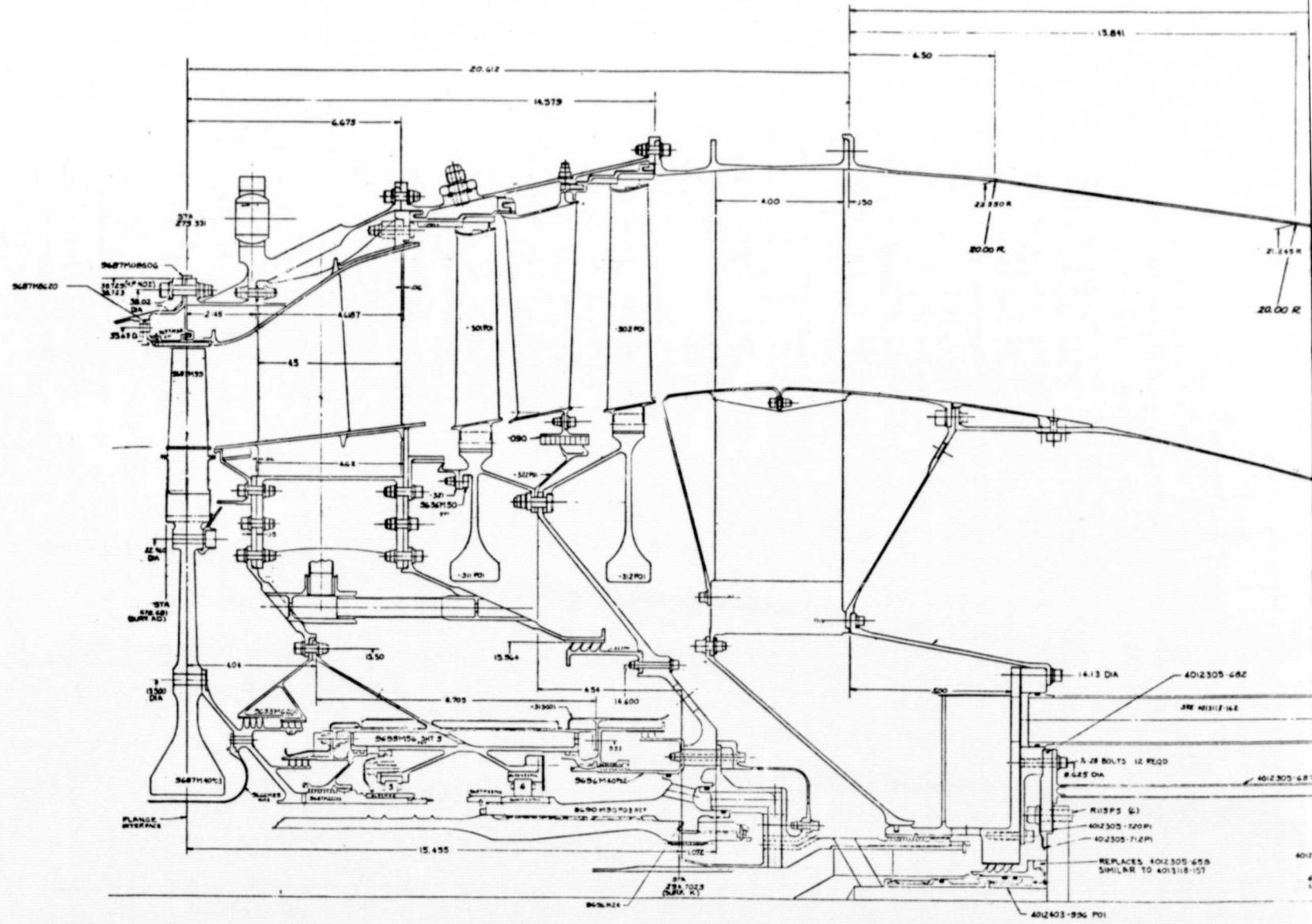
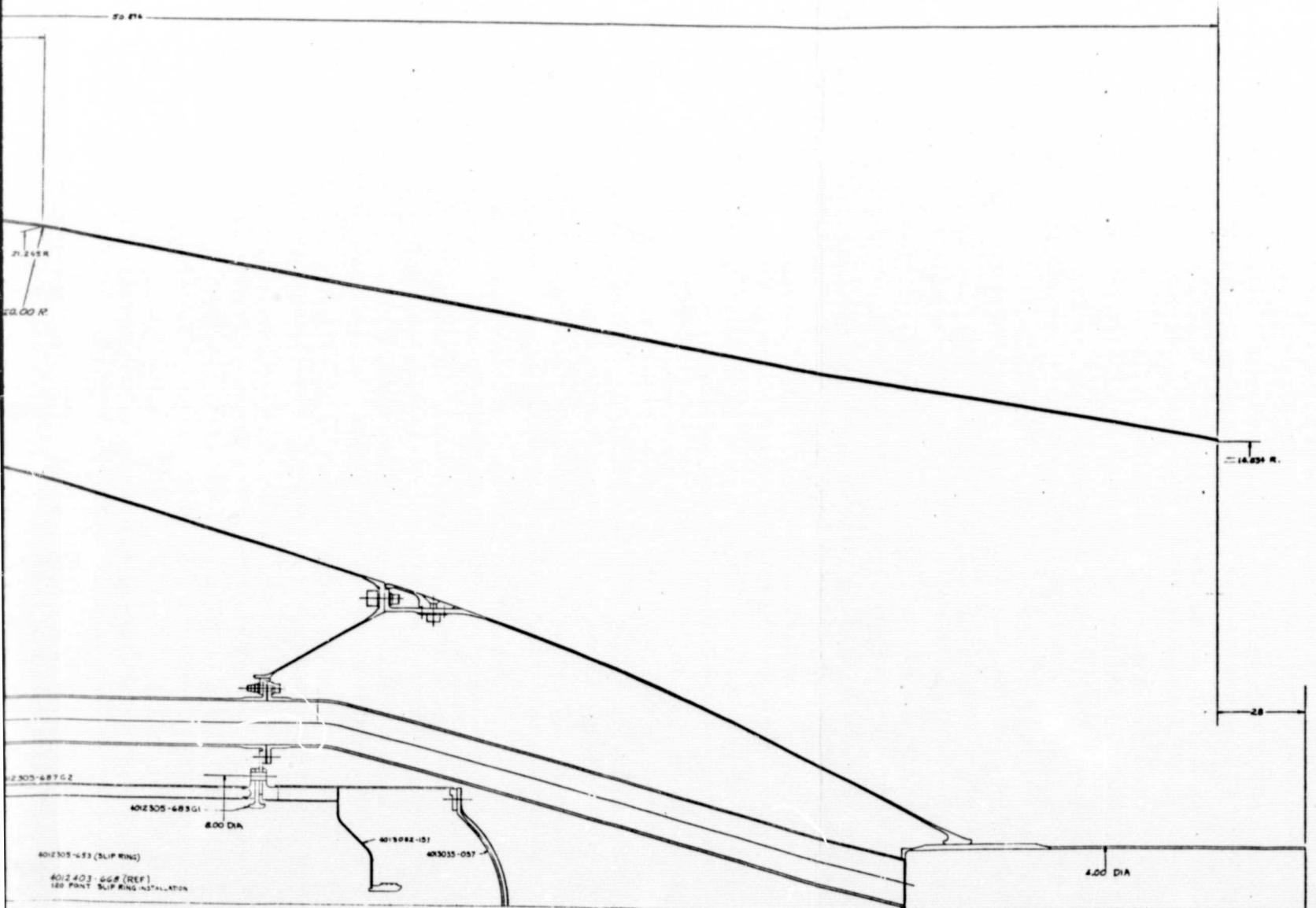


Figure 304. Engine C Low Pressure T

FOLDOUT FRAME

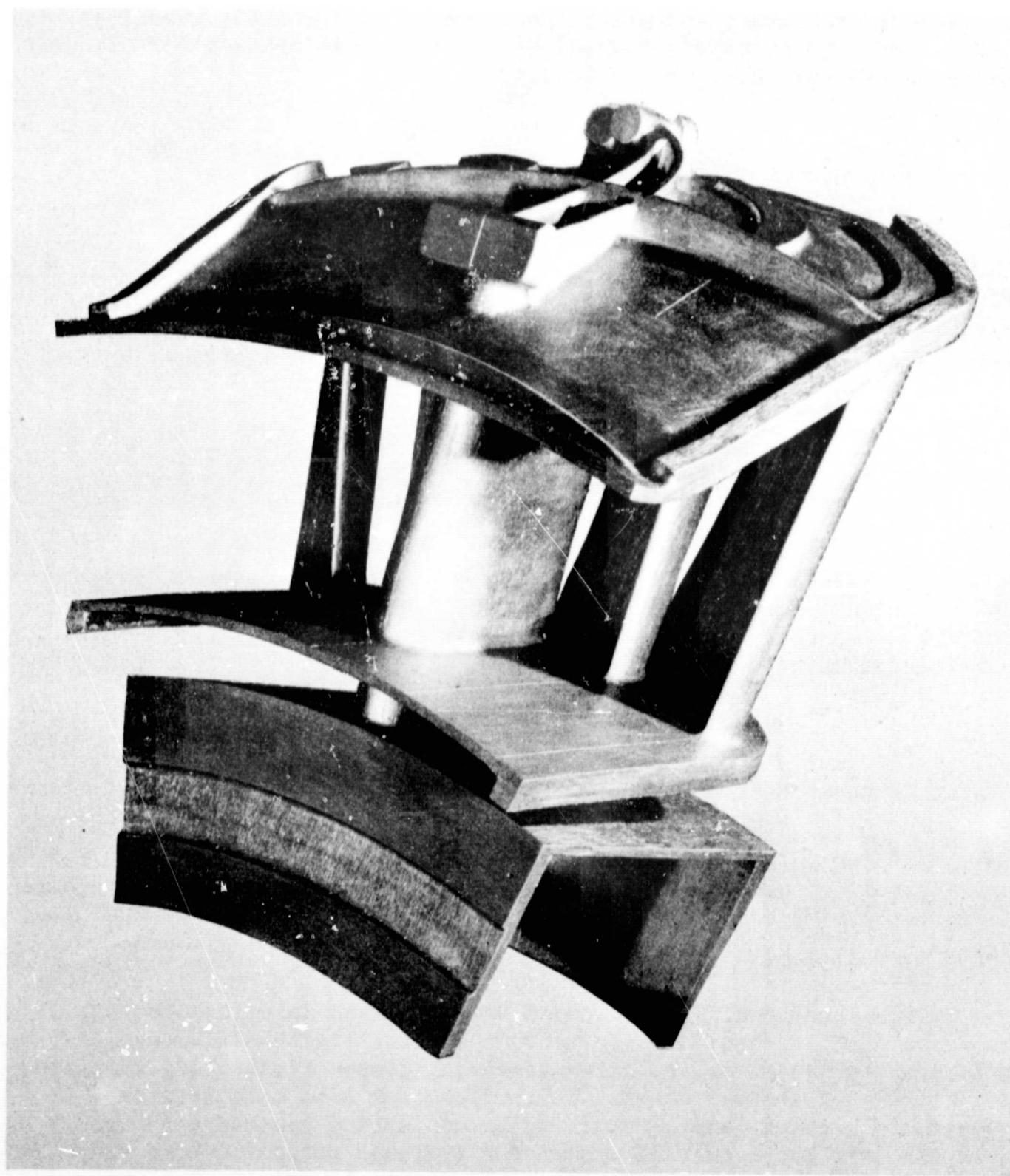


FOLDOUT FRAME

2

Turbine Frame and Exhaust Nozzle Assembly

PRECEDING PAGE BLANK NOT FILMED



PRECEDING PAGE BLANK NOT FILMED

Figure 305. Fan C Turbine Midframe Strut Casting (311788)

A bolted structure permits strut/vane casting interchangeability. The inner rings to which the strut castings are bolted, are Inconel 718 forgings, while the outer aft ring and casing are A-286 forgings. A-286 has a higher coefficient of thermal expansion than Inconel 718 or R-41; therefore, frame steady state and transient thermal stresses, resulting from differential radial thermal growths, can be reduced.

7.3.1.3.2 Engine C Turbine Rear Frame Design

The turbine rear frame for Engine C is identical, in structural design principle, to the Engine A/B turbine rear frame. The primary difference is the frame flowpath configuration. This frame, like the A/B rear frame structure, is an Inconel 718 casting weldment with Hastelloy X inner flowpath liners.

7.3.1.3.3 Engine C Exhaust Nozzle Design

The exhaust nozzle for Engine C is similar in structural design to engine A/B design but slightly different in configuration flowpath contour. As in Engine A/B, the nozzle is a simple Hastelloy X shell-type convergent nozzle.

7.3.1.4 Thermal and Mechanical Stress Analysis - Turbine Frame and Exhaust Nozzles

Thermal and mechanical stress analysis was performed on the turbine midframe, turbine rear frame, and exhaust nozzle for the A/B and C engines.

Conventional analytical methods were utilized in stress evaluating the frames and nozzles. These methods include finite-difference beam and shell computer programs, buckling analysis, computer vibratory analysis, and fundamental thermal stress, deflection, and load calculations. The frame radial, axial, and overturning moment spring constants shown in Table LXXV are the result of a computer analysis method. Here the spring constants were calculated in the usual analytical manner, with CF6 and A/B midframe values obtained from actual static test data.

Table LXXV. Frame Spring Constants

Direction	Spring Constants		
	CF6	A and B	C
Turbine Midframe			
Radial, lb/in.	$*1.28 \times 10^6$	$*1.28 \times 10^6$	1.77×10^6
Axial, lb/in.	$*0.42 \times 10^6$	$*0.42 \times 10^6$	1.15×10^6
Overturning Moment, in.-lb/rad	$*0.63 \times 10^8$	$*0.63 \times 10^8$	0.59×10^8
Turbine Rear Frame			
Radial, lb/in.	0.61×10^6	0.61×10^6	0.63×10^6
Axial, lb/in.	0.147×10^6	0.147×10^6	0.15×10^6
Overturning Moment, in.-lb/rad	0.36×10^8	0.36×10^8	0.29×10^8
*Experimental Data			

7.3.1.4.1 Analysis, A/B Turbine Midframe

The A/B engine will use the present CF6 turbine midframe assembly. This assembly, illustrated in Figure 301, is a bolted structure consisting of eight partially-tangential strut castings bolted to an Inconel 718 outer casing weldment and an Inconel 718 hub ring casting, a Hastelloy X liner assembly, an Inconel 718 C-sump housing casting, and 321 stainless steel piping.

The partially-tangential struts (shown in Figure 302) are used to control thermal stress by permitting the inner ring to rotate (in plane) relative to the casing, thus imposing small bending moments on the strut's flexible minor axis causing low strut bending stresses. The struts are rigidly bolted to the hub ring and bolted to the casing by bolts having expandable-type collars. This type bolt permits strut-casing hole misalignment without sacrificing structural integrity.

Although the midframe for Engine A/B is a CF6 frame, an analysis of the frame was conducted to determine the frame stresses under Quiet Engine simulated flight conditions. Figure 306 shows the ultimate engine mount loads to which the A/B and C midframe will be subjected. From this, a direct comparison can be drawn between the CF6, A/B, and C engine turbine midframe mount loads.

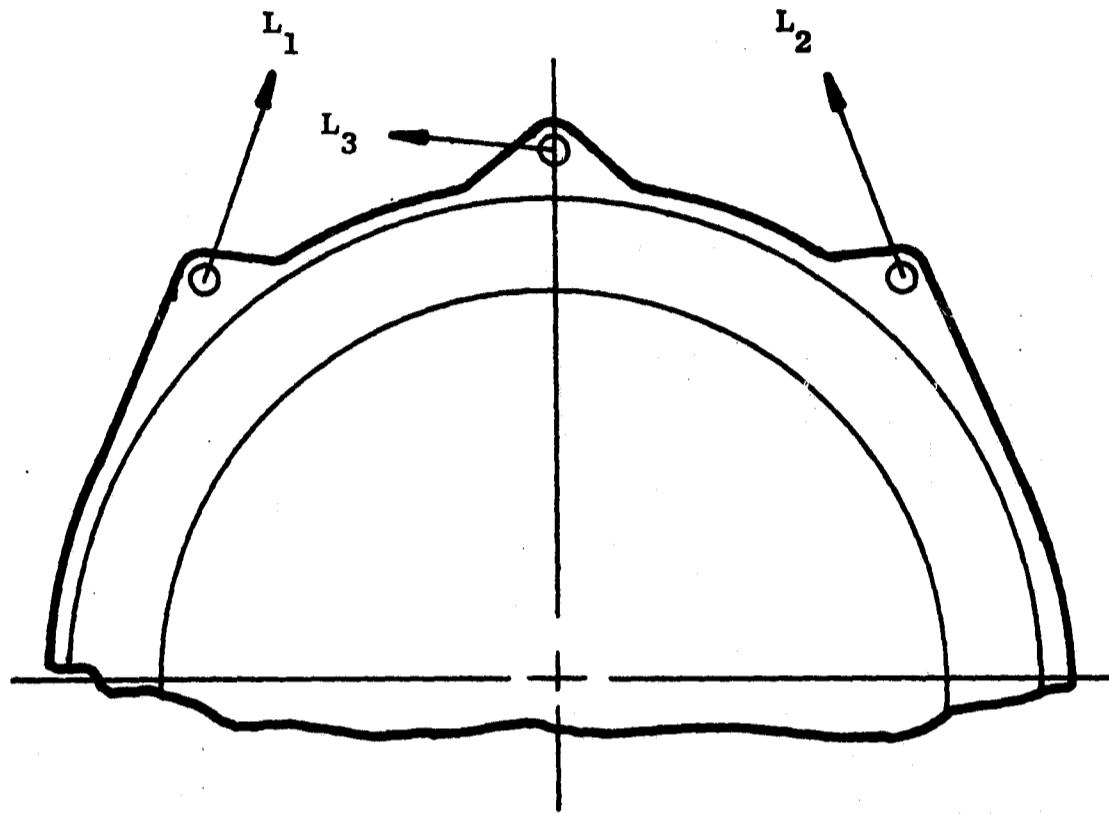
Figure 307 lists a comparison of the ultimate turbine midframe bearing loads and stresses for A/B and C engines. These loads were calculated from maneuver conditions shown in Table LXXVI (and in conjunction with Table LXXVII and Figure 308) and unit bearing loads listed in Table LXXVIII. Figure 309 shows the steady state axial loads which are imposed on the low pressure turbine frame/nozzle assembly.

The maximum stresses in the A/B engine turbine midframe outer shell, hub ring, struts, and engine mounts are shown in Figures 310, 311, and 312. These stresses are the result of maneuver loads which are listed in Table LXXVI under "Landing" maneuver condition and thermal stress. A listing of these peak frame stresses versus material allowable stresses is presented in Figures 313, 314 and 315.

Figures 316 and 317 are the predicted low pressure turbine hot gas temperature profiles. These profiles, both low pressure turbine inlet and exhaust, were used in determining the turbine midframe and rear frame metal temperatures.

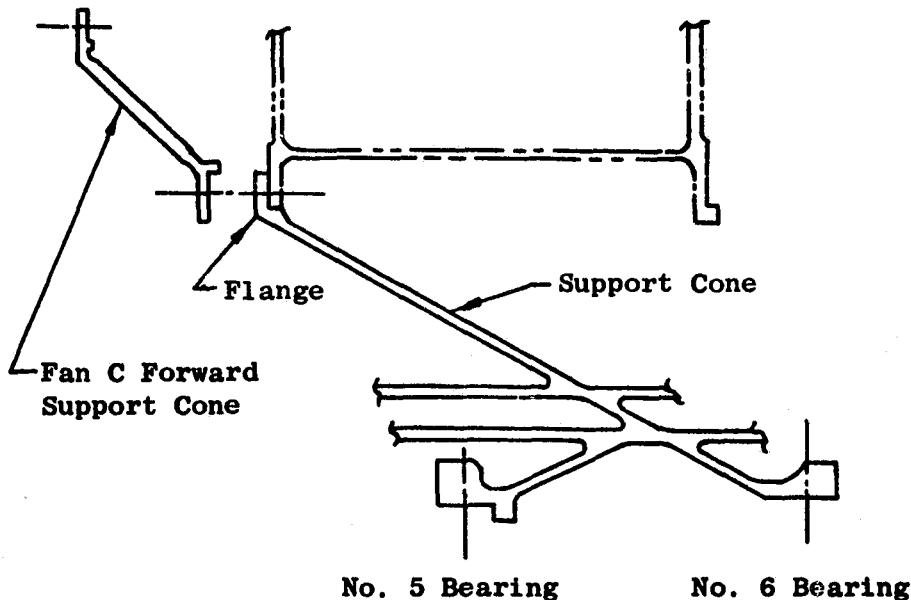
7.3.1.4.2 Analysis, A/B Turbine Rear Frame

The turbine rear frame for Engine A/B, shown in Figure 303, is a CF6 turbine rear frame with a modified inner flowpath.



Engine	CF-6	A/B	C
Conditions	6.5 g's Dn 2 g side Thrust 7° 1 g Fore 3° 11,400 lb Side Gust	6 g's Down Thrust 5° 1 g Fore 2° 11,400 lb Side Gust	1.5 g's side
L_1	91,500	63,200	68,500
L_2	91,500	63,200	68,500
L_3	109,200	35,300	37,800

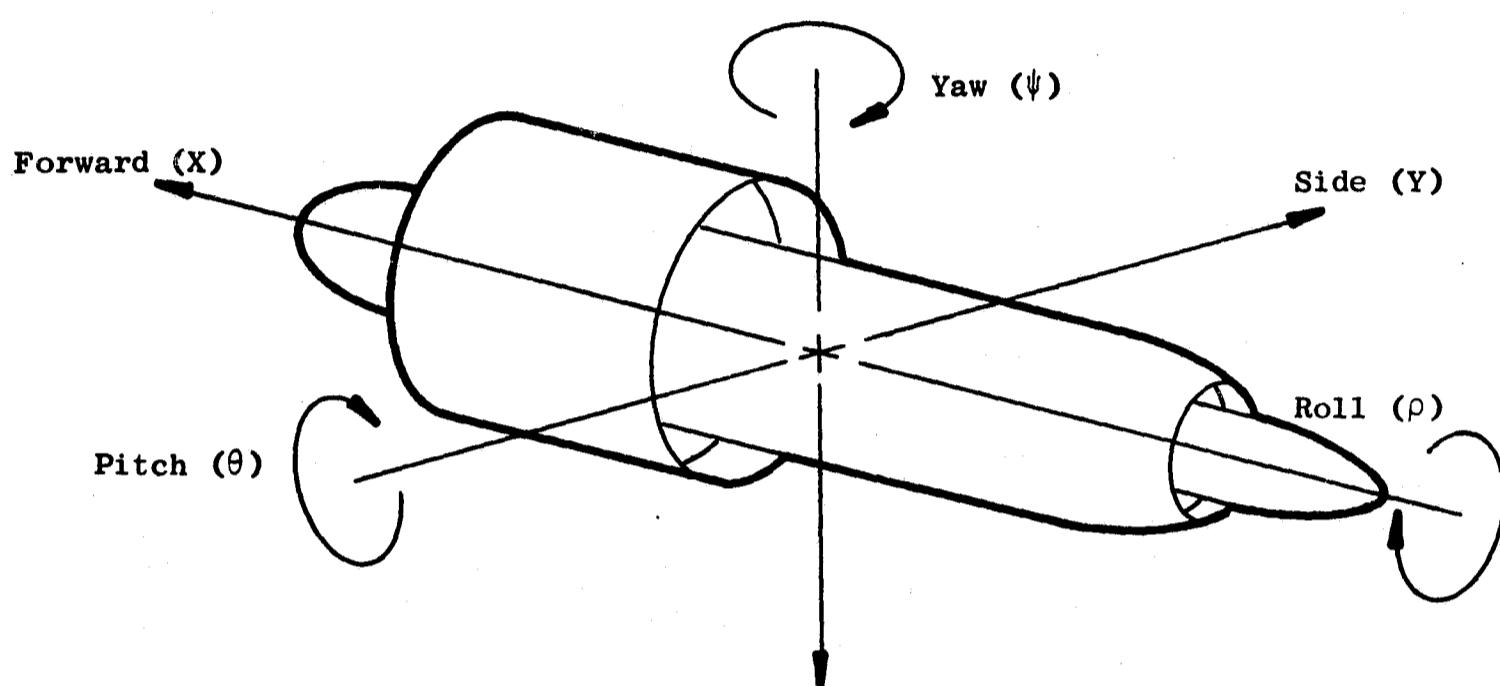
Figure 306. Turbine Midframe Maximum Mount Loads



Component	Ultimate Bearing Load, Pounds		Maximum Stress, PSI		0.2% Allowable Stress, PSI	
	A/B	C	A/B	C	A/B	C
Bolts	7073	7741	17470	19120	147000	147000
Flange	7073	7741	26050	28510	123000	123000
Cone	7073	7741	10822	11844	123000	123000
No. 5 Bearing	2516	2518	18112	18112	123000	123000
No. 6 Bearing	4725	5414	87418	100171	123000	123000
Fwd Cone ID	---	---	---	30850	---	123000
Fwd Cone OD	---	---	---	21400	---	123000
No. 7 Bearing (Turbine Rear Frame)	4485	---	16483	---	106000	---

Figure 307. Bearing Cone Stresses

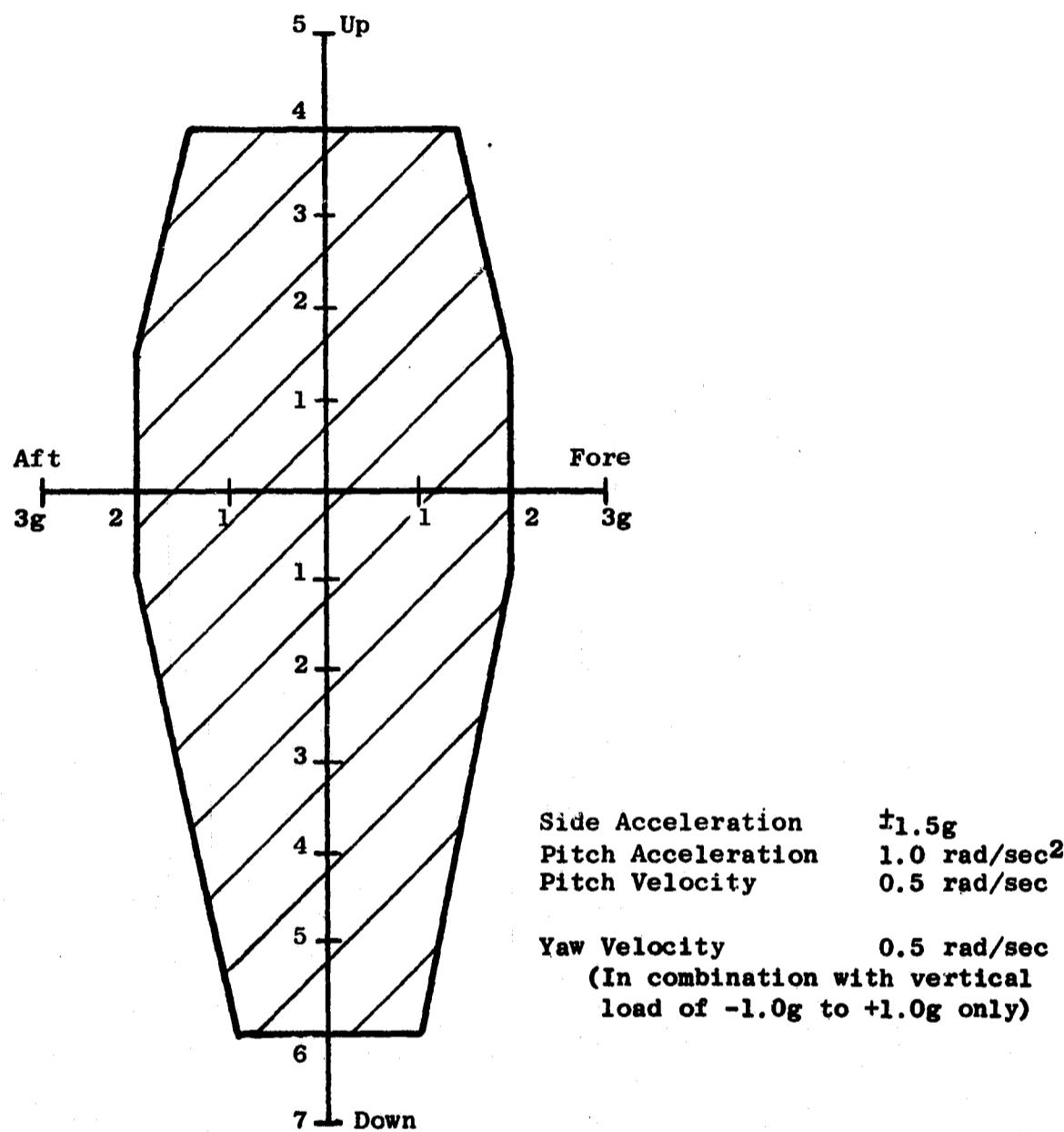
Table LXXVI. Maximum Maneuver Load Combinations



Condition	CF6	Quiet Engine A, B, and C
<u>Landing</u>		
(Fore) N_x	1.0 G	1.0 G
(Side) N_y	$\pm 2.0 \text{ G's}$	$\pm 1.5 \text{ G's}$
(Down) N_z	6.5 G's	6.0 G's
(Pitch) $\dot{\theta}$ Velocity	0	0
$\ddot{\theta}$ Acceleration	$\pm 7.0 \text{ Rad/Sec}^2$	$\pm 5.0 \text{ Rad/Sec}^2$
(Yaw) $\dot{\psi}$ Velocity	0	0
$\ddot{\psi}$ Acceleration	$\pm 3.0 \text{ Rad/Sec}^2$	$\pm 2.0 \text{ Rad/Sec}^2$
<u>Flight I</u>		
(Down) N_z	6.5 G's	6.0 G's
(Pitch) $\dot{\theta}$ Velocity	$\pm 0.5 \text{ Rad/Sec}$	$\pm 0.5 \text{ Rad/Sec}$
$\ddot{\theta}$ Acceleration	$\pm 3.0 \text{ Rad/Sec}^2$	$\pm 1.0 \text{ Rad/Sec}^2$
<u>Flight II</u>		
(Down) N_z	1.0 G	1.0 G
(Yaw) $\dot{\psi}$ Velocity	0.5 Rad/Sec	0.5 Rad/Sec

Table LXXVII. Fan A/B Turbine Midframe Unit Loads

Component Load	1g Down	1g Side (Right)	1g Forward	Thrust T/O	1 Rad/Sec Pitch ($\dot{\theta}$) Nose Up	1 Rad/Sec Yaw ($\dot{\psi}$) Nose Right	1 Rad/Sec ² Pitch ($\ddot{\theta}$) Nose Up	1 Rad/Sec ² Yaw ($\ddot{\psi}$) Nose Right	Side Gust to Right
<u>For. Flght</u>									
Px	0	0	2 600	-8491	0	0	0	0	0
Py	0	-831	0	0	5 920	0	0	-344	9 280
Pz	831	0	2 810	4 060	0	0	0	0	0
Mx	0	176 600	0	-347 900	109 000	0	0	-13 750	392 000
My	55 500	0	-16 310	-23 800	0	-89 200	-4 550	0	0
Mz	0	55 500	0	0	-89 200	0	0	4 550	75 000
<u>Aft Flght</u>									
Px	0	0	-2 130	18 416	0	0	0	0	0
Py	0	-2 498	0	0	3 870	0	0	-182	0
Pz	2 498	0	147	214	0	-3 870	-187	0	0
Mx	0	0	0	296 000	0	0	0	0	0
My	-41 700	0	0	0	0	128 100	4 550	0	0
Mz	0	-4 170	0	0	128 100	---	0	-4 550	0
<u>No. 5 Brg</u>									
Py	0	-107	0	0	2 802	0	0	-66	0
Pz	107	0	243	437	0	-2 802	-66	0	0
<u>No. 6 Brg</u>									
Py	0	-300	0	0	-5 035	---	0	-97.8	0
Pz	300	0	147	212	0	5 035	-97.8	0	0
<u>Strut</u>									
Px	0	---	0	9 582	0	0	0	0	0
Mx	0	0	0	51 900	0	0	0	0	0
<u>Hub</u>									
Px	0	0	0	7 000	0	0	0	0	0
Mx	0	0	0	51 900	0	0	0	0	0
<u>Casing</u>									
Px	0	0	-470	-26 507	0	0	0	0	0
<u>Link Mounts</u>									
L1	2 028	10 830	1 816	2 701	-2 789	-4 100	-375	101	7 115
L2	2 028	-10 830	1 816	2 701	2 789	-4 100	-375	-101	-7 115
<u>Center Mount</u>									
L3	0	12 195	0	0	-9 735	0	0	769	3 725



Notes:

1. Load factors and angular accelerations and velocities are taken about the center of gravity of the engine.
2. Side loads and gyroscopic loads do not act simultaneously.
3. All loading conditions occur over the range from zero to maximum engine thrust.
4. At landing, angular accelerations increase to a limit of 5 rad/sec^2 in pitch and 2 rad/sec^2 in yaw.

Figure 308. Flight Maneuver Loading Diagram

Table LXXVIII. Unit Bearing Loads for Maneuver Case

Direction	Bearing Number						
	1	2	3	4	5	6	7
<u>Engine A/B</u>							
1 G Down	1 075	313	77.51	851.57	106.96	300	225
1 Rad/Sec ²	15 150	-14 950	1 525	1 276	-2 802	5 035	-5 275
1 Rad/Sec ²	126.55	49.08	-16.04	26.70	-66.0	-97.8	-55.7
1000 Lb Thrust	42.95	-54.05	14.29	-34.15	19.86	9.62	-3.07
<u>Engine C</u>							
1 G Down	864	251	77.51	851.57	106.96	367	---
1 Rad/Sec ²	16 700	-16 480	1 537	1 286	-2 825	5 545	---
1 Rad/Sec ²	139.5	54.05	-16.15	26.91	-66.55	-107.90	---
1000 Lb Thrust	36.35	-45.72	14.29	-34.15	19.86	7.32	---

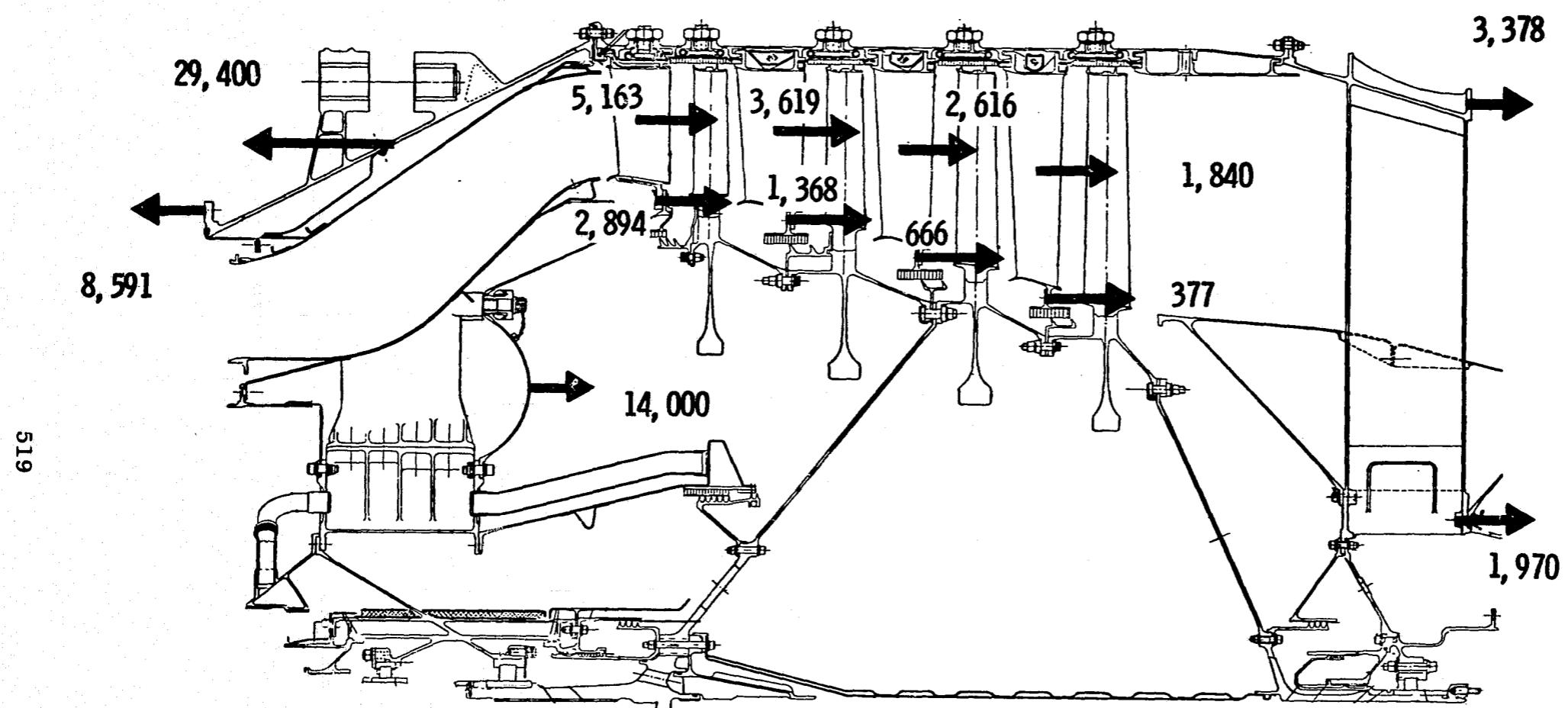


Figure 309. Engine A/B Turbine Axial Loads, Pounds

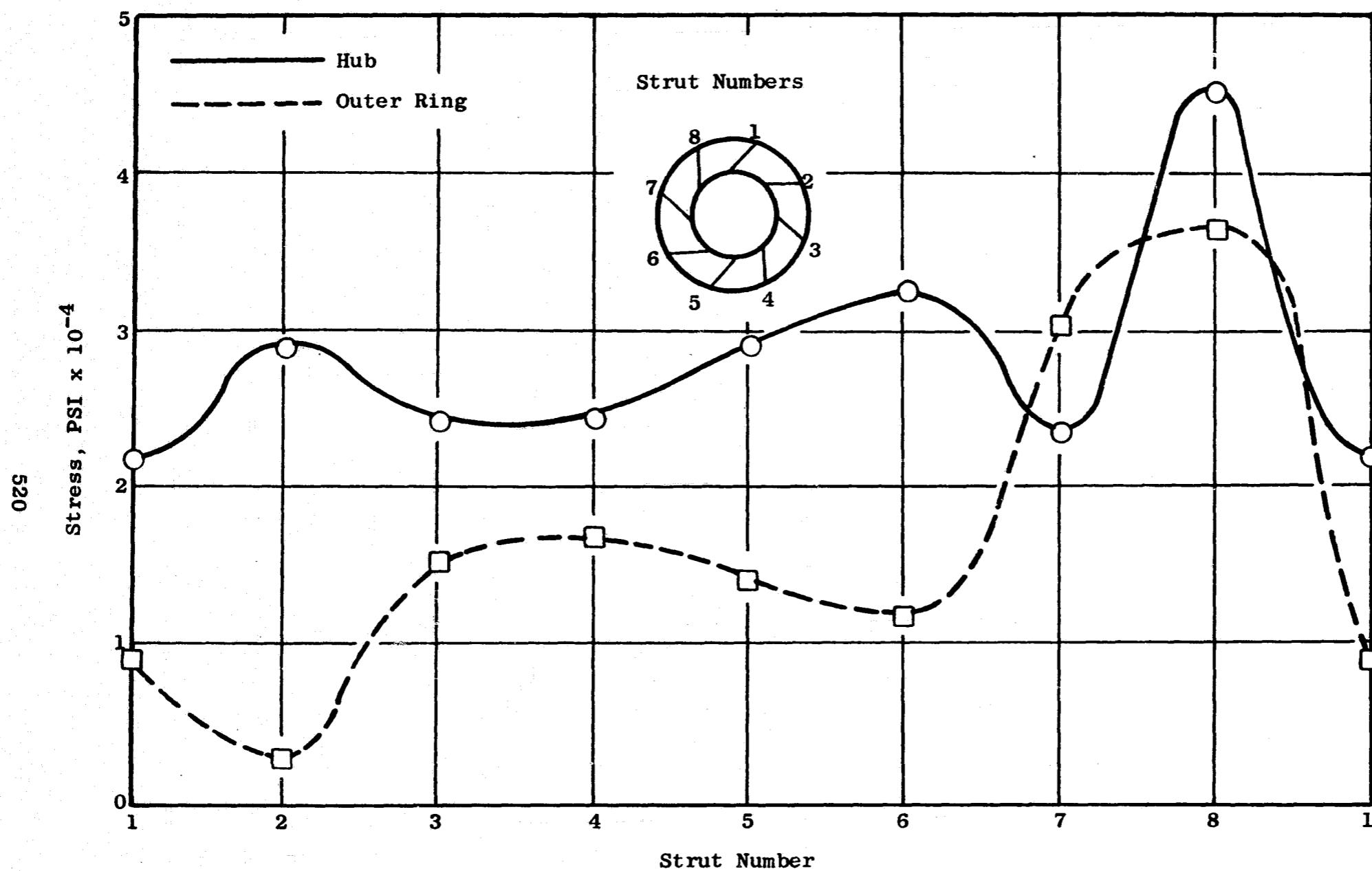
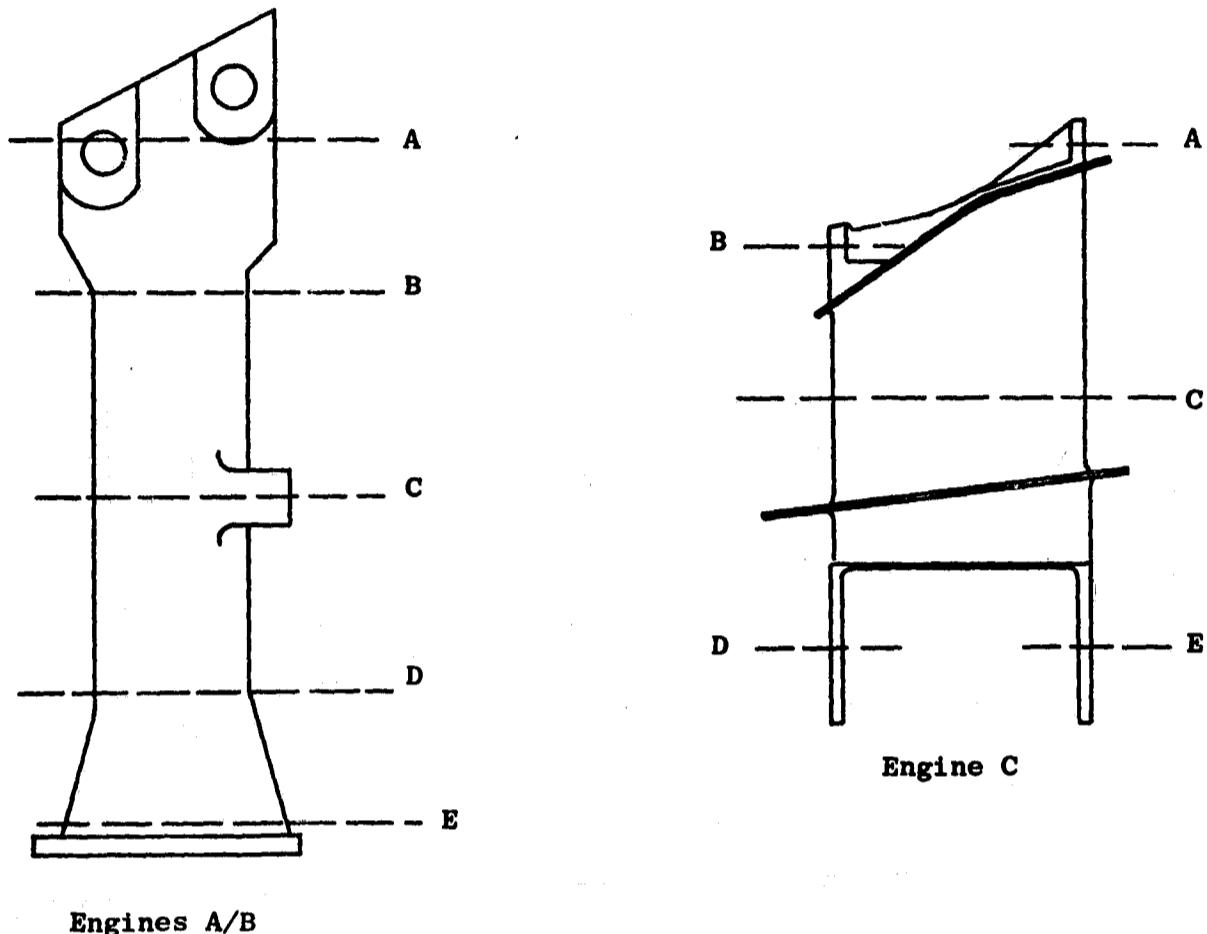


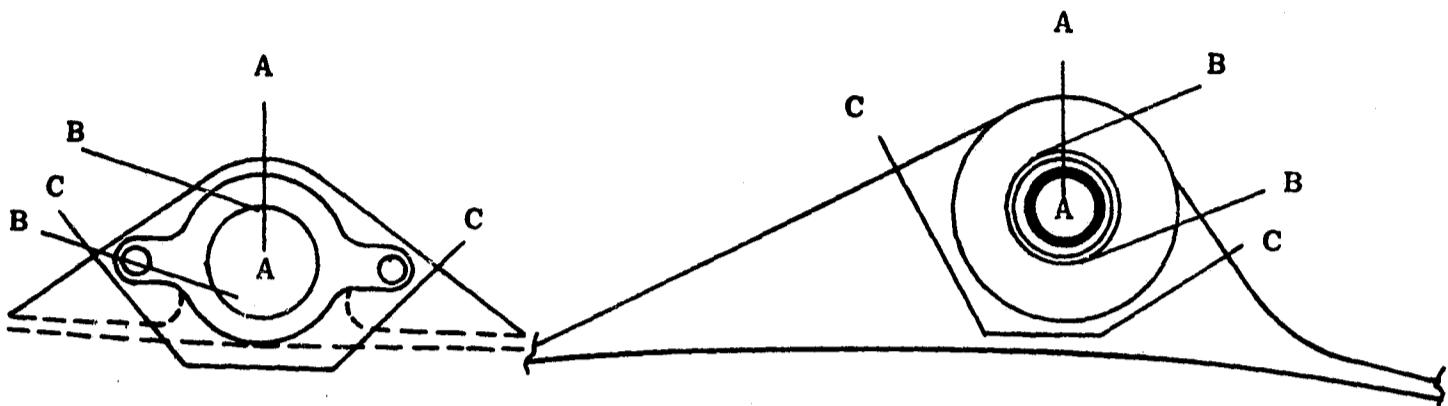
Figure 310. Maximum Stresses Engine A/B Turbine Midframe

TURBINE MIDFRAME



Stress	Location				
	A	B	C	D	E
<u>Engine A/B</u>					
Strut	7	7	7	7	8
Maximum Stress	53,300	22,800	30,500	20,500	9800
Allowable Stress	85,000	85,000	85,000	85,000	85,000
<u>Engine C</u>					
Strut	3	3	5	2	4
Maximum Stress	15,000	32,500	19,400	32,600	58,500
Allowable Stress	88,000	88,000	69,000	102,000	102,000

Figure 311. Strut Maximum Stresses, Turbine Midframe



Section	Ultimate Load, Pounds	Failure Mode	Lug Stress, PSI		Allowable, PSI
			Fwd	Aft	
<u>Engine A/B</u>					
A-A	63,200	Tension	38,340	29,250	111,000
B-B	63,200	Shear	20,780	25,810	63,200
C-C	63,200	Shear	30,380	23,790	63,200
<u>Engine C</u>					
A-A	68,500	Tension		68,000	120,000
B-B	68,500	Shear		34,250	68,300
C-C	68,500	Shear		20,300	68,300

Figure 312. Turbine Midframe Mount Stress Summary

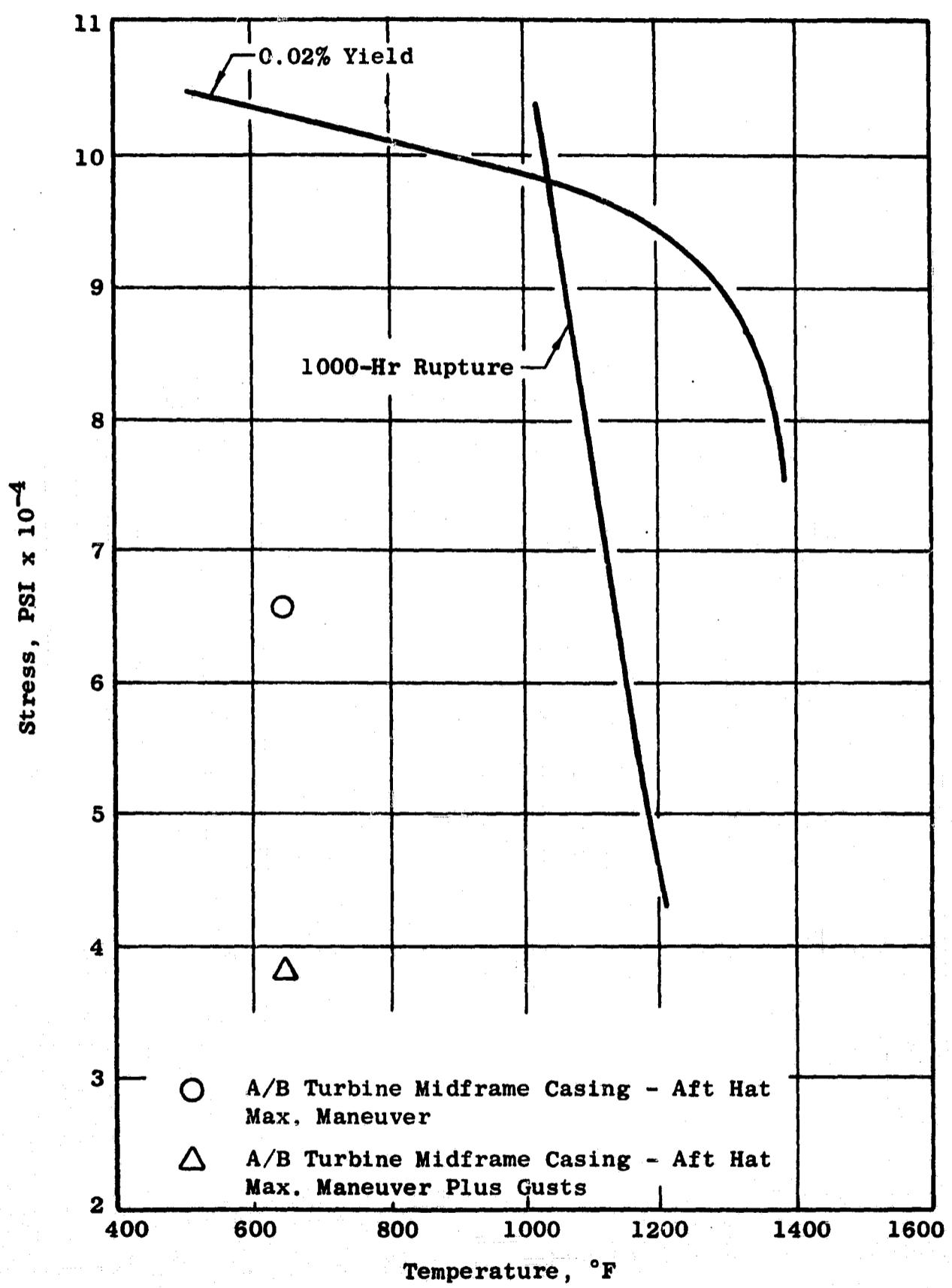


Figure 313. Inconel 718 Cast Material Properties, 3σ Deviations

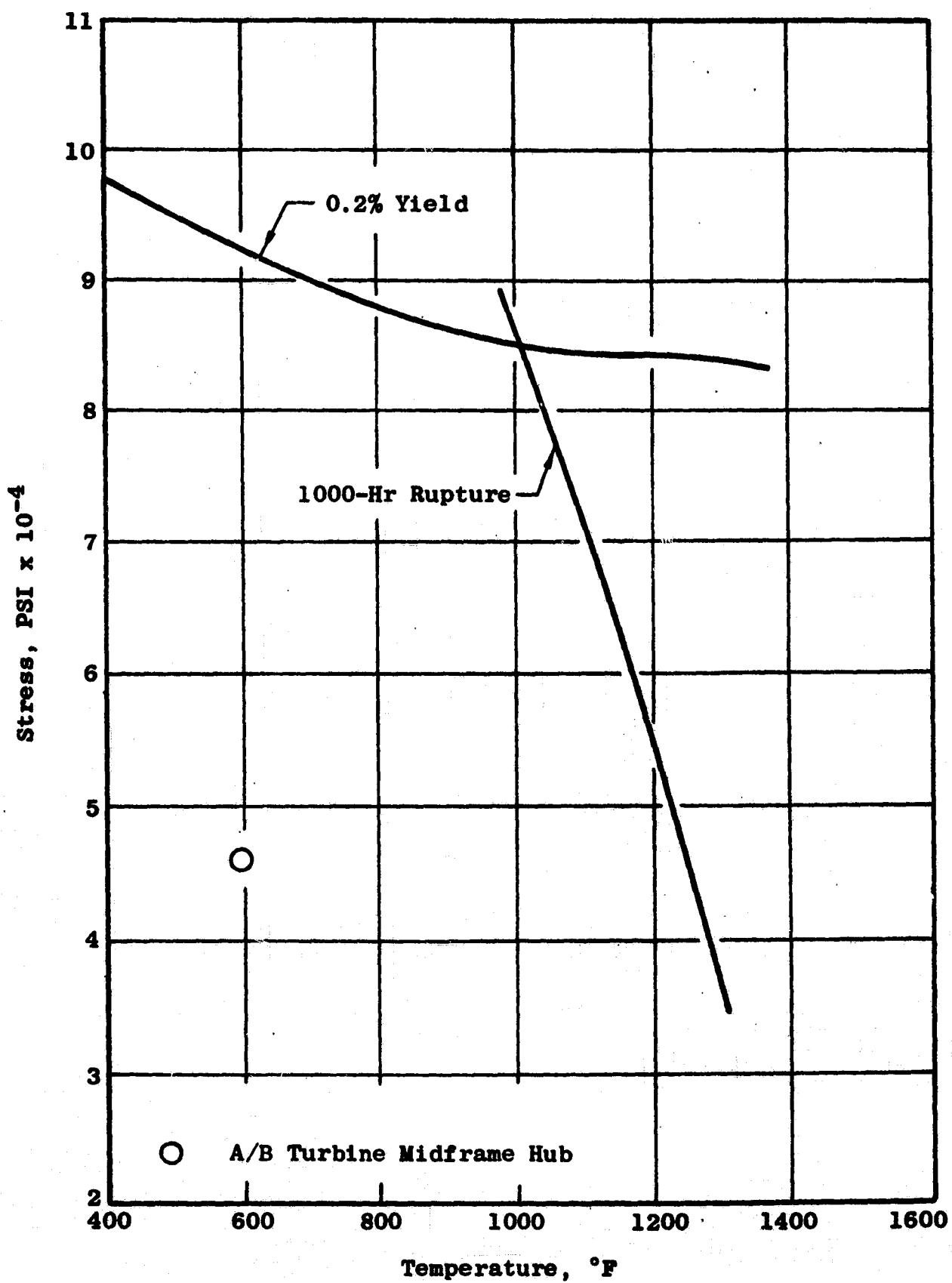


Figure 314. Inconel 718 Cast Material Properties, 3G Deviations

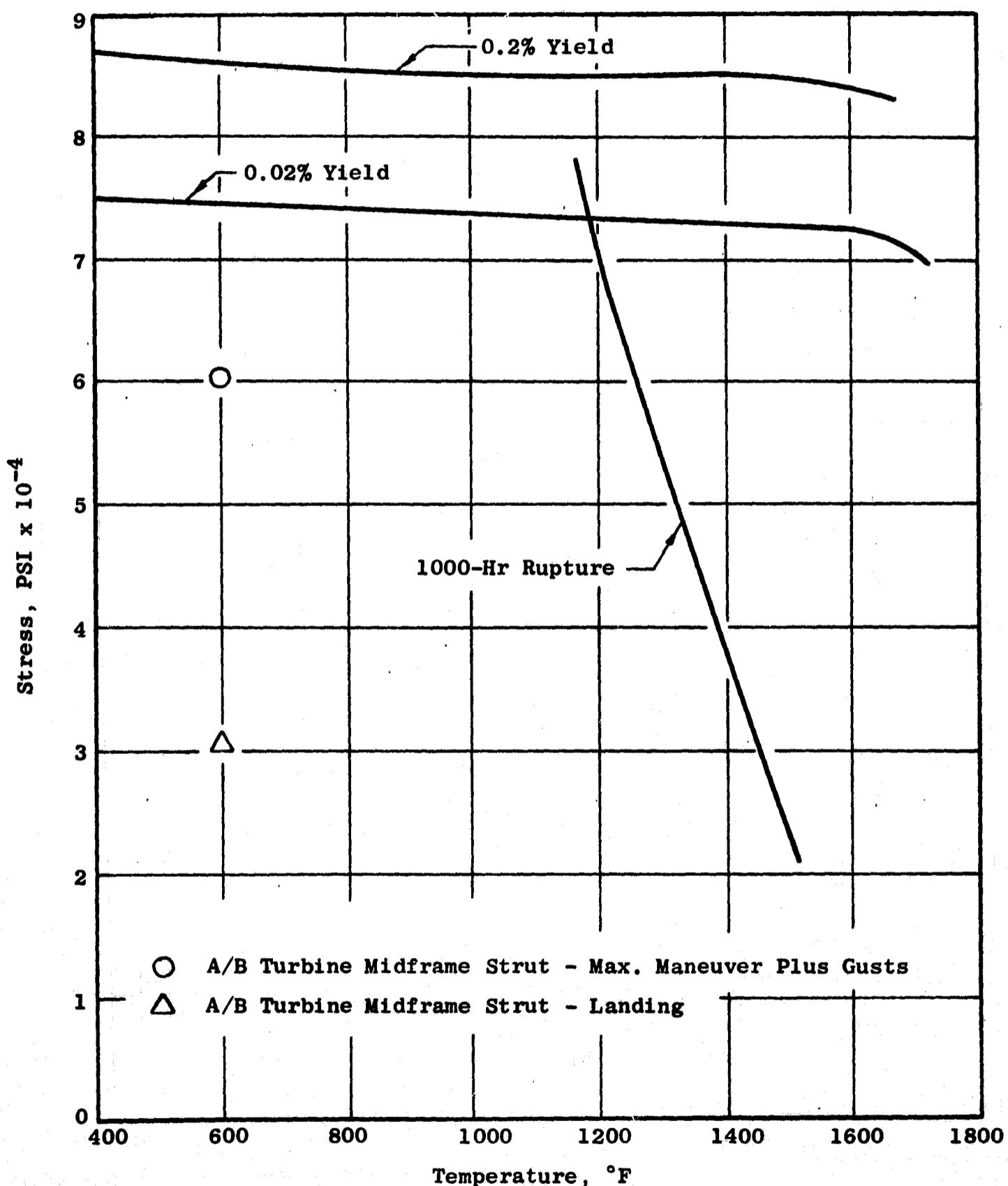


Figure 315. Rene' 41 Cast Material Properties, 30 Deviations

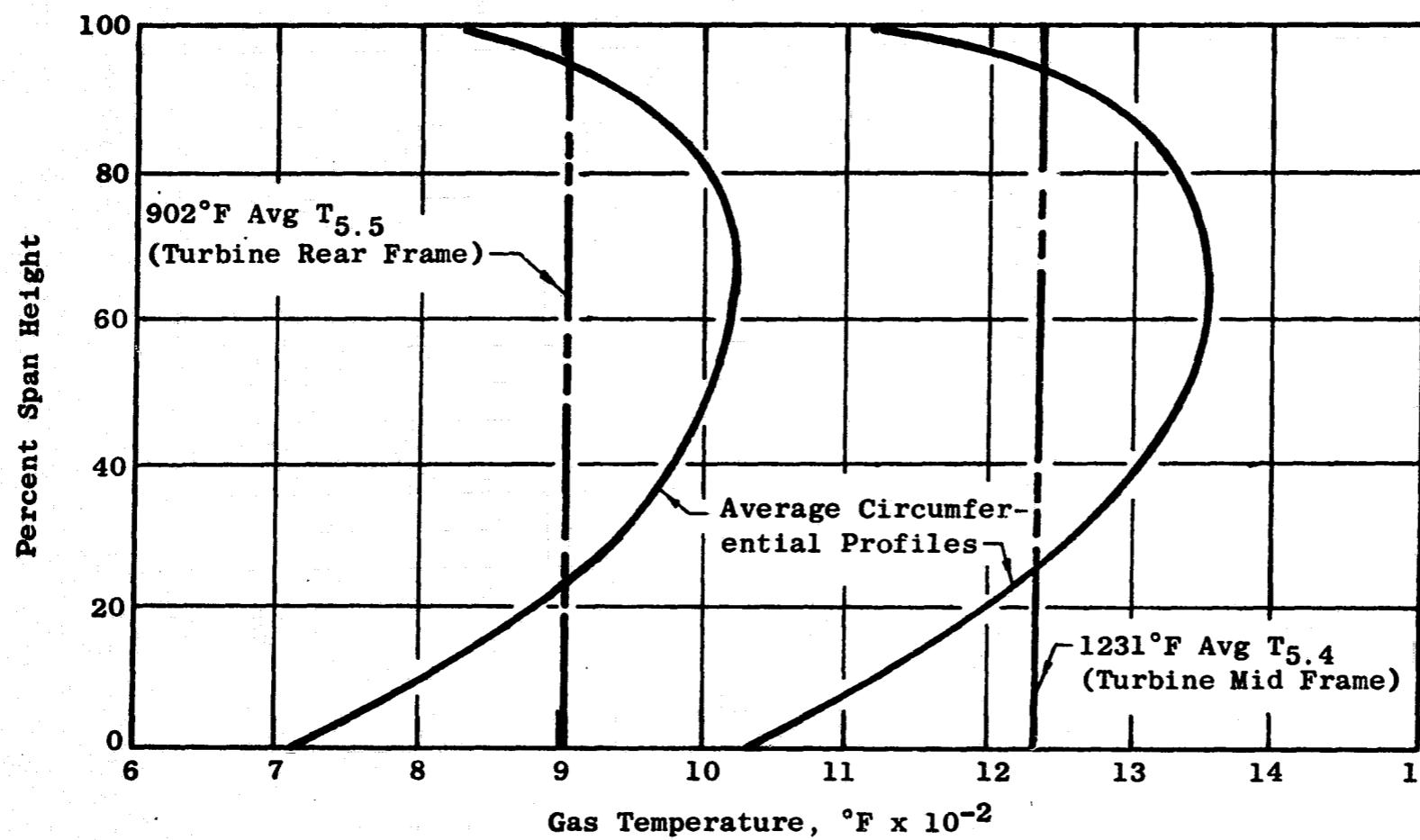


Figure 316. Engine A Integrated Profile of Peaks

527

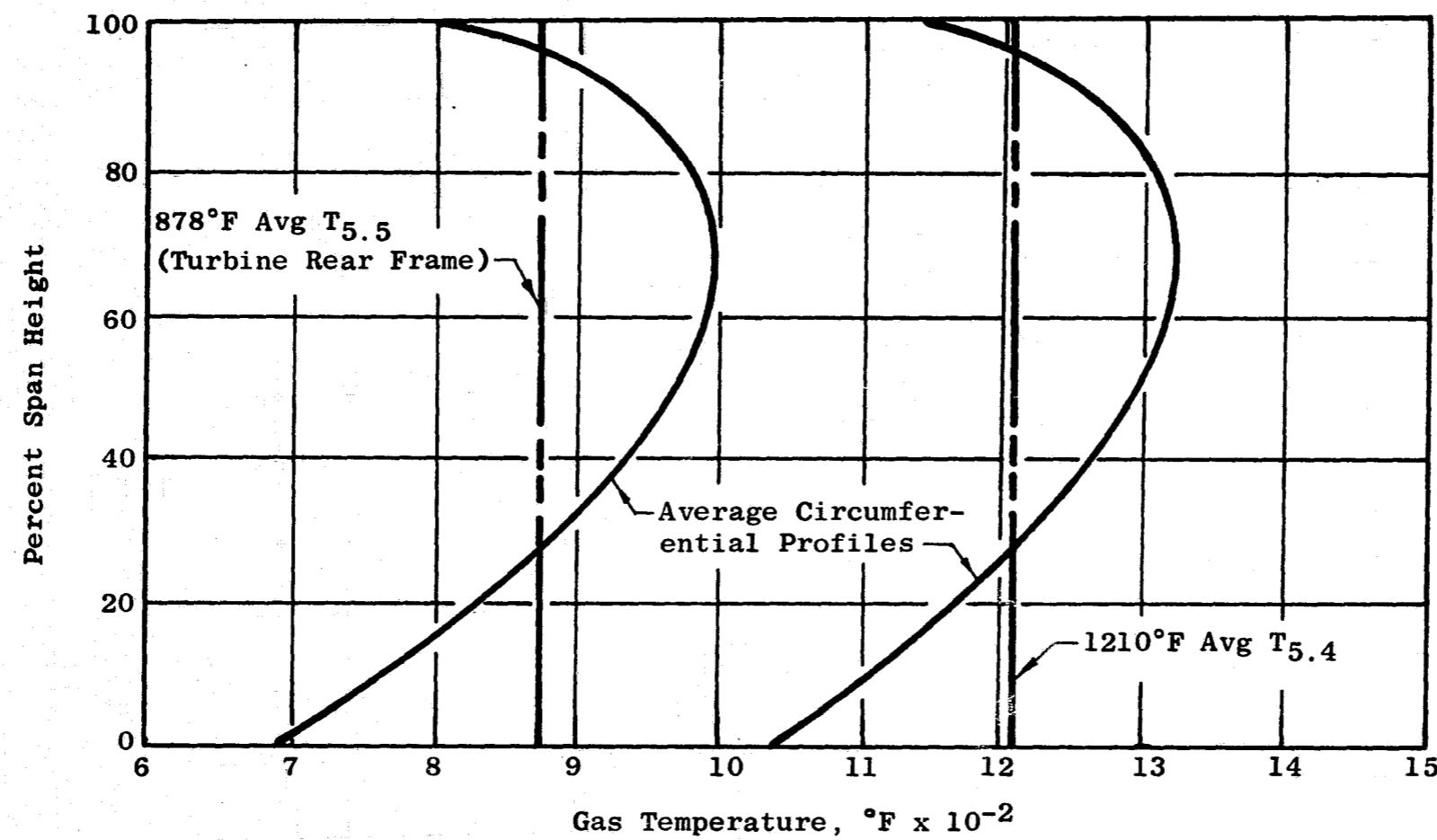


Figure 317. Engine B Integrated Profile of Peaks

The CF6 turbine frame assembly consists of (1) an Inconel 718 casting weldment structure, (2) a Hastelloy X inner flowpath, and (3) a 17-4PH cast sump housing. Four axially-welded 90° cast-arc segments form the frame 360° outer casing. The cast hub ring is joined to the outer casing by eight, partially-tangential strut castings, thus forming the welded structure. The Hastelloy X inner flowpath is a welded two-piece bolted assembly supported by the frame hub.

Engine A/B has a No. 7 (rear frame) low pressure turbine bearing. The unit bearing and maximum bearing loads to which this frame will be subjected are shown in Table LXXVIII and Figure 307.

The maximum stresses which are induced in the A/B rear frame by maneuver loads are shown in Figures 318 and 319. These stresses are the result of the flight condition shown in Table LXVI, the bearing unit loads in Table LXXVIII, and the frame metal temperatures shown in Table LXXIX and Figure 320. Figure 321 is a comparison of the maximum frame stresses relative to the material allowable stress.

7.3.1.4.3 Analysis, A/B Exhaust Nozzle

The exhaust nozzle for Engine A/B is a simple shell convergent nozzle of a type that is utilized on the CF6 engine. This nozzle is basically a utility type nozzle and is subjected to moderate temperature and stresses. The primary mode of failure will be vibratory. Figure 322 shows the shell stability frequency relative to engine operating frequency (engine rpm). The maximum mechanical stresses in this nozzle are relatively low and are compared in Figure 323 with the material allowable stresses.

7.3.1.4.4 Analysis, Engine C Turbine Midframe

The C engine will have a bolted turbine midframe consisting of twelve integral strut/vane R-41 castings which, when bolted to axially spaced A-286 outer and Inconel 718 inner rings, form an aerodynamic cascade structure that functions as the turbine midframe and the Stage 1 low pressure turbine nozzle. The strut vane casting, illustrated in Figure 305, is a frame strut which has integrally cast outer and inner flowpath arc segments. On each side of the strut, and cast integral with the flowpath segments, are two airfoil-shaped turbine vanes. In addition, the trailing edge of the vane strut has the same aerodynamic contour as the vanes. Thus, the structure is a twelve-strut frame/sixty-vane nozzle assembly.

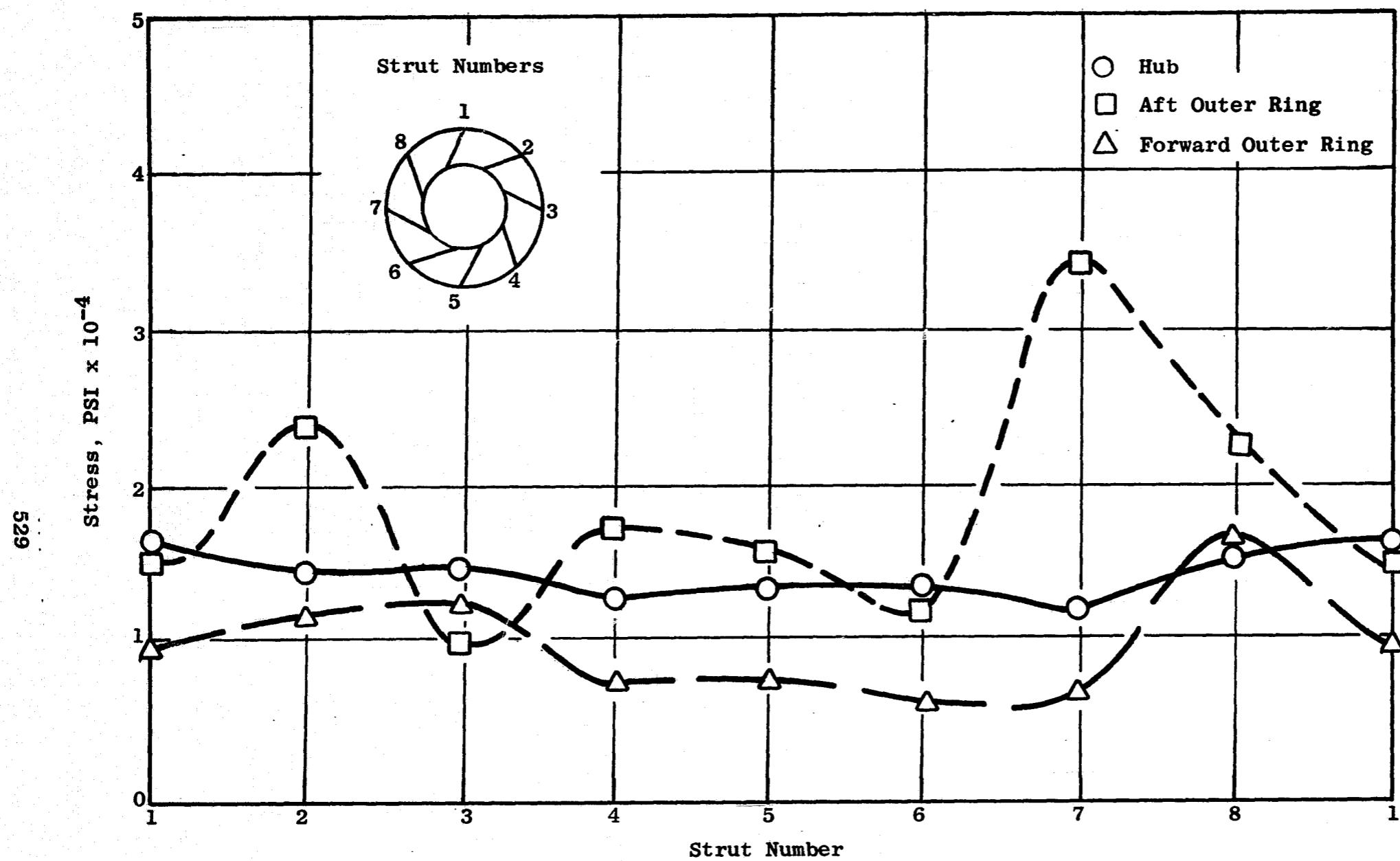
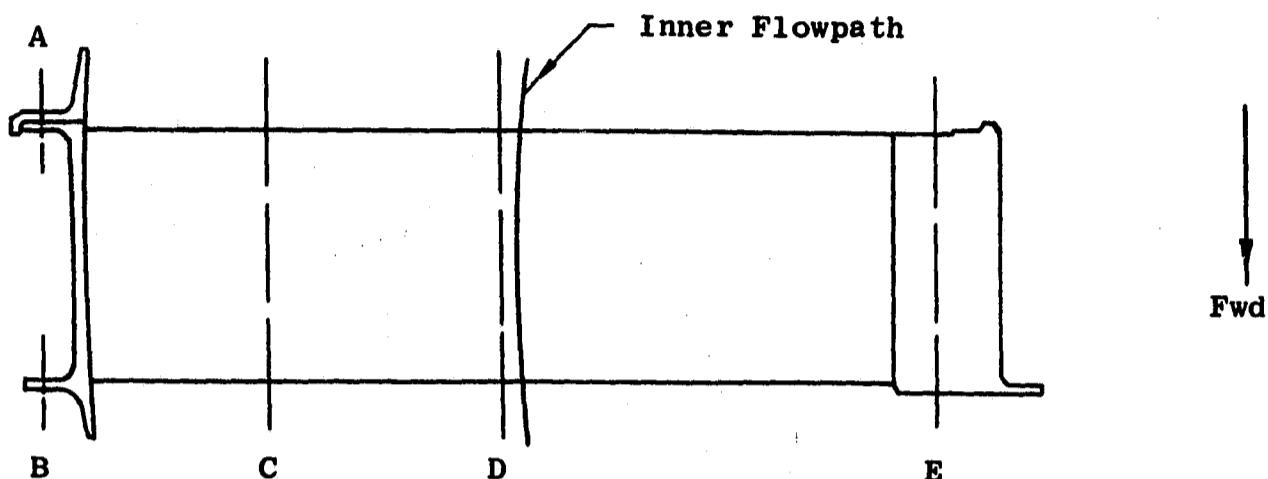


Figure 318. Engine A/B Turbine Rear Frame Maximum Stresses.



Location	Location				
	A	B	C	D	E
<u>Engine A/B</u>					
Strut	7	8	3	7	2
Maximum Stress	22,300	15,600	4200	4500	8800
Allowable Stress	92,000	92,000	87,000	93,000	94,000
<u>Engine C</u>					
Strut	6	1	1	1	1
Maximum Stress	27,100	2800	6400	10,400	4800
Allowable Stress	92,000	92,000	85,000	92,000	94,000

Figure 319. Turbine Rear Frame Maximum Strut Stresses

Table LXXIX. Frame Temperatures, °F

Location	Engines A/B		Engine C	
	SLS	Cruise	SLS	Cruise
T5.4	1182	1075	1171	1050
T5.5	860	717	822	658
1	620	560	750	680
2	700	650	800	730
3	815	750	750	690
4	600	560	1160 (Aug)	1040
5	600	560	720	670
6	1160	1050	1080	970
7	1010	960	1050	950
8	720	620	1080	970
9	775	650	1310 (Peak)	1190 (Peak)
10	840	700	1290 (Peak)	1170 (Peak)
11	700	600	725	650
12	700	600	750	650
13	520	480	920	760
14	---	---	720	650
15	---	---	550	490
16	---	---	550	490
17	---	---	720	650
18	---	---	720	650
19	---	---	600	520
20	---	---	525	470

532

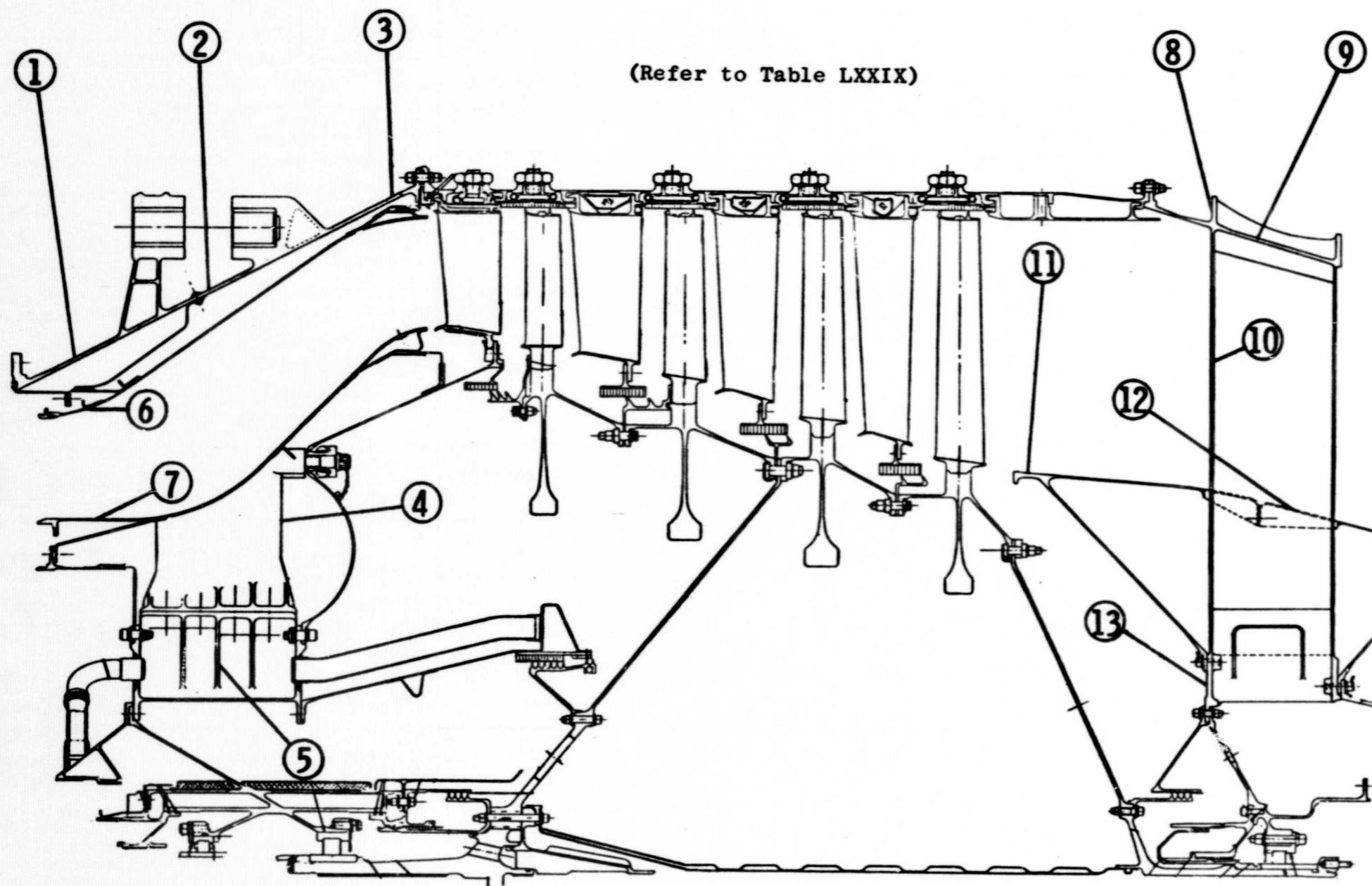


Figure 320. Frame Temperatures, Engine A/B

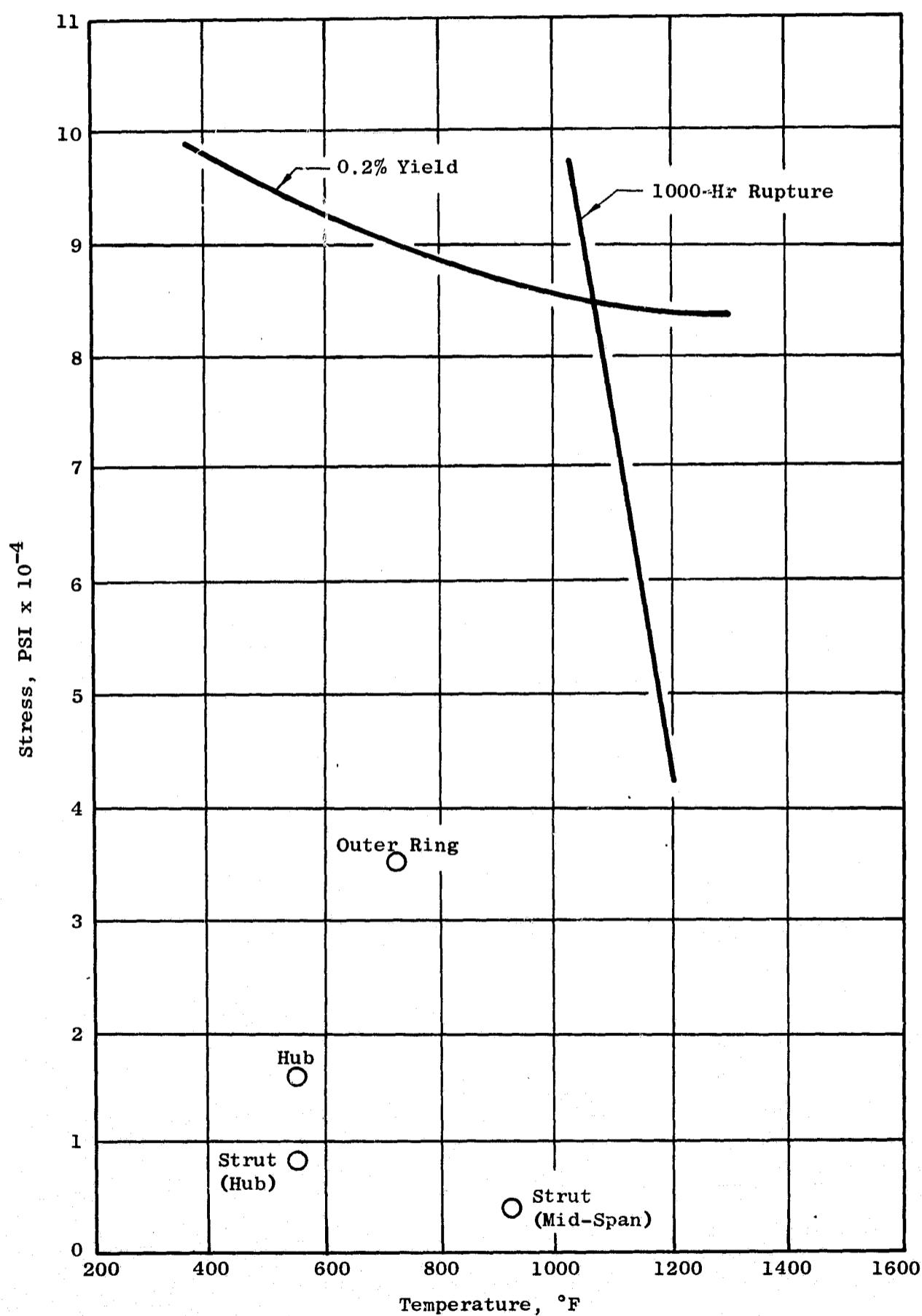


Figure 321. Inconel 718 Cast Material Properties, 30 Deviations

534

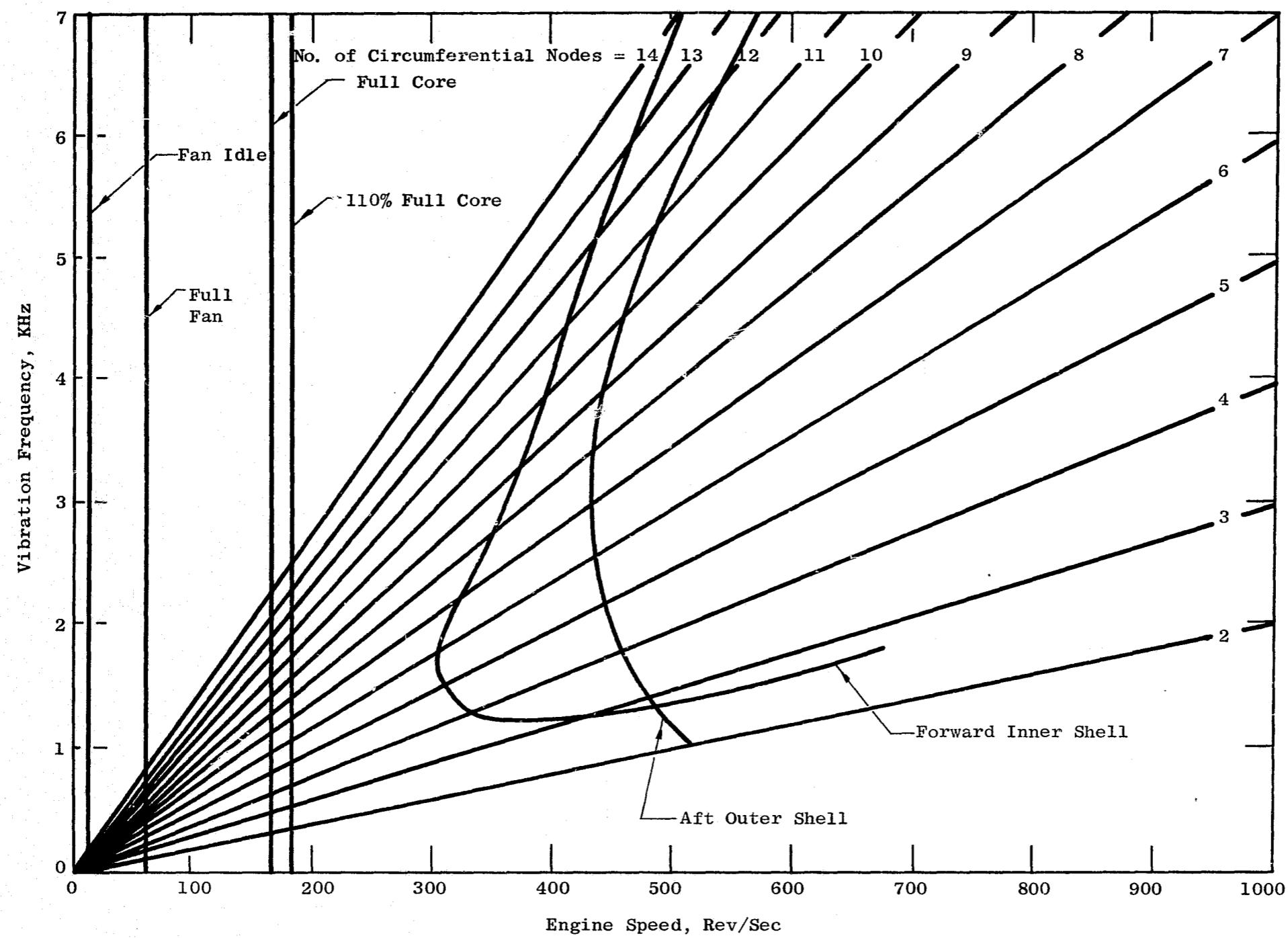


Figure 322. Engine A/B Exhaust Nozzle Shell Stability

535

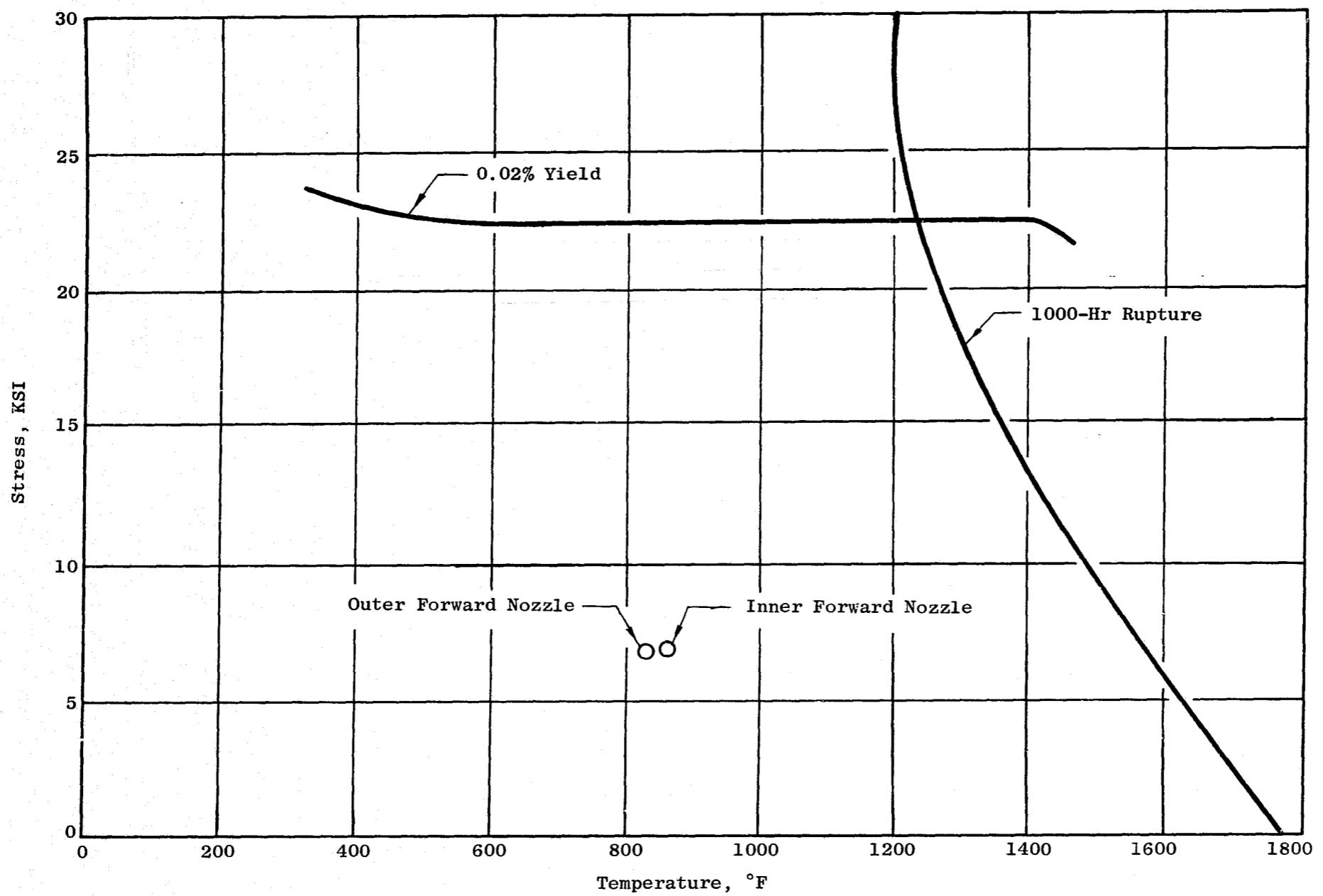


Figure 323. Hastelloy X Yield and Rupture Stresses with 3σ Deviations

The mechanical design philosophy of the Engine C midframe is a structure that is capable of withstanding steady state as well as transient mechanical and thermal stresses. It is the intention that the mechanical stresses imposed on this frame will be approximately 30 percent of the allowable stresses. The remaining 70 percent of the allowable stress is available for thermal transient stress. This low steady state mechanical stress level philosophy is being successfully utilized in the CF6 and TF39 turbine midframe and rear frame structures.

To assist in minimizing the thermal stress, the turbine casing and aft outer ring are A-286 forgings. A-286 material has a higher thermal growth coefficient than R-41 or any R-41 strut casings. The A-286 outer ring and casing will grow, under temperature, faster than the adjacent parts. However, the R-41 struts will be at higher metal temperature under steady state engine operating conditions. The radial growth of the inner ring and strut assembly will be approximately the same as the casing, and steady state thermal stresses will be minimized.

Like the turbine midframe for Engine A/B, the Engine C midframe was completely stress and deflection analyzed. This frame was analyzed using the maximum maneuver combinations shown in Table LXXVI in conjunction with Table XXC and Figure 308 and the frame temperatures in Table LXXIX and Figure 324. The results of these applied maneuver combinations and frame temperatures are the ultimate mount loads shown in Figure 306, the ultimate mount stresses in Figure 312, the maximum bearing load in Figure 307, the maximum frame inner and outer ring (casing) stresses in Figure 325 and the maximum strut stresses in Figure 311. The maximum stresses and associated temperature which occurred in the midframe are compared with the material properties in Figure 326, 327, and 328. Figure 329 shows the steady state axial loads which are imposed on the entire low pressure turbine/frame nozzle assembly.

Engine C low pressure turbine stator vanes are cast integral with the midframe struts and were analyzed for vibratory as well as steady state stresses. Figure 330 illustrates the results of this analysis and also briefly summarizes the stress levels for the fan allowable and the fan steady state alternating allowables and fatigue stresses. A comparison of the vane rupture stress with the material maximum allowable stress is shown in Figure 326.

Figure 331 is the low pressure turbine predicted hot gas temperature profile. This profile (both low pressure turbine inlet and exhaust) was used in determining turbine midframe and rear frame metal temperatures.

7.3.1.4.5 Analysis, Engine C Turbine Rear Frame

The turbine rear frame for engine C is also a CF6 frame with a modified inner flowpath. However, the outer flowpath or frame casing is "cropped" to accommodate the revised flowpath.

Table XXC. Fan C Turbine Midframe Unit Loads

Component Load	lg Down	lg Side (Right)	lg Forward	Thrust T/O	1 Rad/Sec Pitch ($\dot{\alpha}$) Nose Up	1 Rad/Sec ² Yaw ($\dot{\psi}$) Nose Right	1 Rad/Sec ² Pitch ($\ddot{\theta}$) Nose Up	1 Rad/Sec ² Yaw ($\ddot{\psi}$) Nose Right	Side Gust to Right
<u>For. Flight</u>									
Px	0	0	2 250	-18 583	0	0	0	0	0
Py	0	-559	0	0	6 435	0	0	-379	9 680
Pz	559	0	2 040	4 060	0	-6 435	-379	0	0
Mx	0	202 000	0	-203 600	191 720	0	0	-15 145	369 500
My	40 000	0	-11 770	-23 800	0	-96 890	-5 015	0	0
Mz	0	40 000	0	0	-96 890	0	0	5 015	55 000
<u>Aft Flight</u>									
Px	0	0	-1 840	5 840	0	0	0	0	0
Py	0	-1 687	0	0	4 922	0	0	-201	0
Pz	1 687	0	138	214	0	-4 922	-201	0	0
Mx	0	0	0	139 600	0	0	0	0	0
My	-30 100	0	0	0	0	123 068	5 015	0	0
<u>No. 5 Brg</u>									
Py	0	-107	0	0	2 825	0	0	-66.5	0
Pz	107	0	243	437	0	-2 825	-66.5	0	0
<u>No. 6 Brg</u>									
Py	0	-367	0	0	-5 545	0	0	-107.9	0
Pz	367	0	66	161	0	5 545	-107.9	0	0
<u>Strut</u>									
Px	0	0	0	5 387	0	0	0	0	0
<u>Hub</u>									
Px	0	0	0	12 610	0	0	0	0	0
Mx	0	0	0	64 000	0	0	0	0	0
<u>Casing</u>									
Px	0	0	-410	5 254	0	0	0	0	0
<u>Link Mounts</u>									
L1	2 018	13 250	1 352	2 701	-276	-4 688	-410	4.5	7 575
L2	2 018	-13 250	1 352	2 701	276	-4 688	-410	-4.5	-7 575
<u>Center Mount</u>									
L3	0	14 070	0	0	-8 421	0	0	758	4 088

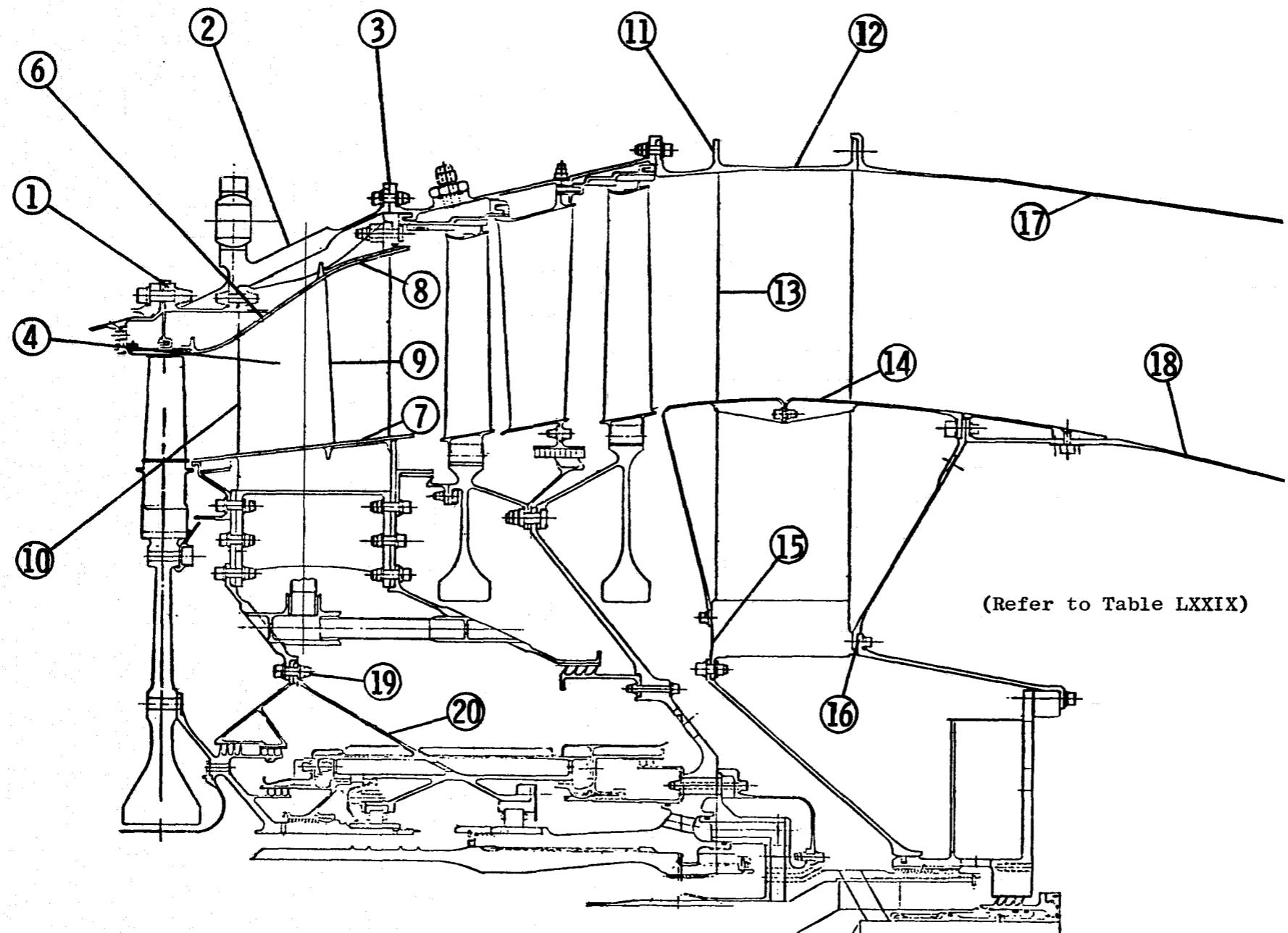


Figure 324. Engine C Frame Temperatures

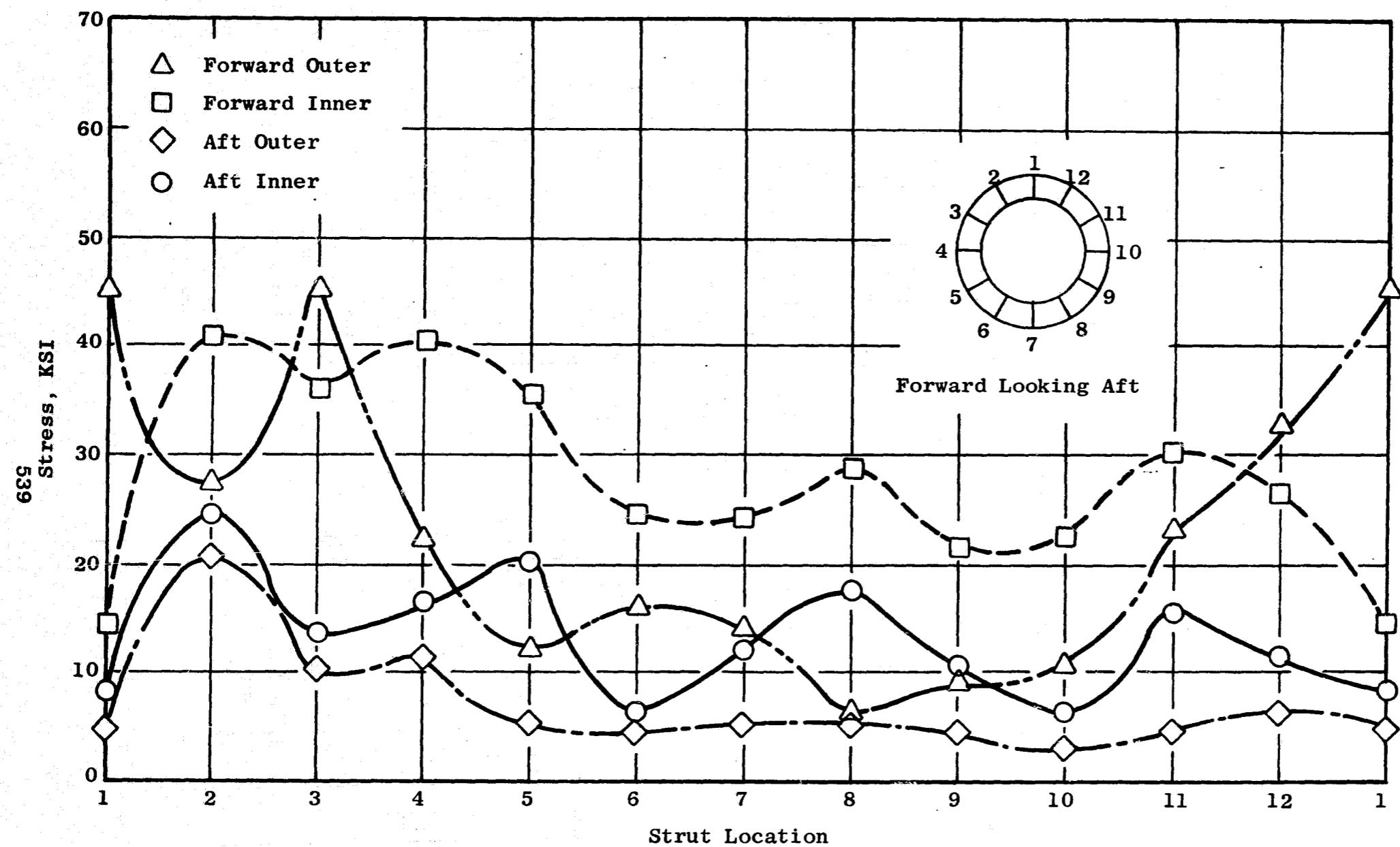


Figure 325. Engine C Turbine Midframe Outer and Inner Ring Stresses

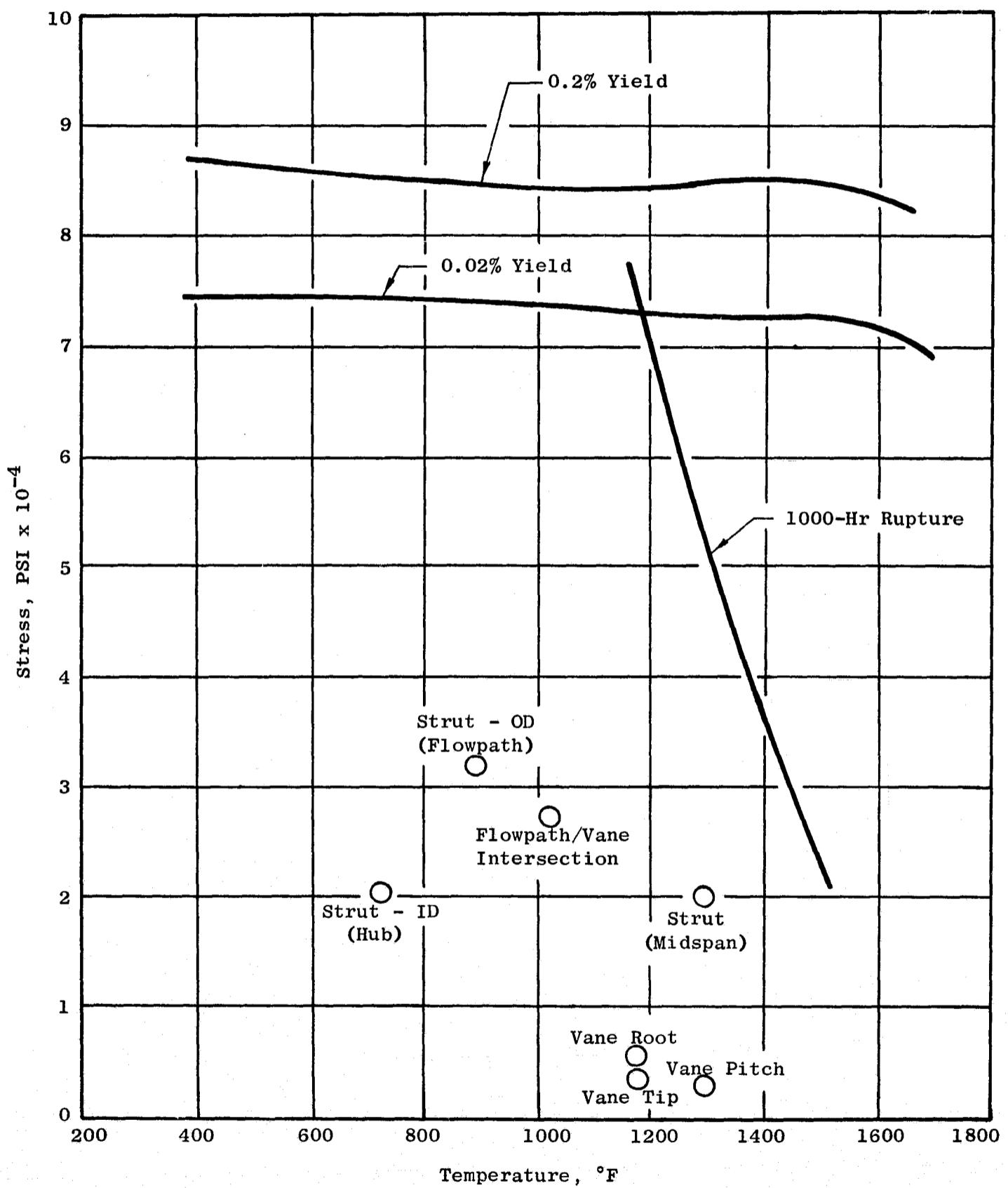


Figure 326. Cast Rene' 41 Material Properties, 3 σ Deviations (Engine C Turbine Midframe Maximum Stresses)

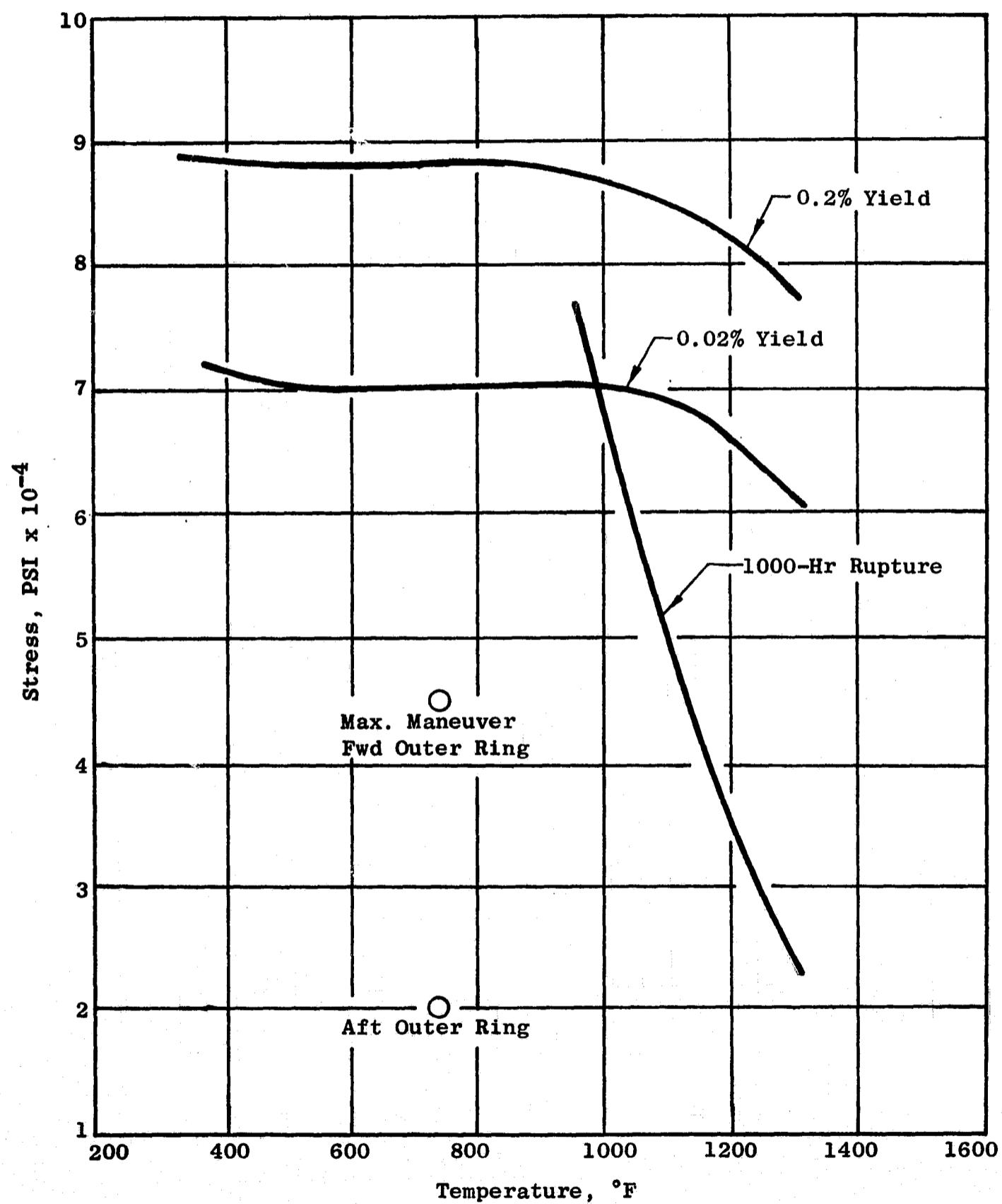


Figure 327. A-286 Forged Material Properties, 30 Deviations

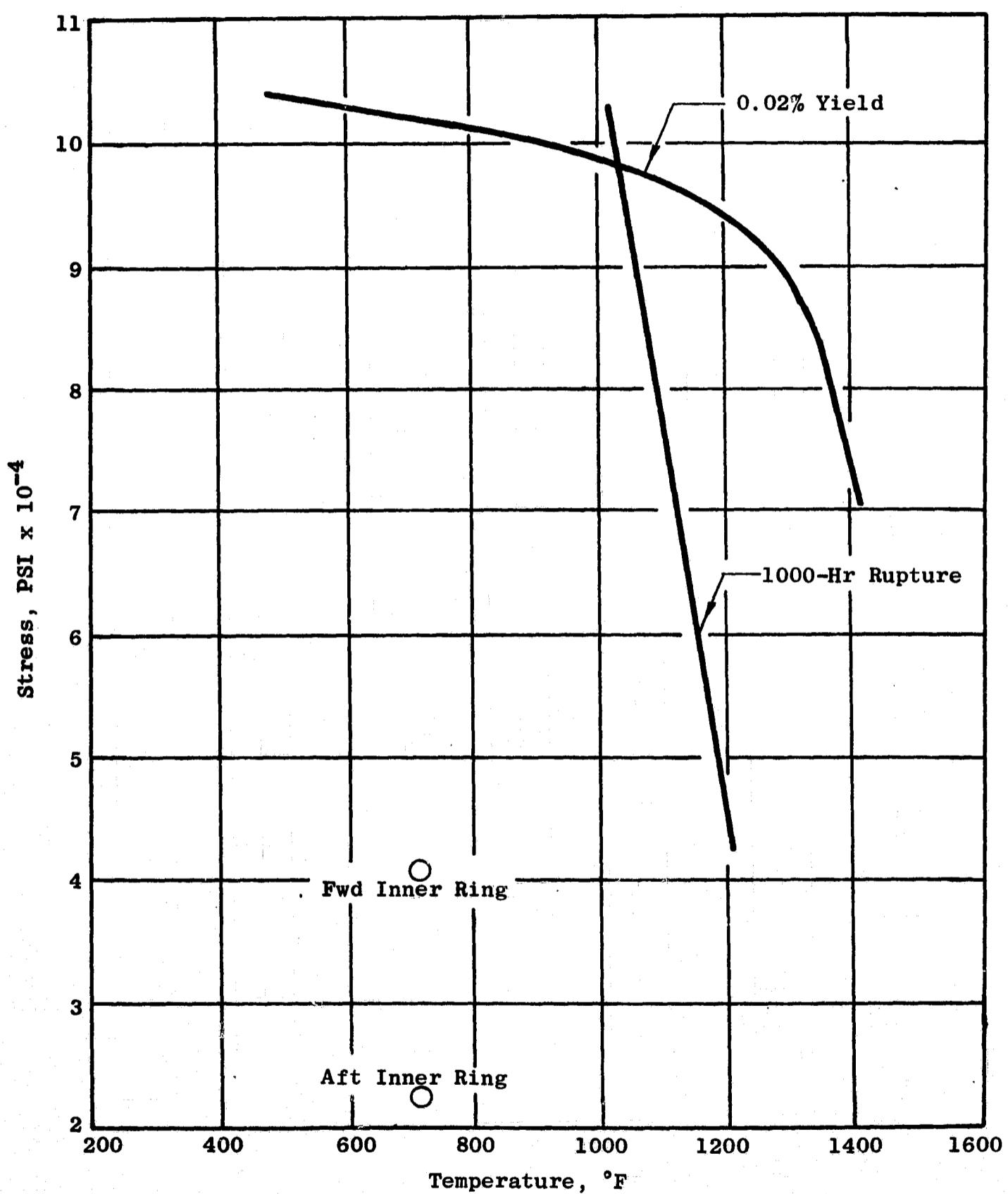


Figure 328. Inconel 718 Material Properties, 3G Deviations (Engine C Turbine Midframe Maximum Stresses)

543

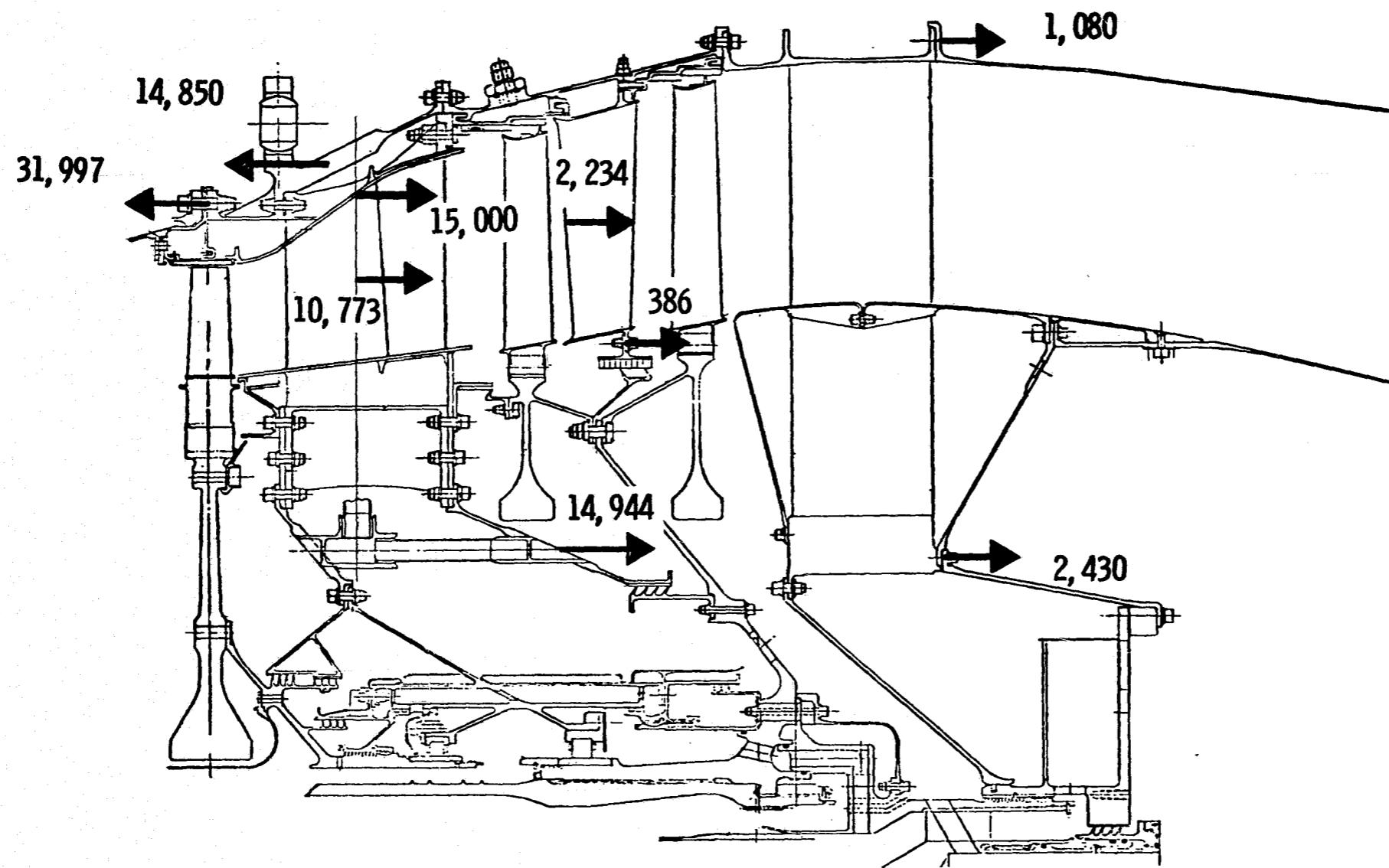


Figure 329. Engine C Turbine Axial Loads, Pounds

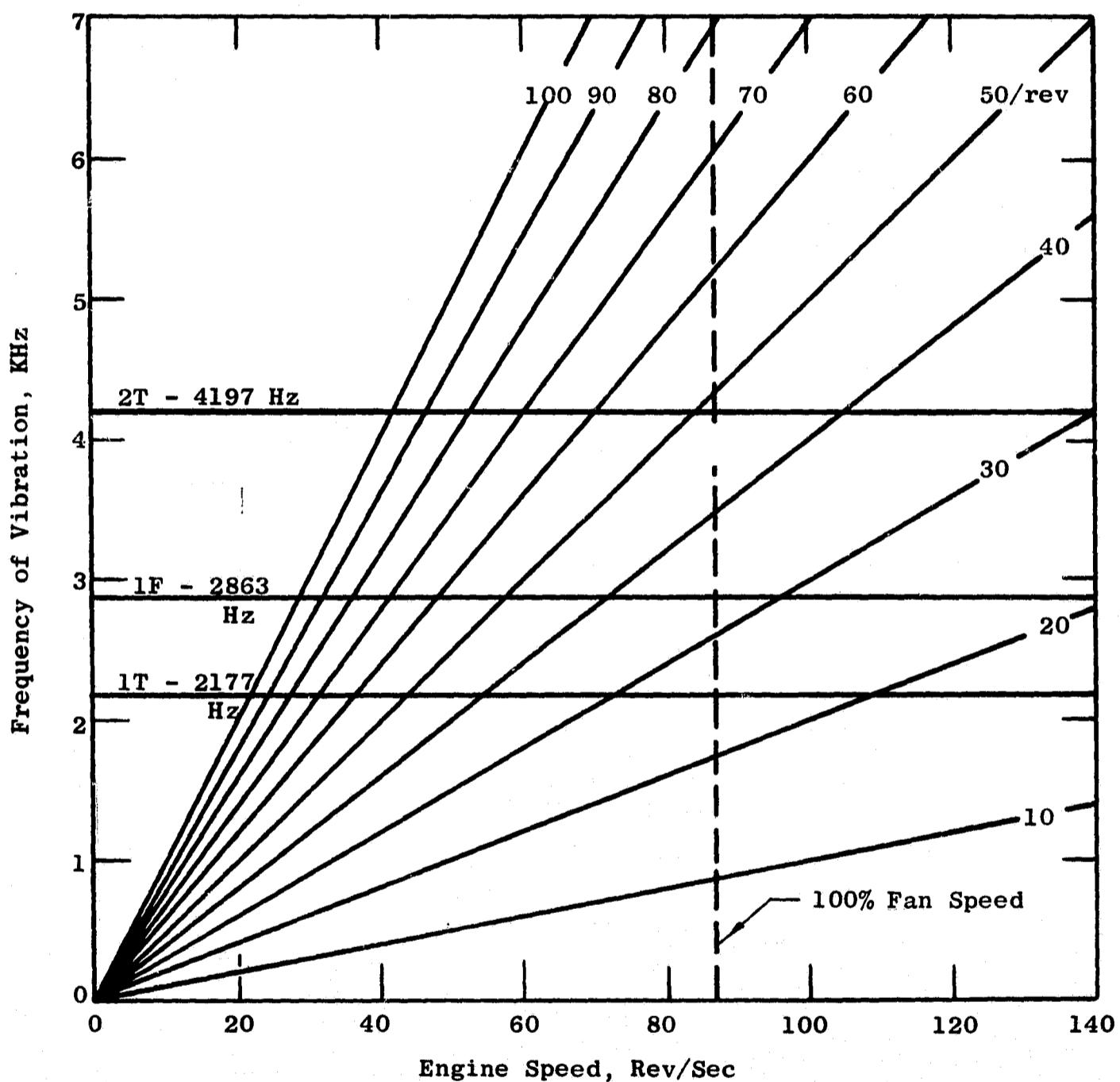


Figure 330. Engine C LP Turbine Stage 1 Vane Natural Frequencies

545

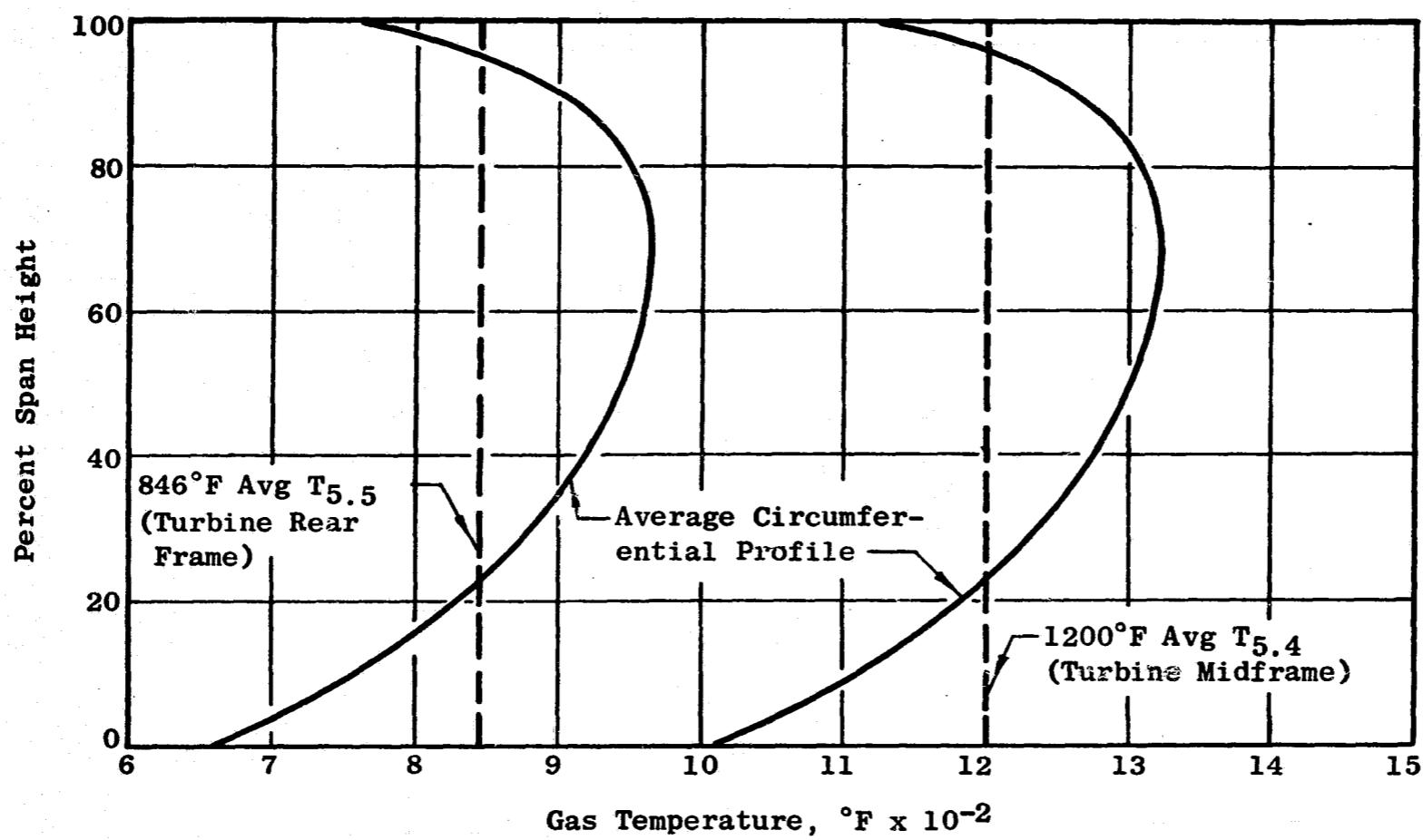


Figure 331. Engine C Integrated Profile of Peaks

The turbine frame assembly consists of an Inconel 718 casting weldment structure and a Hastelloy X inner flowpath. Four axially-welded 90° cast arc segments form the frame 360° outer casing. The cast hub ring is joined to the outer casing by eight, partially-tangential strut castings, thus forming the welded structure. The Hastelloy X inner flowpath is a welded two-piece bolted assembly supported by the frame hub.

The maximum stresses which are induced in the Engine C rear frame by maneuver loads are shown in Figures 319 and 332. These stresses are the result of the flight condition shown in Table LXXVI, the bearing unit loads in Table LXXVII and the frame metal temperatures shown in Table LXXIX. Figure 333 is a comparison of the maximum frame stresses relative to the material allowable stresses.

7.3.1.4.6 Analysis, Engine C Exhaust Nozzle

The exhaust nozzle for Engine C is a simple shell convergent nozzle of a type that is utilized on the CF6 engine. This nozzle is basically a utility type nozzle and is subjected to moderate temperature and stresses. The primary mode of failure will be vibratory. Figure 334 shows the shell stability frequency relative to the engine operating frequency (engine rpm). The maximum mechanical stresses in this nozzle are relatively low and are compared in Figure 323 with the material allowable stresses.

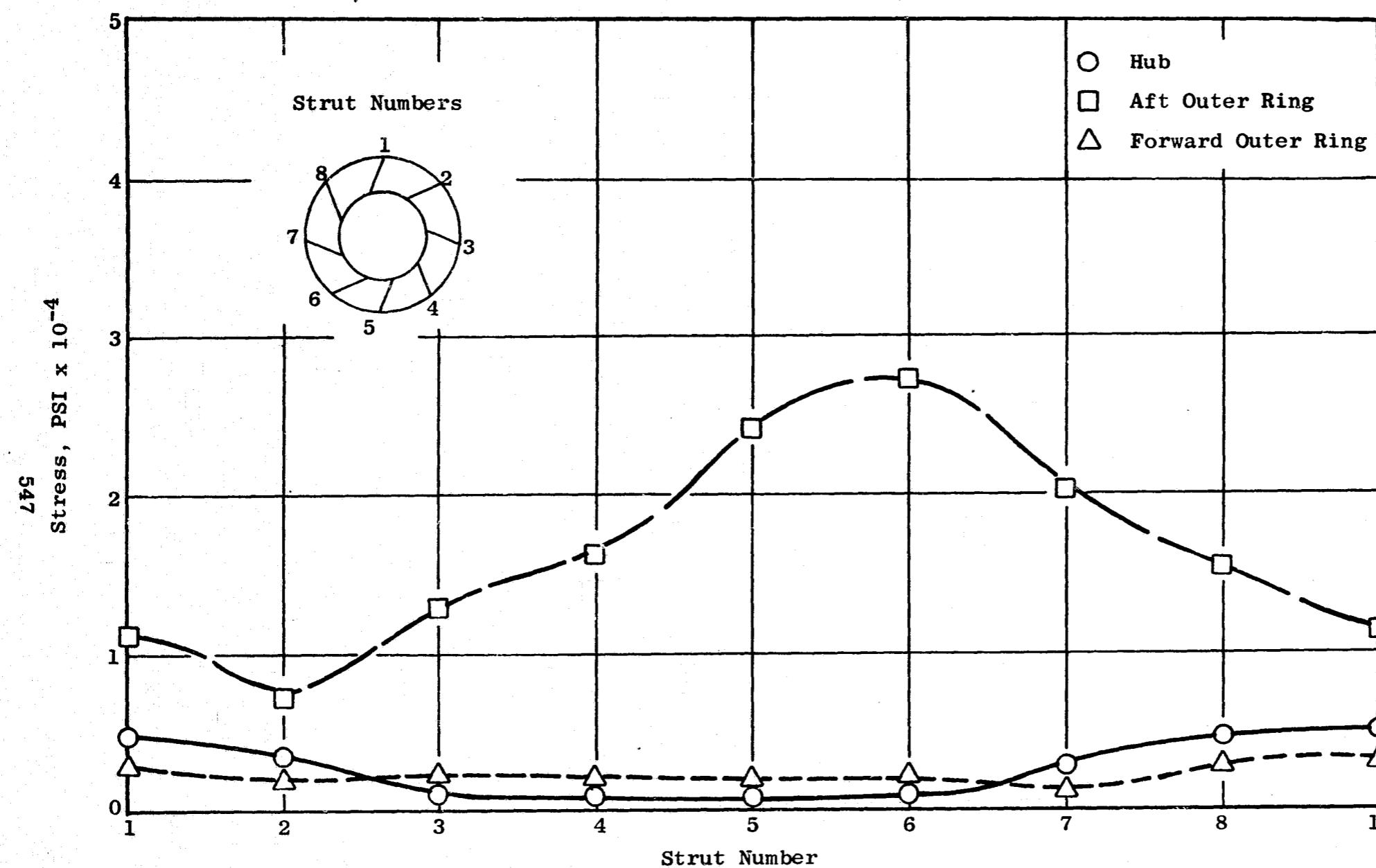


Figure 332. Engine C Turbine Rear Frame Maximum Stresses

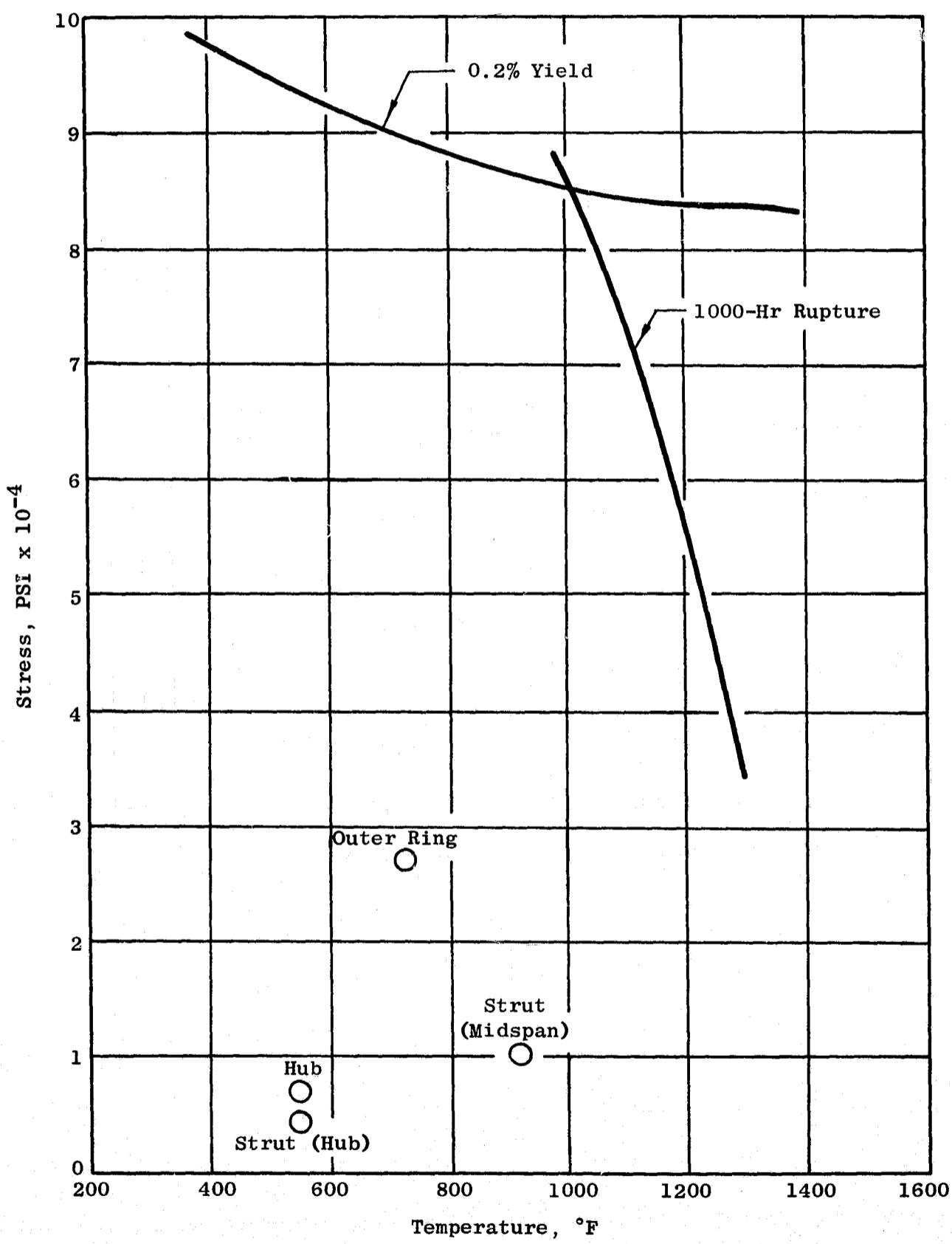


Figure 333. Inconel 718 Cast Material Properties, 30 Deviations
(Engine C Turbine Rear Frame Maximum Stress)

549

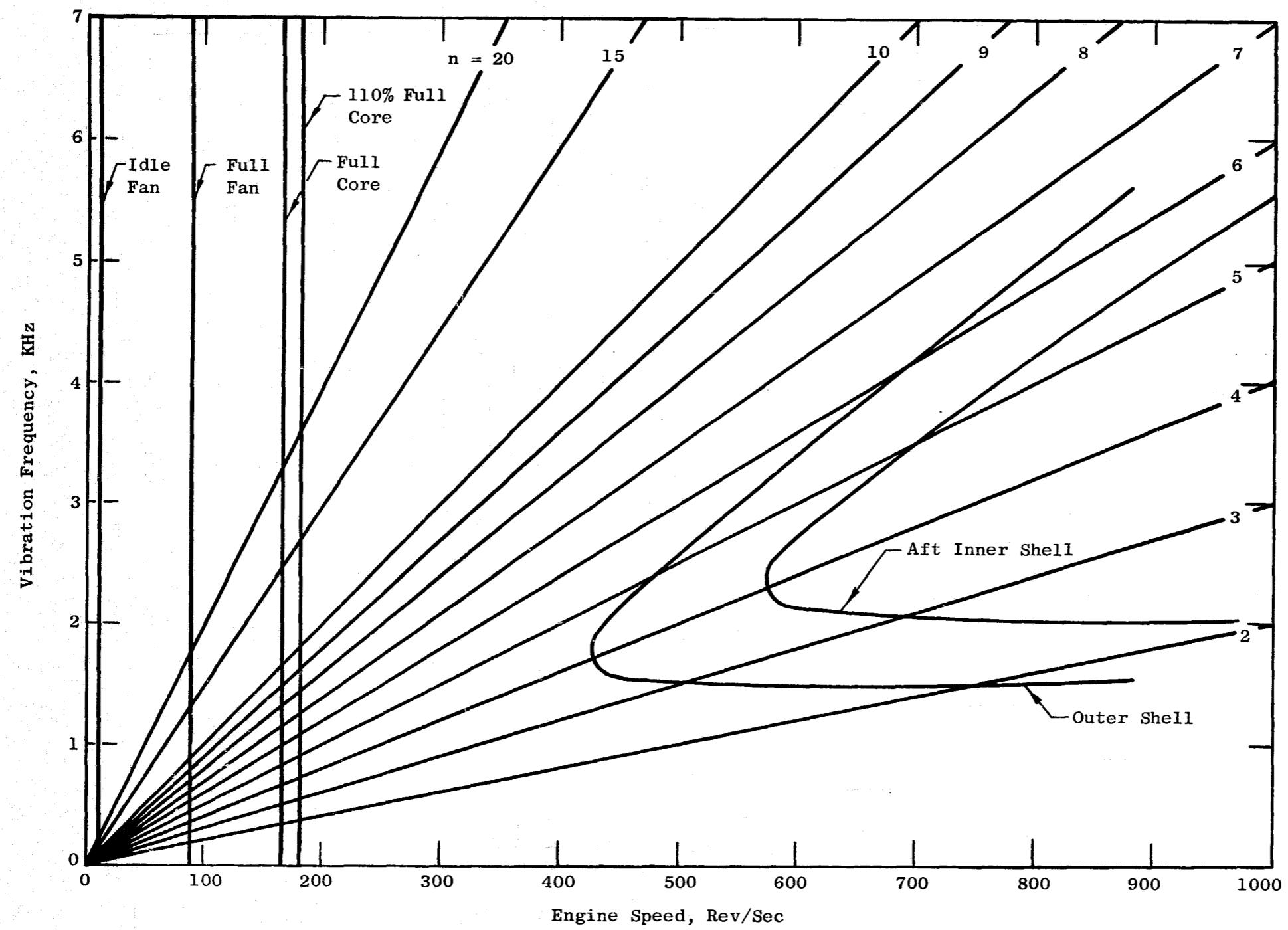


Figure 334. Engine C Exhaust Nozzle Shell Stability

8.0 TURBINE THRUST BALANCE AND PARASITIC FLOW ANALYSIS

8.1 SUMMARY

This section presents the analysis of the bearing thrust forces and parasitic flows of the high and low pressure spools of the Experimental Quiet Engine configurations A, B, and C.

The analysis to determine the bearing thrust loads and parasitic leakage flows of the Experimental Quiet Engines paralleled those successfully used on both the TF39 and CF6 engines. This was possible due to the fact that the Experimental Quiet Engine utilizes a TF39 core and a low pressure system very similar to both the TF39 and the CF6. All seals, holes, tubes, etc., are similar on all of these engines, as is the general design of the air pressurization system.

The analytical tool used successfully on both the TF39 and CF6 engines was the "Rotor Thrust Balance" computer program. This program calculates the net axial force acting on the rotor spool along with the necessary cavity pressures and intercavity leakage flows. Since accuracy of this type of analysis has been proven on the above engine, the same type of analysis was performed on the Experimental Quiet Engines.

Results of the analysis are bearing thrust loads, internal cavity static pressures and temperatures, and intercavity leakage flows throughout the entire network considered. Bearing thrust loads for the high and low pressure systems of the three engine configurations are presented and compared with the bearing thrust loads calculated for the CF6 engine at the same operating point.

8.2 METHOD OF ANALYSIS

The input necessary to run the "Rotor Thrust Balance" program falls into four general categories:

- a) Aerodynamic loads
- b) Network boundary static pressures and temperatures
- c) Engine geometry
- d) Flow resistance characteristics

Input for the analysis was determined for the engine operating at the sea level static, standard day condition. All the flow resistance characteristics (seal clearances, areas, etc.) were calculated for nominal running conditions. No failed-seal or other off-design operation was considered.

Aerodynamic loads were obtained in two ways. All blade and drum forces acting on the low pressure spool for fans A, B, and C were determined from the detailed aerodynamic design analysis of the respective components. The high pressure system (compressor and turbine) blade and drum forces were determined from curves which plot these loads as a function of appropriate cycle parameters. These curves were obtained from actual engine experience on the core engine of the TF39 engine, which is similar to the core used on all three versions of the Experimental Quiet Engine.

The network boundary static pressures and temperatures were obtained in one of three ways:

- a) From the detailed aerodynamic design
- b) From the cycle data and empirical data curves
- c) From the cycle data and empirical equations

Table XIXC lists the location of the various network boundaries, indicates the source for the number input to the program, and tabulates the respective values of static pressure and temperature for the three engines considered. The empirical curves and equations used to obtain these input numbers are based on engine experience on the TF39 and CF6 engines.

The geometrical configuration of the engine was taken from the engine layout and flowpath drawings.

Flow resistance characteristics were taken to be the same as those used in the analysis of the CF6 and the TF39 engines. These characteristics specifically included seal, hole, tube, and leakage path flow resistance as a function of flow area and pressure ratio across the restriction.

8.3 RESULTS OF ANALYSIS

The bearing thrust loads determined by the analysis are shown in Table XVIIIC. Comparison of these loads with those experienced on the CF6 engine indicates that they are well within the allowable bearing limits.

Table XIXC. Flow Network Boundary Conditions

Location	Source	Fan A		Fan B		Fan C	
		P _s	T _s	P _s	T _s	P _s	T _s
Atmospheric	Cycle	14.7	59	14.7	59	14.7	59
Fan Rotor (Root)	Aero Data	14.0	82	13.6	82	14.7	82
Fan Frame Strut Pressurization	Aero Data	19.8	119	19.7	119	20.6	119
HP IGV (Exit, Root)	Empirical Data	16.3	82	17.6	82	18.1	82
9th Stage (Tip)	Empirical Data	76.0	540	78.4	570	82.4	590
Compressor Rotor (Exit, Root)	Empirical Data	198	761	202	772	211.5	785
Combustor Bypass (Cooling)	Empirical Data	219	761	223	772	229	785
HP Turbine Rotor (Root, Inlet Cavity)	Empirical Data	117	761	119	772	125	785
HP Turbine Rotor (Exit)	Empirical Data	45.8	1210	46.6	1219	47.7	1212
LP Turbine Stator (Inlet)	Aero Data	49.9	1124	49.9	1124	49.3	1175
LP Turbine Stator (Tip, Exit)	Aero Data	41.0	1051	41.0	1051	33.8	1034
LP Turbine Stator (Root, Exit)	Aero Data	37.9	1021	37.9	1021	23.7	906
LP Turbine Rotor (Root, Exit)	Aero Data	18.7	802	18.7	802	16.5	810

Table XVIIIC. Bearing Thrust Loads

Spool	Quiet Engine			CF6
	Fan A	Fan B	Fan C	
High Pressure	1331 Aft	1522 Aft	2771 Aft	820 Aft
Low Pressure	5208 Aft	5493 Aft	6980 Fwd	8324 Aft

Cavity static pressures and intercavity flows are shown in Figures 335 through 342. Static pressures shown are in units of psia, and all flows are in units of lbs/sec. All of the engine versions exhibit cavity pressures and flows which are similar to those on the CF6 and TF39 engines. Therefore, no cavity pressurization or internal airflow problems are anticipated.

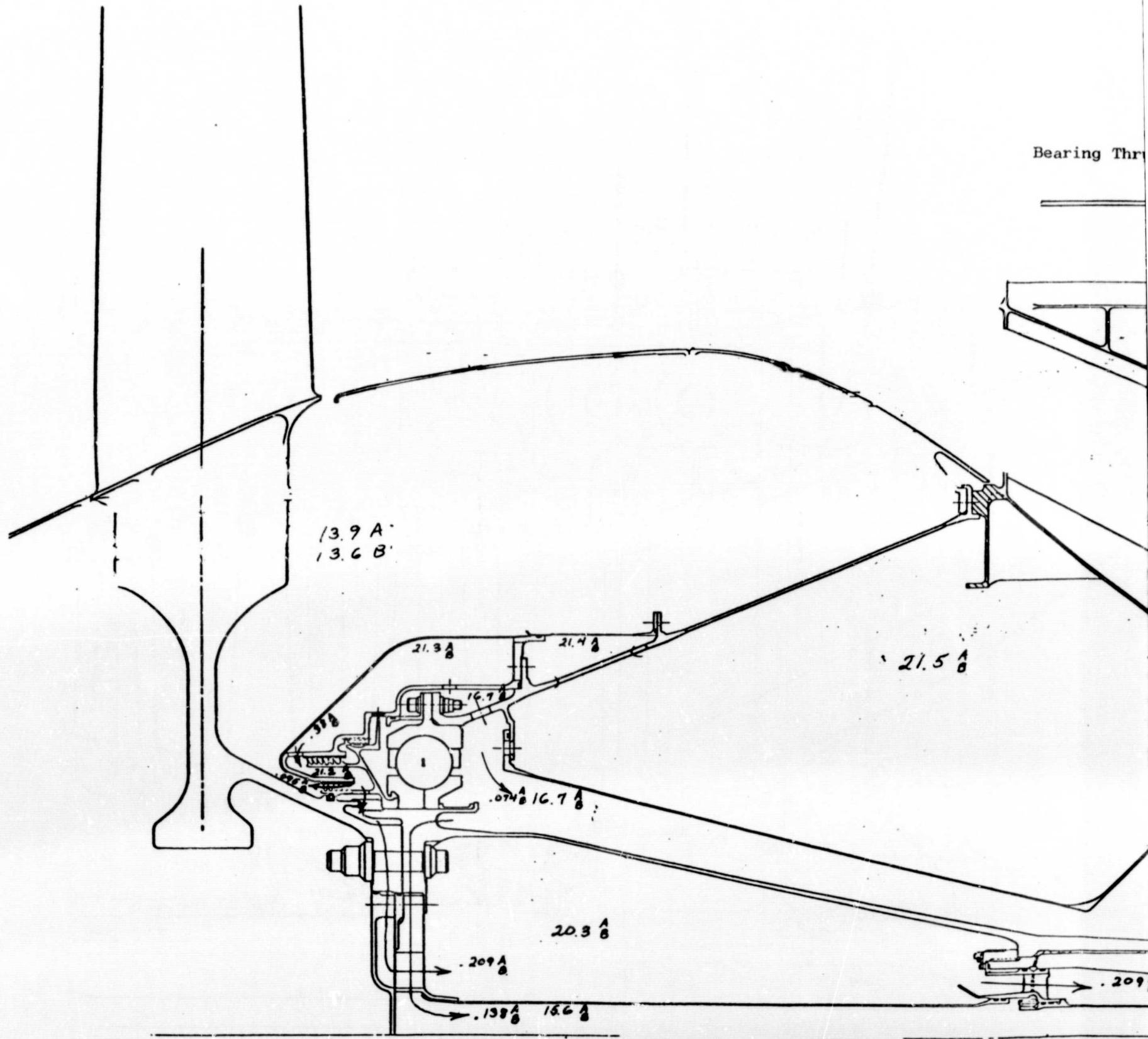
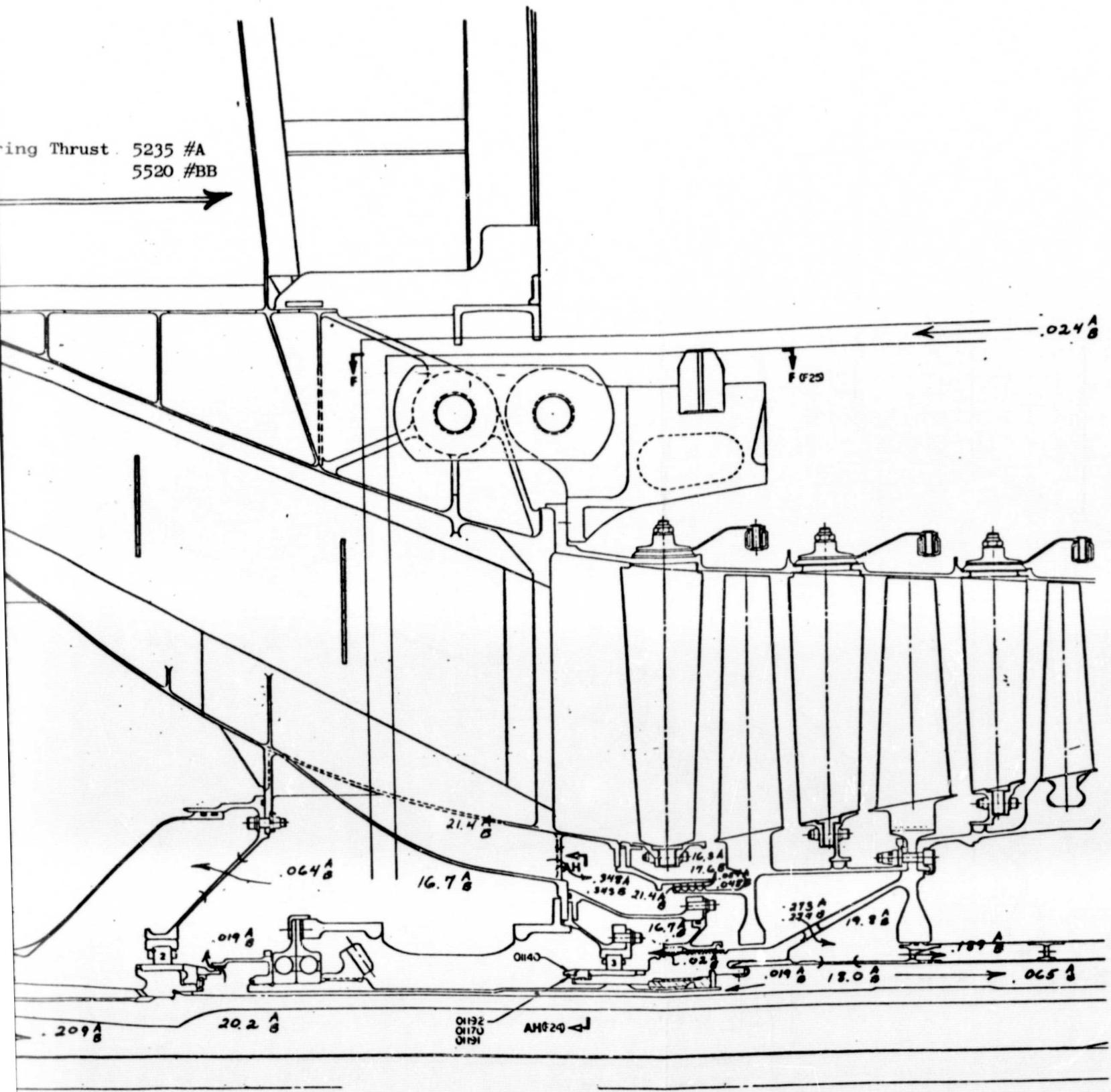


Figure 335. Engine Forward Cavity Press



Pressures and Flows, Fans A/B

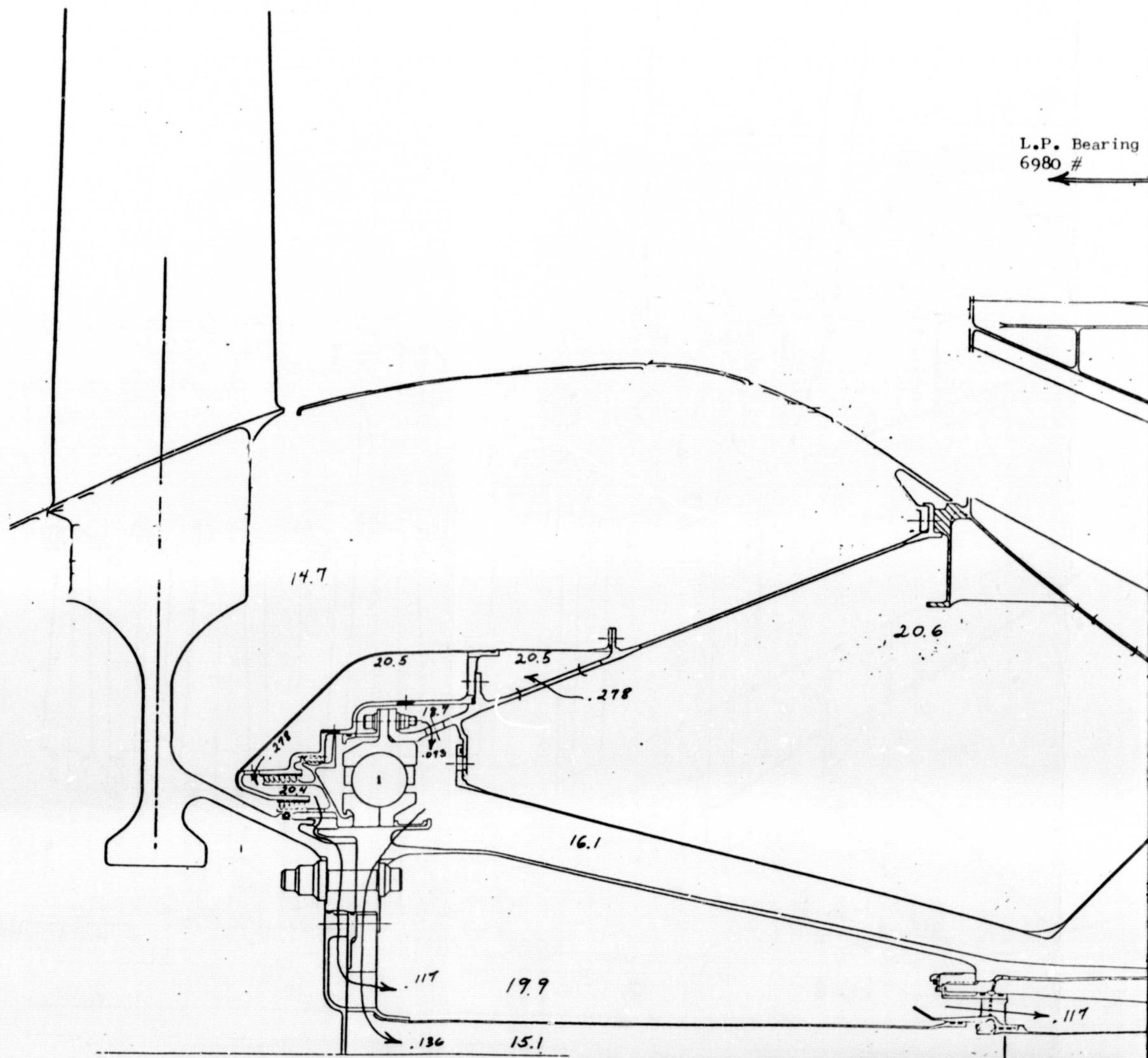
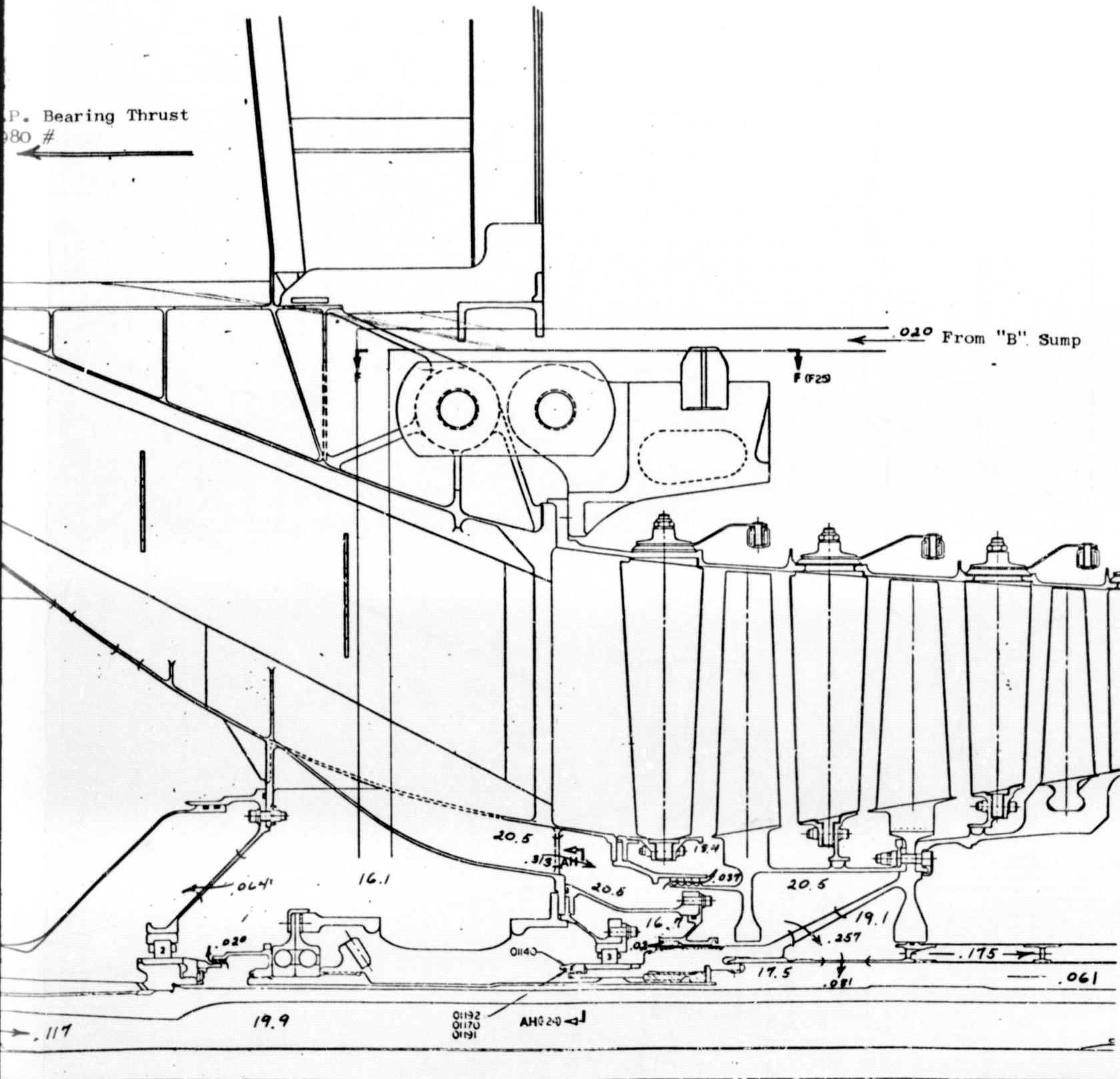


Figure 336. Engine Forward Cavity Pre



Cavity Pressures and Flows, Fan C

FOLDOUT FRAME

2

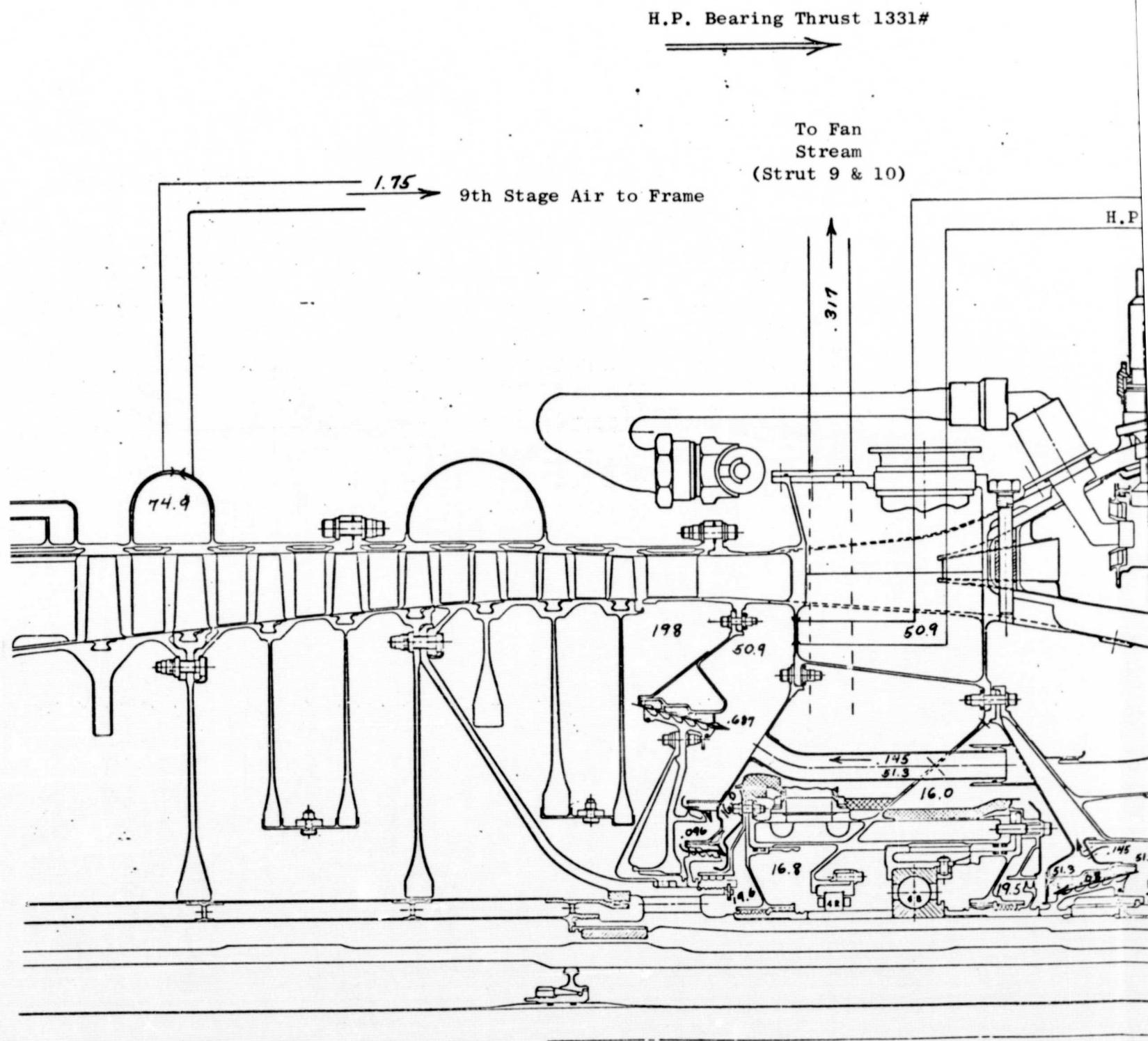
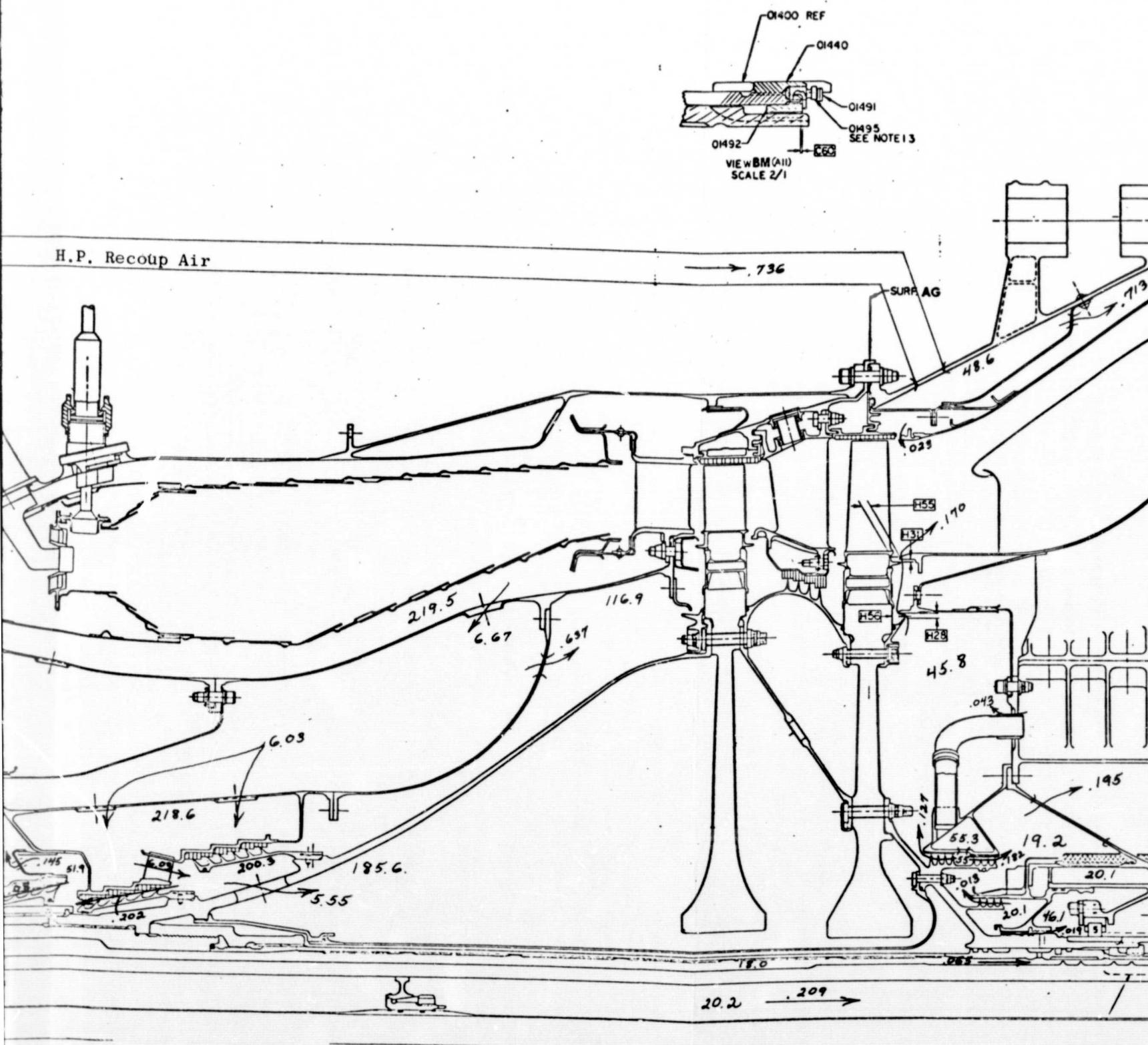


Figure 337. Engine Mid-Cavite



Cavity Pressures and Flows, Fan A

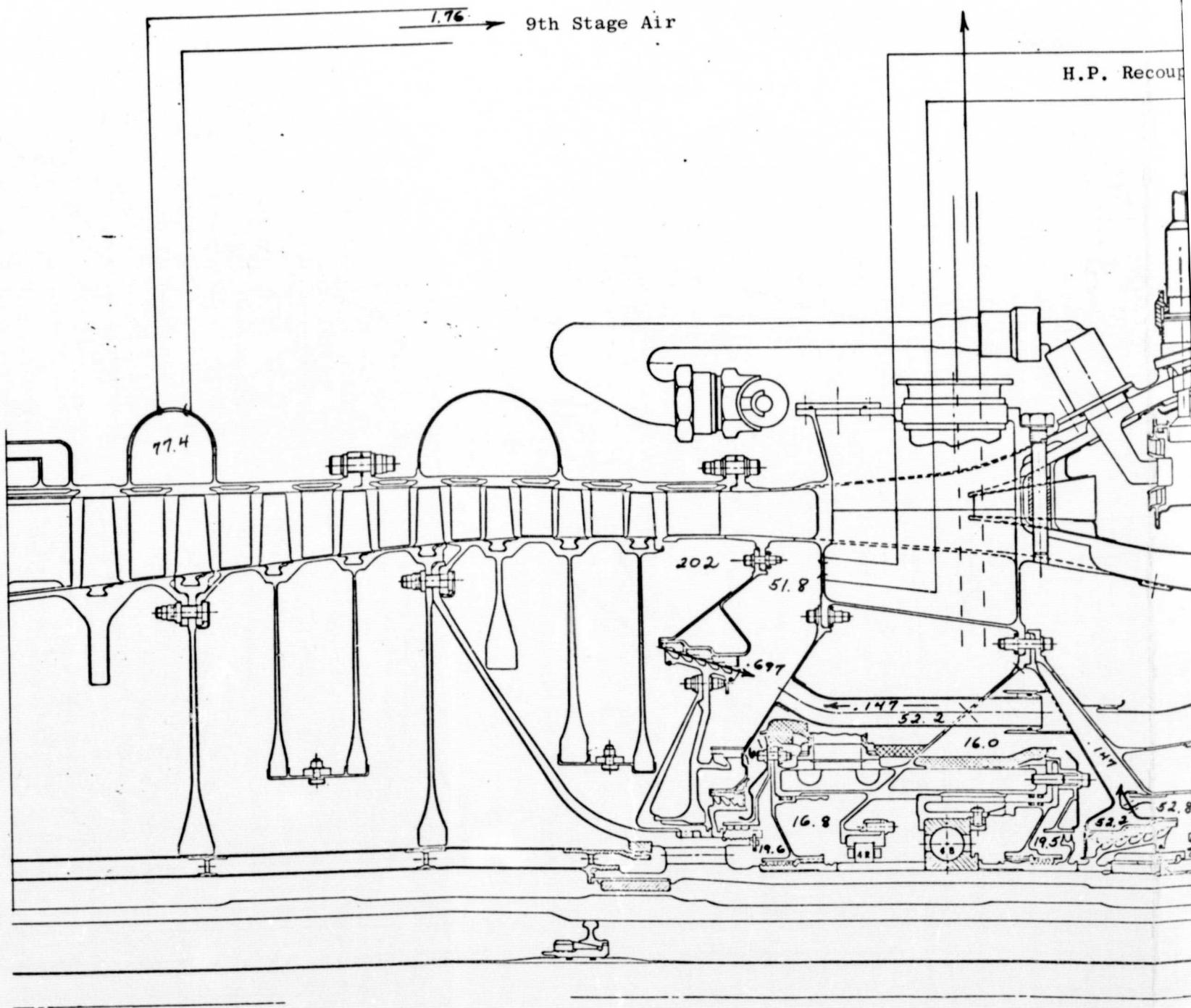
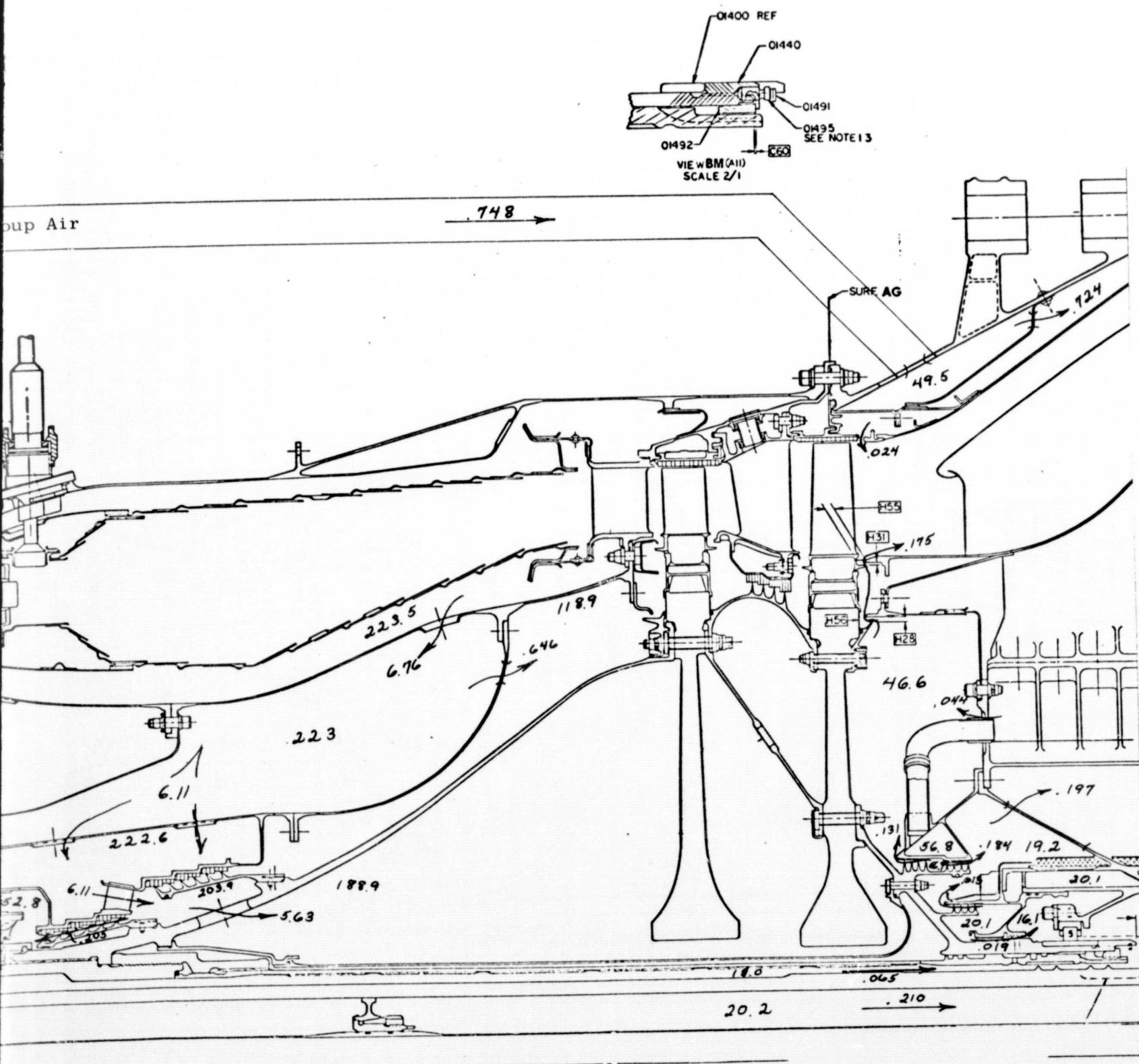


Figure 338. Engine Mid-Cavi



Air cavity Pressures and Flows, Fan B

FOLDOUT FRAME
2

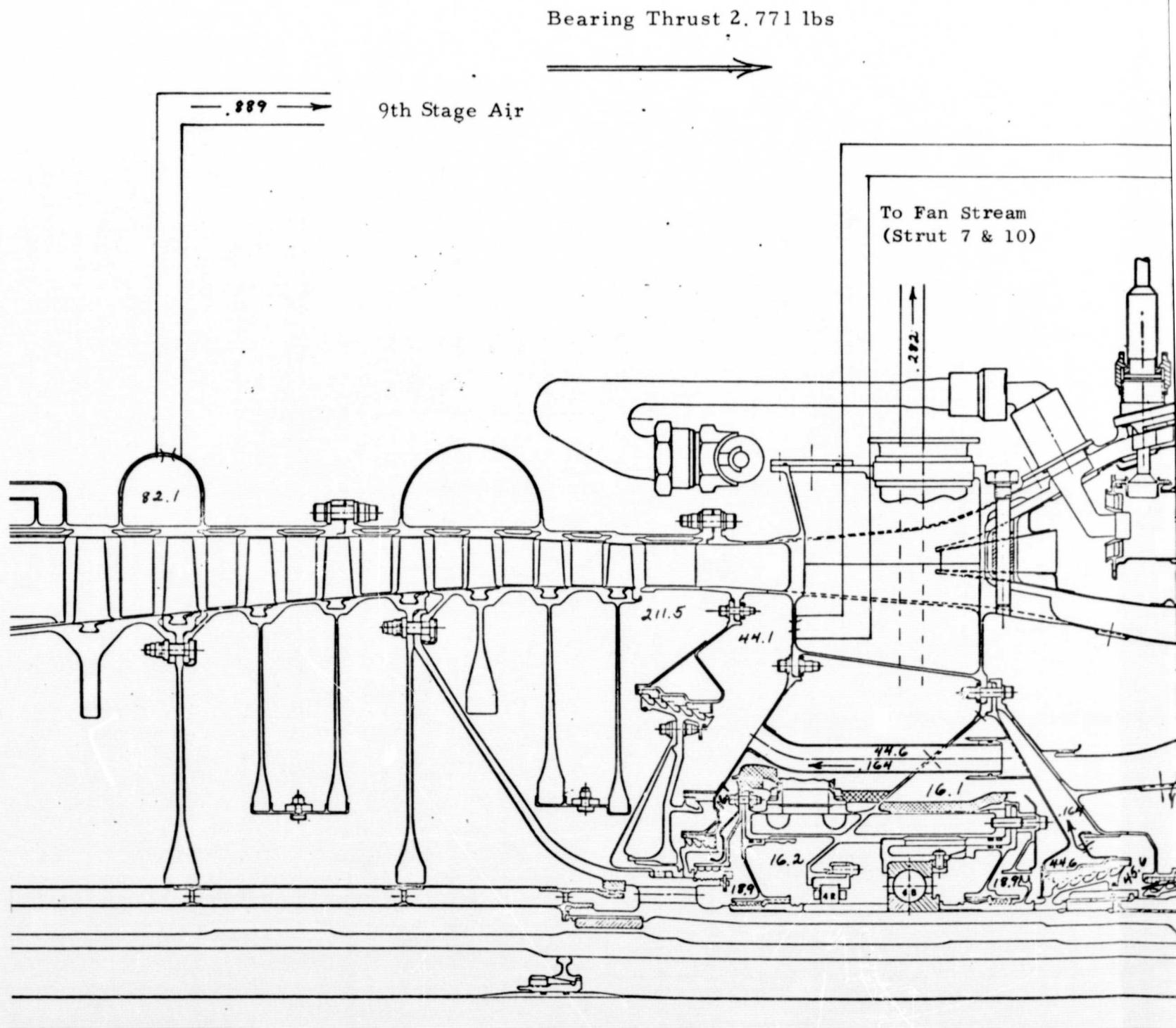
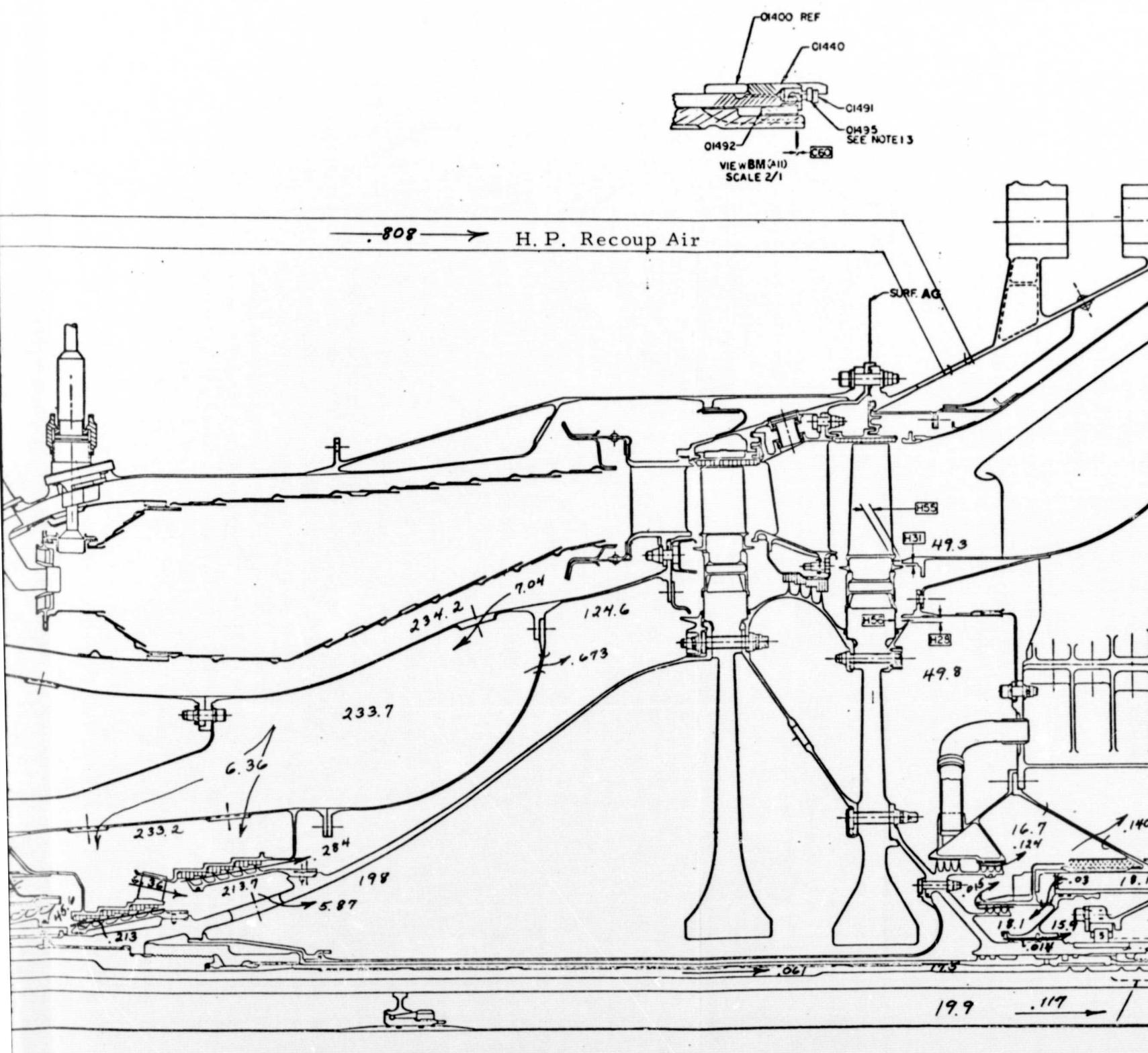


Figure 339. Engine Mid-V Figure 339. Engi



Engine Mid-Cavity Pressures and Flows, Fan C

L.P. Bearing Thrust

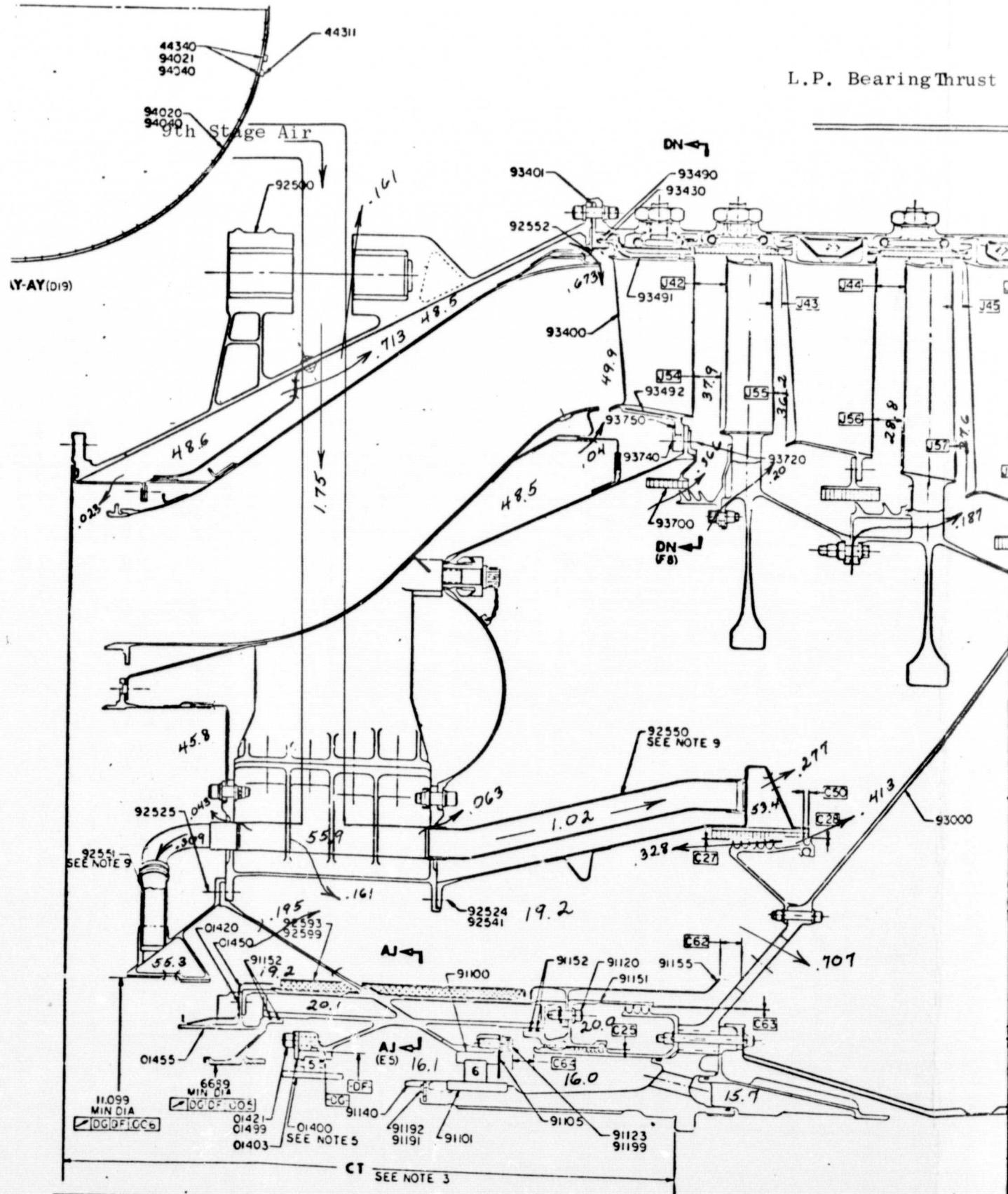
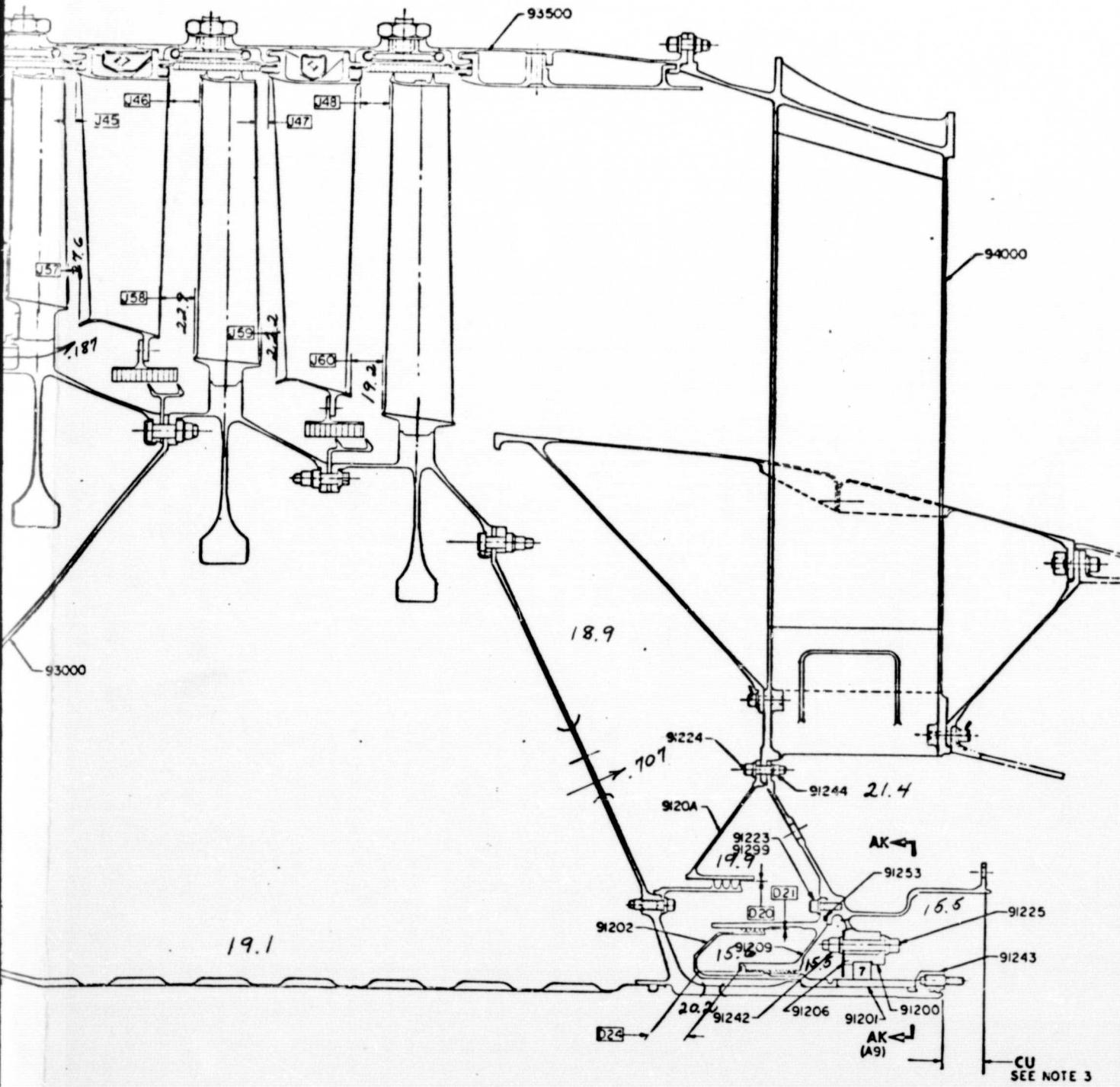


Figure 340. Engine Aft Cavity P

ing Thrust 5272#



Cavity Pressures and Flows, Fan A

FOLDOUT FRAME

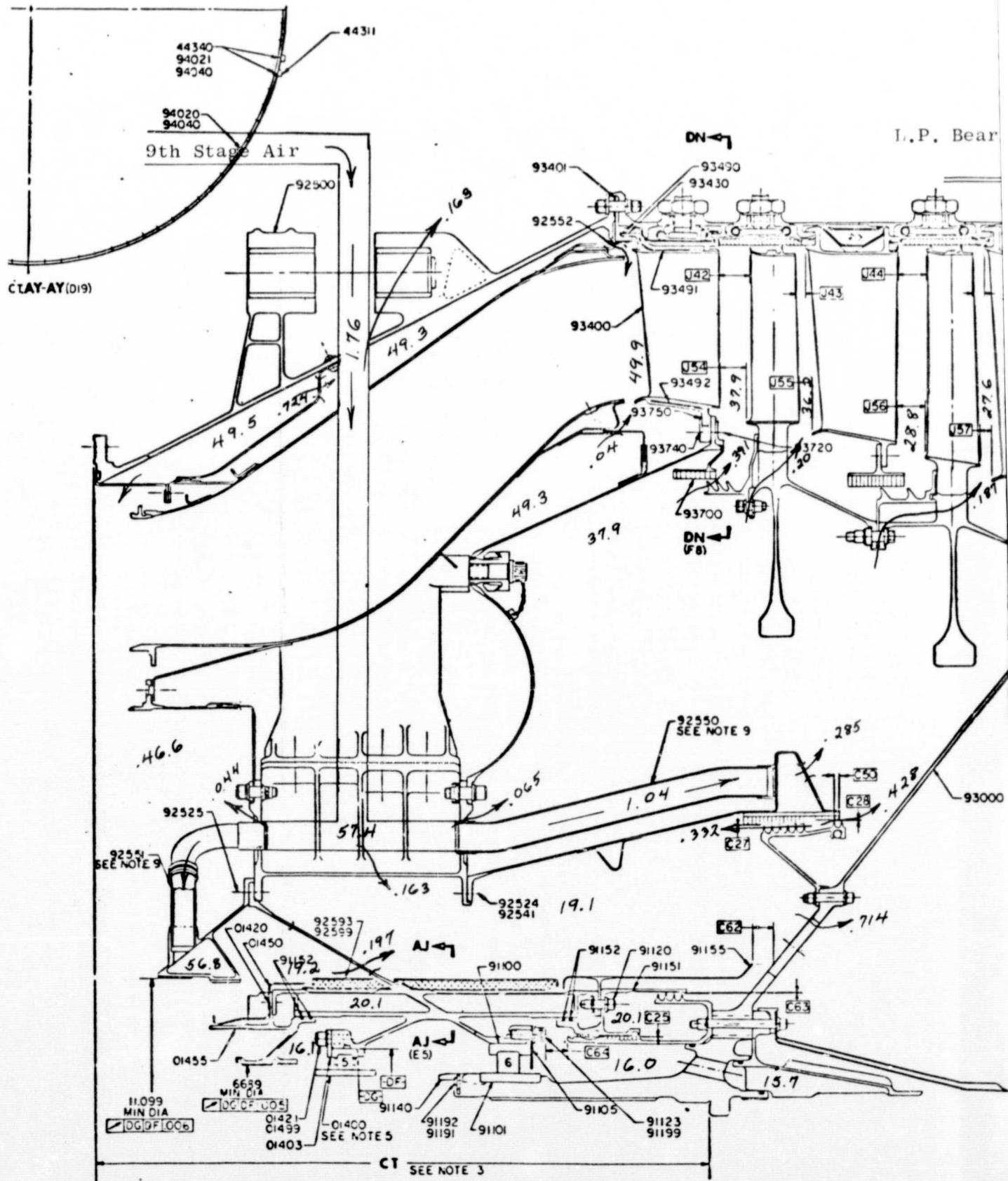
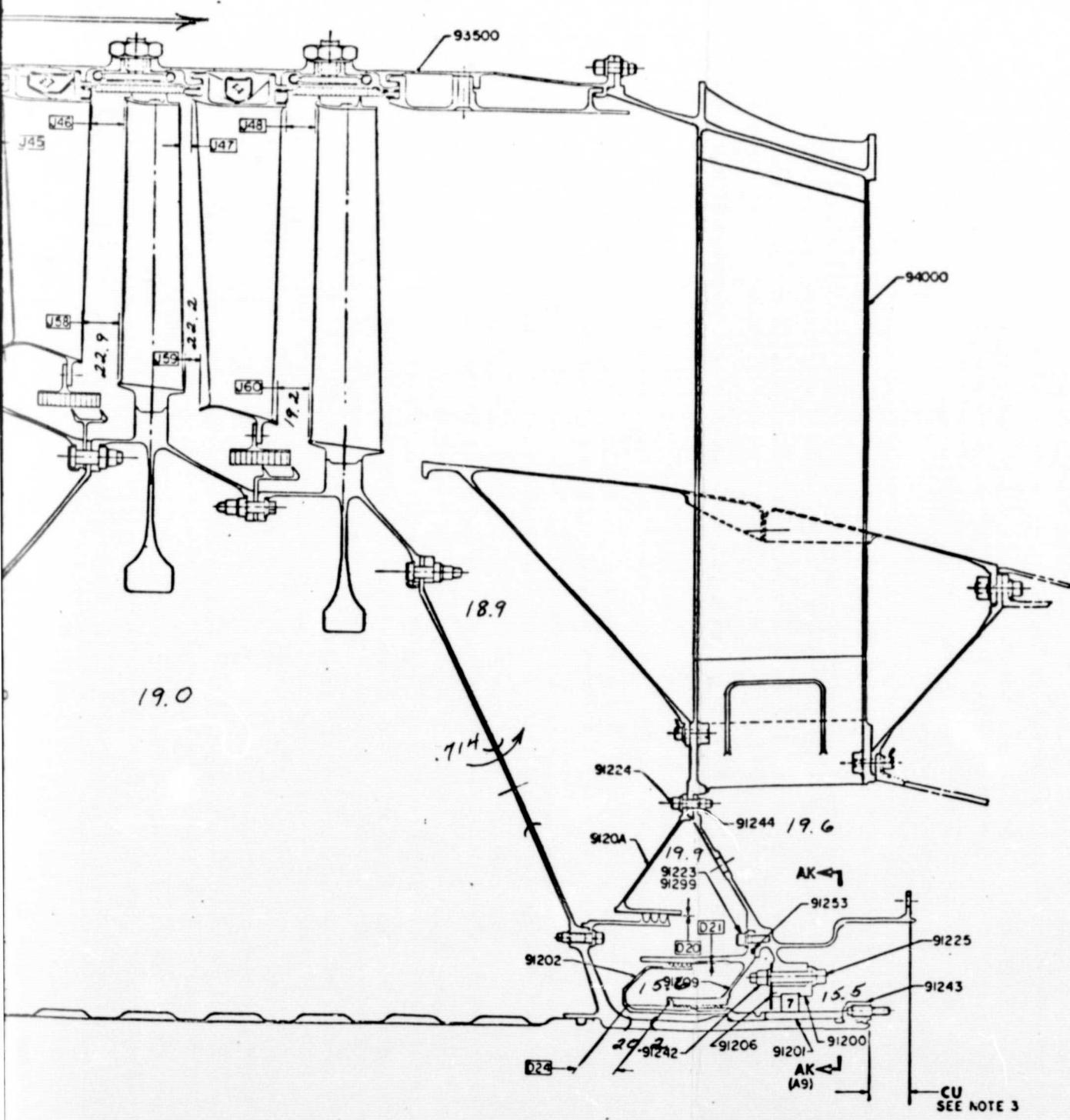


Figure 341. Engine Aft Cavity

ring Thrust 5558#



Pressures and Flows, Fan B

563

PRECEDING PAGE BLANK NOT FILMED

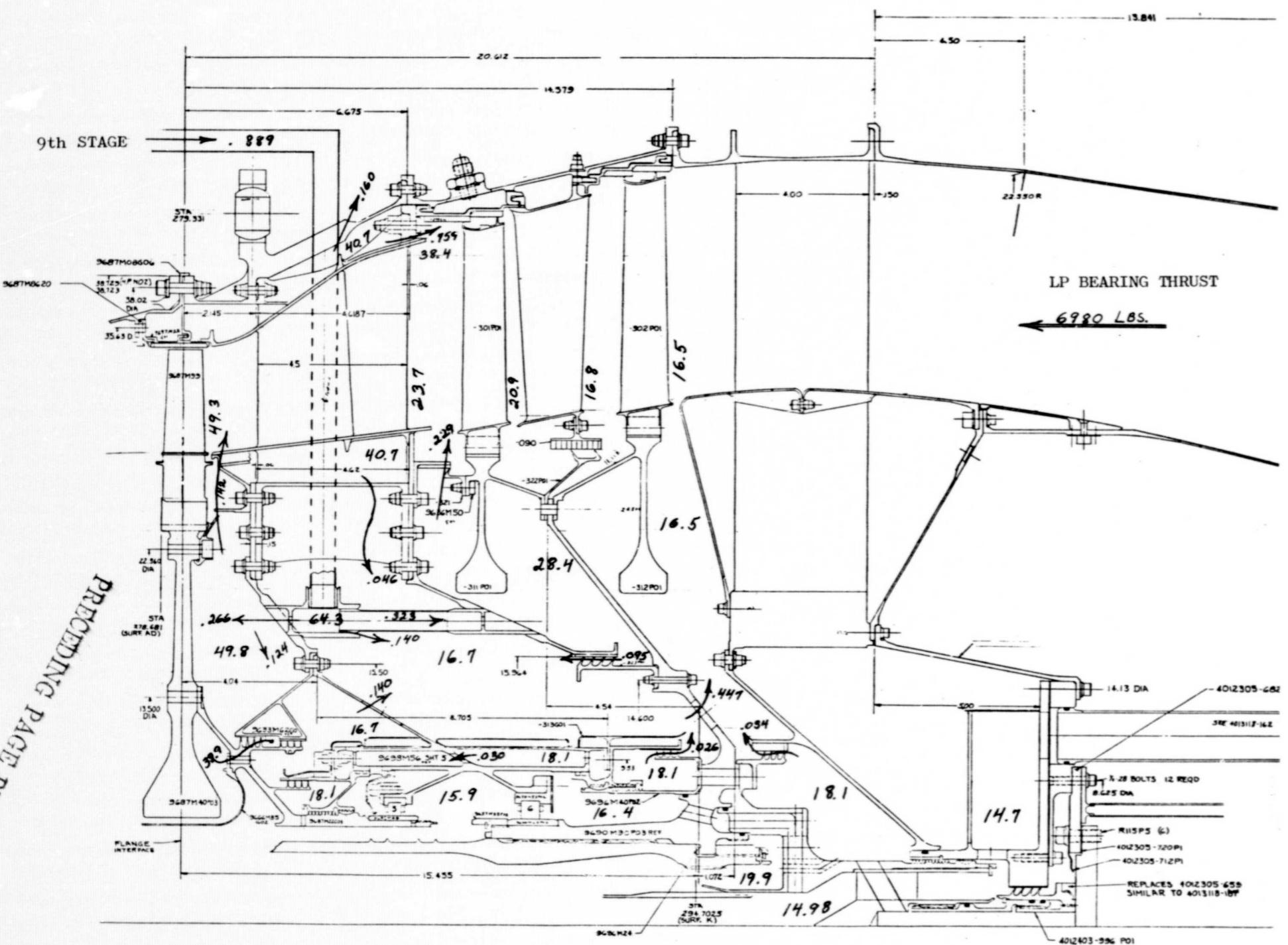


Figure 342. Engine Aft Cavity Pressures and Flows, Fan C

9.0 BEARINGS AND SEALS DESIGN

9.1 SUMMARY

This section delineates the features of the bearings and seals used in the full scale fan components and the experimental engine designs.

The bearings and seals used in the full scale fan components and the experimental engines are essentially identical to those used on the CF6 engine. The lube supply and scavengé system components are identical to those used on the CF6.

Detailed information is provided on the bearings and seals and lubrication system design of the CF6 engine.

9.2 FULL SCALE FAN COMPONENT BEARINGS AND SEALS DESIGN

The sumps for the full scale fan components A, B, and C are essentially identical. Two roller bearings support each of the fan rotors and provide for radial loading, and thrust is taken from each of the rotor systems by a Kingsbury thrust bearing when the fan assemblies are mated with either the General Electric or NASA-Lewis test facility.

The General Electric test facility is shown in Figure 343 with a full scale fan assembled to the forward end of the facility. The test facility is an existing three-bearing machine. In this facility, two roller bearings provide support and radial loading for the rotor, and a Kingsbury thrust bearing provides for bidirectional thrust for both the full scale fans and the facility.

9.2.1 Bearing Design

The roller bearings which support the fan rotors have crowned M50 rollers and M50 races. The outer races retain the rollers while the inner races are separable. Cages are one-piece machined steel with a thin layer of silver plating on all functional surfaces. The forward fan rotor bearing has a 210 MM bore and operates at a maximum speed of 1.15×10^6 DN; the aft fan rotor bearing has a 180 MM bore and operates at a maximum speed of 1.04×10^6 DN. Initial bearing radial plays for the fan rotor roller bearings are set to permit the inner races to run 25°F hotter than the outer races. Table XVIIC lists the pertinent bearing information for the fan roller bearings.

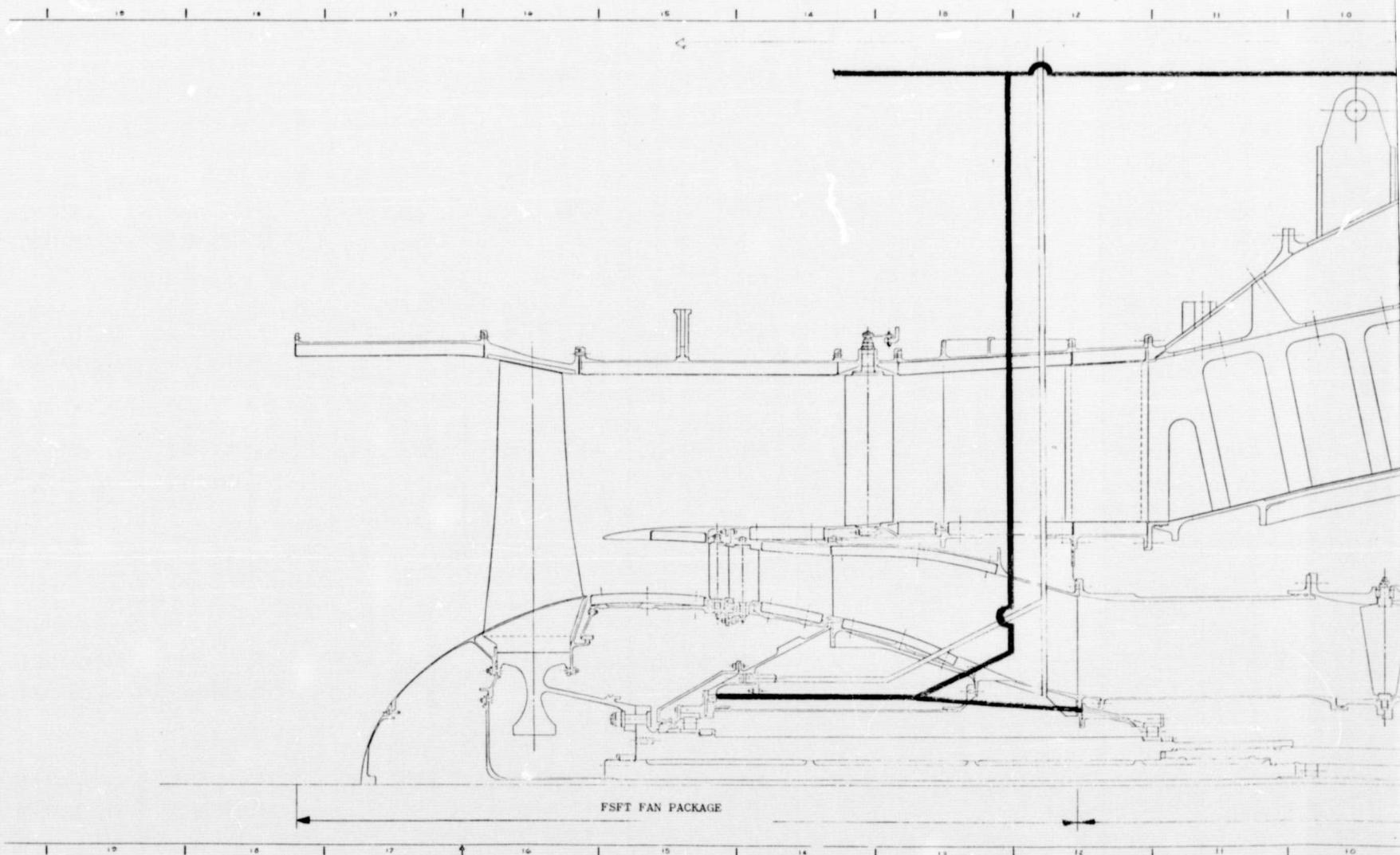
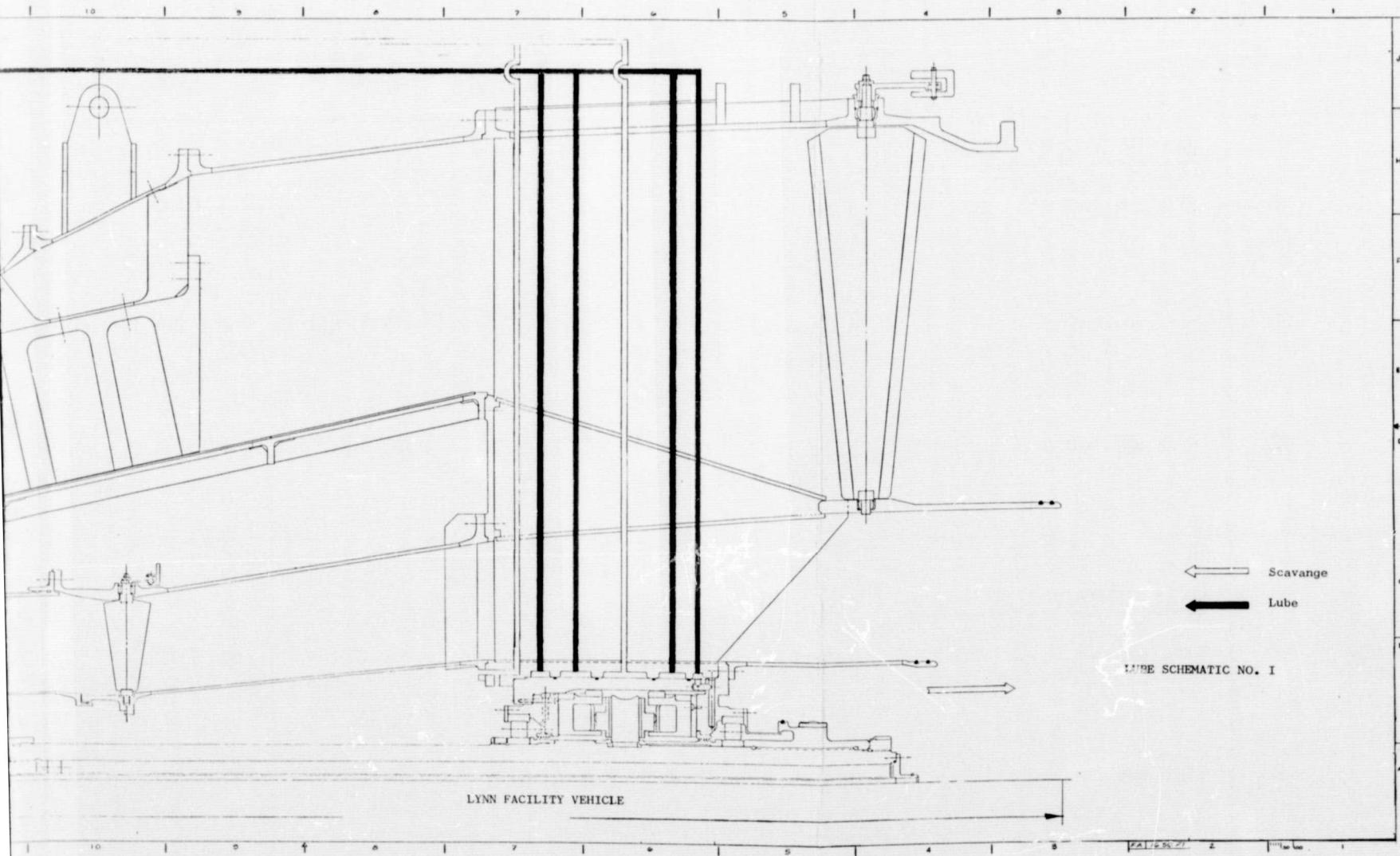


Figure 343. Full Scale Fan Component

FOLDOUT FRAME



Component and Test Facility Assembly

PRECEDING PAGE BLANK NOT FILMED

FOLDOUT FRAME

Page 567

2

Table XVIIC. Full Scale Fans A, B, and C

Description	Type	Speeds	Equivalent Loads, lbs	Dynamic Capacity, Lbs	B ₁₀ Life, hrs	Initial Radial Play
A	<u>Oil-Retained Rollers</u>					
	210 mm Bore	$0.816 \times 10^6 \text{DN}$ (3881 rpm)	6 830	60 000	14 600	0.0038 0.0058
	210 mm Bore	$0.838 \times 10^6 \text{DN}$ (3986 rpm)	8 910	60 000	6 500	0.0038 0.0058
C	210 mm Bore	$1.15 \times 10^6 \text{DN}$ (5460 rpm)	7 290	60 000	8 550	0.0038 0.0058
	<u>Oil-Retained Rollers</u>					
	180 mm Bore	$0.735 \times 10^6 \text{DN}$	5 430	48 000	14 700	0.0038 0.0058
B	180 mm Bore	$0.755 \times 10^6 \text{DN}$	4 100	48 000	33 500	0.0038 0.0058
	180 mm Bore	$1.04 \times 10^6 \text{DN}$	5 400	48 000	10 700	0.0038 0.0058

FOLDOUT FRAME

as A, B, and C Roller Bearing Data

Initial Radial Play	Brg. ΔT , °F	Allowable ΔT Between I/R & O/R, °F	Brg Mat'l	Cage Mat'l	Housing Mat'l	Shaft Mat'l	Shaft Fits' Inch	Housing Fits, Inch
0.0038- 0.0058	33.7	25	M50	AMS 6415	AMS 5062	AMS 6415	0.0019T 0.0006T	0.0009L 0.0002T
0.0038- 0.0058	38.6	25	M50	AMS 6415	AMS 5062	AMS 6415	0.0019T 0.0006T	0.0009T 0.0002T
0.0038- 0.0058	58.5	25	M50	AMS 6415	AMS 5062	AMS 6415	0.0019T 0.0006T	0.0009L 0.0002T
0.0038- 0.0058	33.8	25	M50	AMS 6415	AMS 5062	AMS 6415	0.0017T 0.0006T	0.0009L 0.0002T
0.0038- 0.0058	25.2	25	M50	AMS 6415	AMS 5062	AMS 6415	0.0017T 0.0006T	0.0009L 0.0002T
0.0038- 0.0058	41.3	25	M50	AMS 6415	AMS 5062	AMS 6415	0.0017T 0.0006T	0.0009L 0.0002T

FOLDOUT FRAME

2

FOLDOUT FRAME

9.2.2 Lube and Scavenge System Design

The forward main shaft labyrinth seal (see Figure 343) permits air to leak into the sumps while preventing oil from escaping outward; and, a windback, located between the bearing and seal, serves as a buffer to shield oil spray from the seal. Holes around the bottom half of the windback-supporting cone allow oil to drain into the sump area forward of the bearing, and any oil passing through the windback is slung outward and aft by a rotating slinger. Three axial holes through the outer portion of the forward bearing housing drain oil into the sump area between the two bearings before forward lube levels can reach the labyrinth.

The scavenge tubes in the area forward of the No. 1 bearing connect to the PTO cavity, and all the oil and air entering the PTO cavity at the 6-o'clock position exit at the frame strut. The PTO housing has a cap with a 3-inch tapped hole for a facility connection at this point providing a scavenge passage for air and oil from the fan sump.

Each of the fan roller bearings is lubricated with two oil jets so that if one jet becomes plugged, oil will continue to be supplied to the bearing. These jets are mounted in a one-piece machined lube-jet housing so that problems with fatigue of fabricated jets is eliminated by raising the resonant frequency of the part. A total of two GPM of oil lubricates and cools each bearing.

9.3 CF6 BEARINGS, SEALS, AND DRIVES DESIGN

9.3.1 Bearings and Seals

The CF6 engine bearings, bearing arrangement, seals, and coupling shaft are designed as an integrated mechanical system with the engine rotors and structures to provide the operational features of reliability, maintainability, and long life required for a commercial engine. Some of the features designed into the sumps are:

- a) Cool sump walls bathed in sump pressurization air (fan discharge air)
- b) Labyrinth oil seals
- c) Oil seal slingers and windbacks
- d) Internal sump cavities divided into inner oil sump and outer air sump to reduce the amount of entrained oil in the vent line

- e) Oil seal drain-back and overboard drain provisions
- f) Two lube jets per bearing incorporated into one-piece machined lube jets
- g) Flanged bearing outer races for positive retention
- h) Zero heat rejection from main shaft seals by virtue of labyrinth seal
- i) Center vent system where air-oil separation is accomplished by using the rotational field of the low pressure rotor
- j) Combination roller and ball thrust bearing for gas generator, for control of radial seal clearance

Figure 344 describes the seal design philosophy, indicating how the seals around the bearing are used to provide cavities which will ensure a cool blanket of air around each engine sump. Cool air, bled from fan discharge, is circulated through internal passages in the engine into Cavity No. 1. This cool air is protected from the local ambient temperature and pressure (PS_3) around the bearing by incorporating a cavity which is vented to a low pressure source of air. This source is chosen so that flow will always be away from the bearing in the outer sump pressurization seal. This design ensures a flow of cool air into the oil cavity to prevent leakage through the oil seal adjacent to the bearing and prevents the hot ambient air from coming in contact with the sump walls. This design concept has been used throughout the engine.

Labyrinth seals, used throughout the lubrication system, have adequately vented sumps to ensure positive inward flow and provide a positive, dependable, controlled-wear system. Each labyrinth seal is composed of a stationary member (rub strip) and a rotating member (labyrinth). The rotating member contains sharp-edged teeth for improved performance. The tip clearance of the sharp-edged teeth is chosen so that controlled clearances are assured under normal operational conditions. The seal stator incorporates a rub material, chosen to satisfy the specific temperature requirements of the seal location. All seals that operate at relatively cool temperature (less than 600°F) use either an epoxy or a silver rub strip material. Seal stators of higher temperature, such as the compressor discharge pressure seal, employ open- or filled-cell honeycomb for ease of rub-in.

In each of the sumps, provisions have been made to prevent oil leakage from the seals at low pressure conditions, such as are encountered at idle windmilling, or at extremely high altitude conditions. A slinger has been provided at the entrance of each oil seal to prevent oil from "crawling" along the shaft and entering the seal. In addition, a screw-thread "windback" is used, which consists of a helical thread with the spiral direction chosen to push the oil back into the sump. These two features are provided on each of the oil seals.

571

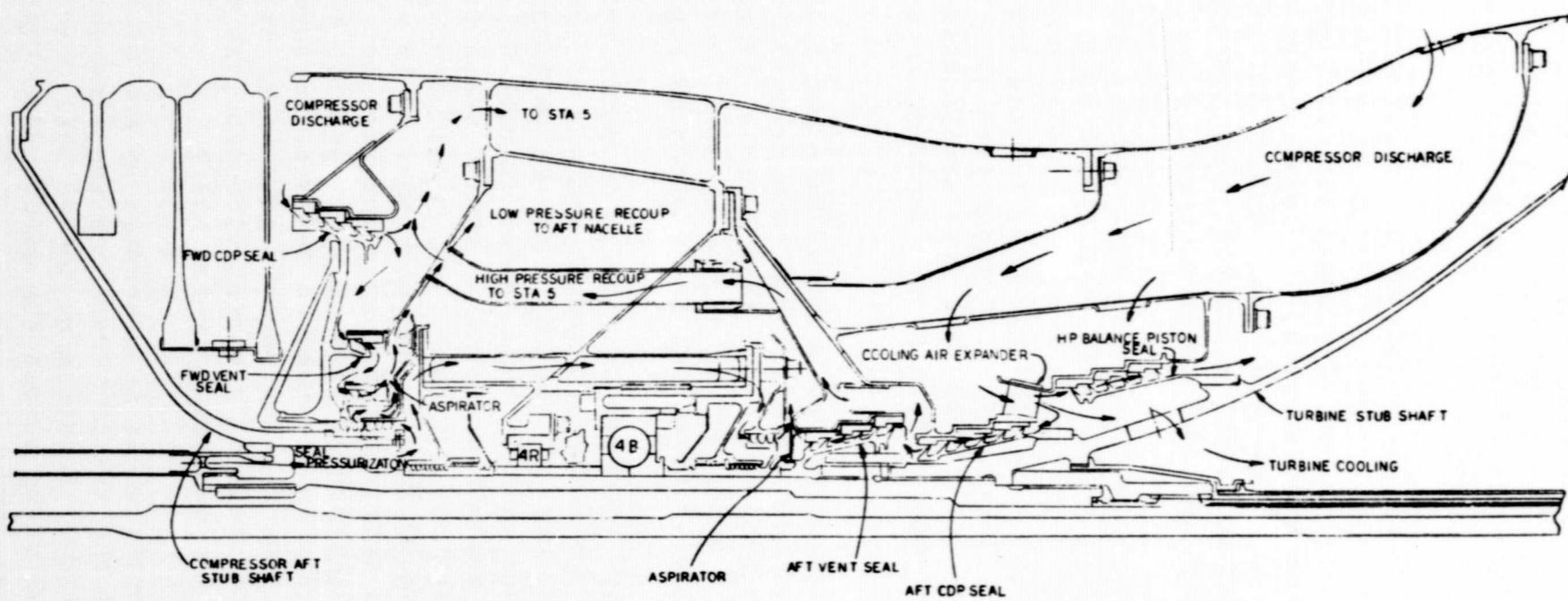


Figure 344. CF6 B Sump

The engine has four basic sumps, which are designated "A", "B", "C" and "D". The Nos. 1, 2, and 3 bearings and inlet gearbox are contained in the "A" sump. The No. 4R and No. 4B bearings are contained in the "B" sump. The Nos. 5 and 6 bearings are in the "C" sump, and the No. 7 bearing and fan tachometer are in the "D" sump.

The roller bearings at all locations are supported by cone structures attached to the engine frame members. Besides providing the stiffness for the engine rotor mounting system, the cones also act to attenuate the thermal deflections and to avoid overstressing the housing connection points to the frame. Cones provide an ideal structural support for main engine bearings because of their radial and axial stiffness, combined with their capability of accommodating thermal deflections at each end.

Each of the bearings is lubricated with two oil jets, so that if one jet becomes plugged, oil will continue to be supplied to the bearing. These jets are mounted in a one-piece machined lube-jet housing so that problems with fatigue of fabricated jets are eliminated by raising the resonant frequency of the part. Another feature is the incorporation of a small collection cavity just behind the oil jet, so that any foreign material which might have found its way into the lube system is not likely to become lodged in a jet orifice.

The bearings are arranged and numbered as shown in Figure 345. M50 and 52100 Consutrode vacuum melt material has been selected as the bearing material. Fatigue tests conducted on this material indicate an improvement in fatigue life of 4 to 6 times that of conventional bearing materials. This material has proven highly successful in previous GE engine designs.

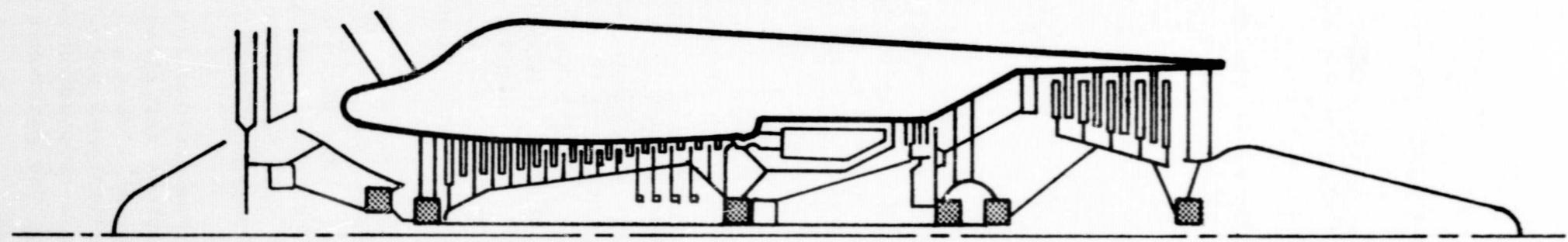
Roller bearings are used predominantly, in order to handle the axial thermal shift between the rotor and stator members of the engine. Thrust is taken from each of the rotor systems by a single ball-thrust bearing. Single-row ball-thrust bearings, rather than tandem (2-row) ball-thrust bearings, were chosen to obtain maximum reliability and to avoid problems of load-sharing between tandem ball bearings. A roller and a ball bearing are used in combination on the high speed rotor. The ball bearing is mounted on cantilever fingers so that it can carry thrust loads, but will not be loaded radially because of the low radial spring rate of the support. This ensures that the load on this bearing will be predictable and will be thrust load only. The roller bearing is located near the forward compressor discharge seal, and positions the seal accurately in a radial direction, as well as accepting all the radial loads from the compressor rotor shaft.

Rotation of the outer races is prevented by one of two methods. On all of the roller bearings and the LP thrust bearing, the outer race is flanged and bolted to the housing. Rotation of the 4B ball bearing is prevented by providing a heavy axial clamp across the outer race. This bearing does not carry appreciable radial load.

573

Legend:

- Ball Bearing
- Roller Bearing



(8 Individual Bearings in 7 Locations - No Differential Bearings)

Figure 345. CF6 Bearing Arrangements

9.3.2 Accessory Drives

The accessory drives for the CF6 engine consist of:

- A right-angled bevel gearbox, located inside the engine front frame and mounted on a flange in the hub of the frame
- The transfer bevel gearbox, mounted on the engine fan casing at the bottom of the engine, outside of the fan flowpath
- Drive shafts, which connect the various gearboxes through involute splines
- Accessory gearbox mounted forward of the transfer bevel gearbox outside of the fan flowpath

Power to drive the accessories is extracted from the compressor stub-shaft and transmitted through a large diameter hollow shaft, which encircles the fan drive shaft, to the bevel gear set in the inlet gearbox. The radial shaft carries the power from the inlet gearbox to the outside of the fan through a radial strut and housing at the engine bottom centerline to the transfer gearbox. The transfer gearbox is connected to the accessory box by a horizontal shaft.

All driven accessories for the engine are mounted on the single engine accessory gearbox. Both spiral bevel gears and involute spur gears are used in the accessory drive system. The bevel gears incorporate a 35-degree spiral angle to obtain a maximum contact ratio, consistent with the smooth operation required for aircraft gearing. High contact ratio means that more teeth are sharing load, and the dynamic overloads are reduced. The bevel set in the inlet gearbox, due to its large diameter, has a maximum pitch-line velocity of approximately 20,000 feet per minute. While this is higher than the 12,000 to 14,000 feet per minute commonly used in turbojet engines, the tooth loading is less than one-half the loading commonly used.

All gears are manufactured from case-hardened steel to precision aircraft standards developed and used by General Electric since the early J47 engines. Bevel gears are manufactured in one piece where possible, or mounted on their shafts with press-fit splines. The press-fit and spline configuration used in this application will eliminate bolt failures sometimes experienced in conventional bolt-and-dowel arrangements.

Spur gears are used throughout the accessory box. The involute tooth form, with its tolerance to center-distance variations and its relatively lower cost of manufacture and mounting, make spur gears a natural choice for this application. Gear meshes are designed with "hunting-tooth" ratios. This prevents repetitive contact on each revolution between the same teeth in the gear mesh and is used throughout the gearboxes to improve life.

Ball and roller antifriction bearings are used to support the shafts of the gears in the accessory drive system. Roller bearings are used where possible because of their higher capacity and smaller size and weight. In applications where it is important to hold axial position, ball bearings are used. Duplex bearings mounted face-to-face are used as thrust bearings on the bevel gears to provide maximum axial stiffness at the meshes. At least one bearing on each shaft is a roller bearing to permit axial thermal expansion without preloading the bearing.

All gearbox oil seals are carbon-face rubbing seals. The carbon element rubs on a hardened flat mating ring, which rotates with the shaft. For ease of removal, each seal is retained from the outside of the gearbox and can be replaced without teardown of the gearbox assembly.

Splined drive shafts are manufactured from AISI 4340 alloy steel with a core hardness of 33-38 Rockwell C, with induction-hardened splines. A shear section in the radial shafts has been incorporated near the inboard end to prevent shaft whip in the event of a shaft failure caused by overload. The critical speed of the shaft has been set so that calculated values are not less than shaft speed at 120 percent engine speed.

The gearbox casings are cast aluminum. Aluminum was chosen in place of the lighter-weight magnesium, to obtain maximum corrosion protection for the gear casings and improved stability.

A pressurized dry sump system is used for lubricating the accessory drive gears and bearings. The system uses engine oil from the main lube pump to jet-lubricate critical gear meshes and bearings. The bevel gear meshes are lubricated on both the incoming and leaving sides, where practical, to ensure adequate lubricant and cooling flow for proper operation. Heavily-loaded bevel gear bearings are lubricated, but the spur gear bearings are mist- and splash-lubricated only from oil directed at the gear meshes.

9.4 CF6 LUBRICATION SYSTEM

The following design philosophy was used in the design of the lubrication system:

- For long-life seals with predictable air leakage rates, use labyrinth seals at the engine main bearings instead of carbon seals.
- To eliminate oil coking and degradation, provide a cool atmosphere around all lubricated components on the engine. Use labyrinth seals which do not reject heat to the oil.

- To eliminate excessive oil consumption, provide large sump vent systems with high capacity air/oil separators.
- To prevent internal engine oil loss, provide generous vent line capacity to control seal pressure drop.
- To prevent internal engine oil contamination, use overboard drains at each sump.
- For maintainability, remove all lube and scavenge pumps and oil filtering and screening equipment from inside the engine and place in accessible zone in accessory compartment.
- For mechanical simplicity, eliminate differential bearings and seals with their complex lubrication requirements on intershaft positions.
- For mechanical integrity, design all tubing and oil system joints to vibration and mechanical limits proved successful on J79, CJ805, and J47 engines.
- For oil tank maintenance, provide a tank which is easy to disassemble.
- To locate and eliminate system faults early in the engine development, plan a comprehensive lubrication system test plan.

The resulting lubrication system will operate on Type I (MIL-L-7808F) or II (MIL-L-23699) oils.

A conventional "dry sump" system, similar to that used on General Electric engines (such as the J47, J79, J93, J85, T64 and T-58), is provided in which oil is pressure-fed to each engine component requiring lubrication and is removed from the sump areas by scavenge pumps. Labyrinth seals are provided as main-shaft oil seals, because of the dependable service such nonrubbing oil seals have demonstrated in subsonic engines such as the J47 and T58.

9.4.1 Lubrication Subsystem

The four subsystems of the engine lubrication system are:

- Lube supply
- Lube scavenge
- Sump air pressurization
- Vent air

9.4.1.1 Lube Supply

The supply subsystem, as shown in the lube system diagram (Figure 346), consists of the lube tank (which serves as the main reservoir of oil in the engine system), the lube pump, the lube supply filter, and the oil supply nozzles. Oil is supplied to the inlet of the lube pump by gravity feed from the oil tank. A tank drain plug is provided in the supply line adjacent to the tank exit. Oil under pressure is supplied by the pump to the filter which serves to protect the lube supply nozzles from contamination. This filter is equipped with a pressure-relief bypass which allows full oil flow to continue to be supplied to the engine after the filter has become plugged.

A pressure relief valve returns oil to the inlet of the lube pump if the pressure exceeds 300 psi. This valve functions only during cold starts. At all pressures less than 300 psi, the entire output from the filter is directed to the engine supply system.

An antistatic leak check valve prevents oil leakage from the pressurized lube tank into the engine gearboxes immediately after engine shutdown. The lube supply lines have been routed so that a failure of the antistatic leak check valve will not result in complete lube tank drainage into the gearboxes during periods of extended engine shutdown.

Immediately downstream of the antistatic leak check valve, a tap is provided to sense the lube system pressure. The pressure is transmitted to the cockpit indicator by a transducer and is referenced to the sump vent internal pressure (measured at the accessory gearbox) in order to record the actual pressure drop across the lube nozzles.

9.4.1.2 Lube Scavenge

The scavenge subsystem, shown in Figure 346, consists of five scavenge elements: the master chip collector, the scavenge filter, the relief valve, the fuel-oil heat exchanger, and the associated piping.

Each of the following major areas of the engine are scavenged by a single scavenge element:

- A sump and transfer gearbox
- B sump
- C sump
- D sump
- Accessory gearbox

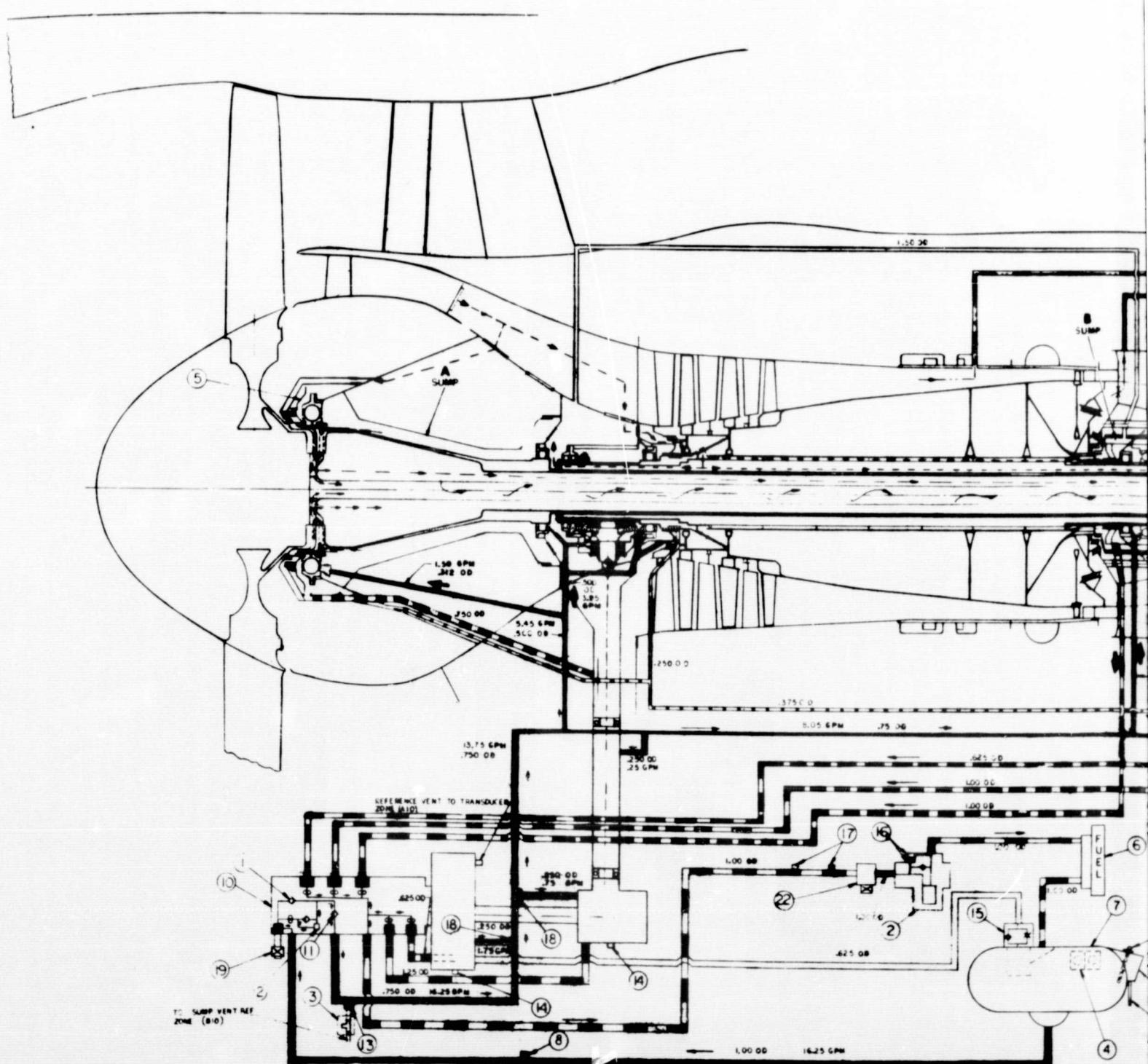
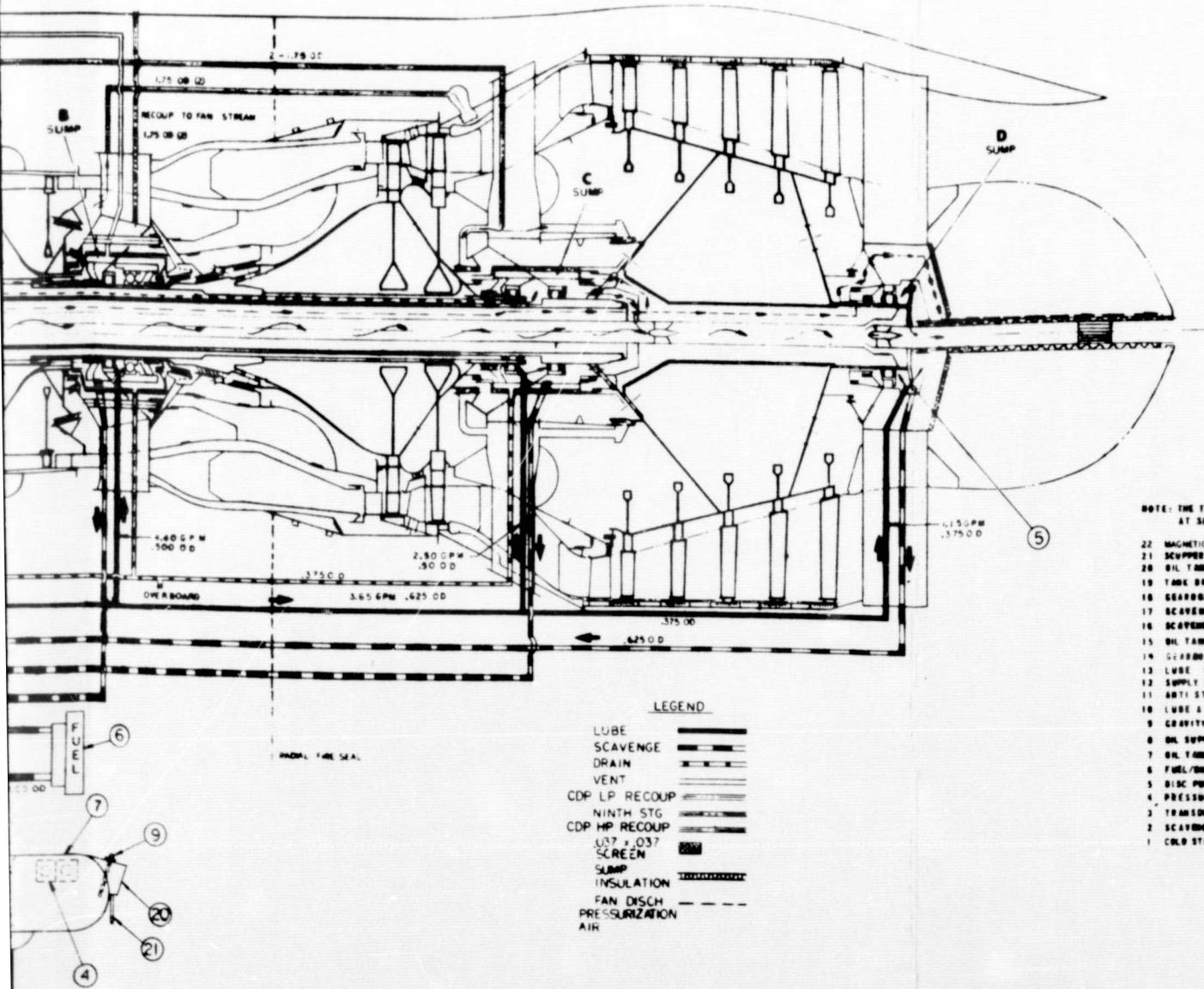


Figure 346. Lube



NOTE: THE TABULATED FLOWS ARE NOMINAL FLOWS
AT SLS, 9750, AND 150°F

1. MAGNETIC CHIP DETECTOR
2. SCUMMER BRAKE FITTING
3. OIL TANK SCUMMER
4. TANK BRAKE VALVE
5. SCARABEE ORIFICE BLOCKS
6. SCARABEE OIL TEMPERATURE TAPE
7. SCAVENGE FILTER OR TAPS
8. OIL TANK PRESSURIZING VALVE (PSI = 10.0 PSID)
9. SCARABEE DRAIN PLUG
10. LUBE SUPPLY PRESSURE TAP (WHN .093/.098 DIA OR FUEL)
11. SUPPLY FILTER (1/2" NOMINAL)
12. ANTI STATIC LEAK CHECK VALVE (PSID MIN. CRACK AT 150°F)
13. LUBE & SCAVENGE PUMP
14. GRAVITY FILL WITH SCREEN & DIP STICK
15. OIL SUPPLY TEMPERATURE TAP
16. OIL TANK
17. FUEL/OIL HEAT EXCHANGER
18. DISC PUMP
19. PRESSURE FILL & OVERFILL PORTS
20. TRANSDUCER PRESSURE TAP
21. SCAVENGE FILTER (1/2" NOMINAL) & CHECK VALVE
22. COLD START BY PASS (1500 PSIID MAX CRACKING PRESS)

Lube System Schematic

PRECEDING PAGE BLANK NOT FILMED

The "A" sump No. 1 bearing and No. 3 bearing areas gravity drain to the radial drive shaft housing and then to the transfer gearbox, where the oil is scavenged by the transfer gearbox scavenge element. The No. 1 bearing area uses a slinger-type disc pump to provide sump draining during excessive dive and roll altitudes. A partition is placed between the No. 1 bearing and center "A" sump areas to prevent oil interchange between the two areas to reduce required No. 1 bearing slinger pump capacity.

Each scavenge element has its own individual inlet screen and provisions for a magnetic chip collector for fault isolation. All scavenge elements have a common discharge port on the pump. The scavenge oil is routed to the common scavenge pump discharge, to the master magnetic chip collector, the scavenge filter, the fuel-oil heat exchanger, and then to the lube tank. The entrained air in the scavenge oil is separated by the tank deaerator and is then directed to the sump vent system through the tank pressurization valve. The scavenge filter contains a bypass relief valve which allows the scavenge oil to bypass the filter element in the event it becomes plugged by contamination. Pressure taps are provided on the filter so that the filter contamination level can be indicated by a Delta P switch and warning light.

9.4.1.3 Sump Air Pressurization

Main shaft oil seals require pressurization air, in order to cause air to flow across the seals and into the sumps at all engine operating conditions to prevent oil leakage past the seals. If air is allowed to flow out of the sump through an oil seal, some oil is carried with it. Such oil leakage must be eliminated in order to prevent excessive oil consumption and possible contamination of the compressor bleed air. Labyrinth seals, composed of a stationary member (rub strip) and a rotating member (labyrinth) provide a positive, dependable, controlled-wear system.

Pressurization air is extracted from the low pressure fan discharge air, where diffusers help to recover a high percentage of the stream total pressure. This air is distributed internally through the engine to each sump pressurization cavity and oil seal. The air tube of the high pressure compressor rotor is utilized to provide pressurization air to the compressor rear frame sump, while the interior of the low speed shaft is utilized to provide air to the two aft sumps of the engine so that no external piping is required for the sump pressurization air. This pressurization air completely surrounds the oil cavities.

The bearing sumps, contained in the compressor rear frame and in the turbine midframe, are isolated from the high pressure and high temperature air of the engine cycle by use of a low pressure cavity placed between the oil seal pressurization air cavity and the high pressure engine cycle air.

The low pressure cavity in the compressor rear frame receives leakage air from the high pressure compressor discharge seals, as well as the seal pressurization air leakage. This leakage air is vented to ambient pressure, to assure that reverse flow will not occur across the pressurization cavity seals and overtemperature the sump.

Pressurization air is supplied to the area between the fan shaft and core engine rotors from the compressor air tube. This air then flows forward and aft to the "A" and "C" sumps, where it provides pressurization air to the fan shaft labyrinth seals which seal the fan shaft cavity from the sumps. Elimination of oil from this area reduces oil system heat rejection and eliminates the possibility of oil leakage into the core engine rotor.

The low pressure cavity in the turbine midframe is vented to the low pressure turbine discharge pressure through the turbine rotor. Using the turbine rotor for this purpose eliminates external piping.

9.4.1.4 Vent Air

Each area of the engine, which requires pressurization of the oil seals, is vented to remove the air which enters the sumps through the oil seals and to keep the sump internal pressure low enough to prevent airflow out through the oil seals during a throttle chop. Generous-size vent lines have been provided for this purpose.

Each sump area and the oil tank are vented overboard to ambient pressure through the exhaust nozzle plug. The "A", "C", and "D" sumps are vented through radial inflow separators, built into the fan and LP turbine shafts, to a center vent tube in the low pressure shafts interconnecting the sumps to the vent exit at the nozzle plug end. The "B" sump is vented externally to the "A" sump, while the tank is vented to the "A" sump through the gearboxes and radial drive shaft housing. A swirler separator, in the center vent tube between the "C" and "D" sumps, is to assure additional air/oil separation at low shaft speeds. The vent system air/oil separators are sized to handle 50 percent more than the expected maximum vent airflow through worn oil seals without the oil loss exceeding the specification limit. This excess capacity is provided to obtain system tolerance to abnormal airflow without a major loss of engine oil.

The vent line from the oil tank contains a tank pressurizing valve which maintains the oil tank pressure and contains a small bleed orifice which will dissipate tank pressure after engine shutdown. The increased tank pressure is provided to pressurize the supply pump inlet and reduce the variation in oil supply quantity to the engine under the varying flight conditions. Airflow through this valve from the scavenging pumps will be sufficient to maintain tank pressure at altitude.

9.5 EXPERIMENTAL QUIET ENGINE BEARINGS AND SEALS DESIGN

Engines A and B use the same bearings and seals as the CF6 engine. Engine C has a cantilevered low pressure turbine, and, therefore, bearing number 7 and the "D" sump are not required.

The fan flowpaths for engines A, B, and C are smaller in diameter than the CF6, and, therefore, it was necessary to shorten the over-all PTO shaft length.

9.5.1 Sumps and Accessory Drives

The sumps and accessory drives designs of the experimental engine are identical to the CF6 engine except as follows:

- (a) For Engines A and B, provisions are made in the fan frame to pipe cool sump pressurizing air into the A-sump cavity. This air then flows aft to the B, C, and D sumps following the same flowpaths as the CF6 design. Engine C uses a sump pressurizing system which is identical to the CF6 design except that the D sump is eliminated.

The external gearbox configuration is identical to the CF6. The gearbox is moved radially inward to be compatible with the new fan designs. Although Fan C is smaller in diameter than Fan A/B, its gearbox is in the same position. Commonality for Engines A, B, and C has resulted in a common PTO shaft and piping arrangement.

- (b) The CF6 uses a three-piece PTO shaft. Two midspan bearings, an internal gearbox bearing, and a transfer gearbox bearing provide the shaft supports. The reduced-diameter flowpaths for Engines A, B, and C allow the transfer gearbox support bearing to move radially inward to the approximate position of the outboard midspan bearing, thus allowing one bearing and one shaft of the CF6 design to be eliminated.

The transfer gearbox for Engines A, B, and C mounts directly on the fan frame. A new PTO shaft housing design provides a continuous sump wall between the frame and transfer gearbox.

9.5.2 Bearing and Seal Design

Engines A, B, and C use the same bearings and seals as are used in the CF6 engine, except on Engine C where the number 7 bearing and D sump are not required.

The analysis performed on the CF6 bearings, which will be used on the experimental engines, shows that the limiting bearing is number 4B in Engine C. The calculated B_{10} life of this bearing at maximum thrust loading is 12,470 hours. Based on this predicted life, no engine bearing problems are expected in the Experimental Quiet Engine.

9.5.3 Lubrication System

The oil supply and scavenge components for the Experimental Engines A, B, and C are identical to those components used on the CF6 engine.

The sump pressurizing air system for Engine A/B will be modified, as fan discharge air (as used on Engine C) does not have pressure levels to assure positive pressurization of the Engine A/B sumps. Air from a low stage of the core high pressure compressor will be used for sump pressurization. This air will be cooled in a heat exchanger, orificed to reduce its pressure, mixed with fan discharge air, and piped into the A-sump cavity. This system of sump pressurization has been successfully used on other engines.

The center vent system is identical to the CF6 engine except in the aft end of the engine. A new piping arrangement is necessary to bypass the vent air around an aft-mounted slip ring. The CF6 swirler-deswirler has been eliminated for all three configurations. Also, since the engine D sump is eliminated in the Fan C configuration, additional modifications were necessary in the aft center vent area. All new passages, including centrifugal separators, aft collector manifold, and piping, are sized for maximum flow requirements.

10.0 CONTROLS AND ACCESSORIES AND CONFIGURATION DESIGN

10.1 SUMMARY

The engine power control system, fuel supply system, and electrical system to be used on the Experimental Quiet Engine are essentially identical to the systems used on the CF6 engine. These components are a direct out-growth of experience derived from the highly successful J79, CJ805, TF39, and GE4/SST engines. The end result is a group of extended-life components which are less complex, less expensive, lighter, and more reliable without sacrificing controlling accuracy or response.

10.1.1 Power Control System

The quiet engine power control system includes the main engine control, compressor inlet temperature sensor, variable stator vane actuators, and the variable stator vane position feedback cable.

The modifications to existing CF6 components for the Experimental Quiet Engine will be as follows:

- a) The CF6 main engine control will have the throttle cam changed to remove the thrust-reverser portion. This will allow increased speed setting accuracy, since a larger change in throttle angle will be used to effect a given speed change. Also, the control will be simplified by removing the power-trim and flight-idle functions which are not required for the Experimental Quiet Engine.
- b) The CF6 compressor inlet temperature sensor will be re-located from the fan duct into the core stream. This allows the same stator schedule to be used on all three engine configurations, since engine-to-engine variations in the relationship between fan duct temperature and the high pressure compressor inlet temperature do not have to be considered.
- c) The variable stator vane position feedback cable will be the same design with respect to materials and construction, as the CF6 design; however, there will be a different length requirement due to the new fan designs.

10.1.2 Fuel Supply System

The fuel supply system includes the main fuel pump, fuel/oil heat exchanger, fuel filter, and pressurizing and drain values. These components will be identical to those used on the CF6 engine.

10.1.3 Electrical System

The electrical functions required for the Experimental Quiet Engine include thermocouples for high pressure turbine discharge temperature measurement; engine speed sensor; fan speed sensor; and ignition exciter, lead, and spark plug. The modifications or changes to existing CF6 components for the Experimental Quiet Engine will be as follows:

- a) The CF6 thermocouple harness will not be used on Engine C configuration due to the new design low pressure turbine. The measurement of turbine discharge temperature will be made with special radial temperature and pressure rakes.

10.1.4 Configuration Design

Each of the Experimental Engine Configurations A, B, and C includes a new fan design and Engine C has a new, smaller diameter, low pressure turbine. The piping and supporting bracketry for these engine configurations required a redesign or modification of 82 tubes and their associated bracketry.

Figures 347 and 348 show the external configuration changes made for the Experimental Quiet Engines as compared to the CF6 engine.

Referring to Figure 347, the left side of the engine, the changes for Engines A/B and C are as follows:

- a) CIT sensor tubes rerouted from the fan duct to the core duct.
- b) Gearbox/pylon tubes are modified (shortened) CF6 tubes, due to relocation of the accessory gearbox.
- c) Feedback cable required length change, due to new fan design and relocation of accessory gearbox.
- d) Customer bleed air manifold not required and removed from engine.

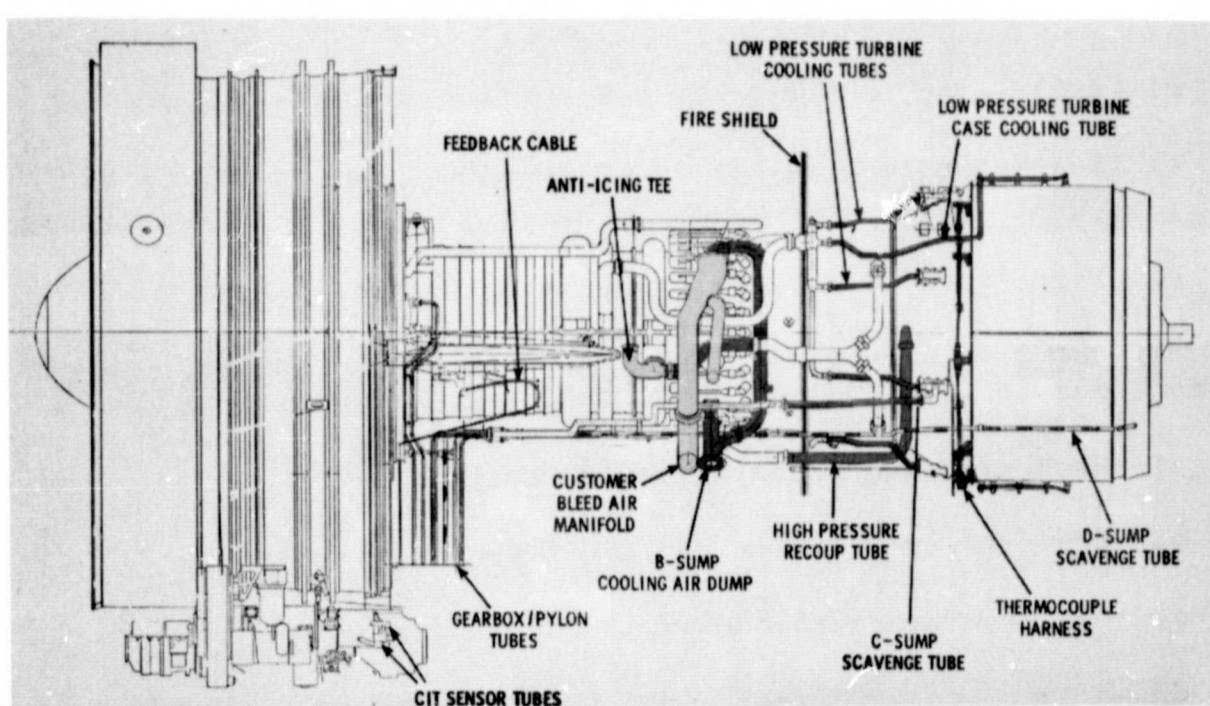


Figure 347. Left Side, CF6 Engine

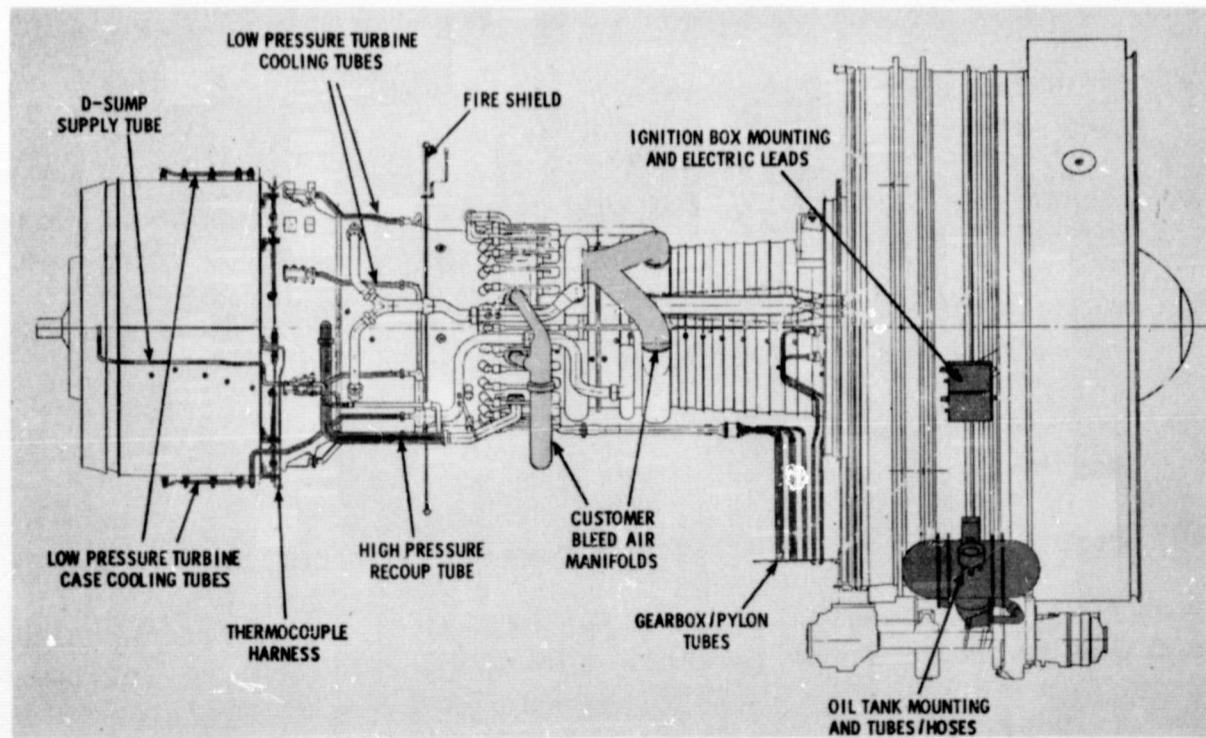


Figure 348. Right Side, CF6 Engine

- e) Anti-icing tee not required and removed from the engine.
- f) B-sump cooling air tubing redesigned, due to fan flowpath contour changes.
- g) Fire shield not required and removed from engine.

Referring to Figure 347, the left side of the engine, the changes for Engine C due to the new low pressure turbine design are as follows:

- a) High pressure recoup tubes redesigned.
- b) Low pressure turbine cooling tubes redesigned.
- c) Low pressure case cooling tubes redesigned.
- d) D-sump scavenge tubing not required and removed from engine.
- e) C-sump scavenge tube redesigned.
- f) Thermocouple harness removed; will use engine test radial temperature and pressure rakes.

Referring to Figure 348, the right side of the engine, the changes for Engines A/B and C are as follows:

- a) Oil-tank mounting and tube/hoses redesigned, due to new fan cases.
- b) Ignition-box mounting and electrical leads redesigned, due to new fan cases.
- c) Gearbox/pylon tubes are modified (shortened) CF6 tubes, due to relocation of the accessory gearbox.
- d) Customer bleed air manifolds not required and removed from engine.
- e) Fire shield not required and removed from engine.

Referring to Figure 348, the right side of the engine, the changes for Engine C due to the new low pressure turbine design, are as follows:

- a) High pressure recoup tubes redesigned.
- b) Low pressure turbine cooling tubes redesigned.
- c) Low pressure turbine case cooling tubes redesigned.

- d) D-sump supply tube not required and removed from engine.
- e) Thermocouple harness removed: will use engine test radial temperature and pressure rakes.

11.0 INSTALLATION AERODYNAMICS AND PERFORMANCE

11.1 Summary

This section presents the installation aerodynamic design for the three Experimental Quiet Engine configurations. The design is based on current standard design practices for bypass turbofan engines and state-of-the-art installations. The design includes definition of flowlines for the inlet, fan bypass duct and nozzle, core cowl, core nozzle, wing pylon, and fairing for the leads to the accessory package in the fan cowl.

Performance of the installations evaluated for cruise and take-off conditions. This includes calculation of fan duct and primary total pressure losses, as well as core cowl and pylon scrubbing drag.

In addition to the engine, installation designs were made for the NASA-Lewis Test Facility.

11.1.1 Inlet Cowl and Diffuser Aerodynamic Design

Most of the Experimental Quiet Engine testing will be with a standard bellmouth inlet; however, two flight inlets (thick lip and thin lip) will be used for some of the Engine B testing. This will provide data on the effects of flight inlets on noise reduction. The inlets were patterned after inlets selected for aircraft application and represent the current state-of-the-art in inlet design technique. The inlets are lengthened to permit use with the Fan B design. The D_{max}/D_{lip} ratio for the thin lip inlet was increased to allow 4 inches for structure at the fan rotor.

The throat is sized by cruise airflow requirements; and, therefore, the same diffuser section is used for both inlets. The only deviation from flight diffuser design practice is the incorporation of a 13-inch cylindrical section ahead of the fan rotor to assure interchangeability with the bellmouth inlets normally used for testing.

The thick-lip inlet, with area and Mach number distributions for standard day takeoff, is shown in Figure 349. The thin-lip inlet variable geometry design has not been finalized. Equivalent conical diffusion angle is shown in Figure 350 for the diffuser section with and without the 13-inch cylindrical section.

11.1.2 Fan Bypass Duct and Nozzle Aerodynamic Design

The fan bypass duct and nozzle is the region of fan exhaust from the

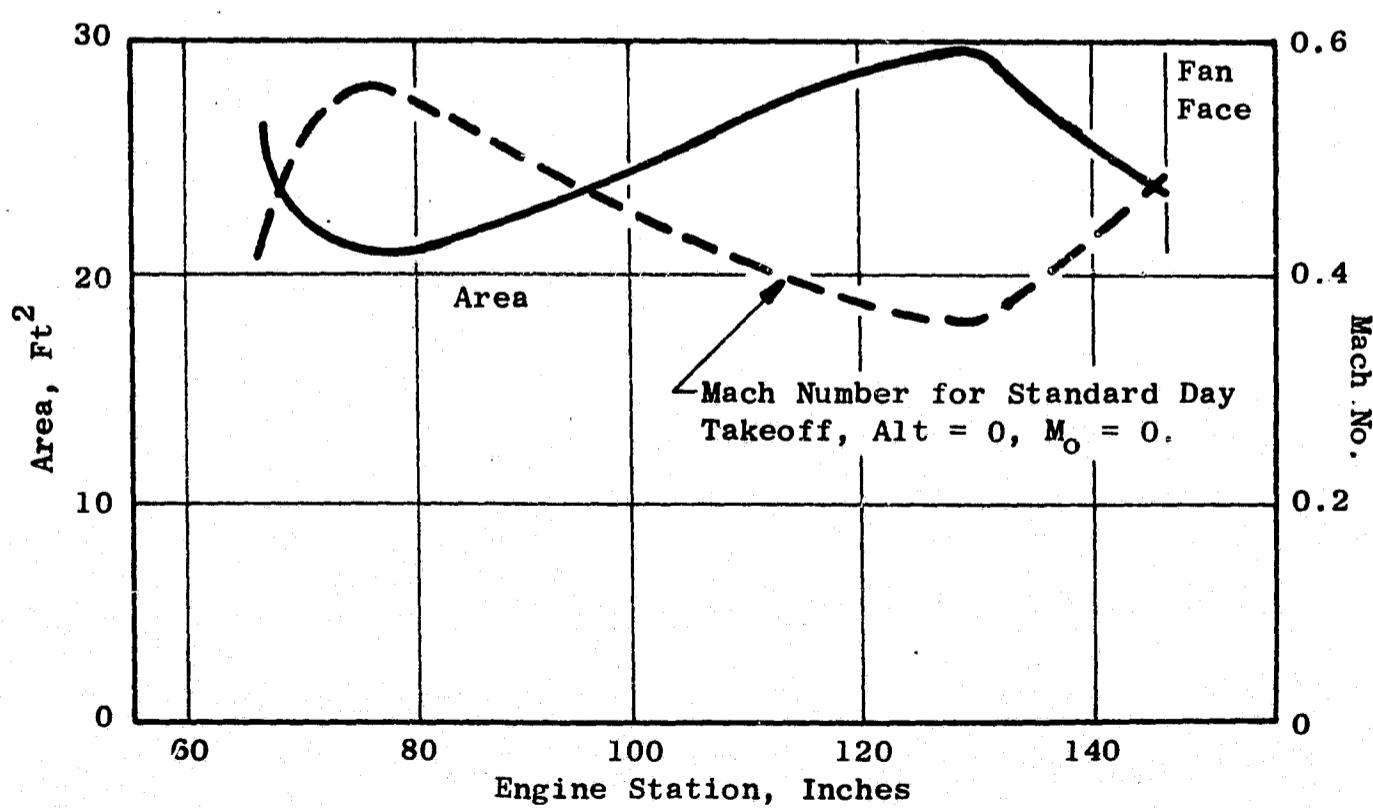
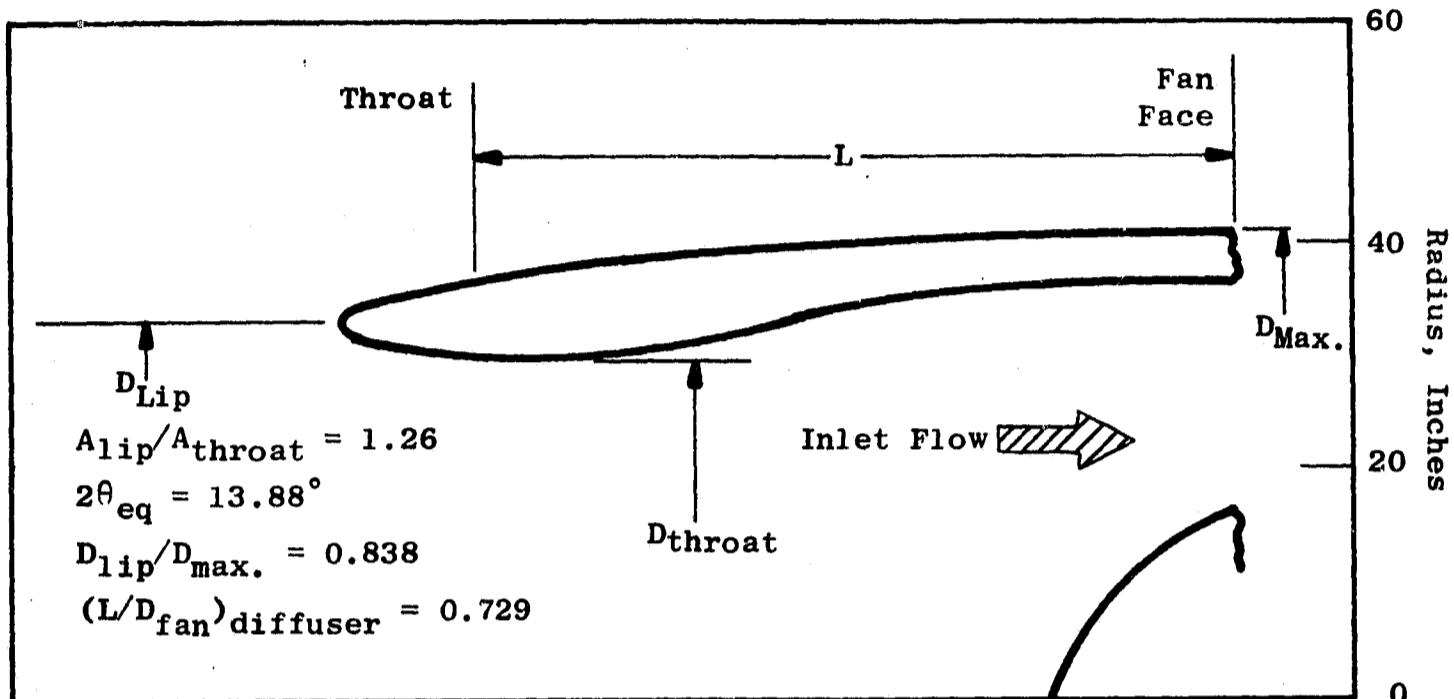


Figure 349. Schematic of the Thick-Lip Inlet for Engine B

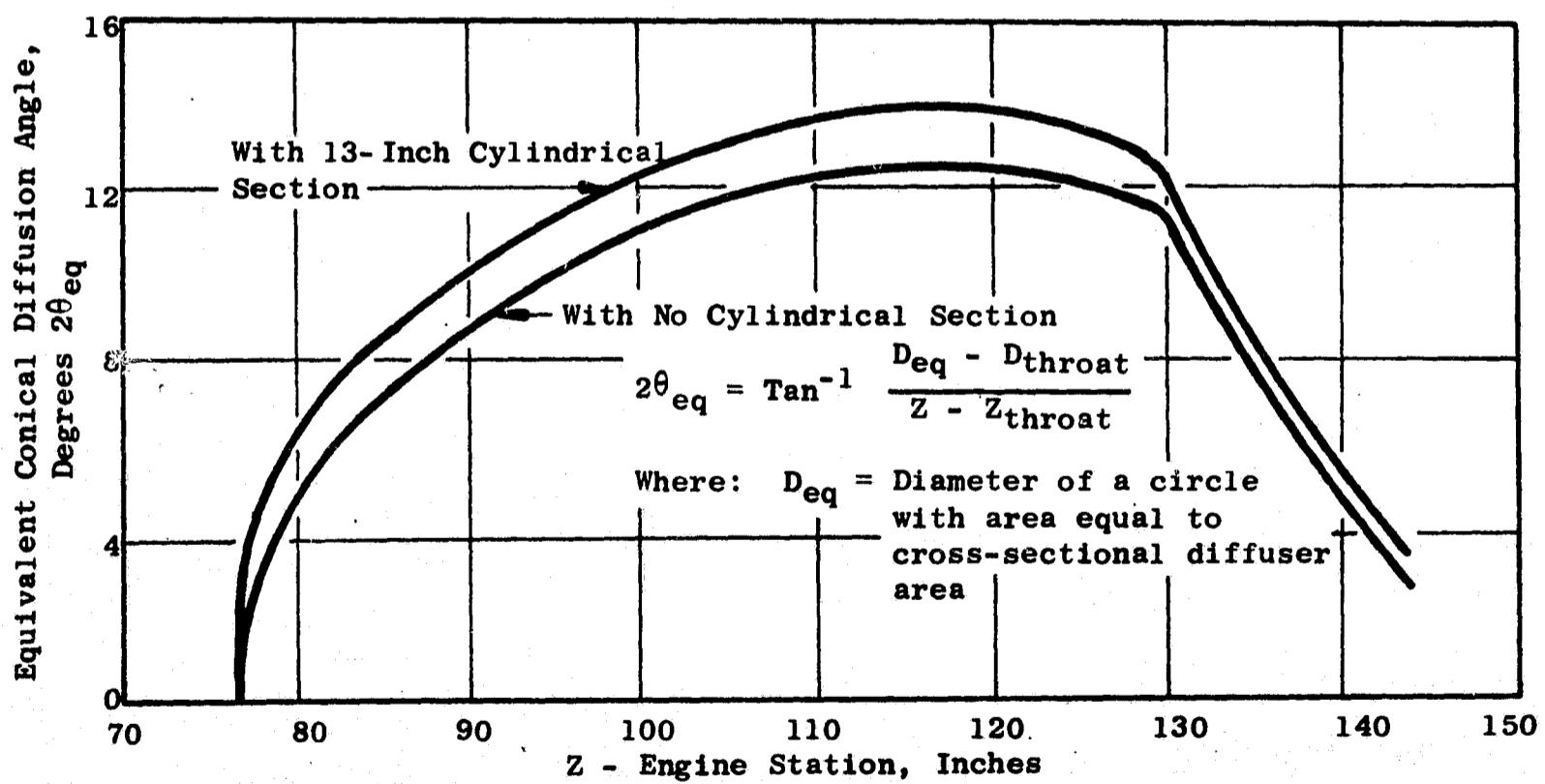
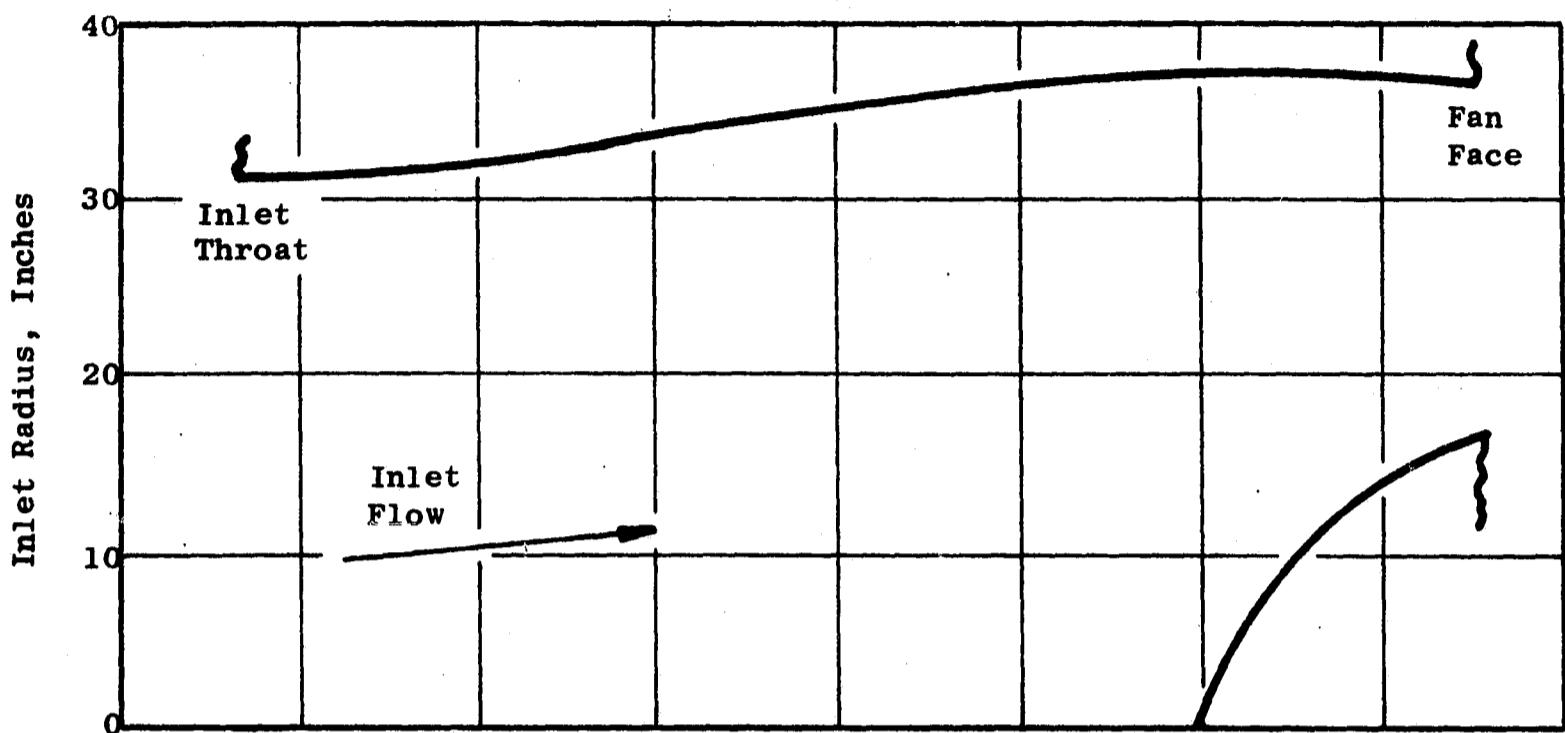


Figure 350. Fan B Inlet Diffuser and Equivalent Conical Diffusion Angle With and Without the 13-Inch Cylindrical Section

outlet guide vanes to the exit of the duct (Figure 351). Similarity between Engines A and B permits the use of the same fan ducts for both, and the use of fan nozzles that differ only slightly in length to account for small differences in throat area.

Duct surfaces are defined using straight lines where possible. However, smooth curved surfaces are required to maintain a smoothly-varying flow area. The final design represents a compromise between these two design approaches. The outer surface is defined by two straight lines from the outlet guide vanes to the bypass nozzle, where a smooth curve is used. The inner surface is defined by three straight lines for the first twenty inches aft of the outlet guide vanes, and a smooth curve for the remainder of the inner surface.

Duct flow areas are sized to give Mach numbers near 0.5 for a major portion of the duct. Because of the Mach number existing at the engine outlet guide vanes (0.55) and the desire to keep diffusion losses to a minimum, duct Mach numbers of 0.52 and 0.54 resulted for Engines A/B and C, respectively. Figures 352 and 353 are comparisons of the Mach number distributions of the engines and indicate the close similarity between the flows of all engines. Plots of flow area vs engine station for the engines (Figure 354) illustrate the smooth flow area variation along the ducts.

The total fan duct losses are listed in Table XVIC for the Experimental Quiet Engines. These loss estimates included duct and pylon smooth skin friction, pylon interference, radial strut loss, step and gap loss, and acoustic treatment loss. Hot day conditions were used in the calculations at both takeoff and cruise. Because the fan ducts for Engines A and B differed only slightly in length, the difference in total loss for the two ducts is negligible. Duct loss for Engine C is somewhat higher ($0.08\% \Delta P_T / P_T$ higher at cruise conditions) because of the slightly higher Mach numbers and the increased ratio between surface area and flow area.

11.1.3 Core Duct and Nozzle Aerodynamic Design

The CF6 core engine is used for the Experimental Quiet Engine. The flow is lower than that for the CF6, because of lower design thrust, resulting in a relatively small primary nozzle throat area compared to the low pressure turbine diameter. The combination of a small throat and aerodynamic limitations on the surface of the core cowl produces a slightly longer nozzle than would ordinarily be required.

Core duct surfaces were defined using straight lines where possible. As in the case of the fan duct, Engines A and B have the same core nozzle except for a slight difference in length to account for a variation in the nozzle throat area. In Engines A and B, the outer surface consists of three straight-line segments, while the inner surface is a smooth curve. Engine C has a single straight line for the outer surface and a smooth curve for the inner surface.

595

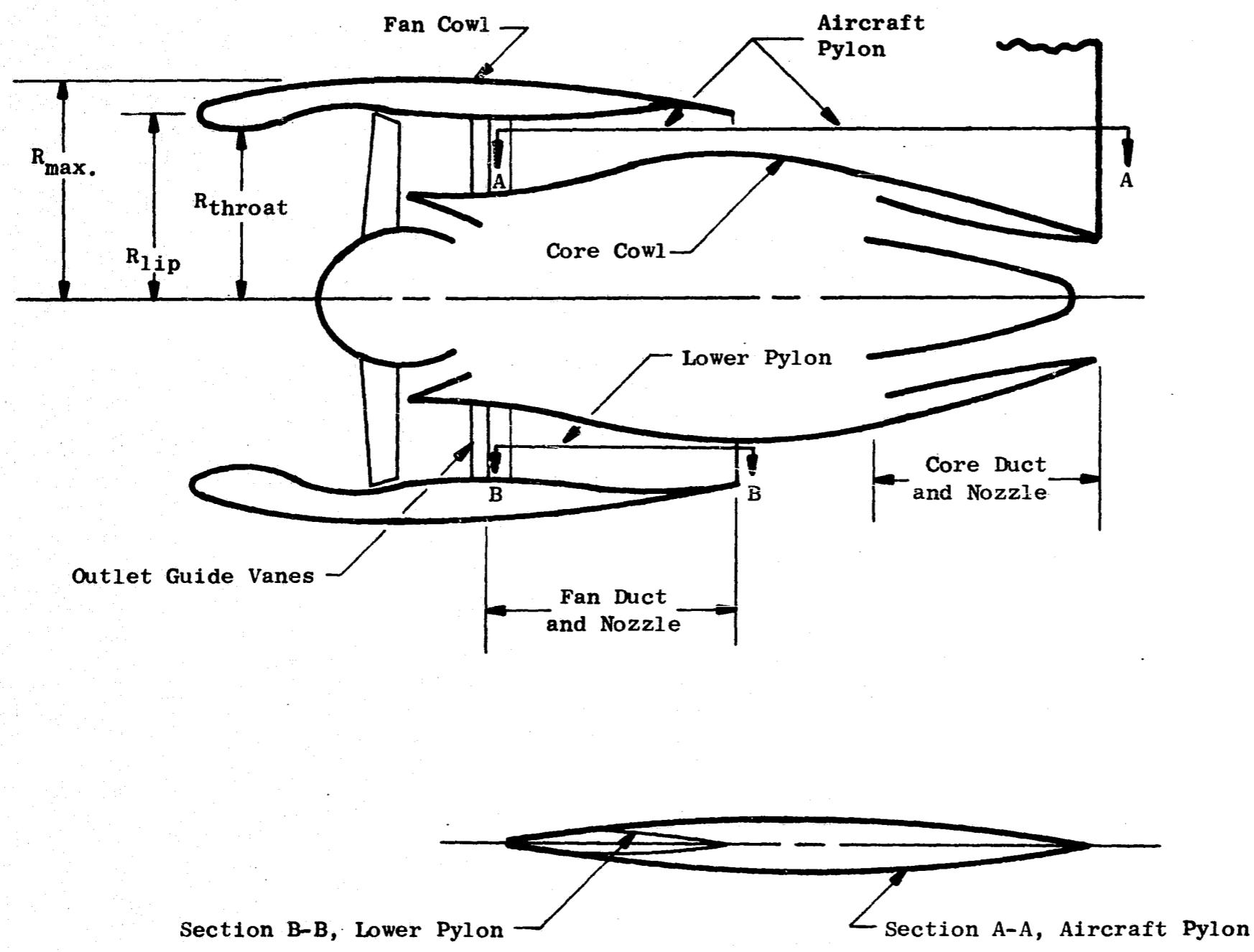


Figure 351. Schematic of the Experimental Quiet Engine Installation

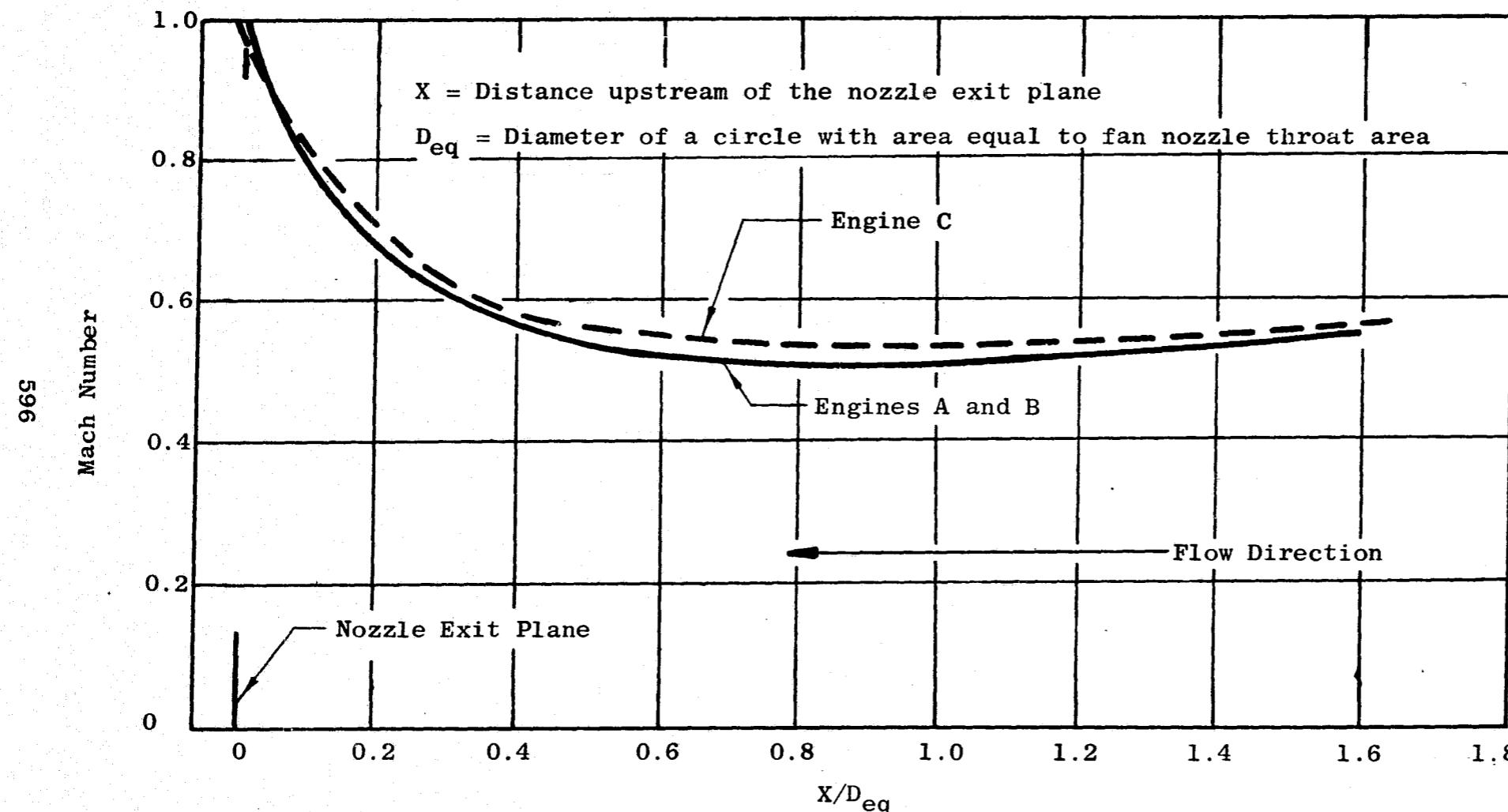


Figure 352. Fan Duct and Nozzle Mach Number Distribution for Engines A, B, and C at Cruise Conditions

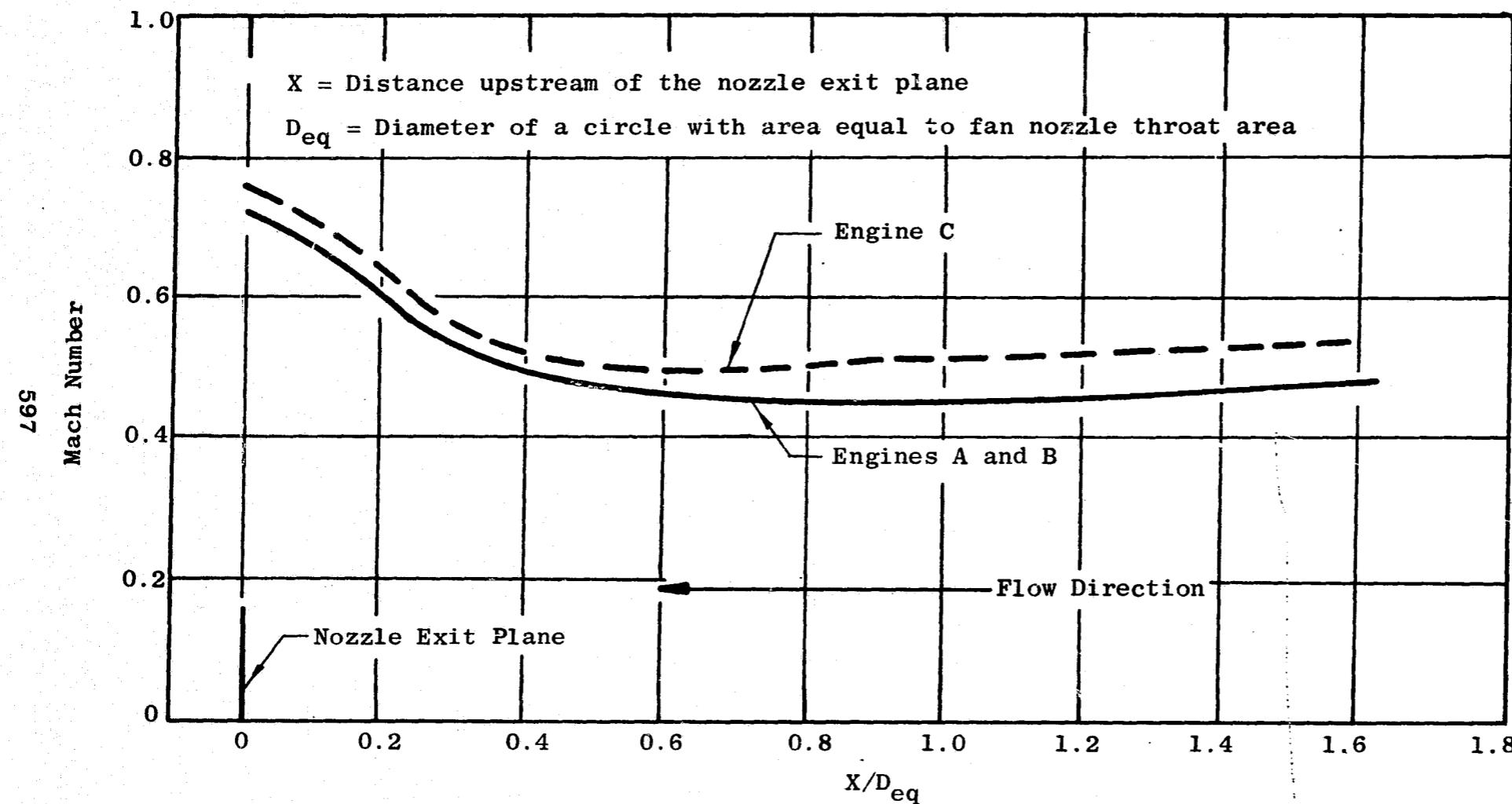


Figure 353. Fan Duct and Nozzle Mach Number Distribution for Engines A, B, and C at Take-off Conditions ($M_0 = 0$)

869

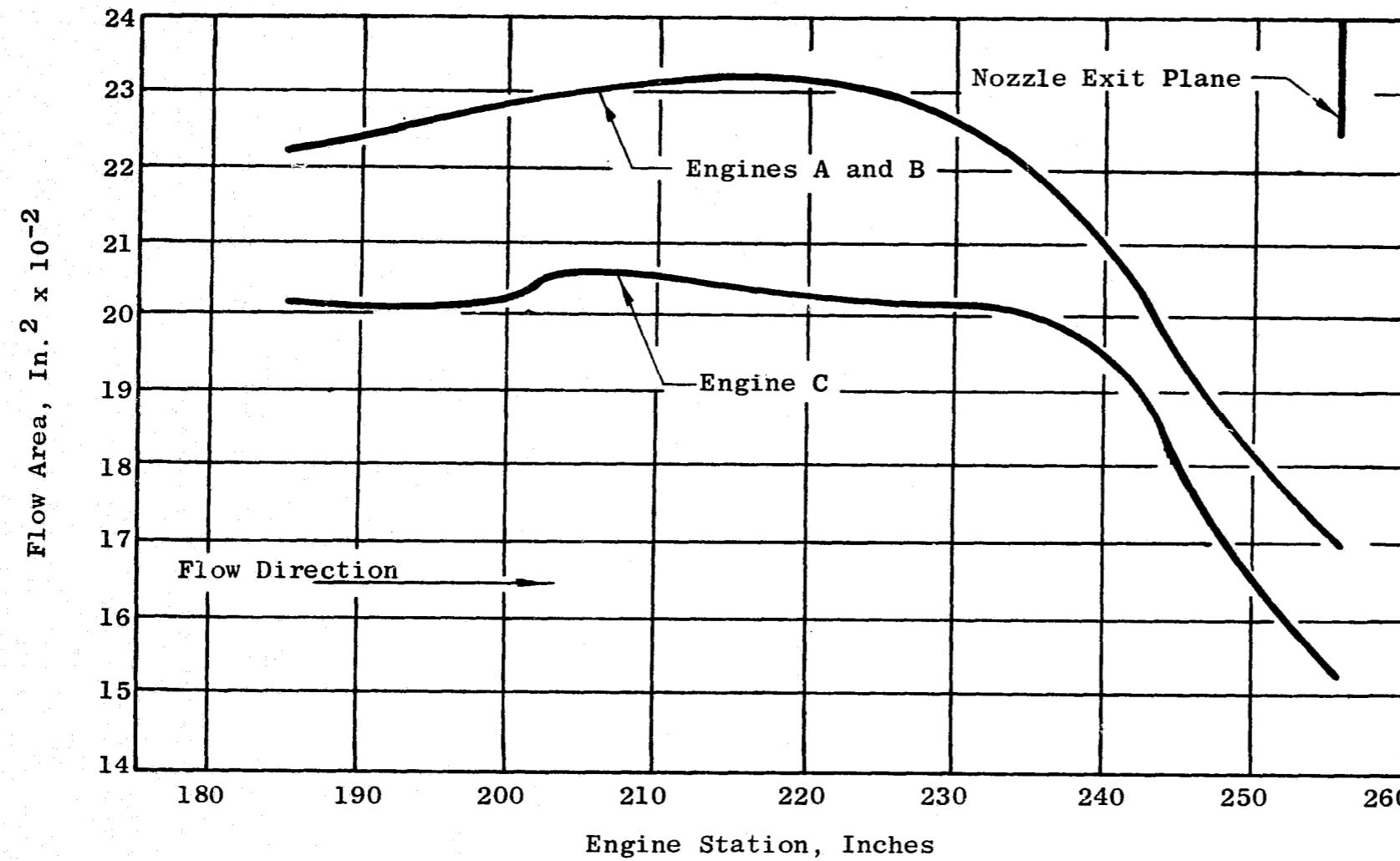


Figure 354. Flow Area Distributions for Engines A, B, and C Fan Duct and Nozzle

Table XVIC. Experimental Quiet Engine Installation Exhaust Losses

Condition	Engines		
	A	B	C
<u>Cruise</u>			
$M_0 = 0.82, 35\,000 \text{ Feet, Hot Day}$			
Net Thrust, F_N (Lb)	4 900	4 900	4 900
Core Cowl Drag (% F_N) (Lbs)	3.11 152.2	3.08 151.1	2.62 128.2
Pylon Scrubbing Drag (% F_N) (Lbs)	0.37 17.9	0.36 17.7	0.31 14.9
Fan Duct Loss (% $P_{T_{23}}$)	1.82	1.82	1.90
Core Duct Loss (% $P_{T_{55}}$)	1.67	1.67	1.30
<u>Takeoff</u>			
$M_0 = 0, 0 \text{ Feet, Hot Day}$			
Net Thrust, F_N (Lb)	22 000	22 000	22 000
Core Cowl Drag (% F_N) (Lbs)	0.98 215.9	0.97 214.3	0.86 188.5
Pylon Scrubbing Drag (% F_N) (Lbs)	0.13 27.8	0.12 27.4	0.11 24.0
Fan Duct Loss (% $P_{T_{23}}$)	1.67	1.66	1.83
Core Duct Loss (% $P_{T_{55}}$)	0.69	0.69	0.62

Figures 355 and 356 illustrate Mach number distribution in the core nozzles of the engines. The plots of flow area vs. engine station for the engines in Figure 357 illustrate the smooth flow area variation along the nozzles.

Performance losses of the engine core nozzles are listed in Table XVIC. The losses include friction loss, turbine rear frame strut loss, and step and gap losses. Because of their similarity, core nozzles for A and B have the same loss level. Core nozzle friction loss for C is higher because of the increased ratio of surface area to flow area and higher Mach numbers; however since the turbine rear frame struts were designed specifically for this engine, the over-all core duct losses are lower than in Engines A and B.

11.1.4 Core Cowl Aerodynamic Design

The core cowl design for Engine A/B has a small primary nozzle throat area resulting in longer cowls than the smaller diameter and shorter low pressure turbine of Engine C.

Although the Quiet Engine core cowls for A and B are long, they are at a lower radius (less surface area). The net result is that the core cowl drag for Engines A/B and C is low at cruise conditions. The core cowl losses of the engines are listed in Table XVIC. The total core cowl loss includes surface friction, steps and gaps, and base drags. Note that core cowl pressure drag was not included in the losses quoted. The effects of core cowl static pressures are included in the fan nozzle velocity coefficient.

11.1.5 Aircraft Pylon and Lower Pylon Fairing Aerodynamic Design

The aircraft structural pylon fairing and the lower pylon fairing (used for accessory drive shaft and pneumatic, hydraulic, and electrical lines) were designed with the same leading edge. An included angle of 29 degrees was used to insure proper clearance of the drive shaft leading to the accessory gearbox.

The lower pylon fairing was closed smoothly from a maximum width of 7.38 inches, so that the trailing edge occurred at the fan nozzle exit. The aircraft pylon was maintained at a maximum thickness of 12.00 inches for a distance of 60 inches and then closed smoothly so that the trailing edge occurred at the primary nozzle exit.

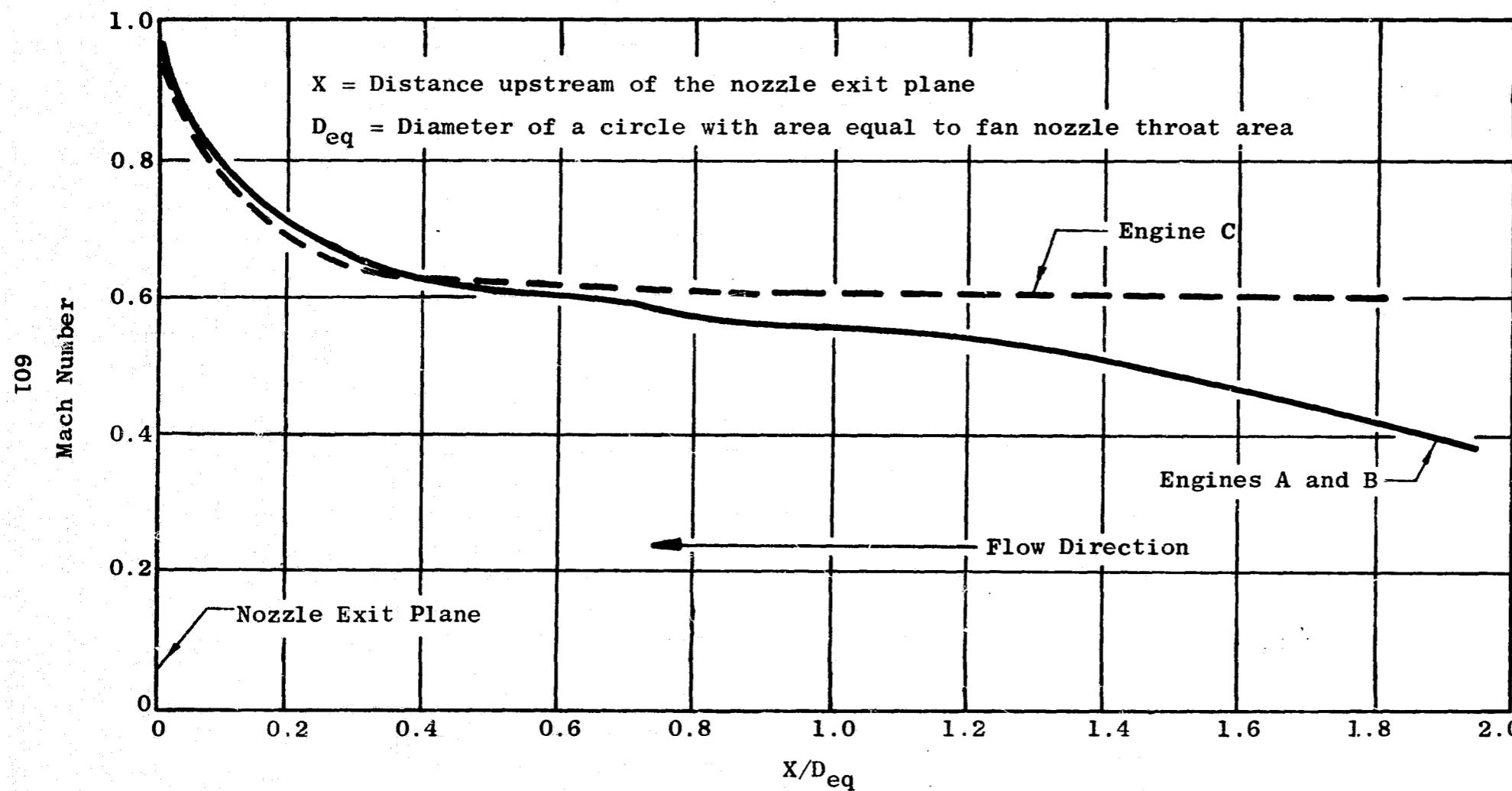


Figure 355. Core Duct and Nozzle Mach Number Distribution for Engines A, B, and C at Cruise Conditions

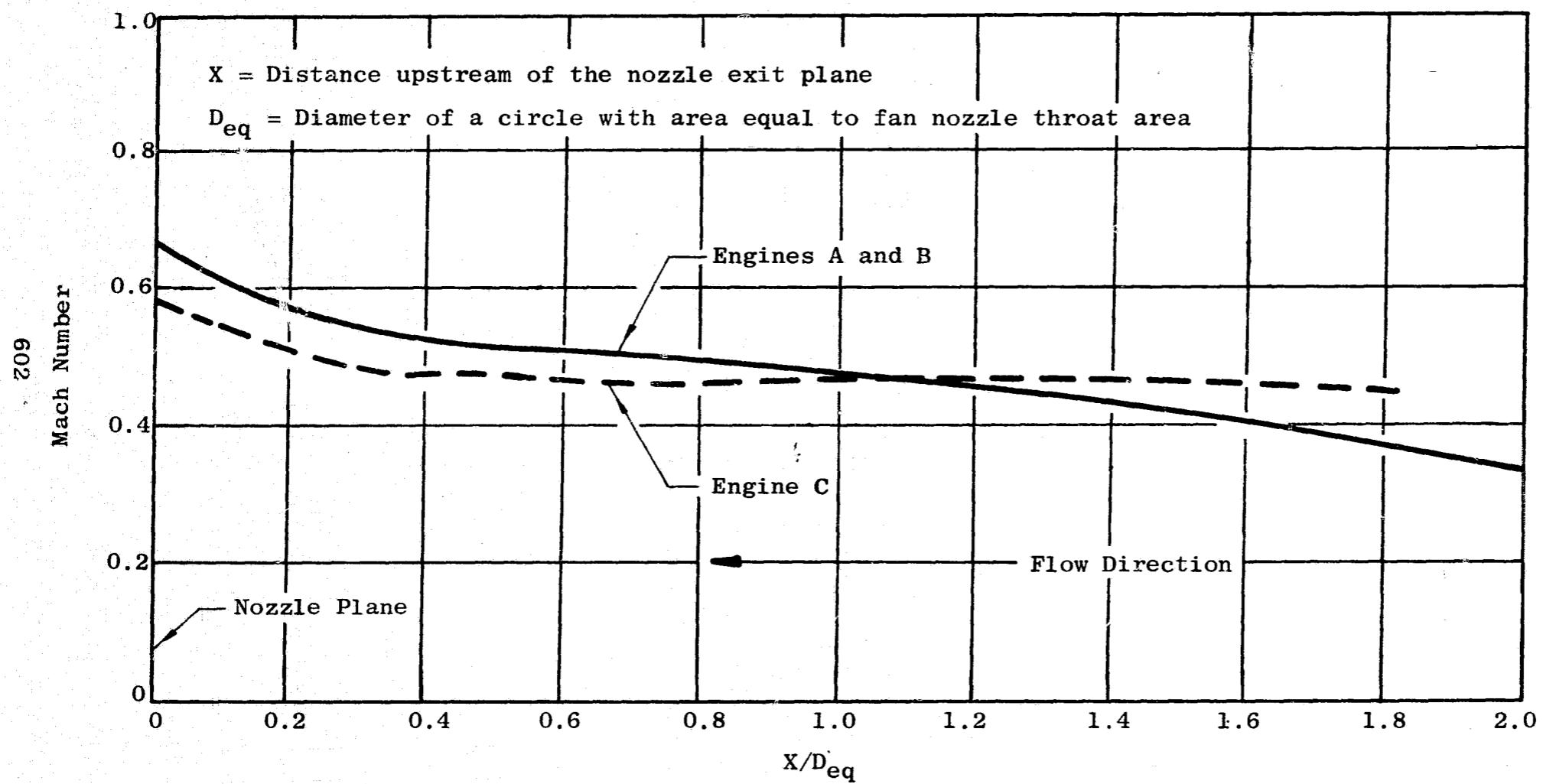


Figure 356. Core Duct and Nozzle Mach Number Distribution for Engines A, B, and C at Take-Off Conditions ($M_0 = 0$)

E09

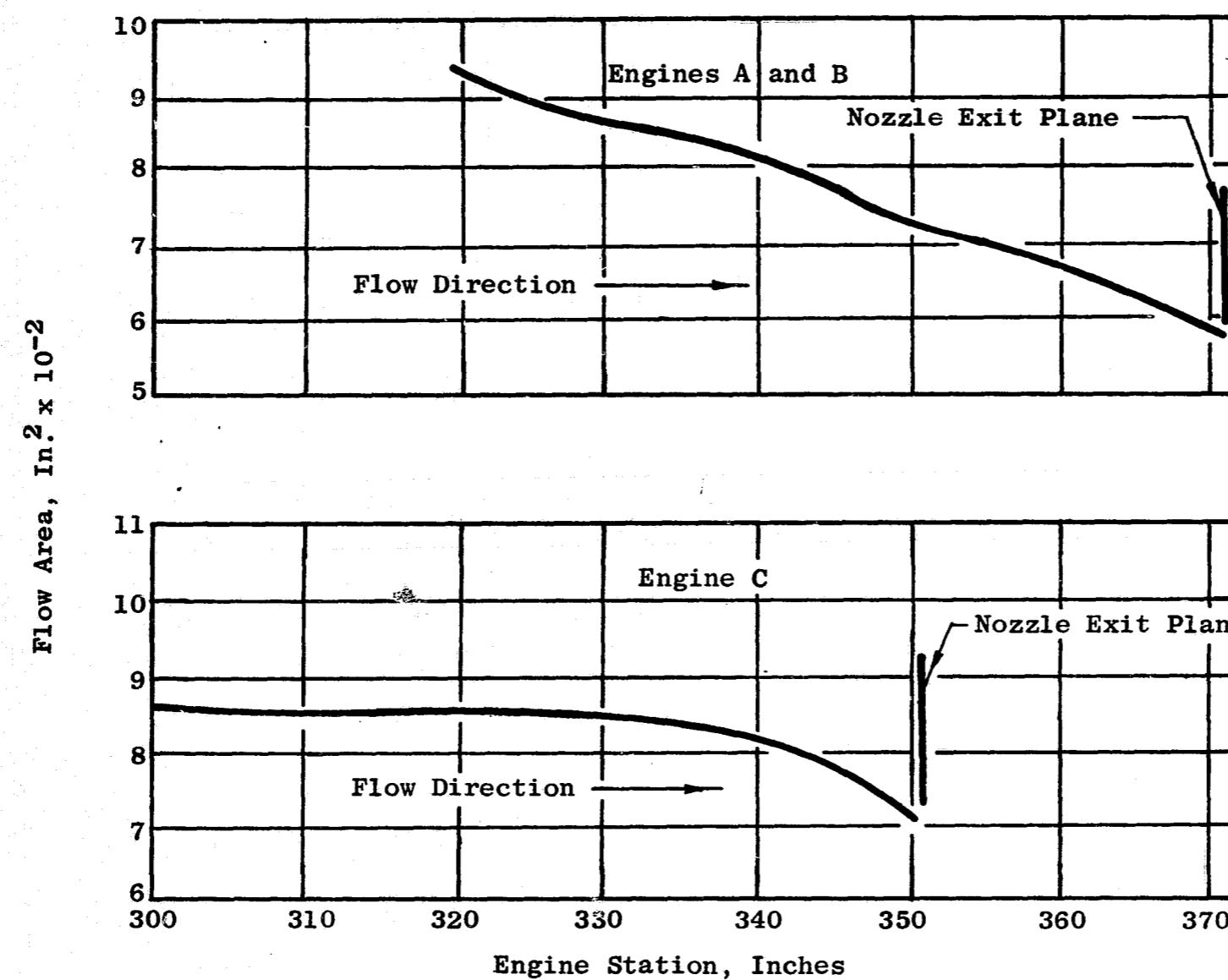


Figure 357. Flow Area Distributions for Engines A, B, and C Core Duct and Nozzle

The pylon scrubbing drag for the engines is listed in Table XVIC. As in the case of the core cowl, pressure drag effects are included in the fan nozzle velocity coefficient.

11.1.6 NASA-Lewis Facility Installation Aerodynamic Design

The fan component tests at NASA-Lewis will be conducted on an existing facility. In order to simulate the fan flow of the engines, facility installation flowpaths were designed to simulate the effects of the actual engine installations.

The facility installations consist of core and bypass ducts and nozzles. The core nozzle is the same for all installations, while there are two designs for the fan nozzles - one for A/B, and one for C. The fan and core nozzles are designed to simulate engine flows and back pressures on the fans.

The installations were designed with as many straight line segments and common parts as possible. At the same time, care was taken to avoid sacrificing any aerodynamic or noise performance. The bypass duct is the same for Fans A/B, but the forward end of the Fan C bypass duct is different because of the smaller Fan C diameter. Figure 358 illustrates the common parts of the bypass ducts.

The possible addition of sound suppression splitters at a later date was taken into consideration in the design of the bypass ducts. Flow areas are large enough to permit the installation of splitters, with their accompanying blockages, without causing excessive losses due to high Mach numbers. The flow area was established considering diffusion losses when the splitters were not used.

Flow areas of the ducts in the NASA-Lewis facility installations are shown in Figures 359, 360, and 361. Figure 362 shows the fan bypass duct Mach number distributions.

The loss estimates for the NASA-Lewis facility installation fan bypass and core ducts are summarized in Table XVC. The bypass duct for C has a lower loss than the duct for A/B, because of lower diameters and lower Mach numbers existing along portions of the duct.

605

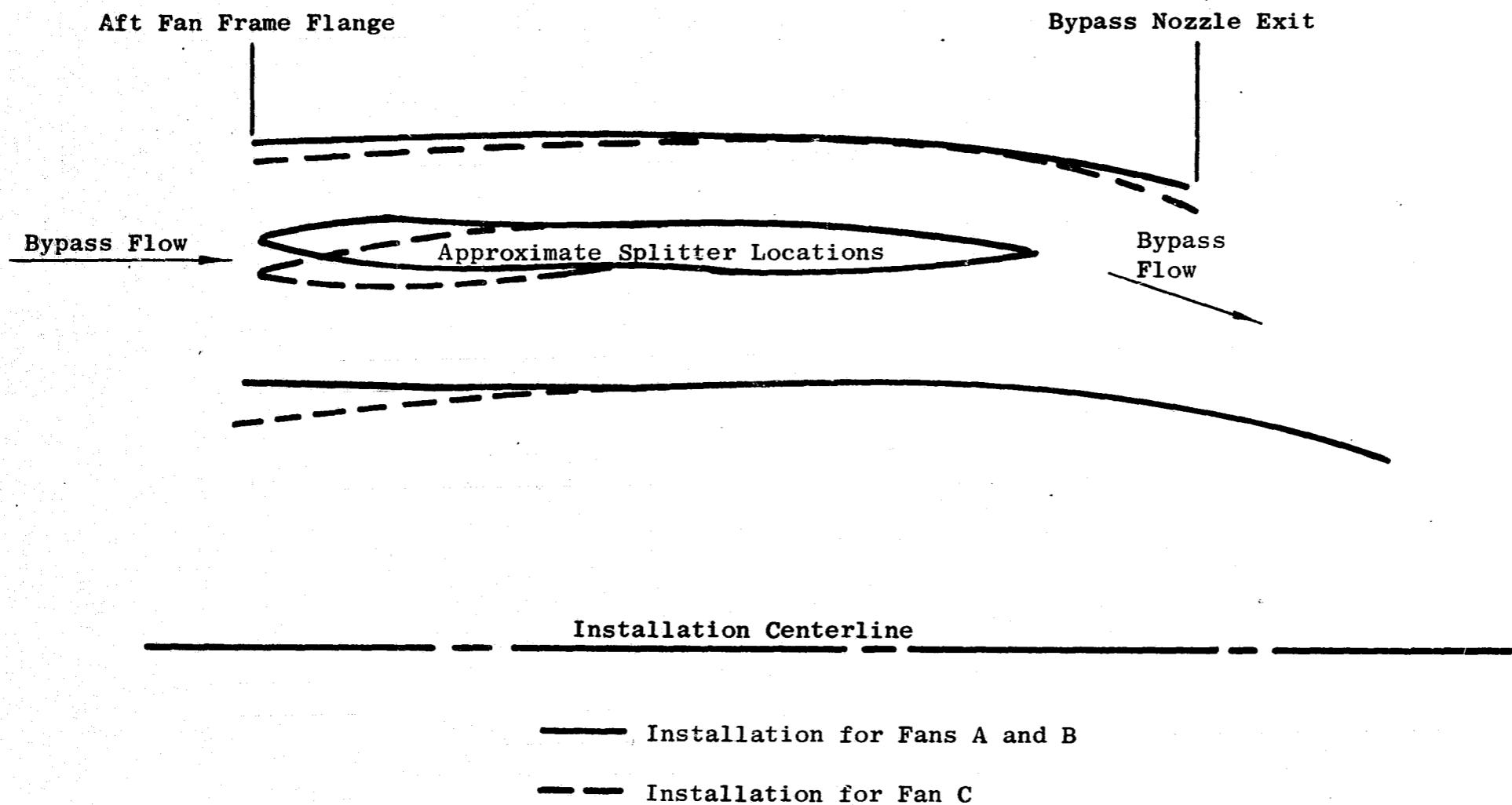


Figure 358. Schematic of the NASA-Lewis Installations Bypass Ducts, Indicating Common Parts and the Proposed Locations of Splitters Used to Increase the Amount of Duct Acoustic Treatment

909

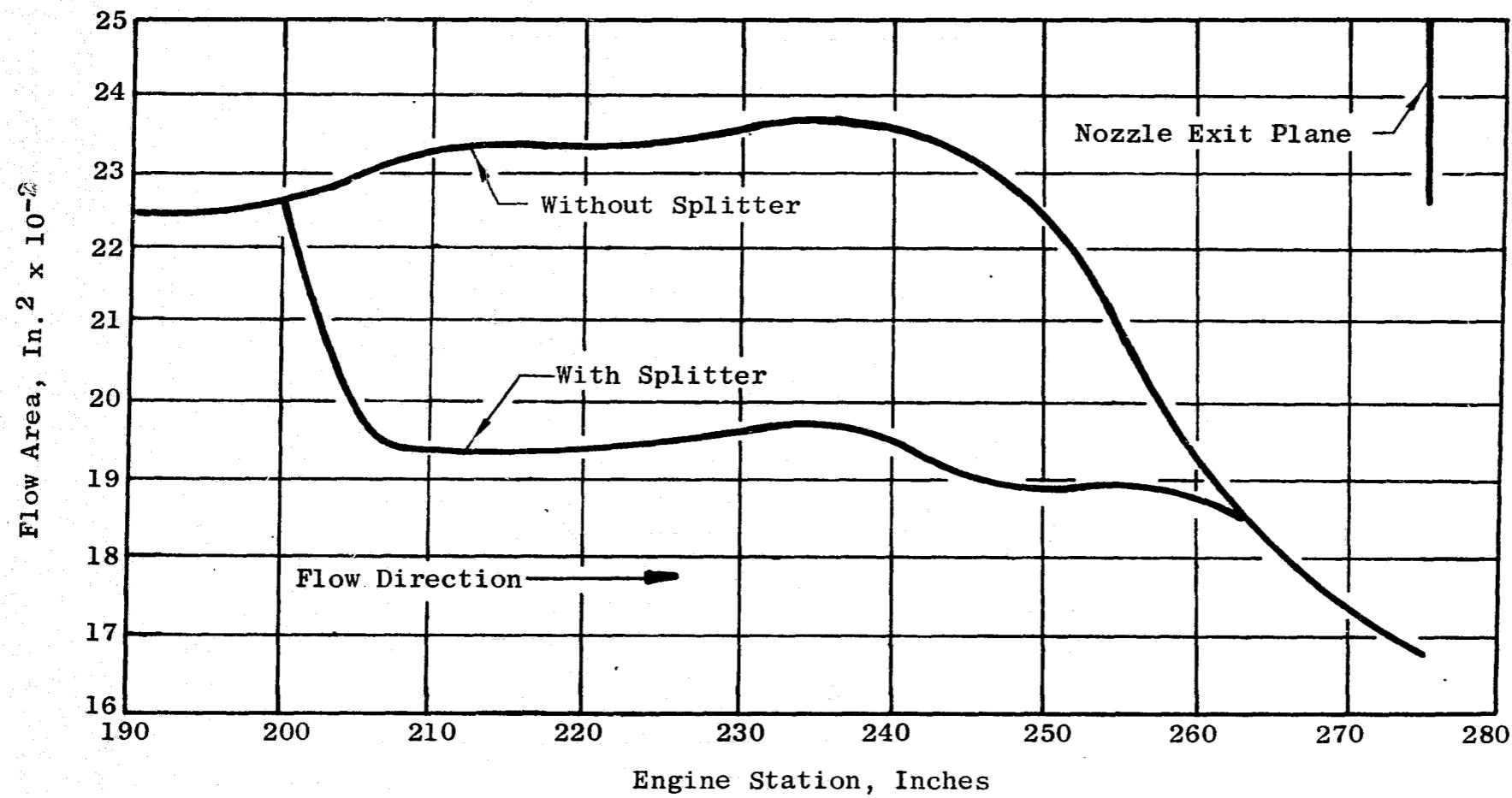


Figure 359. Bypass Duct Flow Area Distribution of the NASA-Lewis Installation for Fans A and B

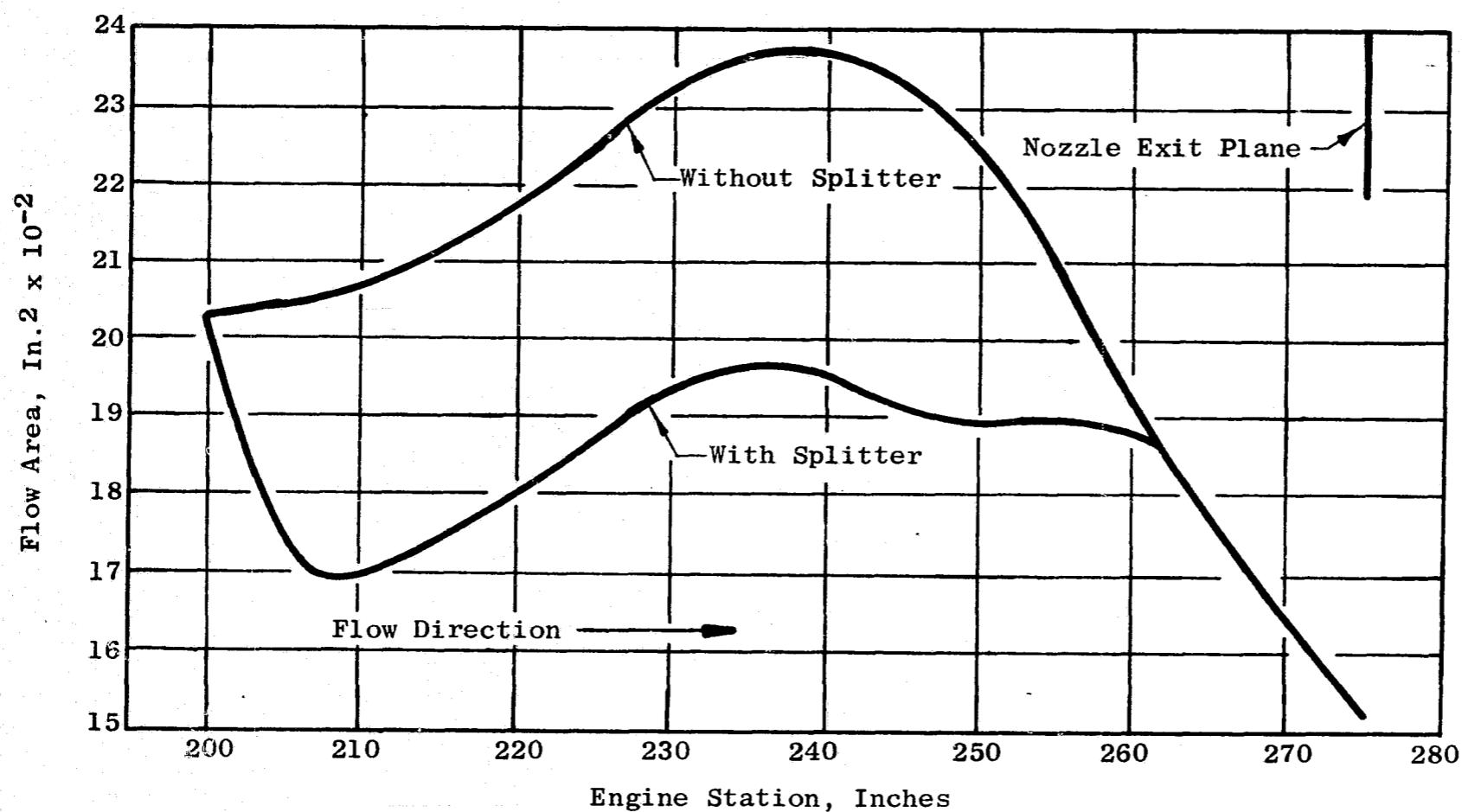


Figure 360. Bypass Duct Flow Area Distribution of the NASA-Lewis Installation for Fan C

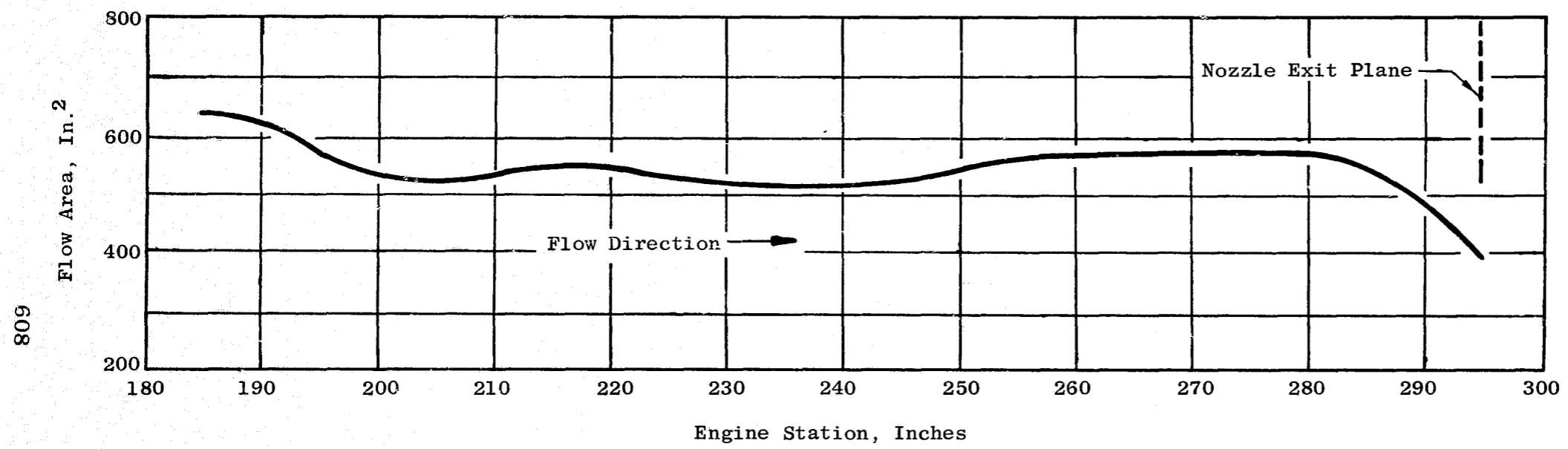


Figure 361. Core Duct Flow Area Distribution of the NASA-Lewis Installation for Fans A, B, and C

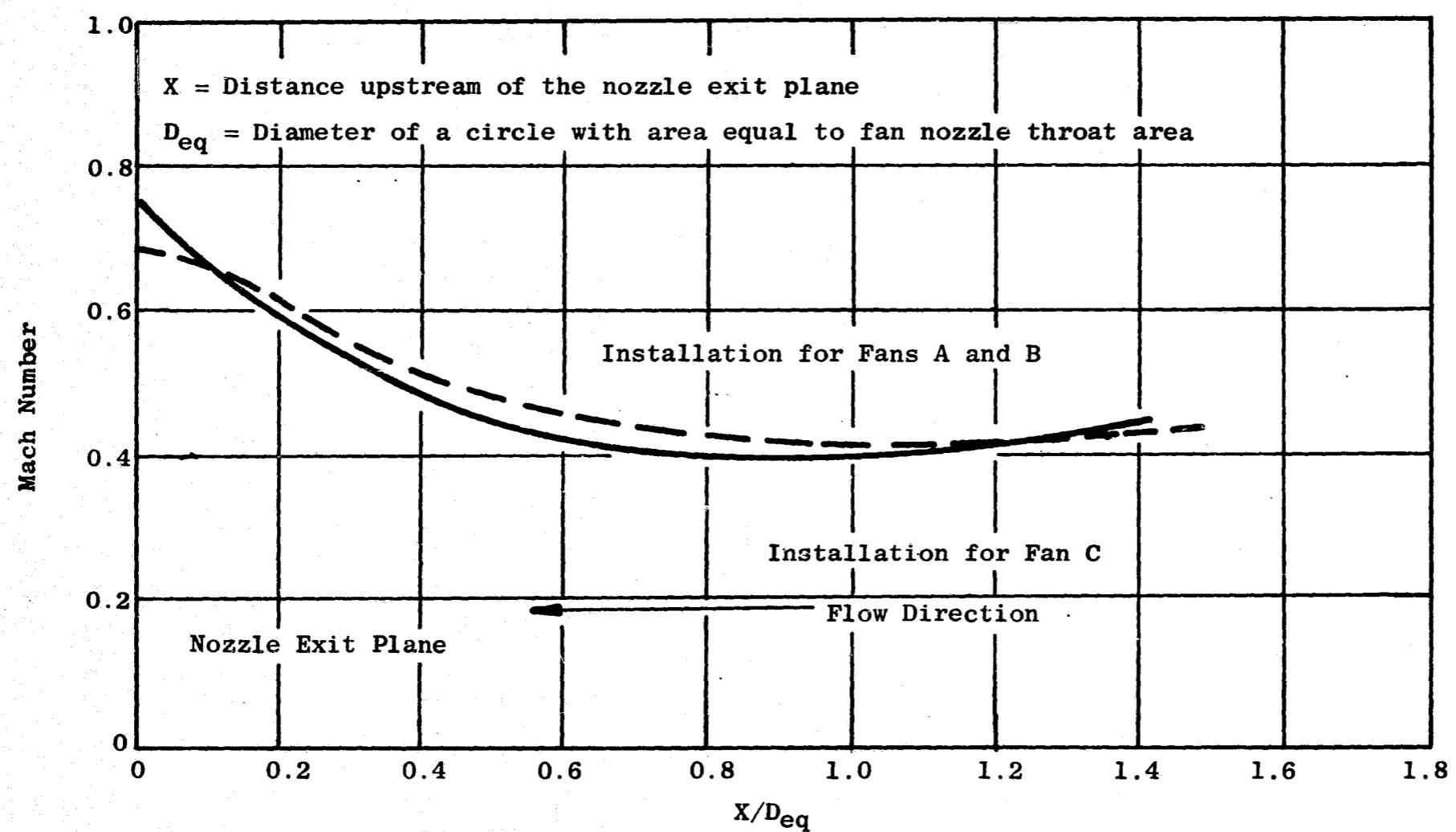


Figure 362. Bypass Duct Mach Number Distribution for the NASA-Lewis Installations

Table XVC. NASA-Lewis Facility Installation Duct Losses

Condition

Takeoff

Hot Day

$M_\infty = 0$

Alt = 0 ft

<u>Component</u>	<u>Engines</u>		
	<u>A</u>	<u>B</u>	<u>C</u>
Fan Duct (%P_{T23})	1.61	1.61	1.39
Core Duct (%P_{T55})	0.80	0.80	0.80
Core Cowl Drag (lbs)	35.6	35.6	40.5

12.0 TEST AND INSTRUMENTATION

12.1 SUMMARY

This section presents the test and instrumentation planning required for acquisition of acoustic and aerodynamic data for the full scale fan components, scale model vehicles, and full scale engine tests. The over-all test objectives for each area of test, as well as the instrumentation requirements, are specified. Also, the safety instrumentation required for adequate protection of the test vehicles is detailed. The three major test areas are:

- a) Component Development Testing, which covers the full scale fan testing at Lynn, Massachusetts.
- b) Scale Model Acoustic Testing, which covers the scale model vehicles testing at Peebles, Ohio.
- c) Full scale Engine Testing, which covers the engine testing at Peebles, Ohio.

12.2 FULL SCALE COMPONENT TESTING OF FANS A, B, C AND X

The three full scale fans, A, B, and C, will be first aerodynamically tested at General Electric's full scale fan test facility at Lynn, Massachusetts. Subsequently, these fans will be delivered to the NASA-Lewis for test in the Lewis far field acoustic test facility.

A fourth full scale fan will be aerodynamically tested in the Lynn facility. The design of this fan will be based upon aero/acoustic results from the previous full scale fans, as well as results from the acoustic scale model program.

12.2.1 Test Objectives

For each of the full scale fan vehicles, the test objectives are:

- a) Determine fan aerodynamic performance by obtaining a complete operating map, including surge limits and adiabatic efficiencies for both the bypass portion and the hub portion of the fan.
- b) Determine the effects of inlet distortion.

- c) Confirm the mechanical integrity of the fan components throughout each vehicle's operating range.
- d) Investigate the fan pure tone sound propagation.

12.2.2 Instrumentation

For each of the full scale fan vehicles, the instrumentation planned is shown in Figure 363 and is specified as follows:

12.2.2.1 Aerodynamic Instrumentation

Plane 0

24 (Min.) - Inlet screen thermocouples

Plane 0.5

4 - 6-element pitot-static rakes
8 - Outer wall static pressure taps

Plane 2.0

3 - Inlet distortion rakes, each rake having four static pressure immersions and twelve total pressure immersions.

Plane 2.5

5 - Static pressure taps equally spaced about the circumference
1 - Boundary layer rake
1 - 3-parameter radial traverse probe (cobra probe)
1 - 2-parameter radial traverse probe (wedge static probe)
The radial traverse probes will be axially located in a plane as close to the rotor hub as possible.

Plane 2.5 to 23

- A. Fans B and C
 - 10 - Kistler probes axially spaced over the rotor
 - 10 - Static pressure taps axially spaced over the rotor
- B. Fan A
 - 10 - Static pressure taps axially spaced over the rotor

Plane 23

- 5 - Static pressure taps equally spaced about the outer walls
- 1 - 3-parameter radial traverse probe (cobra probe)

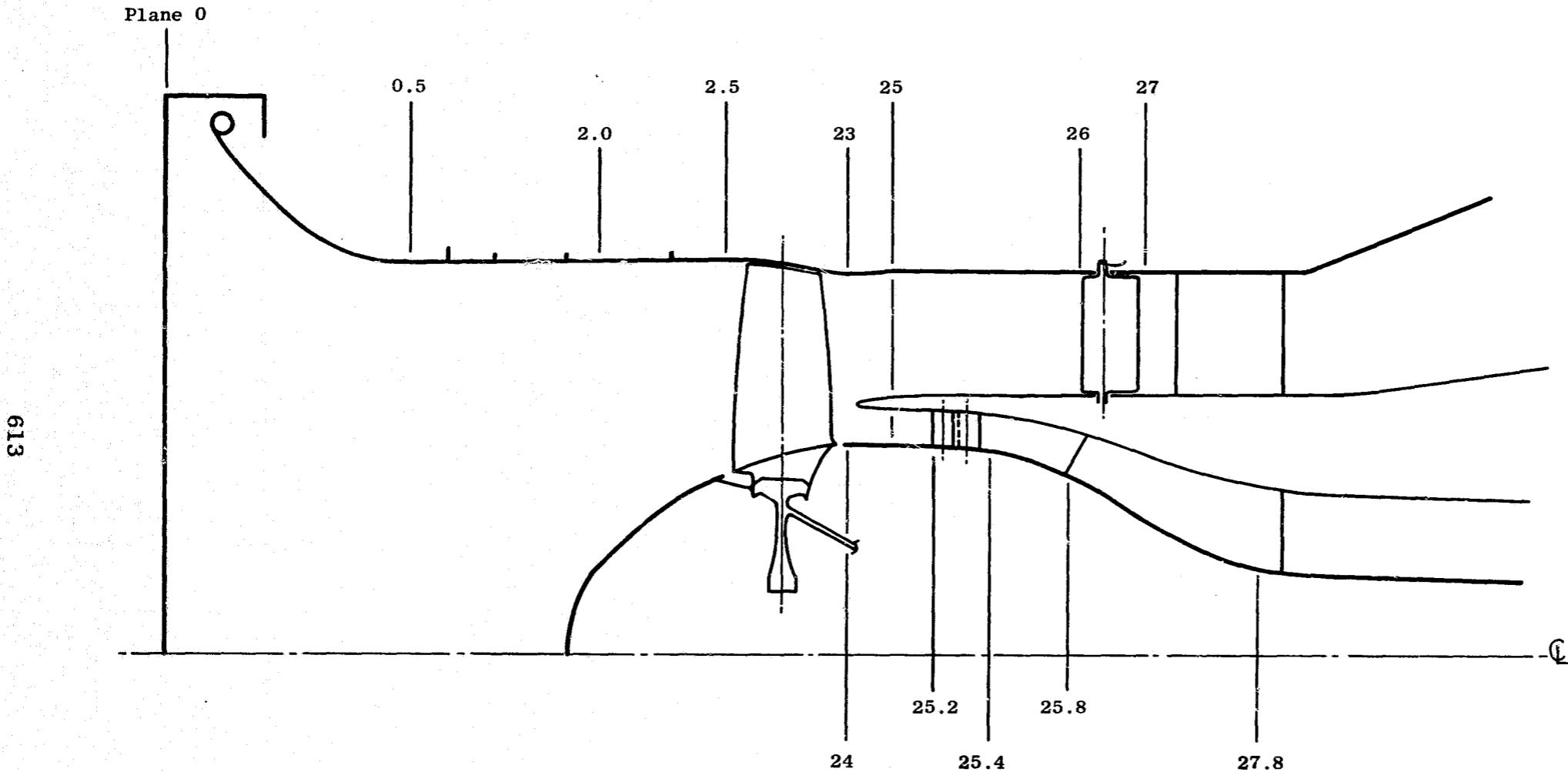


Figure 363. Full Scale Fan Installation Schematic

Plane 23 cont'd.

- 1 - 2-parameter radial traverse probe (disc static probe)
- 1 - High dynamic response radial traverse (either a hot-film or hot-wire probe)

Plane 23 to 25

- 5 - Static pressure taps axially spaced along the splitter in both the fan bypass and core flowpaths

Plane 24

- 5 - Static pressure taps equally spaced about the inner wall circumference

Plane 25

- 1 - Boundary layer rake in the fan bypass flowpath of the splitter
- 3 - 5-element total pressure rakes with elements located on centers of equal mass flow. These rakes will be located in the core flowpath.

Plane 23 to 26

- 4 - Static pressure taps axially spaced along the bypass outer wall and inner wall

Plane 24 to 25.2

- 5 - Static pressure taps axially spaced along the core inner wall

Plane 25.2

- 5 - Static pressure manifold groups on the core inner and outer walls, each group spanning one core OGV inlet passage. Provisions for traversing a yaw probe forward of the core OGV's and used only if needed.

Plane 25.4

- 5 - Static pressure manifold groups on the core inner and outer walls, each group spanning one core OGV exit passage
- 5 - 18-element combination total pressure total temperature wake rakes located approximately three-fourths core OGV chord length from the core OGV trailing edge. Each rake will be centered on immersions of equal mass flow.

Plane 25.4 to 25.8

- 5 - Static pressure taps axially spaced along the core inner and outer walls

Plane 27.8

- 6 - Static pressure taps circumferentially located about the core inner and outer walls.
- 5 - 5-element total pressure rakes with the elements located on centers of equal mass flow.
- 5 - 5-element total temperature rakes with the elements located on centers of equal mass flow.

Plane 26

- 5 - static pressure manifold groups on the bypass inner and outer walls, each group spanning one bypass OGV inlet passage.
- 1 - Yaw traverse probe

Plane 27

- 16 - Static pressure taps spaced about the inner and outer walls of the bypass OGV exit.
- 5 - Static pressure manifold groups on the bypass inner and outer walls, each group spanning one bypass OGV exit passage.
- 7 - 24-element combination total pressure/total temperature wake rakes, located approximately three-fourths of one bypass OGV chord length from the bypass OGV trailing edge. Each rake will be centered on immersions of equal mass flow.

12.2.2.2 Acoustic Instrumentation

One acoustic traverse located at fan inlet
One acoustic traverse located at bypass discharge

12.2.2.3 Safety Instrumentation

Rotor strain gages - 35 each

Stator Strain Gages - 15 each per stator system

- a total of 45 on Fans B and C

- a total of 30 on Fan A

The exact location of the strain gages will be determined by frequency and stress distribution investigations.

Clearanceometers - 4 each on Fan B and Fan C (2 each located over the rotor blade leading and trailing edges)

Vibration Pickups - 3 each on fan forward bearing housing
- 2 each on the bellmouth
- 2 each on the fan rotor casing

Lube oil static pressure taps

Lube oil thermocouples

Bearing race thermocouples

12.3 SCALE MODEL ACOUSTIC TESTING OF CONFIGURATION B AND C

Concurrent with the full scale fan test program, planning is in place for carrying out a comprehensive acoustic scale model fan evaluation program wherein unique noise reduction features will be evaluated. This acoustic scale model fan testing will be accomplished at the existing test setup at General Electric's Peebles, Ohio, far field acoustic test facility.

12.3.1 Test Objectives

The development test objectives for the acoustic scale model Fans B and C are:

- a) Evaluate the acoustic characteristics of the different fan acoustic configurations as a result of incorporating noise reduction features.
- b) Evaluate the effects of the acoustic modifications on the aerodynamic performance of each configuration.
- c) Confirm the mechanical integrity of each acoustic configuration.

12.3.2 Instrumentation

For scale model acoustic vehicles B and C, the instrumentation planned is shown in Figure 364 and is specified as follows:

12.3.2.1 Aerodynamic Instrumentation

Inlet - Plane 22

- 4 radial rakes with each rake having a 6-element immersion
- 3 parameters at each immersion (equal area)
 - a) Total
 - b) Static
 - c) Temperature
- 5 boundary layer rakes (15 elements each)
- 6 bellmouth wall statics
- 3 wall statics 4 inches forward of the fan

Fan Discharge - Plane 23

- 6 arc rakes (2 6-element rakes, 4 12-element rakes)

617

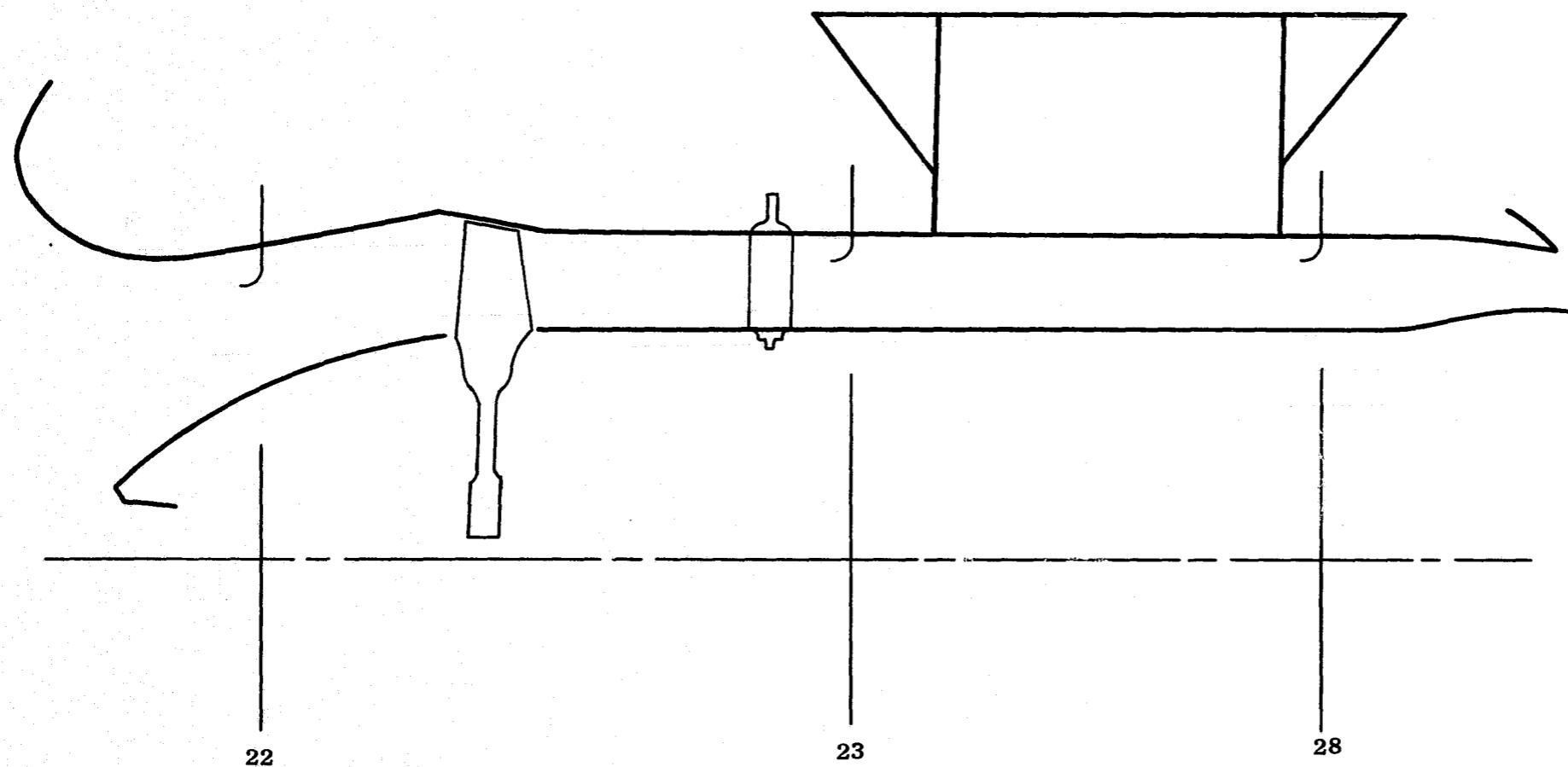


Figure 364. Instrumentation Planes, Acoustic Scale Model Vehicles

Fan Discharge - Plane 23

Each element has two parameters:

- a) Total pressure
- b) Temperature

6 radial rakes consisting of:

- 3 - 11-element rakes for boundary layer
- 3 - 7-element slanted rakes for total pressure

Fan Nozzle - Plane 28

3 14-element total pressure rakes (outer wall)

12.3.2.2 Acoustic Instrumentation

Sound Probes (Total of 3)

Inlet
Fan Discharge
Fan Nozzle

12.3.2.3 Safety Instrumentation

Strain Gages

On rotating parts, requiring slip ring
On nonrotating parts

Sump Instrumentation

14 bearing and seal thermocouples
8 static pressure taps
6 vibration pickups

12.4 FULL SCALE ENGINE TESTING

The aero/acoustic evaluation of the full scale bypass fan engines will be accomplished at General Electric's full scale far field acoustic facility at Peebles, Ohio.

12.4.1 Test Objectives

For each of the full scale engines tested, the test objectives are:

- a) Demonstrate the mechanical integrity of the basic engine system under sea level static conditions.
- b) Determine the engine aerodynamic and thermodynamic performance characteristics.
- c) Evaluate the noise characteristics of the engine.

12.4.2 Instrumentation

For each of the full scale engines, the instrumentation planned is shown in Figure 365 and is specified as follows:

12.4.2.1 Aerodynamic Instrumentation

Fan Inlet (Station 2.0)

Bellmouth Configuration

Total pressure	4 radial rakes with 6 elements per rake
Static pressure	4 radial rakes with 6 elements per rake
Total temperature	Rake-mounted thermocouples
Wall static pressure	4 wall static pressure taps

Flight Inlet Configuration

Total pressure	Inlet rake system similar to that used on CF6 or TF39 engines with flight-type inlets
Total temperature	
Static pressure	6 wall static pressure taps

Fan Discharge (Station 2.3)

Total pressure	7 arc rakes with 13 elements per rake
Total temperature	7 arc rakes with 13 elements per rake
Wall static pressure	10 wall static pressure taps

620

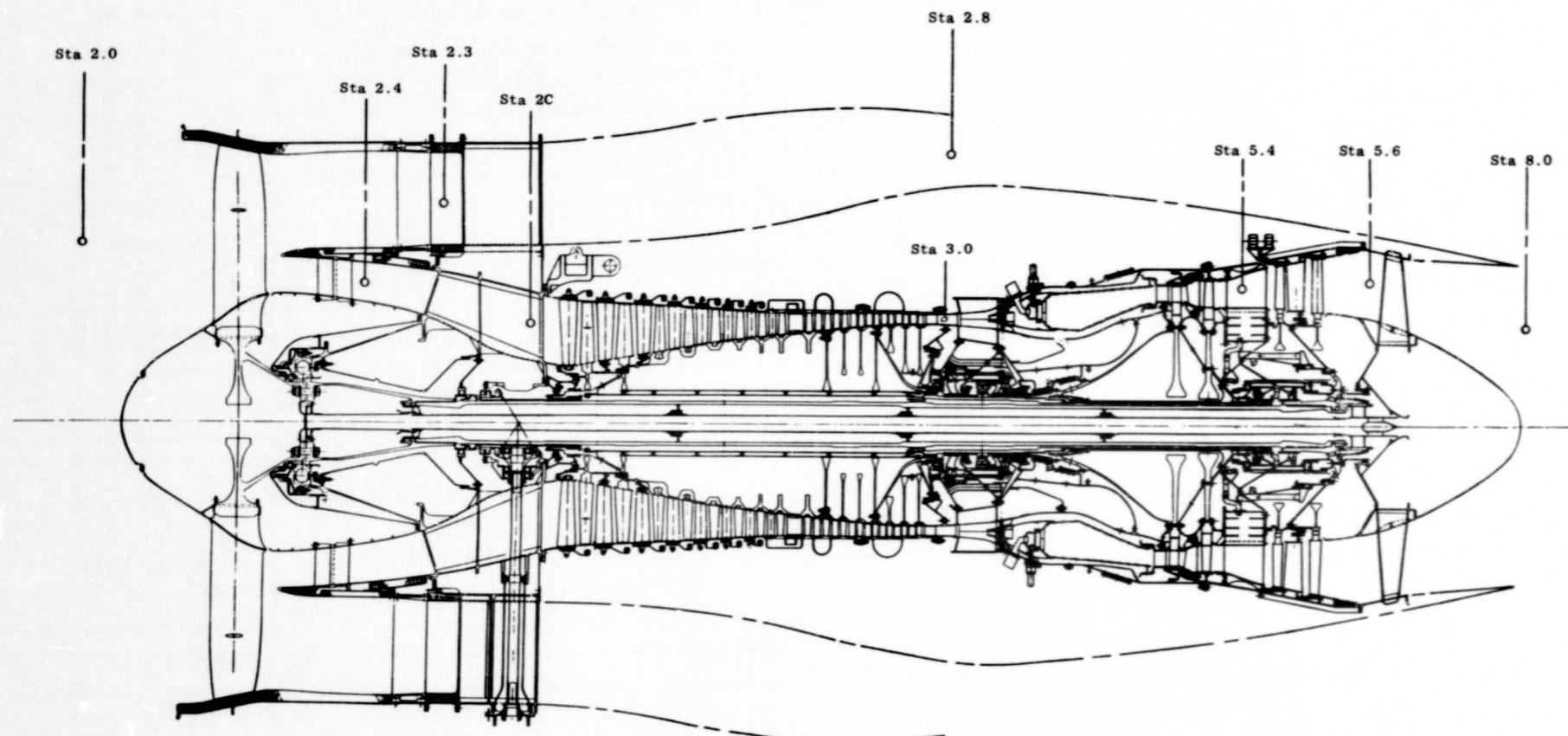


Figure 365. Typical Station Designations for Aerodynamic Instrumentation

Core Compressor Inlet (Station 2C)

Total pressure	6 radial rakes with 5 elements per rake
Total temperature	5 radial rakes with 5 elements per rake
Wall static pressure	12 wall static pressure taps

Core Compressor Discharge (Station 3.0)

Total pressure	5 radial rakes with 5 elements per rake
Total temperature	5 radial rakes with 5 elements per rake
Wall static pressure	5 wall static pressure taps

LP Turbine Inlet (Station 5.4)

(Configuration A and B)

Total pressure	CF6 pressure harness - average of 25 elements
Total temperature	CF6 temperature harness - average of 22 elements

LP Turbine Inlet (Station 5.4)

(Configuration C)

Total pressure	6 radial rakes with 5 elements per rake
Total temperature	6 radial rakes with 5 elements per rake

Low Pressure Turbine Discharge (Station 5.6)

Total pressure	4 radial rakes with 5 elements per rake
Total temperature	4 radial rakes with 5 elements per rake

Primary Nozzle Throat (Station 8.0)

Smoke level	1 smoke sampling probe
Total pressure	5 radial rakes with 5 elements per rake
Total temperature	5 radial rakes with 5 elements per rake
Static pressure	4 axial wall taps

12.4.2.2 Acoustic Instrumentation

Fan Inlet (Station 2.0)

Acoustic radial traverse probe

Fan Discharge (Station 2.3)

Acoustic radial traverse probe

Fan Nozzle Discharge (Station 2.8)

Acoustic radial traverse probe

12.4.2.3 Safety Instrumentation

To insure safe operation of the engine, standard safety instrumentation will be used and will consist of vibration pickups, lube pressures, fuel pressures, bearing and seal temperatures, and sump pressures. Strain gages will be incorporated to monitor stress levels, but will be limited to those engine configurations which contain components on which strain gages would be considered necessary.

13.0 ENGINE CYCLE PERFORMANCE

13.1 SUMMARY

This section presents an abbreviated cycle performance tabulation to provide over-all engine A, B, and C performance data. The performance shown is based on the predicted component performance maps determined under Phase I of the Experimental Quiet Engine design and on the measured core engine performance established from TF39/CF6 engine and component tests. A more extensive engine performance tabulation, covering a range of flight Mach numbers and altitudes will be included in separate report to be issued in April 1970.

13.2 ENGINE CYCLE PERFORMANCE

The data shown in Table XIVC are based on U.S. Standard Atmosphere, 1962, standard day inlet conditions and 100 percent ram recovery. The thrust levels shown are uninstalled values based on ideal exhaust nozzle performance. Fan duct and tailpipe pressure losses, representative of predicted values for the test engine configurations, are included. The fuel heating value used was 18400 BTU/lb. No customer bleed or power extraction is assumed in the data shown.

The three engines are sized for 4900 pounds thrust at the engine design point, Mach 0.82, 35 000 feet. Fans A and B have the same fan pressure ratio and airflow at this flight condition. Fan C, which has a higher fan pressure ratio commensurate with it's higher fan tip velocities, is sized for a smaller airflow. At the design point, the difference in specific fuel consumption (SFC) for the three engines is approximately 1.5 percent, with the Fan B cycle having the lowest level. Although the bypass ration of Fan B is lower than that of Fan A, this effect on SFC is offset by the combination of higher cycle pressure ratio and reduced turbine inlet temperature of Fan B. Fan C has the highest cycle pressure ratio and lowest temperature; however, the lower bypass ratio results in an increased SFC relative to the other cycles.

With the engines sized at the Mach 0.82, 35000-foot flight condition, the performance at sea level static was established by operation to a thrust level of 22 000 pounds. At this condition, the fan and core speeds are reduced from the cruise levels, and the cycle pressure ratio is lower.

Table XIV.C. Predicted Cycle Performance Data

Parameter	Mach 0.82, 35000'			Sea Level Static			Mach 0.25, Sea Level		
	Standard Day			Standard Day			Standard Day		
	A	B	C	A	B	C	A	B	C
Net Thrust*, Lbs	4900	4900	4900	22000	22000	22000	16139	16120	16237
Specific Fuel Consumption, (Lbs/Hr)/Lb	0.644	0.641	0.651	0.358	0.356	0.368	0.473	0.470	0.487
Total Airflow, Lbs/Sec	374	374	361	827	826	804	859	858	832
Total Corrected Airflow, Lbs/Sec	949	949	915	827	826	804	827	827	801
Bypass Ratio	5.52	5.32	4.87	5.33	5.18	4.70	5.53	5.37	4.86
Fan Pressure Ratio	1.5	1.5	1.6	1.41	1.42	1.48	1.39	1.39	1.45
Duct Exhaust Nozzle Pressure Ratio	2.29	2.29	2.44	1.39	1.40	1.45	1.43	1.43	1.49
Duct Exhaust Velocity	1012	1011	1025	795	796	848	829	830	881
Cycle Pressure Ratio	17.67	18.12	18.97	15.27	15.58	16.57	14.68	14.98	15.94
Turbine Inlet Temperature, °F	1738	1714	1689	1896	1873	1859	1882	1859	1847
Core Exhaust Nozzle Pressure Ratio	2.06	2.07	1.78	1.36	1.36	1.27	1.36	1.36	1.28
Core Exhaust Velocity	1552	1538	1442	1168	1158	1019	1171	1161	1023

* Uninstalled net thrust, based on ideal exhaust nozzle performance

Performance at the take-off condition (Mach 0.25, sea level) is established by holding the core gas generator speed constant at the level defined by the sea level static condition. At the take-off condition, all three engines provide comparable thrust levels.

14.0 REFERENCES

1. Benzakein, M. J. and Kazin, S. B.: "Fan/Compressor Noise Reduction," ASME Paper 69GT-9.
2. Benzakein, M. J. and Morgan, W. R.: "Analytic Prediction of Fan/Compressor Noise," ASME Paper 69WA/GT-10.
3. Seyler, D. R. and Smith, L. H.: "Single Stage Experimental Evaluation of High Mach Number Compressor Rotor Blading Part 1 - Design of Rotor Blading," NASA CR-54581, April 1, 1967.
4. Smith, L. H. and Yeh, Hsuan: "Sweep and Dihedral Effects in Axial-Flow Turbomachinery", Journal of Basic Engineering, Trans. ASME, Series D, Vol. 85, 1963, pp. 401-416.
5. Reddy, J. L. and Klapproth, J. F.: "Advanced Fan Development for High Bypass Engines," AIAA Paper Number 68-563, June 1968.
6. Gostelow, J. P., Krabacher, K. W. and Smith, L. H.: "Performance Comparisons of High Mach Number Compressor Rotor Blading," NASA CR-1256, December, 1968.
7. Rockenbach, R. W. : "Single Stage Experimental Evaluation of Slotted Rotor and Stator Blading," Part 1X-Final Report, NASA CR-54553.

PRECEDING PAGE BLANK NOT FILMED